Conf-790854

336
1-2-80

Lh. 466

U[illegible]EPARTMENT OF ENERGY
Division of Energy Storage Systems

MASTER

Coordinated by the Pacific Northwest
Laboratory for the Assistant Secretary for
Conservation and Solar Energy

Proceedings of the 1979 Mechanical and Magnetic Energy Storage Contractors' Review Meeting

M-22

August 1979
Washington, D.C.

Published December 1979

DISCLAIMER

790854
Conf-790584-
Dist. Category UC-94b

U.S. DEPARTMENT OF ENERGY
Division of Energy Storage Systems
Washington, D.C. 20545

Coordinated by the Pacific Northwest Laboratory for the Assistant Secretary for Conservation and Solar Energy

Proceedings of the 1979 Mechanical and Magnetic Energy Storage Contractors' Review Meeting

August 1979
Washington, D.C.

Published December 1979

TABLE OF CONTENTS

Papers are grouped by session in the order they were presented at the conference.

Compressed Air Energy Storage (cont.)

UNDERGROUND PUMPED HYDRO STORAGE

SOLAR MECHANICAL ENERGY STORAGE

FLYWHEELS

SESSION 1: SUPERCONDUCTING MAGNETIC ENERGY STORAGE

THIS PAGE

WAS INTENTIONALLY

LEFT BLANK

PROJECT SUMMARY

Project Title:	"Development of Standards for Superconducting Materials and Superconductors"
Principal Investigators:	A. F. Clark and F. R. Fickett
Organization:	National Bureau of Standards Boulder, CO 80303 (303) 499-1000, X3253
Project Goals:	The superconductor standards program is a cooperative effort funded by: NBS and four division of DOE (Energy Storage, Fusion Energy, High Energy Physics, and Magnetohydrodynamics through the Francis Bitter National Magnet Laboratory). The goal of the program is to arrive at a set of voluntary standards for modern practical superconductors that will be acceptable to both manufacturers and users. The need for such a set of standards increases as more and more large superconducting magnet systems are designed and constructed. The primary areas in which standards are now being developed are: critical current, critical temperature, critical field, and physical and mechanical properties of conductors.
Project Status:	Four papers presenting interim definitions for superconducting parameters have been completed. Three have been published. An ASTM subcommittee on superconductors has been formed and task groups appointed. A national survey of measurement techniques has been made. Extensive studies have been made of the effect on results of various practices in common methods of measuring critical current. A comparison of three techniques for measuring critical temperature (calorimetric, susceptibility and resistive) has been made.
Contract Number:	02-79-ET-26603,000
Contract Period:	FY'79
Funding Level:	$185K
Funding Source:	U.S. Department of Energy

STANDARDS FOR SUPERCONDUCTORS

F. R. Fickett and A. F. Clark
Thermophysical Properties Division
National Bureau of Standards
Boulder, Colorado 80303

ABSTRACT

This report describes the present state of the superconductor standards program and includes a brief historical introduction. The need for standards in this area is described with particular attention paid to the need for consensus among all interested parties and our techniques for achieving it. Early results from the experimental research projects are presented and the scope of the entire program is outlined.

INTRODUCTION

The superconductor standards program is a cooperative effort funded by: NBS, four divisions of DOE (Energy Storage, Fusion Energy, High Energy Physics, and Magnetohydrodynamics through the Francis Bitter National Magnet Laboratory), and the Air Force Aeropropulsion Laboratory. The goal of the program is to arrive at a set of voluntary standards for modern practical superconductors that will be acceptable to both manufacturers and users. The need for such a set of standards increases as more and more large superconducting magnet systems are designed and constructed.

The basis for the program was set several years ago at meetings called by NBS at The ASM Conference on the Manufacture of Superconducting Materials and the Applied Superconductivity Conference, 1976. The manufacturers, users, and researchers present all made extensive suggestions as to how the work should proceed. In the years that followed a small program was initiated, with NBS funding, to make a more formal survey of the needs and desires of the research community. From this study and several related meetings, the following conclusions were drawn:

> For all concerned, standards were both necessary and desirable.
>
> The small size and financial position of the wire manufacturing industry (and its competitive nature) precluded industrial developments of standards in a reasonable period of time.
>
> The NBS Cryogenics Division (now Thermophysical Properties Division) was an "unbiased third party" with the charter, the desire, and the expertise to carry out a superconductor standards program of a sufficient size that significant progress could be made in a time span of several years.
>
> The problem, as always, was funding.

Fortunately, there appeared to be agreement with our conclusions among a variety of agencies, and cooperative funding of the program as described above was arranged. The full project started in mid-FY 79.

The development and promulgation of standards can be a very sensitive issue, for sound financial reasons. Because of this, our program relies heavily on continuing interactions

between all interested parties to assure that, as far as possible, a consensus will be developed on any proposed standard. To this end a portion of the funding is subcontracted to each of the U.S. wire manufacturers to promote development of their research capability, to provide us with needed data, and to provide a source of funding for their participation in work associated with test development. Furthermore, a new ASTM subcommittee on superconductors (ASTM B1.08) was formed earlier this year with excellent participation from manufacturers, funding agencies, and the national laboratories. The first formal report of the various task groups will be presented at the International Cryogenic Materials Conference in late August. Minutes of the organizational meeting are available from the authors.

The term Standards as used here may indicate any or all of four quite different aspects of standardization:

1. Unambiguous definition of terminology,
2. Detailed description of measurement technique,
3. Development of common experimental apparatus,
4. Preparation and characterization of reference materials.

The role of each of these aspects in our program is described in the following sections, where more specific examples are discussed.

DEFINITION OF TERMS

It was decided early that the first step in any standards program should be the development of a uniform terminology. To this end an extensive review of existing terminology was made and several review iterations were performed involving more than 50 reviewers both in this country and abroad. The result was four papers containing proposed definitions, three of which have now been published in the open literature. They deal respectively with:

1. Fundamental states and flux phenomena[1]
2. Critical parameters[2]
3. Fabrication, stabilization and transient losses[3]
4. Josephson phenomena[4].

The ASTM committee described above is now reviewing some of the terms and each of the published papers solicits responses from the readers. Ultimately all definitions will be collected in a NBS document that will serve as the guide for their application.

A specific example of problems created by ambiguous definitions is illustrated in Fig. 1 which shows the effect of stress on the critical current of a commercial high field superconductor measured at NBS[5]. The separate curves indicate the critical current behavior one observes using the indicated criterion or definition for critical current. Note that not only the magnitude, but also the shape of the curve is affected. All of the definitions shown have been used. Our studies have led us to conclude that the use of either the electric field criterion or the resistivity criterion will provide a maximum of information with minimum effort.

MEASUREMENT TECHNIQUES

The measurement of critical parameters of superconductors (current, field, and temperature) as well as other phenomena of importance in applications (ac losses, effects of stress and fatigue, etc.) require complex apparatus that usually must be constructed by the experimenter. In such measurements it is not uncommon for the results from different laboratories to be quite different even though everyone agrees on the definitions of the appropriate terms and similar apparatus is used. One solution to this problem is the use of a very detailed and reproducible experimental technique that has been developed from extensive experimentation. This type of development is one of the strong thrusts of our program.

To again use our experimental critical current investigation as an example, consider Fig. 2, which shows the effect of the use of grease as a means of holding the test specimen in a "conventional" hairpin test rig machined from linen phenolic[6]. Clearly, this apparently rather innocuous (and common) laboratory technique greatly influences the result.

In support of the program segment on standard measurement techniques, we are now surveying all of the laboratories that make these measurements routinely to determine the details of their technique and apparatus. We intend to publish the results as a NBS report if the information developed appears to be of sufficiently wide interest. A similar survey of techniques

used in Japan, a leader in new materials technology, has been prepared by a guest worker on the program (Dr. Genshiro Fujii of the Institute for Solid State Physics, University of Tokyo) and will be published later this year.

APPARATUS DEVELOPMENT

It is often desirable to have a standard apparatus design available for a given test. Frequently the technique and apparatus descriptions are a single document (e.g. ASTM Standards). Care is needed in the design phase to insure that the device is suited to all potential users and that a given measurement can be completed in a reasonable time. Our first design in this category is for a critical current apparatus and work has just started. The final design will be subjected to a detailed evaluation by interested parties. If possible, apparatus will then be sent to various laboratories for field trials of the design.

Another aspect of apparatus development occurs in the situation where widely different techniques are used to measure what is ostensibly the same quantity. Determining the causes of disagreement among the techniques can be a very difficult task. A specific example is provided by the ac loss phenomena in superconductors. The losses may be determined by a calorimeter, a wattmeter, or a flux integration technique. All of these measurements are difficult and agreement between any two is rare; among three it is essentially nonexistent. One of our experimental projects has started to research the problem and preliminary experimental data are shown in Fig. 3 from one of our latest publications[7]. These results are very encouraging, but much work remains to be done before we understand all of the parameters.

A similar project is also underway at NBS (Gaithersburg) to compare several techniques commercially used for the measurement of critical temperature.

REFERENCE MATERIALS

Evaluation of apparatus and test techniques employed at different locations is greatly simplified by the use of standard reference materials. In the case of testing of practical superconductors, such materials are nearly essential. The acquisition and characterization of superconductors representing a range of properties is an important part of the program plan, but one that will be pursued later in the program. An informal inventory of available materials at various manufacturers has been made as a first step.

CONCLUSIONS

All aspects of the superconductor standards program are progressing well in spite of a rather late start this year. The experimental projects at NBS are already producing useful data and our subcontractors are well along at setting up their respective experiments. The response of the users and suppliers to our efforts at involving them in all aspects of the program has been gratifying. In FY 80 we anticipate much greater visibility for the program as more experimental results become available and our activities in definitions and apparatus standardization receive further distribution.

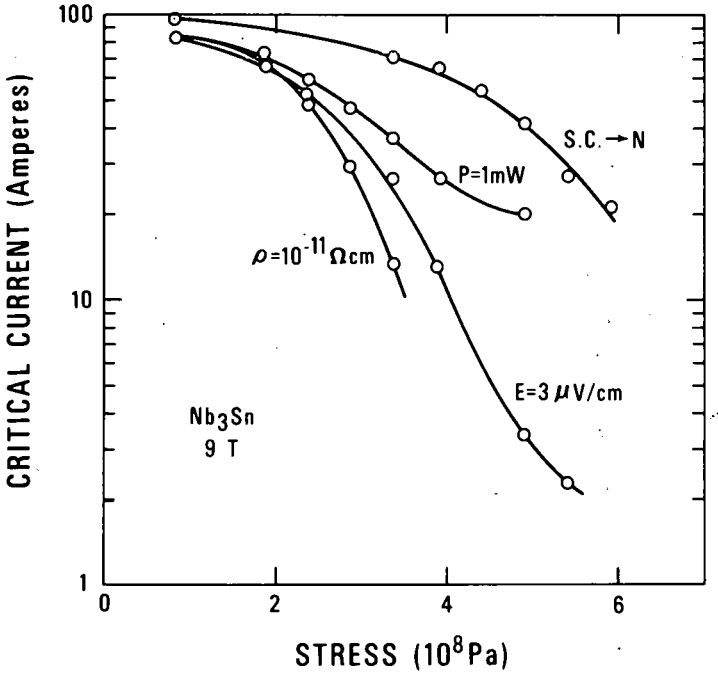

Fig. 1 The critical current of a Nb_3Sn multifilamentary conductor as a function of applied stress for various critical current criteria.

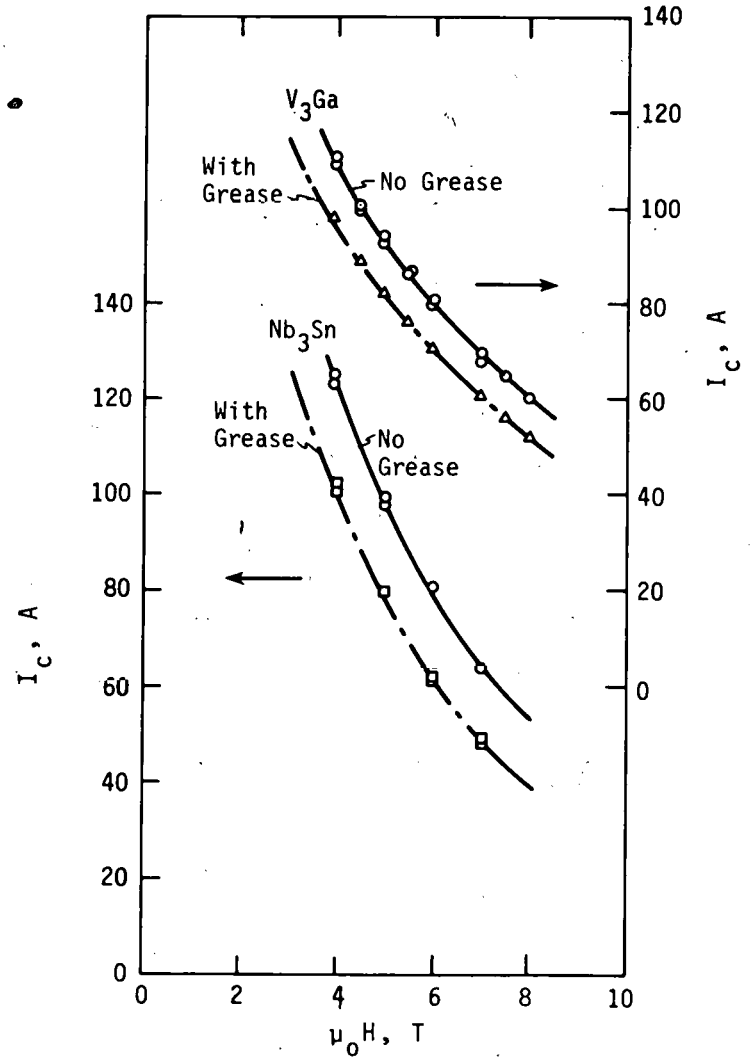

Fig. 2 Critical current degradation of Nb_3Sn and V_3Ga fixed with grease to a phenolic sample holder with fiber direction perpendicular to the sample.

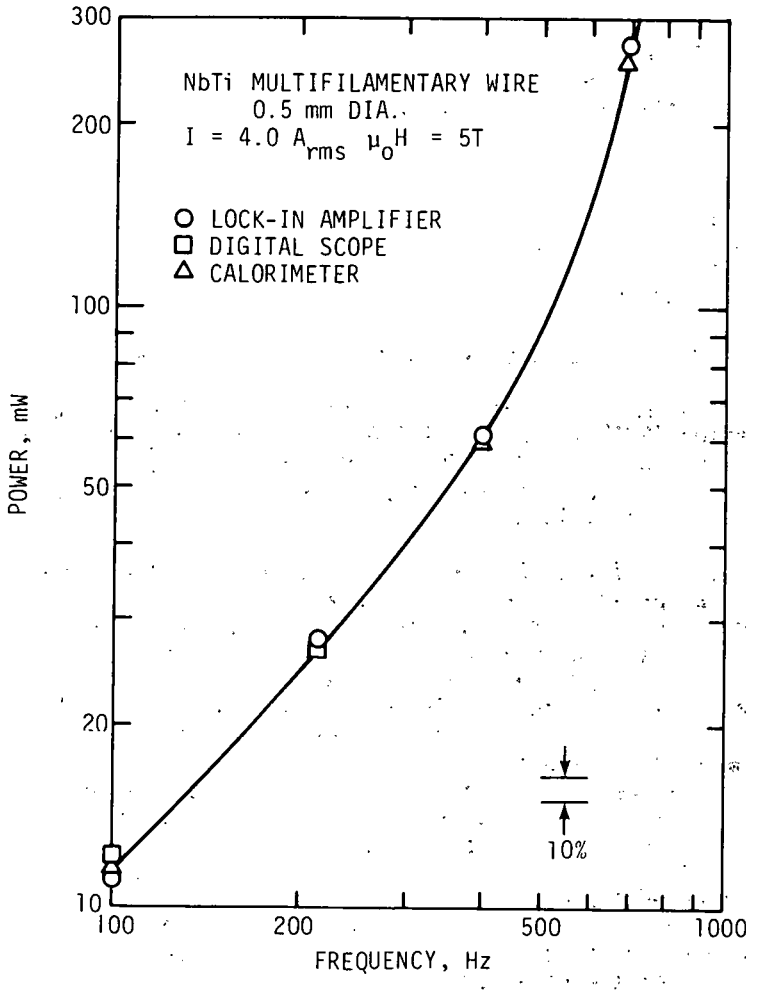

Fig. 3 The ac loss as a function of frequency for a multifilamentary NbTi superconductor. A calorimetric value at 215 Hz is not shown since it agrees almost exactly with the digital value.

REFERENCES

1. R. L. Powell and A. F. Clark, Cryogenics 17, 697 (1977).
2. R. L. Powell and A. F. Clark, Cryogenics 18, 137 (1978).
3. D. T. Read, J. W. Ekin, R. L. Powell, and A. F. Clark, Cryogenics 19, 327 (1979).
4. R. L. Powell, S. B. Kaplan, R. Radebaugh, and F. R. Fickett, Cryogenics (To be published).
5. A. F. Clark and J. W. Ekin, IEEE Trans. Mag. MAG-13, 38 (1977).
6. G. Fujii, J. W. Ekin, R. Radebaugh, and A. F. Clark, Paper No. FA-19, Cryogenic Engineering Conference/International Cryogenic Materials Conference, University of Wisconsin, August 21-24, 1979.
7. R. Radebaugh, G. Fujii, D. T. Read, and A. F. Clark, Paper presented at the XVth International Congress on Refrigeration, Venice, Italy, September 23-29, 1979.

PROJECT SUMMARY

Project Title:	Superconducting Magnetic Energy Storage (SMES)
Principal Investigator:	John D. Rogers
Organization:	University of California Los Alamos Scientific Laboratory Los Alamos, NM 87545 (505) 667-5427; FTS 843-5427
Project Goals:	The goals of the SMES program are two-fold. These are to design, fabricate, and place into operation a 30-MJ, 10-MW SMES unit for electric utility transmission line stabilization on the Bonneville Power Administration (BPA) system by 1982-83. The second goal is to design and have constructed a 10-to-50-MWh SMES unit. This unit will be for a completely detailed engineering prototype demonstration of an electric utility diurnal load-leveling system.
Project Status:	The engineering design of the BPA SMES transmission line stabilization system is in an advanced state. Many large hardware items are determined and on order. The refrigerator has passed the acceptance test. It is being installed in a trailer obtained for this purpose. The superconducting wire for the 30-MJ coil has been obtained. A contract was placed with General Atomic Co. for design of the 30-MJ coil. The design is about 80% complete. Lengths of 5-kA cable have been received and tested. Additional cable development is necessary. The converter has been ordered and all components for the protective energy dump circuit have been received. Surplus high-pressure gas-recovery compressors have been obtained and are to be trailer mounted. Similarly, an evaporative cooler has been obtained and will be trailer mounted for a heat-rejection unit. Detailed controls design and operating logic are being addressed for remote microwave-link operation of the SMES unit in the BPA system. An RFQ has been issued for the power transformer. The reference design for a 1-GWh diurnal load-leveling SMES unit was completed. The costs extrapolated to a 10-GWh unit were determined to be \$77 to \$111/kWh. Recommendations, based on the study, are made for extending the large SMES unit work.
Contract Number:	W-7405-ENG-36
Contract Period:	Continuing
Funding Level:	\$1,385,000 FY79
Funding Source:	Department of Energy, Division of Energy Storage Systems and Division of Electrical Energy Systems.

THE STABILIZATION UNIT FOR BONNEVILLE POWER ADMINISTRATION

R. I. Schermer
Los Alamos Scientific Laboratory of the
University of California
Los Alamos, New Mexico 87545

ABSTRACT

The Bonneville Power Administration operates the transmission system that joins the Pacific Northwest and southern California. A 30-MJ (8.4 kWh) Superconducting Magnet Energy Storage (SMES) unit with a 10-MW converter can provide system damping for low frequency oscillations. The unit is scheduled to operate in 1982. Progress during FY 79 is described, including the details of mechanical and electrical testing of prototype conductors and the design, specification, and procurement activities for the energy storage coil, nonconducting dewar, electrical system and cryogenic system.

INTRODUCTION AND SUMMARY

The Pacific Northwest and southern California are part of the Western US Power System and are connected by two 500-kV, ac-power transmission lines, collectively referred to as the Pacific AC Intertie, and one ± 400-kV dc-transmission line, the Pacific HVDC Intertie. The two ac lines have a thermal rating of 3500 MW, and the dc line has a rating of 1440 MW.

The stability of the Western Power System is affected by relative weakness of the tie provided by the 905-mile-long Pacific AC Intertie. In fact, studies made before energization of the Pacific AC Intertie showed that negatively damped oscillations with a frequency of about 20 cpm were likely to occur. In 1974 negatively damped oscillations with a frequency of 21 cpm (0.35 Hz) were observed. The peak-to-peak oscillation on the Pacific AC Intertie was about 300 MW. Subsequent to these instabilities, the Bonneville Power Administration (BPA) installed equipment to modulate the power flow on the HVDC Intertie as a means of damping the oscillations. The maximum possible power modulation on the HVDC Intertie is 40 MW, about 3 percent of the HVDC power rating. The modulation of the HVDC Intertie has increased the stability limit of the Pacific AC Intertie from about 2100 MW to 2500 MW whenever the HVDC Intertie is operating. However, the HVDC Intertie does not operate continuously. The line availability is 89.5%, and the southern terminal was down for six months as a result of earthquake damage. A back up stabilizing system could be used. Late in 1975, representatives of BPA and the Los Alamos Scientific Laboratory (LASL) developed the concept of installing a small SMES unit for the purpose of providing system damping similar to that now available through modulation of the Pacific HVDC Intertie. The design parameters of the unit to be installed at the Fite Substation near Tacoma are summarized in Table 1.

TABLE 1. Design Parameters of a 30-MJ System Stabilizing SMES Unit

Maximum power capability, MW	10
Operating frequency, Hz	0.35
Energy interchange, MJ	9.1
Maximum stored energy, MJ	30.0
Coil current at full charge, kA	5
Maximum coil terminal voltage, kV	2.18
Coil operating temperature, K	4.5
Coil lifetime, cycles	$>10^7$
Heat load at 4.5 K, W	<150
Coil diameter, m	3.0

Several technical descriptions of the project have appeared previously,[1,2] and should be consulted for details. This report will concentrate principally on the work done in FY 79 and on the current status of hardware procurement.

Figure 1 is a schematic that shows the main components of a SMES system. The coil will be immersion cooled in liquid helium at 4.5 K and will have an open wound construction very similar to that employed in existing coils. The unusual features of the coil are the very low heat generation allowed, despite the unusually short cycle time, and the very large number of operating cycles expected over its life. The conductor originally proposed for this application is a modification of the conductor used by Westinghouse[3] in a pulsed superconducting coil constructed for the Controlled Thermonuclear Reactor development program at LASL. The superconducting wire has been obtained and tested. The coil designer, General Atomic,[4] has recently proposed a pancake coil design rather similar to that used in a number of successful bubble chambers.

Most of the other components of the unit are well within the state of the art. The converter, a scaled-down version of the thyristor units now used on high-voltage dc-transmission lines, is under construction. The control system for regulating the power flow between the ac system and the SMES system has been developed and demonstrated in the laboratory. The refrigerator is a standard unit and is under test. The dewar, similar to one that has operated successfully for a period of several years, must be made of a nonconductive material such as epoxy fiber glass to avoid eddy current heating as the coil is charged and discharged.

The only items on the critical path are the coil and conductor. Final verification testing of the conductor is preceeding in parallel with engineering design of the coil. Coil construction is scheduled to start 1/80 and to be completed in 18 months. Converter delivery is now scheduled for 12/79, largely because of modifications for the energy dump circuit; refrigerator acceptance testing has been delayed four months to 9/79. There is sufficient time to check the electrical and cryogenic system at LASL before the coil is manufactured.

SITE SELECTION

The SMES unit will be located at the Fite Substation of the BPA transmission system, which is situated in an industrial area several miles east of Tacoma, WA. A small masonary building on the site was originally proposed to house the system, but after an inspection by a team from LASL and BPA, it was decided that a flat area, 300 ft x 300 ft, in the center of the substation will be much more suitable. The site should avoid complaints about noise, esthetics, or magnetic field affects. A liquic-nitrogen supplier is located within a few miles. The site has limited water, so that a closed-loop system must be used to supply cooling water for the refrigerator components.

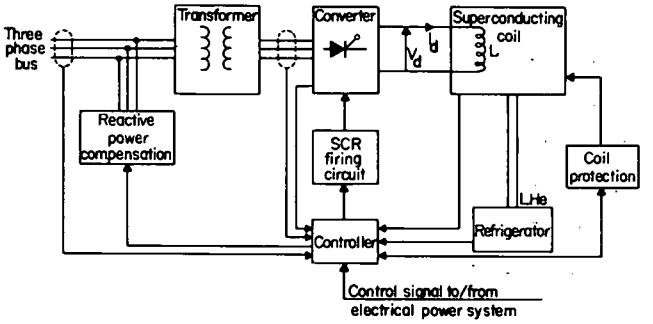

Fig. 1. Components of a Superconducting Magnetic Energy Storage System

The only problem with the substation is that it is manned only 4 hours per day. This has led to an unanticipated requirement for automated control of the entire system, which will increase the hardware cost of the system by roughly $250,000. There are no sites available, however, at stations which are manned around the clock. BPA has argued, in addition, that any SMES system which operates commercially will certainly need a high degree of automation, and that there is no reason not to solve the problem at this time.

A draft memorandum of understanding (MOU) has been circulated among the BPA and LASL staffs. The MOU gives the responsibilities of both parties in the installation and operation of the equipment.

CONDUCTOR DEVELOPMENT

The cable design for the 30-MJ coil, as shown in Fig. 2, has been modified somewhat from that described in previous presentations[1,2] as a result of the on-going program of ac loss tests, stability tests, mechanical tests, and detailed engineering discussions held with the coil designer, General Atomic. Geometric specifications for the various elements are given in Table 2. The first subcable consists of a superconducting component core, around which are cabled six strands of oxygen-free copper that acts as a stabilizer. If a length of superconducting core should become normal, that is, become non-superconducting, the current will transfer into the copper, allowing the core to regain the superconducting state. In the original proposal, the first subcables were solder-filled and wrapped with Kapton* tape. Neither of these steps presently appears necessary. Furthermore, eliminating these steps results in a gain in performance and a savings of $100,000 in fabrication costs. Insulation must be added to the second subcable, as shown, to limit ac losses. For the pancake design proposed by GA, the stainless steel strap no longer forms an integral element of the cable. The cable core consists of a thin strip of Kapton or Mylar* that serves to prevent fretting of the interior cable surfaces. It is expected that the modified conductor will be far easier to wind than the original conductor.

*DuPont trademark

TABLE 2. Conductor Specifications for 30-MJ Coil

A. Superconductor Composite Core	
Area of NbTi, mm^2	4.85×10^{-2}
Filament diameter, μm	6.5
Number of filaments	1464
Strand diameter, mm	0.511
Cu to NbTi ratio	2.94:1
Twist pitch, mm	5.0
B. First Subcable (Six copper wires cabled about one core)	
Uncompacted diameter, mm	1.39
Overall Cu to NbTi ratio	26.7:1
C. Second Subcable (Insulated)	
Six first subcables around a copper core	
Diameter, mm	4.59
D. Finished Conductor	
Ten second subcables around a Kapton strip	
Strip dimension, mm	18 x 0.25
Conductor dimension, mm	23 x 9.2

Most of the development work which has gone into the original conductor concept is directly applicable to the modified conductor. Samples of original conductor are undergoing the entire series of qualification tests so that the original concept will be available for use if necessary.

ELECTRICAL TESTING PROGRAM

Stability tests on a mock-up conductor array using second subcable with Kapton insulated first subcable show that the original conductor concept is stable at the BPA operating point. Tests will be done on samples of modified cable as they become available, although it is expected that the modified cable will be stable at an even higher current than the original conductor.

A simple test of electrical resistivity at 20 K (boiling point of liquid hydrogen) has been developed for use as a quality control procedure during cable fabrication. It has been found that the first subcable must be annealed at 600°F for 2 hours to recover the original low electrical resistivity of the stabilizing copper. This procedure does not affect the superconductor. Forming the second subcable and final conductor results in only a further 10% increase in the resistivity.

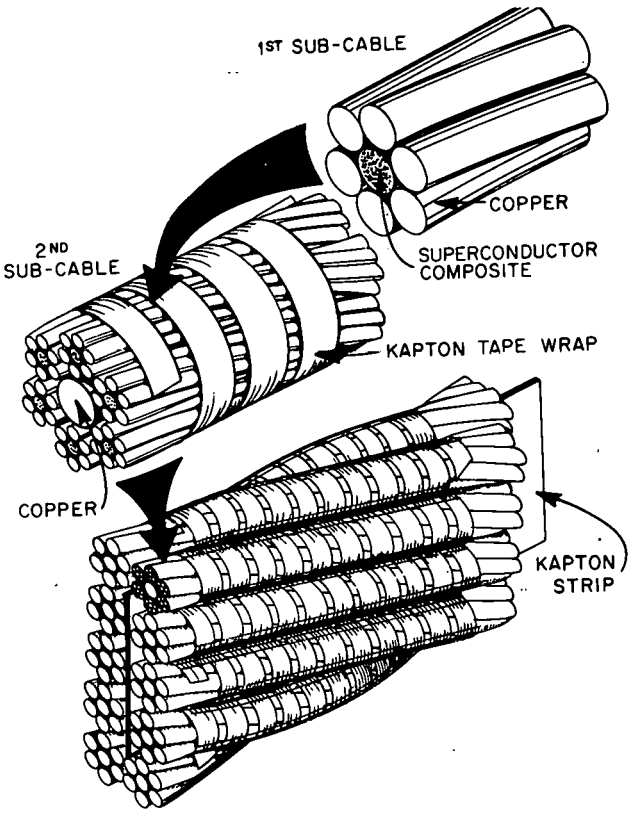

Fig. 2. Low-Loss Cryostable Cable for 30-MJ Pancake Coils

Ac losses have been measured as a function of frequency and cable geometry to define the separate contributions due to superconductor hysteresis, coupling currents, and copper eddy currents. With soldered first subcable the losses are approximately equal to those calculated in the original 30-MJ system proposal. With nonsoldered cable, the contact resistance between the copper wires is sufficient to reduce the coupling and eddy current losses by a factor of ten, with no detectable effect on conductor stability. Further, the contact resistance between first subcables is large enough that they need not be insulated before the second subcables are formed. Leaving the first subcables bare reduces cost, increases stability, and solves a number of problems related to current sharing between insulated strands in a cable. The present design calls for each of the 10 second subcables to have a separate power lead from the liquid helium bath to a common, room-temperature, bussbar. The lead resistance forces each second subcable to carry the same current, while the uninsulated first subcables within each second subcable automatically share the current. It is possible to use short lengths of superconductor cold-welded together, and even a complete break in the superconductor can be tolerated.

Acceptance tests have been performed on 64 samples of superconducting composite core wire, drawn from 90% of the wire order. All samples met the specified current carrying performance of 110 A at 4.2 K, 3 T and 1×10^{-12} Ω-cm. The average performance was 20% higher.

MECHANICAL TESTING PROGRAM

The behavior of the conductor for transverse compression is nonlinear. The apparent odulus of elasticity in the expected 30-MJ load range is 10 000 to 20 000 psi. This low odulus is apparently caused by the conductor taking the load by elastic bending of the umerous short arches in the wires and subcables that remain in the cable after fabrica- ion. Mechanical hysteresis, if any, will be within design limits. The low modulus causes o unusual problems in coil design, although it does produce larger absolute values of con- uctor displacement than previously anticipated.

Magnetomechanical forces will cause individual first subcables to deflect radially out- ard in the space between the support teeth. For the worst case of unsoldered, fully- nnealed first subcables, there may be some plastic deformation in the highest field region, ith a small but negligible effect on the electrical resistivity. Cyclic loading will be in he elastic region in all cases.

Three types of fatigue tests are being run on the conductor. Jack Ekin, of the ational Bureau of Standards (NBS), Boulder, has recently completed work on his contract to easure how cyclic strain affects the electrical resistivity of the copper stabilizer in the PA conductor. He used samples of soldered and unsoldered first subcable with various nitial resistivity ratios representing differing degrees of hardness. A cyclic strain mplitude of 0.25%, which is several times the design amplitude in the 30-MJ coil, is neces- ary to see any effect. At 10^5 cycles the resistivity change is less than 5% in all ases, including a dead-soft, unsoldered cable. A plot of $\Delta\rho/\rho$ verses log N is linear, ermitting extrapolation to higher N.

Also at NBS, mockup coil sections at 4 K are subjected to compressive cyclic loads in xcess of those predicted for the 30-MJ operation, for up to 10^6 cycles. So far, a ection of the original conductor-coil configuration has withstood 500 000 cycles between 000 and 1500 psi with no degradation of the interstrand insulation or of the fiber-glass/ poxy structure. A similar test is underway at the University of Wisconsin, using a lightly different sample configuration. This test will accumulate 10^7 cycles at 77 K.

PROCUREMENT EFFORT

All of the superconducting wire has been delivered by Magnetic Coporation of America, epresenting an expenditure of $74 000. An order has been placed with Phelps Dodge Corp. or the required 13 000 lb. of stabilizing copper wire. This material, certified to have an lectrical resistance at 4 K of 1/180 of the room-temperature value, will cost $20 000.

COIL DESIGN AND CONSTRUCTION

Four responses were received to the RFQ for design and construction of the 30-MJ super- onducting coil, which would include procurement of the conductor. Phase I of the contract, or $288 000, has been awarded to General Atomic Company of San Diego, CA. The result of hase I will be an engineering design, including working drawings, material specifications, nd quality control plans. The following paper, by J. Purcell, describes the design effort t GA. Phase II can also be awarded to GA at the option of LASL. All the Phase I funds ill be expended in FY 79.

DEWAR

A preliminary inquiry to locate manufacturers who are interested in fabricating the arge fiber-reinforced-plastic dewar elicited six positive responses. Conceptual drawings ave been prepared for two different design options. In the first, the dewar is simply a arge cylindrical tank with dished ends, designed according to the ASME code for

pressure-vacuum vessels. To save helium, a second, evacuated, chamber would be placed inside the bore of the coil. In the second option, the dewar is toroidal, with a roughly rectangular cross section and a flat lid. In both cases, there must be liquid nitrogen cooled shields in the vacuum spaces and in the helium gas space above the coil and superinsulation in the vacuum spaces. The superinsulation must be arranged not to form a conducting ring encircling the coil. At least one vendor has successfully fabricated the second type of dewar, 10 feet in diameter and 3 feet deep. Currently, the two sets of drawings are being circulated among the vendors for comments, following which modifications and more specific design will be made and a formal RFQ will be issued.

ELECTRICAL SYSTEM

A schematic of the electrical system is shown in Fig. 3. A contract for the 10-MW converter was let to Robicon Corp., Pittsburgh, PA, and was subsequently extended for modifications to include integrating the energy dump circuit for a combined total cost of $180 000. The final design review for the converter has been held, detailed drawings approved and fabrication begun. Scheduled delivery date is November 30, 1979.

The 108 SCR's for the converter were purchased for $38 000 at the end of FY 78 from Westinghouse Electric Corp. An additional order has been placed for 48 SCR's at a cost of $17 000, with delivery scheduled before the end of FY 79. The additional SCR's are for the energy dump circuit and for spares.

Considerable effort on the part of the LASL staff went into the design of the energy dump circuit, which is based upon a circuit developed for switching applications in the magnetic fusion program.[5] By placing the interrupter in series with the converter, rather than in parallel, it is possible to discharge the coil at a higher voltage and therefore in a shorter time. The entire electrical system is arranged so the 30-MJ coil can be protected under any conceivable failure mode. The 5-KA dc vacuum interrupter is formed by a parallel combination of the three-phase contacts of a commercially available ac vacuum breaker. This $12 000 item has already been shipped by GE to Robicon for integration into the converter modules. The remaining components of the energy-dump circuit are presently being fabricated by various vendors.

Bids have been received and are being evaluated for the 12-MVA converter transformer, which is a $100 000 to $200 000 item. It is expected that the contract will be let very shortly, with delivery scheduled for the end of FY 80.

The four firing cirucits shown in Fig. 3 are built into the converter. The control circuitry, which forms the logic interface with the BPA network, will be designed and built by LASL. Experiments with a prototype circuit have been described previously.[6]

Present plans call for all the electrical system components to be delivered to Los Alamos except for the transformer, which will be delivered to Tacoma, WA. Power at Los Alamos will be supplied by an existing 3.25-MVA rectiformer. The control circuit will be integrated into the system and the computer controlled operation will be tested.

CRYOGENIC SYSTEM

Figure 4 shows a block diagram of the cryogenic system, with the components arranged for the Tacoma site. All the components are mounted on trailers, so that the entire system is portable. In particular, the system will be assembled at Los Alamos in mid FY 80, which will permit an extensive testing of the automatic operation and which should limit the amount of plumbing that needs to be done at Tacoma.

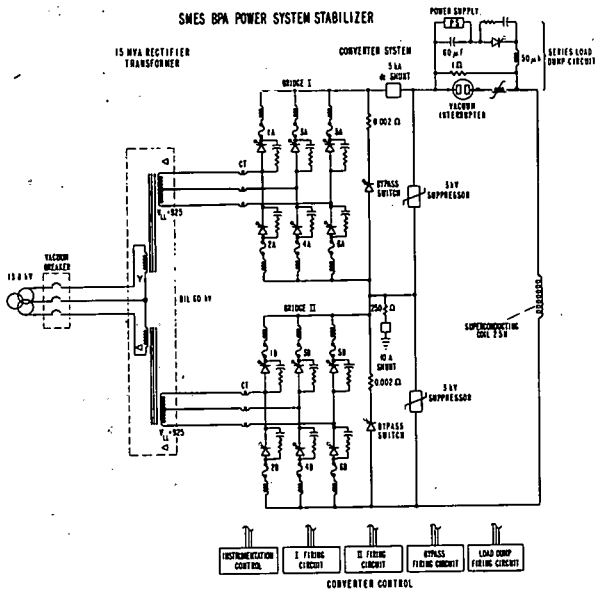

Fig. 3 Electrical System for SMES BPA System Stabilizer

The refrigerator is a CTI - Cryogenics model 2800 with Sulzer gas bearing turbines, three variable flow compressors, and liquid nitrogen precooling. The refrigerator will produce 75 ℓ/hr of liquid helium or 320 W of refrigeration at 4.2 K, or any linear combination of the two. The expected load, 15 ℓ/hr of liquid and less than 150 W should be within the system capability with only two compressors running. Initial tests are scheduled momentarily. The refrigerator and compressors installed in the trailer and equipped for automatic remote control cost $450 000. This includes two spare gas-bearing turbines. Two-thirds of this amount has been expended.

The refrigerator trailer, fabricated by Aluminum Body Corp., Los Angeles, CA, cost $24 000 and has been shipped to CTI. Still outstanding is an RFQ for refrigerator modifications to allow long-term unattended operation and automatic remote control.

The liquid nitrogen trailer was obtained as excess equipment and will be reconditioned at Los Alamos.

A minimum inventory of 108 000 SCFM of helium is required to operate the system at a cost of $10 000. It is assumed that there will be intervals during which the refrigeration plant will not be running when the gas will be recovered and stored. The gas recovery subsystem consists of any one of the refrigerator compressors, three Corblin 2500 psi compressors, a 100 W heater in the coil dewar, and a high pressure tube trailer. One Corblin will handle the gas flow resulting from the normal heat load on the dewar, which evaporates the liquid helium in 86 hours. The heater and additional Corblin compressors permit the dewar to be emptied in one day, if desired.

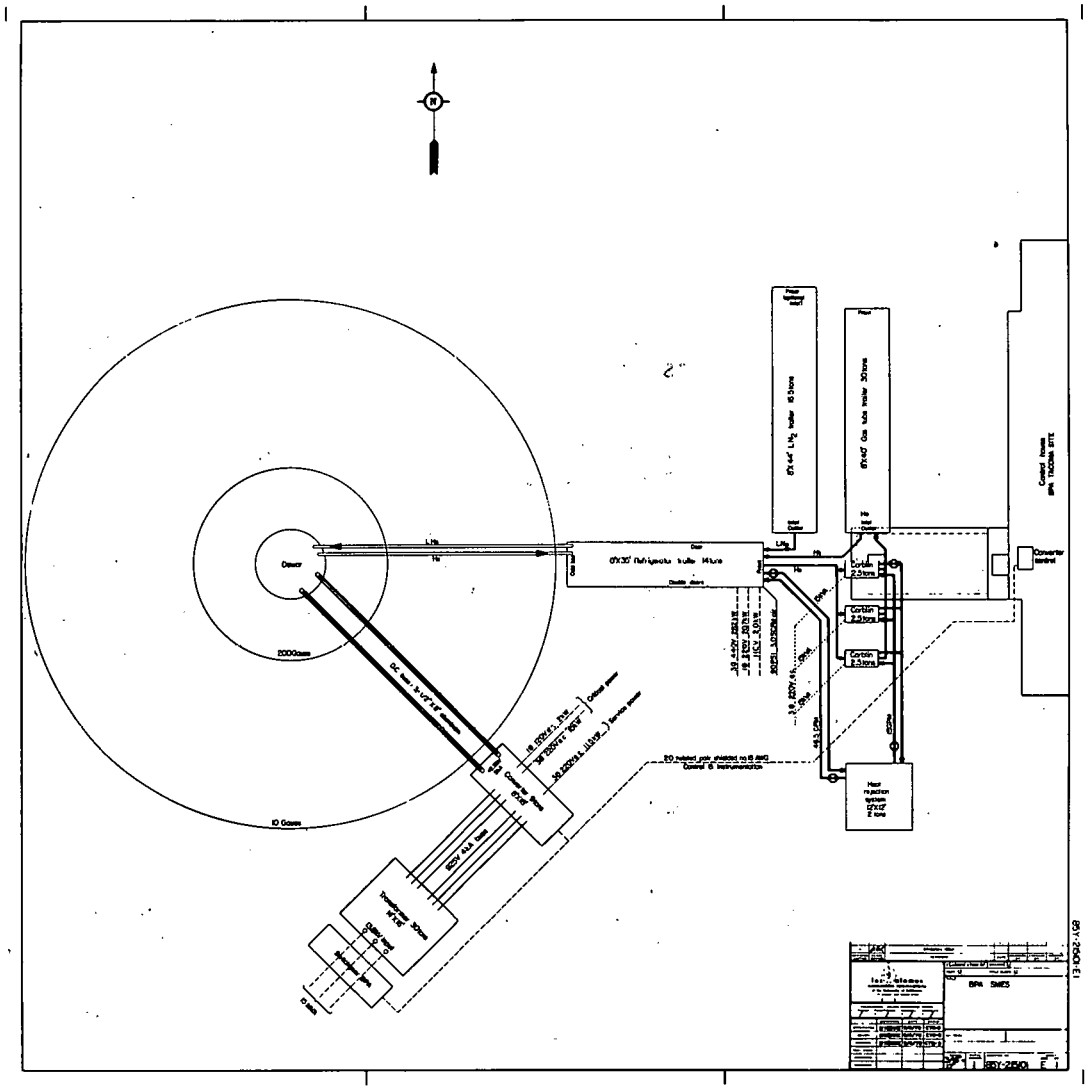

Fig. 4. Layout of SMES System at Fite Substation, Tacoma, WA

The Corblin compressors were obtained from excess property and are currently being serviced. A suitable trailer to contain them exists at Los Alamos. A bid of $100 000 was received for the tube trailer but acceptance has been deferred to allow for a search of excess property lists for this item. Tube trailer delivery is only 60 days. If all the compressors run simultaneously, they require 60 gpm of cooling water, which is too much for once-through cooling. An evaporative cooling tower has been located at Los Alamos which appears suitable for this application. A flat-bed trailer to hold the cooling tower has also been located as excess property.

CONCLUSION

The 30-MJ SMES transmission line stabilization project is proceeding with the critical items on schedule. Verification testing has been performed on one version of the original conductor. Much of this testing also applies to a modified conductor that promises to perform even better and which will be easier to fabricate. The refrigerator and converter systems will be completed early in FY 80 and tested at LASL.

REFERENCES

1. H. J. Boenig, J. C. Bronson, D. B. Colyer, W. V. Hassenzahl, J. D. Rogers, R. I. Schermer, June 1978, "A Proposed 30-MJ Superconducting Magnetic Energy Storage Unit for Stabilizing an Electric Transmission System," Los Alamos Scientific Laboratory report LA-7312P.

2. J. D. Rogers, H. J. Boenig, J. C. Bronson, D. B. Colyer, W. V. Hassenzahl, R. D. Turner and R. I. Schermer, Jan. 1979, "30-MJ SMES Unit for Stabilizing An Electric Transmission System," IEEE Trans. on Magnetics, Vol. MAG-15, Jan. 1979, pp. 820-823.

3. J. D. Rogers, D. J. Blevins, J. D. G. Lindsay, G. A. Miranda, C. E. Swannack, D. M. Weldon, and J. J. Wollan, C. J. Mole, E. Mullan, P. W. Eckels, H. E. Haller III, M. A. Janocko, S. A. Karpathy, D. C. Litz, P. Reichner, Z. N. Sanjana, and M. S. Walker, "0.54-MJ Superconducting Magnetic Energy Transfer and Storage," Adv. Cryo. Eng. 23, 57 (1978).

4. J. Purcell, following paper, this conference.

5. R. Warren, M. Parsons, E. Honig, and J. Lindsay, "Tests of Vacuum Interrupters for the Tokamak Fusion Test Reactor," April 1979, Los Alamos Scientific Laboratory report LA-7759-MS.

6. H. J. Boenig and W. S. Ranken, 1977, "Design and Tests of a Control System for Thyristorized Power Supplies for Superconducting Coils," Proc. 7th Symp. Eng. Problems of Fusion Research, Knoxville, TN, Oct. 25-28, 1977, IEEE, Inc., Piscataway, NJ, IEEE No. 77CH1267-4-NPS, p. 484.

THIS PAGE

WAS INTENTIONALLY

LEFT BLANK

PROJECT SUMMARY

Project Title:	Superconducting Magnetic Energy Storage (SMES)
Principal Investigator:	John D. Rogers
Organization:	University of California Los Alamos Scientific Laboratory Los Alamos, NM 87545 (505) 667-5427; FTS 843-5427
Project Goals:	The goals of the SMES program are two-fold. These are to design, fabricate, and place into operation a 30-MJ, 10-MW SMES unit for electric utility transmission line stabilization on the Bonneville Power Administration (BPA) system by 1982-83. The second goal is to design and have constructed a 10-to-50-MWh SMES unit. This unit will be for a completely detailed engineering prototype demonstration of an electric utility diurnal load-leveling system.
Project Status:	The engineering design of the BPA SMES transmission line stabilization system is in an advanced state. Many large hardware items are determined and on order. The refrigerator has passed the acceptance test. It is being installed in a trailer obtained for this purpose. The superconducting wire for the 30-MJ coil has been obtained. A contract was placed with General Atomic Co. for design of the 30-MJ coil. The design is about 80% complete. Lengths of 5-kA cable have been received and tested. Additional cable development is necessary. The converter has been ordered and all components for the protective energy dump circuit have been received. Surplus high-pressure gas-recovery compressors have been obtained and are to be trailer mounted. Similarly, an evaporative cooler has been obtained and will be trailer mounted for a heat-rejection unit. Detailed controls design and operating logic are being addressed for remote microwave-link operation of the SMES unit in the BPA system. An RFQ has been issued for the power transformer. The reference design for a 1-GWh diurnal load-leveling SMES unit was completed. The costs extrapolated to a 10-GWh unit were determined to be $77 to $111/kWh. Recommendations, based on the study, are made for extending the large SMES unit work.
Contract Number:	W-7405-ENG-36
Contract Period:	Continuing
Funding Level:	$1,385,000 FY79
Funding Source:	Department of Energy, Division of Energy Storage Systems and Division of Electrical Energy Systems.

DESIGNING THE MAGNET FOR THE BONNEVILLE POWER ADMINISTRATION*

John R. Purcell
General Atomic Company
P.O. Box 81608, San Diego, California 92138

ABSTRACT

This paper describes the design of the Bonneville 30 MJ superconducting stabilizing coil. The various components in the coil are described along with the rationale for materials choice.

INTRODUCTION

The 30 MJ coil is a solenoid with a winding bore of 107 inches. It will be 48 inches tall and have an outside diameter of 134 inches. Peak field on the conductor will be about 2.7 T at full current of 4900 amperes and the stored energy will be 32 MJ. Total weight of the finished coil will be 36,000 pounds.

CONSTRUCTION

The coils will be constructed by winding a superconducting cable and a stainless steel strip in parallel. The stainless steel strip will support the hoop stress generated by the magnetic field. An overall view of the coil is shown in Fig. 1. The windings will be flat discs, or pancakes, shown in Fig. 2, that consist of outward spiraling turns of superconductor and stainless steel. Forty of these pancakes (23 turns each) are stacked, one above the other to form the complete coil. The coil stack is clamped together with tie bolts and clamp rings. Connections are made between the pancakes to place all the windings in series. Current flows into one end of the coil, spirals in and out through the pancakes, and out the other end of the coil to produce the magnetic field.

CONDUCTOR

Since the coil will be operated in a pulsed mode at a frequency of 0.35 Hz, it is important to minimize the heating produced by the pulsed fields and current. The heating aspect has the largest impact on the conductor itself. To reduce the ac losses, the superconductor must be finely divided, twisted, and parallel paths must be electrically insulated and be further twisted. The copper stabilizing material must also be divided into small wires and twisted.

In addition to having low ac losses, the conductor must be stabilized against thermal and electrical perturbations. Stabilization is the purpose of the additional copper wires that are twisted into the cable along with the superconductor. In the event a short length of superconductor goes "normal" for a short period of time, the current in that short section is bypassed into the neighboring copper until the superconducting state is resumed. The copper provides a low resistance path, to minimize heating during the current bypass, and allows the conductor to return to the superconducting state. Considerations of stability and ac loss have led to a conductor design as shown in Fig. 3.

MECHANICAL

The pancakes are separated by perforated spacers as can be seen in Fig. 2. The spacers must be perforated to allow free circulation of the liquid helium and be strong enough to support the large compressive load between coils. Epoxy glass laminate is a good material for this service.

*Work support by Department of Energy, LASL Agreement X49-6722H-1.

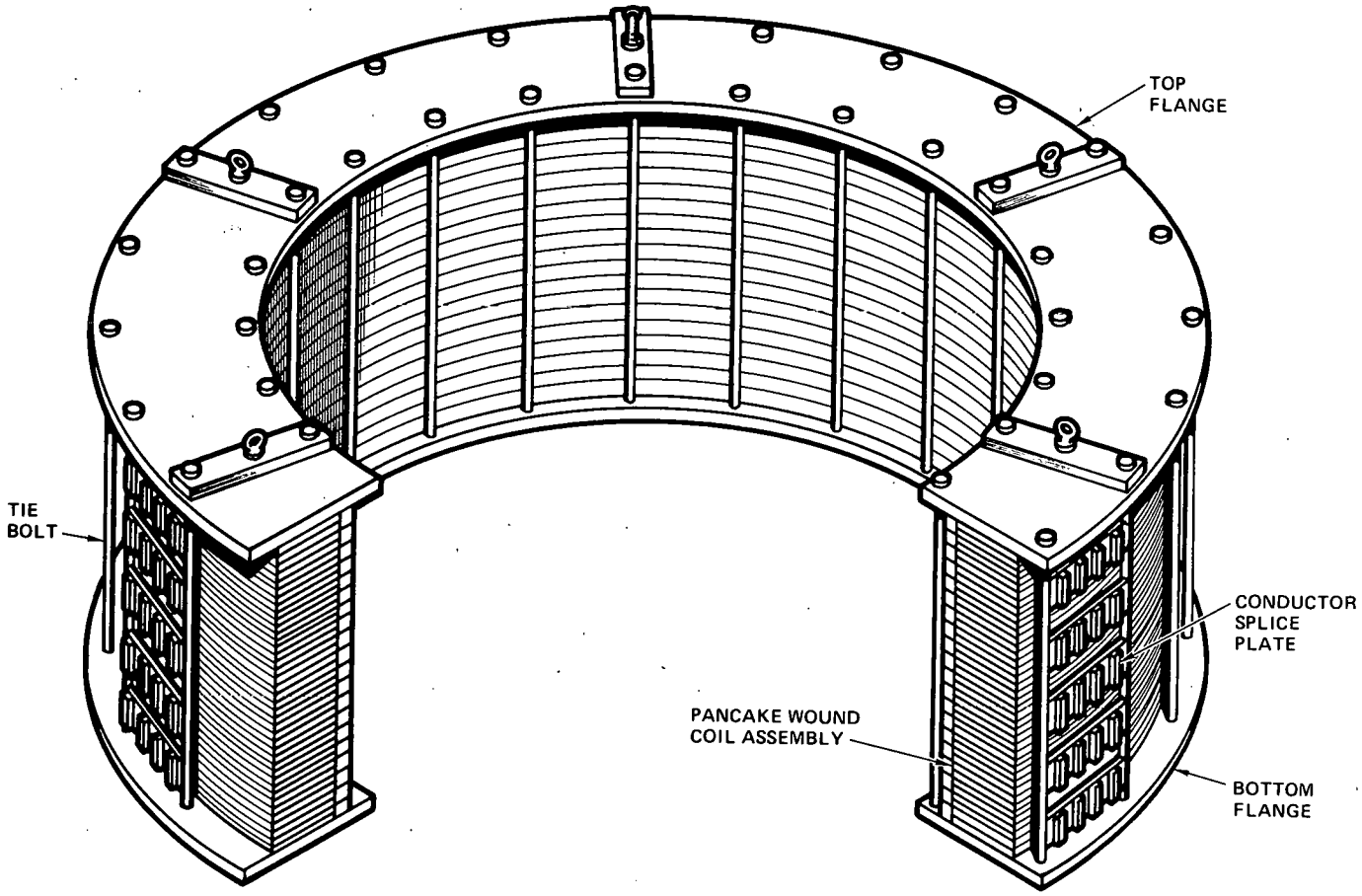

Fig. 1. Isometric view of 30 MJ magnet with a 90^{o} sector removed

One of the forces generated by a solenoid winding when it is energized is a bursting force, called the hoop force, that tries to make the coils grow in diameter. The hoop force is supported by tension in the stainless steel strips wound into the pancake coils. In addition to the hoop force, the magnetic field produces another force that pushes two coils together tending to make the coil stack shorter. This force is transmitted from pancake to pancake through the width of the stainless steel strip. The fragile conductor is thus protected from large forces, both along its length and across its width, by the stainless steel strip.

The coil assembly will be tied together with aluminum bolts between epoxy glass laminate plates at the top and bottom of the coil. Aluminum is a desirable material for these tie bolts because its thermal coefficient matches the composite thermal coefficient of the coil stack and the tension will be the same at low temperature as it is at room temperature. In addition, the low elastic modulus of aluminum results in considerable stretch of the bolts during tightening. This stretch in the aluminum tie bolts will allow them to maintain a clamping force even when the magnet is energized and the coil stack is shortened somewhat due to magnetic forces.

Joints between the pancakes will be made by soldering with about a 12-inch overlap. The joints will not be superconducting; however, the resistance will be very low and the total heat generated by the joints at full current will be only 2–3 watts.

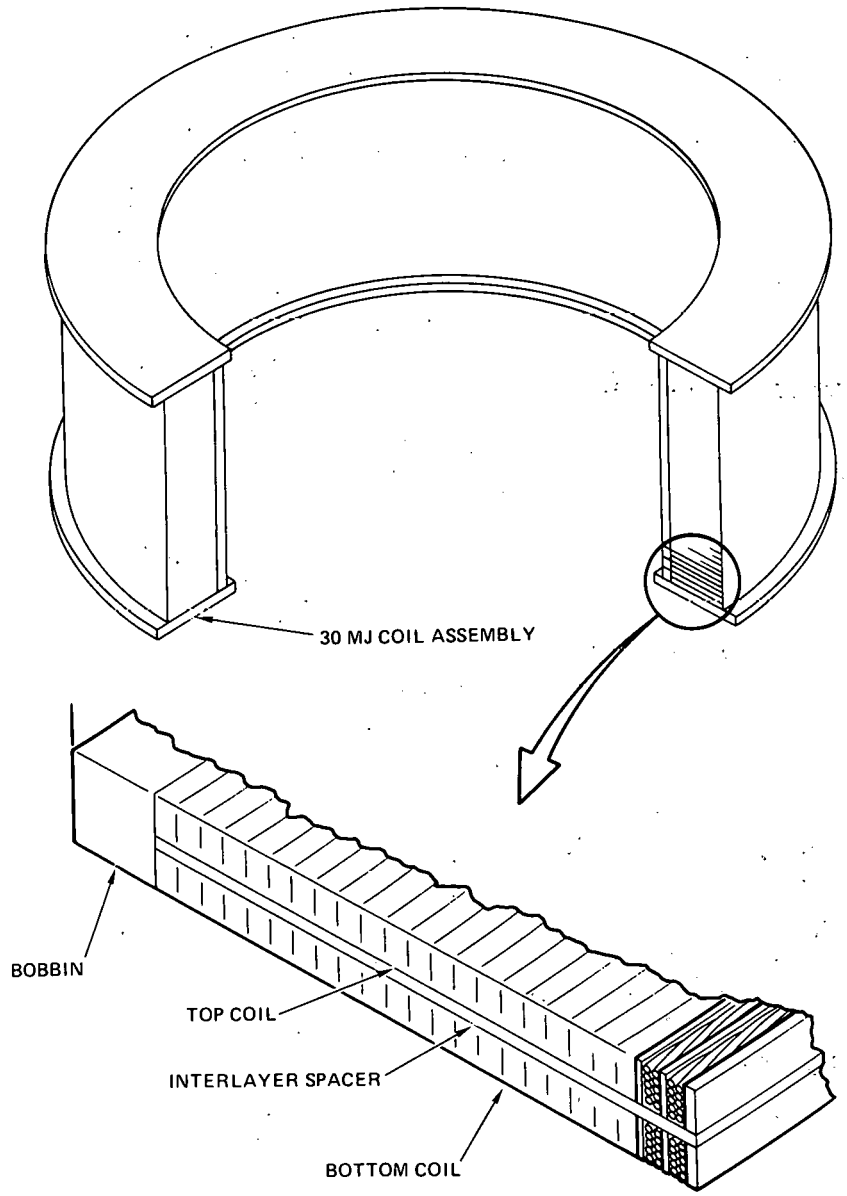

Fig. 2. Isometric end view of double pancake assembly

LIFETIME

The energy storage coil is designed to operate for 30 years and to tolerate 10^8 cycles from 80% to 100% current. The coil will normally be in an ideal environment for long life. It will be kept in an inert atmosphere (helium) at 4°K, well below the temperature that any chemical reactions or corrosion can take place. The occasional warmup to room temperature and subsequent cooldown to 4°K present very little thermal fatigue effect. Only the effect of mechanical fatigue is seen as a design problem and this is being considered very carefully. The design eliminates all sliding and inelastic motion during coil energization and all materials that are subjected to stress will operate at conservative stress levels to insure reliability.

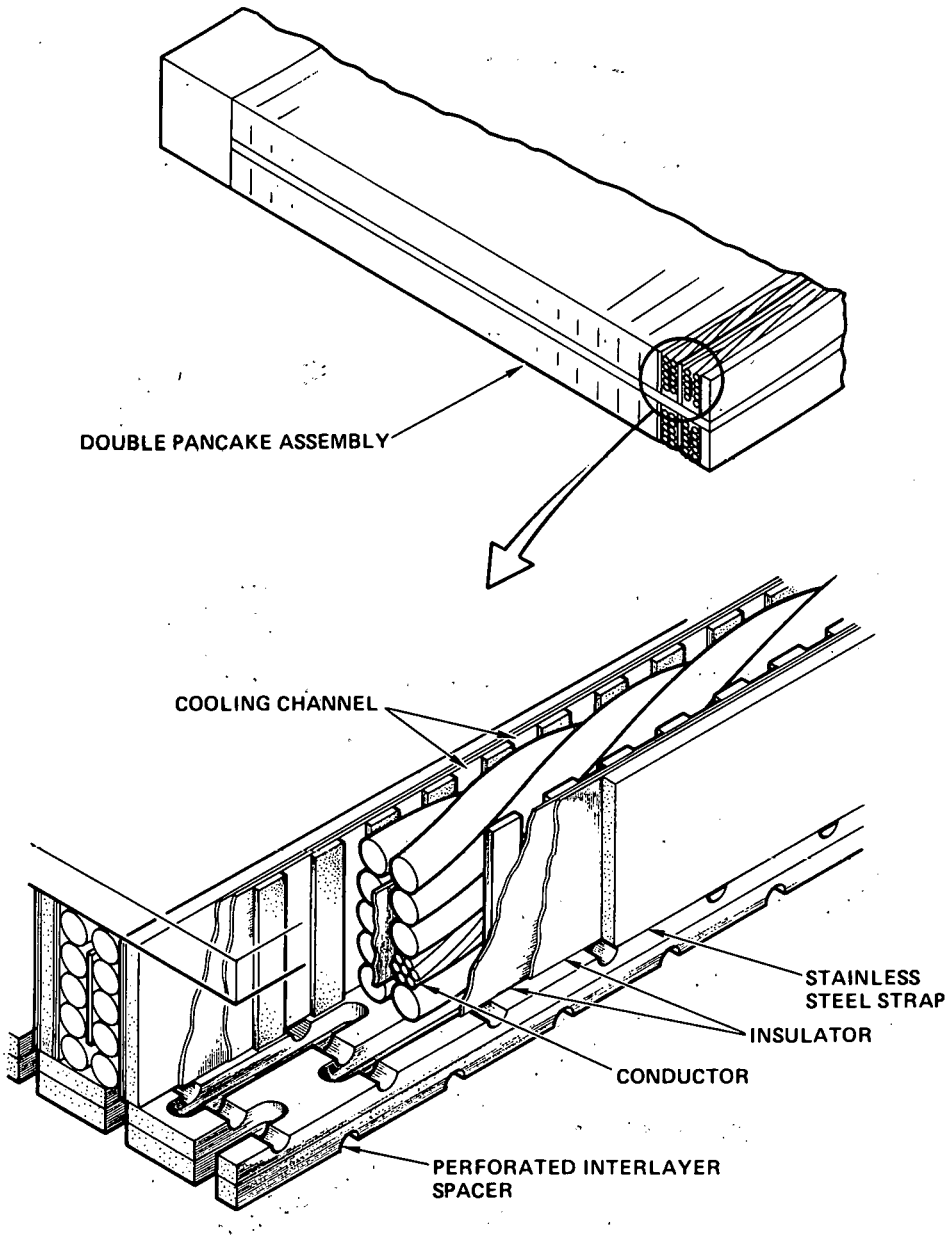

Fig. 3. Isometric view of conductor assembly showing stainless steel support strap, insulator strips and 10-cable conductor

THIS PAGE

WAS INTENTIONALLY

LEFT BLANK

PROJECT SUMMARY

Project Title:	Superconducting Magnetic Energy Storage (SMES)
Principal Investigator:	John D. Rogers
Organization:	University of California Los Alamos Scientific Laboratory Los Alamos, NM 87545 (505) 667-5427; FTS 843-5427
Project Goals:	The goals of the SMES program are two-fold. These are to design, fabricate, and place into operation a 30-MJ, 10-MW SMES unit for electric utility transmission line stabilization on the Bonneville Power Administration (BPA) system by 1982-83. The second goal is to design and have constructed a 10-to-50-MWh SMES unit. This unit will be for a completely detailed engineering prototype demonstration of an electric utility diurnal load-leveling system.
Project Status:	The engineering design of the BPA SMES transmission line stabilization system is in an advanced state. Many large hardware items are determined and on order. The refrigerator has passed the acceptance test. It is being installed in a trailer obtained for this purpose. The superconducting wire for the 30-MJ coil has been obtained. A contract was placed with General Atomic Co. for design of the 30-MJ coil. The design is about 80% complete. Lengths of 5-kA cable have been received and tested. Additional cable development is necessary. The converter has been ordered and all components for the protective energy dump circuit have been received. Surplus high-pressure gas-recovery compressors have been obtained and are to be trailer mounted. Similarly, an evaporative cooler has been obtained and will be trailer mounted for a heat-rejection unit. Detailed controls design and operating logic are being addressed for remote microwave-link operation of the SMES unit in the BPA system. An RFQ has been issued for the power transformer. The reference design for a 1-GWh diurnal load-leveling SMES unit was completed. The costs extrapolated to a 10-GWh unit were determined to be $77 to $111/kWh. Recommendations, based on the study, are made for extending the large SMES unit work.
Contract Number:	W-7405-ENG-36
Contract Period:	Continuing
Funding Level:	$1,385,000 FY79
Funding Source:	Department of Energy, Division of Energy Storage Systems and Division of Electrical Energy Systems.

1-GWh DIURNAL LOAD-LEVELING SUPERCONDUCTING MAGNETIC ENERGY STORAGE SYSTEM REFERENCE DESIGN

J. D. Rogers
Los Alamos Scientific Laboratory
of the University of California
Los Alamos, NM 87545

ABSTRACT

A point reference design has been completed for a 1-GWh Superconducting Magnetic Energy Storage system. The system is for electric utility diurnal load-leveling; however, such a device will function to meet much faster power demands including dynamic stabilization. The study has explored several concepts of design not previously considered in the same detail as treated here. Because the study is for a point design, optimization in all respects is not complete. The study examines aspects of the coil design; superconductor supported off of the dewar shell; the dewar shell, its configuration and stresses; the underground excavation and related construction for holding the superconducting coil and its dewar; the helium refrigeration system; the electrical converter system; the vacuum system; the guard coil; and the costs. This report is a condensation of the more comprehensive study which is in the process of being printed.

INTRODUCTION

A study has been undertaken to evaluate the magnitude in size, technical difficulty and detail, and cost of a 1-GWh Superconducting Magnetic Energy Storage (SMES) system for diurnal load-leveling for electric utility application. A 1-GWh size was chosen as being sufficiently large to make extrapolation to a larger size reliable and, unto itself, to be a size for which there could be considerable demand, cost permitting. Extrapolation of cost per unit of energy stored is, to the first order, inversely proportional to the maximum energy stored to the one-third power. The approach, used in the design, has been to explore some variations to already conceived details of a SMES unit. These details are particularly those related to the dewar structure and the support and design of the conductor. Before any commitment is made to these or other concepts, a careful comparison is needed. To aid the study and establish credibility in areas in which unusual expertise is required, industrial consultants were used to assess the nature of converters, underground excavation for locating the superconducting storage coil, and high-purity aluminum to establish both methodology and costs.

Several aspects of a large SMES unit determined by earlier work are retained as features of this reference design. These include the concept of operating with the superconductor in a 1.8-K 1-atm superfluid helium bath to reduce the cost of the superconductor; contoured, modular cold- and warm-wall helium dewar to accommodate thermal expansion and reduce material thickness; location of the storage coil underground to reduce coil support construction costs; and the use of a simple solenoid with a height-to-diameter ratio of about one-third.

Table 1 gives some of the characteristics of the storage system. The technology base of this reference design is considered to be within the state of the art. No discoveries or unusual inventions are needed to design and construct such a SMES system. At the same time, technology development is required to establish methods of construction which will be reliable. Also, improvements in the technology base could considerably alter the economics of such a major capital project.

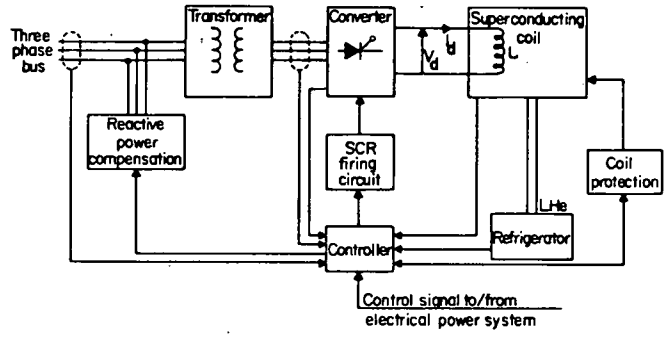

Fig. 1. Components of a Superconducting Magnetic Energy Storage System

TABLE 1. 1-GWh SMES System Parameters

Energy exchanged	3.6×10^{12} J (1.0 GWh)
Maximum energy stored	3.96×10^{12} J (1.10 GWh)
Coil diameter	132 m
Coil height	44 m
Coil thickness	20 cm
Tunnel width	3.0 m
Coil inductance	3170 H
Maximum current	50 kA
Minimum current	15 kA
Maximum field	4.5 T
Temperature	1.85 K
Minimum voltage	5.0 kV
Maximum voltage	16.7 kV
Maximum power	250 MW

ENERGY STORAGE COIL AND CONDUCTOR

At the heart of a SMES unit is the conductor, which carries the current that in turn establishes the magnetic field in which energy is stored. The conductor itself consists of two functional parts: (1) the superconductor, in which all the current flows under normal operating conditions, and (2) the stabilizer, which forms a parallel path of normal conductor in which the current can flow in an abnormal, transient condition when a length of superconductor becomes resistive. The proposed conductor is a 50-kA superconducting cable sandwiched between two parallel stabilizing elements, consisting of high-purity aluminum jacketed with cold-worked copper. See Fig. 2. The interaction of current and magnetic field creates a transverse force on the conductor, which, therefore, must be located in a coil structure that transmits these forces to external support members. Coil characteristics are given in Table 2.

The superconductor is multi-filament NbTi, extruded in copper with a copper-to-NbTi ratio of 1.33, drawn to a strand diameter of 0.147 cm, and formed into a 23-strand flat, transposed cable, 0.277 cm by 1.67 cm.[2] One advantage of designing with this conductor is that its cost can be rather accurately defined, and it is well within the state of the art of the superconducting wire industry to produce this cable. Current density in the aluminum stabilizer is set at 15 kA/cm^2 by the requirement that if external protective action is required, 1% of the stored energy can be removed with a turn-to-turn potential of 100 V and a temperature rise in the aluminum of 100 K.

TABLE 2. 1-GWh Coil Characteristics

Average radius	66 m
Height	44 m
Radial thickness	0.20 m
Inductance	3170 H
Operating current at full charge	50 kA
Cryogenic coolant	Helium at 1.8 K, 1 atm
Number of turns	4280
Number of radial turns	5
Winding pattern	pancake
Radial turn spacing	0.60 cm
Axial turn spacing, midplane	2.69 cm
Axial turn spacing, end	11.7 cm

The conductor is designed to be fully stable, such that the heat generation with all the current in the stabilizer is equal to the heat which can be carried away by the helium in contact with the exposed surface. A study has been performed by ALCOA on the cost of high-purity aluminum as a function of purity, based on the use of a proprietary process that they developed.[3] The cost of copper is taken as $1.50/kg.

In a superconductor, when the magnetic field is varied, the electric fields produce eddy current losses that must be removed by the liquid helium. The time averaged losses total 131 W with the coil holding full charge and 12 W with the coil holding minimum charge, both entirely due to joints, and 303 W with the coil either being charged or discharged.

The radial and axial forces on the individual conductors are transmitted through the conductor stack to the helium vessel and thence to the support struts. While the accumulated radial load is small, the accumulated axial load may become very large. With a strain limit of 10^{-3} in the aluminum stabilizer, the maximum load is 84 MPA (12.2 ksi). The load within eachhelium vessel section accumulates to a large value.[4] It is, therefore, proposed that the conductor stack within each section be divided vertically into two sections. The half nearest the coil midplane bears on the vessel end, while the half away from the midplane bears on ledges fitted to the inner and outer helium vessel walls.

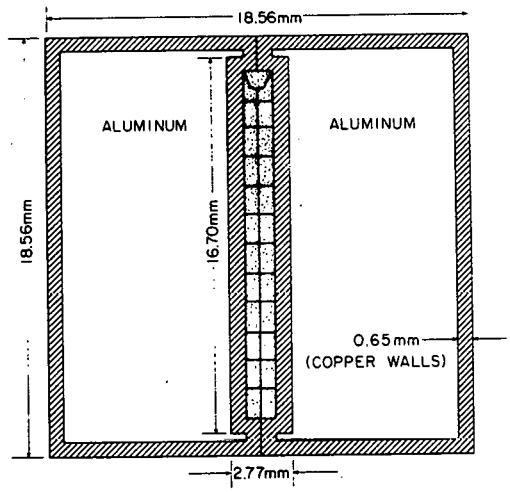

Fig. 2. Cross Section of a Conductor Array Showing Dimensions

Material costs for the conductor support within the dewar are taken as $2.50/kg for either aluminum alloy or stainless steel; and the fabricated, insulated cost is taken as twice this. Placement costs are included in the coil winding estimate. Aggregate costs of the various elements discussed in this section are given in Table 3.

TABLE 3. Costs for Conductor and Coil

Item	Cost 10^6
50 kA, graded and fabricated superconducting cable	43.2
Copper jacketed, aluminum stabilizer; materials	7.3
fabrication	7.3
Supports and spacers; material	6.2
fabrication	6.2
Coil winding labor	2.7
Total	72.9

DEWAR AND STRUCTURAL SUPPORT

The general dimensions for the 1-GWh excavation cross section are shown in Fig. 3. The excavation is made to house a large underground vacuum vessel. Inside this vacuum vessel are the inner vessels that serve as structural support for and contain the superconducting coil. The upper and lower ends of the outer vacuum vessel are sealed by means of an aluminum 5083 bellows that joins to an end seal structure. The upper end seal structure will have the necessary penetrations for construction purposes and piping, and personnel access to the tunnel will be through the radial access drift tunnel.

The inner, helium vessel is shown segmented into 13 sections with numbers 1 through 6, above the central segment and 7 through 12 below. The central segment is numbered 13. The helium vessel is a rippled structure in the plan view. See Fig. 4. Support struts, located every 2 m on centers circumferentially, transmit the radial and axial magnetic forces to the outer wall of the excavation. The general concept is based upon struts proposed by the University of Wisconsin.[5] The struts have been divided axially into an 18.2-m central section, in which the axial loads are very small, plus two 12.9-m end sections in which the axial loads are greater than the radial loads.

The vacuum vessel is to be constructed of aluminum 5083 in the H-38 condition. The vessel will be a continuous shell except for required penetrations with bellows closures for piping, conductors, and access. This shell will be constructed from seam-welded aluminum plate 2.5 mm thick. The shell will be supported by 0.3-m-long rock anchor-type supports on a 1- by 1-m spacing pattern. The material for the vacuum vessel and bellows is expected to cost $245 000 and $123 000, respectively.[6] The strut components and materials are shown in Fig. 5.

The installed costs of this system and the per unit materials costs are given in Table 4. A factor of three times the computed material cost has been used to determine the installed cost. This factor may be somewhat high and its effect is discussed below.

Potential savings in material cost can be investigated through design changes in some areas. Three such major changes are evident. Stainless steel is considered for the dewar structural material because of the known available technology for handling with some confidence in the vacuum reliability of welds, etc. If similar technology for aluminum sections can be made available, there are potentially large material cost savings.

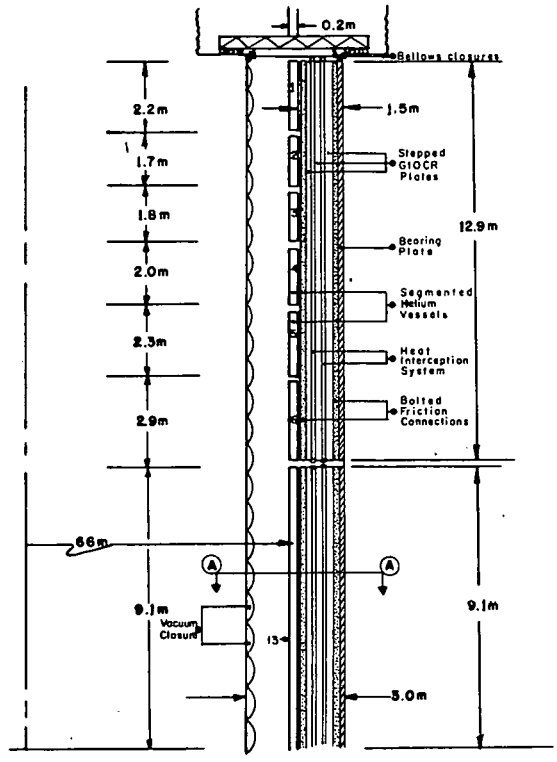

Fig. 3. Basic Dimensions and Cross Section of the 13-Segment Vessel Concept

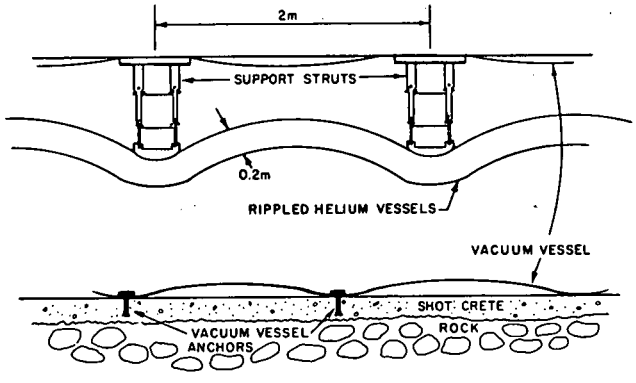

Fig. 4. Section AA Plan View of Fig. 3 Showing Proposed Vessel Concept

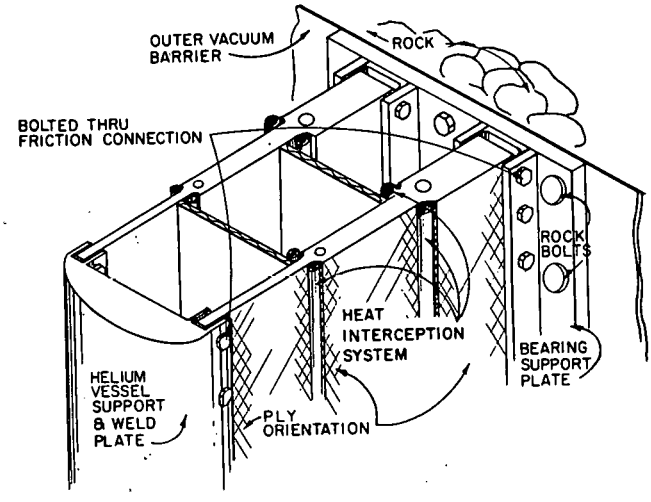

Fig. 5. Low-Thermal Conductivity Support Components

TABLE 4. In-Place Cost for 1-GWh SMES Structural Components

Component	Cost, 10^6
Vacuum walls	0.74
Vacuum-wall anchor system	1.54
Bellows seals, upper and lower enclosure structures	0.68
Low-conductivity support struts	53.7
Helium vessels	33.9
Total	90.56

Material Cost

Aluminum	$4880/m^3$ ($0.80/lb)
G-10 CR	$8/kg
A-304 Stainless	$17300/m^3$ ($1.00/lb)

The second promising concept is the wire rope conductor design.[6] Such a self-supporting conductor design would be a highly efficient structure, eliminates the dewar as a load-carrying member, and is the easiest proposed conductor to fabricate.

The third possibility is to use considerably less expensive oriented fiber reinforced polyester or other reinforced support structure material rather than the G10CR fiber-glass reinforced epoxy.

UNDERGROUND EXCAVATION

Superconducting magnetic energy storage devices are planned for installation in underground tunnels. See Fig. 6. Structural supports from the cold inner helium dewar to the 300-K rock make use of the rock as an economical load-bearing material. The rock is under compression from its own weight and the earth's overburden. Elastic analyses of granite under the coil load distribution generate compressive stresses having maximum values of ~103 bars and shear stresses of ~17 bars in the surrounding granite. These values are ~10% or less of limiting strength criteria; hence, the tunnels should be stable.

Consideration of effects of cyclic loading during the 30-yr history, hydrologic conditions, or locating the dewar in weaker rocks suggests induced stresses may approach failure; and rock bolting for wall stabilization is a necessity. Rock properties for isotropic granite were chosen to allow comparisons with calculations of Fuh et al.[7] for a different tunnel design.

The first dewar segment is physically connected to the wall so the loads are taken more than 3.1 m away from the end access room. Segments two through six are attached for a distance of 12.9 m vertically along the tunnel wall. The axial pressure is transmitted to the wall as constant axial components equal to 108 bars (1580 psi). The radial load is a minimum at the top and bottom of the coil tunnel and is a maximum at the midplane of the tunnel. The effect is to increase incrementally the radial pressure from 12.5 bars (182 psi) to a peak value of 100.5 bars (1470 psi) along the entire outer tunnel surface. The total force from the field is resolved into radial and axial components. Figure 7 is an illustration of the resolved components.

The maximum principal compressive stress given as a negative value on Fig. 8 is 103 bars (~1495 psi) occurring ~15 m below the top of the room. Similar contours were calculated for other stresses. The minimum principal stress is compressive and is 75 bars (~1090 psi). The hoop stress is compressive with a maximum value of 26 bars (~380 psi). The shear stress of ~17 bars increases approaching the midplane.

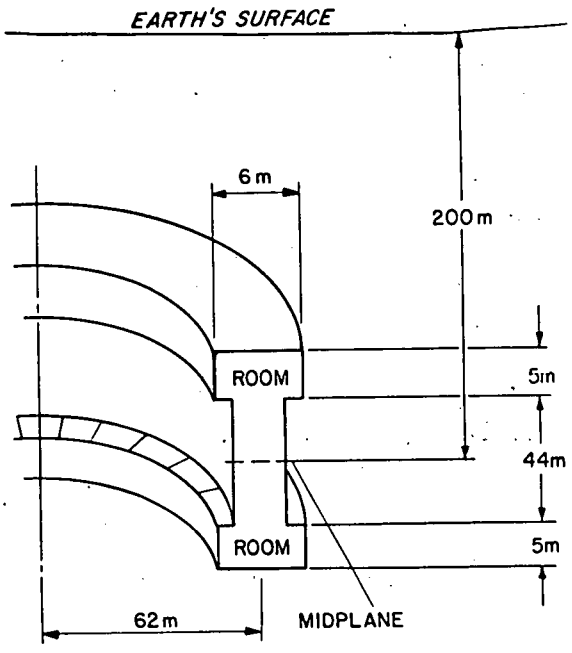

Fig. 6. Schematic of Quarter Section of Tunnel to Contain SMES Device

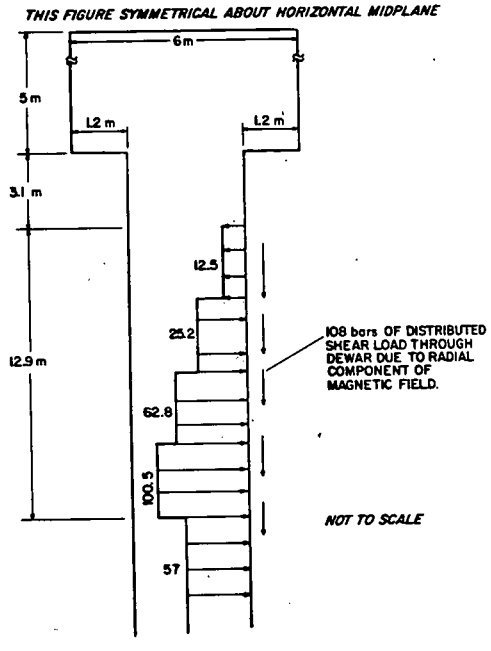

Fig. 7. Loading System with Coil Supported by Outer Wall

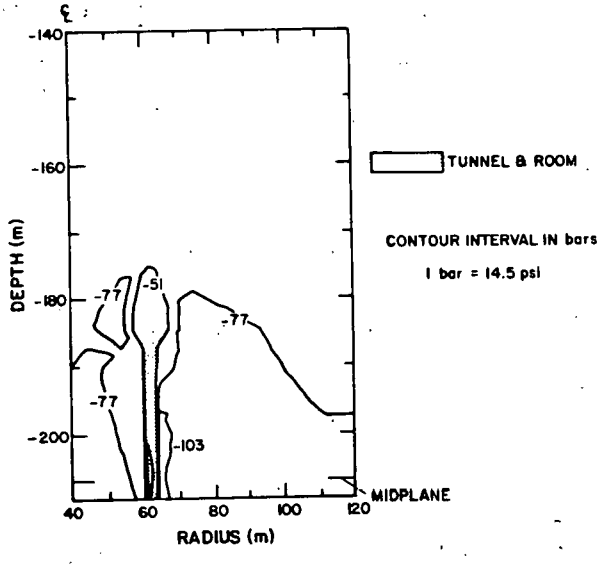

Fig. 8. Maximum Principal Compressive Stress with Coil Supported by Outer Wall

A consulting contract was placed with Fenix and Scisson, Inc., a mining engineering firm, to make a SMES tunnel excavation and construction study and to obtain costs for same. The tunnel conforms to the configuration of Fig. 6. The study considered locating the coil depths of 200, 300, and 400 m. Only the cost estimates for the 200-m depth are presented here.

The excavation study originally called for six, 1.82-m-diam drill holes with steel linings for vacuum pump-out lines; a production shaft, 3.96-m by 3.35-m with concrete lined stabilized walls and a skip hoist for subsequent use in assembling the storage coil; a horizontal shaft, 3.7-m by 3.7-m, extending 250-m horizontally from the center line of the tunnel axis to an equipment room at the 227-m level; and an equipment room, 20 m by 20 m by 10 m high, with its own 3.9-m by 3.9-m vertical service shaft. The rock walls throughout the excavation are to be stabilized with rock bolts.

The main storage coil tunnel is lined with impermeable load-bearing concrete walls with a minimum compressive strength of 422 to 563 kg/cm^2. Steel load bearing plates are mechanically anchored to both walls with 50-mm-diam by 1-m long zinc-plated rock bolts. The zinc plating is required for a 30-year life. Twenty-five-millimeter copper pipes on 1-m centers are imbedded in the concrete lining of the tunnel walls. These supply heat to prevent freezing of the concrete and rock due to the heat leaks into the dewar. Provision was made to remove ground water seepage from behind the concrete. An underground equipment room was found to provide a saving in the refrigerator system. Its remote location from the coil was necessary to have the equipment in a low fringe field of $200 G for maintenance.

Fenix and Scisson estimated the total cost of the above work at $48.5 million. Subsequent analysis and redesign resulted in a significant cost saving. The major design changes follow. These are:

1. Locating the vacuum pumps in the underground equipment room make the six drilled shafts unnecessary, provided the equipment room and the horizontal drift leading to it are somewhat enlarged. The net saving is $9 million.

2. The vertical shaft to the equipment room can be eliminated and the main production shaft used for all mining and maintenance functions, provided the main shaft is relocated and the horizontal production drifts are extended. The net saving is 0.7 million.

3. The excavation study was performed at a stage in the design when the axial magnetic forces were to be transmitted to both inner and outer tunnel walls. Under the final concept, in which load-bearing struts do not contact the inner wall, this wall need not have a thick concrete lining, can be of lower quality, and does not require heating pipes. The associated cost reduction is $2.0 million.

4. The study included a steel bearing plate at the base of each support strut, at a cost for material and placement of $3 million. These plates have since been redesigned and their cost has already been included in Table 4, although the cost of the rock bolts which fasten these plates to the tunnel wall are still counted in this section. These bolts, at $8 million, are a major cost item.

The adjusted cost for excavating and preparing the tunnel, after considering the savings of items 1 through 4, becomes $33.8 million.

CRYOGENIC SYSTEM

Cooling of the superconducting coil is accomplished by means of a two-fluid system. The coil is immersed in a superfluid bath at 1.8 K that is maintained with an overpressure of 1 atm. The 1.8-K temperature is achieved by two means. The first is a thermal barrier located in a small cross-sectional area portion of the dewar. This barrier sustains a temperature gradient with a small heat leak to an overlying layer of 4.5-K liquid helium. The

4.5-K liquid is then pressurized at about 1 atm with cold helium gas. The second device is merely a heat exchanger, a set of vertical pipes, located within the 1.8-K 1-atm liquid helium bath. This heat exchanger operates at 1.8 K and 12.5 torr on the refrigerant side. The largest heat load to be removed is that due to thermal conduction along the support struts. The refrigerator provides the liquid helium and cold gas to the system, which distributes liquid helium to cool the coil to 1.8 K and cold gas to cool the support struts and dewar radiation shield. The refrigerator consists of the helium compressors, cold box, low pressure pumps, transfer lines, and helium storage facility. Some of the liquid at 4.5 K cools the power leads. The liquid is vaporized by the leads and returned to the helium compressor at approximately 300 K.

The support struts and dewar radiation shield are cooled with high-pressure helium gas from the cold box at temperatures of 63 K and 12 K. This 18.0-atm gas undergoes a 10.0-K temperature rise across the parts to be cooled and is then recirculated through the cold box. Low-pressure helium pumps provide the continuous pumping power to move 12.5-torr helium gas through the transfer lines and cold box for heat exchange and to raise the pressure to about 1.0 atm at 300 K to feed the main helium compressors. The pumps are located underground in the equipment room with the cold box.

Equipment that will need routine servicing and maintenance must, for occupational reasons, be in a magnetic field of 200 G or less. Hence the below-ground equipment room for the cold box and pumps must be at a distance of 250 m from the center of the magnet. Adjacent to the compressors at the surface will be a helium storage facility and a water cooling system.

Liquid helium will be stored at 4.5 K on the surface in eight dewars during periods when the coil and coil dewar must be nonoperational for maintenance. A liquid-helium pump, located beneath the coil dewar, provides a 225-m head to transfer the liquid, in reverse direction, through the 4.5-K coil-dewar heat exchanger supply line and a vertical transfer line.

The major features that have been evaluated are given in detail in Ref. 8. The heat loads are listed in Table 5. The characteristics of the cryogenic system and costs are given in Tables 6 through 8. The heat exchanger cost is estimated to be \$1 million. The helium inventory for the system is 1.4×10^6 m^3 and will cost \$1.68 million if purchased as gas. A double-flow wood cooling tower with a 50-hp motor is required. The installed tower would cost \$30 000.

TABLE 5. Cryogenic Heat Loads, kW

		Temperature Level, K		
	ℓ/hr	1.8	12.0	63
Power leads (4.5 K)	250			
Coil losses		0.30		
Support struts		1.44	9.3	127
Dewar radiation		0.50		16
Transfer lines				1
Total	250	2.24	9.3	144

TABLE 6. Transfer Line Parameters

	4.5-K Liquid Supply	4.5-K Liquid Storage	4.5-K Vapor Return	12-K Supply and Return	63-K Supply and Return
Pressure, atm	1.0	1.0	0.0164	18	18
Diameter, cm	7.6	7.6	30.5	4.8	15.2
Length, m	250	350	250	500	500
Friction pressure drop	0.029 psi	0.30 psi[b]	0.312 torr	4.8 psi	3.7 psi
Heat load, W	0.291[a]	2.8[a,b]	16.5[a]	6.2	1100
Cost, 10^6	0.52	0.73	1.56	0.43	1.80
Total cost, 10^6					5.04

[a]Includes frictional pumping power.

[b]Includes lateral supply line used for transfer to storage.

TABLE 7. Cryogenic Refrigerator Summary

				Totals
Temperature, K	4.5	12.0	63.0	
Total refrigeration loads, kW	4.1	9.3	144	
Ideal refrigeration work ratio, W/W	65.7	24.0	3.76	
Ideal refrigerator input power, kW	269	223	541	
Carnot efficiency fraction	0.25	0.25	0.25	
Actual refrigerator input power, kW	1080	893	2170	4140
Volumes, m^3	464	145	38	647
Weights, kg	102 500	33 700	9 600	145 800
Costs, 10^6	2.64	2.31	4.30	9.25

TABLE 8. Liquid-Helium Storage System

Dewars	
Volume, ℓ (gal)	227 000 (60 000)
Quantity	8
Cost, 10^6	3.6
Pump	
Flow rate, g/s	375
Head, m (psi)	225 (40)
Efficiency, %	60
Power, kW	1.39
Cost, 10^6	1.0
Total cost, 10^6	4.6

ELECTRICAL SYSTEM

The power conversion equipment forms the interface between the utility bus and the superconducting magnetic energy storage coil. The equipment consists of several parallel-connected converter transformers, each tied to a line-commutated converter. The transformers provide the voltage transformation from the high-voltage level of the utility bus to the medium-voltage level at the converter input. The converter provides bidirectional power flow between the three-phase ac system and the dc coil. The rating of the power

conversion equipment requires that it be divided into two identical modules, each of which in turn consists of four identical submodules. The heart of each submodule is a converter transformer and two parallel-connected Graetz bridges forming one 12-pulse bridge. The assumption is made that a 230-kV system with a short-circuit capacity of over 4000 MVA is adequate to be used for the installation of a 1-GWh 250-MW SMES unit.

Different circuit configurations suitable for SMES converters are presented elsewhere.[9] From consideration of these circuits the series-parallel switching scheme as shown in Fig. 9 results in the lowest installed converter power and cost for a constant power system. This circuit configuration results in a 40% reduction in the converter size compared to a converter unit which is designed for maximum voltage and maximum current. A constant-voltage converter would not require switching and would need less reactive-power compensation.

The design calls for an energy exchange of 3.6×10^{12} J in four hours at a constant-power rate with a maximum charging or discharging power of 250 MW. Maximum and minimum current and voltages are respectively 50 kA and 15 kA and 16.7 kV and 5.0 kV. Figure 10 shows the voltage, current, and power relationship for the SMES system in per unit and absolute parameter values. A line-commutated converter with silicon controlled rectifiers, SCRs, as switching elements is uniquely qualified as the power conditioning equipment for a SMES unit. Two converter modules with a current rating of 25 kA and a voltage rating of 10 kV at 12.5 kA are required to guarantee 250 MW output power under all load currents. The area bordered by dashed lines in Fig. 10 represents the operating range of the two converter modules. A voltage drop of 1.0 kV at 25 kA results in a module rating of 11 kV and 25 kA. The total installed converter power is 2 x 11 kV x 25 kA = 550 MW. If two 8.33-kV 25-kA converter modules are used and a 10% voltage increase of the no-load voltage over the rated voltage is allowed, then the installed converter power is reduced to 2 x 9.16 kV x 25 kA = 458 MW. However, the converter would not be capable of providing 250 MW in the current range of 25 kA to 28.8 kA. The darkened area in Fig. 10 indicates the insufficient converter power for this case. At 25 kA the maximum power would be 218.6 MW instead of 250 MW. The smaller converter rating is justified in spite of the 12.6% reduction in output power within a small current range because of the substantial saving of 92 MW of converter power. At 40 $/kW this results in a saving of $3.68 million. The total installed converter power has been reduced by 52 MW; but, in addition, the mixed mode of operation allows the use of the module by-pass switching scheme at a lower per unit cost of $35/kW. Table 9 summarizes the converter characteristics.

Line-commutated converters, working in both the rectifier and the inverter mode of operation, require reactive power to compensate for the reactive-power demand of a SMES unit and to improve the power factor. A recent study by General Electric (GE)[10] shows that the static VAR generator with a controlled inductance should be used when the SMES unit is for

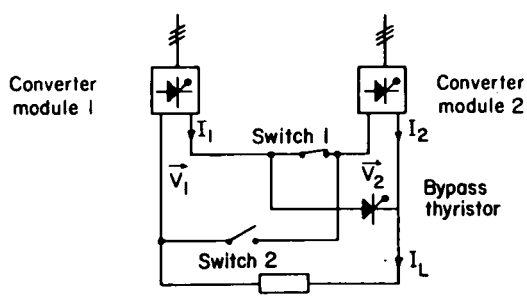

Fig. 9. Series-Parallel Converter Module Switching Circuit

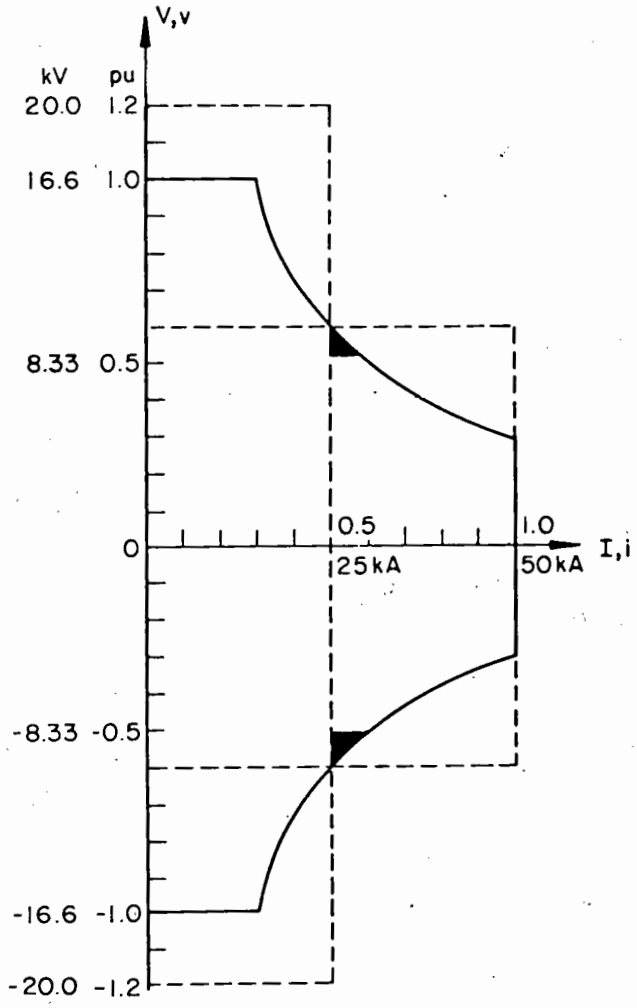

Fig. 10. Current-Voltage Diagram of SMES Unit and Converter

storage purposes and system stabilization and if only for storage, less expensive switching capacitors are adequate for VAR compensation.

The reactive-power requirement is 58.1 MVAR. Commutation reactive power must be added to the displacement reactive power and is estimated to be about 50 MVAR. The total reactive power is, therefore, about 100 MVAR. For a converter operated in mixed mode, the reactive power is reduced by 20%. An additional cost of $25/kVA occurs for the VAR generator.

Table 10 summarizes the cost for the total converter system. The costs are in 1977 dollars; however, if the converter cost development over the last 10 years is an indication for the future, then the converter cost will stay constant for the next 5 to 10 years.

TABLE 9. Converter Parameters[a]

Converter module	
Maximum current	25 kA
Load voltage at 25 kA	8.33 kV
No-load voltage	9.16 kV
Power rating	229 MW
Number of converter modules	2
Number of submodules in a converter module	4
Submodule	
Maximum current	25 kA
Load voltage at 25 kA	2.08 kV
No-load voltage	2.29 kV
Power rating	57.25 MW
Number of Graetz bridges in a submodule	2
Graetz Bridge	
Maximum current	12.5 kA
No-load voltage	2.29 kV
Power rating	28.63 MW
Number of 2000-V 1400-A, watercooled SCRs, 3 in series, 4 in parallel for each leg of the bridge	72
Submodule Transformer	
High voltage	230 kV
Low voltage	1.68 kV
Secondary phase current	10.21 kA
Power rating	60 MVA

[a]Two converter modules in series-parallel switching arrangement for 250-MW output power.

TABLE 10. Cost for Power Conditioning Equipment for the 1-GWh 250-MW SMES Unit

	Constant Power Mode 458 MW, 50 MVAR		Mixed Mode 406 MW, 40 MVAR	
	Unit Cost $ /kVA	Total Cost 10^6	Unit Cost $ /kVA	Total Cost 10^6
Converter including transformers SCR bridges, filters, by-pass switches, and building	40	18.3	35	14.2
VAR generator	25	1.3	25	1.2
		19.6		15.4

VACUUM SYSTEM

The dewar is located 200 m below the surface of the earth. Three pairs of diffusion pumps are located at this lower level and are coupled as closely as possible to the dewar wall. They are located, equally spaced, around the lower circumference of the dewar and are connected by appropriately sized lines to a single line that runs to the equipment room and the mechanical blowers and pumps. See Fig. 11. Only the diffusion pumps, right angle valves, and the refrigerated baffles are located immediately adjacent to the dewar. Pumping capacity of the system is set by the surfaces to be outgassed, the volume of the vacuum space, and the nature of the materials. Table 11 gives the dewar volume and surface area.

TABLE 11. Dewar Volume and Surface Area

	Vacuum Vessel	Helium Vessel
Volume, m^3	5.4×10^4	3.8×10^3
Net volume, m^3	5.0×10^4	2.0×10^3
Surface area, m^2	4.0×10^4	3.7×10^4

In the vacuum vessel there will be 960 tonnes of fiber-glass reinforced epoxy or polyester struts with a surface area of 1.3×10^4 m^2 and 32 tonnes of aluminized Mylar superinsulation. From these two items, together with the stainless steel and aluminum surfaces, an out-gassing load can be expected after one hour of pumping of 1.6×10^5 torr-liter/s.

Cost of the vacuum system hardware, including instrumentation, is set at $830 thousand. Installation is an equal cost.

GUARD COIL

The effect of constraints on the magnetic field beyond the fence enclosing the 1-GWh SMES coil on the land requirements and a possible guard coil were examined . If the property line can be at a field of 10^{-3} T or greater an economical guard coil will have little effect on the location of the boundary. A guard coil can reduce the land requirement by at least a factor of 4 if the property line is at a field of 3×10^{-5} T. A guard coil located at the same depth

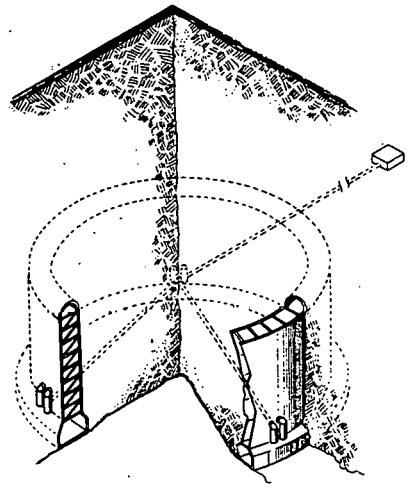

Fig. 11. Schematic of Dewar and Vacuum System

as the main storage coil is more effective than a guard coil at ground level; but neither has much effect on the field at ground level directly over the main coil. This field can only be controlled by locating the main coil deeper. The parameters of the reference guard coil are presented in Table 12. Use of the same 50-kA conductor as in the main storage coil has been assumed.

TABLE 12. Guard Coil Parameters

Vertical location	ground level
Mean radius, m	330
Height, m	0.574
Radial thickness, m	0.191
Number of turns	110
Conductor length, m	2.30×10^5
Maximum current, kA	50
Maximum field, T	4.9
Self inductance, H	39
Mutual inductance to main coil, H	7.6
Energy change, MWh	8.3
Operating temperature, K	1.85
Vacuum vessel minor diameter, m	1.0

The resulting pressure from the magnetic forces is approximately 10^7 MPa (1400 psi) and is well below the stress limit of the conductor. The fields at the guard coil at maximum charge are $B_R = 6.9 \times 10^{-3}$ T and $B_Z = -1.56 \times 10^{-2}$ T. The guard coil itself contributes -1.47×10^{-2} T to B_Z. The resulting force components are 3.78×10^4 N/m upward and 8.58×10^4 N/m outward. The upward force should be compared to a conductor weight of 1.73×10^3 N/M.

The vector sum of F_Z and F_R can be supported in hoop tension by 0.11 m^2 of alloy aluminum at a stress of 280 MPa (40 ksi) and a material cost of \$1.76/kg. The upward force must be transmitted to the outer vessel wall by means of fiber-glass straps set into long, re-entrant tubes in the outer wall. The upward force can be balanced by several meters of earth. For cost purposes the weight of the concrete foundation is taken to be equal to this levitating force. A total of 3330 m^3 of concrete is required, at an installed cost of \$500/m^3. With cold support, the heat leak into the guard coil is very small compared to the main storage coil. Thus the refrigeration requirement and the helium inventory have been neglected.

Component costs of the guard coil are given in Table 13, where the same cost factors have been used as in Ref. 2 and 3. The superconductor is not graded, and the dewar is constructed of 0.5-cm-thick aluminum alloy. A vacuum vessel 1.0-m in cross-sectional diameter leaves more than enough space for insulation and for construction tolerances.

TABLE 13. Component Costs for Guard Coil

Item	Cost \$$10^6$
50-kA superconducting cable	7.8
Stabilizer, fabricated	1.9
Coil winding labor	1.5
Structural support	3.3
Dewar	1.5
Concrete foundations	1.7
Total	17.7

COSTS

The costs provided in the several tables are not on a common basis because of their diverse origins and because different contributors were involved with the design. This section compiles the costs and adds profit, installation costs, and engineering design costs for those items and facilities in which they have not already been incorporated. Engineering is considered to include complete design and specification for manufacture, fabrication, field operations, installation, and construction; architectural services; and project management of the SMES system. In Table 14, if profit, installation, and engineering design costs are not listed, they are already included in the base number. For all items, additional cost detail can be found in Ref. 2-6 and 8-10. No land costs are included.

TABLE 14. Cost of 1-GWh SMES Unit

	$10^6
Conductor and coil	72.90
Profit on aluminum matrix	0.57
Engineering at 15%	11.02
Winding machine	3.50
Dewar and structural support	90.56
Engineering at 15%	13.58
Cavern	33.80
Cryogenic system	
Transfer lines	5.04[a]
Valves	2.00[a]
Low-pressure (12.5-torr) pumping system	3.58[a]
1.8-K heat exchanger	1.00
Cooling tower	0.03
Helium storage dewars	3.60
Liquid helium storage pumps	1.00
Refrigerator	9.25[a]
Installation[a]	5.96
Engineering[a]	2.98
Helium gas	1.68
Electrical system	15.40[b]
Vacuum system	0.83
Installation	0.83
Engineering at 15%	0.25
Guard coil	17.70
Engineering at 15%	2.66
Total	299.72
	$300/kWh

[a]Installation and engineering are included for these items at 30 and 15%, respectively, of their cost. Similar costs for the other items of the cryogenic system are included in their base costs as given.
[b]This item is often assigned as a cost to power instead of energy.

The principal costs for the system occur in five areas. These areas are the coil and conductor, the dewar and structural support, the cavern or excavation, the cryogenic system, and the electrical system. The costs represent current technology and are for a base reference design. Materials selection has been for those requiring the least development, such as a built-up welded stainless steel dewar. Costs are based upon information obtained on recent purchases, contracts, major installations, and studies conducted for this reference design. In some instances the sources of cost data are confidential and the amounts must be taken at face value. Engineering costs not originally included in the base numbers are added

at 15%. Certain indications of possible reductions are developed and a lower cost list is presented in Table 15.

The single largest cost for the conductor and coil at $72.9 million is the 50-kA, graded superconducting cable at $43.2 million. See Table 3. This amount is based on present-day costs of NbTi superconductor for projects such as the energy-doubler magnets for the Fermi National Accelerator Laboratory and the Brookhaven accelerators. The prospect of reducing this cost a factor of 2 in a large scale operation is credible. The superconducting cable cost included in the $51.3 million for conductor and coil in Table 15 is thus $21.6 million. The major cost saving of using aluminum stabilizer is already incorporated in Table 14. No other significant cost reduction is anticipated in this item.

The dewar and structural support costs listed in Table 14 are for a stainless steel dewar and G10CR epoxy fiber-glass structural supports. The fabricated-shape materials cost of $4 880/$m^3$ ($0.80/lb) for aluminum is from an uninflated 1977 price list[11] and of $17 300/$m^3$ ($1.00/lb) for A304-LN stainless steel is from a Lawrence Livermore Laboratory bid quotation for the Mirror Fusion Test Facility. The cost of G10CR currently ranges from $6 to $17/kg. This design study uses $8/kg in Table 14.

TABLE 15. Revised Cost of 1-GWh SMES Unit

	10^6
Conductor and coil	51.30
Profit for aluminum matrix	0.57
Engineering at 15%	7.78
Winding machine	3.50
Dewar and structural support	42.49
Engineering at 15%	6.37
Cavern	30.00
Cryogenic system	
Transfer lines	5.04[a]
Valves	2.00[a]
Low-pressure (12.5-torr) pumping system	3.58[a]
1.8-K heat exchanger	1.00
Cooling tower	0.03
Helium storage dewars	3.60
Liquid helium storage pumps	1.00
Refrigerator	9.25[a]
Installation[a]	5.96
Engineering[a]	2.98
Helium gas	1.68
Electrical system	15.40[b]
Vacuum system	0.83
Installation	0.83
Engineering at 15%	0.25
Guard coil	10.40
Engineering at 15%	1.56
Total	207.40
$207/kWh	

[a]Installation and engineering are included for these items at 30 and 15%, respectively, of their cost. Similar costs for the other items of the cryogenic system are included in their base costs as given.
[b]This item is often assigned as a cost to power instead of energy.

The revised costs of Table 15 incorporate other changes. These are a change from a stainless steel dewar to aluminum, a support structure material cost of $4/kg based on quantity production, and the use of a multiplier of 2 for the installed cost of polyester-fiber glass composite and other materials. The change from stainless steel to an aluminum dewar requires a change from a 13-segment to a 25-segment dewar. This occurs because the thermal stress is exceeded for an aluminum dewar with fewer segments.

The cavern costs are fixed mostly by the materials and mining equipment. If the rate of excavation is doubled without additional labor and equipment, then a saving of about $3.8 million can be made.

The cryogenic system cost indicates an area for which engineering optimization would be most productive. Transfer line costs are based on estimates made available by Cryenco. The refrigerator cost, the installation cost, and the engineering cost are based upon a reasonable extrapolation of large liquid helium plants presently being installed in the United States. Optimization would possibly reduce the cryogenic system cost by 15 to 30%; however, there would be a compensating increase in the structural support cost for a lower overall net saving. Refrigerator costs corresponding to a reduced structural support thermal conductivity by a factor of 2 would change the last line of Table 7 to $2.00, 1.42, 2.86, and 6.28 million. The total saving in refrigerator cost is $2.96 million . Such an optimization is not included in Table 15.

The guard coil cost has been reduced by changes in both the superconductor and dewar costs corresponding to those made above for the main energy storage coil.

Thus, based upon the point reference design and on the material and fabrication costs presented in this report, the capital cost of storing energy in a 1-GWh SMES system ranges from $207 to $300/kWh. These values extrapolate inversely as the maximum energy to the one-third power. For a 10-GWh SMES unit the corresponding costs become $96 and $139/kWh. Clearly, the economy of size is important.

The possibility of this type of saving being made without an associated increase for some other part of the system is unlikely. A more realistic percentage reduction by optimization has been judged to be nearer to 20%, although even this appears high for optimization of the entire system. On this basis the unit installed costs for a 10-GWh system would then range from $77 to $111/kWh. These costs must be recognized as being higher by factors of 2 to 3 than previously developed numbers.

CONCLUSIONS

A SMES system has the potential of providing a very advanced and efficient energy storage system for electric utility diurnal load-leveling. The cost of constructing such a system may be high. Nevertheless a more thorough engineering design is warranted. SMES efficiency has been reevaluated in a utility operational scenario in a recent study by Arthur D. Little, Inc.[12] Comparison with battery storage underground pumped hydrostorage, compressed air energy storage, and conventional generation capacity shows that SMES is economically competitive and is the most attractive of the large systems when the rated energy delivered per year per unit power capacity is above about 1750 kWh/yr per kW. See Figs. 3.8 and 3.9 of Ref. 12. This result is predicated upon system costs lower than those developed here.

REFERENCES

1. F. R. Kahlhammer, "Energy Storage: Applications, Benefits and Candidate Technologies," Proc. of the Symp. on Energy Storage of the Electrochemical Society, March 1976, pp. 1-20.

2. R. I. Schermer, "1-GWh Diurnal Load-Leveling Superconducting Magnetic Energy Storage System Reference Design; Appendix A: Energy Storage Coil and Superconductor," Los Alamos Scientific Laboratory report LA-7885-MS Vol. II (1979).
3. C. N. Cochran, R. K. Dawless, and J. B. Whitchurch, "1-GWh Diurnal Load-Leveling Superconducting Magnetic Energy Storage System Reference Design; Appendix B: Cost Study, High-Purity Aluminum Production," Los Alamos Scientific Laboratory report LA-7885-MS Vol. III (1979).
4. J. G. Bennett and F. D. Ju, "1-GWh Diurnal Load-Leveling Superconducting Magnetic Energy Storage System Reference Design; Appendix C: Dewar and Structural Support," Los Alamos Scientific Laboratory report LA-7885-MS Vol. IV (1979).
5. R. W. Boom, ed., "Wisconsin Superconductive Energy Storage Project," Vol. I and II, Engineering Experiment Station, College of Engineering, University of Wisconsin, Madison, WI (1974 and 1976).
6. J. G. Bennett and F. D. Ju, "1-GWh Diurnal Load-Leveling Superconducting Magnetic Energy Storage System Reference Design; Appendix C: Dewar and Structural Support," Los Alamos Scientific Laboratory report LA-7885-MS Vol. IV (1979).
7. G. F. Fuh, T. Doe, and B. C. Haimson, "Design of Underground Tunnels for Superconductive Energy Storage," Supplemental Volume, Eighteenth US Symposium on Rock Mechanics, US National Comm. Rock Mech., National Acad. Sci., F. Wang, and G. Clark, Eds., (Colorado School of Mines Press, Boulder, CO, 5A5-6 1977).
8. D. B. Colyer and R. I. Schermer, "1-GWh Diurnal Load-Leveling Superconducting Magnetic Energy Storage System Reference Design; Appendix E: Cryogenic System," Los Alamos Scientific Laboratory report LA-7885-MS Vol. VI (1979).
9. H. J. Boenig, "1-GWh Diurnal Load-Leveling Superconducting Magnetic Energy Storage System Reference Design; Appendix F: 1-GWh Electrical System Design," Los Alamos Scientific Laboratory report LA-7885-MS Vol. VII (1979).
10. C. B. Lindh, R. V. Pohl, and H. T. Trojan, "1-GWh Diurnal Load-Leveling Superconducting Magnetic Energy Storage System Reference Design; Appendix G: Design Study: Thyristor Converter Stations for Use with Superconducting Magnetic Energy Storage Systems," Los Alamos Scientific Laboratory report LA-7885-MS Vol. VIII (1979).
11. Materials Jour., Materials Selector 84, No. 6, 26 (1977).
12. "An Evaluation of Superconducting Magnetic Energy Storage," Arthur D. Little, Inc. report to be published.

PROJECT SUMMARY

Project Title:	"Superconductive Energy Storage"
Principal Investigator:	R.W. Boom
Organization:	531 Engineering Research Building University of Wisconsin Madison, Wisconsin 53706 (608)263-5027
Project Goals:	To develop hardware components, produce engineering system designs, procure manufacturing and assembly equipment designs, revise cost estimates, and assess operational efficiencies for large underground superconductive storage systems.
Project Status:	Component development in three areas: cryogenics, conductor and structures is under way to be completed in FY-81. Rock mechanics design and experimentation is under way to be completed in FY-81. Parallel efforts supported by the Wisconsin Utilities are under way on the same schedule in five other areas: magnetics, environmental studies, system design, electrical, and safety.
Contract Number:	EY-76-C-02-2844-000
Contract Period:	FY-78
Funding Level:	$600 K
Funding Source:	U.S. Department of Energy Division of Energy Storage

COMPONENT DEVELOPMENT FOR LARGE MAGNETIC STORAGE UNITS

S. W. Van Sciver and R. W. Boom
University of Wisconsin
Madison, Wisconsin 53706

ABSTRACT

A survey of University of Wisconsin research and development on components for large scale superconductive energy storage units is presented. The major activities involve development of the aluminum stabilized-NbTi composite conductor and the fiberglass reinforced polyester strut. Scale models of these components have been produced and tested. Design activities have been directed toward consideration of a 15 tunnel design to reduce axial structure. Rock mechanics studies of the 15 tunnel design are also reported.

INTRODUCTION

The Superconductive Energy Storage Project at the University of Wisconsin was described in papers by R. W. Boom and S. W. Van Sciver in the Proceedings of the 1978 Mechanical and Magnetic Energy Storage Contractors' Review Meeting, DOE Report CONF-781046.[1,2] Those two papers include a review of technical progress from 1970 to 1978 in the evolution of system design and the development of components. The conclusions given at that time are:

1. A one layer, thin wall, high current superconductive solenoid is probably the best design.

2. Bedrock structure is needed.

3. Pool cooling with superfluid helium is preferred.

4. The conductor is a composite of NbTi and high purity aluminum which has full cryogenic stability.

5. The conductor, dewar and associated structure are to be rippled at approximately a one meter radius of curvature.

6. The design is a multi-tunnel sectored solenoid to save on axial structure.

In FY-79 the design has been refined, more detailed tunneling cost studies have been undertaken and work on system assembly has been initiated. The conductor and strut development has continued through scaled sample tests. Electrical system studies, unit size preference and bridge cost estimates have also continued and are presented in a companion paper by J. J. Skiles.[3]

Our present preference is for units of 5000 MWh size. This size is a compromise between less expensive larger units and the need for several redundant smaller units for reliability. Relative costs are given in Table 1. The Wisconsin Electric Utility companies have a combined peak capacity of 8880 MW installed in 1979. It has been assumed for several years that 10,000 MWh from storage would be an appropriate amount for Wisconsin. In the past year it has

been tentatively decided that the use of two 5000 MWh units would be preferable. Each unit would be rated at 500 MW for 10 hour discharge at constant power level and would be discharged to 10% of its stored energy daily. To account for a residual 10% energy always in storage and to account for losses the actual storage capacity of a unit is 10~15% larger than the amount used. Thus the actual size recommended for construction is approximately 5500 MWh.

TABLE 1. Relative Capital Costs* of Superconductive Magnetic Storage Units

Size (MWh)	Relative Capital Cost/ Unit Energy
10,000	1.00
5,000	1.26
1,000	2.16
100	4.63

*Based on scaling relations presented in Ref. 4.

We tentatively recommend a 100 MWh model unit as the first storage device to be built after the component development and fabrication phase is completed in FY-83. Successful completion of the 100 MWh model would probably be followed by the construction of a 1000 MWh demonstration plant.

DESIGN

The design of the Wisconsin superconductive energy storage unit has emphasized the demonstration unit size of 1000 MWh discharge capabilities.[5] Recent work has been directed toward a new design which reduces the need for axial structure in the unit. A sketch of this design is shown in Fig. 1. There are 15 tunnels arranged in a circular pattern. The resultant forces are primarily radial directed outward along the 40 m radii. The orientation of the forces normal to the rock structure greatly reduces the shear loading and the need for axial structure. The use of many tunnels reduces the accumulation of axial forces by transferring these forces to the bedrock more frequently.

The central tunnels would have their turns wound perpendicular to the minor radius. The two tunnels at ±69° would have the turns inclined at about 10° from horizontal. The end tunnels at ±90° are 20% larger in diameter with 20% more turns which are inclined at about 40° from perpendicular. The above distribution of turns reduces end fields in each tunnel and generally makes the overall flux lines parallel to the winding layer in each tunnel. The parameters are listed in Table 2.

In comparison to earlier designs approximately the same amount of radial strut material is required to carry the magnetic force to the rock face. The axial strut material is only 4% of the previous designs. The savings of axial strut materials is due to the multi-tunnels and the circular configuration. The axial cold structure is only 1/8 as much as the cold structure for previous three tunnel designs.

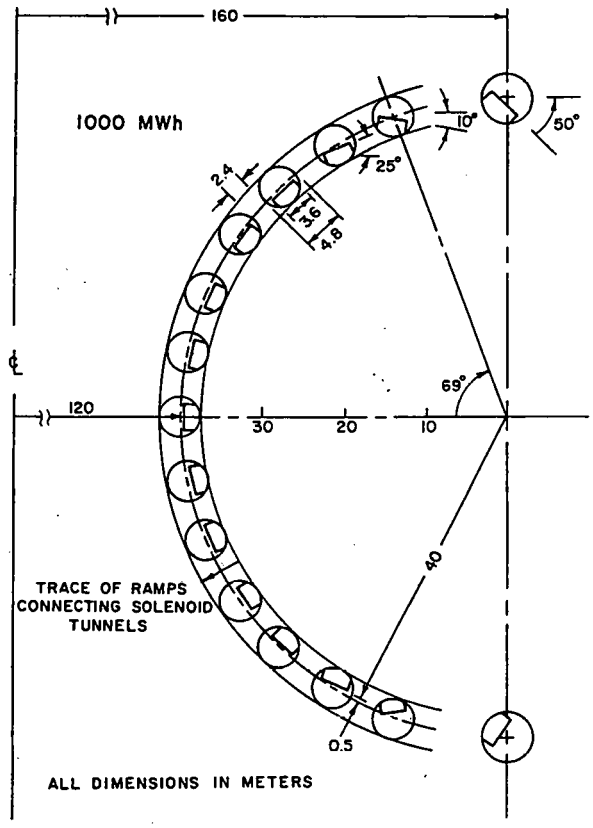

Fig. 1. Cross Section of New 15 Tunnel Energy Storage Magnet Design

TABLE 2. Fifteen Tunnel Solenoid

Energy Stored	1186 MWh
Major Radius	120 m
Minor Radius	40 m
Total Turns	554
Turns per Central Tunnel	36
Turns per End Tunnel	43
Current per Turn	300,000 A
Central Average Field	2.5 T
Maximum Field	4.0 T
Total Radial Force	4.4×10^{10} N
Total Axial Force	1.7×10^{9} N
Radial Strut Material*	0.79×10^{6} Kg
Axial Cold Structure*	1.2×10^{6} Kg
Axial Strut Material*	0.03×10^{6} Kg

*Material is polyester fiberglass used at 1.9×10^{8} N/m^2 (27,000 psi).

ROCK SUPPORT*

The tunnels shown in Fig. 1 would be constructed by a Tunnel Boring Machine (TBM) in the Sinnipee dolomite of eastern Wisconsin. Such construction is much less damaging to the rock fabric at the tunnel perimeter with consequently fewer anomalies in the effective rock properties such as rock modulus.

The support requirements are not onerous. It is anticipated that there will be no difficulty in ensuring the integrity of rock-bolt support for the life of the facility. All bolts are fully encapsulated in resin, which serves both to develop a full anchorage and to protect the bolts from ground water. Carbonate rock is a passive environment not conducive to electrochemical corrosion of bolts. The rock permeability is generally low enough to ensure that inflow of ground water will be minimal and controllable by grouting. No need is foreseen for structural lining of tunnels.

The average magnetic pressure is 360 psi at 2.5 tesla and 1440 psi at 5 tesla. Taking 15,000 psi as a rock compressive strength and derating by 50% for 250 years of daily cycling we see that a field of 5 tesla can be tolerated with a safety factor of 5. It should be anticipated that the effective rock strength is higher than this for Sinnipee dolomite as in crystalline rocks and dolomites occurring elsewhere in the U.S.

The cost estimates are approximately $40,000,000 for the tunnels of a 1000 MWh unit. This study includes the cost of shaft construction, support and lining; installation of shaft and tunnel equipment; construction of adits, tunnels and inter-tunnel ramps; tunnel support, drainage and grouting; and ventilation, temporary lighting, cleanup and equipment operation. There are sufficient rock-bolts to provide tunnel support and hangers for mechanical and electrical installation ($\sim$250,000). The construction period is estimated at four to six years with one TBM and three to five years with two TBM's.

In general, the civil work can be regarded as straightforward without novel techniques. The only item which is non-routine is to transfer the TBM from level to level by ramping, a maneuver which has been accomplished on numerous projects. The loadings are large but well within the capacity of the rock mass to sustain. Fully resin encapsulated rock bolts and dowels should have an indefinite life, especially in carbonate rock. Water inflow can be controlled by grouting and drained or evaporated away. Earthquake effects are slight for buried structures if shears and faults are avoided.

COMPONENT DEVELOPMENT

Research and development has been carried out over the past year in two key areas: conductor and structure. An artist conception of how these components fit into the energy storage magnet is shown in Fig. 2. The strut, which is approximately one meter in length, is an A-frame of fiberglass polyester. Cooling tubes are attached to the strut at two locations to minimize the heat load at the magnet temperature of 1.8 K. Magnetic force is transferred through the strut to bedrock at discrete locations, thus minimizing the need for expensive cold structure.

The conductor is 80 mm in diameter and carries approximately 300,000 A at 2.5 T.[6] Structurally, it is designed to carry the hoop tension between struts and the bearing stress over the discrete load transfer points. The conductor is to have full cryogenic stability and to be cooled in 1.8 K superfluid helium.

---

* - Wisconsin Electric Utility Research Foundation study by T. G. McCusker.

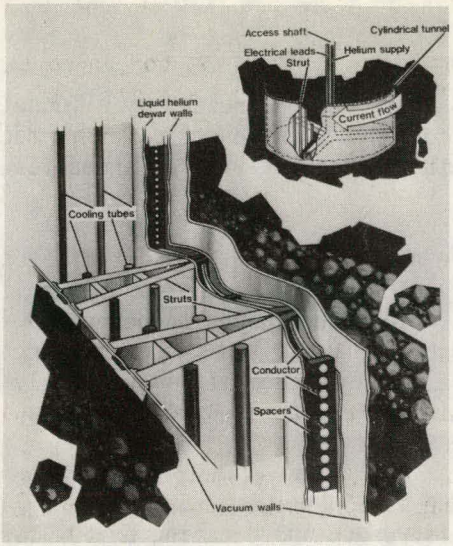

Fig. 2. Artist Sketch of Magnet and Support Structure

Structural research has been in the selection of candidate materials and compressive testing of model struts. Conductor work has involved studies of stabilizer, superconductor and helium heat transfer as well as fabrication and testing of assembled model conductors. This section surveys the recent work in these two developmental areas.

CONDUCTOR

The Wisconsin conductor design for energy storage contains four components. Current is carried by a composite of NbTi in an aluminum stabilizer. The conducting elements are held together by an internal structural member or cruciform which is made from high strength aluminum alloy. To restrict the high purity aluminum from excessive plastic flow the superconductor, stabilizer and cruciform are surrounded by an aluminum alloy skin.[7]

In an effort to understand enhanced current densities in NbTi, transmission electron microscopy of four commercial multifilamentary composites of varying composition in the range Nb 46.5 to 53 w/o Ti has been carried out.[8] Detailed investigation of the structures found in these composites has shown that α-precipitates play at least as important a role as dislocation cell size in the critical current density. Although this type of study is complex, it represents the only reliable method to study changes in current density that result from small variations in fabrication and heat treatment.

To insure stability the sectored composite conductor must have adequate thermal conductivity in the radial direction. The thermal resistance of the bond between the stabilizer and the skin, the thermal conductivity of the skin and the heat transfer to the helium will govern the radial flow of heat. The method of joining the conductor components and the selection of a skin alloy are thus important considerations.

The bonding between conductor components is under investigation to develop the best manufacturing and assembly procedure.[9] Radial heat transfer and electrical resistivity studies of two component specimens have shown that drawing is far superior to swaging for conductor assembly. Swaged samples typically have thermal or electrical boundary resistances between components which are one to two orders of magnitude greater than occurs in drawn specimens. As a result of these studies, swaging has been eliminated as a manufacturing technique for the conductor.

Heat transfer studies in superfluid helium have continued to develop further understanding of conductor stability in this cooling medium. As was discussed in the 1978 contractors' review meeting, peak heat fluxes in superfluid helium have the potential of being two to three times that which occurs in normal helium. Design values for full cryogenic stability equate the critical heat flux, q, with the joule heat generated when the current in the stabilizer

$$I^2\rho/A = qS \qquad (1)$$

where ρ is the resistivity of the stabilizer and S is the surface area. Higher heat fluxes translate directly to higher overall current densities.

Recent transient heat transfer studies at Wisconsin have shown further advantage to superfluid helium. An extended period of "transient stability" appears to exist at higher heat fluxes than the steady state peak value. For example, under conditions where the steady state peak may be less than 1 W/cm^2, heat can be transferred at the rate of 4 W/cm^2 for 250 msec without burnout.[10]

The above subcomponent studies have led to the fabrication and preliminary testing of a model conductor.[11] A photomicrograph of the assembled conductor is shown in Fig. 3. The conductor was prepared in the University of Wisconsin fabrication facilities.

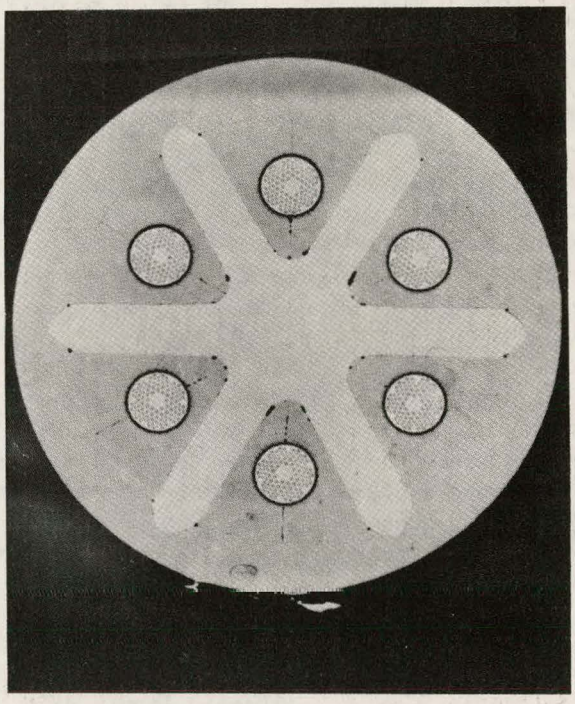

Fig. 3. Photomicrograph of Assembled Model Energy Storage Conductor

The conductor component was chosen to match as closely as possible the full scale conductor. A standard NbTi-Cu multifilament composite was chosen as the superconducting component. The conductor contains six wires, each capable of 900 A at 4.2 K and 2.1 T. The six web 6061-T6 aluminum alloy cruciform was manufactured in industry in 4.5 m lengths. The cruciform has a 9.3 mm diameter and a cross sectional area of 23 mm^2. The skin and wedge were extruded from high purity aluminum with a modest resistance ratio (RRR = $\rho_{273K}/\rho_{4.2K}$) of 150.

The fabrication procedure for the conductor is shown in Fig. 4. All components are chemically cleaned and mechanically abraided to break the oxide surface. The cruciform, superconductor and wedges are then drawn down in the tubing which forms the skin. The first drawing step brings the skin in contact with the other components. The second and last drawing step brings the conductor to final size and pierces the cruciform into the skin. The piercing process insures the formation of an integral conductor with good mechanical and electrical properties.

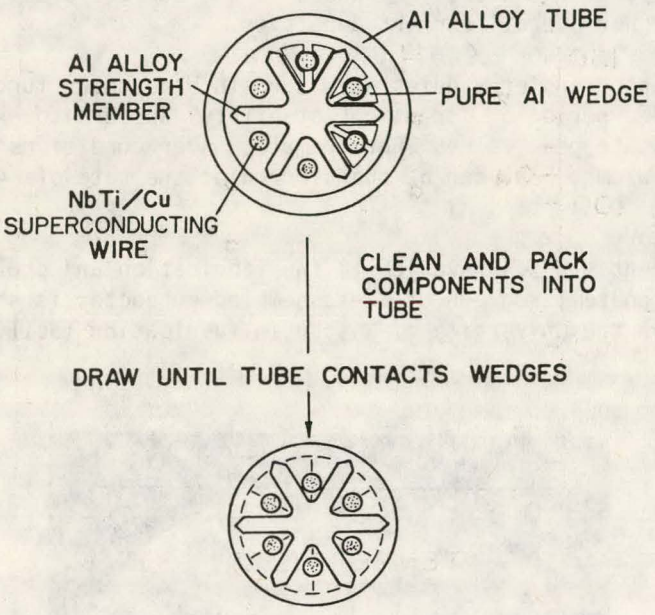

Fig. 4. Fabrication Procedure Used in Making the Model Conductor

Planning is under way to test the model conductor in a magnetic field. The design capabilities of the conductor are 5400 A at 2 T and 4.2 K with full cryogenic stability.

STRUCTURES

The structural requirement for superconductive energy storage are for a large quantity of low thermal conductivity, high load carrying support structure to transfer the radial and axial load from the 1.8 K magnet to the bedrock. The following is a list of important criteria for choosing the appropriate material for supporting the magnet: low thermal conductivity, high compressive strength, moderate fatigue life, and low cost.

In order to determine the best candidate material, numerous commercial fiber reinforced composites have been tested, both for ultimate strength as well as fatigue life. This work has been carried out at room temperature as well as in liquid nitrogen and liquid helium. Glass fiber reinforced polyester has evolved as the best material available, because it has comparable strength to epoxy-fiberglass and is substantially less expensive. Additionally, the polyester appears more resistant to thermal stock than the other composites.

Most of these compressive tests have been carried out in rod material. However, the strut design which has evolved uses sheets or plates of composite materials. Recent studies have begun to look at sheet material both machined into rod and with rectangular cross section.[12] The ultimate strengths of these materials along with previous measurements are shown in

Fig. 5. The polyester sheet material is seen to have a lower ultimate strength which appears to result from layer delamination. Further work is under way to consider other alternatives including the potential of a different strut design.

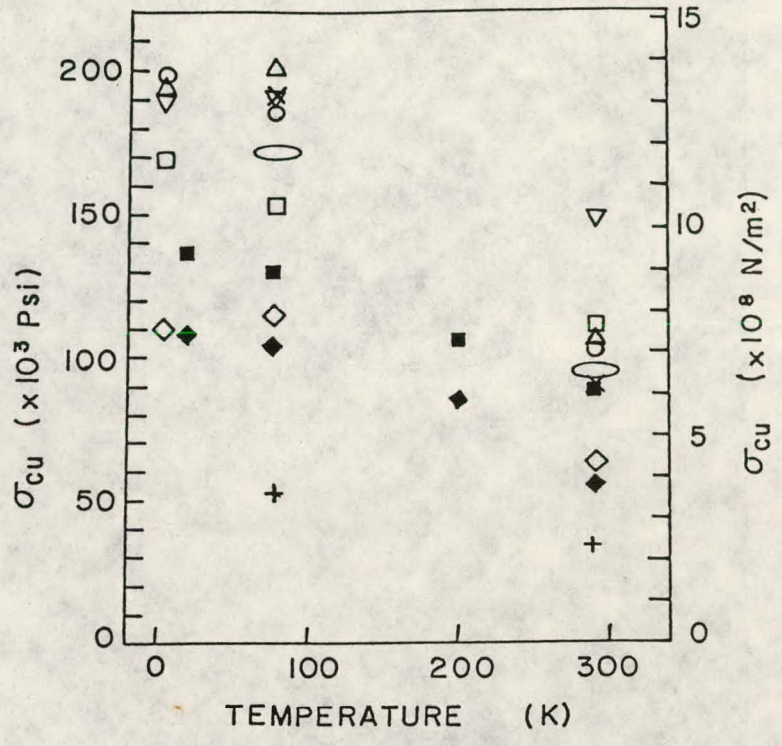

Fig. 5. Ultimate Strength of Composite Materials Tested in Selecting Strut Material

Recently structures experimental testing has moved from the material selection to emphasizing testing of actual model struts. One such test, shown in Fig. 6, is a compressive loading of the A-frame structure made from EXTREN polyester mat material. A 1/8th scale strut, 1/2 scale in all linear dimensions, has been tested in compression at room temperature. Without the cross support shown in the figure, the failure mode is buckling since the sheet material is too thin compared to its length. This theory was verified in the experimental tests. The maximum load that the strut without cross support would carry was 250,000 lbs.

Buckling problems are serious concerns in the present strut design. These factors have led to the possibility of alternative designs using tubes or rod material. This suggestion of using rod material is further encouraged by the experimental testing which gave better results for rods.

CONCLUSIONS

The major achievements during the past year's component development program has been in fabricating and testing model conductor and struts. Future work will be directed toward more tests of these components and subsequent improvements in design and fabrication based on these studies. Further design work will involve studying the multi-tunnel design more closely, both for structural requirements as well as assembly possibilities. The ultimate goal of these activities is to develop the best components and fabrication technique so that a model superconductive energy storage unit can be built.

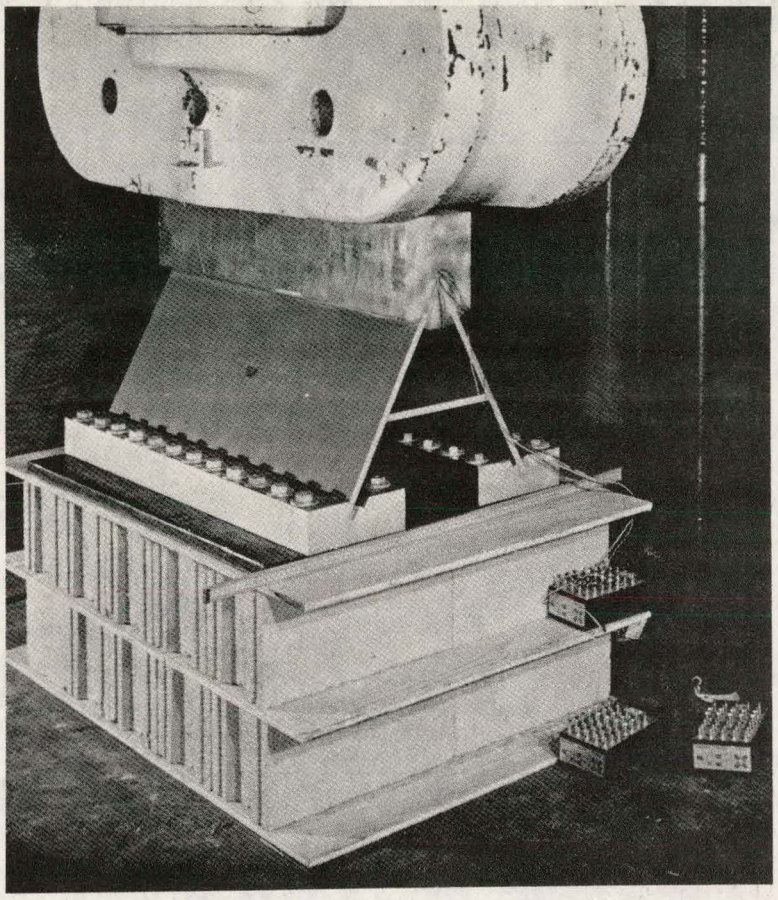

Fig. 6. Model Strut Showing 1/8 Scale Strut Under 1,000,000 lb. Press

REFERENCES

1. R. W. Boom, Proceedings of the 1978 Mechanical and Magnetic Energy Storage Contractors' Review Meeting, CONF-781046, 237 (1978).

2. S. W. Van Sciver, Proceedings of the 1978 Mechanical and Magnetic Energy Storage Contractors' Review Meeting, CONF-781046, 247 (1978).

3. J. J. Skiles and J. B. Prince, 1979 Mechanical and Magnetic Energy Storage Contractors' Review Meeting.

4. Wisconsin Superconductive Magnetic Energy Storage Project, Vol. I, University of Wisconsin July , 1974.

5. Wisconsin Superconductive Magnetic Energy Storage Project, Vol. II, University of Wisconsin January, 1976.

6. Wisconsin Superconductive Magnetic Energy Storage Project, Annual Report, University of Wisconsin, May, 1977.

7. S. G. Ladkany and W. C. Young, IEEE Trans. on Magnetics, Mag-13, 105 (1977).

8. A. West and D. C. Larbalestier, 1979 Cryogenic Engineering/Materials Conference, Paper BA-4.

9. S. W. Van Sciver and K. T. Hartwig, 1979 Cryogenic Engineering/Materials Conference, Paper KA-3.

10. S. W. Van Sciver, Cryogenics, 19, 385 (1979).

11. K. T. Hartwig, 1979 Cryogenic Engineering/Materials Conference, Paper KA-2.

12. Z.G. Khim, 1979 Cryogenic Engineering/Materials Conference, Paper EB-6.

THIS PAGE

WAS INTENTIONALLY

LEFT BLANK

PROJECT SUMMARY

Project Title:	"Superconductive Energy Storage"
Principal Investigator:	R.W. Boom
Organization:	531 Engineering Research Building University of Wisconsin Madison, Wisconsin 53706 (608)263-5027
Project Goals:	To develop hardware components, produce engineering system designs, procure manufacturing and assembly equipment designs, revise cost estimates, and assess operational efficiencies for large underground superconductive storage systems.
Project Status:	Component development in three areas: cryogenics, conductor and structures is under way to be completed in FY-81. Rock mechanics design and experimentation is under way to be completed in FY-81. Parallel efforts supported by the Wisconsin Utilities are under way on the same schedule in five other areas: magnetics, environmental studies, system design, electrical, and safety.
Contract Number:	EY-76-C-02-2844-000
Contract Period:	FY-78
Funding Level:	$600 K
Funding Source:	U.S. Department of Energy Division of Energy Storage

ELECTRICAL ENGINEERING CONSIDERATIONS FOR DIURNAL SUPERCONDUCTIVE STORAGE DEVICES

J. J. Skiles
Energy Research Center
University of Wisconsin
Madison, Wisconsin 53706

J. B. Prince, Jr.
Wisconsin Electric Power Company
231 W. Michigan Avenue
Milwaukee, Wisconsin 53201

ABSTRACT

A report is given of electrical studies at the University of Wisconsin associated with the design and operation of superconductive magnetic energy storage (SMES) systems utilized for electric utility load leveling. The power delivery capability of the phase controlled thyristor inductor-converter (I-C) bridge and the necessity for minimizing or compensating for the reactive power drawn from the power system by the I-C unit are identified as major power system considerations. A System Planning Analysis for Evaluating SMES is suggested.

INTRODUCTION

Superconductive magnetic energy storage (SMES) designs for load leveling on power systems are based on a superconductive coil in a liquid helium dewar which stores dc magnetic energy and is interfaced to an electric power system through a full-wave, three-phase, Graetz bridge capable of reversible converter or inverter operation[1] as shown in Fig. 1.

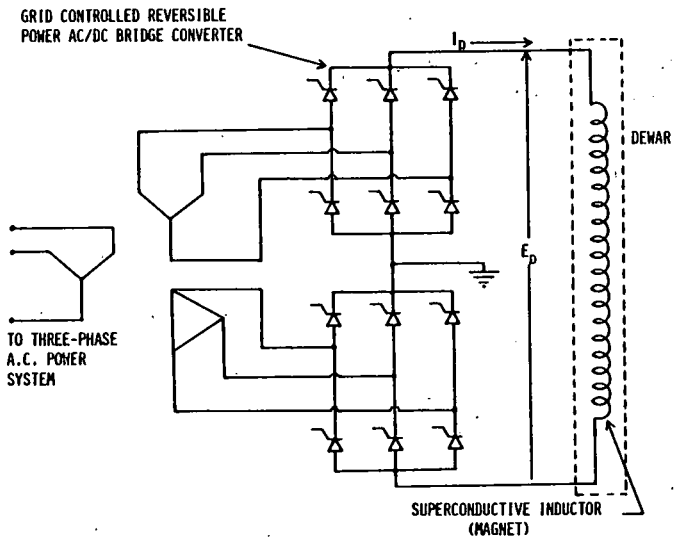

Fig. 1. Basic Circuit Elements for Superconductive Energy Storage Inductor-Converter (I-C) Unit for Power System Applications

The electrical insulating properties of helium limit the allowable dc voltage across the superconductive coil from less than 10 KV to a few tens of KV in most designs. The economics of scale[2] favor large energy storage capability and units as large as 10,000 MWh capacity have been proposed, with power ratings as high as 300 MW to 500 MW. This corresponds to dc coil currents in the range of 300,000 amperes or more.

The Graetz bridges use commercially available power thyristors with phase angle control to regulate the power through the bridge. Available thyristors do not have 10 KV or 300,000 amp capacities in single units and consequently the bridges are constructed of a number of thyristor modules in series and in parallel to obtain the necessary voltage and current rating of the bridge. Continued progress in power semiconductor technology will probably result in simpler designs with individual thyristors with higher voltage and current ratings than are currently available.

The requirement for series and parallel connection of modules, although complicating the design, is not all on the negative side. Isolation of failed thyristor modules will permit continued operation of the unit at reduced power rating. Also, a variety of control schemes are possible with multiple modules that is advantageous in controlling reactive power drawn from the system and in minimizing power frequency harmonics introduced into the system.

The favorable experience with high voltage inductor-converter (I-C) phase controlled thyristor bridges in high voltage dc transmission terminals and with heavy current pulsed power supplies suggests that the Graetz bridge circuit will not be a major design problem in full-size SMES storage units suitable for power system use. As will be discussed later, a complicating design consideration is the possibility that the I-C bridge should be designed for constant power capability while the coil is in the discharge mode.

MAJOR ELECTRICAL CONSIDERATIONS

A number of major electrical problems have been identified and reported in the literature. Many are interrelated. These problems include:

1. Bridge kW capability
    a. Constant power
    b. Constant voltage
    c. Hybrid design
2. Consequences of phase control
    a. Introduction of harmonics
    b. Reactive power problems and power factor control
    c. Choice of control algorithms
3. Power system operation
    a. Steady-state peak shaving and choice of operating cycle
    b. Use as a regulating machine
    c. Transient over-voltage behavior
    d. System stability considerations
    e. Reliability; forced outage rates and duration of outages
    f. Generation reserve requirements

BRIDGE kW CAPABILITY

Conventional fossil-fueled and nuclear-fueled generating units can be operated at almost all times up to the maximum power capability of the generator. As it is common to think of an SMES unit as equivalent to a conventional generator when discharging stored energy, the power capability of an SMES unit should be examined.

The power transferred between the I-C bridge and the superconducting coil is given by

$$P = E_D I_D$$

where E_D is voltage across the coil and I_D is current in the coil.

Conventional converters would operate at constant voltage and thus the power capability would vary linearly with the coil current. As the SMES unit is discharged, the capability of delivering three phase ac power to the power system is similarly reduced. This varying power capability, dependent on the state of charge of the storage system, represents a new variable in the planning and operation of power systems with SMES installed.

A solution, but costly, is to design the bridge for constant power capability. Transrex Division of Gulton Industries has investigated one possible constant power design for the University of Wisconsin SMES project. Series-parallel switched groups of converter modules were also investigated by General Electric in a study for the Los Alamos Scientific Laboratory.[3] The configuration investigated by Transrex uses three different thyristor converters (A, B, and C), of different sizes, that can be bypassed or connected in series or paralleled to approximate a constant power capability as shown in Fig. 2.

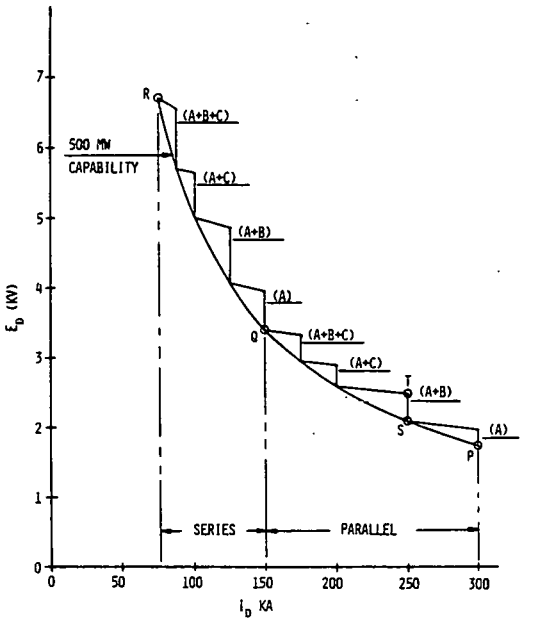

Fig. 2. Power Capability Curve

The conceptual design used to approximate a constant power capability also provides another approach to controlling the reactive power drawn by the converter.

A hybrid approach to converter design has also been proposed[4] that would operate at constant power from 1.0 pu I_D down to 0.6 pu I_D, and at constant voltage with linearly decreasing current and power capability for I_D less than 0.6 pu.

CONSEQUENCES OF PHASE CONTROL

Inherent in phase control of thyristor (or other controllable device) bridges is the generation of harmonics of the power frequency and a variation in the reactive power drawn by the converter as the power is controlled.

Harmonic Generation in phase-controlled rectifier-converter circuits is well understood. Well known are the techniques of converting three phase power to 12, 24 or higher number of phases to eliminate low order harmonics and to minimize the magnitudes of the remaining harmonics in bridges. Analog filtering and shielding to further reduce the effects of harmonics on power and communication systems are well known. Active filters have also been studied.[5] Experience in solving high voltage dc transmission and converter terminal harmonic problems is directly applicable to SMES converter harmonics.

Reactive Power requirements of I-C bridge units require careful consideration because of the effect on the associated power system.

Phase control of a bridge with single thyristor elements in each arm of the bridge gives the semicircular power and reactive power locus shown in Fig. 3.

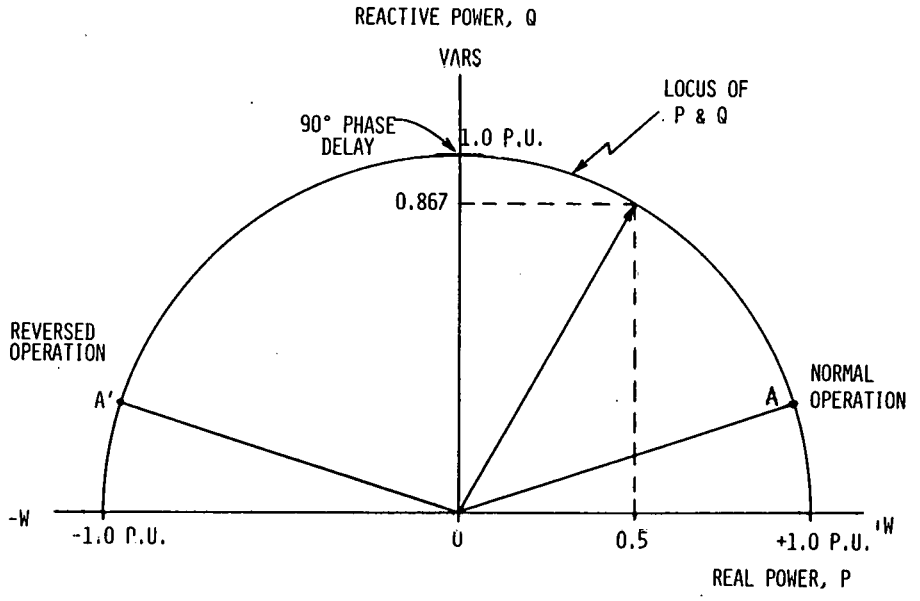

Fig. 3. Vars Versus Watts

Normal operation is shown as point A for maximum practical power capability. The reactive power (VARS or Q) drawn under normal operation at point A is a function of the effective commutating reactance even with nominal thyristor control phase angles close to zero.

As power is reduced, using phase angle control, the real power P and reactive power Q follow the semicircular locus to a new operating point A' where the direction of power flow

through the converter has been reversed. Reactive power is still drawn from the system, however. To minimize the reactive power drawn from the system the phase angle should be close to 180° (150° or more). Note that operation at low values of real power with phase angles near 90° results in excessive reactive power demands on the power system (near 1.0 pu) and must be avoided if possible.

Minimizing or compensating for the reactive power drawn from the power system is a major concern. Possible approaches include:

1. Special phase angle control and/or switching of series-parallel combinations of converter bridge thyristor and transformer modules that keep most units operating with near 0° or 180° phase angles on the thyristor controls at any time to minimize reactive power.[6]

2. Voltage tap changing of the transformers connecting the converter to the power system.

3. Switched power factor correcting capacitors.

4. Synchronous condensers.

Voltage tap changing transformers, switched capacitors, and synchronous condensers have the disadvantages of cost and operational reliability considerations. The effectiveness of power correcting capacitors is reduced during periods of low voltage troubles on the system when they may be needed the most.

POWER SYSTEM OPERATION

Numerous studies have been conducted on the application of SMES units to peak shaving. A.D. Little investigated several alternative storage cycles in a study for the Department of Energy.[7]

The dynamic performance of SMES units on power systems and transient over-voltage behavior have been studied.[8,9]

SMES units have the capability of improving the transient stability of power systems because they can respond within a few cycles to damp oscillations on the system.[10,11]

Little attention has been given to the reliability, forced outage rates prediction, or system reserve requirements with SMES units on a system. However, these characteristics must be studied in more detail for proper evaluation of the value of SMES units and operating characteristics of associated power systems.

SYSTEM PLANNING ANALYSIS OF SMES

Much of the research to date on SMES has been related to component development and system design, studies of the electrical effects on power system and performance of the I-C bridge, and system optimization to reduce construction and operational costs. Most of the work on system economics has been concerned with general studies of typical systems.

The optimum kW and kWh ratings of storage units, and indeed their worth to a utility, can only be determined by detailed studies of the particular utility system involved. Utilities serving neighboring geographic areas may have quite different daily, weekly, seasonal and annual load factors, generation mixes, fuel costs, load projections, etc.

Whenever a storage unit is first added to a system it is likely that the economics will not be optimum if the bulk of the existing generation was selected without consideration for

storage. The economics may improve in later years as older generation is retired or displaced by newer generating units installed for use with storage on the system.

Realistic system planning studies of the possible use of storage should cover a time period starting when storage could first be available and continuing over a period of perhaps 25 years.

Parameters for a planning study would include:

- Start with a 1988, or later, system
- A 25 year planning period
- Use load forecasts including anticipated impacts of time-of-use rates and load management
- Study different storage cycles; daily, 5 day, 7 day cycles
- Study constant power, constant voltage and hybrid I-C alternatives (unless one alternative is clearly established beforehand as the best)

The planning study can be conveniently divided into four major categories:

1. Preliminary Analysis: Determine
   a. Tolerable range of MW and MWh ratings
   b. Timing of need
   c. Transmission requirements
   d. Regulatory interface: licensing and accounting

2. Operational Analysis: Study
   a. System losses
   b. System reliability
   c. System stability
   d. System reserve requirements
   e. Operational cycle to be used
   f. Institutional problems
   g. Intangible benefits and costs
   h. Maintenance scheduling

3. Economic Analysis
   a. Capital requirements/year
   b. Operational costs/year
   c. Fuel requirements/year

4. SMES Unit Design Recommendation
   a. MW and MWh ratings
   b. Storage cycle
   c. Reactive power compensation
   d. Design reliability

CONCLUSIONS

The focus of research and development efforts on SMES to date at Wisconsin has been primarily on development of components, optimization of designs to lower costs, and on studies of the operating characteristics of SMES units in power systems under normal and abnormal system

conditions. These studies have led to refinements in component designs and to better estimates of the cost of constructing SMES units.

Future efforts will include more detailed system planning analysis of SMES units in actual power systmes. As SMES units have some characteristics that are not identical to normal system generation, new analysis techniques will have to be evolved to aid the system planner.

The progress of SMES component development, SMES system design and SMES electrical interface design will continue to be closely coordinated and integrated with the SMES electrical power system use studies reported on in this paper.

ACKNOWLEDGEMENTS

The authors wish to acknowledge the contributions of H. A. Peterson to the understanding and solutions to many of the electric power system problems associated with SMES. Al Mihm, Bruce Erickson and Lloyd Grove of the Wisconsin Electric Power Company have also contributed to this report.

REFERENCES

1. H. A. Peterson, N. Mohan and R. W. Boom, "Superconductive Energy Storage Inductor-Converter Units for Power Systems," IEEE Transactions on Power Apparatus and Systems, Vol. PAS-94, No. 4, July/August 1975, pp. 1337-1346.

2. University of Wisconsin Superconductive Energy Storage Project Report, Vol. 1, July 1, 1974, p. IX-6.

3. "Design Study: Thyristor Converter Stations for Use with Superconductive Magnetic Energy Storage," Electric Utility Systems Engineering Department-General Electric, for the Los Alamos Scientific Laboratory.

4. H. A. Peterson, private correspondence.

5. University of Wisconsin Superconductive Energy Storage Project Report, Vol. II, January 1976, pp. VIII-10 to VIII-18.

6. University of Wisconsin Superconductive Energy Storage Project Report, Vol. 1, July 1, 1974, pp. II-1 to II-34.

7. "An Evaluation of Superconductive Magnetic Energy Storage," Draft Final Report, A. D. Little, Inc., April 19, 1979, pp. 3.2-3.5.

8. Reference 2, pp. IV-1 to IV-28.

9. University of Wisconsin Superconductive Energy Storage Project 1976 Annual Report, May 1, 1977, pp. VIII-1 to VIII-29.

10. P. C. Krause and D. M. Triezenberg, "Hybrid Computer Study of a SMES Unit for Damping Power System Oscillations," Proceedings of the 1978 Mechanical and Magnetic Energy Storage Contractors' Review Meeting, DOE, October 1978, pp. 264-269.

11. R. L. Cresap and J. F. Hauer, "Power System Stability Using Superconducting Magnetic Energy Storage Dynamic Characteristics of the BPA System, Proceedings of the 1978 Mechanical and Magnetic Energy Storage Contractors' Review Meeting, DOE, October 1978, pp. 254-262.

PROJECT SUMMARY

Project Title:	An Evaluation of Superconducting Magnetic Energy Storage Systems
Principal Investigator:	James Nicol
Organization:	Arthur D. Little, Inc. Acorn Park Cambridge, MA 02140
Project Goal:	To evaluate the degree to which the nation and its electric utilities might benefit from the development of Superconducting Magnetic Energy Storage Systems and to evaluate the nature and severity of the technical barriers which must be overcome.
Project Status:	The investigation has been essentially completed; the only remaining tasks involve editorial modifications of the Draft Final Report. Two general questions were examined, they were 1) if the present conceptual designs and the associated costs are correct, will the SMES system be of benefit to the electric utilities? and 2) can equipment built according to the present conceptual designs meet the utilities' operating requirements? To answer the first question, we extended the comparison methodology beyond its present state of development. Our analysis shows that the SMES system may compete favorably with alternate storage systems when all systems are sized to deliver the same amount of energy to the load. This favorable outcome is the direct result of the high efficiency with which SMES can accept and deliver energy. To answer the second question, the subsystems and proposed designs for the superconducting magnetic energy storage system were reviewed. It was clear that several major technical barriers must be overcome before a successful SMES unit can be constructed on the scale envisioned by the proponents. Although there is little reason to doubt that the technical problems can eventually be solved, it is not clear at this point that the solutions will be economically acceptable. The major problem areas appear to lie in developing a design which can be constructed in the field to meet the stringent vacuum performance requirements, with adequate reliability and with the ability to be maintained in the event of failure.
Contract Number:	31-109-38-4917
Contract Period:	FY '79
Funding Level:	$55,000
Funding Source:	U.S. Department of Energy, Energy Storage Systems Division, Via Argonne National Laboratories

AN EVALUATION OF SUPERCONDUCTING MAGNETIC ENERGY STORAGE

Bette M. Winer
Arthur D. Little, Inc.
Acorn Park
Cambridge, MA 02140

ABSTRACT

The object of this investigation into the benefits and likely costs of Superconducting Magnetic Energy Storage (SMES) Systems was to determine if continued R&D support by DOE is justified. The results of the study indicate that due to the high efficiency with which the SMES System could accept and regenerate ac electrical energy, an SMES unit can compete economically with alternative advanced storage technologies if 1) its capital costs and the efficiencies are within the estimated range, and 2) the unit is sized so as to allow it to perform the same task proposed for alternative generator types and no more. However, the present SMES System design is unlikely to be able to meet the electric utilities' requirements of reliability, maintainability and system protection;and the costs of a unit which could meet these requirements are unknown. In addition, there is considerable uncertainty about the design and cost of major subsystems and the environmental impact of the magnetic field. Thus, while continued support of R&D programs for the SMES system may appear to be justified, the goal of this work should be providing information to allow a final assessment of the ability of SMES to help meet the nation's future energy needs.

INTRODUCTION AND SUMMARY

This investigation was undertaken to help decide if additional support from DOE for the development of an SMES System could be justified by the benefits that might accrue. Superconducting magnetic energy storage involves converting electrical energy into energy stored in the magnetic field of an electromagnet constructed of superconducting wire. The key to this process is that the storage is essentially lossless because superconducting wire has no electrical resistance to dissipate energy. The chief difficulties lie in the fact that superconducting materials lose their electrical resistance only at temperatures near absolute zero; thus the entire system must be enclosed in a refrigerated vacuum vessel. Most of the losses in SMES are the energy used for running the refrigerator and in converting ac power to dc and back again. The following areas were addressed:

1) The present state of technical development; additional development required; technical and environmental problems to be solved; realism of assumption that problems can be solved at acceptable costs; likely cost of an SMES unit built to the present conceptual design.

2) Usefulness and economic desirability of SMES to the electric utility industry; assuming cost to be within the specified range.

To address the first area, the major subsystems and the proposed designs for the SMES magnet were reviewed. Several major technical barriers must be overcome before a successful SMES unit can be constructed on the scale envisioned by its proponents. There is little doubt that the problems can be solved, but it is not clear that the solutions will be economically acceptable. The major problem areas appear to lie in designing reliable and maintainable hardware which can be constructed to meet the stringent vacuum performance requirements. (The present design requires the magnet to be placed underground with significant impact on fabrication and maintainability.) There is also need for a better understanding of rock behavior under diurnal pressure fluctuations over a period of years. The range of capital costs estimated for the present SMES System design are in reasonable agreement with those presented in previous studies; the capital cost of equipment designs which meet utility requirements for maintainability and system

protection are unknown.

To decide if SMES systems built to present designs could be useful and economically attractive to the electric utility industry, a new comparison technique was developed. We compared alternative storage systems sized to deliver the same amount of energy to the load each year; except for the storage systems under evaluation, the power system characteristics were the same for each case. This approach extends the techniques previously used to compare energy storage systems to the next level of complexity. The results of our analysis show clearly that SMES systems may indeed compete economically with alternative storage and conventional power systems. This favorable outcome is the direct result of the efficiency with which SMES can accept and deliver energy.

SMES SUBSYSTEMS

An SMES system will consist of the following major subsystems.*

- o The superconducting magnet
- o The cryogenic container
- o Structural containment for the magnet
- o Refrigeration and vacuum systems
- o Power conditioning equipment

These will each be discussed in the following paragraphs.

The Superconducting Magnet System

The Superconducting Conductor

Historically, whenever a superconductor, like NbTi or Nb_3Sn, is expected to carry large currents, it is stabilized by encasing it in copper to prevent thermal run-away should the superconductor revert to the normal phase with normal ohmic resistance.

In principle, aluminum is an attractive alternative to copper because it is much less expensive. Unfortunately the successful use of aluminum-cladded superconductor requires the resolution of unsolved metallurgical problems. If these are resolved, the cost of aluminum stabilized conductor should be reasonably close to the predictions of its proponents. If copper must be used, conductor costs will be substantially greater.

Two types of conductor designs have been considered for use in the SMES magnet: modular, copper stabilized conductor and monolithic, aluminum stabilized conductor. The modular design is attractive because the basic modules could be manufactured off-site and shipped to the site in relatively long lengths for final assembly. Thus, critical processing would be performed in a facility designed for quality production. Monolithic conductors would need either on-site manufacture or manufacture in short lengths and on-site assembly with a large number of conductor joints. Both of these alternatives are riskier than the modular design.

Magnet Design

The present conceptual designs for the magnet are scaled-up versions of smaller magnet designs, i.e. either a single solenoid or the segmented solenoid shown in Figure 1. However, the designs have been driven by economic considerations to sizes for which there is no experience (See Figure 2). Thus, it cannot be stated unequivocally that a large SMES magnet can be built; nor is there experience to determine the service reliability of equipment built to these specifications. The cost of a more self-evidently maintainable design might eliminate the SMES from economic competition.

* R. W. Boom, "Superconductive Diurnal Energy Storage Studies," Proc. of the 1978 Mechanical and Magnetic Energy Storage Contractors' Review Meeting, Oct. 1978, Luray, VA., U.S. Dept. of Energy Report CONF-781046 and personal communication giving revisions to March 1979.

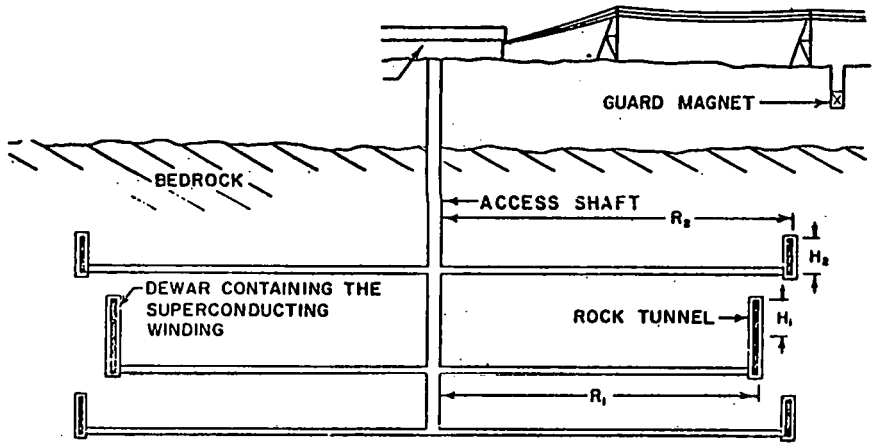

Figure 1. Schematic of SMES System Installed in Bedrock (University of Wisconsin)

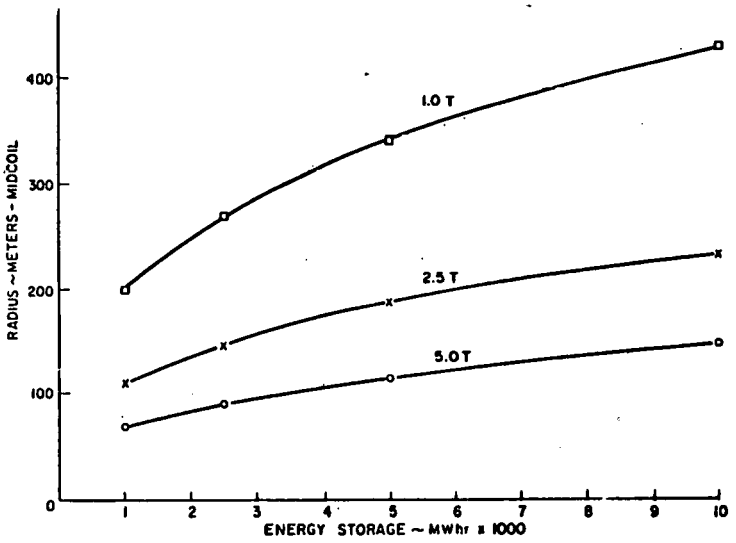

Figure 2. Radius of SMES vs. Energy Storage Capacity and Magnetic Field for Solenoid

The University of Wisconsin has considered how to provide for magnet protection and continued operation should a portion of the superconductor fail. The magnet is to be separated into twenty-four independent sections (with separate dewars and leads) with multiple shorting switches to allow each section to be discharged independently. However, the discharging of one section and the shorting of others would result in unbalanced forces. The integrity of the support struts and rock under these conditions is questionable; if the failed section is not to collapse, additional inter- and intra-coil structure may be required. The cost of this structure might be prohibitive.

The proposed underground placement of the SMES resulted from analyses indicating that the cost of structural containment above ground would be prohibitive. The proposed use of rock confinement and support implies that a large portion of the magnet might have to be disassembled in order for any repairs to be affected. Providing for component replacement in the underground environment may well cost more than above-ground placement. Another option might be to reduce or internally balance the forces sufficiently so as to allow for above-ground placement at reasonable cost.

Cryogenic Container

The proposed cryogenic container design is notable in three important aspects:

1) its size and the fact that it must be erected in the field;

2) a requirement to withstand substantial diurnal pressure variations, and

3) the liquid superfluid helium bath at 1.8°K.

Despite the very large scale-up from existing dewar systems, it appears that a large-scale system can successfully retain superfluid helium for long periods of time provided (1) the mechanical details of the system are thoroughly tested in the laboratory and on small-scale production assemblies; (2) the field fabrication is performed by skilled technicians under close supervision; and (3) as the system is constructed, the plating and welds are rigorously tested by x-ray and vacuum mass spectrometer leak detectors.

The existing designs for the superfluid helium dewar and vacuum container could probably not be rigorously tested for vacuum leaks under field assembly, or, in the event of failure, be repaired in the field. It is not clear how closely a more self-evidently reliable design will resemble those used for cost estimates and for this evaluation. Thus it is difficult to put limits upon a variation from present cost estimates. Little is presently known about the ability of aluminum cryogenic containers to withstand flexing for many cycles over long periods (10^4 cycles in 30 years) and retain their integrity.

Structural Containment of the Magnet

There is very little information available on the ability of rock to withstand the large, daily-cycled stresses proposed to be imposed on the walls of the cavern which cycle daily. This question has been investigated at the University of Wisconsin, but few definitive answers have been obtained to date.

Two recent independent engineering estimates of the cost of excavation agree reasonably well both in cost estimate (about 25% of the total SMES project) and in acknowledged uncertainty (about a factor of two). The large cost uncertainty derives from the difficulty in estimating subsurface conditions in advance. In addition, these estimates rest on a number of optimistic assumptions concerning the following areas:

(1) the excavation volume required for a reliable and field maintainable SMES,

(2) water seepage during the construction and operation phases,

(3) the rock treatment required to resist cyclic magnet loads over many years.

It appears technically feasible to place a SMES under ground but with large uncertainty in cost. It is imprudent to assume that no new geotechnical problems will arise during system life; accessibility to the underground space after the magnets are installed may be critical. These factors make it extremely difficult to reliably determine excavation costs at this time.

Refrigeration and Vacuum Systems

The refrigeration and vacuum systems being considered for SMES differ from current commercial and industrial practice only in scale and performance. The refrigeration system is the source of the major energy loss in the system and must therefore be designed for optimum efficiency. No major scale-up difficulties are expected.

Power Conditioning Equipment

The two types of power conditioning systems (ac/dc convertors) investigated for SMES are characterized either by:

- constant voltage across the magnet - implying that the unit's power delivery or charging rate capability will depend on the SMES state of charge, and

- o constant input/output power capability - independent of SMES state of change but implying higher cost.

Both approaches use relatively conventional Graetz bridges with solid-state thyristors. All present utility generators have a constant power capability. Units may be derated temporarily because of maintenance problems, but this is easily accommodated. A unit whose power rating varies continuously during the day is far beyond utility experience and would require additional system reserves to maintain system integrity. General Electric estimates that constant power conditioning (I_{max}/I_{min} = 3,) will cost $60-80 per kW. More importantly, the General Electric converter design requires the magnet to withstand 17 kV across the terminals. The present University of Wisconsin SMES design could not tolerate such a high voltage. The baseline design being investigated by Los Alamos could tolerate such a voltage and is more expensive.

The conversion efficiency at these high-current, low voltage systems has been estimated between 96.5% and 98.5%. This would yield a round-trip efficiency between 93% and 97%. As will be shown later, the economic analysis is relatively insensitive to the exact magnitude of the efficiency for most of the situations considered.

System Costs

In accordance with the conditions of this study, we have not developed SMES capital or other costs ab initio. The starting point was the costs estimated by the University of Wisconsin for its most recent "Revised Design, 1978."* We have scrutinized the methods of estimation and the date supporting these costs. For each subsystem we used University of Wisconsin scaling laws to develop our own estimates of potential cost variations. (The "baseline" unit for cost estimation purposes had a storage capacity of 10 GWh at a magnetic field of 2.5 T**) The results of these calculations are presented in Figure 3. The capital cost may be as high as $120/kWh for the smallest unit considered and as low as $34/kWh for the largest. These costs are very similar to those estimated by previous reviewers of this technology.

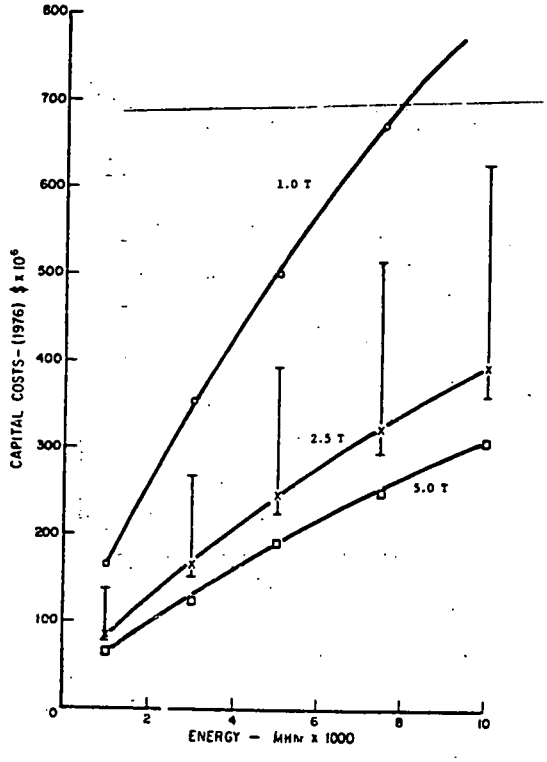

Figure 3.
SMES System Capital Costs (1976$) vs Storage capacity and Magnetic Field

* Ibid. page 2.

** R.W. Boom et al; "Magnet Design for Superconductive Energy Storage for Electric Utility Systems," Proc. of Conference on Superflywheel and Superconductive Storage, Asilomar, CA., Feb. 8-13 1976.

Environmental and Safety Problems

These problems stem from the presence of the stray magnetic field of the solenoid. At ground level the magnetic field of the baseline design ranges from approximately twice that of the earth's field at a distance of 2,800 meters from the center of the solenoid to 1,600 times the earth's field directly above the magnet.

The field of the coil will remain at 1 Gauss (2 times the earth's field) or higher within a volume which extends to a height of approximately 2,600 meters above the surface of the earth directly over the center of the coil. The presence of this field may affect: animal life (particularly birds), mankind and devices which mankind uses, and instrumentation (e.g. magnetic compasses used by aircraft). Available information suggests that human exposure to fields as high as 100 Gauss may not be harmful provided the exposure is not excessively long; other information indicates also that equipment such as cardiac pacemakers may operate in fields up to 10 Gauss. There is no information on the effects on animals of magnetic fields. Clearly then it would be desirable to ensure that a region at least 1,200 meters in radius (the 10 Gauss radius) should be closed to access by man and perhaps animals at ground level. Air space closure is a more different question requiring further investigation.

COMPARATIVE ANALYSIS OF ELECTRIC UTILITIES STORAGE SYSTEMS

Generation capacity, once purchased, is scheduled for operation to minimize the operating costs of the system; thus, operating decisions are based only on the variable or deferrable operating costs* of the various facilities. Thus, the energy any generating plant will deliver during its life depends on 1) system load as a function of time and 2) the relative operating costs of all other generators in the utility system. The "cost" of energy from a storage generator is equal to the cost of the energy delivered to storage during the charging portion of the cycle (M_c) divided by the cycle efficiency; the "value" of energy from a storage generator is equal to the cost of delivering this same energy from conventional sources (M_d). Storage use is determined by the criterion that the marginal "cost" of the stored energy should be less than or equal to its marginal "value". Additionally, the limits on power and energy capacity cannot be exceeded and the energy placed into storage multiplied by the cycle efficiency must equal the energy taken out of storage. These constraints are indicated in Figure 4.

The limited energy capacity of the storage reservoir can help determine the "value" of the stored energy. When the energy in the reservoir is limited, the schedule is set so as to obtain the highest possible "value" for the stored energy. Higher "value" for the limited stored energy can be obtained by saving it to displace only the most costly conventional generation. When the "value" of the stored energy is increased, the maximum acceptable "cost" of the stored energy is also increased when considering storage operating over a weekly cycle (see Figure 5). This fact results in a strong interdependence between the efficiency, reservoir capacity and the amount of energy delivered.

The two curves beginning at point A in Figure 5 are for two different types of storage units with different cycle efficiencies but charged with the same amount of energy at the beginning of the week. Since the amount of week-night recharge energy that can be economically justified for the less efficient unit is less than that for the more efficient unit, the less efficient unit runs out of energy before the end of the week. In order to avoid this, it would have had to start with more energy in the reservoir (dotted line beginning at point B). If the reservoir of a particular type of storage unit is small enough to justify full charge and discharge of the unit each day, the amount of energy that can be delivered becomes a simple function of the reservoir capacity. However, if there is either an increase in the amount of energy to be delivered or a decrease in the amount of high cost energy to be displaced, the less efficient machines will have to be larger, possibly large enough to operate over the weekly cycle and then the required storage capacity would be an extremely sensitive function of cycle efficiency.

In this study, the economics of various storage systems are compared; each system is sized so that it delivers the same amount of energy to the load under simulated utility operations. The major difference between the present study and previous comparative analyses of storage systems is that previous studies assume that the amount of energy delivered from storage depends only on the size of the storage reservoir and not on cycle efficiency. For example, Public Service Electric & Gas** (PSE&G) assumed that all storage systems sized to be capable of producing power at full power capacity for two hours without recharging would deliver energy to the load equivalent to discharging at full capacity for 400 hours a year. Similarly, if a unit was sized to be able to produce power for five hours without interruption, it would deliver energy equivalent to operating the unit at full capacity for 1,000 hours per year.

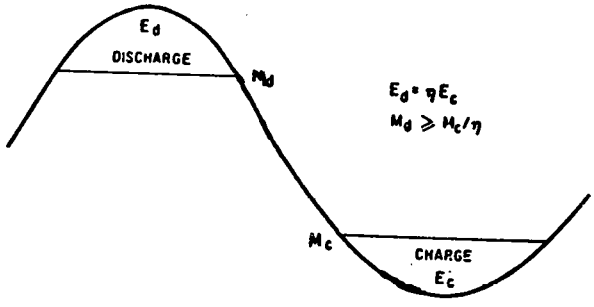

Figure 4. Constraints on the Economic Use of Storage

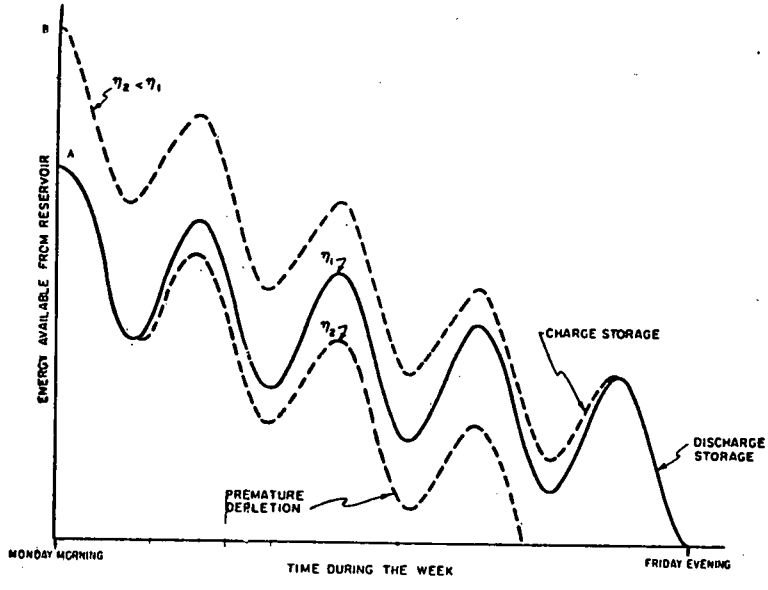

Figure 5. Energy in Reservoir as a Function of Time During the Week for Two Storage Systems with Different Cycle Efficiencies - Equal Energy to the Load

*The cost of operating the SMES refrigeration is a constant, not a variable or deferrable cost.

**"An Assessment of Energy Storage Systems Suitable for Use by Electric Utilities", PSE&G, EPRI EM-264, ERDA E(11-1)2501, July 1976.

The present study does not accept the previous assumptions, but extends the analysis to the next level of complexity. Using a model utility and a model load, we first calculate the capacity of storage generators required to deliver specific amounts of energy to the load as a function of the cycle efficiency of the storage system. The economic comparisons between different types of storage and conventional generators are then performed for these appropriately (not equally) sized units and, thus, makes the correct allowance for storage efficiency.

While the storage cycle efficiency, the ratio of the amount of energy available from the storage reservoir to the amount of energy delivered to the storage reservoir, is an important determinant of system usefulness, it is neither the only efficiency associated with storage nor need it be the only determinant of the "value" of the stored energy for a specific utility. This distinction is important for two of the candidate storage systems - Superconducting Magnetic Energy Storage and Compressed Air Energy Storage (CAES). The former requires electrical energy in order to maintain its low temperature but this is unrelated to the decision to operate, and the latter requires the use of costly fuel in order to discharge; neither of these requirements is reflected in the cycle efficiency. The cost of the fuel required to discharge CAES needs to be considered when calculating the marginal "cost" and "value" of the stored energy.

SIMULATION OF UTILITY OPERATIONS

In this study we used simplified models of the utility load and generation costs in order to obtain an estimate of the energy economically available from a specific storage unit. The following assumptions were made:

A) Assumptions Concerning Power Demand

- The fractional variation of power demand with time would not change with the years, i.e., the shape of the load curve is constant from year to year.
- The ratio of storage capacity to the model utility's yearly peak demand would not change. (This would be the case if there were no growth in power demand or if sufficient storage generation capacity were added each year to keep pace with power demand growth.)

B) Assumptions Concerning the Economics of Conventional Generation

- The operating costs of all conventional generators will increase at the same exponential rate.
- Additions of generating capacity would maintain the assumed dependence of incremental operating costs on power delivered.
- Units are removed for scheduled maintenance so as to leave unchanged the dependence of the incremental cost of energy from conventional generators on the power delivered, expressed as a percent of seasonal peak demand.

The composite result of these assumptions is that a simulation of utility operations for one year is equally valid for all years within the planning horizon. In these calculations it was assumed that the utility generation mix contained a storage system with a power capacity of 500 MW_e (6.25% of the yearly peak demand.* Using these assumptions the amount of energy that can be economically delivered to the load from a storage system with a given size of reservoir and input/output efficiency can be calculated. These values can be manipulated and plotted to yield Figure 6, a plot of the storage reservoir capacity (in units of hours of storage capacity) required for the delivery of specific amounts of energy each year plotted against the cycle efficiency. The curves in

*For a complete description of the assumed electric utility load and costs, see "An Evaluation of Superconducting Magnetic Energy Storage - Draft Final Report", ADL, July 1, 1979.

Figure 6 have a number of interesting characteristics. These characteristics, their origins and implications are pointed out in the following paragraphs.

A maximum useful reservoir capacity will exist for every type of storage system. The maximum useful reservoir capacity for any type of storage system is a function of the cycle efficiency. The higher the efficiency of the storage unit, the greater the amount of storage capacity that can be economically used. As the efficiency increases, the amount of energy that can be economically diverted to storage increases and, consequently, the greater the amount of energy that can be delivered.

There is a value of efficiency for which the maximum useful reservoir capacity is identically zero. It is defined as the minimum marginal cost of off-peak energy (10 mills for the sample utility) divided by the maximum marginal cost of the peaking energy (30 mills for the sample utility), both from the conventional generators. Thus, for the sample utility, storage systems with cycle efficiencies less than 33% would have a maximum useful reservoir size identically equal to zero. This implies that no matter what its size, it would never be economically desirable to operate a unit with this efficiency.

Storage systems with very small reservoir capacities are emptied and refilled each day. For these units, the marginal value of stored energy need only be greater than its marginal cost; thus, the amount of energy delivered during the week is only a function of the size of the reservoir and is insensitive to the magnitude of the efficiency (the flat portions of contours in Figure 6 are for daily cycling). If the efficiency is low enough so that, for fixed values of marginal value and delivered energy, the marginal costs and values are equal, the system must operate over the weekly cycle; the size of the required storage reservoir must rise in order to allow this. Once the weekly cycle, rather than the daily charge/recharge cycle, is required in order to deliver the specified amount of energy, the situation corresponds to that illustrated in Figure 5 and the required size of the reservoir becomes very sensitive to the value of the cycle efficiency.

The Compressed Air Energy Storage (CAES) system requires the burning of fuel to discharge the reservoir and thus does not have a well defined cycle efficiency. The size of the reservoirs required to deliver the specified amounts of energy to the load were calculated for the postulated system energy requirements; the results are plotted as x's in Figure 6.

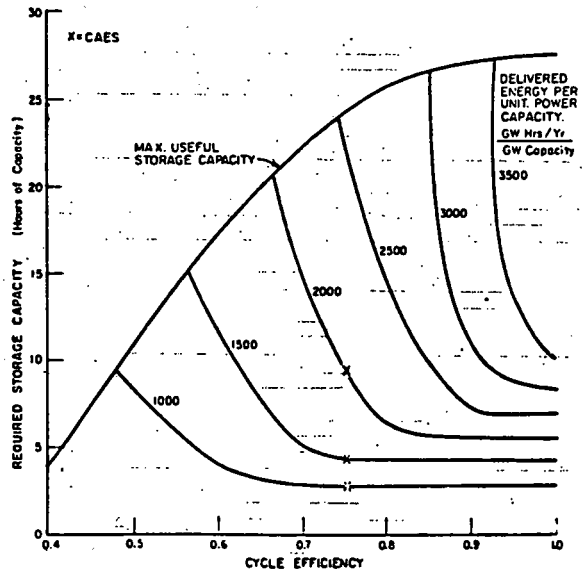

Figure 6. Required Storage Capacity as a Function of Cycle Efficiency for Assumed Values of Delivered Energy -- $P_d(max) = .0625 \times L(max)$

No matter how large the storage reservoir, for any given utility there is a maximum amount of energy that can be delivered economically from a storage generator having a specific cycle efficiency. For the utility modeled here, a storage generator with cycle efficiency of .8 and maximum power rating of 500 MW_e cannot economically deliver more than 1300 GW-hrs per year; it would be cheaper to use conventional generation capacity to meet a greater need.

The storage reservoir capacity needed to allow a storage system with a certain efficiency, to deliver a specific amount of energy each year to the load is obtained from Figure 6 and listed in Table 1 for the different types of storage. Using the storage system costs given in Table 2, the range of total capital costs for each type of unit was calculated. The "present worth of all future revenue requirements" (pwafrr) for each type of plant operating in the expected manner were calculated using specific financial assumptions.*

The assumption was made that the cost of off-peak energy is the same for all candidate storage systems. The assumption is very close to being strictly true if all storage systems are operating on a daily cycle; the amount of off-peak energy required is very small and its cost varies very slowly with variations in the amount required (the amount required is inversely proportional to the cycle efficiency). When comparing one storage system operating over a daily cycle with another operating over a weekly cycle, the situation becomes more complex; the energy used to partially recharge the reservoir during weeknights has a higher cost than the energy used to completely recharge this same unit during the weekend. Calculations of the weighted average of the marginal costs of off-peak energy for a number of circumstances indicates that they are all within 1 mill/kWh of the assumed 15 mills/kWh. The weighted cost of the off-peak energy for the more efficient equipment (e.g., the SMES) sized to operate over a daily cycle, is less. Ignoring this difference introduces a slight bias against the more efficient equipment.

A second assumption was that the type of generation capacity displaced by storage depends only on the amount of energy delivered from storage; this assumption acknowledges those provisions of the Industrial and Utility Fuel Use Act of 1978 which do not allow the construction of oil-fired generators expected to operate more than 1500 hours per year. Thus, the type of facility being displaced and its value can be assumed to depend only on the amount of energy delivered by the storage unit.

The "pwafrr" for each type of storage system was divided by the total energy delivered during the life of the plant and subtracted from the appropriate levelized life cycle costs for conventional generators performing the same service. The results are presented in Figure 7. The empty boxes are the values for these storage systems if their cycle efficiencies are at the high end of the ranges** indicated in Table 1; the shaded boxes are the results if the lower efficiency had been used. The width of the boxes reflects the uncertainties in the capital costs of the various units (Table 2).

Figure 7 indicates that if the SMES system can be constructed for the estimated costs and if the SMES system cycle efficiency is above 90%, it will be able to compete economically both with conventional generation capacity and with the other candidate storage systems. That it can compete when the reservoirs are small and the amount of energy delivery each year is low is not surprising; several previous studies have shown this to be true. The prediction that the SMES can compete for high energy delivery rates is a new result; its competitive edge derives from the fact that the other storage systems require a weekly cycle and a large reservoir to perform a task while the SMES system can perform the same task using a series of daily cycles and a small reservoir.

---

*For a detailed listing of the financial assumptions, see "An Evaluation of Superconducting Magnetic Energy Storage - Draft Final Report", ADL, July 1, 1979.

**For CAES, the empty box represents the situation where extra fuel is required to discharge the reservoir and the shaded box represents the situation where no fuel is required and the cycle efficiency is 70%.

Table 1. Required Storage Reservoir Size Storage Generation Equals 6.25% of Maximum Load

Storage Type	Efficiency	Energy Delivered Per Year (kWh per kW cap.)	Required Storage Cap. (kWh cap. per kW cap.)
Underground Pumped Hydrostorage	.67 - .72	1000	3
		1500	4.5 - 7.5
		2000	9.5 - 20
Compressed Air Energy Storage	.7 - (A)	1000	3
		1500	4.5 - 5
		2000	9.5 - 14.5
Batteries	.75 - .8	1000	3
		1500	4.5
		2000	6.5 - 9.5
		2500	14.5 - 22
Superconducting Magnetic Energy Storage	.93 - .97	1000	3
		1500	4.5
		2000	5.5
		2500	7
		3000	8.5 - 9.5
		3500	11.5 - 17

(A) Every kilowatt-hour removed from storage requires .742 kWh of electrical energy to be placed into storage plus the combustion of 3980 Btu's of fuel.

Table 2. Assumed Costs of Storage Alternatives

Storage Type	C_p $/kW	C_s $/kW	Fixed[1] Charge Rate	O&M[1]
UPH	115-150[2]	12-16[2]	.21	$1.6/kW/yr
CAES	215-305[2]	2-5[2]	.18	$5.3 mills/kWh
P_b/H+ Batt.	60-90[2]	50-70[2]	.21	$2.7 mills/kWh
Adv./Batt.	60-90[2]	20-40[2]	.18	$2.7 mills/kWh
SMES	60-80[3]	36-124[4]	.22	$3.2/kW/yr[5]

1. Source: Public Service Electric and Gas Co., "An Assessment of Energy Storage Systems Suitable for Use by Electric Utilities", EPRI EM-264 and ERDA E(11-1)-2501, July 1976.
2. Source: The Aerospace Corporation, "Characterization and Applications Analysis of Energy Storage Systems", Aerospace Report No. ATR-77(7538-1), December 1977.
3. Source: General Electric, "Design Study - Thyristor Converter Stations for Use with Superconducting Magnetic Energy Storage Systems", Order No. L68-27996-1, Nov. 1978.
4. Source: Costs used included economies of scale and are indicated in Figure 3.
5. Source: $3.2 kW/yr plus the cost of energy used to run the vacuum and refrigeration equipment. The latter is assumed to be 2¢/kWh and to increase at the rate of 8% per year. The fixed O&M cost is twice the O&M cost assumed by PSE&G. Both figures are relatively arbitrary; we are slightly more pessimistic than was PSE&G.

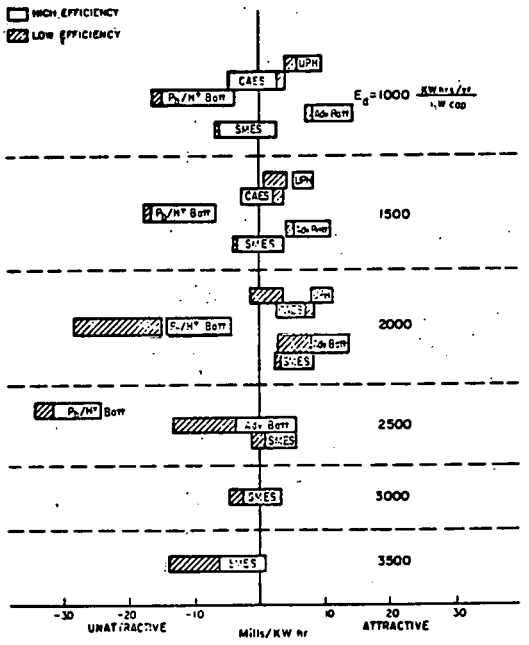

Figure 7. Levelized Life Cycle Cost Difference Between Storage and Conventional Generation

FUTURE R&D REQUIREMENTS

Any future work to develop a large capacity SMES for utility load leveling service should logically contain the following four elements.

1. Development of a baseline system design to meet utility operating requirements and specified objectives for constructability, maintainability and system protection.

2. Experimental and analytical research in key areas to achieve the objectives of the baseline system at reasonably predictable costs.

3. Revision of the baseline design in light of the research results.

4. If the revised baseline design appears to meet cost contraints, the construction, test and operation of a small demonstration unit.

The first two elements should be done at the same time and in close collaboration, the results of each acting as a guide for the other.

THIS PAGE

WAS INTENTIONALLY

LEFT BLANK

PROJECT SUMMARY

Project Title:	"Force Balanced Magnetic Energy Storage Coil"
Principal Investigator:	O.K. Mawardi
Organization:	Case Western Reserve University University Circle Cleveland, Ohio 44106
Project Goals:	A preliminary feasibility study has been completed to determine the economics of a novel design of a superconductivity coil to be used for magnetic energy storage. The Force Compensated coil is made up of two coil systems with a mechanical structure tying them together and subject to opposing forces generated by the two coils. Since the structure is self-contained within its cryostat, it is possible to exceed the fundamental material limitation on inductor size. Furthermore, the structure can be made considerably smaller than that needed for conventional coils. The economies of this system is shown to be capable of achieving savings of upwards of 40% when compared to a conventional system.
Contract Number:	LASL - 1996H
Contract Period:	FY'78
Funding Level:	$40K
Funding Source:	U.S. Department of Energy, Division of Energy Storage Systems through the Los Alamos Scientific Laboratory

A FORCE BALANCED MAGNETIC ENERGY STORAGE SYSTEM

O. K. Mawardi, H. Nara and M. Grabnic
Case Western Reserve University
Cleveland, Ohio 44106

ABSTRACT

A novel scheme of constructing coils suited for inductive storage system is described. By means of a force-compensating method, the reinforcement structure can be made considerably smaller than that needed for conventional coils. The economics of this system is shown to be capable of achieving savings of upwards of 40% when compared to a conventional system.

INTRODUCTION

The use of energy storate systems is recognized, nowadays, as an accepted procedure for the load levelling of an electric power generating network.[1] One specific scheme of energy storage, viz., the superconducting magnetic energy storage systems (SMES) has attracted a great deal of attention.[2] This is because SMES offer some very desirable operational features from the point of view of siting advantages, minimal environmental impact, rapid dynamic response and high efficiency of performance.

The earlier studies on SMES concentrated on inductors of conventional shapes.[3] Although several magnetic and support structure configurations were considered with a view towards minimizing costs, it became apparent that for the energy storage capacities of interest to the utilities (i.e., in the range 10 to 10,000 Mwh) the cost of the support structure for the magnet exceeded by far the cost of the cryogenics as well as that of the superconductors.

In order to sustain the very large mechanical forces between the conductors it was proposed [4] to use bedrock for the former of the magnets. The resulting increased cost of this method of construction places SMES at an economic disadvantage by comparison to other energy storage systems, hydroelectric for instance.[5]

Recently, a novel scheme for an economically acceptable magnet support structure was suggested.[6] Preliminary calculations indicated that with this scheme the cost of the structure could be reduced by a substantial fraction. In this paper more precise estimates for the cost of the structure have been obtained. These estimates were derived on the basis of a preliminary feasibility study which is described here.

UNDERLYING CONCEPT OF NEW SCHEME

The concept of a force-free coil is not new. Fermi and Chandrasekhar[7] in particular have speculated on the configuration of current carrying plasmas in which the currents and their induced magnetic fields are everywhere parallel. This idea was later extended to coil design. The configuration of a force-free coil is inferred from the solution of the equation

$$\underline{J} \times \underline{B} = 0 \qquad (1)$$

One special solution of Eq. (1) is a helical conductor of infinite length and wound with a pitch of 45° on a cylindrical former (Fig. 1a). The combination of several helical conductors all wound with the same pitch and on the same cylindrical former is also force-free. It is noticed that all these coils are equivalent to a current in the axial direction and another current in the azimuthal direction.

Suppose that one constructs an array of two sets of conductors. The first consists of axial conductors placed on a cylindrical former, while the second set consists of circular coils wound on the same cylindrical former but nested inside it (Fig. 1b). If the surface current densities for the two sets of conductors are equal, then the combination of the two coils is force-free. In this manner the single force-free coil has been transformed in two coils which are force-compensated.

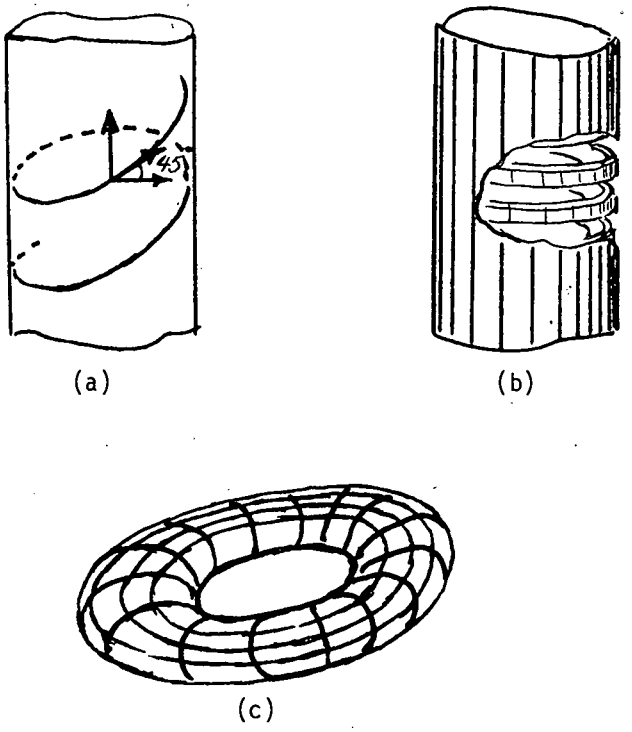

Fig. 1(a). Helical force-free coil wound with a pitch of 45° on a cylindrical former; Fig. 1(b) Force-compensated coils consisting of azimuthal and axial conductors; Fig. 1(c) Force compensated coils of toroidal shape.

Whereas coils of infinite length are truly force-compensated, coils of finite length are not because of the fringing of the magnetic field at the ends. To obtain a physically realizable force-compensated system of finite dimensions, the infinitely long cylinder is transformed into a torus. It can be shown, that the transformation required to preserve Eq. (1) will lead to a torus with a cross section as shown in Fig. (1c). By inspection of Fig. (1c) it appears that indeed the forces from the two sets of coils (poloidal and toroidal) do oppose and compensate each other. The details of a formal proof has been published elsewhere.[8]

DESIGN FEATURES OF THE SYSTEM

The feasibility study reported here was performed for a SMES of 10 Mwh capacity and for which the maximum magnetic field was 5 teslas. Since, half of the energy is stored inside the torus (i.e., contributed by the poloidal coils) while the other half contributed by the toroidal coils is ouside the torus, one readily finds that the mean major radius required is 20 m. The accurate shape and dimensions for the poloidal coils are shown in Figure 2. The

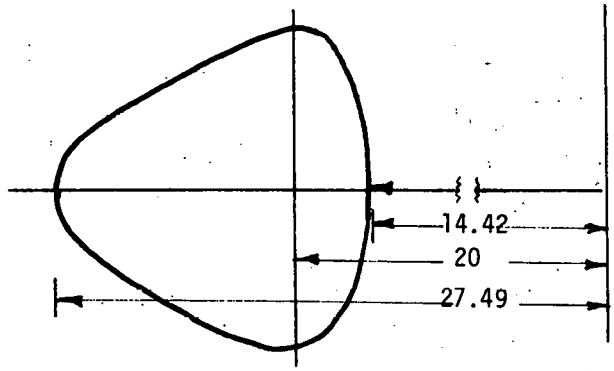

Fig. 2 Shape of poloidal coils and critical dimensions.

profile of the cross section is given in parametric form by the cartesian coordinates (see Ref. 8)

$$x = \exp\,(60.99 - 6.6\cos\phi)/20.36) \tag{2}$$

$$y = 6.6 \sin \phi \tag{3}$$

where ϕ varies between 0 and 2π.

a) DESIGN OF POLOIDAL COILS

Having defined the dimensions of the poloidal coils one needs to determine the cross section of the conductors, as well as the number of poloidal coils to store the stated energy. It is convenient to design the coils such that one layer of conductors will be sufficient to produce the required magnetic field of 5 T. It can be shown that if one defines the conductor size by a x b where a is the thickness of the conductor and b its width then one can show that the number of turns N satisfies the equations

$$N = \frac{2\pi\ \mu_o\ R_{min}}{B_{max}}\ \frac{b}{a}\ q^2 J \tag{4}$$

and

$$N = 2\pi\ R_{min}\ q/a \tag{5}$$

In the above R_{min} = 16.53 m, B_{max} = 5 T, $\mu_o = 3\pi \times 10^{-7}$, q is the space factor for winding and taken as 90%; and J the allowed current density is 3000 amps/cm^2. The total current on the other hand is found from

$$I = \frac{4.16 \times 10^8}{N} \qquad (6)$$

If we set $I = 10^5$ amps, it follows that N = 4160 turns, a = 2.28 cm and b = 14.6 cms. The conductors are proposed to be constructed of individually insulated subconductors each of whick is separately cryostable when carrying a fraction of the total current.

b) DESIGN OF TOROIDAL COILS

When the number of discrete toroidal coils is selected, the number of turns for toroidal coil is fixed from the force-compensation requirement. A more stringent criterion, however, is found from stress considerations. Each of the poloidal coils is approximated to a beam subjected to a number of concentrated forces located at the contact "points" with the toroidal coils. A structural matrix analysis program was developed and the cases of 10, 20, 40 and 60 toroidal coils were investigated. On the basis of the stresses found in the poloidal coils it was decided that at least 60 toroidal coils are needed for a safe design.

Having decided on the number of toroidals there remains to be determined the turns per coil as well as the cross section of the toroidal coils. The distribution of the number of turns follows at once from the force compensation criterion. The cross section of the conductors on the other hand has to satisfy the stability requirement, viz., that any one coil will not collapse should it quench and hence carry no force compensating current.

It is known from the theory of elasticity[9] that a circular ring subjected to a uniform force on its rim will collapse if the pressure exceeds a critical value that varies inversely with the cube of the radius. Using this criterion one obtains the following minimum sizes for the toroidal coils.

Coil position	Radius (m)	No. of turns	Conductor Dimensions (cms)
1	14.42	24	2.26 x 14.6
5	14.94	24	2.28 x 14.6
10	17.24	20	2.28 x 17.52
15	20.00	20	2.28 x 17.52
20	23.21	20	2.28 x 17.52
25	26.07	18	3.04 x 14.6
30	27.49	18	3.04 x 14.6

STRUCTURAL STABILITY OF THE SMES

In the previous section, the number and cross sections of the toroidal coils were selected to satisfy the criteria for static stability. Since the critical force for the collapse of a ring varies inversely with the cube of the radius it is obvious that the poloidal coils constructed with conductors of comparable cross sections would satisfy the stability criterion if the toroidal coils do. Indeed, this was found to be the case.

What remains to be checked is whether the SMES is statically stable under its own dead weight and when no current circulates in the coils. In addition one must determine the effects of the thermal stresses on the SMES.

Numerical computations were made with a coded program referred to as STRESS for the statics of the poloidal coil under a variety of constraints. The effect of the toroidal coils on the poloidal coils was represented by 60 springs as shown in Fig. 3. It was observed that use of "roller" supports on all four anchoring locations of the perimeter of the poloidal coils allows the maximum release of the thermal stresses. It was also observed that the conductors provide adequate stiffness to have the structure maintain its shape under its dead weight.

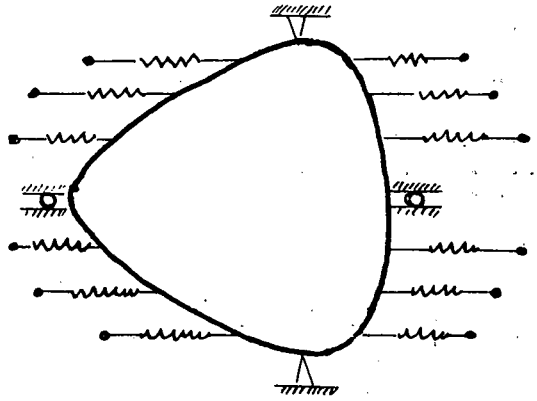

Fig. 3. Effective schematic representation of constraint and boundary conditions on poloidal coils.

The manner in which the "roller" supports are constructed in practice is shown in Fig. 4.

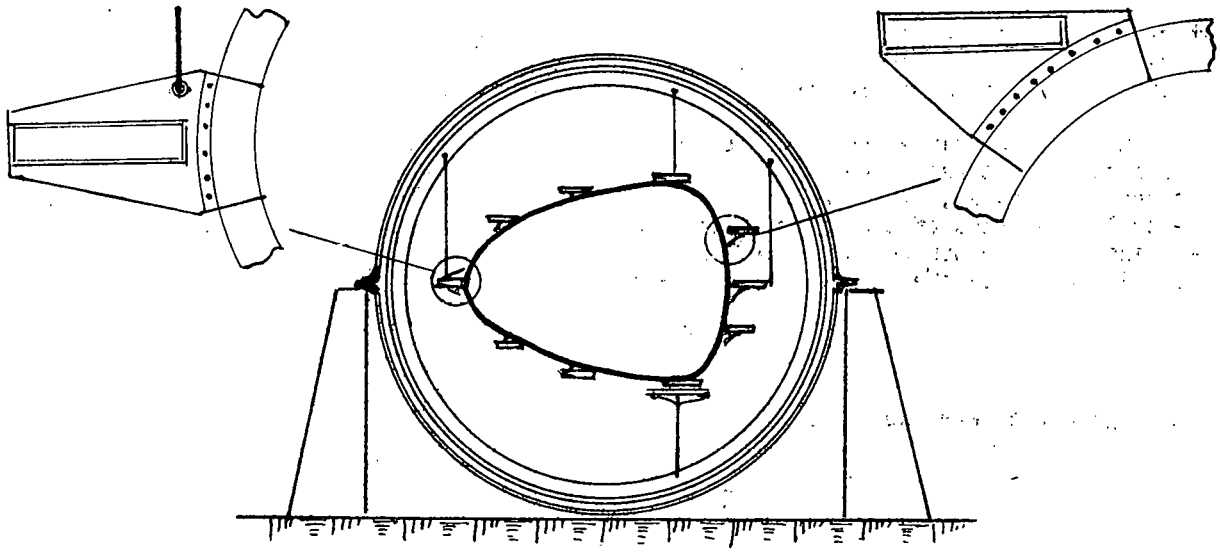

Fig. 4. Details for the support of the SMES in the vacuum chamber.

CAPITAL COST OF FORCE-COMPENSATED SMES

The items which significantly contribute to the cost of the system are

a) superconductors
b) reinforcement structure
c) dewar
d) refrigeration
e) interface to the power system.

Hassenzahl et al., have already carried out the economics for a toroidal SMES.[10] A large fraction of their calculations can be adapted to the present case after important modifications are introduced as explained below.

a) SUPERCONDUCTORS

It is well known to magnet designers that cylindrical coils satisfying the Brooks criteria[11] have the optimum design from the point of view of cost of conductor per unit of magnetic energy stored. It turns out that coils wound on a torus in the poloidal direction would use almost twice as much conductors as a Brooks coil storing the same magnetic energy.

In our case, the SMES stores half the energy in poloidal coils and the other half in toroidal coils. The winding factor for the toroidal coils is only slightly less than that of the Brooks coil.[12] Consequently, our system would use approximately 1.5 times the amount of conductors needed in a Brooks coil and not twice. The conductors needed hence cost 1.5/2.0 = 75% of that of a conventional toroidal system.

b) REINFORCEMENT STRUCTURE

In all previous SMES considered, the magnetic forces were contained through structures extraneous to the coils. An estimate of the mass of reinforcement structure needed can be obtained by means of the theorem of the virial which leads to the expression

$$M_s = \kappa \frac{E \rho_s}{\sigma_w} \tag{7}$$

where κ is a dimensionless constant relating to the efficiency of the use of support structures, $\kappa \geq 1$, ρ_s is the density of the support material, σ_w is the working stress in the material, E is the magnetic energy stored and M_s is the mass of the support.

In our case, since the magnetic forces are compensated by the coils themselves, no extraneous structures, other than the connecting straps described in the previous section, are needed. Indeed, it is easy to check that when the criterion of Eq. (7) is applied to the coils, the mass of conductors alone is more than adequate to sustain the stresses. Defining a mean minor radius r and mean major radius R for the torus, and a mean magnetic field intensity in the torus the right hand side of (7) is

$$\kappa((2\pi R \times \pi r^2) \frac{B^2}{2\mu_o}) \frac{\rho_s}{\sigma_w} \tag{8}$$

Rearranging the terms we can write the above

$$\kappa(2\pi R \times 2\pi r\, ab\, \rho_s) \frac{B^2}{2\mu_o \sigma_w} \frac{r}{a\alpha b} \tag{9}$$

b is the width of the conductors as defined in section III, and α the space factor for the winding. We now notice that the quantity between parenthesis is the mass of the poloidal coils.

Now for fields of the order of 5 teslas, r is approximately 6m, b is 14.60 cm., α = 90%, and σ_w is 30,000 lbs/in^2. Introducing all these quantities in (9) and using κ = 1.1, i.e., assuming a 10% factor of safety it appears that 92% of the mass of the conductors would have been sufficient to accomodate the internal stresses. When the connecting straps estimated to be 10% of the mass of the conductors are added to the conductors, we secure a margin of safety of 20%.

The actual cost of the structure is hence taken to be 10% of the cost of the conductors.

c) DEWAR

The cost of the Dewars used in conventional SMES is high because of the reinforcement needed when warm reinforcement is used. Cold reinforcement leads to considerably lesser amounts. The lowest costs quoted in Hassenzahl's report are for forced helium flow in hollow conductors and for cold reinforcement.

In our case, since the structure is freely suspended and does not need extraneous reinforcement, we will assume the cost of 1750 \$/m^2 for the dewar as though it used forced flow since the cryogenic installation for our system is simple.

The summary of the cost are given below. All costs are 1975 prices. We have extrapolated our costs to the larger rating of 3.9 x 10^7 MJ. Our system is compared to that of two conventional SMES of toroidal geometry with warm and cold reinforcement structure respectively. The numbers are taken from Hassenzahl, et al. (Ref. 10).

TABLE I

	Conventional		
	Warm Reinforcement	Cold Reinforcement	Force Compensated
Energy Stored (MJ)	3.9 x 10^7	3.9 x 10^7	3.9 x 10^7
Superconductor Cost	342	222	166
Dewar Cost	340	300	300*
Structure Cost	228	1,014	25
Mining Cost	105	-	-
ac-dc Convertor	54	54	54
Misc. Costs	51	51	51
Total (x 10^{6}s)	1,120	1,641	595

* It is believed that the cost of the dewar is overestimated as it included a certain amount of reinforcement which is not needed.

CONCLUSION

The simplicity of construction of the force-compensated coil is reflected in the substantial reduction in the cost of the system. In addition, to the several advantages already mentioned in the introduction, the new system has the convenient feature of easy accessibility since the whole system is at ground surface.

ACKNOWLEDGEMENT

This work was supported in part by the Energy Storage Division, Department of Energy, through the Los Alamos Scientific Laboratory.

REFERENCES

1. G. D. Friedlander, IEEE Spectrum 1, 58, (1964); Wisconsin Superconductive Energy Storage Project (1974).

2. W. V. Hassenzahl et al., "The Economics of Superconducting Magnetic Energy Storage Systems for Load Levelling", LA-5377-MS, Los Alamos Scientific Laboratory, New Mexico, (1973).

3. M. S. Lubell, et al., "The Economics of Large Superconducting Toroidal Magnets for Fusion Reactors", Oak Ridge National Laboratory Report ORNL-TM-3927.

4. J. R. Powell et al., "Warm Reinforcement and Cold Reinforcement Magnet Systems for Tokomak Rusion Reactors: A Comparison", Brookhaven National Laboratory BNL-17434 (1972).

5. R. A. Huse et al., "International Conference on Large High Voltage Systems", 31-07 (1976).

6. O. K. Mawardi, "Design of a Force-Free Inductive Storage Coil", Los Alamos Scientific Laboratory LA-5953-MS (1976).

7. E. Fermi and S. Chandrasekhar, Astrophys. J. 118, 116, (1953).

8. O. K. Mawardi, "Force Compensated Magnetic Energy Storage Systems". Report submitted to Energy Storage Division, Department of Energy (1979). Also publication in press.

9. A. E. Love, "Treatise on the Mathematical Theory of Elasticity" (Dover Publications, NY) p 424.

10. See Ref. 2.

11. F. W. Grover, "Formulas for Mutual and Self Inductance", Bulletin of the Bureau of Standards 8, 1 (1912), p 112.

12. See Ref. 6.

THIS PAGE

WAS INTENTIONALLY

LEFT BLANK

PROJECT SUMMARY

Project Title:	Energy Storage in Superconductive Magnets: A demonstration
Principal Investigator:	Carl H. Rosner
Organization:	Intermagnetics General Corporation P.O. Box 566, New Karner Rd Guilderland, NY 12084
Project Goals:	To provide a ready-visual understanding of superconductive magnetic energy storage (SMES) and its potential.
Project Status:	To demonstrate the interest, versatility and reliability of electro-magnetic energy storage systems, a model demonstration system was designed and built by Intermagnetics (IGC) to the specifications of Los Alamos Scientific Laboratory. The system consists basically of a small 50K gauss superconductive magnet with an associated cryostat, a charging power supply and an energy conversion circuit. On-going studies at the University of Wisconsin, Los Alamos National Laboratory and elsewhere are becoming increasingly more optimistic in their assessments of the advantages of using SMES systems. The electric energy stored in the magnet virtually without loss until needed, operates a 50 W light bulb, a spark discharge system or a tape recorder. Provision has been made to connect any one of these items, all of them simultaneously or any other suitable appliance requiring a 12 V or 110 volt power source. This system has already been operated for many cycles and has a virtually unlimited and undiminished cycling capability. The drawback is, of course, the requirement for continuous cooling. There appear to be no insurmountable problem that would prevent the ready scale-up of this system by factors of 10 to 10,000 times the level of energy stored in this system. The engineering and economic challenges are being addressed in the aforementioned studies. To confirm the utility of SMES it is expected that systems storing 10-1000 Mj will be constructed within the next 3-5 years. In addition, the ongoing developments of even larger superconductive magnets, superconductive motors and generators, etc. will allow a more realistic assessment of the practical and economical potential of SMES systems during the same time-frame.
Contract Number:	4-L69-2475L-1
Contract Period:	July-August 1979
Funding Level:	$24.9K plus Intermagnetics Corporate Support
Funding Source:	U.S. Department of Energy, Division of Energy Storage Systems

ENERGY STORAGE IN SUPERCONDUCTIVE MAGNETS: A DEMONSTRATION

Carl H. Rosner
Intermagnetics General Corporation
P.O. Box 566, New Karner Road
Guilderland, NY 12084

ABSTRACT

The possible utilization of superconductive magnets as efficient energy storage systems has been proposed and explored a number of times during the past 15 years. In order to clearly demonstrate the salient features of such a system, an operational model was constructed. Using a superconductive magnet having a stored energy capability of 20,000 joules, the system includes a cryostat as well as charging and discharge equipment. The energy can be discharged in a 50 w light bulb, a spark-gap, a tape-recorder, or any appliance that can operate at 12 or 110 volts.

INTRODUCTION

In its simplest form, an electro-magnet can be considered to be an "all electric battery," where electric energy is stored in the form of magnetic flux, maintained by a continuously circulating electric current. Such magnets in the form of inductors have been useful in electro-technology ever since the discovery of electricity. Using conventional copper wire has involved the acceptance of associated power losses.

Since the early 1960's the use of superconductive magnets as more efficient energy storage medium has repeatedly been advocated and explored. In addition the inherent energy conservation potential of superconductive technology has wide-ranging application possibilities in the electric power industry as well as for signal/computing devices. The principal approaches to energy storage in electrical systems are shown in Fig. 1.

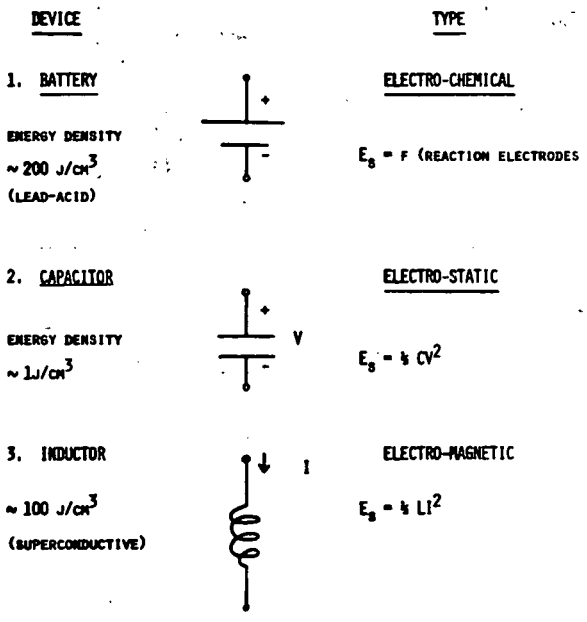

Fig. 1. Approaches to Energy Storage in Electrical Systems.

Their relative merits are indicated by comparing the energy density in joules per cubic centimeters. The ready availability of superconductors presents an opportunity that is addressed in this article.

SUPERCONDUCTIVE ENERGY STORAGE

Electro-magnetic energy storage systems (EM-ESS) utilizing superconductors would require large and ideally loss-less inductances. Progress made in the understanding of design and fabrication problems associated with ever-larger superconducting magnets is directly applicable to the development of EM-ESS systems. Many of the earlier studies have concluded that technical complexities and resultant high first costs would seemingly rule out EM-ESS systems for practical application. However, recent technical developments, as well as dramatic price increases in oil supplies and realization of its finite availability, has rekindled strong interests in more closely examining the real merits of EM-ESS.

To demonstrate the interest versatility and reliability of EM-ESS, a model demonstration system was designed and built by Intermagnetics (IGC). The system consists basically of a small 50 k gauss superconductive magnet with an associated cryostat, a charging power supply and an energy conversion circuit. The system components are shown in Fig. 2.

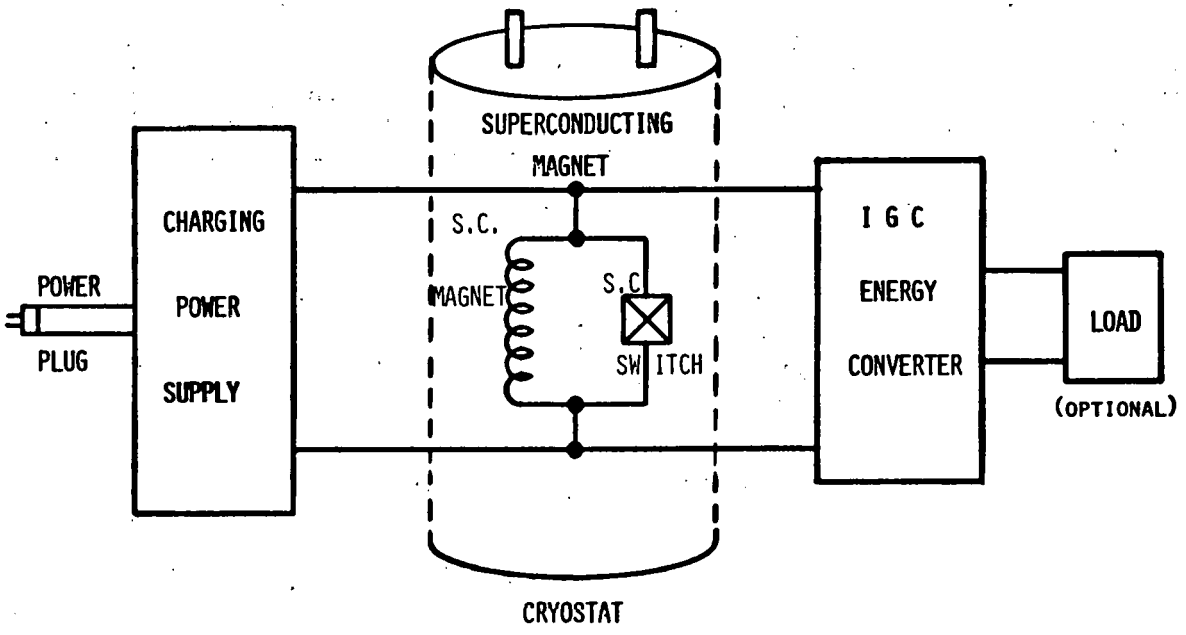

Fig. 2. Intermagnetics S.C. Energy Storage System.

In view of the fact that the demonstration magnet only stores about 20,000 joules and that none of the components were specially designed for EM-ESS applications, no claims as to economic or small size accomplishments can be made here. Nevertheless, if one examines the list of advantages and disadvantages shown in Fig. 3, a meaningful set of possibilities emerges that invites closer scrutiny.

ADVANTAGES	AND	DISADVANTAGES
TECHNICALLY PROVEN		EXPENSIVE AT LOW POWER LEVELS
READILY SCALABLE FROM KW TO 10,000 MW RANGE		REQUIRES CONTINUOUS CRYOGENIC REFRIGERATION
UNLIMITED NUMBER OF CHARGE/ DISCHARGE CYCLES		REQUIRES SHIELDING OF STRAY-MAGNETIC FIELDS
HIGHLY EFFICIENT		REQUIRES MECHANICAL SUPPORT STRUCTURES FOR CONTAINMENT OF MAGNETIC FORCES
NO MOVING PARTS		REQUIRES ELECTRICAL CONVERSION EQUIPMENT
ALL ELECTRIC INPUT/OUTPUT		SYSTEM COMPLEXITY MAY LIMIT USEFULNESS TO SPECIAL PURPOSE APPLICATIONS
ENVIRONMENTALLY ATTRACTIVE		RELATIVELY HIGH FIRST COST
CAN BE LOCATED ALMOST ANYWHERE		
EASE OF MAINTENANCE		
LOW OPERATING COST		
VARIABLE DUTY CYCLE		
POSSIBLE TO CHARGE AND DISCHARGE FROM 1 TO 1,000 HOURS		
COMPARABLE TO HYDRO-ELECTRIC POWER STORAGE		

Fig. 3. Energy Storage in Superconductive Magnets: Advantages and Disadvantages.

In particular, on-going studies at the University of Wisconsin, Los Alamos National Laboratory and elsewhere are becoming increasingly more optimistic in their assessments.

The demonstration system shown here contains all the features and requirements of almost any EM-ESS systems. Its operation Fig. 4. is quite straight forward.

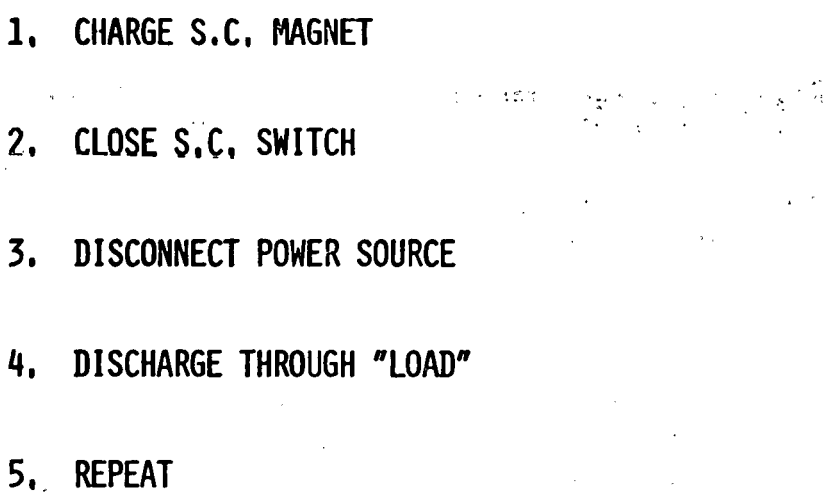

Fig. 4. Superconductive Magnetic Energy Storage: Principle of Operation.

A power supply converts a-c power from the power line outlet into a d-c current used to charge the superconductive magnet. When the magnet is fully charged, it can be "short-circuited" with a superconducting switch, whereupon the power line source can be disconnected. As long as the system remains cold, the energy in the EM-ESS system is virtually loss-less.

When it is desired to extract the energy from the superconductive magnet, the "load" is connected across the magnet and the superconductive switch is opened. Electric current now flows through the "load." In the demonstration system, we have provided for this load to be either a 50 w light bulb, a spark discharge system or a tape recorder. Provision has been made to connect any one of these items, all of them simultaneously or any other suitable appliance requiring a 12 V or 110 volt power source.

The system has already been operated for many cycles and has a virtually unlimited and undiminished cycling capability. The major drawback is, of course, the requirement for continuous cooling.

There appears to be no insurmountable problems that would prevent the ready scale-up of this system by factors of 10 to 10,000 times the level of energy stored in this system. The engineering and economic challenges are being addressed in the aforementioned studies. To confirmthe utility of EM-ESS it is expected that systems storing 10-1000 Mj will be constructed within the next 3-5 years.

In addition, the ongoing developments of every larger superconductive magnets, superconductive motors and generators, etc. will allow a more realistic assessment of the practical and economic potential of EM-ESS systems during the same time-frame.

ACKNOWLEDGEMENT

The fabrication of the superconductive energy storage demonstration system was sponsored, in part, by the Advanced Physical Methods Branch, Division of Energy Storage Systems, Department of Energy.

SESSION 2. COMPRESSED AIR ENERGY STORAGE

THIS PAGE

WAS INTENTIONALLY

LEFT BLANK

PROJECT SUMMARY

Project Title:	Compressed Air Energy Storage Technology Program
Principal Investigator:	W.V. Loscutoff
Organization:	Pacific Northwest Laboratory P.O. Box 999 Richland, Washington 99352 (509) 946-2768
Project Goals:	Reservoir Stability Studies - Develop design and stability criteria for long-term operation of underground reservoirs used for CAES in order to accelerate the commercialization of the concept. Advanced Concepts Studies - Develop and assess advanced technologies for CAES that require little or no supplementary firing by petroleum fuels in order to eliminate the dependence of CAES on these fuels.
Project Status:	The reservoir stability criteria studies are progressing satisfactorily. Program milestones attained have been the development of preliminary design and stability criteria for the three major types of storage reservoirs from surveys of existing information and completion of some of the initial porous rock and salt numerical studies. All subcontracts are in place for the numerical and laboratory studies. Field studies project plans are being prepared and are scheduled for initiation during FY-1980. The advanced concepts studies are screening the major advanced technologies, thermal energy storage (TES), fluidized bed combustion (FBC) and coal gasification. The screening should be completed in FY-1980. Decisions on more comprehensive studies and development of one or more advanced concepts are planned for late FY-1980 or early FY-1981. Development and evaluation of equipment for all CAES concepts is continuing.
Contract Number:	EY-76-C-06-1830
Contract Period:	FY1979
Funding Level:	$65 K
Funding Source:	Department of Energy, Division of Energy Storage Systems

COMPRESSED AIR ENERGY STORAGE PROGRAM OVERVIEW

W.V. Loscutoff
Pacific Northwest Laboratory
Richland, Washington 99352

ABSTRACT

The DOE Compressed Air Energy Storage (CAES) Technology Program consists of a group of interrelated studies directed at developing a new technology to improve the cost and efficiency of electrical power utilization and reducing the consumption of petroleum fuels. The program has two major elements -- Reservoir Stability Studies and Advanced Concepts Studies. The Reservoir Stability Studies are aimed at developing long term design and stability criteria for underground reservoirs used in CAES plants. The Advanced Concepts Studies are directed at development of CAES configurations that will require little or no petroleum fuels for firing of the turbines.

In this overview, we summarize the program efforts during FY-1979, outline specific tasks, indicate current progress, identify future activities, and point out milestones and accomplishments.

INTRODUCTION

Compressed air energy storage is a technique for supplying electric power to meet peak load requirements of electric utility systems. It incorporates a modified state-of-the-art gas turbine and an underground reservoir --- an aquifer, a salt cavity or a mined hardrock cavern. The compressor and turbine sections of the gas turbine would be alternately coupled to a motor/generator for operation during different time periods. During nighttime and weekend off-peak periods, low-cost power plants not using petroleum fuels would be used to compress air which would be stored in the underground cavern. During the subsequent daytime peak-load periods the compressed air would be withdrawn from storage, mixed with fuel, burned and expanded through the turbines to generate peak power. This concept reduces the consumption of premium fuels by more than 60 percent for conventional CAES systems. Some advanced CAES concepts do not require any premium fuels at all.

Studies have shown that the CAES concept is technically feasible and, with a proper utility power generation mix, is economically viable. CAES systems offer several advantages over conventional systems used by utilities for meeting peak load requirements. Replacement of current gas turbines by CAES plants could result in annual savings of more than 100,000,000 barrels of oil. The net annual oil saving would be greater in the future. CAES plants are not limited to the same degree of siting difficulties faced by conventional pumped hydro plants. Finally, a well designed CAES plant should have a smaller adverse impact on the environment compared to a conventional peaking plant.

In view of the potential benefits that the concept offers, the Department of Energy (DOE) has undertaken a comprehensive program in order to accelerate commercialization of the technology. The Pacific Northwest Laboratory (PNL) was selected by DOE as the lead laboratory for the CAES Technology Program. As such, PNL is responsible for assisting the DOE in program responsibilities for planning, budgeting, contracting, managing, reporting and disseminating information. Under subcontract to PNL are a number of companies, universities and consultants that are responsible for various facets of the program. The funding for this program was $2,235K, broken down into $1,600K for Reservoir Stability Studies, $575K for Advanced Concepts and $60K for Environmental Concerns. This report presents an overview of the activities by PNL and its subcontractors during FY-1979 on the Reservoir Stability Studies and Advanced Concepts Studies.

OBJECTIVE AND SCOPE OF WORK

The CAES Technology Program has evolved into two basic research and development elements and a supporting effort on environmental concerns. Recognizing that long term reservoir stability is a key issue to successful commercialization of CAES technology, the Reservoir Stability Studies element has the major emphasis in the early phases of the program. Recognizing also that the petroleum fuel requirements of conventional CAES systems may be an obstacle to large scale acceptance of the concept, the Advanced Concepts Studies element has been established and will dominate the research and development activity during the latter phases of the program. In support of the two major program elements, a study of potential environmental concerns associated with the commercialization of CAES has also been initiated.

The objectives of the program are as follows:

- Reservoir Stability Studies - Establish design and stability criteria for large underground air reservoirs in salt domes, hard rock, and porous rock formations that may be used for air storage in utility applications.
- Advanced Concepts Studies - Develop advanced CAES technologies that would eliminate the dependence of CAES systems on petroleum fuels.
- Environmental Concerns - Identify and evaluate potential environmental impacts associated with commercialization of CAES technology.

The Pacific Northwest Laboratory leads this program and is providing the required program management effort. Under subcontract to PNL, Re/Spec is providing support on behavior of hard rock caverns; Serata Geomechanics and Louisiana State University are studying the behavior of salt cavities; University of Wisconsin and Los Alamos Scientific Laboratory are supporting the studies on porous rock reservoirs; United Technologies Research Center, Argonne National Laboratory, Massachusetts Institute of Technology and Knutsen Research Services are supporting the advanced concepts research efforts. The program organization is shown in Fig. 1.

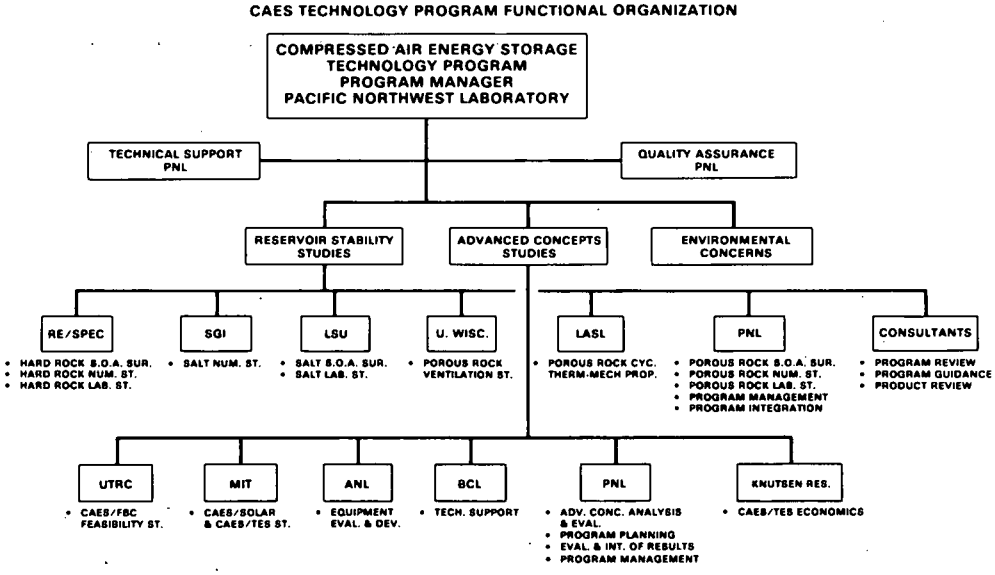

Fig. 1. CAES Technology Program Functional Organization

The program is organized into tasks and associated subtasks, as shown graphically in Fig. 2. It should be noted that while the task entitled "Environmental Concerns" appears as part of the work structure outline, it is funded by the Division of Environmental Control Technology and, thus, outside the responsibility of the Division of Energy Storage Systems. No presentations on this task will be made in this report.

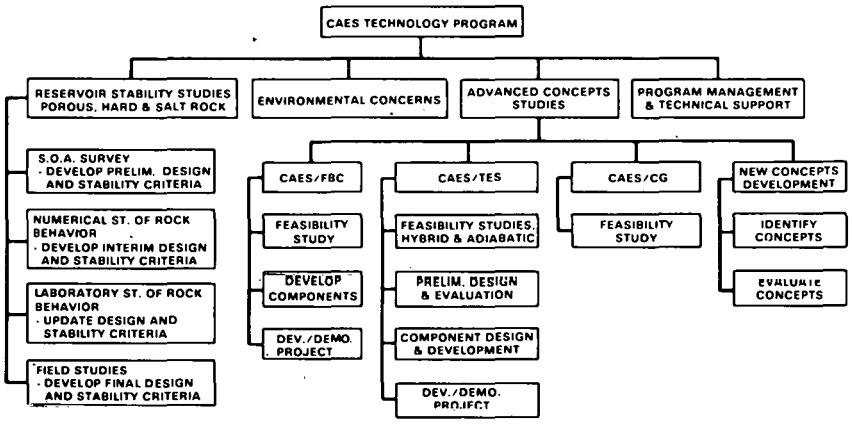

Fig. 2. CAES Technology Program Work Structure Outline

The master schedule of milestones and activities developed to accomplish the planned tasks in a timely fashion is shown in Fig. 3. The overall program effort is keyed on developing the required design and stability criteria for underground reservoirs, and to developing CAES concepts that do not require any petroleum fuels.

The first milestone marks the development of preliminary design and stability criteria for underground CAES reservoirs. These criteria are updated as numerical and laboratory studies are completed. The final reservoir design and stability criteria are scheduled to be developed following the completion of field studies.

In the Advanced Concepts Studies, the major point is a decision by DOE, backed by the feasibility studies, to proceed to a commercial-scale development/demonstration program. The initiation of one or more of the advanced CAES projects marks the major milestones in the program.

PROGRESS TO DATE

RESERVOIR STABILITY STUDIES

FY-1979 has seen a number of new activities start and milestones reached. These include the following elements:

- Develop preliminary design and stability criteria for
  - porous rock reservoirs
  - salt cavities
  - hard rock caverns
- Complete initial numerical model development for the behavior of salt cavities.
- Complete initial laboratory studies of air-water-rock interactions.

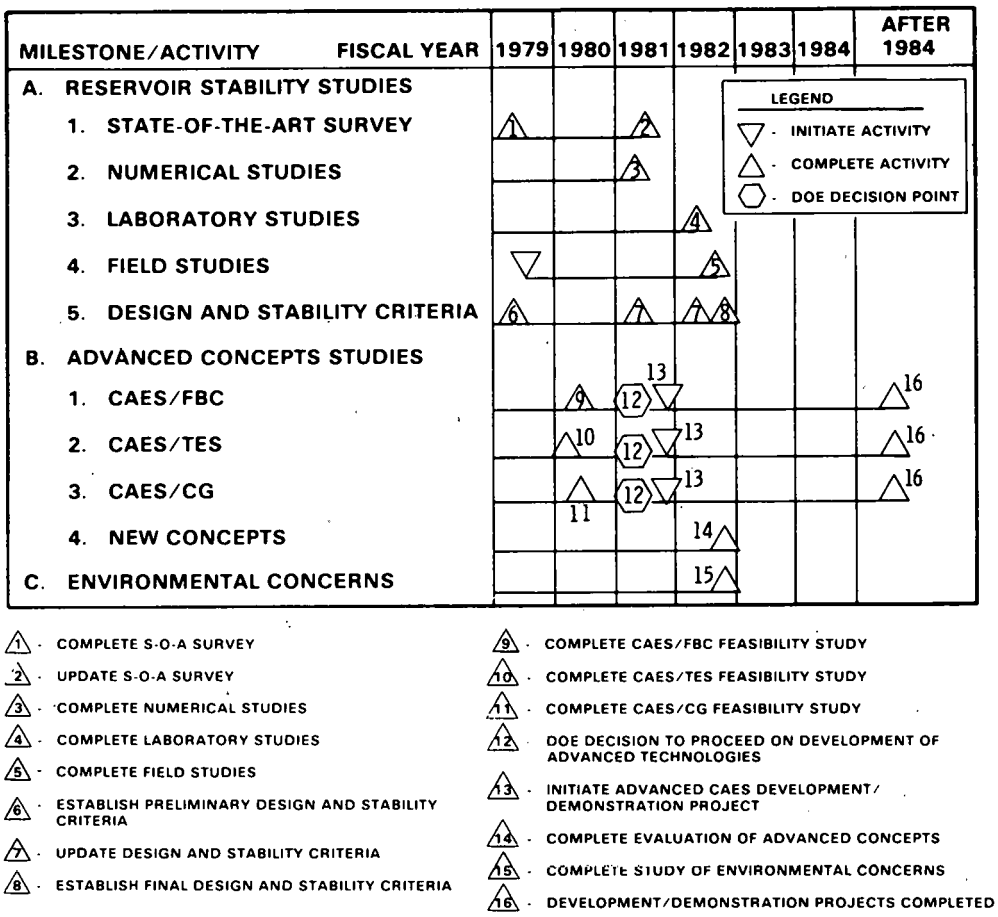

Fig. 3. CAES Technology Program Milestones

- Complete numerical studies of moisture effects on air storage in porous rock.
- Complete a study of wellbore thermal effects on a porous rock reservoir.
- Initiate laboratory studies of salt.
- Initiate laboratory studies of hard rock.
- Design a flow facility for laboratory studies of porous rock.
- Develop initial project plans for field studies.

Those tasks that have been identified as being completed have been documented and reports on these subjects are available from PNL.

Major activities in FY-1979 that are not listed as milestones or accomplishments but that will impact milestones in FY-1980 and FY-1981 include the following:

- Numerical hard rock cavern studies.
- Numerical porous rock reservoir studies.
- Laboratory hard rock studies.
- Laboratory salt studies.

- Laboratory porous rock studies.
- Initiation of field studies.

A summary of the foregoing activities is shown in the milestone chart in Fig. 3 together with anticipated completion dates, where applicable. The final milestone in this series of studies is the development of realistic design and stability criteria for CAES reservoirs that would facilitate the commercialization of CAES technology.

ADVANCED CONCEPTS STUDIES

The major milestones, accomplishments and activities in the Advanced Concepts Studies during FY-1979 were the following:

- Complete CAES/TES and CAES/solar studies by MIT.
- Select preferred FBC concept for CAES systems.
- Obtain preliminary results from studies of effects of hot air injection on porous rock.
- Compare major CAES/TES studies using standard methods, parameters and values.
- Initiate DOE-TVA study of advanced CAES systems.
- Continue evaluation of coal gasification as an alternative fuel for CAES systems.
- Examine and evaluate a number of novel advanced CAES concepts, e.g., two tank low pressure ratio system.
- Summarize rotating machinery requirements for advanced CAES.
- Initiate preliminary conceptual designs of CAES plants for the three types of air storage reservoirs.

Future major activities in the Advanced Concepts Studies project include the following:

- Complete feasibility studies of the major types of advanced CAES technologies.
- Select the preferred technologies for further development, leading to a demonstration of the technologies.
- Complete evaluation and initiate development, when necessary, of equipment for advanced CAES technologies.

SUMMARY AND CONCLUSIONS

In this overview, I have outlined the current CAES Technology Program and indicated its progress. In conclusion of this overview, I would like to state a number of conclusions resulting from previous and current studies.

- Low risk component design exist for near-term CAES plants.
- While near-term CAES plants can save significant amounts of petroleum fuels, they are still dependent on these fuels. It is important to eliminate this dependence in the near future. Fortunately, it appears that we do have this option.
- Economic attractiveness of CAES, especially advanced technologies, is enhanced relative to simple cycle gas turbines by the continuing escalation of petroleum fuel prices.

The papers that will follow this overview will be more specific and detailed on some of the major topics and conclusions regarding CAES technology.

PROJECT SUMMARY

Project Title:	Numerical Modeling to Predict Behavior of Underground Hard Rock Caverns Used for Compressed Air Energy Storage
Principal Investigator:	Dr. Arlo F. Fossum
Organization:	RE/SPEC Inc. P.O. Box 725 Rapid City, SD 57709 (605) 343-7868
Project Objectives:	Develop numerical models to evaluate the thermal/mechanical/hydrological behavior of compensated CAES caverns in hard rock and perform numerical modeling to establish stability and design criteria.
Project Status:	This project is divided into the following phases and tasks: (1) TASK I-1: Establish Major Generic Rock Property Characteristics (2) TASK I-2: Formulate Conceptual Numerical CAES Simulation Model (3) TASK II-1: Establish CAES Criteria/Modeling Procedures (4) TASK II-2: Parametric Evaluations by Use of Numerical CAES Simulation Model (5) TASK II-3: Formulation of CAES Stability and Design Criteria The project status is as follows: (1) The major generic rock property characteristics have been identified and quantified to the extent possible through an extensive literature survey. (2) A conceptual numerical CAES simulation model has been formulated which can be used in an integrated or a discrete manner. (3) Modeling procedures have been established for the construction phase of a CAES cavern and are currently in development for the operational phase. (4) Parametric evaluations by use of discrete elements of the numerical CAES simulation model are underway. (5) The formulation of CAES stability and design criteria is in progress. Current work is centered around air leakage considerations.
Contract Number:	Special Agreement No. B49407-A-H/Prime Contract EY-76-C-06-1830
Contract Period:	August 31, 1978 - November 30, 1979
Funding Level:	$150,551
Funding Source:	Pacific Northwest Laboratories, Battelle Memorial Institute

NUMERICAL STUDIES OF COMPENSATED CAES CAVERNS IN HARD ROCK

Paul F. Gnirk
Terje Brandshaug
Gary D. Callahan
Joe L. Ratigan
RE/SPEC Inc.
P. O. Box 725
Rapid City, SD 57709

ABSTRACT

The primary purpose of this paper is to present some results of thermal, mechanical, and air leakage modeling analyses for compensated CAES caverns in hard rock. Particular attention is drawn to the influence on the in situ (pre-mining) stress state on pre-operational cavern stability and operational air leakage. Consideration is also given to the region of cyclic temperature perturbation around an operational CAES cavern and the time required to achieve a quasi-steady temperature field in the rock mass. Where possible, the implications of the modeling results are qualitatively confirmed by comparison with case history data and observations.

INTRODUCTION

The underground layout of a compensated compressed air energy storage (CAES) system in hard rock can be visualized as a collection of parallel storage caverns, each of which is connected at either end by inclined entries to common (air and water) crosscut tunnels. As shown in Fig. 1, the crosscut (air) tunnel on the upward inclined end is connected to the surface compression and generation equipment by an air shaft. On the downward inclined end, the crosscut (water) tunnel is connected to a water inlet/outlet shaft which in turn connects to a surface water reservoir. Water from the surface reservoir provides a compensating head for maintenance of constant air pressure (with varying volume) in the storage caverns. This is designated a "wet" system due to the rise and fall of water in the caverns during the withdrawal (generation cycle) and injection (compression cycle) of compressed air. In order to prevent air ejection through the water shaft, the base of the shaft, as well as any intermediate water storage caverns, must be situated at greater depth than that of the air storage caverns. Due to turbine machinery limitations and pressure losses during the generation cycle, a maximum air pressure of about 7 to 7.5 MPa (1,000 to 1,080 psi) is allowed, which dictates a facility depth of about 715 to 765 m (2350 to 2500 ft.).

Although the internal pressure in the storage caverns is constant, the rock is subjected to a daily temperature cycle due to alternating contact with hot air (compression cycle) and water at "ambient" temperature (generation cycle). More specifically, the operational cycle will involve a period of seven days with compression/inactive cycles on Saturday and Sunday and compression/inactive/generation/inactive cycles on each weekday. For design purposes, the useful life of a compensated CAES cavern system is designated to be 30 years, or approximately 11,000 temperature cycles. Although generation will occur only on week days, temperatures will fluctuate in the caverns during the weekend due to cooling of the compressed air and fall of the water in the caverns.

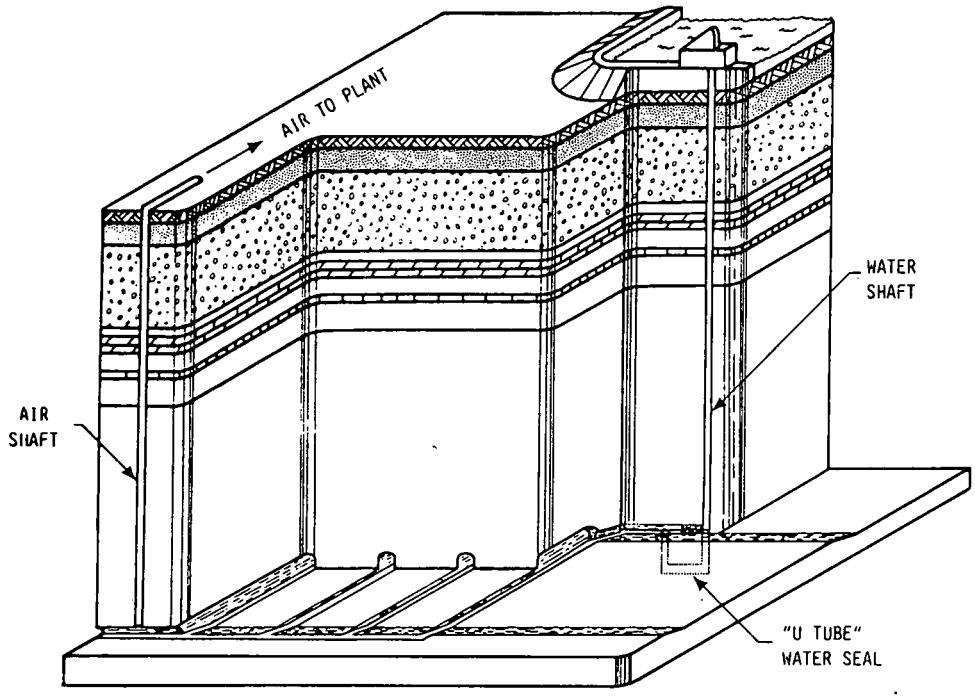

Fig. 1. Schematic Representation of a Compensated CAES Cavern System.

The purpose of the numerical modeling program is to establish procedures for predicting the thermal/mechanical/hydrological response of caverns to compensated CAES operating conditions, and to develop corresponding design and stability criteria for such cavern systems in hard rock. This effort is complimentary to past and present programs involving preliminary definition of stability and design criteria (1-5) and laboratory studies of appropriate rock properties (6). The basic elements of a CAES numerical simulation model and of the probabilistic approach to cavern design for the excavation phase have been discussed previously (5,7).

Over the course of the numerical modeling program, a dual approach has been selected, leading to the same end point, viz.:

(1) Integrated (Conceptual) Approach: Development of a comprehensive numerical model of coupled thermal/mechanical/hydrological behavior for compensated CAES caverns, incorporating the probabilistic design approach, with case history simulations and parametric evalutions.

(2) Discrete (Practical) Approach: Use of discrete elements of an overall numerical model to perform parametric evalutions of post-excavation and operation cavern stability, thermal perturbation into the cavern rock, drawdown during cavern construction, and air leakage.

The distinction between the two approaches lies in the relative level of sophistication. The integrated or conceptual approach seeks to incorporate a creative blend of theory and experience from cavern construction through operation, such that theoretical projections can be employed as a design tool when the base of empirical knowledge is restricted. The discrete or practical approach seeks to provide parametric information of immediate use to the designer for distinct phases of construction and operation; the generalization of this information to situations involving event complexity and strong coupling of phenomena, however, is not immediately straightforward. The two approaches do have commonality in that phenomenological mechanisms of rock behavior must be identified in the sense of constitutive laws and used appropriately in the modeling efforts to formulate criteria for rock stability and air leakage.

For the purpose of this paper, we have chosen to present some results that have been achieved in this study by use of the discrete approach. The stability of CAES caverns after excavation and prior to operation is discussed from the viewpoints of geometry and in situ stress state, followed by incorporation of those results into design criteria based on extensive case history knowledge. Preliminary results are given for the extent of thermal perturbation in the rock around compensated CAES caverns for extreme limits of temperature fluctuation during operation. Finally, a comparison between predicted and observed air leakage from a cavern in hard rock in Sweden is presented. For completeness, the above topics will be preceded by brief discussions of the appropriate generic rock properties and the essential numerical techniques. It must be emphasized that much of the information presented in this paper represents results obtained during the early phases of this program.

GEOTECHNICAL AND THERMAL/MECHANICAL ROCK PROPERTIES

In general, the vertical *in situ*, or pre-mining, stress in a hard rock mass can be taken as the weight of the overburden. For a collection of all rock types and groups of the hard rock variety (igneous, metamorphic, and sedimentary), the vertical stress gradient averages about 0.0268 MPa/m on the basis of bulk density[2]. This value is reasonably consistent with those given by Brown and Hoek[8] of 0.027 MPa/m and Haimson[9] of 0.025 MPa/m. For igneous and metamorphic rocks in particular, we have deduced average values of 0.0269 MPa/m and 0.0282 MPa/m, respectively [2].

Although the vertical stress is relatively easy to quantify on the basis of rock density, the horizontal *in situ* stress is quite variable over North America, and may range from 0.5 to 2.0 or greater at depths of 700 to 800 m, as shown in Fig. 2. Clearly, this *in situ* stress is site specific, and, as shown later, its influence on cavern stability can be significant.

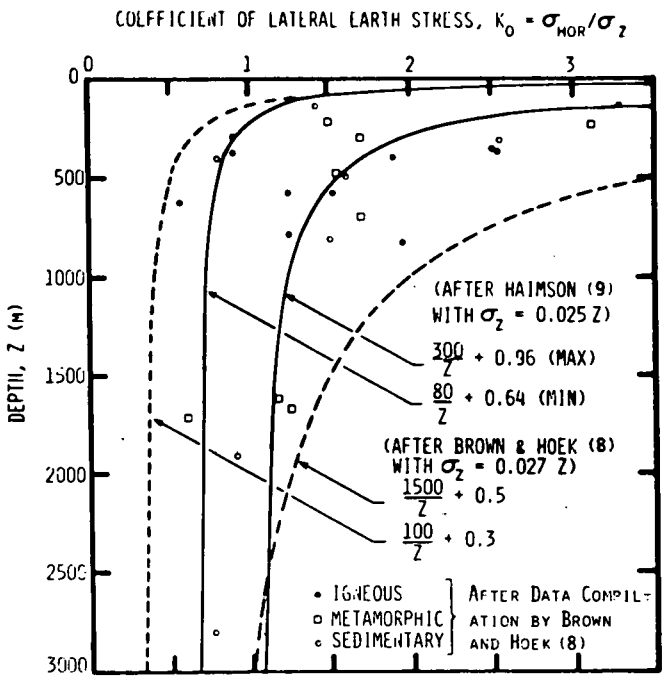

Fig. 2. Coefficient of Lateral Earth Stress (Average Horizontal In Situ Stress) as a Function of Depth.

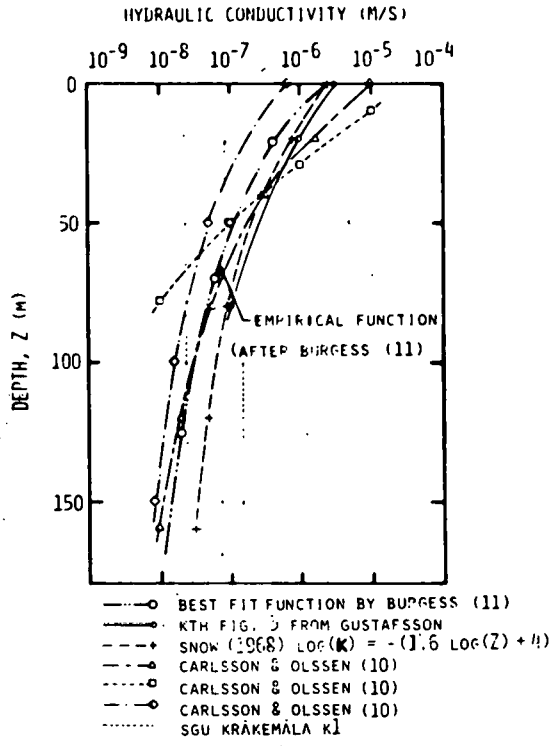

Fig. 3. Compilation of Field Data and Empirical Relationships for Hydraulic Conductivity as a Function of Depth for Igneous and Metamorphic Rock Masses (After Stille, et al.(12)).

Carlsson and Olsson[10] have investigated hydraulic conductivity as a function of depth for some Swedish rock masses which have virtually no primary permeability, only secondary permeability. Their investigation indicated a decrease in hydraulic conductivity with depth, but the data were highly scattered and limited to relatively shallow depths (generally less than 175 m). Employing data from the above study and others, Burgess[11] and Stille, et al.[12] have developed a mean relationship for hydraulic conductivity as a function of depth (see Fig. 3). We note that a single measurement by Carlsson and Olsson[10] at a depth of about 300 m indicates a hydraulic conductivity which is approximately two orders of magnitude less than calculated from the preceding relationship. For the present study, as well as for other similar studies, little permeability and fissure deformation data have been found in the literature for hard rock regions at depths below 400 m.

For the purpose of this study, we have chosen the mean and extreme values given in Table 1 for the material properties of a generic hard rock. In general, the extreme values encompass the range of measurements reported in the literature for igeneous, metamorphic, and sedimentary rocks.

TABLE 1

Mean and Extreme Values of Thermal/Physical/Mechanical Properties for Generic Hard Rock

PROPERTY	MEAN	EXTREMES
Young's Modulus (GPa)	50	25/75
Poisson's Ratio	0.25	0.15/0.40
Cohesion (MPa)	35	10/60
Angle of Internal Friction (Deg.)	35	20/50
Density (kg/m^3)	2,730	2520/2875
Thermal Conductivity (W/m-K)	2.90	1.85/3.95
Thermal Diffusivity ($10^{-6}m^2/s$)	1.15	0.90/1.35
Specific Heat (J/kg-K)	935	835/1035
Coefficient of Thermal Expansion (1/K)	8.0	6.25/9.75

NUMERICAL SIMULATION PROCEDURES

For the purpose of the numerical modeling discussed in this paper, use was made of the SPECTROM series of finite-element codes as developed by RE/SPEC over the past eight years.

SPECTROM is particularly applicable to problems in rock mechanics, involving discrete or coupled phenomena in the thermal, mechanical, and hydrological realms of rock behavior. Use is made of isoparametric elements, with capabilities for handling nonlinear and anisotropic material properties, time-independent and time-dependent nonlinear material response through post-failure, and two and three dimensional geometries. Each of the codes within the series has been extensively validated with closed-form analytical solutions and available commercial finite-element codes on CDC CYBERNET, and with laboratory and in situ (or field) case history data where available.

POST-EXCAVATION CAVERN STABILITY

OBJECTIVES AND RANGE OF PARAMETERS

The purpose of this aspect of the study was to evaluate the influence of cavern geometry and spacing and coefficient of lateral earth stress on the stability of caverns prior to CAES operation. The computed stress fields in the rock mass following excavation are applicable strictly to an elastic medium which is devoid of joints or other structural discontinuities. When inelastic deformation of the medium is not considered, or does not occur, the stress perturbation is independent for all practical purposes of the sequence of excavation. In addition, the solutions are strongly statically determinate, which implies negligible dependence on elastic properties.

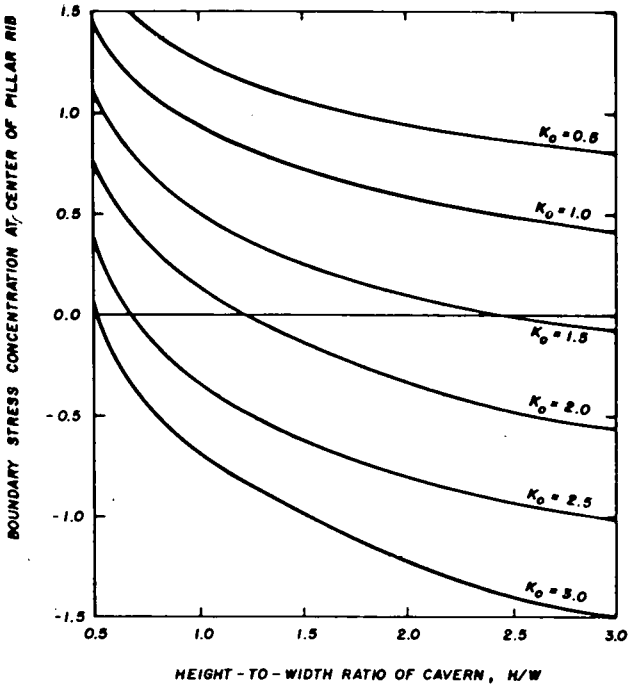

Fig. 4. Boundary Stress Concentration in the Rib of a Single Cavern for a Range of Height-to-Width (H/W) and In Situ Stress (K_o) Ratios.

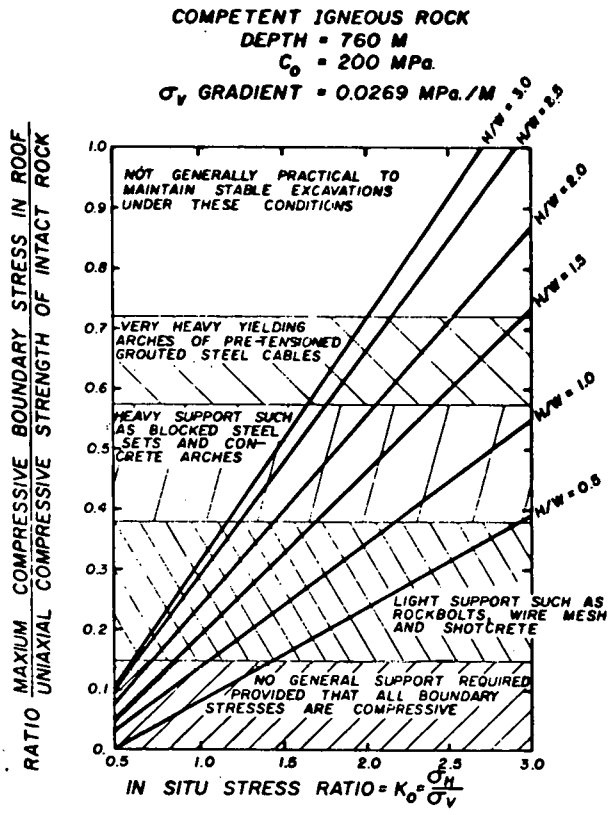

Fig. 5. Post-Excavation Stability of a Single Cavern in Competent Igneous Rock at a Depth of 760 m (Support Requirements after Hoek (14)).

The cavern excavation is assumed to be situated at a floor depth of 760 m, and the vertical in situ stress gradient is taken to be 0.0269 MPa/m. Consideration was given to single caverns with height-to-width ratios ranging from 0.5 to 3.0, and to a sequence of three caverns in parallel with height-to-width ratios of 1, 1.5, and 2 and extraction ratios of 20, 40, and 60%. In all instances, the cavern width was chosen as a constant 10 m, with the radii of the arched crown and rib-floor intersections being 10% of the cavern height and 5% of the cavern width, respectively. In the discussions that follow we have chosen compressive stress to be algebraically positive.

SINGLE CAVERNS

Figure 4 illustrates the influence of height-to-width ratio H/W and in situ stress ratio K_o on the stress concentration factor in the central rib boundary (side wall) of a single cavern. The stress concentration factor is defined as the ratio of the tangential (in this case, vertical) stress in the rib and the in situ (pre-mining) vertical stress. Clearly, as both H/W and K_o increase, the vertical stress in the rib changes from compression to tension. For high values of K_o, the induced arching action above and below the cavern tends to "stretch" the rib. As demonstrated later in this paper, this stretching action will give rise to zones of predominate air leakage in the rib sections of the cavern.

As a point of qualitative validation of the results given in Fig. 4, as regards caverns stability, we draw attention to the Flygmotor CAES caverns in Sweden which have a height to width ratio of approximately 0.3 and are situated at a depth of about 90 m (see Bergman, et al.[13]). For the generally high horizontal in situ stresses at that depth, as illustrated previously in Fig. 2, the ribs of the caverns have remained exceptionally stable over many years of daily operation (we note that the temperature fluctuations in the caverns are only nominal). For this case history situation, the boundary stress concentration in the rib is probably compressive, but of relatively low magnitude.

Figure 5 is an illustration of the application of the elastic stress results to practical design considerations as regards need for artificial support. We have plotted the ratio of the maximum compressive boundary stress in the cavern roof and the uniaxial compressive strength of a competent igneous rock (200 MPa) to K_o for a range of values of H/W. Superposed on this plot are the artificial support needs, as deduced from correlations by Hoek [14] based on extensive case history data. For an H/W of 1.5 to 2, which is of interest to CAES cavern design, the in situ stress ratio must be less than 1.3 to 1.5 in order to avoid the use of heavy artificial roof support, such as blocked steel sets and concrete arches.

MULTIPLE CAVERNS

Figure 6 illustrates the influence of extraction ratio and in situ stress ratio on the vertical stress concentration in the rib of the central cavern in a three-cavern array, for a cavern height-to-width ratio of 2. For extraction ratios of 20 to 40% and a range of K_o from 1 to 2, the vertical pillar stress is compressive and of the order of 50 to 140% of the in situ vertical stress. For extremely high horizontal stresses, such as may occur at shallow depth, one could anticipate a vertical tensile stress in the pillar rib. As a point of qualitative validation, we draw attention to the case history described by Anttikoski and Saraste [15] for three oil storage caverns in parallel near Helsinki. The caverns have a H/W of 2 and an extraction ratio of 30 to 40%, and are situated in an in situ horizontal stress field of about 15 MPa (K_o = 10 to 15). Through a combination of field observation and finite element analysis, they concluded that perhaps 60 to 90% of the pillars were in a state of tension and the cavern roofs were heavily stressed in compression. The formation of horizontal fractures across the pillars was deduced from the adjustment of oil levels between adjacent caverns to a common elevation.

In Fig. 7, we have combined the results for the stress concentrations in the cavern roofs with the uniaxial compressive strength of a competent igneous rock to illustrate the need for artificial roof support for ranges of H/W and K_0 and a constant extraction ratio of 40%. The artificial support needs have been deduced, as before, from case history correlations by Hoek (14). For an H/W of 1 to 2, only light support in the form of rock bolts and wire mesh is required to maintain cavern roof stability after excavation, for a value of K_0 between 1.25 and 1.75.

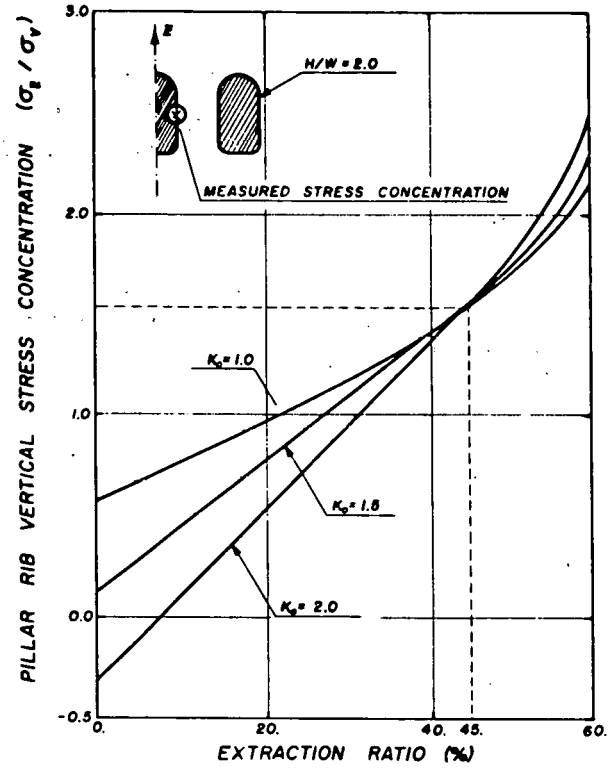

Fig. 6. Boundary Stress Concentrations in the Pillar Rib of the Central Cavern in a Three-Cavern Array.

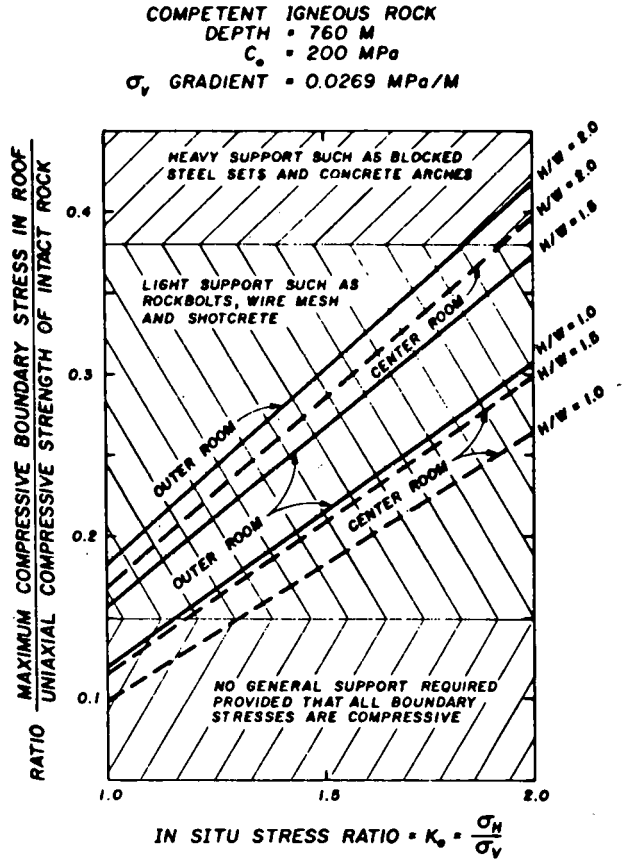

Fig. 7. Post-Excavation Stability of an Array of Three Caverns in Competent Igneous Rock at a Depth of 760 m (Support Requirements after Hoek (14)).

GENERAL REMARKS

The preceding results, although only a representative sample of those accumulated to date in this study, clearly indicate the need for site specific in situ stress data for the design of CAES caverns. A slight alteration in cavern geometry in relation to the artificial support needs can be perhaps an economic trade-off which deserves thoughtful attention from the viewpoints of rock stability and air leakage. In general, the results indicate that enhanced rock stability can be achieved with an array of caverns as compared to a single cavern, at least from the viewpoints of pre-operational considerations for CAES in hard rock.

THERMAL PENETRATION INTO CAES CAVERN WALL

In order to investigate the cyclic thermal effects in the rock during CAES operation, a cavern was chosen with a height and width of 20 m and 10 m, respectively. The compensated cavern was considered to be initially full of water at 10°C. The top 2 m were assumed to contain compressed air at all times and the bottom 0.5 m to contain water at all times. Thus, the operational height of the cavern over the compression and generation cycles was 17.5 m. The cycle time was taken to be one day, with the compression and generation cycles separated into alternating 12 hour periods. The air/water interface was supposed to move at a constant velocity over the operational height of the cavern. Compressed air inlet temperatures of 75°C and 150°C were considered. The cavern was assumed to be 750 m deep and the geothermal gradient was taken to be 25°C/km. Finally, the rock type was chosen to be igneous, with the following thermal properties: thermal conductivity = 2.9 W/m-K; specific heat = 935 J/kg-K; thermal diffusivity = 1.3 E-06 m^2/s.

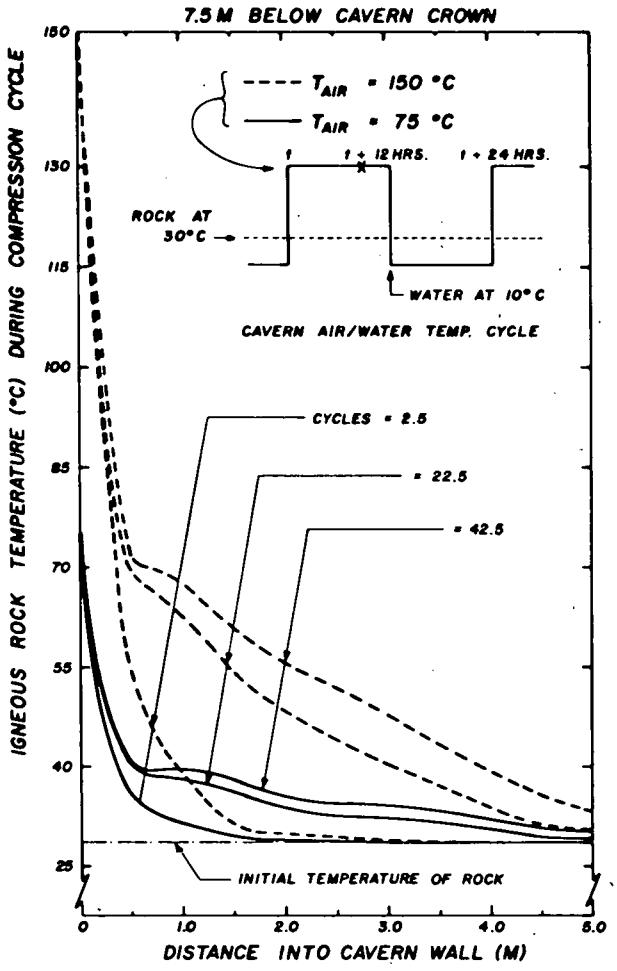

Fig. 8. Temperature Distribution in a CAES Cavern Wall in Igneous Rock During the Compression Cycle.

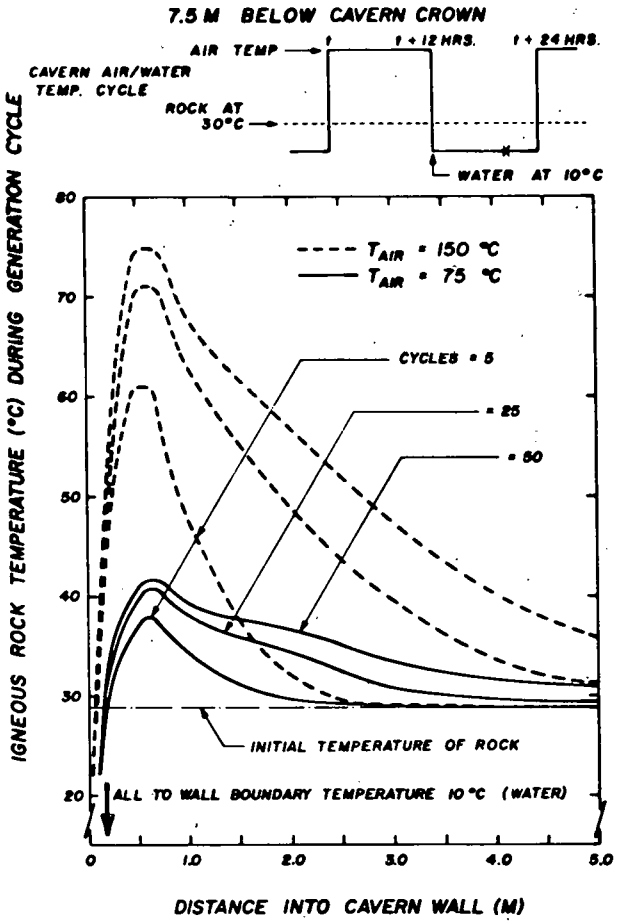

Fig. 9. Temperature Distribution in a CAES Cavern Wall in Igneous Rock During the Generation Cycle.

Figures 8 and 9 illustrate the temperature distributions along a horizontal line into the rock at a distance of 7.5 m from the crown of the cavern. The cavern wall (depending on elevation) is defined to be at the water temperature (10°C) or the compressed air temperature (75°C or 150°C) throughout the compression and generation cycle periods. The temperature in the first meter of the cavern wall is seen to rise substantially within the first five cycles of cavern operation. The region beyond one meter is relatively unperturbed by the cyclic temperature boundary on the cavern wall and undergoes continuous heating. The temperature rises between the twentieth and fiftieth cycles are much less. At the fiftieth cycle, temperature increases are quite small and the first meter of the cavern wall is near a steady oscillatory temperature distribution with small temperature increases.

If the initial temperature of the material is the same as the mean of the oscillatory surface temperature, the temperature distribution reaches a steady oscillatory motion much more rapidly than if the initial temperature of the medium is above or below the mean of the harmonic surface temperature. For the CAES system discussed above, the analytical solution indicates that the transient portion of the solution will contribute to thermal oscillation within 5 meters of the cavern wall for the life of the cavern. However, the majority of the transient is damped within the first one hundred cycles.

One of the more important aspects of this simulation is the location and magnitude of the thermal gradients. The largest thermal gradients occur early in time and within the first meter of the cavern wall, indicating that this region will be the most critical as regards thermally induced stresses.

CASE HISTORY SIMULATION OF CAVERN AIR LEAKAGE

In an effort to provide a test case for our proposed numerical model for air leakage, RE/SPEC subcontracted with Hagconsult AB to document the history and geometry of the Flygmotor CAES cavern system near Trollhatten, Sweden (Bergman, et al.[13]). The CAES system is used to supply compressed air for wind tunnel testing of aircraft engines.

The Flygmotor cavern system was excavated in a biotite gneissic rock mass at a depth of about 90 m during 1949-51 and has a volume of approximately 12,000 m^3 of usable storage. The system is water-compensated, and due to the low height of the individual caverns (3.8 m), essentially provides a constant air pressure source. The cavity is normally charged five to six times a day and has experienced approximately 30,000 unload-load cycles since construction.

Following cavity excavation, a tightness test was performed in September of 1951. The cavern was pressurized to 830 kPa without water compensation and the pressure drop was monitored for 24 hours. This test was repeated twice for a total of three continuous tests. The results are given as follows:

TEST NO.	PRESSURE DROP kPa/day	AIR LEAKAGE %/day
1	29.4	3.6
2	27.0	3.3
3	39.2	4.8

Although these air leakage rates are high and might well be unacceptable in most CAES applications, they were acceptable to Flygmotor.

Initial efforts to simulate the air leakage tests have been performed under the following assumptions:

- the cavern can be modeled as an equivalent single drift;
- the air pressure drop in the cavern can be neglected;
- air transport is governed by the single phase compressible gas transport equation for isothermal conditions in porous media (the rock mass was reported to have been extensively drained of water during construction).

All of the above assumptions will result in greater air leakage than actually occurred during the tests. The degree of over-estimation resulting from these assumptions, is, however, presently being evaluated where possible. Four simulations of the Flygmotor air leakage tests have been performed. The first two simulations assumed that the permeability of the porous media was isotropic. The two permeabilities used in these simulations were 10^{-14} and 10^{-16} m^2 which are equivalent to hydraulic conductivities of 10^{-7} and 10^{-9} m/s. The porosity of the rock mass was taken to be 0.01% (Bergman, et al.[13]) in all cases. The cumulative cavern air loss for the simulation with 10^{-9} m/s is illustrated in Fig. 10 along with the measured cumulative air leakage. In this regard, the error in the simulation at the end of the third test is an accumulation of error from all the proceeding tests.

It should be noted that the simulation with a permeability of 10^{-14} m^2 (recommended by Bergman, et al.[13]) resulted in air leakage rates of much greater magnitudes than measured. However, at this point, it is not clear which permeability (if either) is applicable to the rock mass containing the Flygmotor caverns.

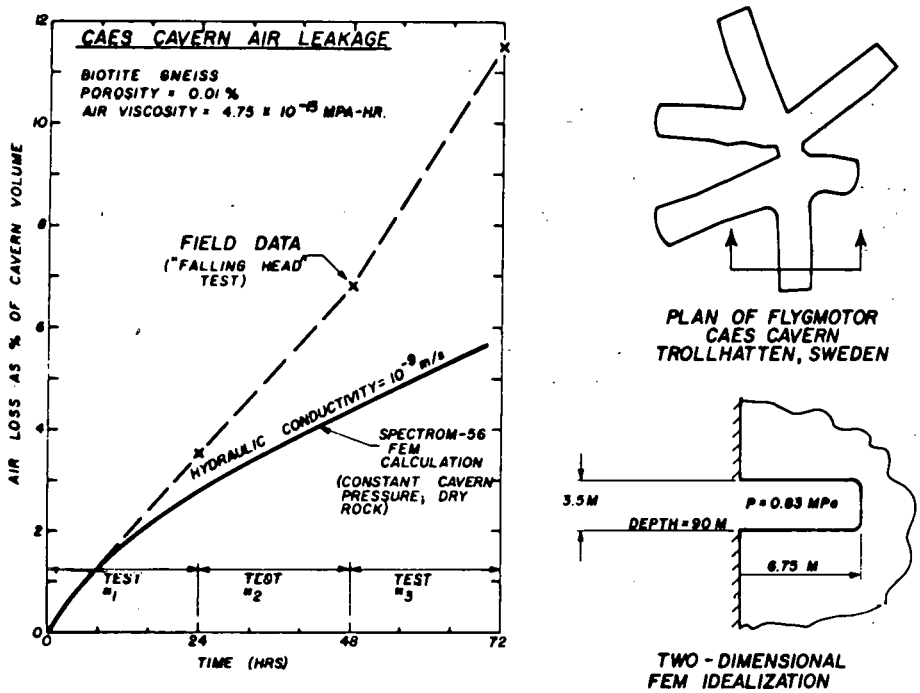

Fig. 10. Comparison of Calculated and Measured Air Leakage from the Flygmotor CAES Cavern System in Sweden.

The final two simulations used the empirical permeability/normal stress relationship developed by Burgess[11]. This formulation assumes that:

- equivalent porous media permeability is a function of the normal stress across a joint set at an assumed orientation.
- the relationship can be determined from field measurements which preferentially measure horizontal permeability wherein normal pressure on the discontinuities is equal to the weight of the overburden.

Prior to making the air leakage calculations with the empirical permeability relationship, an elastic stress analysis of the Flygmotor caverns was performed for the purpose of obtaining the normal stress distributions across assumed joint sets at vertical and horizontal orientations. The analysis was undertaken for coefficients of lateral earth stress of 5.5 and 10, which are typical measured values in hard rock at a depth of about 100 m (see Fig. 2). With these stress results and the stress-dependent permeability relationship, the air leakage was found to be approximately a factor of 30 greater than that measured. In effect, the coefficient of lateral earth stress was found to have only a minor influence on the volume of air leakage. However, the location of leakage in the cavern (roof versus rib) is strongly dependent on the in situ stress ratio, with the higher value giving rise to a greater loss of air through the cavern ribs.

The over-estimation in the air leakage is due to several factors. Firstly, the empirical permeability/stress relationship was derived with a bias towards the greater values of permeability (Stille, et al.[12]). Secondly, the assumed two-dimensional model of the Flygmotor cavity is extremely important in evaluating the percent air loss. In this regard, the cavern system was modeled as an equivalent volume disc with a height of 3.5 m. The air loss from this simulation was significantly lower than that obtained with the two-dimensional analysis.

ACKNOWLEDGMENTS

The contents of this paper are derived from work performed under Special Agreement No. B-49407-A-H (Prime Contract EY-76-C-06-1830) with Pacific Northwest Laboratories of Battelle Memorial Institute for the U.S. Department of Energy. The authors are indebted to Landis D. Kannberg, Terry J. Doherty, and Walter V. Loscutoff of BPNL for their technical guidance and assistance; to Arlo F. Fossum for his constructive suggestions and varied technical assistance; and to Julie S. Annicchiarico for her thoughtful attention in typing the manuscript.

LIST OF REFERENCES

1. D. S. Port-Keller and P. F. Gnirk: "CAES and UPHS in Hard Rock Caverns: I. Geological and Geotechnical Aspects", RE/SPEC Project Summary Rpt. RSI-0076, Prepared for Battelle Pacific Northwest Lab. (1979).

2. P. F. Gnirk, D. S. Port-Keller, and H. Waldman: "CAES and UPHS in Hard Rock Caverns: II. Thermal/Mechanical/Chemical Rock Properties", RE/SPEC Project Summary Rpt. RSI-0078, Prepared for Battelle Pacific Northwest Lab. (1979).

3. P. F. Gnirk and D. S. Port-Keller: "Preliminary Design and Stability Criteria for CAES Hard Rock Caverns", Proc. DOE 1978 Mech. and Magnetic Energy Storage Contractors' Review Mtg., Luray (1978), pp. 364-373.

4. P. F. Gnirk: "CAES and UPHS in Hard Rock Caverns: III. Preliminary Stability and Design Criteria for Compressed Air Energy Storage Caverns", RE/SPEC Project Summary Rpt. RSI-0079, Prepared for Battelle Pacific Northwest Lab. (1979).

5. A. F. Fossum: "On the Analysis Procedures for Formulation of Stability and Design Criteria for CAES in Hard Rock Caverns: I. Excavation Phase", RE/SPEC Topical Rpt. RSI--0077, Prepared for Battelle Pacific Northwest Lab. (1979).

6. A. F. Fossum: "Laboratory Testing of Hard Rock Specimens for Compensated CAES Caverns", Proc. DOE 1979 Mechanical and Magnetic Energy Storage Contractors' Review Mtg., Washington D.C. (1979).

7. P. F. Gnirk and A. F. Fossum: "On the Formulation of Stability and Design Criteria for Compressed Air Energy Storage in Hard Rock Caverns", 14th Intersociety Energy Conversion Engrng. Conf., Boston (1979), V. 1, pp. 429-440.

8. E. T. Brown and E. Hoek: "Trends in Relationships Between Measured In Situ Stresses and Depth", Int. J. Rock Mech. Min. Sci., V. 15 (1978), pp. 211-215.

9. B. C. Haimson: "The Hydrofracturing Stress Measuring Method and Recent Field Results", Int. J. Rock Mech. Min. Sci., V. 15 (1978), pp. 167-178.

10. A. Carlsson and T. Olsson: "Variations of Hydraulic Conductivity in Some Swedish Rock Types", Rockstore 77 (1977), V. 2, pp. 301-307.

11. A. Burgess: "Groundwater Movements Around a Repository: Regional Groundwater Flow Analyses", KBS Teknisk Rapport 54:03 (1977).

12. H. Stille, A. Burgess, U. E. Lindblom: "Groundwater Movements Around a Repository: Geological and Geotechnical Conditions", KBS Teknisk Rapport 54:01, (1977).

13. M. Bergman, J. Lundberg, and K. Windelhed: "Case History Examination of Compensated Compressed-Air Storage Caverns in Gneissic Rock at Trollhattan, Sweden", RE/SPEC Topical Rpt. RSI-0091, Prepared for Battelle Pacific Northwest Lab. (1979).

14. E. Hoek: "The Role of Modeling in the Design of Nuclear Waste Repositories: The Design Engineer's Viewpoint", LLL/ONWI Workshop on Thermomechanical Modeling for a Hardrock Waste Repository, Berkeley (1979).

THIS PAGE

WAS INTENTIONALLY

LEFT BLANK

PROJECT SUMMARY

Project Title:	Establishment of Design and Stability Criteria Through Laboratory Testing of Hard Rock Specimens Subjected to Loadings and Environmental Conditions Appropriate to a Compressed Air Energy Storage Cavern
Principal Investigator:	Dr. Arlo F. Fossum
Organization:	RE/SPEC Inc. P.O. Box 725 Rapid City, SD 57709 (605) 343-7868
Project Objectives:	Investigate the properties of hard rock specimens, from formations suitable for CAES under the cyclic conditions imposed by a CAES installation, by means of laboratory scale testing and formulate preliminary design and stability criteria for CAES caverns.
Project Status:	This project is divided into the following five phases: (1) Determine Significant Rock Properties (2) Procure Specimens (3) Select Specific Procedures for Rock Characterization before and after Testing (4) Conduct Laboratory Scale Testing of Rock Specimens (5) Formulate Stability and Design Criteria The project status is as follows: (1) The significant rock properties have been determined for which data are lacking and a study is nearing completion which seeks to find representations between certain rock properties and the rock petrography. (2) Large quantities of quarry rock have been obtained from four major generic rock groups. Additional granitic specimens will be obtained from at-depth conditions. (3) Specific procedures for rock characterization before and after testing have been selected and are proceeding according to the project plan. (4) Sample preparations, conditioning, and laboratory scale testing are all underway. (5) The methodology for formulating stability and design criteria based on this testing program, the state-of-the-art survey, and the numerical modeling program is being formulated.
Contract Number:	Special Agreement No. B-51295-A-E/Prime Contract EY-76-C-06-1830.
Contract Period:	March 2, 1979 - August 5, 1980
Funding Level:	$205,925
Funding Source:	Pacific Northwest Laboratories, Battelle Memorial Institute

LABORATORY TESTING OF HARD ROCK SPECIMENS FOR COMPENSATED CAES CAVERNS

A. F. Fossum
RE/SPEC Inc.
P. O. Box 725
Rapid City, SD 57709

ABSTRACT

Laboratory scale testing and its role in the formulation of compressed air energy storage (CAES) cavern stability and design criteria are discussed with viewpoints toward fundamental and special tests. Fundamental testing provides numerical values of parameters between stress and strain. In addition to the initial elastic constants, six fundamental coefficient material functions are identified of which five require data fitting. The constitutive equations deemed appropriate are inelastic but incrementally linear and involve a combination of incremental plasticity and fracturing material theory. Special testing provides answers to specific questions related to rock behavior in thepresence of CAES operating conditions. For example, "How is the load bearing capacity and stiffness of rock affected by thermomechanical cycling in the presence of moisture under pressure?" These and other similar questions must be answered by testing rock in systems which reproduce the operating conditions as closely as possible.

INTRODUCTION

Laboratory scale testing provides a means for addressing those unknowns which may affect the technical and economic feasibility of Compressed Air Energy Storage (CAES) from the standpoint of the response of underground caverns to pressure, temperature, and moisture fluctuations occurring during the periodic charge and discharge operations. Results from such testing, together with other Pacific Northwest Laboratory sponsored programs, should culminate in the formulation of design and stability criteria for CAES caverns to ensure their long lifetime suitability and encourage early commercialization of the CAES concept.

The pertaining CAES operating conditions of primary interest include the following:

(1) Initial vertical and horizontal in situ stresses and hydraulic pressures corresponding to cavern depths of 500 to 1000 meters (vertical stress gradients range from 0.0282 MPa/m for metamorphic rocks to 0.0247 MPa/m for sedimentary rocks with an intermediate value of 0.0269 MPa/m for igneous rocks).[1] In general, for these depths, the maximum horizontal in situ stress may be substantially greater than the vertical in situ stress, by a factor of two or more.[1] The water pressure may be taken as 0.01 MPa/m;

(2) Inlet air temperatures from 50 to 150°C,

(3) Compensating water temperatures from 0 to 20°C,

(4) Initial rock temperatures (the geothermal gradient varies from region to region with an average value of approximately 28°C/Km[1]);

(5) A useful life of approximately 10,000 cycles, or 30 years.

The specification of CAES caverns in hard rock immediately categorizes the situation to one involving igneous (granitic), possibly metamorphic, and certain sedimentary (limestones, marbles, dolomites) rocks. At the pressures and temperatures mentioned above, these rocks behave in a brittle manner in which the modes of inelastic behavior are microcracking and frictional sliding on fissure surfaces. This type of behavior is dominant for crustal conditions as opposed to at-depth conditions where the pressure-temperature regime is conducive to ductile rock behavior involving dislocation processes. Thus, consideration must be given to the influence of joints or planes of weakness, permeability, and groundwater presence. In addition, the cyclic temperature fluctuations will induce cyclic thermomechanical stresses which may degrade the strength and stiffness properties of the rock structure and lead to progressive global and/or local instabilities.

ROLE OF LABORATORY TESTING

The role of laboratory scale testing in the formulation of stability and design criteria is two-fold. On the one hand, parameters necessary in conducting analyses must be determined experimentally by testing rock specimens in systems which induce homogeneous stresses and strains. These parameters are fundamental parts of the expressions relating stress and strain and as such characterize the rock under consideration. Such expressions are derived within the realm of general theories, the structure of which must satisfy a number of physical principles. Many times these fundamental physical requirements are conceived following the observation of experimental behavior.

On the other hand, laboratory scale testing can provide an understanding of some characteristics of the real world in the absence of a theory encompassing the known behavior and for which analytical or numerical solution techniques fail. In this case testing seems to be, and often is, the only available approach possible within the time limitations imposed. In the study at RE/SPEC, testing is being conducted for both purposes. For discussion purposes, reference will be made to fundamental testing and special testing in the context of the above definitions.

FUNDAMENTAL TESTING

The essence of an analysis of a CAES cavern, for the purpose of formulating stability and design criteria, is the ability of the engineer to predict the mechanical behavior of a rock mass supported and loaded in a specified manner from controlled experiments on simple rock bodies. This requires the engineer to formulate constitutive equations and to solve boundary value problems.

In the current context, constitutive equations are the relations between stress and strain. In addition to stress and strain, the constitutive relations for rock are likely to involve other measurable physical quantities such as time, temperature, and quantities called internal parameters for which a direct measurement cannot be made. However, the effects of internal parameters can usually be expressed in terms of stress or strain history.

A knowledge of the deformation mechanisms is valuable in suggesting particular forms for phenomenological constitutive relations. Since CAES caverns are proposed for the brittle temperature-pressure regime, the observed macroscopic inelastic strain may be considered as the outcome of a chain of events including frictional sliding on microscopic fissures, attended by the outgrowth of localized tensile cracks from the tips of the fissures, and overriding of asperities. Dilatancy is thought to be the cumulative effects of these latter features. The criterion separating elastic from inelastic behavior for rock is pressure dependent because of the frictional nature of rocks. This type of pressure dependence is different than that which has been observed in metals arising from microporosity. The latter is characterized by a description in which the pressure dependence of the criterion separating elastic from inelastic behavior is fully matched by inelastic dilatancy. This type of behavior is not observed in the laboratory testing of rocks.

In general, the behavioral aspects of rock are complicated indeed and the phenomenological approach to the description of rock behavior leads to sophisticated constitutive relations. But, in order for the analyst to obtain realistic results, the use of such relations is in fact necessary. Fortunately finite element methods render structural analyses with sophisticated constitutive relations feasible. Nonetheless, one must be mindful of the degree of accuracy called for in a particular rock mechanics analysis and simplify the description in a judicious manner, such that the important or dominant characteristics which affect the structural behavior significantly under the prevailing conditions are considered.

The two broad categories of constitutive relations are those in which increments of stress and strain are linearly related, and those in which the relation is nonlinear. The first includes the incremental or flow theories, the total or deformation theories, and hypoelasticity. The second includes the endochronic theory. The premise is taken here that incrementally linear inelastic constitutive laws are appropriate for the degree of accuracy called for in the analysis of CAES caverns under the pertaining conditions.

Fundamental Requirements of an Incremental Approach

The essential ingredients of an incremental approach to rock behavior are the following:

(1) A criterion marking the onset of inelastic rock behavior;

(2) Rules relating the stress and stress increments or decrements to the strain increment;

(3) Hardening and softening rules;

(4) Limit or failure criteria at which instability results.

In much of the rock mechanics literature, a tacit equivalence seems to exist between item (4) and item (1) and as a result little data exist for items (1)-(3). Constitutive laws exist however which include all of the essential features for a structural analysis and which are appropriate to the study of CAES caverns[2]. These constitutive laws combine familiar incremental plasticity and fracturing material theory and provide nonlinear triaxial constitutive relations which are incrementally linear. The dominant characteristics accounted for in these relations, which may be important to CAES cavern performance, are internal friction, pressure sensitivity, inelastic dilatancy due to microcracking and friction, strain hardening, strain softening, degradation of elastic moduli due to microcracking, and hydrostatic nonlinearity due to pore collapse. In addition, special hardening rules can be incorporated which permit

inelastic response during unloading, reloading, and cyclic loading, as experienced at the periphery of a CAES cavern during the periodic charge and discharge operations. For compensated systems, which are of interest in this study, cyclic loading is induced by the periodic heating and cooling of the cavern wall corresponding to charging when hot air is injected into the cavern, and discharging when cold water displaces the hot air.

Generally speaking, the constitutive relations mentioned above require, in addition to the initial elastic constants, six independent scalar coefficients. These coefficients are material functions of the invariants of stress and strain. The initial elastic constants are shear modulus and bulk modulus. The six inelastic material functions are identified as follows:

(1) Plastic hardening modulus;

(2) Fracturing compliance;

(3) Internal or plastic friction coefficient;

(4) Volumetric fracturing compliance coefficient;

(5) Plastic dilatancy factor;

(6) Fracturing dilatancy factor.

Of these six functions, only one has been determined theoretically[3]. The fracturing dilatancy factor has been determined by a theoretical argument based on a micromechanics model in which the effective elastic constants of a randomly microcracked elastic material are calculated by the self-consistent method for composites[3]. The remaining five functions must be determined empirically by the fitting of test data.

Figure 1 demonstrates how incremental plasticity is combined with fracturing material theory to obtain a realistic plastic-fracturing theory. The behavior depicted in Fig. 1b prevails at very low confining pressure as well as in the later stages of uniaxial compression.

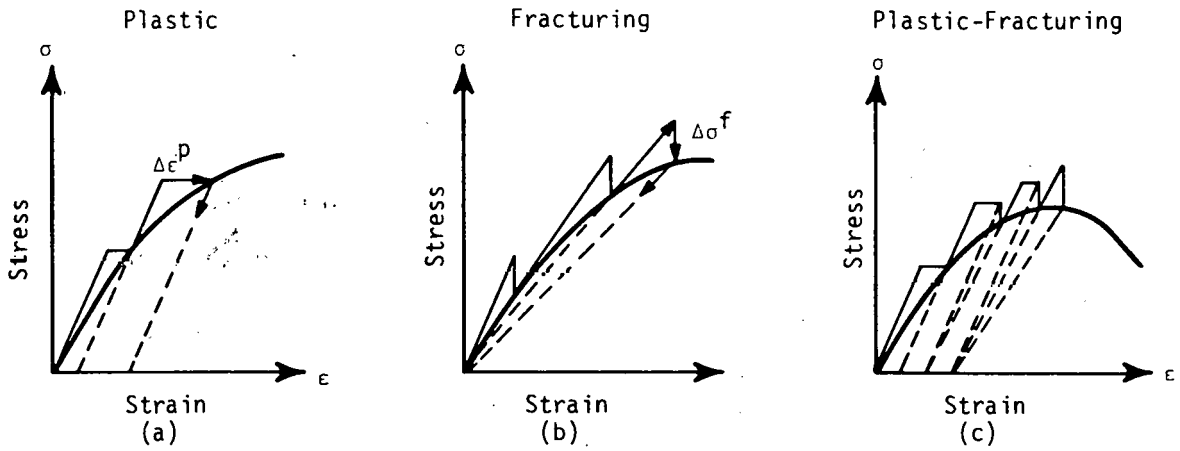

Fig. 1. Elements of Elastic-Plastic-Fracturing Behavior.

The behavior depicted in Fig. 1a is pronounced at high confining pressure and in the early stages of the uniaxial compression test. During testing, the individual contributions consisting of plastic slip and microcracking are estimated with an observation of the unloading slopes. The inelastic strain will be essentially plastic if the unloading slope is nearly equal to the initial loading slope. The inelastic strain due to microcracking or fracturing will be the strain due to an unloading slope decline. This notion is illustrated in Fig. 2.

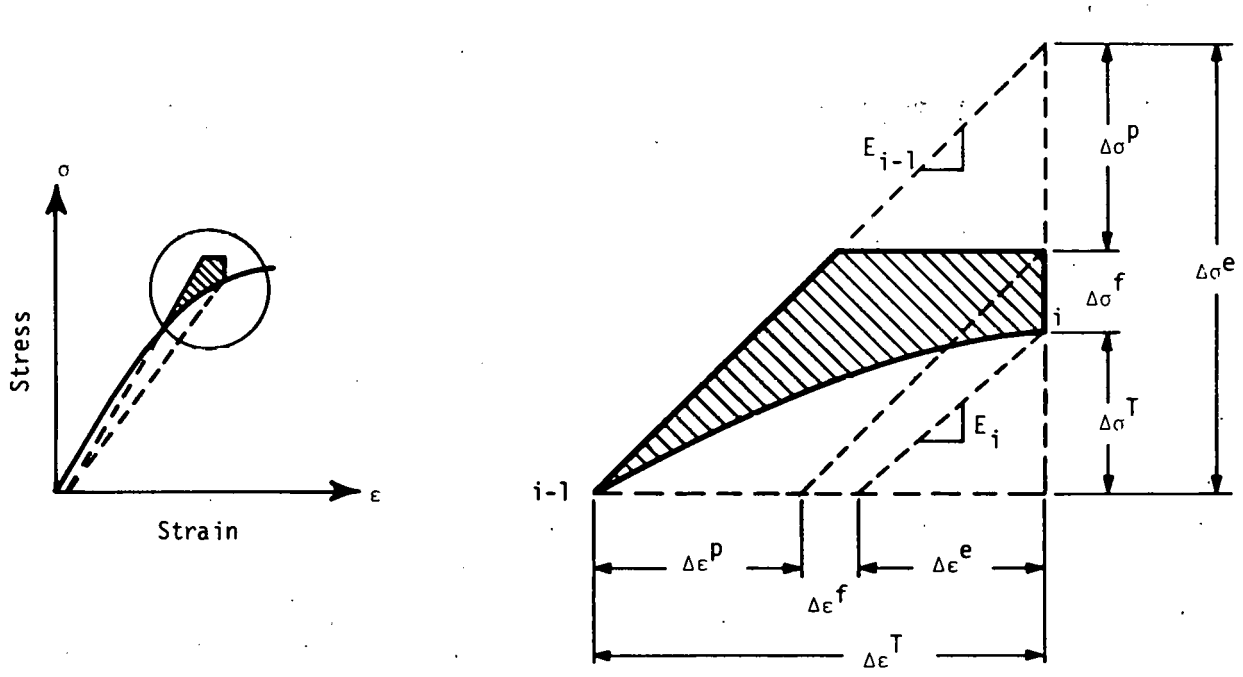

Fig. 2. Components in Total Stress and Strain Increments for Plastic-Fracturing Behavior.

The fundamental laboratory testing at RE/SPEC is, for the most part, being carried out with the use of triaxial (axially symmetric) compression machines. In principal, two fundamentally different types of deviant stress states can be achieved with this type of machine, namely triaxial compression and triaxial extension. In practice, however, the triaxial extension mode is difficult to execute because of sealing problems and of the requirement for confining pressures which usually exceed the machine's capacity. This is unfortunate since these two types of stress states give bounds on the criterion separating elastic from inelastic behavior (for materials exhibiting initial isotropy). Fig. 3 illustrates the stress states associated with these two tests. In the triaxial compression test, the axial stress exceeds the uniform lateral stress, and in the triaxial extension test, the lateral stress exceeds the axial stress. If the criterion separating elastic from inelastic behavior is known for all possible stress states, then a hypersurface can be constructed which

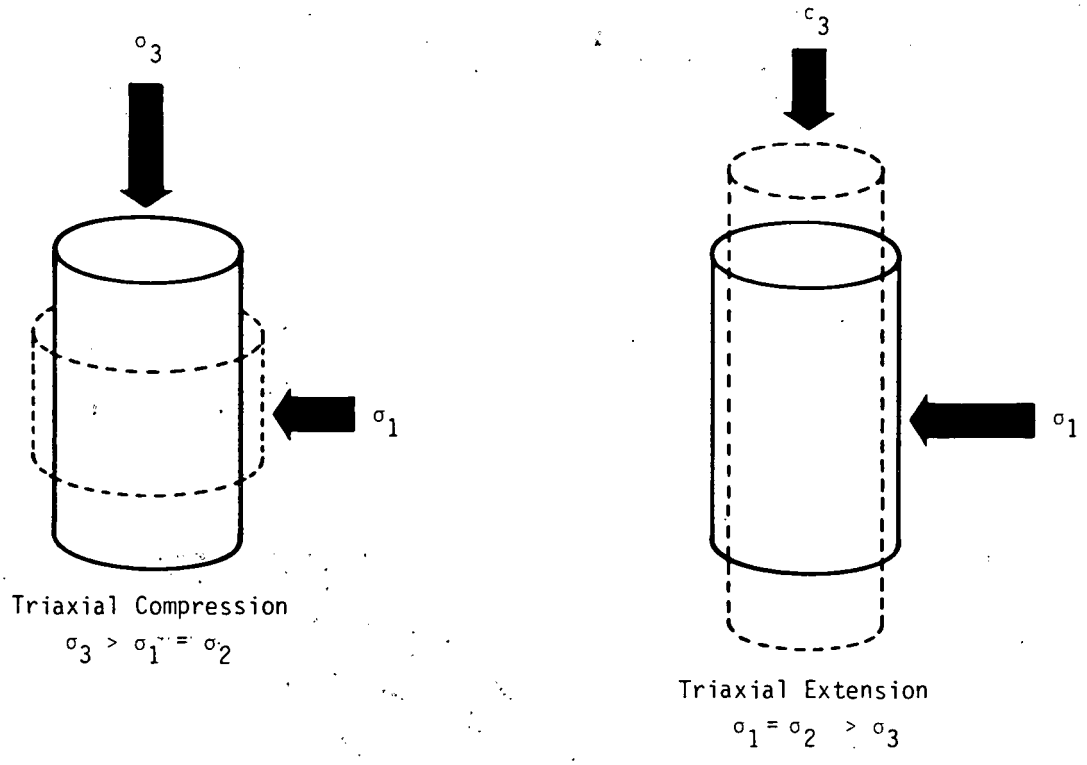

Fig. 3. Stress States Associated with Triaxial Compression and Extension Tests.

bounds the elastic region in a stress space with principal stresses as coordinates. Figure 4a shows the projection of such a region on the plane which intersects the principal stress axes with equal angles for a Mohr-Coulomb criterion and a Drucker-Prager type of criterion. The axes passing through the outer vertices correspond to the triaxial compression stress states and those passing through the inner vertices correspond to the triaxial extension stress states identified in Fig. 3. For a given mean stress, geological materials are generally stronger in compression than in extension. Thus, a cone constructed from triaxial compression data circumscribing the Mohr-Coulomb criterion will give inflated strength values for other stress states. One can, however, use triaxial compression data to construct other cones such as one passing through the inner vertices, or one which is tangent to the individual sides of the Mohr-Coulomb surface. Obviously the cone, or circle in the plane shown in the figure, is a conjecture with regard to the actual strength values for any stress state other than triaxial compression. The Mohr-Coulomb criterion may come closer to the actual situation, but without triaxial extension data or data from other stress states, its adequacy is not known with any certainty. The Mohr-Coulomb criterion can also be evaluated in terms of triaxial compression data.

Fig. 4b depicts a CAES cavern with a height to width ratio and a horizontal to vertical initial stress ratio of two. Near the corners of this cavern, the state of stress is in pure shear. In the roof, the stress state is near pure shear on the triaxial extension side. In the floor the stress state is near pure shear on the triaxial compression side. The state of stress along the wall is at or near triaxial extension. Thus the importance of interpreting triaxial compression data is clear; states of stress near triaxial compression may not even exist near the periphery of the cavern where inelastic behavior is most important.

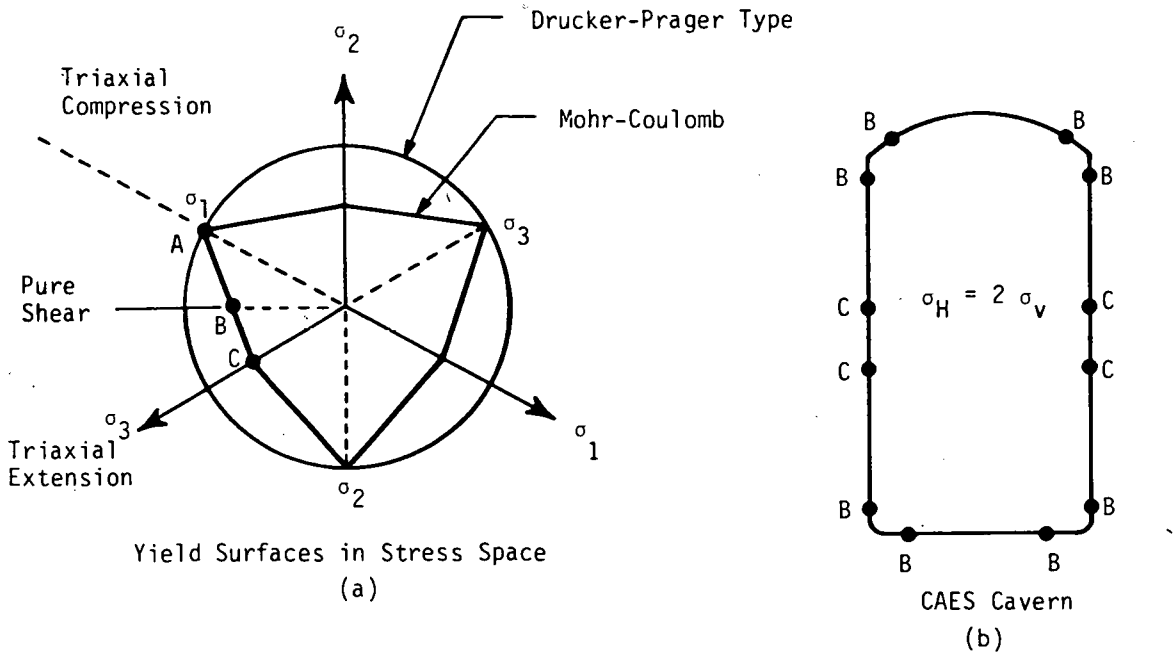

Yield Surfaces in Stress Space
(a)

(b)

Fig. 4. Types of Stress States Around a Cavern and Their Location in Stress Space.

With this awareness, the material functions mentioned earlier are being evaluated with the use of triaxial compression tests. A determination of the type of hardening that exists and the study of intrinsic corners that may develop in the loading surface (hypersurface in stress space) cannot be accomplished with this test.

Other aspects which are being considered include the following:

(1) Influence of temperature and moisture on rock properties;

(2) Influence of type, orientation, and spacing of joints on rock properties;

(3) Degradation of strength and stiffness of rock under cyclic loading with and without the presence of temperature, moisture, and confining pressure.

These considerations fall under the realm of special testing.

SPECIAL TESTING

Special testing refers to those tests which have rather a singular purpose. These tests are somewhat out of the ordinary but provide information which can be used as the basis for an understanding of rock behavior under circumstances which are difficult to model, or for which a sufficiently general theory does not exist. Although a compensated cavern will not experience much internal pressure change, the thermally-induced stress variations can be substantial. Therefore, the reduction in strength and stiffness and the change in permeability of rock is being investigated as a function of stress cycles.

Generally speaking, the fatigue life of a specimen consists of three phases, namely, nucleation, progagation, and rupture. There is not a clear distinction between nucleation and propagation, but rupture refers to fracture under a quarter cycle of loading.

Rocks exhibit several damage mechanisms which can progress independently or in interaction with each other. Because of the complex microstructural nature of rocks, the characterizing and monitoring of the damage process during cyclic loading is difficult at best. The likely damage mechanisms include matrix cracking, grain boundary cracking, and fracture of embedded minerals. For a brittle material such as rock, rupture is due to the formation, growth, and coalescence of microcracks. Since one expects, for this type of material, that the nucleation period is long compared with the propagation period, the Palmgren-Miner rule is probably adequate for prediction of fatigue life. Correspondingly, one of the types of fatigue testing being conducted at RE/SPEC is the uniaxial load controlled fatigue test. The data from these tests can be presented graphically as stress-life (S-N) curves. Since the fatigue life depends on numerous variables including mean stress (steady component stress), range of stress, loading frequency, temperature, moisture content, and specimen size, a method for screening, as outlined by Plackett and Burman[4], is being employed involving a design of optimal multifactorial experiments.

In addition to the cycles-to-failure data, cyclic stress-strain curves are being obtained periodically throughout the test so that modulus decay can be characterized. These data are important to thermal stress calculations since these stresses are directly proportional to the modulus of elasticity.

Another special cyclic loading test which will be conducted at RE/SPEC is one in which a cylindrical test specimen is subjected to a confining pressure and a cyclic axial load. The confining fluid, which will be alternately cold water and hot air, will be allowed to make contact with the test specimen. By maintaining the preloaded test specimen at a constant length, cyclic thermal stresses will be induced by the exchange of hot air and cold water. If failure does not occur after a specified number of cycles, the specimen will be broken and the residual strength recorded. The axial preload, confining pressure, and water and air temperatures will be chosen to be representative of an operating CAES cavern.

Other testing either in progress or proposed for the future include the guarded hot plate test for the determination of thermal conductivity as a function of temperature, and characterization tests for the determination of bulk density, grain size range, porosity, and permeability. In addition, modal petrographic and chemical analyses are in progress.

Finally, upper and lower bound representations have been established which give effective thermal conductivity of a generic rock as a function of the thermal conductivities and volume fractions of the constituent minerals.

REFERENCES

1. Debra S. Port-Keller and Paul F. Gnirk, "CAES and UPHS in Hard Rock Caverns: I. Geological and Geotechnical Aspects", Project Summary Report RSI-0076, Prepared for Pacific Northwest Laboratories, Battelle Memorial Institute under Special Agreement No. B-51225-A-L, Prime Contract EY-76-C-06-1830, (January 19, 1979).

2. Zdenek P. Bazant and Sang-Sik Kim, "Plastic-Fracturing Theory for Concrete", Journal of the Engineering Mechanics Division, ASCE, Vol. 105, No. EM3, pp. 407-428, (1979).

3. B. Budiansky and R. J. O'Connell," Elastic Moduli of Cracked Solids," International Journal of Solids and Structures, Vol. 12, pp. 81-97, (1976).

4. R. L. Plackett and J. P. Burman, "The Design of Optimal Multifactorial Experiments", Biometrika, Vol. 33, pp. 305-325, (1946).

THIS PAGE

WAS INTENTIONALLY

LEFT BLANK

PROJECT SUMMARY

Project Title:	Air-Water-Rock Interactions
Principal Investigator:	J.A. Stottlemyre
Organization:	Pacific Northwest Laboratory P.O. Box 999 Richland, Washington 99352 (509) 946-2733
Project Goals:	To investigate potential physical and chemical property alterations under simulated CAES reservoir conditions. Establish a CAES porous media laboratory for future site specific evaluation. Generate data in support of site selection and reservoir stability criteria.
Project Status:	Quartzose sandstones are exhibiting good property stability in heated, humidified air environments as simulated in autoclave systems. Due to this observation and the inherent inability to adequately simulate field conditions in autoclaves the following course is being pursued: 1) Autoclave tests will be used to screen CAES candidate rock types only, 2) Successful candidate rocks will then be tested in a heated, triaxially loaded pressure vessel which permits adequate control of temperatures, stresses, advective flow rates, humidities and cycling frequencies, 3) Future emphasis will be on making measurements under carefully simulated field conditions and investigating the phenomena of thermal fatigue and hydrolytic weakening of potential CAES reservoir rocks.
Contract Number:	EY-76-C-06-1830
Contract Period:	FY1979
Funding Level:	$50K
Funding Source:	Department of Energy, Division of Energy Storage Systems

PERMEABILITY AND FRIABILITY ALTERATIONS IN QUARTZOSE SANDSTONES EXPOSED TO ELEVATED TEMPERATURE HUMIDIFIED AIR

J.A. Stottlemyre, R.L. Erikson, and R.P. Smith
Pacific Northwest Laboratory
Richland, Washington 99352

ABSTRACT

The feasibility of elevated temperature Compressed Air Energy Storage concepts may depend, to a major extent, upon the physical and chemical stability of reservoir rocks to new environmental conditions. This paper is based on preliminary autoclave studies of quartzose sandstones exposed to simulated CAES subsurface conditions. The properties of primary concern are absolute gas permeability, friability, and compressibility. Independent variables include temperature (50-300°C), pressure (20-120 bars), experiment duration (14-56 days), and environment (dry air, humidified air, or brine). Preliminary observations, based on a very limited data set, are: 1) quartzose sandstones exposed to dry air exhibit excellent property stability under all test conditions, 2) samples undergo significant disaggregation when exposed to brine at temperatures as low as 100-150°C, and 3) when exposed to humidified air at elevated temperature. Preliminary results indicate sandstones may be suitable storage media for heated, humid air as long as elevated temperature zones are relatively free of mobile liquid phase water.

INTRODUCTION

The economic and technical feasibility of Compressed Air Energy Storage (CAES) technology depends to a major extent on locating, developing, and maintaining a suitable subsurface reservoir. One area of uncertainty is the physical and chemical stability of the reservoir medium, e.g., sandstone aquifer or crystalline rock to new subsurface environmental conditions associated with CAES operations. Of primary interest are potential changes in permeability, friability, and compressibility of sandstone due to elevated temperatures, humidities, and oxidation potentials.

This paper is a synopsis of a recent laboratory investigation concerning the potential effects of heated, humidified air on quartzose sandstones. Information is presented in the following sequence: 1) anticipated reservoir environment, 2) experimental facilities and procedures, 3) multivariate experimental strategy, 4) data analysis and conclusions, and 5) summary recommendations.

ANTICIPATED RESERVOIR ENVIRONMENTS

Numerical models[1] have been utilized to estimate the temperature, pressure, and moisture levels as a function of injection air temperature, radial distance from any given well, and time. Example curves for temperature and pressure are shown in Figs 1 and 2 and are based on the reference data presented in Table 1. In a CAES reservoir, moisture will be derived from two sources: 1) residual or irreducible water left in the porous rock after initial air bubble expansion, and 2) water vapor entrained in the injected air stream. This moisture will be gradually removed from the near well zones via evaporation with undersaturated injection air. Fig. 3 presents a possible dehydration history for the reference reservoir.[1]

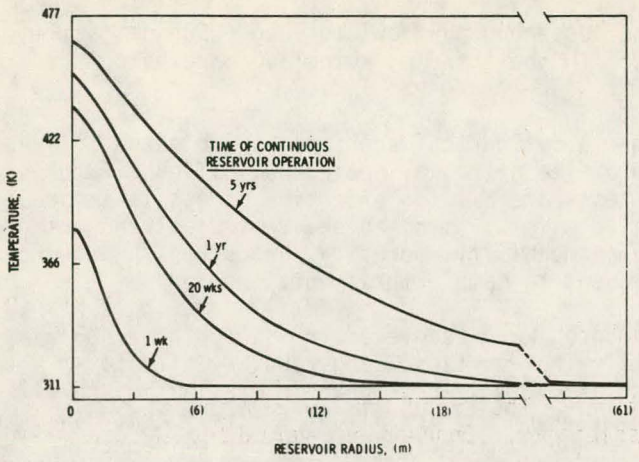

Fig. 1. Thermal Development Around An Injection/Production Well.

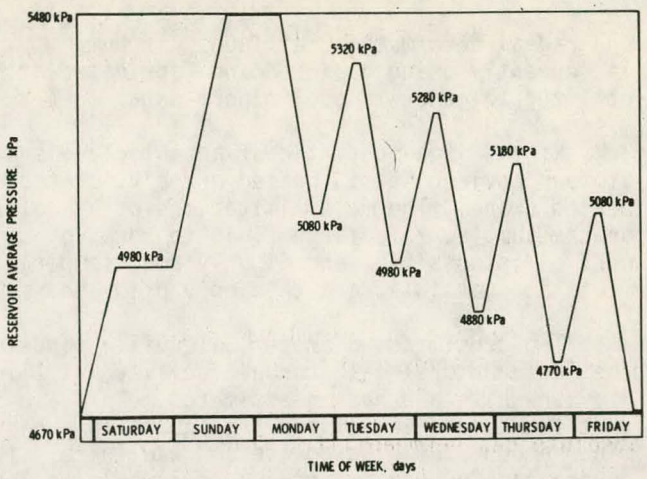

Fig. 2. Reservoir Air Pressure Variations

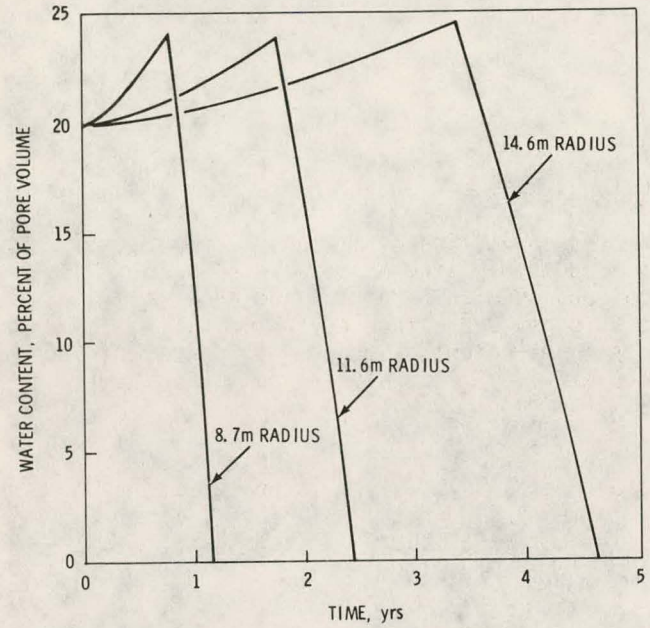

Fig. 3. Possible Dehydration History for Reference Reservoir

TABLE 1. Reservoir Parameters for Base Case Computer Simulation (Wiles 1979)

Parameter	Reference Value
Geometry	
Reservoir Diameter (m)	122
Well Diameter (cm)	18
Properties	
Porosity (%)	20
Permeability (m^2)	5.0×10^{-13}
Rock Thermal Conductivity (w/m·°C)	2.16
Rock Thermal Capacity ($MJ/m^3 \cdot °C$)	2.62
Operating Conditions	
Nominal Pressure (MPa)	5.07
Mass Flow Rate	
Injection (kg/s·m)	0.18
Extraction (kg/s·m)	0.16
Initial Reservoir Temperature (K)	312
Air Injection Temperature (K)	505

These computations are necessary to establish limits on the expected subsurface reservoir conditions. From this data, it appears that a certain zone of rock surrounding each well will be exposed to heated humidified air for an extended period of time. It is therefore necessary to simulate these environmental conditions, to the degree possible, in laboratory investigations.

EXPERIMENTAL FACILITIES AND PROCEDURES

To adequately simulate anticipated field conditions, the sample should be heated, loaded triaxially, and ventilated with air of known humidity, temperature, and flow rate. Measurements of principal concern include the pressure drop along the axis of the rock core, axial

and radial deformation, effluent air humidity, and suspended particulate load. Such a facility is currently being designed and fabricated at PNL. In the interim, autoclaves are being utilized to generate preliminary data.

Fig. 4 is a schematic of an autoclave system. A cylindrical specimen is subjected to one of four environments: heated dry air, heated humidified nitrogen, heated humidified air, or heated brine. The main limitations of autoclave tests are: 1) no effective stress is imposed on the sample, 2) a large fluid to rock volume ratio exists, 3) no advective fluid transport control is possible, and 4) only room temperature permeability, porosity, and strength measurements are possible, and then only prior and subsequent to sample treatment.

Ten centimeter diameter Galesville sandstone cores were recovered from a depth of 685 m at the Media natural gas storage facility in Illinois. The quartzose sandstone is white to grayish-white and has an estimated mean grain size of 0.5 mm. Petrographic examination reveals that the subangular clasts are equant to subequant in form and are almost entirely quartz with minor amounts of plagioclase and kaolinite. The cementing material is also predominantly crystalline quartz. The rock as a whole is moderately well sorted and exhibits cyclic parallel bedding of thin, coarse-grained layers and thicker, fine grained layers. Fig. 5 is a micrograph of a typical Galesville sample. Fig. 6 shows a range of permeability values for the Galesville samples. Galesville sandstone is currently under consideration as a candidate rock type for a CAES field demonstration.

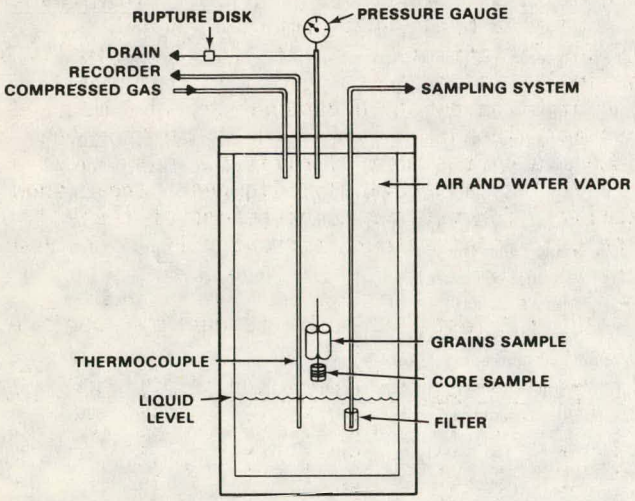

Fig. 4. Schematic of an Autoclave System

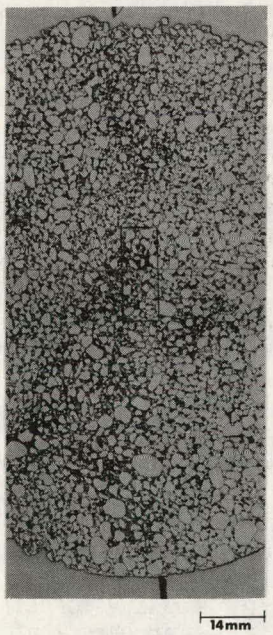

GALESVILLE SANDSTONE

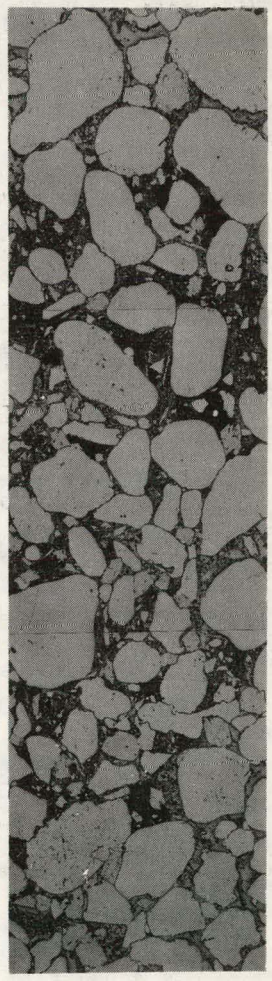

Fig. 5. Micrograph of Typical Galesville Sample

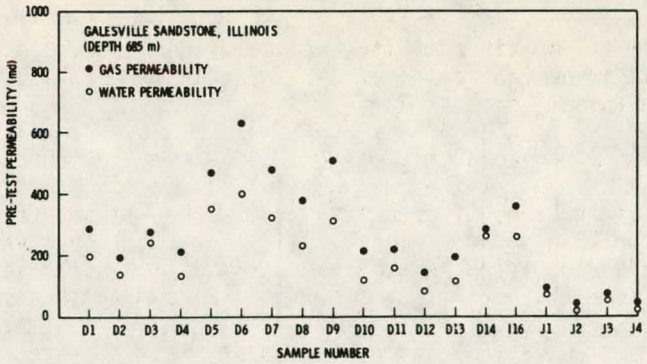

Fig. 6. Range of Permeability Values for Galesville Samples

MULTIVARIATE EXPERIMENTAL STRATEGY

The main objectives of the experiments are: 1) identify independent variables that have significant impact on the response of the rock, 2) identify those independent variables that have relatively small influence and therefore can be held constant in future experiments, and 3) identify trends in the data pertaining to CAES reservoir design and/or operating criteria. A Placket-Burman experimental design was selected to systematically investigate the main response characteristics of the dependent variables to various combinations of the maximum and minimum magnitudes of the independent variables. The variables and their ranges are listed in Table 2.

The cores are reacted in: 1) a dry air environment, 2) a water vapor and pure nitrogen environment, 3) a water vapor and air environment, and 4) a brine environment. Table 3 illustrates the percent change in gas permeability and "friability". Friability is basically a qualitative term which refers to the potential for individual grains to dislodge from the rock matrix. The friability test involves a carefully controlled point loading of the specimen and is designed to address changes in intergranular contact strength. Temperature, liquid water saturation, and duration of the experiment were found to be the most significant independent variables controlling permeability, porosity and friability alterations. Figures 7 and 8 show the percent changes in gas permeability and "friability" for various combinations of these three variables. The changes are listed inside the circles as either increasing (↑) or decreasing (↓) a certain percentage over the pretest level.

TABLE 2. Range of Independent Variables

Independent Variable	Minimum Value	Maximum Value
Pressure (bars)	60	120
Temperature (°C)	50	300
Time (months)	0.5	2.0
Oxygen content (%)	0.0	21.0
Carbon dioxide content (%)	0.0	0.1
Stirring frequency (per day)	0	8
Liquid saturated environment	No	Yes
Air and vapor saturated environment	No	Yes

*Dependent Variables - Gas permeability, Liquid permeability, Friability, Porosity

TABLE 3. Test Matrix for Screening Experiments

Trial	Pressure (bars)	Temperature (°C)	Time (mths)	Oxygen (%)	CO_2 (%)	Stirring (Yes-No)	Liquid (Yes-No)	Vapor (Yes-No)	Permeability (% Change) Gas	Permeability (% Change) Liquid	Friability Index (% Change)
1	120	300	0.5	21	0.1	Y	N	N	↓03	00	↑ 27
2	120	50	2.0	21	0.1	N	N	N	↓02	↓04	↑ 41
3	60*	300	2.0	21	0.0	N	N	Y	↑31	↑78	↑ 222
4	120	300	2.0	0	0.0	N	Y	N	↑65	↑73	↑ 474
5	120	300	0.5	0	0.0	Y	N	Y	↑76	↑38	↑ 185
6	120	50	0.5	0	0.1	N	Y	Y	↓17	↑37	↑ 29
7	60	50	0.5	21	0.0	Y	Y	N	↓03	↓08	↑ 43
8	60	50	2.0	0	0.1	Y	N	Y	↑18	↑31	↑ 26
9	60*	300	0.5	21	0.1	N	Y	Y	↑96	↓36	↑ 171
10	120	50	2.0	21	0.0	Y	Y	Y	↓11	↑51	↑ 61
11	60*	300	2.0	0	0.1	Y	Y	N	↑12	↑28	↑ 480
12	60	50	0.5	0	0.0	N	N	N	↓02	↓14	↑ 31

*Actual pressure increased to prevent flashing

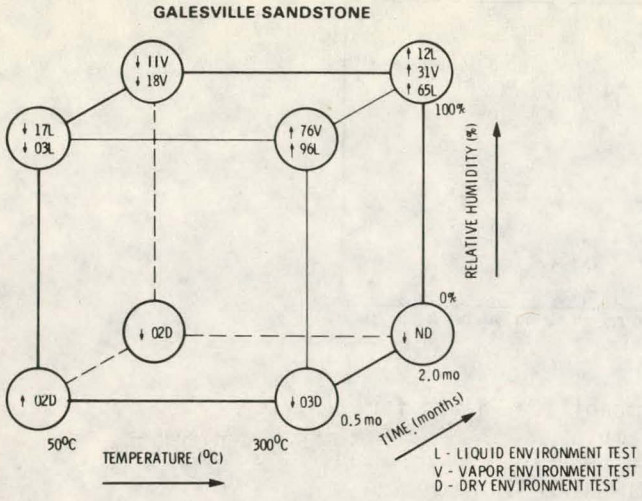

Fig. 7. Air Permeability Percent Change Without Gold Shielding

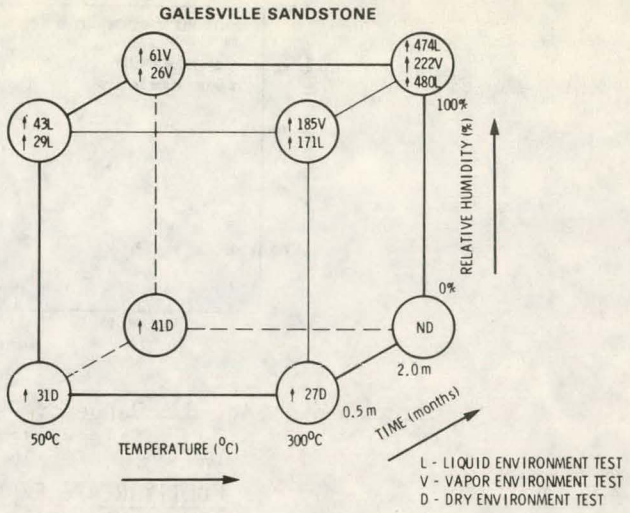

Fig. 8. Friability Index Percent Change Without Gold Shielding

DATA ANALYSIS AND CONCLUSIONS

Figs. 9 through 11 present data on the effects of temperature on apparent porosity, gas permeability, and "friability". The triangular symbols are the dry air tests, the open circles are the brine tests and the closed circles are the humidified air tests. During the course of the investigation it was discovered that in the humidified air experiments, vapor was condensing on the roof of the pressure vessel, dripping onto the core, and presumably dissolving the sandstone cement. This chemical dissolutioning resulted in subsequent disaggregation of the sample, increased "friability", and increased permeability. To prevent this anomalous effect, the specimen was shielded from the condensate by gold foil as shown in Fig. 12. For the specimen on the left, the corner of the shield was purposely placed in contact with the rock and the resulting dissolution is apparent. The specimen on the right, however, is adequately protected from the condensate and reveals good visual appearance even after treatment with humidified air. Results from the "gold shield" experiments all fall within the arbitrary stability zones shown in the figures. Those humidified air tests without shielding resulted in the anomalous data points outside the stability zone.

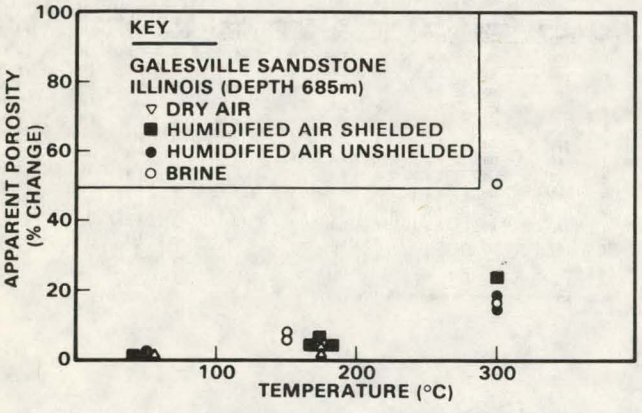

Fig. 9. Percent Change in Apparent Porosity with Temperature

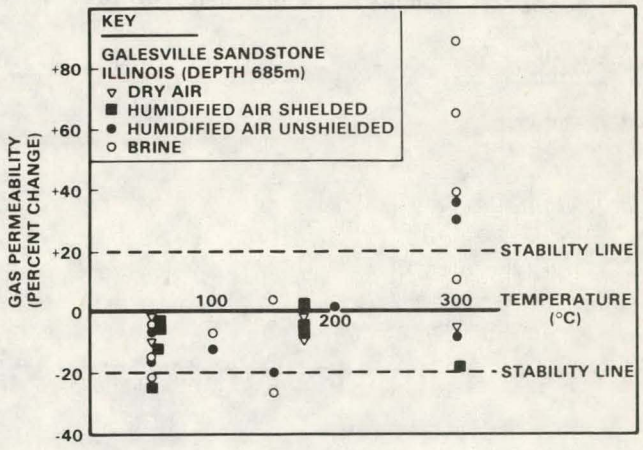

Fig. 10. Percent Change in Gas Permeability with Temperature

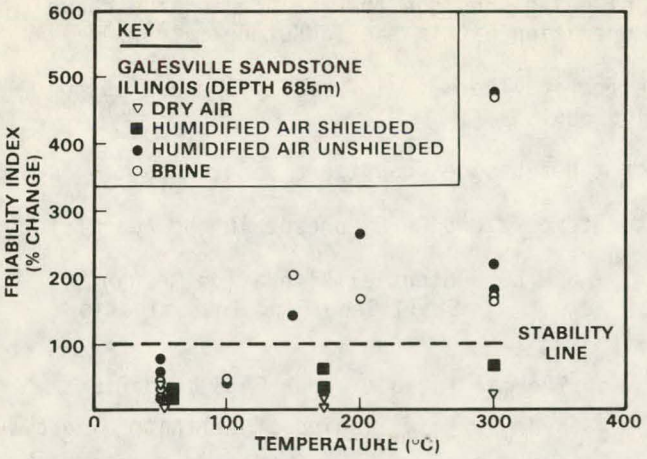

Fig. 11. Percent Change in the Friability Index with Temperature

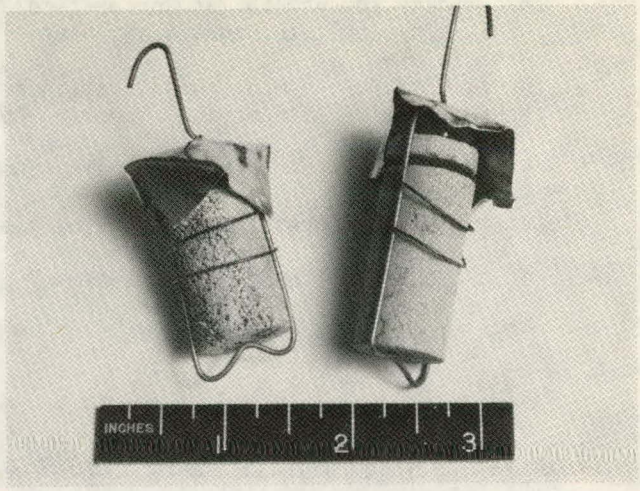

Fig. 12. Left-Condensate Dissolutioning Right-Totally Shielded Core

Based on preliminary autoclave data the following is concluded:

1. Samples exposed to dry air demonstrate excellent stability under all autoclave test conditions.

2. Samples exposed to humidified air also support good property stability. However, the nature of autoclave experiments and the length of the tests are such that the possibility of hydrolytic weakening and time delayed grain dislocations can not be presently dismissed. Similarly, the phenomenon of thermal fatigue may require investigation.

3. Unconfined samples exposed to heated brine reveal increased friability probably due to dissolutioning of the intergranular cement. This disaggregation could result in increased permeability; however, it is possible that the dislodged particles may ultimately reduce the permeability by plugging the formation.

4. Statistically meaningful conclusions are not possible based on existing autoclave data.

SUMMARY RECOMMENDATIONS

Based on literature reviews, consultant interactions, laboratory investigation, and numerical modeling efforts, preliminary conclusions concerning sandstone property stability can be formulated. Currently, it is concluded that most of the potential alteration mechanisms identified previously[2] can be dismissed as insignificant for an adequately designed and operated CAES facility. Table 4 is a list of the potential alteration mechanisms that for one reason or another fall into this category.[3] Table 5 is a list of potential mechanisms that cannot be tabled at this point and require additional investigation. This includes thermal fatigue and hydrolytic weakening. Thermal fatigue refers to a reduction in material strength due to thermal stress cycling. Hydrolytic weakening refers to a reduction in strength due to water vapor induced chemical attack of silicate mineral bonds. If active, either or both mechanisms could conceivably result in the generation of particles or fines and subsequent reduction in permeability.

As a result of investigations to date, the following is recommended:

1. Quartzose sandstone should be subject to more extensive autoclave experiments in order to yield data of more statistical significance.

2. Investigate the phenomena of thermal fatigue and hydrolytic weakening in laboratory experiments designed to simulate anticipated field conditions.

3. Investigate the possibility of particulate plugging should either or both of the above mechanisms result in significant particle generation within the sandstone matrix.

4. Investigate porous media desaturation and effective thermal diffusivity properties to ensure validity of numerical modeling conclusions.

5. Extend analyses to other potential CAES rock types besides quartzose sandstones.

6. Initiate field investigations of the elevated temperature CAES concept in the near future.

TABLE 4. Potential Alteration Mechanisms Considered Unlikely Under CAES Conditions

- Clay swelling and dispersion
- Mineral dissolutioning and scaling
- Fluids incompatibility
- Increased compressibility
- Redox reactions
- Casing corrosion
- Well completion cement degradation

TABLE 5. Potential Alteration Mechanisms Still Requiring Investigation

- Thermal fatigue under CAES conditions
- Hydrolytic weakening of silicate minerals under CAES conditions
- Particulate plugging
- Thermo-mechanical plugging (marginal)

REFERENCES

1. L.E. Wiles, The Effects of Water on Compressed Air Energy Storage in Porous Rock Reservoirs. PNL-2869, Pacific Northwest Laboratory, Richland, WA, March 1979.

2. J.A. Stottlemyre and R.P. Smith, "Potential Air/Water/Rock Interactions in a Porous Media CAES Reservoir", PNL-SA-7284, Proceedings of the 1978 Mechanical and Magnetic Energy Storage Contractor's Review Meeting. CONF-781046, Luray, VA, Oct. 1978.

3. J.A. Stottlemyre, R.P. Smith and R.L. Erikson, Potential Physical and Chemical Property Alterations in a Compressed Air Energy Storage Porous Rock Reservoir. PNL-2974, Pacific Northwest Laboratory, Richland, WA, September 1979.

BIBLIOGRAPHY

J.A. Apps, E.L. Madsen and R.L. Hinkins, The Kinetics of Quartz Dissolution and Precipitation, 1978.

J.D. Blacic, Hydrolytic Weakening of Quartz and Olivine, Ph.D. Thesis, University of California, Los Anageles, CA, 1971.

J.J. Day, B.B. McGlothlin, and J.L. Huitt, Laboratory Study of Rock Softening and Means of Prevention During Steam or Hot Water Injection, Gulf Research & Development Co., Pittsburgh, PA, May 1967.

E.C. Donaldson, B.A. Baker and H.B. Carroll, Particle Transport in Sandstones, Energy Research & Development Administration, SPE 6905, 1977.

D.T. Griggs, "Hydrolytic Weakening of Quartz and Other Silicates", Geophys. J. Roy. Astron. Soc., 14: 19-21, 1967.

C.H. Hewitt, Analytical Techniques for Recognizing Water Sensitive Reservoir Rocks, Marathon Oil Co., Littleton, CO, August 1963.

T. Marshall and A. Hugill, "Corrosion by Low-Pressure Geothermal Steam", Corrosion by National Association of Corrosion Engineers, Vol. 13, May 1957, p. 329t.

G.W. Morey and J.M. Hesselgesser, The Solubility of Some Minerals in Superheated Steam at High Pressures, The Geophysical Laboratory, Carnegie Institution of WA, Washington, D.C., June 1951.

W.H. Somerton, A.H. El Shaarani and S.M. Moharak, "High Temperature Behavior of Rocks Associated with Geothermal Type Reservoirs", Preprint 4897, Soc. Pet. Engrs., April 1974.

W.H. Somerton and A.K. Mathur, "Effects of Temperature and Stress on Fluid Flow and Storage Capacity of Porous Rocks', Proceedings 17th Rock Mechanics Symposium, 1976.

J.A. Stottlemyre, Preliminary Stability Criteria for Compressed Air Energy Storage in Porous Media Reservoirs. PNL-2456, Pacific Northwest Laboratory, Richland, WA, June 1978.

J.A. Stottlemyre and R.P. Smith, "Potential Air/Water/Rock Interactions in a Porous Media CAES Reservoir", PNL-SA-7284, Proceedings of the 1978 Mechanical and Magnetic Energy Storage Contractors' Review Meeting. CONF-781046, Luray, VA, Oct. 1978.

R.M. Weinbrandt, H.J. Ramey, Jr., F.J. Casse', "The Effect of Temperature on Relative and Absolute Permeability of Sandstones", SPE 4142, Soc. Pet. Eng. J., July 1975.

THIS PAGE

WAS INTENTIONALLY

LEFT BLANK

PROJECT SUMMARY

Project Title:	Fluid/Thermal Analysis for Porous Media Reservoirs
Principal Investigator:	L.E. Wiles
Organization:	Pacific Northwest Laboratory P.O. Box 999 Richland, Washington 99352 (509) 946-2049
Project Goals:	Develop a two-dimensional (r-z geometry) model for dry porous media reservoirs to predict the reservoir pressure and temperature response under conditions of daily air mass cycling. Use this data to provide design guidelines for the efficient and stable operation of the reservoir. Provide the data to parallel efforts that also will provide such guidelines. These efforts are the structural analysis, experimental work, and field studies.
Project Status:	The model was applied to the parameters that entered the analysis by virtue of inclusion of the vertical dimension. These parameters included the wellbore heat transfer and conditions that caused vertical flow perturbation in the porous zone. The analysis of these parameters was completed and a topical report should be available soon.
Contract Number:	EY-76-C-06-1830
Contract Period:	FY1979
Funding Level:	$94K
Funding Source:	Department of Energy, Division of Energy Storage Systems

TWO-DIMENSIONAL FLUID AND THERMAL ANALYSIS OF DRY POROUS ROCK RESERVOIRS FOR CAES

L. E. Wiles
Pacific Northwest Laboratory
Richland, Washington 99352

ABSTRACT

The analysis of the hydrodynamic and thermodynamic response of a Compressed Air Energy Storage (CAES) dry porous media reservoir subjected to daily air mass cycling is described. The analysis is based upon a numerical computer model that uses a finite difference method to solve the two-dimensional (r-z) conservation equations for the transport of mass, momentum, and energy in the below ground system. The investigation quantifies the behavior of those parameters that enter the model by virtue of inclusion of the vertical dimension. The topics that were evaluated were the wellbore heat transfer and the pressure and temperature response of the reservoir. The wellbore heat transfer was evaluated with respect to insulation, preheating (bubble development with heated air), and air mass flow rate. The wellbore heat transfer reduces thermal energy recovery while offering the advantage that the temperatures and thermal cycling at the reservoir were reduced. The most severe thermal cycling occurred in the wellbore near the earth surface. The pressure and temperature responses of the reservoir were found to be largely dependent on the producing length of the wellbore within the porous zone. Reduced producing lengths resulted in increased reservoir pressure losses as well as nonuniform temperature distributions. Other reservoir parameters that were evaluated that had less significant effects were anisotropic permeability and stratified permeability, heat losses to the vertical boundaries, and natural circulation.

INTRODUCTION

The analysis of the hydrodynamic and thermodynamic response of CAES porous media reservoirs subjected to daily air mass cycling is intended to provide design guidelines for the efficient and stable operation of the air storage reservoir. Previous investigations performed at PNL[1,2] have been based on one-dimensional (radial) modeling. Several parameters were subsequently identified that required two-dimensional (radial, vertical) modeling to be able to quantify their effect on reservoir performance. These parameters included heat transfer between the wellbore and the caprock and overburden, heat transfer between the porous zone and its vertical boundaries, natural circulation in the porous zone, anisotropic and stratified material properties (specifically, permeability) and the producing length of the wellbore. The two-dimensional model and the analysis of these parameters is the subject of this paper.

THEORETICAL DEVELOPMENT

BASIC ASSUMPTIONS AND GOVERNING EQUATIONS

The important basic assumptions that were applied to this analysis are:

- The fluid and solid phases are in local thermal equilibrium.
- The transport of mass, momentum, and energy occurs in the radial and vertical directions.
- The reservoir and the air are dry.
- The Darcy equation for low velocity flow is applied.

Additional assumptions are described in a topical report to be issued by PNL. The application of these assumptions results in the following set of equations that describe the transport of mass, momentum and energy in the reservoir.

- Conservation of mass

$$\frac{\partial}{\partial t}(\phi\rho) + \frac{1}{r}\frac{\partial}{\partial r}(r\phi\rho u) + \frac{\partial}{\partial z}(\phi\rho w) = 0 \qquad (1)$$

- Conservation of momentum in the radial direction

$$\left(\frac{\mu\phi}{k_r\rho}\right)(\phi\rho u) = -\phi\frac{\partial P}{\partial r} \qquad (2)$$

- Conservation of momentum in the vertical direction

$$\left(\frac{\mu\phi}{k_z\rho}\right)(\phi\rho w) = -\phi\frac{\partial P}{\partial z} + \phi\rho g_z; \quad \text{and} \qquad (3)$$

- Conservation of energy

$$\frac{\partial}{\partial t}\left\{(1-\phi)\rho_s C_s T + \phi\rho C_v T\right\} + \frac{1}{r}\frac{\partial}{\partial r}(r\phi\rho u C_p T) + \frac{\partial}{\partial z}(\phi\rho w C_p T) - \frac{1}{r}\frac{\partial}{\partial r}\left(rK_r\frac{\partial T}{\partial r}\right) - \frac{\partial}{\partial z}\left(K_z\frac{\partial T}{\partial z}\right) = 0 \qquad (4)$$

A definition of nomenclature is given in Table 1.

BOUNDARY CONDITIONS

The reservoir geometry used in this study is shown in Fig. 1 where the region of influence of a single well is shown as a vertical cylinder with the wellbore at the center. The applicable regions of the overburden, caprock, porous rock and basement rock are shown. The producing length of the wellbore is the section of the wellbore in the porous zone through which air can pass. At the wellhead the mass flow rate is continuously specified. During the reservoir charge cycle the temperature is specified. During reservoir discharge or when the reservoir is closed, the temperature at the wellhead is obtained from local equilibrium conditions. The outer radial boundary of the single well reservoir is insulated to the transport of mass and energy. The vertical boundaries of the porous zone are insulated to the transport of mass. The earth surface and the bottom of the basement rock are insulated to the transport of energy. The schedule for weekly air mass cycling is depicted in Fig. 2.

REFERENCE CONDITIONS

The foundation of the analysis is a set of reference conditions for the reservoir geometry, material properties and operating conditions. The values given to these parameters are provided in Table 2. Unless otherwise specified, these values apply throughout the discussion of results.

SOLUTION

A detailed outline of the solution method of the governing equations will be provided in a topical report to be issued by PNL. Briefly, the solution is achieved with a numerical computer model which is based on finite difference techniques.

ANALYSIS AND RESULTS

The development of the multi-dimensional numerical model has provided the capability to investigate several important aspects of reservoir behavior that were previously beyond the consideration of the available one-dimensional models. The additional phenomena that could be evaluated were generally related to either the wellbore heat transfer problem or to those parameters that introduced vertical fluid and thermal perturbations in the porous zone.

TABLE 1. Nomenclature

C_s	-	Heat capacity of rock
C_p (C_v)	-	Constant pressure (constant volume) specific heat of air
g_z	-	Gravitational acceleration in vertical direction
k_r (k_z)	-	Permeability in radial direction (vertical direction)
K_r (K_z)	-	Effective thermal conductivity of porous rock in radial direction (vertical direction)
P	-	Pressure of air
r	-	Radial coordinate
t	-	Time
T	-	Temperature
u	-	Radial velocity of air
w	-	Vertical velocity of air
z	-	Vertical coordinate
ϕ	-	Porosity
ρ (ρ_s)	-	Density of air (rock)
μ	-	Viscosity of air

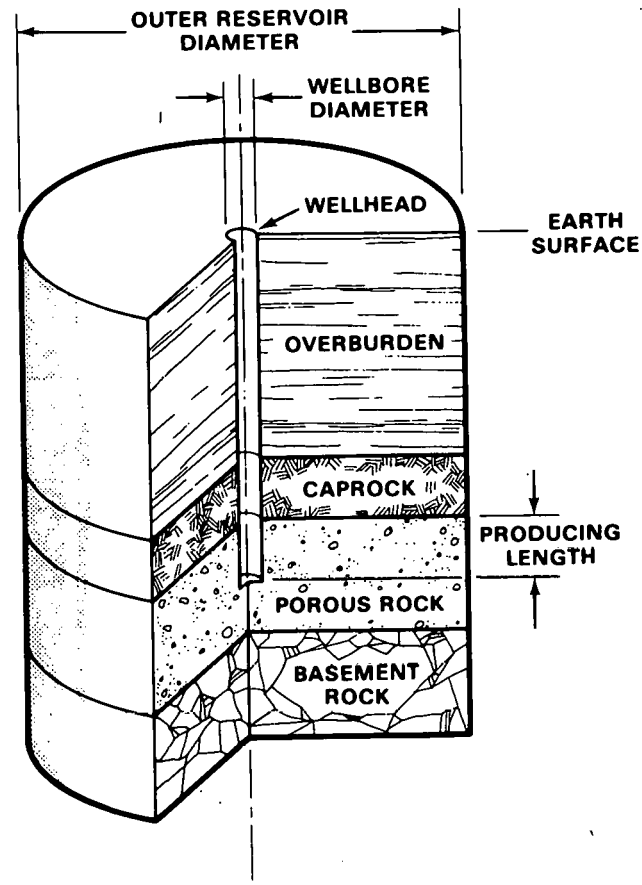

Fig. 1. Geometry for Two-Dimensional Analysis

TABLE 2. Reference Reservoir Conditions

Parameter	Reference Value	
Geometry		
Reservoir Depth	518.2 m	(1700 ft)
Vertical Thickness	30.5 m	(100 ft)
Reservoir Diameter	121.2 m	(400 ft)
Well Diameter	0.17 m	(7 in)
Completion Length	30.5 m	(100 ft)
Properties		
Porosity	20%	
Permeability	500 md	
Rock Thermal Conductivity	2.16 $\frac{W}{m \cdot °C}$	(1.25 $\frac{Btu}{hr\text{-}ft\text{-}°F}$)
Rock Thermal Capacity	2.62 $\frac{MJ}{m3 \cdot °C}$	(39.1 $\frac{Btu}{ft3\text{-}°F}$)
Operating Conditions		
Nominal Pressure	5070 kPa	(50 atm)
Air Flow Rate		
Injection	5.45 $\frac{kg}{sec}$	(12.0 $\frac{lbm}{sec}$)
Extraction	7.17 $\frac{kg}{sec}$	(15.8 $\frac{lbm}{sec}$)
Percent of Air Cycled	12%	
Injection Temperature	232°C	(450°F)
Earth Surface Temperature	21.1°C	(70°F)
Geothermal Gradient	0.0017°C/m	(0.001°F/ft)
Initial Reservoir Temperatures Determined by Geothermal Conditions		

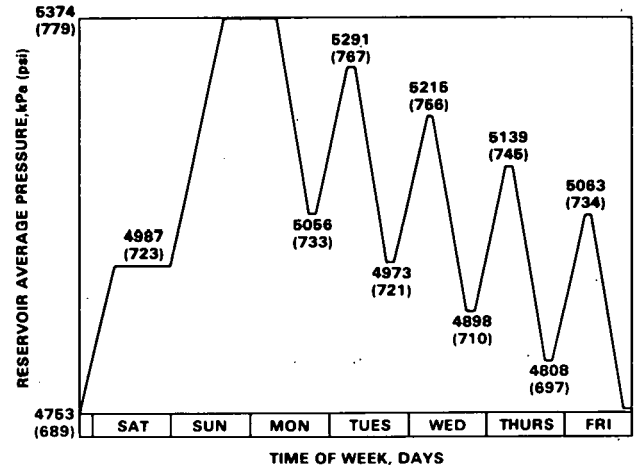

Fig. 2. Reference Weekly Reservoir Pressure Cycle

WELLBORE HEAT TRANSFER

Heat losses between the wellhead and the reservoir can have a significant impact on thermal energy recovery, thermal cycling, and thermal distributions. The parameters that were identified as having an impact on the wellbore heat transfer included wellbore insulation, preheating, air storage volume and reservoir depth. Wellbore insulation involves the modeling of an annular region of insulating material around the wellbore. Preheating refers to the heating of the underground system by injecting heated air during bubble development. The air storage volume and reservoir depth will affect the optimum air mass flow rates and, therefore, the thermal energy entering the underground system. The depth also establishes the length over which the heat transfer may occur. To characterize the thermal response for these parameters, six cases were defined for analysis. These are outlined in Table 3. Each case was simulated for 1-yr of air mass cycling. Only the results for the insulated and preheated conditions are provided here. The cases involving storage volume and depth (cases 5 and 6, respectively) basically only involve the rate of thermal energy entering the underground system. This will affect the magnitude of the results compared to the reference conditions but the same characteristic behavior is observed. Details of the analysis of these parameters is left to the topical report to be issued by PNL.

TABLE 3. Parametric Cases for Wellbore Heat Transfer Analysis

Case	Initial Thermal Conditions	Wellbore Insulation	Reservoir Depth (m)	Reservoir Depth (ft)	Reservoir Thickness (m)	Reservoir Thickness (ft)	Other Conditions
1	Geothermal	No	518.2	(1700)	30.5	(100)	Reference
2	Preheated	No	518.2	(1700)	30.5	(100)	
3	Geothermal	Yes	518.2	(1700)	30.5	(100)	
4	Preheated	Yes	518.2	(1700)	30.5	(100)	
5	Geothermal	No	518.2	(1700)	61.0	(200)	Double Air Mass Flow Rates
6	Geothermal	No	1036.3	(3400)	30.5	(100)	Double Air Mass Flow Rates

A summary of the results for the thermal energy recovery is shown by Fig. 3. The results are compared with the results obtained by the one-dimensional model which employed essentially the same reservoir and operating conditions. The one-dimensional result essentially represents, for comparative purposes, a perfectly insulated wellbore.

Thermal cycling of the air in the wellbore during the first week of simulated reservoir operation is shown in Fig. 4 for the reference conditions. Thermal development doesn't change the shape of the cycles although the amplitude of the cycles diminishes and the temperatures generally increase in time.

Insulation

The insulation is represented by a 10.2 cm (4.0 in) annulus with an I.D. of 20.3 cm (8.0 in). The conductivity of the insulation was 0.216 W/m-°C (0.125 Btu/hr-ft-°F). The volumetric heat capacity of the insulation ($\rho_i C_i$) was 0.724 MJ/m^3-°C (10.8 Btu/ft^3-°F).

Thermal cycling of the air in an insulated wellbore is shown in Fig. 5 for the first week of simulated reservoir operation. The interesting point of this result is that the thermal cycling of the air in the wellbore is actually greater for the insulated case than for the reference case for which there is no insulation. One explanation that serves to support this result is based upon consideration of the controlling heat transfer medium. During a charging cycle the heat transfer between the air in the wellbore and the surrounding material is controlled by the heat conductance of the surrounding material. During reservoir closure the heat transfer is controlled by the low conductance of the air in the wellbore. Also, this cycling only represents the cycling of the air temperature in the wellbore. The heat capacity of the surrounding material is so large by comparison to the heat capacity of the air that the

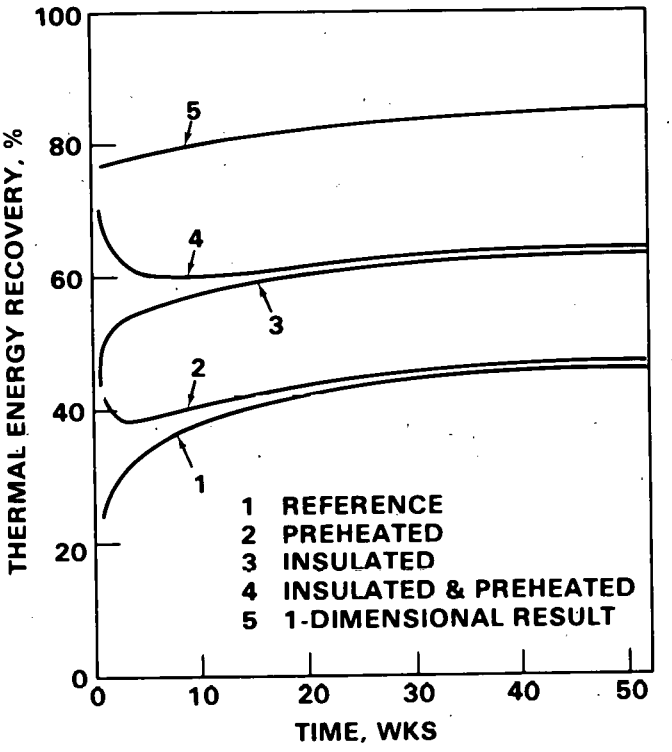

Fig. 3. Effect of Wellbore Heat Transfer on Thermal Energy Recovery

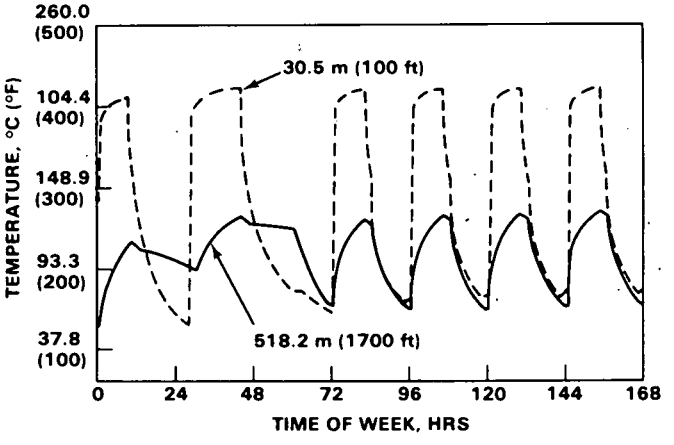

Fig. 4. Thermal Cycling in the Reference Reservoir, Week 1

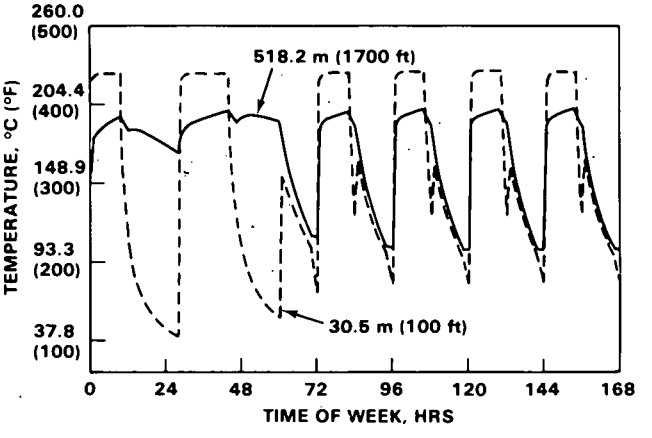

Fig. 5. Thermal Cycling for an Insulated Wellbore, Week 1

amplitude of the thermal cycling in the surrounding material decreases rapidly from the surface of the wellbore.

Preheating

In Fig. 3 the effects of preheating are shown by curves 2 and 5 which should be compared to curves 1 and 4, respectively. The effects of preheating on thermal energy recovery are seen to dissipate after only about 20 weeks. In addition to the initial improvement of thermal energy recovery, preheating reduces the amplitude of the initial thermal cycling although temperatures are generally higher. However, the effects of preheating dissipate rapidly so that after 1 year the thermal cycling of the preheated case is indistinguishable from the nonpreheated case.

RESERVOIR ANALYSIS

The reservoir analysis was intended to characterize the fluid and thermal response of the reservoir to conditions that were encountered in the porous zone by virtue of inclusion of the vertical dimension. The principal measure of the fluid response was the quasi-steady-state difference between the wellbore boundary pressure and the reservoir average pressure. This pressure difference represents the work required to overcome fluid friction in the porous zone. The thermal response that was of interest was the temperature distribution. In general, factors which perturb the flow field and the resultant quasi-steady-state pressure difference also affect the temperature distributions because the primary mode of energy transport is by convection.

Pressure Response

The parameters that were identified as important to the pressure response that required the inclusion of the vertical dimension to permit their evaluation were the producing length of the wellbore, and anisotropic and stratified permeability. The producing length of the wellbore proved to be the more important of these parameters. In Fig. 6 the quasi-steady-state pressure difference is plotted against the permeability ratio. The large effect of the producing length on the pressure loss suggests that the flow area at the wellbore-porous material interface is extremely important. At this interface the porous zone flow velocities are at their maximum values. The series of lines in Fig. 6 are drawn for various producing lengths in a 30.5-m-thick (100-ft-thick) reservoir. The producing lengths begin at the top of the porous zone.

The large effect of the producing length on the pressure loss suggests that the flow area at the wellbore-porous material interface is extremely important. At this interface the porous zone flow velocities are at their maximum values. These flow velocities dominate the reservoir pressure loss. The results dealing with producing length suggest the importance of extending the producing section of the wellbore through the entire reservoir thickness, to the extent possible, to avoid excessive flow losses.

The results shown in Fig. 6 suggest that the permeability ratio has a much smaller impact on pressure loss in the reservoir. For these cases the horizontal permeability was fixed at 500 md. Since flow from the wellbore is predominantly radial, for the case of the producing length being equal to the reservoir thickness, there is no noticable effect of the reduced vertical permeability on the pressure response. For producing lengths less than reservoir

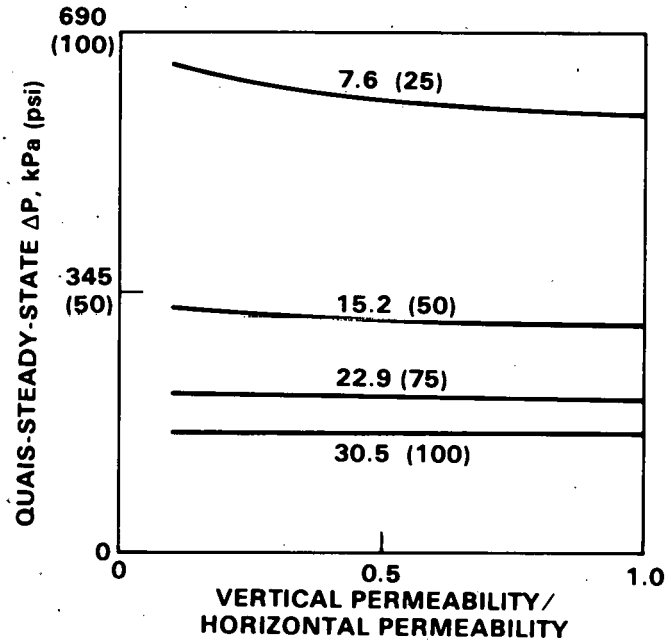

Fig. 6. Quasi-Steady-State Pressure Difference Versus the Permeability Ratio for Various Producing Lengths m (ft), Reservoir Thickness = 30.5 m (100 ft)

thickness, a portion of the air must expand vertically after entering the porous zone. As the air moves away from the wellbore, the vertical flow area increases dramatically so that vertical flow velocities are small. As a result, the contribution of the vertical flow to the pressure drop is small even for cases of significantly reduced vertical permeability and reduced producing lengths.

The effects of stratification of permeability were evaluated by modeling a 3.81-m-thick (12.5-ft-thick) layer of 100 md material, the top of which was 15.2 m (50 ft) from the top of the porous zone. The surrounding material was fixed at 500 md. A series of cases were evaluated whereby the producing length of the wellbore, beginning at the top of the porous zone, terminated above, within, and below the low permeability layer. The effect on the pressure response for these cases was similar in magnitude to the effect of the permeability ratio.

Thermal Response

Since the primary mode of energy transport in the porous zone is by forced convection, the thermal behavior of the porous zone will be largely determined by the mass transport. Factors affecting the mass transport that would affect the radial uniformity of the flow and that required the two-dimensional modeling for analysis included the producing length of the wellbore and stratified permeability. In addition, phenomena is present, even in homogeneous reservoirs, that adds to the maldistribution of thermal energy in the reservoir. These include natural circulation, heat losses to the vertical boundaries and non-uniform flow distribution from the wellbore. However, these additional effects are of less importance. A discussion of their analysis will be provided in the topical report to be issued by PNL.

An example of the effect of the flow disturbance on the thermal distribution is shown in Fig. 7 where vertical temperature profiles for various radii are shown for the reference reservoir and for a case in which the producing length is 7.62 m (25 ft). This flow disturbance concentrates the thermal energy at the top of the reservoir. The thermal energy concentration and the steep thermal gradients may present problems from the standpoint of the structural and geochemical stability of the reservoir. Figure 7 is composed of data taken during the first weekly cycle.

Even in the homogeneous reference reservoir vertical temperature gradients exist, as shown in Fig. 7. These result from non-uniform flow distributions caused by the headering effect of the wellbore. These temperature gradients, once developed, stablize quickly, apparently due to the balancing effect of other heat transfer mechanisms.

CONCLUSIONS AND RECOMMENDATIONS FOR FURTHER STUDY

The results of the computer analysis have led to quantification and characterization of certain behavior of the underground CAES system that could only be addressed by a multi-

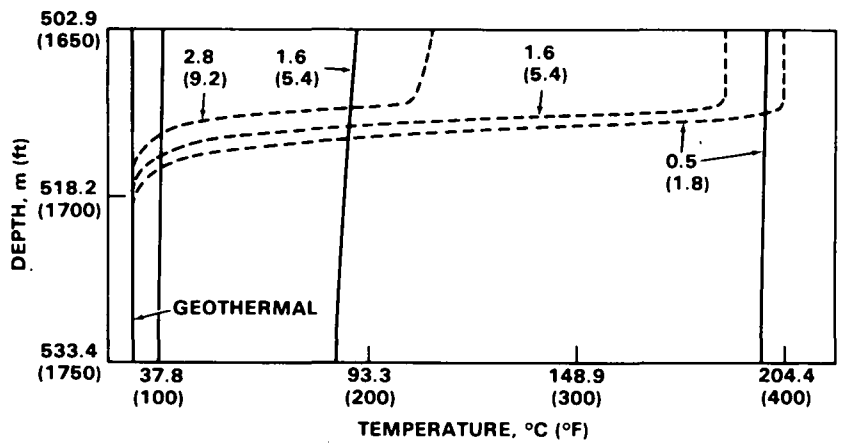

Fig. 7. Vertical Temperature Distributions at Various Radii (m (ft)) for Producing Lengths of 30.5 m (100 ft) (Solid Lines) and 7.62 m (25 ft) (Dashed Lines)

dimensional model. According to the results obtained by the numerical modeling, the following statements can be made regarding the effects of the vertical parameters of the reservoir. With regard to wellbore heat transfer:

- The recovery of thermal energy can be significantly reduced due to heat losses in the wellbore.
- Wellbore thermal insulation was shown to provide significant potential for improving thermal energy recovery.
- Heat losses from an uninsulated wellbore reduce the thermal cycling and lower the temperature in the porous zone.
- While wellbore insulation improves thermal energy recovery, the wellbore and porous zone are exposed to greater extremes of thermal cycling and higher temperatures.
- Preheating the reservoir may result in significantly improved thermal energy recovery and reduced thermal cycling during the initial weeks of reservoir operation.
- The effects of preheating are rapidly dissipated.

With regard to thermal behavior in the porous zone:

- The most important factor in determining the thermal distribution in the porous zone is the forced convection flow field.

With regard to the fluid behavior in the porous zone:

- The producing length should be maximized to avoid excessive pressure losses.
- Reduced vertical permeability does not significantly affect the overall pressure loss in the porous zone.
- Stratification of permeability has a greater effect on pressure loss in the reservoir when the producing section extends through the layer.

The results of this investigation led to the next phase of model development. The importance of the producing length of the wellbore with regard to reservoir pressure loss was shown. For porous zones having a liquid phase water boundary below the air storage zone, the producing length will necessarily be less than the storage zone thickness. This will be required to prevent the production of water in the wellbore due to water coning. The degree of water coning will depend on such parameters as producing length, air mass flow rates, permeability/saturation relationships, storage zone thickness, and water zone thickness. Development of the model and the analysis of these and other subsequently identified parameters will constitute the next step of this research effort.

REFERENCES

1. G.C. Smith, L.E. Wiles and W.V. Loscutoff, Numerical Analysis of Temperature and Flow Effects in a Dry, One-Dimensional Aquifer Used for Compressed Air Energy Storage. PNL-2546, Pacific Northwest Laboratory, Richland, WA, February 1979.
2. L.E. Wiles, The Effects of Water on Compressed Air Energy Storage in Porous Rock Reservoirs. PNL-2869, Pacific Northwest Laboratory, Richland, WA, March 1979.
3. G.C. Smith and L.E. Wiles, "Analysis of Underground Porous Reservoirs for Compressed Air Energy Storage", Proceedings 1978 Compressed Air Energy Storage Symposium, Vol 1, Pacific Grove, CA, 1978.

THIS PAGE

WAS INTENTIONALLY

LEFT BLANK

PROJECT SUMMARY

Project Title: "Testing of Galesville Sandstone under Compressed Air Storage Conditions"

Principal Investigator: James D. Blacic

Organization: Geological Research Group, G-6
Los Alamos Scientific Laboratory
P. O. Box 1663, MS 978
Los Alamos, NM 87545
FTS 843-6815

Project Goals: To determine the thermomechanical properties of Galesville sandstone at temperatures, pressures and cyclic stresses appropriate to an aquifer compressed air energy storage system.

Project Status: Laboratory tests have demonstrated that the elastic and strength properties of Galesville sandstone are temperature and pressure dependent. Young's modulus varies in a nonlinear fashion with respect to differential stress and effective confining pressure. Modulus increases with increasing effective pressure over the range 0-31 MPa, and with increasing temperature over the range 37-120°C. Poisson's ratio decreases markedly to values as low as 0.1 with both increasing effective pressure and increasing temperature.

Preliminary tests indicate that compressive strength variation with effective pressure can be expressed in terms of a linear Mohr-Coulomb relation at 37°C, but a nonlinear Mohn-Coulomb behavior is exhibited at 120°C.

The effect of cyclic compressive stress at 37°C on thermomechanical properties is mainly a strong reduction in Poisson's ratio. There is no apparent effect of cyclic loading on compressive strength or Young's modulus for up to 10,000 cycles of 20 MPa differential stress.

Contract Number: Battelle P.O.#63737-A-H, directed under "Reservoir Stability Criteria Studies," #C8-01-01-03-2 PNL 85002.

Contract Period: March, 1979 - Sept., 1980

Funding Level: $133K

Funding Source: Battelle PNL, Energy Programs Division

THERMO-MECHANICAL PROPERTIES OF GALESVILLE SANDSTONE

J. D. Blacic, P. H. Halleck, and P. D'Onfro
Geosciences Division, G-6
Los Alamos Scientific Laboratory
Los Alamos, New Mexico 87545

ABSTRACT

Elastic and strength properties of Galesville sandstone are temperature and pressure dependent over the range appropriate for an aquifer compressed air energy storage system. At 37°C, Young's modulus increases from 23 GPa at ambient pressure to 47 GPa at 31 MPa effective pressure while Poisson's ratio decreases from 0.30 to 0.22. At 120°C, Young's modulus increases from 28 GPa at ambient pressure, to 60 GPa at 33 MPa effective pressure while Poisson's ratio decreases from 0.22 to 0.08. Under ambient conditions, tensile strength is 4 MPa. At 37°C, ultimate compressive strength increases from 70 MPa at ambient pressure to 200 MPa at 32 MPa effective pressure. At 120°C, strength increases from 56 MPa at ambient pressure to 262 MPa at 30 MPa effective pressure. Cyclic loads of 20 MPa at 37°C and 10.4 MPa effective pressure indicate no effect on Young's modulus and ultimate strength up to 10,000 cycles; Poisson's ratio is reduced 28%.

INTRODUCTION

As part of the evaluation of water-saturated aquifers for a compressed air energy storage (CAES) system, we have determined elastic and strength properties of a sandstone. The goal of this work is to evaluate the effects of temperature, pressure, and cyclic loading on thermo-mechanical properties to support modeling studies of an aquifer CAES system.

The sample material is Cambrian Galesville sandstone from Warren County, Illinois obtained from Illinois Power Company cores. Reservoir analysis indicates that our samples range in permeability from 100 to 600 millidarcies and in porosity from 15 to 24%. The average grain size is approximately 0.1 millimeters. Composition is 98% quartz nonuniformly cemented by dolomite.

EXPERIMENTAL TECHNIQUE

Test samples are right circular cylinders 2.5 cm diameter by 6.3 cm long. Jacketed samples are tested in a triaxial, externally heated pressure vessel using silicone oil as pressure transmitting medium. Axial load is applied at a constant displacement rate with a servo-controlled hydraulic testing machine. Sample strains are determined with an internal system consisting of three axial and three radial LVDT displacement gages. Volume strain is calculated from the average axial and radial strains.

Normal test procedure is as follows: the jacketed sample is first saturated by pumping water through it at low pressure. Confining pressure is then applied followed by argon pore pressure and finally the sample is heated. The gas pore pressure is applied through a small separate reservoir. At temperatures above boiling, water vapor may pass

into this separate vessel from the sample and condense. In this way a relatively constant-humidity pore pressure is maintained during the test. This also simulates, to some extent, pressurization of an air bubble in a saturated reservoir. Differential stress is then applied at a constant displacement rate.

Displacement versus load records are digitized and stress-strain values are calculated and plotted. Tangent Young's modulus is determined by linearizing small segments of the stress-strain curves in a running least squares scheme and plotted versus stress. Poisson's ratio is determined in a similar way.

ELASTIC PROPERTIES

The stress-strain curves shown in Fig. 1 are typical of the mechanical response of Galesville sandstone. Young's modulus derived from the axial stress-strain curve is shown in Fig. 2. Typically, the modulus increases from a low value and stabilizes when about 25 percent of the failure stress is attained. The initial low value is mainly due to compliance of the sample-platten interface. The stable values are those reported below. As load increases towards failure Young's modulus continually decreases. Poisson's ratio derived from the test data of Fig. 1 is shown in Fig. 3. Again, values are unstable at low loads followed usually by a broad, stable region and then Poisson's ratio increases rapidly as failure is approached.

The variation of Young's modulus with temperature and effective pressure (confining pressure minus pore pressure) is shown in Fig. 4. At a given temperature, modulus increases by about a factor of two from ambient to 30 MPa effective pressure. This can

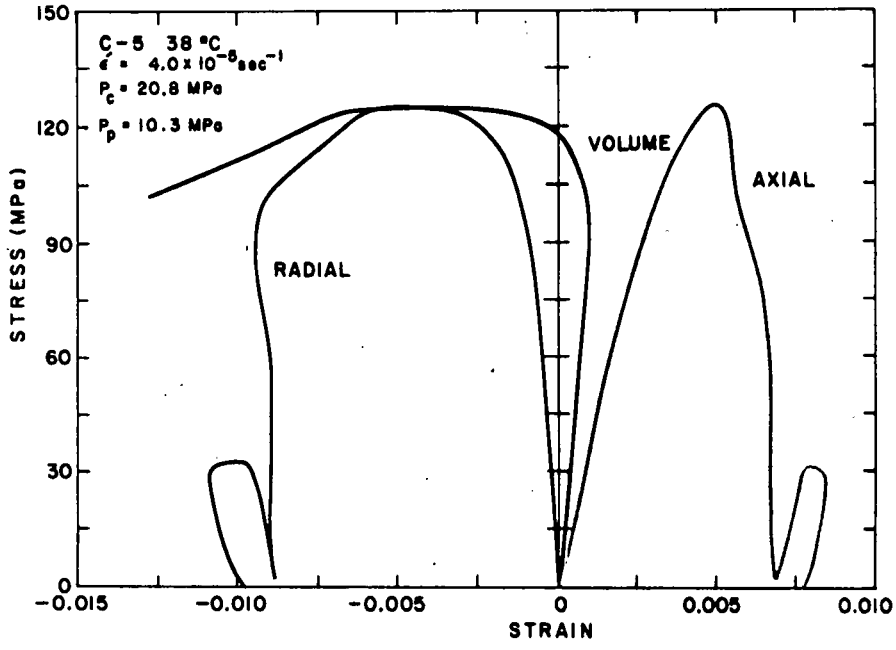

Fig. 1. Stress-strain curves for experiment #C-5; Galesville sandstone. $\dot{\epsilon}$ = strain rate, P_c = confining pressure, P_p = pore pressure.

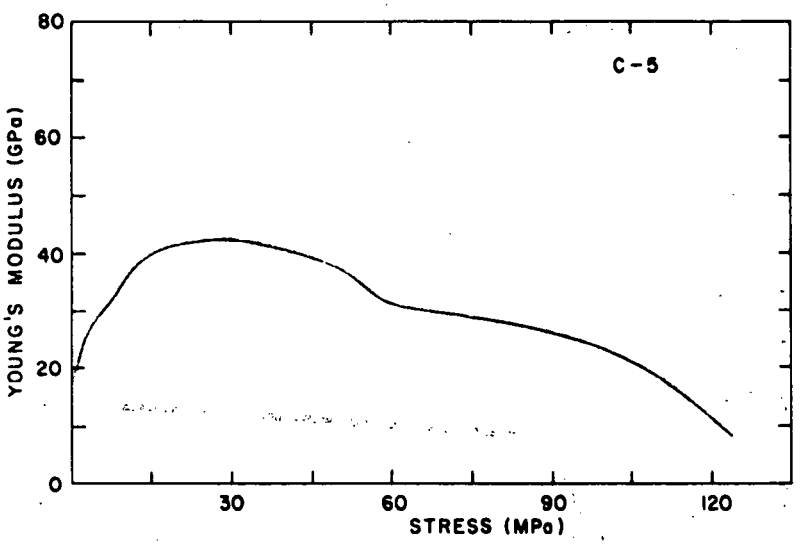

Fig. 2. Young's modulus as a function of differential stress for experiment #C-5.

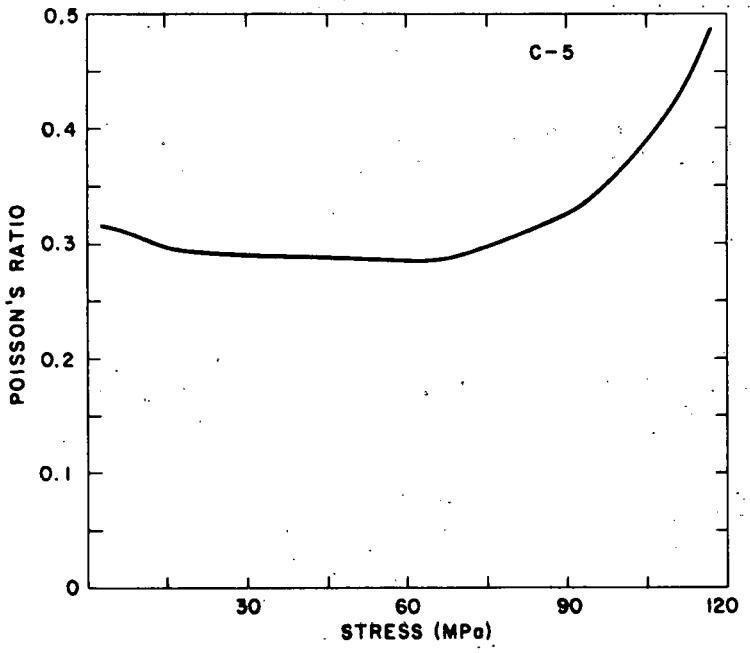

Fig. 3. Poisson's ratio as a function of differential stress for experiment #C-5.

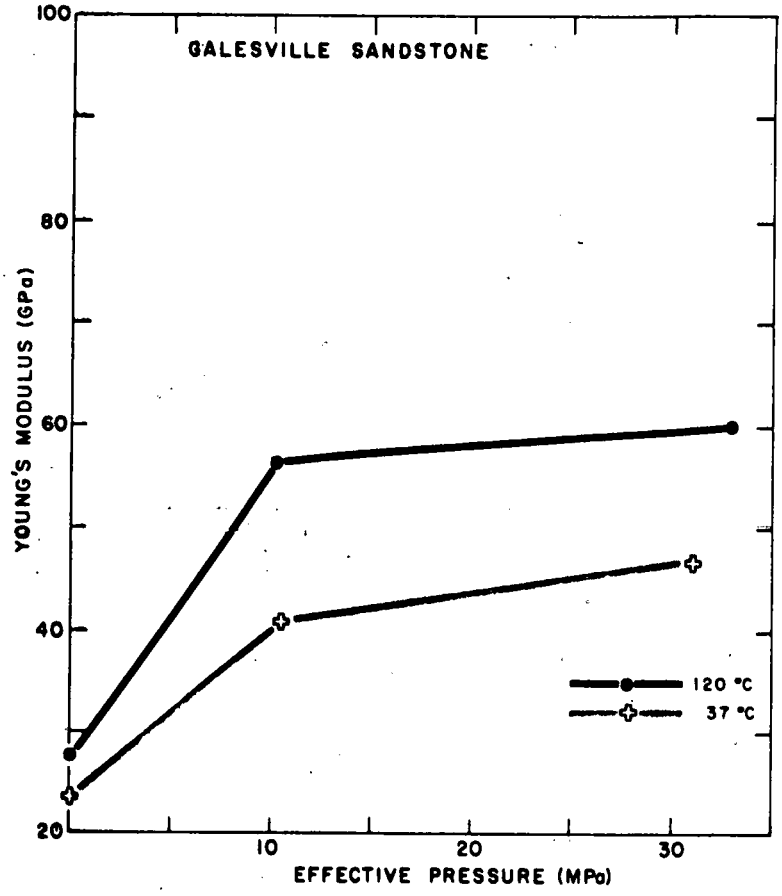

Fig. 4. Young's modulus of Galesville sandstone as a function of temperature and effective pressure.

reasonably be explained as being due to crack and pore closure at pressure. Somewhat surprisingly, modulus also increases substantially with increasing temperature. A possible explanation is that porosity is reduced as a result of differential thermal expansion but we have no evidence as yet that this is so.

Variation of Poisson's ratio with pressure and temperature is shown in Fig. 5. Poisson's ratio is significantly reduced by both increasing pressure and temperature. This suggests that at the maximum temperature and pressure conditions of a CAES environment very low values of Poisson's ratio are likely for this sandstone.

STRENGTH PROPERTIES

As shown in Fig. 1, failure of the samples is reflected in onset of nonlinear stress-strain behavior. There is substantial "plasticity" at the highest pressures and temperatures. Failure occurs by faulting on one or more inclined shear zones accompanied by considerable crushing and disaggregation. The effective principal stresses at the ultimate strength of each test is represented in Mohr circle plots in Figs. 6 and 7. At

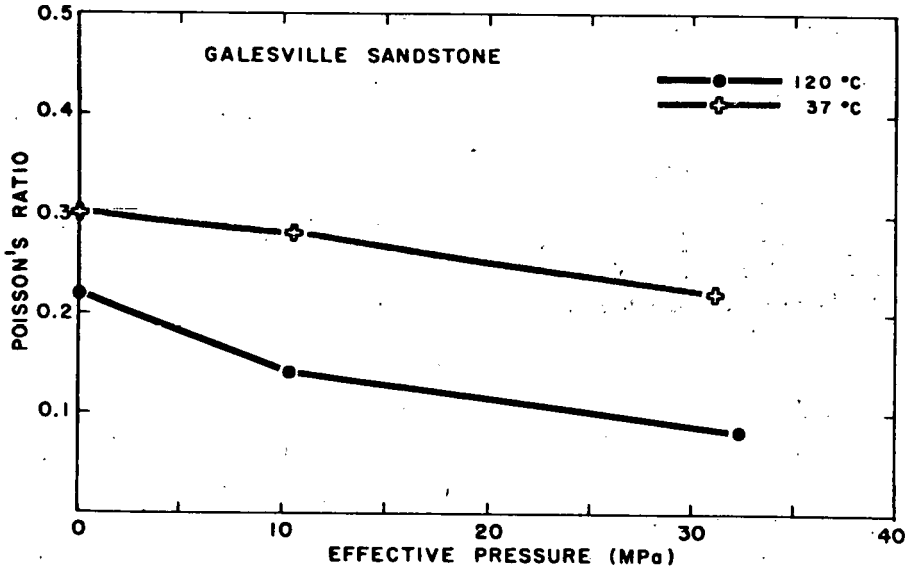

Fig. 5. Poisson's ratio of Galesville sandstone as a function of temperature and effective pressure.

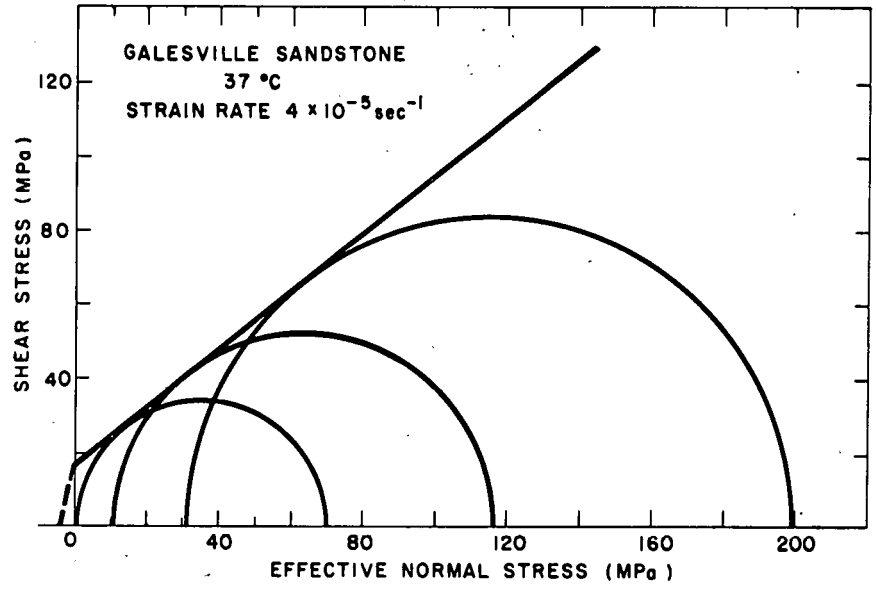

Fig. 6. Mohr circle diagram for Galesville sandstone at 37°C.

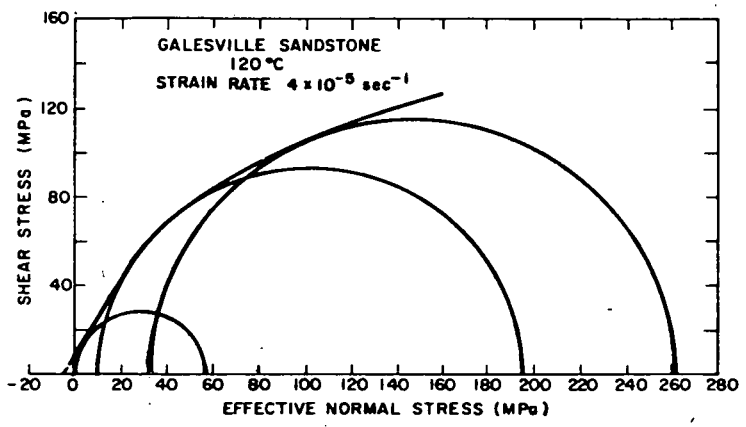

Fig. 7. Mohr circle diagram for Galesville sandstone at 120°C.

38°C, results are well represented by a linear Mohr envelope with a cohesion of 18 MPa and coefficient of internal friction of 0.78. However, at 120°C the Mohr envelope is highly nonlinear. Increasing temperature reduces the uniaxial strength but apparently increases the triaxial strength. In view of the limited amount of data, this result could be indicative of sample variability.

The tensile strength at ambient conditions was determined to be 4 $\pm$0.5 MPa. This is an average of 15 indirect measurements using the Brazilian test.

CYCLIC LOADING

The effects of cyclic loading have been evaluated at 37°C, 20.7 MPa confining pressure and 10.3 MPa pore pressure (Table 1).

TABLE 1. Stress Cycles of 20 MPa: Effect on Young's modulus (ΔE) and Poisson's Ratio ($\Delta\nu$)

Cycles	ΔE%	$\Delta\nu$%
100	+9	-6
1,000	0	-12
10,000	-1	-28

There is no consistent effect of a 20 MPa cyclic load on Young's modulus. The observed variation is judged to be due to sample variability. There appears to be a consistent reduction of Poisson's ratio due to cyclic loading with up to a 28% reduction at 10,000 cycles. No effect on ultimate strength was observed outside that judged to be due to sample variability.

THIS PAGE

WAS INTENTIONALLY

LEFT BLANK

PROJECT SUMMARY

Project Title:	Reservoir Stability - Structural Analysis for Porous CAES
Principal Investigator:	J.R. Friley
Organization:	Pacific Northwest Laboratory P.O. Box 999 Richland, Washington 99352 (509) 946-2295
Project Goals:	Acquire/develop analysis capabilities to treat the structural behavior of porous rock reservoirs subject to CAES type load conditions. Apply this capability in analyzing a generic site to assess the structural response and thus gain insight into potential areas of concern (or lack of same) regarding reservoir stability.
Project Status:	After briefly reviewing several modeling techniques (finite difference method, BIE method, finite element method), it was decided that the finite element method was the logical analysis tool to address porous structural modeling. An existing finite element program (ADINA) developed by K. Bathe of MIT was studied and subsequently modified to enable treatment of pore pressure structural effects. In addition, graphics enhancements were added. Utilizing this analysis tool, site loading conditions of a generic site were utilized to study site response during the first year of site operation. Tensile stresses were found to exist only in the cap rock region. The effects of this on reservoir performance, however, is as yet unknown. Fatigue stresses of any significant magnitude were found to exist only in the well bore vacinity. The significance of this behavior, however, cannot be assessed until (1) well casing/rock interaction capability has been added to the code, and (2) fatigue (at temperature) data becomes available. Porous rock stress levels were evaluated using Mohr Coulomb data for Galesville sandstone (100^{o}F) obtained from LASL. A safety factor of 3 resulted. "At temperature" MC evaluations have not as yet been made, however. In FY-80, the addition of well casing/rock interaction capability and the acquisition of "at temperature" material properties will substantially improve our response prediction capabilities.
Contract Number:	EY-76-C-06-1830
Contract Period:	FY1979
Funding Level:	$2,175K BO/$2,715K BA
Funding Source:	Department of Energy, Division of Energy Storage Systems

STRUCTURAL RESPONSE OF A GENERIC POROUS SITE

J. R. Friley
Pacific Northwest Laboratory
Richland, Washington 99352

ABSTRACT

Structural response of a hypothetical compressed air energy storage (CAES) porous rock site was investigated. Emphasis was placed on gross response of the porous rock site rather than detailed behavior in the wellbore vicinity. Structural loading conditions considered nonuniform thermal loading, pore pressure loading, in situ and overburden effects. Loading conditions corresponding to several stages of site development and operation were investigated.

Both mean and cyclic structural response of the reservoir were investigated by utilizing thermal and pore pressure loadings corresponding to various times of a one year thermal/flow simulation. Attention was focused on several areas of site structural behavior. These included tensile stress levels in the site caprock, fatigue stress levels in the cap and porous rock massess, and margin of safety values for the porous rock based upon a Mohr-Coulomb failure envelope for Galesville sandstone.

Results from these investigations indicate that zones of significant structural response are concentrated in the wellbore vicinity. This is especially true of the caprock mass and is attributed largely to the assumption of casing insulation made in the thermal/flow simulation.

INTRODUCTION

Structural response of a porous compressed air energy storage site is not as yet fully known. Undoubtedly, these response characteristics will depend heavily on influences which are site dependent. These influences include elastic and inelastic properties of the rock thicknesses, geometries of the rock forms involved, and placement techniques used during well completion.

In order to gain some insight into the structural behavior of such a site, computer based analyses of a hypothetical site have been performed. The purpose of this presentation is to describe these analyses and to indicate what response modes might be anticipated in an actual site based upon these results.

Structural features of a porous CAES site will now be described with reference to Fig. 1. Most likely, the porous reservoir to be used is initially saturated with water. If this is the case, then an initial drying period or "bubble development" will be necessary before cyclic operation of the site occurs. It is anticipated that this initial pressurization will be of moderate temperature and pressure levels and that no significant damage to the rock forms will occur.

After some initial charging, the reservoir will be loaded in a cyclic fashion by the utility. Hot pressurized air will be produced and stored during periods of excess generating capacity. During periods of peak demand, air will be drawn from the reservoir and utilized by some turbomachinery system for generation of additional power. It is anticipated that such a periodic operation will have both daily and weekly components.

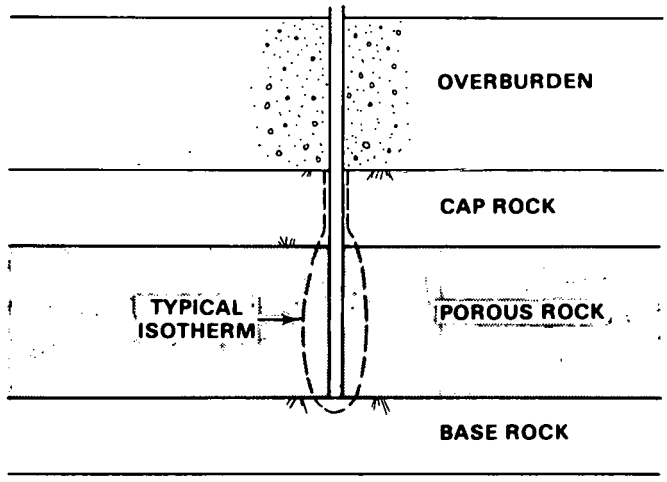

Fig. 1. Cross Sectional View of a Generic Porous Site

ANTICIPATED STRUCTURAL TRENDS

During the initial period of site operation, the temperature of the various rock masses will be very nearly equal to the ambient temperature at the site depth. During operation heated areas will be concentrated in the central regions of the site adjacent to the wellbore. For rock types felt to be suitable for applications such as this, air pressure in the porous zone will be quite uniform and is thought not to be a significant contributor to site loading.

Heated regions will be wider in the porous rock than in the cap rock since thermal energy is transferred by flow as well as conduction in this region. In addition, insulating grout material will likely be used in well completion to reduce thermal losses. As a result, typical isothermal contours will likely be as shown in Fig. 1. This heated region is likely to be small during initial periods of site operation and gradually increase in expanse as site operation continues.

In the porous zone, the heated central regions will expand against the cooler confining outer regions both axially and radially and give rise to central compressive stress levels. Some tensile hoop stress components in the outer region can thus be anticipated as a result of this behavior.

Vertical thermal expansion of this central core in the porous zone well bear against the cap rock. The effect this has on cap rock stress will depend to a large extent on the cap rock stiffness and perhaps more importantly, the stiffness of the overburden directly above the cap rock. For relatively weak overburden, this vertical loading will tend to cause tensile stress levels at the top surface of the cap rock due to flexure.

Since thermal effects are more pronounced in the porous zone than in the cap rock or base rock, some radial stretching of the cap and base rock regions can be anticipated due to radial expansion of the porous zone. This radial expansion will likely cause tensile hoop stresses in the cap and base rock regions and compressive stresses in the central porous zone.

In addition to stress contributions due to thermal and pore pressure loading, in-situ stress levels initially existing at the site depth will be a contributor to rock stresses. While in-situ stresses vary with geographic location, they are in general compressive (vertically and laterially) and tend to increase with site depth. Thus, tensile components caused by behavior modes described previously will likely be reduced partially or totally by in situ stress effects.

ANALYSIS DESCRIPTION

Structural investigations were performed for loading conditions incurred during the first year of simulated site operation. Thermal and pressure loading conditions used in these analyses were taken from independently performed thermal/flow investigations.[1] Thus, no coupling effects between the structural and flow modeling were considered. While this assumed decoupling might lead to questionable results for liquid flow cases, the assumption seems reasonable in view of the compressibility ratio of air to porous rock. Further discussions of flow in an elastic porous material may be found in references 2, 3, and 4.

The analysis procedure used to model structural behavior made use of the poro-elastic formulation (Ref. 2). In this formulation, stress-strain equations and equilibrium equations take the following form using indicial notation:

$$\sigma_{ij} = (Pf)\delta_{ij} + E_{ijkl}\,(\varepsilon_{kl} - \varepsilon_o\delta_{kl})$$

$$\varepsilon_o = \frac{1-2\nu}{E}\,(1 - \beta)P + \alpha T$$

$$\left[\sigma_{ij} - (Pf)\,\delta_{ij}\right],_j = 0$$

- σ_{ij} - stress tensor
- P - pore pressure
- E_{ijkl} - elasticity tensor
- δ_{kl}, δ_{ij} - Kronecker delta
- ε_{kl} - total strain
- ε_o - initial strain
- E - Young's modulus
- β - Bulk modulus ratio of porous rock to interpore material (assumed to be .25 after Reference 2)
- ν - Poisson's Ratio
- T - temperature above stress/strain free temperature
- f - rock porosity

The structural analyses performed made use of the finite element method.[5] The computer program used was a modified version of the ADINA code.[6,7] The axisymmetric model used with this program is shown in Fig. 2. All elements are quadratic isoparametric elements and two point Gaussian quadrature was used throughout. Initial calculations were performed with boundary conditions as illustrated in Fig. 2 and with material properties shown in Table 1.

Since the purpose of this investigation was to model gross reservoir response, the structural effects of the well casing were neglected and the central region was considered to be solid. It was felt that while this assumption will cause some inaccuracy in localized regions close to the wellbore, the overall response of the reservoir will only be slightly affected.

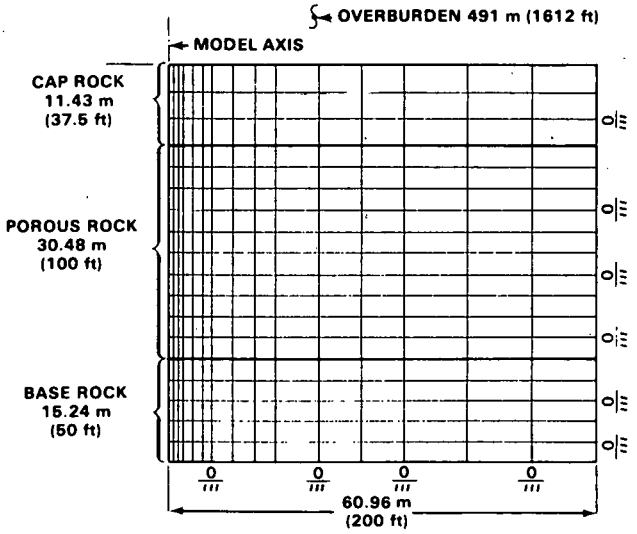

Table 1. Rock Properties

	Porous Rock	Cap Rock and Base Rock	
E (MPA)	3.0×10^4	3.2×10^4	(Ref. 9)
ν	.25	.25	(Ref. 9)
α ($°C^{-1}$)	10^{-5}	10^{-5}	(Ref. 9)
f	.20	--	

Fig. 2. Finite Element Mesh

In situ stress levels were simulated by using two methods. The first method utilized pressure loads (11.12 MPA) applied at the top surface of the cap rock. This produces a compressive lateral stress due to fixed constraints of the outer radius of the model. This method is likely to overestimate the amount of cap rock flexure due to vertical expansion of the porous zone. A second method used vertical restraints at the top surface of the cap rock in conjunction with superimposed in situ stresses equivalent to those resulting from using the first method.

Horizontal stress for this condition is equivalent to about a third of the vertical stress. Most geological data indicates that while vertical stresses are closely approximated by overburden weight, lateral stresses are often times greater than one third of the vertical stress. Thus the in situ stress assumptions should be conservative with respect to tensile stress prediction.

As previously mentioned, structural investigations were carried out for load conditions occurring at various times during a one year thermal flow simulation. Daily charging temperatures varied between 143°C and 204°C for this simulation period, and charging pressures varied between 4.48 MPA and 5.17 MPA. The reservoir temperatures occurring at the end of one week and one year are shown in Figs. 3 and 4, respectively. Here the growth of the thermally affected zones can be clearly seen. It should be mentioned that an additional plot of temperatures at week 26 of the simulation showed thermal distributions very similar to those of week 52. Thus, the rate of thermal growth seems to diminish with site operation.

Tensile stress results for the load conditions described are shown in Figs. 5 through 7. Figs. 5 and 6 show one week and one year results for the in situ conditions simulated by cap rock pressure loading. Fig. 7 shows the tensile stress field after one year assuming the top of the cap rock to be vertically restrained. Tensile stresses were observed only in the cap rock for all times and boundary conditions analyzed.

Some hoop tensile stress exists in the cap rock after only one week of simulated operation. The relatively large zone affected in Fig. 6 shows the effects of cap rock flexure stress caused by a larger heated zone in the porous rock after a year of simulation time. The tensile stress level is reduced substantially as shown in Fig. 7 by restraining the cap rock with vertical constraints along the top edge.

The severity of stress levels in the porous zone was assessed by comparing the state of stress with failure levels of the Mohr-Coulomb envelope shown in Fig. 8. This Mohr-Coulomb was obtained by testing Galesville sandstone (100°F) using confining pressures and pore pressures

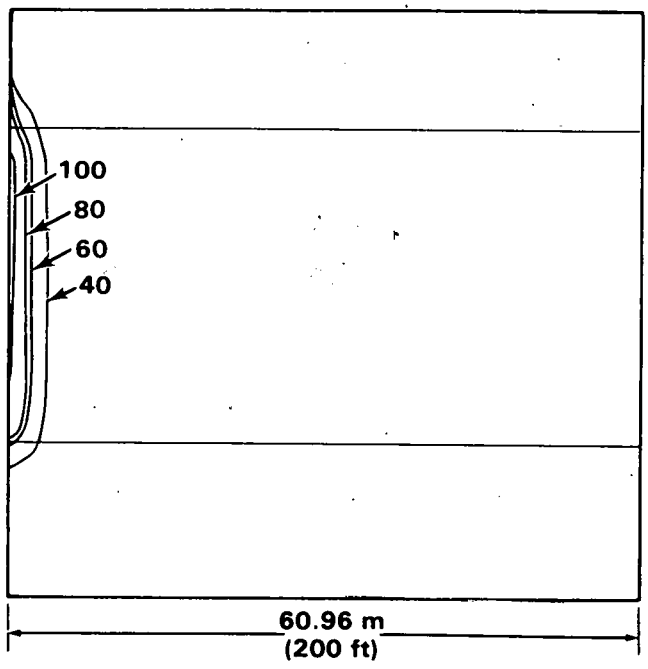

Fig. 3. Temperature Contours (°C) at the End of One Week

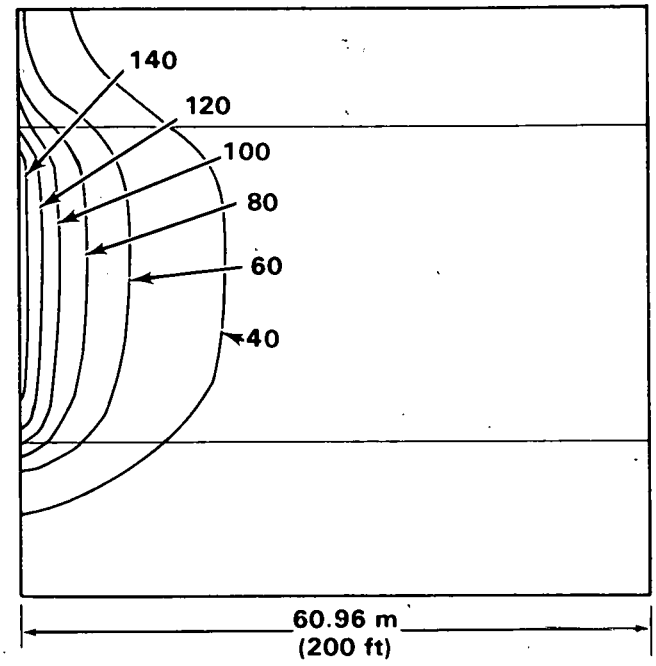

Fig. 4. Temperature Contours (°C) at the End of One Year

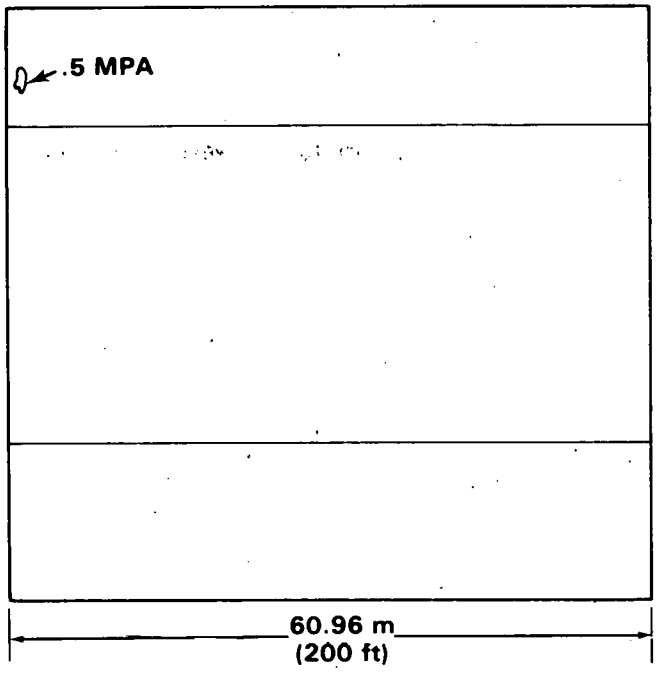

Fig. 5. Tensile Stress at the End of One Week

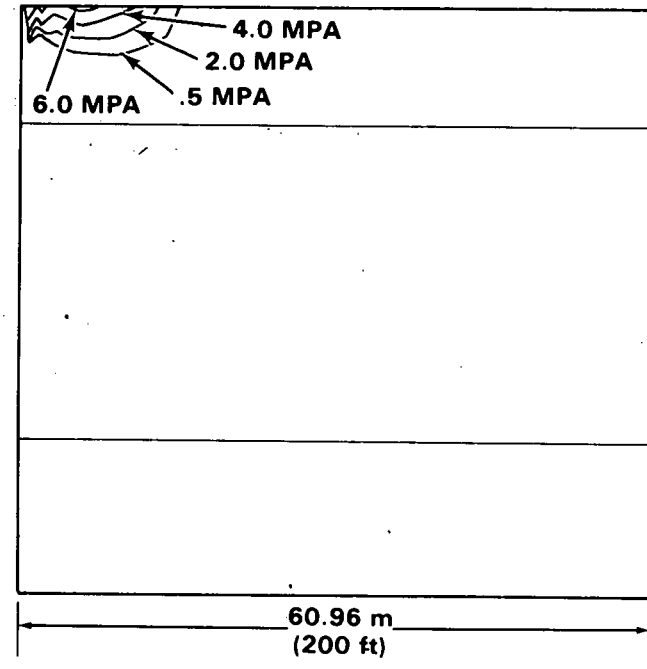

Fig. 6. Tensile Stress at the End of One Year

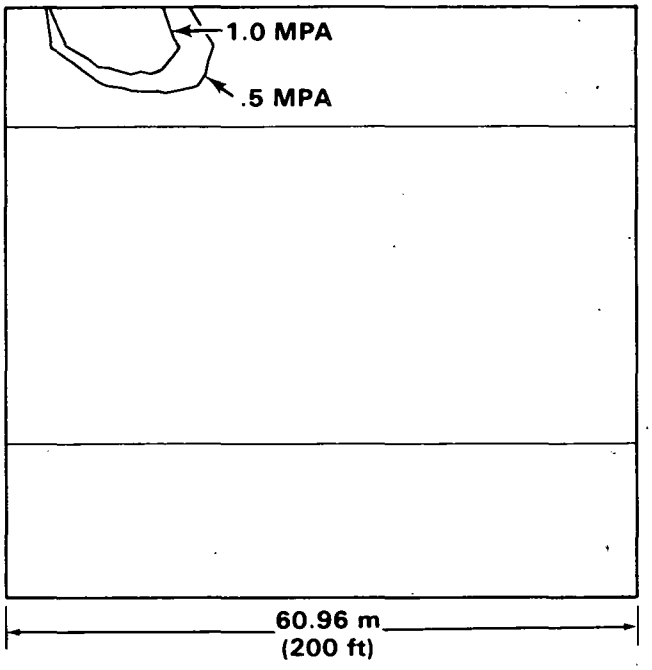

Fig. 7. Tensile Stress at the End of One Year (Cap Rock Restrained)

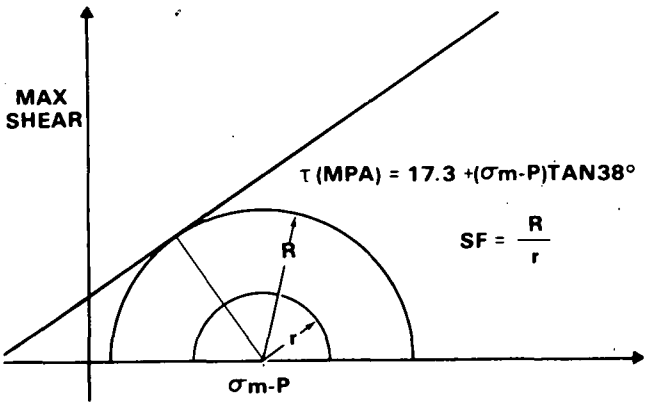

Fig. 8. Mohr Coulomb Failure Envelope for Galesville Sandstone (Ref. 8)

similar to those of the model.[8] Safety factors were defined the radius ratio of two circles. The denominator being the radius of Mohr's circle (three dimensional) for the point in question and the numerator being the radius of the concentric circle which is tangent to the Mohr-Coulomb envelope. This is illustrated in Fig. 8. Contour plots of Mohr Coulomb safety factors are shown in Figs. 9 and 10 for weeks one and 52, respectively. These safety factor values corresponded to the model of Fig. 2 with axial loading to simulate the overburden. The corresponding values for the case of vertical constraints were very similar, however. As can be seen from these figures, failure based upon this criteria will not occur.

Unlike most geologic structures, loading of a porous CAES site will be cyclic in nature and fatigue damage is a potential failure area to be addressed. In order to gain some insight into fatigue severity, the model shown in Fig. 2 was analyzed by applying differential thermal loading experienced during a 24 hour cycle. This differential loading was obtained and corresponding analyses were performed for several times during the one year simulation so that fatigue stress trends as a function of time could be studied. Resulting shear stress values for the middle of the cap and porous regions are shown in Figs. 11 and 12, respectively.

These figures suggest that fatigue stresses of any significant magnitude in the cap rock are very concentrated in the well bore vicinity. Due to the assumption of neglecting the casing, however, the magnitude shown in Fig. 11 is only of qualitative value. Fatigue stress levels are somewhat greater in the porous rock than in the cap rock. As could have perhaps been anticipated, the central region is the most severely stressed. Due to the assumption mentioned above, these stress levels too should be considered only qualitatively.

CONCLUSIONS

Structural response trends are described with considerations given to the assumptions made in carrying out the analyses. In this context, stress levels in the cap rock and porous rock zones in the well bore vicinity should not be considered quantitatively accurate. These stress levels will be influenced by:

- The size and wall thickness of the casing
- The locations along the casing which are grouted into place

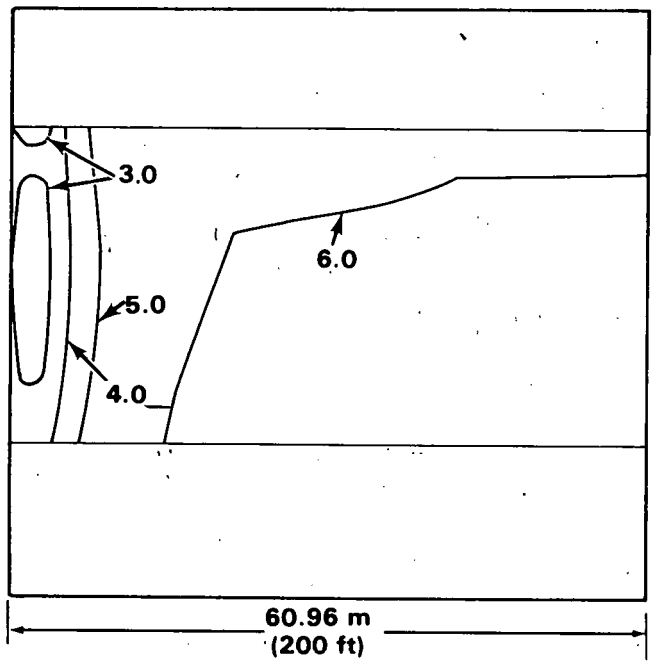

Fig. 9. Mohr Coulomb Safety Factors at the End of One Week

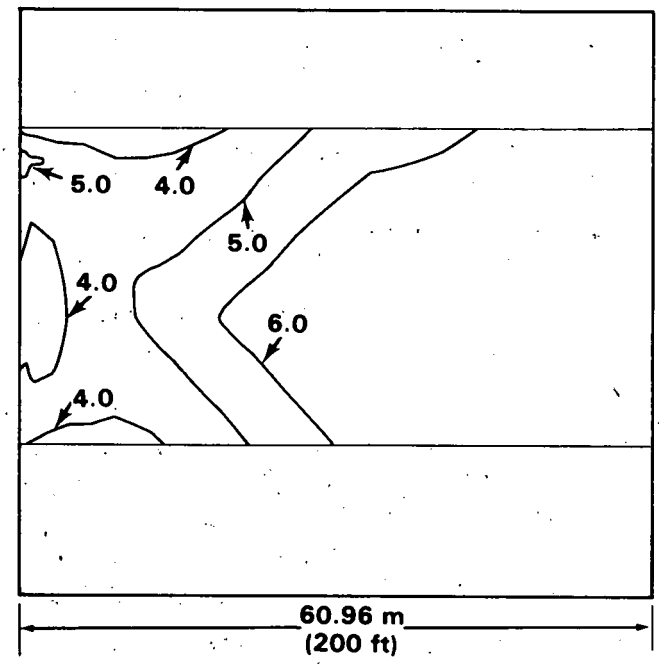

Fig. 10. Mohr Coulomb Safety Factors at the End of One Year

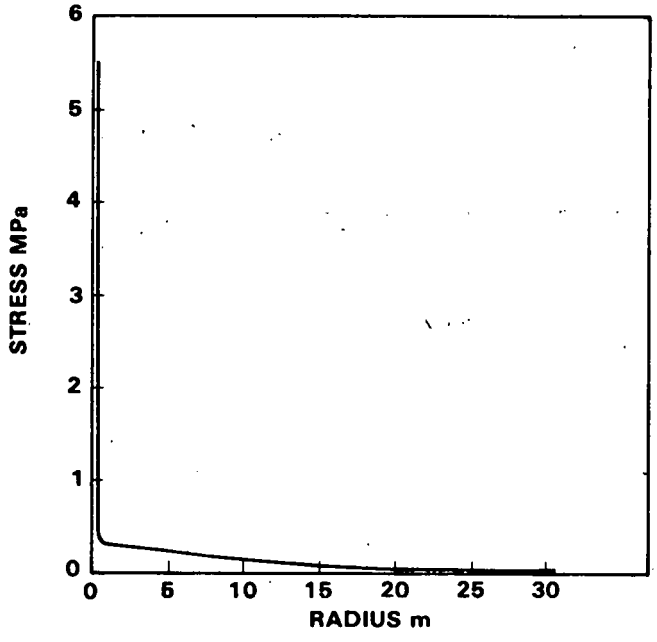

Fig. 11. Cap Rock Cyclic Shear Stress

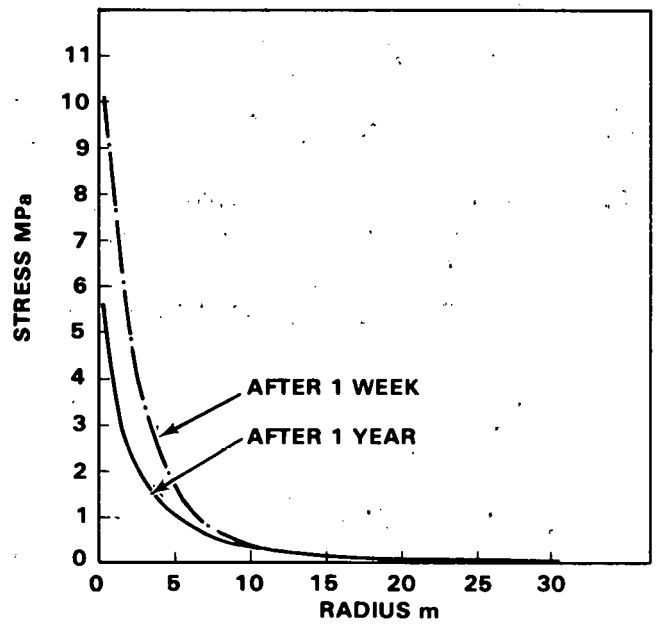

Fig. 12. Porous Rock Cyclic Shear Stress

- The degree of fracturing produced during the well drilling
- The termination level of the casing in the porous zone.

Plans are underway to address some of these localized features in FY-80.

Certain general response trends described in this paper, however, are thought to be somewhat general and independent of well completion details. These response trends are:

- Significant tensile stresses if existing at all will likely occur within the cap rock away from the porous media interface.
- Fatigue stress levels are markedly higher in the near wellbore porous zone rather than in the cap rock.

REFERENCES

1. L.E. Wiles, "Fluid Flow and Thermal Analyses for CAES in Porous Rock Reservoirs", Proceedings of the 1978 Mechanical and Magnetic Energy Storage Contractor's Review Meeting. NTIS CONF-781046

2. A. Lubinski, "The Theory of Elasticity for Porous Bodies Displaying a Strong Pore Structure", Proceedings of the Second U.S. Congress of Applied Mechanics, 1954.

3. K. G. Stagg and O.C. Zienkiewicz, Rock Mechanics in Engineering Practice, John Wiley & Sons, New York, NY, 1968.

4. R. P. Mordgren, "Strength of Well Completions", Eighteenth Symposium on Rock Mechanics, Johnson Publishing Co., Boulder, CO, 1977.

5. O.C. Zienkiewicz, The Finite Element Method, 3rd Edition, McGraw Hill, 1977.

6. K.J. Bathe, Static and Dynamic Geometric and Material Nonlinear Analysis Using ADINA. MIT Report 82448-2, 1977.

7. K.J. Bathe, ADINA-A Finite Element Program for Automatic Dynamic Incremental Nonlinear Analysis, MIT Report 82448-1, 1976.

8. J. Blacic, "Cyclic Thermo-Mechanical Properties of Aquifers", Proceedings of the 1979 Mechanical and Magnetic Energy Storage Contractors Review Meeting. NTIS CONF-781046, 1979.

9. CRC Handbook for Applied Engineering Science, 2nd Edition, CRC Press, Cleveland, OH, 1973.

THIS PAGE

WAS INTENTIONALLY

LEFT BLANK

PROJECT SUMMARY

Project Title: "Laboratory Test of Salt Specimens Subjected to Loadings and Environmental Conditions Appropriate to a Compressed Air Energy Storage Reservoir".

Principal Investigator: Robert L. Thoms

Organization: Louisiana State University (LSU)
Institute for Environmental Studies
Baton Rouge, Louisiana 70803
(504) 388-8521

Project Goals: To test rock salt and develop a data base for long-term stability criteria for compressed air energy storage (CAES) caverns in rock salt. Long-term stability criteria also will be formulated on the bases of test data.

Project Status: The test program is divided into two phases, i.e., (1) cyclic temperature and pressure tests on cylindrical rock salt specimens at LSU, and (2) in-situ tests on boreholes in salt in the Jefferson Island mine in south Louisiana.

Six laboratory test units have been assembled to the extent that conventional triaxial "strength" tests and uniaxial creep tests can be performed on 100 mm (4 in.) diameter cyclindrical specimens of rock salt. Controls and thermal loading components for simulating cyclic CAES environments are being assembled into the test units. Preliminary cyclic uniaxial testing has been performed on salt from the Avery Island dome in the LSU laboratory.

Salt specimens suitable for laboratory tests have been obtained from four Louisiana domes, and also from the Huntorf salt dome in West Germany. The Huntorf dome is the site of the world's first operational CAES facility. The Huntorf cores will be used for baseline tests corresponding to apparently successful CAES reservoirs in dome salt. The probability appears high also for obtaining test specimens from bedded salt in the Permian Basin of the U.S.

Four boreholes (or coreholes) have been drilled at a test site in the Jefferson Island mine. The holes will be used for in-situ tests, and have diameters and lengths of 108 mm (4.25 in.) and 760 mm (30 in.) respectively. Cores taken from these holes are part of the specimens on hand at LSU. A protective shed with lighting and 110 AC power has been erected over the site. A hydraulic stress cell has been installed in an observation borehole to determine the lateral state of stress in the mine floor.

In-situ tests on slant holes drilled beneath mine pillars (so as to encounter large confining stresses) have been delayed because the Jefferson Island mine was classified to be "gassy" by the Mining Safety and Health Administration (MSHA) in mid summer, 1979. This work will be implemented when access to an appropriate site becomes available.

Contract Number:	Subcontract B-67966-A-H, Prime Contract EY-76-C-06-A-H.
Contract Period:	Oct. 77 - Dec. 78.
Funding Level:	$198,631
Funding Source:	Battelle- Pacific Northwest Laboratories

LABORATORY STUDIES OF SALT RESPONSE TO CAES CONDITIONS

R. L. Thoms
Louisiana State University
Institute for Environmental Studies
LSU, Baton Rouge, LA 70803

ABSTRACT

A testing program is described for establishing a data base on rock salt response and for formulating long-term stability criteria for cyclic loadings typical of operational compressed air energy storage (CAES) caverns. The program is divided in two generalized laboratory phases, i.e., (1) cyclic temperature and triaxial stress tests at LSU, and (2) in-situ cyclic temperature and pressure tests in boreholes in salt mines. Accomplishments to date and work still to be done are reported and summarized.

INTRODUCTION

Currently there is no significant data in the literature on the response of rock salt to cyclic loading conditions which simulate the environment around a compressed air energy storage (CAES) cavern. A relevant data base is prerequisite for rational design and operation of CAES cavern systems. The foregoing report summarizes accomplishments to date and work still to be done on establishing a data base from generalized laboratory tests appropriate to CAES applications. When adequate, the data base will be used to formulate long-term stability criteria for CAES cavern systems in salt formations.

OBJECTIVES AND SIGNIFICANCE OF STUDY

The objectives of the current study include: (1) performing laboratory tests, in a generalized sense, on rock salt under CAES cavern loading conditions; and (2) subsequently establishing a data base and formulating long-term stability criteria for CAES caverns in salt formations.

Considerable interest has been shown recently in geostorage in salt formations. Without going into detail, most frequently considered storage applications in salt, e.g., oil or gas, involve cavern pressure loadings of only a relatively small number of cycles. Further, storage of liquids generally involves only small rates of pressure change in storage caverns; and storage of solid wastes obviously would not ordinarily involve loading rate effects. Thus, little work has been done or reported on cyclic loading or loading rate effects for salt. However, at least one case has been reported where rapid depressurization of a test cavern in salt caused associated roof collapse.[1] Also, from considerable work on other polycrystalline materials, i.e., structural metals, it can be anticipated that cyclic loadings could cause possible undesirable "fatigue" effects in rock salt caverns.

Rational engineering design implicitly requires realistic and relevant data on material behavior. Thus a specialized test program has been initiated to obtain data suitable for design of CAES caverns. The data will be reported in a format which should be generally useful for planning and operating CAES cavern systems. Long-term stability criteria for CAES caverns also will be presented as a logical extension of the data analysis. It should be noted that site

specific tests generally will still be required to furnish input for the long-term stability criteria which will be formulated through this study. However, the present study will provide a basis for testing and data analysis relative to CAES in salt formations in general.

SCOPE OF TEST PROGRAM

As noted previously, the study includes two major testing phases: a series of tests at LSU on salt specimens from a number of locations; and in addition, a series of in-situ tests on boreholes in south Louisiana salt mines. Both of these series of tests are included in the scope of "generalized" laboratory testing for this study. Further, limited numerical modeling is incorporated in planning of tests and for data correlation and analysis.

The series of tests at LSU will be carried out principally with six triaxial test machines capable of exerting coupled cyclic temperature fields and axial and confining stresses on cylindrical salt specimens. "Standard" salt test specimens have diameters and lengths of 10 cm (4 in.) and 20 cm (8 in.) respectively. Confining stresses (pressure) up to 34,500 kPa (5004 psi) and axial stresses up to 77,625 kPa (11,259 psi) can be applied. This is adequate to simulate most stress environments for salt caverns at depths ranging from 610 m (2001 ft) to 1524 m (5000 ft). This range extends over the most likely depths for construction of CAES caverns.

For the second testing phase, in-situ cyclic pressure and temperature tests will be performed in boreholes in the floor and possibly beneath pillars in salt mines. Tests performed in boreholes beneath pillars would include effects of relatively large confining pressures in the essentially undisturbed surrounding salt. Possible deterioration of the surrounding rock salt fabric versus numbers of loading cycles will be monitored.

Effects to be monitored in both the triaxial and borehole tests include related displacements (strains), loading environments, and microseisms versus time or numbers of load cycles.[2] In addition, possible deterioration of the surrounding rock salt fabric will be noted.

The geological setting of the salt specimens tested also will be described. For example, possible effects of gas entrapped in the salt will be noted. Gas entrapped in salt can cause blowouts (gas outbursts) such as the one that occurred recently at the Belle Isle salt mine in south Louisiana. Blowouts should be a significant concern in site selection for CAES caverns, and thus are included as factors in long-term stability criteria for storage in salt. [3]

A large number of index tests are planned for correlation of data from more time consuming triaxial tests. Uniaxial tests and the "split cylinder" or "Brazil" tests will be used for this purpose. The split cylinder test employs the failure load of diametrically loaded short, e.g., 2.5 cm (1 in.), cylinders.

Applied test loads will be selected on the basis of preliminary numerical modeling so as to span loading environments anticipated for CAES caverns. Basic test parameters will incorporate sufficient detail to uniquely define typical loading cycles for particular tests. For example, Fig. 1. is a schematic of a typical loading cycle for a triaxial extension cycle creep test performed in the laboratory.

Anticipated results from the testing program will include "failure surfaces" associated with stress environments and numbers of load cycles. Long-term stability criteria will be deduced for CAES caverns based on the test program results.

WORK PLAN

The preceeding text has included some detail on the overall objectives, significance, and scope of the study. Therefore, only major topics in the general work plan are listed in this section. The topics essentially follow in order the time sequence of the major steps in the study.

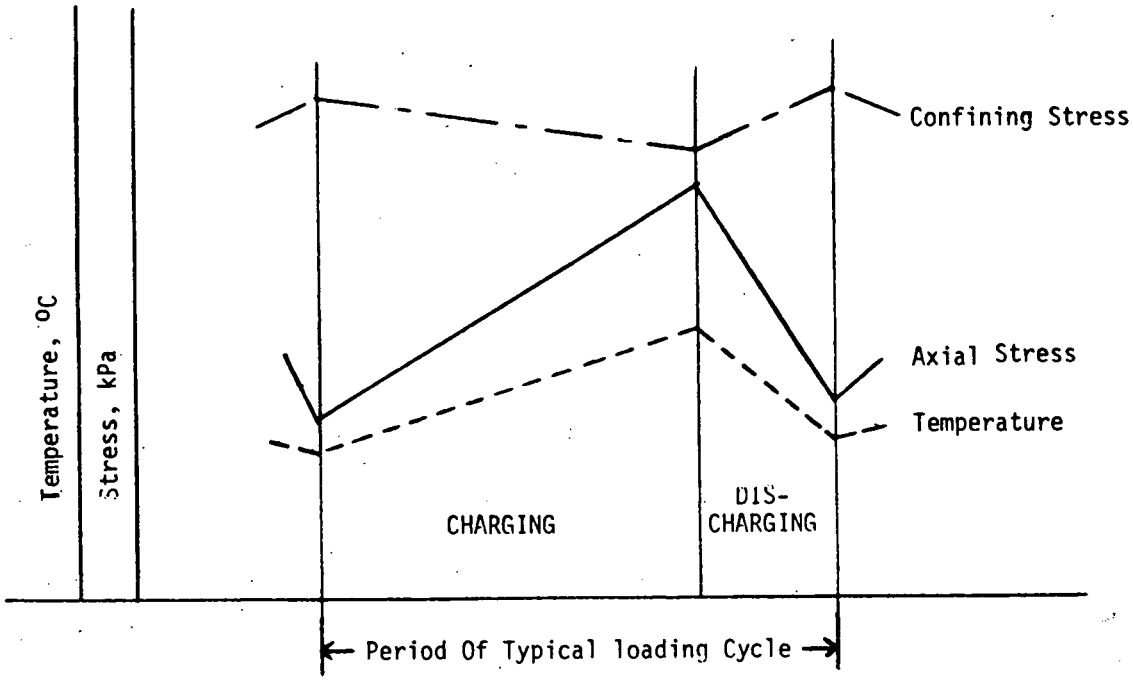

Fig. 1. Typical Cyclic Triaxial Extension Test Loading

1. Obtain salt cores for testing from south Louisiana salt mines and other opportune sites significant for CAES.
2. Test cores in LSU laboratory under simulated CAES loading environments.
3. Test boreholes for in-situ behavior in salt mines.
4. Correlate laboratory and in-situ test data.
5. Report data and present stability criteria.

A more detailed project plan has been prepared for this study which incorporates the above major steps.

ACCOMPLISHMENTS TO DATE

Major Accomplishments to date include the following items.

1. Salt core acquisition from: south Louisiana salt mines (Jefferson and Avery Islands), north Louisiana coreholes (verbal approval - Vacherie and Rayburn's domes), West Germany (Huntorf dome, gas storage wells, with operational CAES plant in same dome).
2. Laboratory at LSU for cyclic CAES loadings, with six test units, is approximately 75% complete.
3. Boreholes and enclosing shed have been completed for testing in the floor of the Jefferson Island salt mine.
4. Plans have been completed for performing tests in boreholes slant-drilled beneath mine pillars. Implementation of this effort has been delayed because of recent "gassy-mine" classification of Jefferson Island salt mine.
5. Preliminary testing has been performed on Avery Island salt. There are some indications that cyclic loading causes more severe effects than static loading. Figure 2

depicts results for a uniaxial creep test on Avery Island salt. It corresponds very closely to test results obtained by other workers for salt from the Tatum dome in south Missippi.(4)

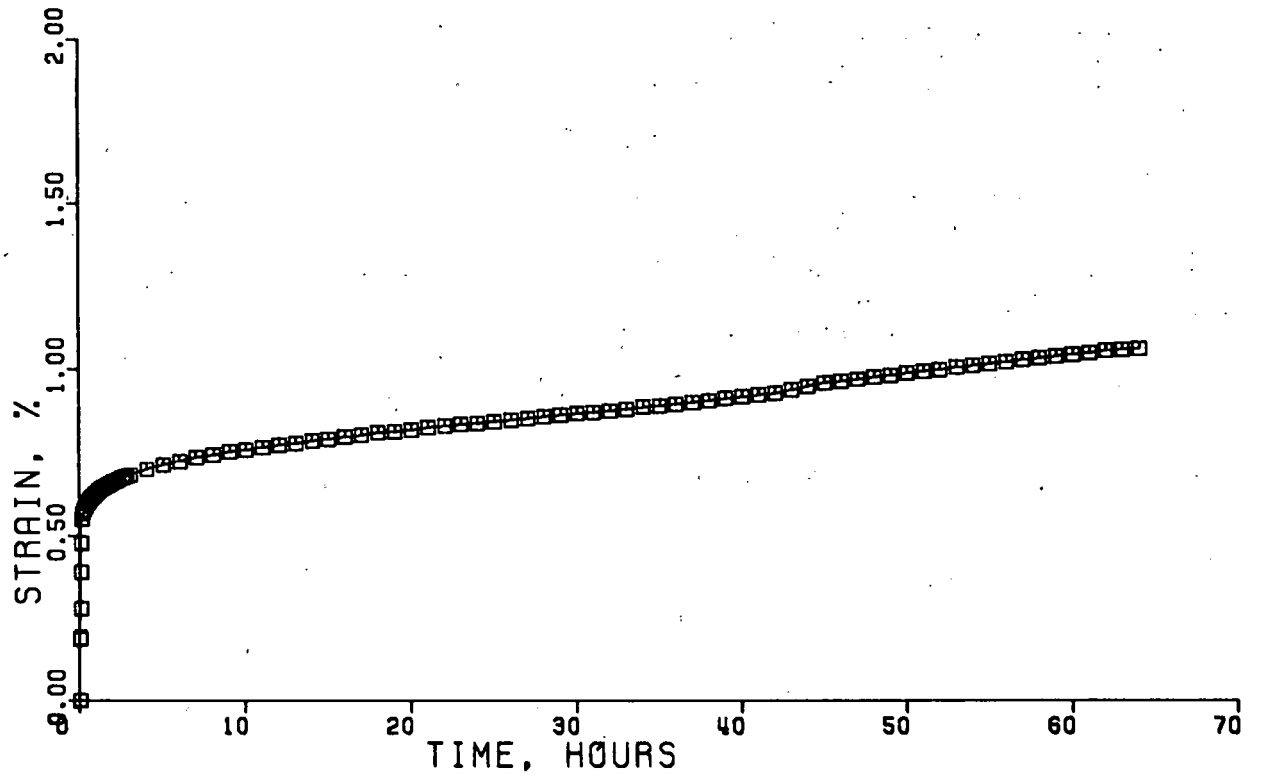

Fig. 2. Uniaxial Creep Test for Avery Island Salt, 1750 psi (12064 kPa)

WORK TO BE DONE

Work remaining to be done under this study includes the following items at the time of this review.

1. The laboratory at LSU, now approximately 75% finished, will be completed. Late equipment delivery has delayed completion of the laboratory.
2. Loading and monitoring system for boreholes in the floor of the Jefferson Island mine will be installed and tests initiated. Tests in slant holes beneath pillars have been delayed because of a recent gassy mine classification; however, this test may be moved to another mine or carried out at a later date.
3. Test data from a variety of salts, including the Huntorf salt, will be analyzed. The Huntorf salt should furnish highly significant data because the first operational CAES plant is located in that dome.
4. Results will be reported along with long-term stability criteria based on test data.

SUMMARY

Work is well along on providing generalized laboratory test facilities for simulating effects of CAES caverns in rock salt. A unique feature of the facility is the parallel development of in-situ testing in salt mines. Testing of salt specimens has been initiated at LSU, and testing in a south Louisiana mine is close to initiation. Tests will become increasingly sophisticated and specific as equipment now on order is received and assembled into testing units.

REFERENCES

1. H. U. Rohr, "Mechanical Behavior of a Gas Storage Cavern in Evaporitic Rock," Proc. 4th International Symposium on Salt, V. II, Northern Ohio Geological Society, 1974, p. 93-100.

2. B. C. Haimson and K. Kim, "Acoustic Emission and Fatigue Mechanism in Rock," Proc. First Conference on Acoustic Emission/Microseismic Activity in Geologic Structures and Materials, H. R. Hardy, Jr., and F. W. Leighton, Eds., Trans Tech Publications, 1977, p. 35-55.

3. R. L. Thoms and J. D. Martinez, "Preliminary Long-Term Stability Criteria for Compressed Air Energy Storage Caverns in Salt Domes," Report for Battelle-PNL, Special Agreement B-54804-A-L, Prime Contract EY-76-C-06-1830, Institute for Environmetal Studies, Louisiana State University, August 1978, p. 7.

4. A. P. Boresi and D. C. Deer, "Creep Closure of a Spherical Cavity In An Infinite Medium (With Special Application to Project Dribble, Tatum Salt Dome, Mississippi)." For: Holmes and Narver, Inc., Las Vegas Division, May, 1963, p. P.10.

ACKNOWLEDGEMENT

This work was performed for Battelle-Pacific Northwest Laboratories, under Prime Contract EY-76-C-06-A-H, Subcontract No. B-67966-A-H.

THIS PAGE

WAS INTENTIONALLY

LEFT BLANK

PROJECT SUMMARY

Project Title:	Field Studies Planning, Salt and Porous Media
Principal Investigator:	T.J. Doherty
Organization:	Pacific Northwest Laboratory P.O. Box 999 Richland, Washington 99352 (509) 946-2793
Project Goals:	To plan field studies in salt and porous media with the two objectives of extending reservoir stability numerical and experimental studies in situ conditions and supporting reservoir evaluation efforts of the utilities in the development program.
Project Status:	Directed small scale studies are being conceptualized to validate the design and stability criteria inside time and cost constraints. Liaison with the utilities performing salt and porous media CAES system development projects is underway.
Contract Number:	EY-76-C-06-1830
Contract Period:	FY1979
Funding Level:	$65K
Funding Source:	Department of Energy, Division of Energy Storage Systems

COMPLEMENTARY AND POTENTIAL CAES FIELD STUDIES

T.J. Doherty
Pacific Northwest Laboratory
Richland, Washington 99352

ABSTRACT

Field studies at PNL form an integral part of the transition from concept examination and applied research to development and demonstration of CAES technology. Small scale directed studies for three media types are presently in a conceptual phase. Porous media work is directed towards determining in situ permeability changes and wellbore desaturation. A shallow aquifer high temperature injection test is in planning. The key concern in salt is the effect of air penetration and temperature at high strain, low confining stress conditions. Bench scale or small in-situ cavern experiments are being examined for feasibility and cost. An in situ study of hard rock reservoir parameters is awaiting detailed prioritization of key areas of concern.

INTRODUCTION

Studies of reservoir stability seek to establish design and stability criteria that will allow efficient utilization of geologic structures for compressed air energy storage over useful facility lifetimes. Four types of studies will contribute to the identification of final design and stability criteria.

The first phase of the reservoir stability studies was a state-of-the-art-survey (Fig. 1) of existing knowledge in the field of geologic storage, with supplemental knowledge from related technologies. This baseline information was condensed into preliminary design and stability criteria and was evaluated to direct later studies in the areas of insufficient knowledge. These criteria will be confirmed, modified, or updated as results of later studies become available.

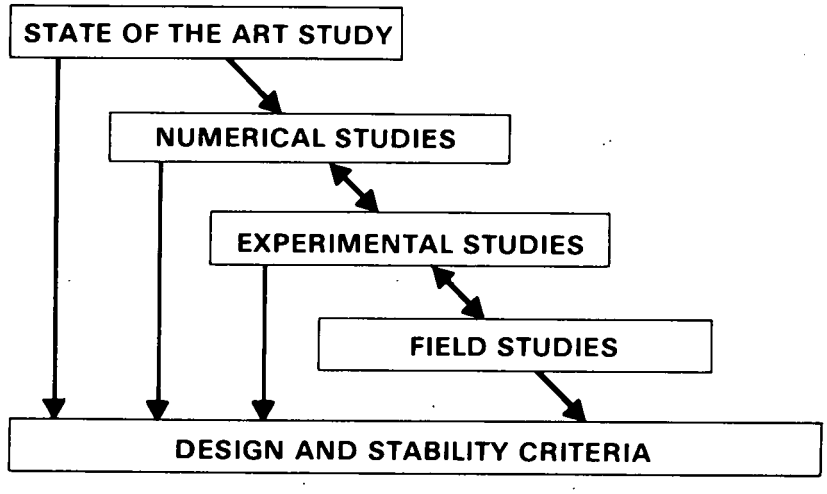

Fig. 1. Reservoir Stability Structure

The next two phases are experimental studies and numerical studies of the response of the geologic storage media to CAES operational loadings. Experimental and numerical studies are being carried out concurrently, and are phased in such a way that numerical work can support and guide the experimental studies and results from tests of material response can be incorporated into numerical modeling. Both of these phases are making contributions to the design and stability criteria as the results of their studies confirm or deny the initial postulates. Also, as a direct result of numerical and experimental studies, new ground is being covered in the field of geological engineering which allows a prioritization of the key areas of concern for each type of geologic structure under CAES operational conditions. These studies are well underway for porous media aquifer storage and for domal salt storage schemes, and are in the preliminary stages for hard rock materials. Results from these studies have indicated that many of the postulated failure mechanisms will not present problems. A few critical items have indicated potential for problems. These are being carefully examined.

The fourth phase of the criteria generation and confirmation process is the area of field studies. Field studies form an integral part of the transition from concept examination and feasibility determination to actual development and demonstration of CAES technology. The products of this series of studies, from numerical through experimental to field studies, are design and stability criteria for long life utilization of geological reservoirs for CAES applications.

The field studies project is within the PNL Reservoir Stability Study, which concentrates on determining geological constraints to CAES operation. Also, ongoing, is a joint development program with DOE-STOR and EPRI that is to demonstrate conventional CAES plants in the U.S. in different geologic media. This program is performing preliminary system design and is in the process of site selection and exploration. Total system development is the purpose of this demonstration program.

The CAES field studies task has two responsibilities that are necessary to the validation and acceptance of the design and stability criteria being formulated with Reservoir Stability Studies:

1. Extension of CAES numerical and experimental results and conclusions to in situ conditions.

2. Support of baseline studies dealing with exploration and monitoring of the geological reservoirs currently ongoing in the development program.

Two methods have been chosen to address these responsibilities in a timely and cost-effective manner. The first method entails performance of directed small scale field studies of parameters that have been identified as critical to CAES reservoir operation. A full scale operational test facility for conventional and advanced CAES reservoir testing would require long time periods for siting and construction, and would not fit within the budget, scope or time frame of the technology program as presently outlined. Data from such a facility would also not be available in sufficient time to be useful to the design process in the parallel development program. Knowledge of reservoir response has increased greatly since initiation of the reservoir studies and it is felt that the critical parameters affecting the integrity of CAES storage reservoirs have been identified. Directed small scale studies to examine these critical items in situ, can be performed in relatively short time periods and within a reasonable budget.

The second method involves establishing a working relationship with the development program in that area of their project that is concerned with exploration and monitoring of their reservoir. The data needs and operational conditions of the development program do not coincide exactly with that of the technology program. Operational conditions planned for the demonstration reservoirs do not cover the range of temperatures, pressures, and other conditions that should be covered in order to determine constraints on CAES reservoirs. Nevertheless, the data resulting from the development program will provide full scale baseline information to the small scale field studies.

DIRECTED SMALL SCALE FIELD STUDIES

Small scale tests are planned for design and construction that will examine the key parameters of CAES reservoir behavior. Numerical and experimental tools developed as part of the program will be utilized to aid test design and will themselves be verified. This will be done by utilizing these tools to predict performance of the tests to determine the level of accuracy or utility they have with respect to in situ conditions. Pre and post test coring and/or material examination will be performed to quantitatively evaluate correlation between lab and field testing conditions.

Upon completion of a testing sequence, comparisons between prediction and performance will be made, and correlation noted. From these, conclusions about the validity of the design and stability criteria or recommendations and modifications can be made.

The three media for CAES reservoirs being examined by Reservoir Stability Studies are porous formations, domal salt, and hard rock. This discussion addresses field study concepts being developed for porous media and domal salt.

POROUS MEDIA STORAGE RESERVOIR

The concept under development for porous media is based on utilizing near surface Lower Paleozoic sandstones. These formations, particularly the Galesville, have been studied by CAES researchers and are fairly well characterized. The specific formations should be within 100 meters of the surface, primarily so that drilling and casing costs (Fig. 2) will be reasonable. Formation closure and caprock seal integrity will be considerations but may not be primary ones. The present thinking is to develop a reasonably small bubble at moderate pressure over a period of a few months by cool air injection. Once a bubble has been developed sufficiently to clear water from a two well doublet, hot air injection would be initiated in one well and air withdrawal in the other, maintaining some overpressure to insure crossflow. This process would be reversed after some cycle time, and the heated region about the now reversed injection well would be cycled by the opposite cool air flow. Once established, this procedure will result in a crossflow that will deposit heat at the injection well and pick up heat at the withdrawal well. This should closely simulate flow, temperature, and drying conditions in a porous medium near the wellbore region under warm air cycling during the early period of CAES operation.

Confined moist air flow tests on down hole cores are planned for FY-1980. Laboratory versus in situ permeability from aquifer study and gas storage experience have been found to be somewhat different, often markedly so. An in-situ test under CAES conditions will indicate if permeability trends remain consistent with lab results. Numerical studies indicate that near wellbore stresses due to the temperature gradient[1] are much higher than in-situ stresses and that the heated area near the wellbore is well within the desaturated area[2]. These trends can be confirmed in-situ by establishing a flow thermal gradient in an aquifer.

Well instrumentation and a small hole array in the bubble region, as indicated by Fig. 3, will allow monitoring of pressure, temperature and saturation in the formation. Well head temperature, pressure and flow monitoring will be the key measurements for monitoring permeability changes. Other tools to aid permeability change and desaturation rates that are available for data gathering before and during testing are listed below:

- Thermistor - An electrical resistor using a semiconductor whose resistance varies in a known manner with temperature.
- Thermocouple psychrometer - Measures the dewpoint at high relative humidities and gives temperature and saturation data.
- Heat dissipation units - Short time temperature drop is measured after a heat source pulse. Thermal diffusivity correlates with degree of saturation.

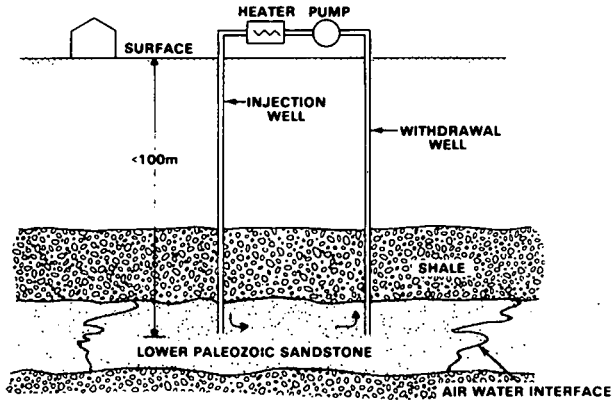

Fig. 2. Porous Media Field Test Schematic

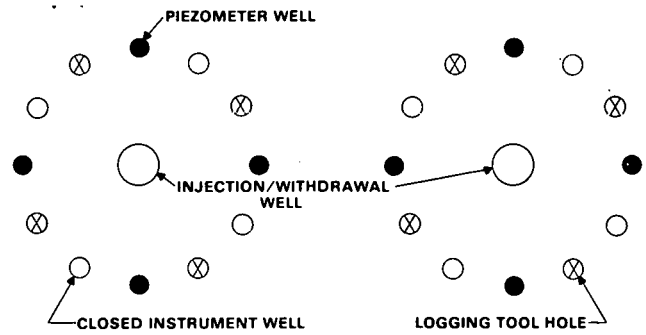

Fig. 3. Test Site Layout

- Piezometer - Hollow tubes at various depths to indicate hydrostatic pressures and allow for sampling.
- Tracer test - A fluorinated hydrocarbon gas is mixed with the injection air in known concentration. Water and air samples are taken from piezometer wells periodically to be analyzed by a gas chromatograph. Tracer concentrations indicate air movement patterns.
- Electric logs - Used in the wells before casing so that the surrounding formation may be defined.
- Single point resistivity - This log will establish the boundary between strata of differing resistivity and aid in lithologic correlation.
- Spontaneous potential log - This log records natural potentials which enhance data from the resistivity log for lithology and bed thickness evaluation.
- Radiation logs - These logs are used in open wells to monitor saturation and porosity in the areas of interest during testing.
- Neutron-Gamma log - This is a porosity log used for baseline data.
- Neutron-Epithermal Neutron log - This log measures water content, indicating porosity below a water surface and formation moisture above.
- Cement bond log - This log detects gaps in the cement between casing strings.
- Galvanic instrumentation - Detection of casing deterioration during testing.

As stated previously, this plan is in a conceptual phase, but some progress has been made. The key test parameters have been identified and a work plan to complete the conceptual design by December has been formulated and implemented. Technical management will be handled at PNL along with some instrumentation related functions and test operation, but the major site selection exploration, drilling and construction will be placed with consultants and subcontractors familiar with the geology and working environments.

SALT TEST CONCEPT

Numerical and experimental studies to date have indicated that stable performance can be expected under CAES operation, but both modeling and experiment indicate that the key item ensuring good performance is the surface quality of the wall cavity. In this area, the numerical models predict high strain, which affects salt permeability. Experimental results indicate an onset of opacity affecting the salt quality under high strain cyclic loading. A

change in permeability, such as increase in secondary permeability, also results in some air penetration into the rock structure, which reduces the confinement (Fig. 4). This could further lower the salt performance in the near well region. Salt is very sensitive in its strength and flow parameters to changes in temperature. Minor temperature changes from compression/extraction or moderate injection temperatures would also affect the near surface region. These phenomena are under investigation in ongoing numerical and experimental work, but these studies, due to limited sample size, may not be able to address sufficient scale to indicate the true field performance of a domal salt.

The pertinent operating parameters for such a study would require a well confined salt body, a solutioned cavity surface, and cyclic air pressure and temperature within the cavity. Examination methods could include wall coring or visual methods. Closure displacement measurements would also be important.

The requirement for a confined salt body has led investigators to address two concepts. Both are fairly flexible at this stage as the key issue to be resolved is whether mine owner/operators will allow development of the test concepts within their facilities.

The first concept is extension of the LSU[3] in-mine borehole tests to a small solution cavity (Fig. 5). This concept would be convenient for instrumentation and advanced boring. Coring from adjacent openings could be utilized to obtain post test cores. It is possible the cavity could be located so that it can be mined directly from a lower level allowing direct access. Some contacts have been made on general feasibility with mine operators but no indication of commitment has been received as most of the operators are presently dealing with the new gassy mine classification problems.

The other concept would be to utilize the early startup phase of a standard solution mine. The small cavity (Fig. 6) could be cycled at an accelerated time rate. Some available optical instruments have been identified for visual and dimensional examination of the cavern and the possibility of post-test side coring the smaller cavern is under investigation. One disadvantage of the concept is that the test area becomes the property of the mine operator after his mining commences.

Progress on getting approval of this general concept has been good. Preliminary discussions with mine management on details and schedules are in progress and it is hoped that test development can be initiated in FY-1980. A conceptual design report, with a mine operator approved site, is planned for inclusion in the December 1979 salt field studies plan.

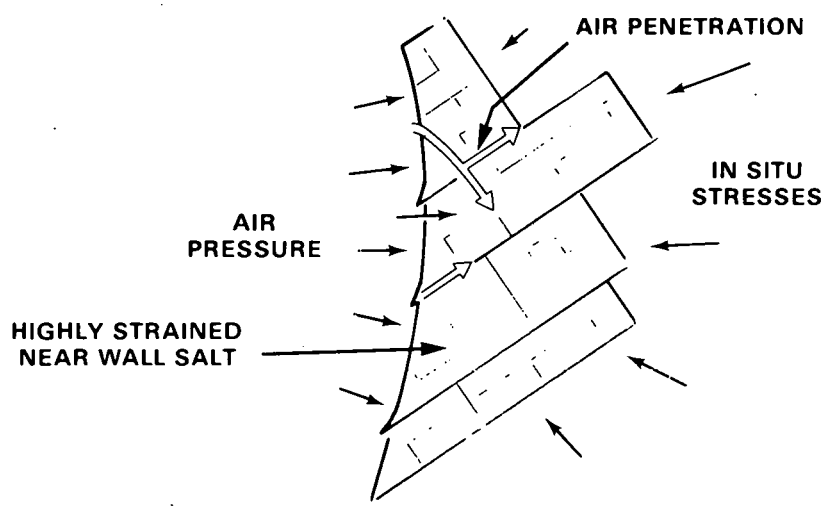

Fig. 4. Mechanism for Reducing Effective Confinement

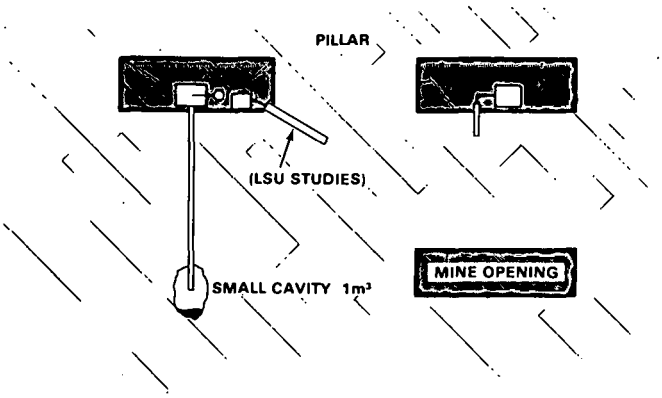

Fig. 5. Salt Concept In-Mine

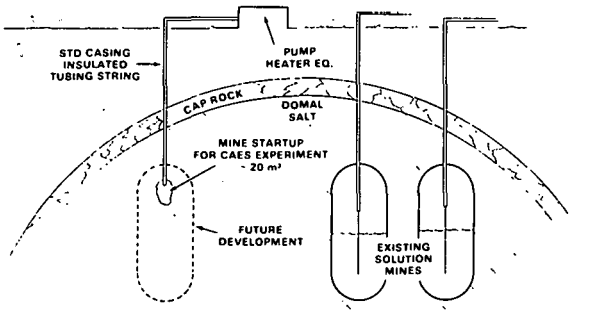

Fig. 6. Salt Concept in Solution Mine

DEVELOPMENT PROGRAM RELATIONSHIP

The DOE-EPRI CAES development programs, presently being performed by utilities, have as their purpose total system demonstrations. Public Service Indiana (PSI) has responsibility for the porous media CAES concept. Middle South Services (MSS) is carrying out its study on CAES application to domal salt structure. Both of these programs are at the stage of site selection and are formulating site exploration plans. The reservoir stability studies can support the utility studies and benefit from these studies by:

1. Facilitating interchange of data and providing special test data on demonstration site exploration cores.

2. Providing technical support with numerical and experimental tools.

3. Proposing instrumentation supplements at demonstration sites to extend the exploration and monitoring data base beyond minimum needs.

We have initiated liason with both PSI and MSS and have requested information on their exploration phases. The level of involvement in the development program will be determined once we have the opportunity to examine the exploration and site selection decisions of the utilities and they respond and comment on our proposals. Firm arrangement for mutually beneficial cooperation could be included in the December 1979 field studies plan documents.

CONCLUSION

Directed small scale field studies for salt and porous media are being identified to confirm design and stability criteria developed in the Reservoir Stability Study. In addition utility direction is being sought in order to create a field study demonstration program relationship that will be mutually beneficial.

REFERENCES

1. J.R. Friley, Structural Response of a Generic Porous Site. PNL-SA-7918, presented at the 2nd Annual Mechanical & Magnetic Energy Storage Contractors Review Meeting, Washington, D.C., 1979.

2. L.E. Wiles, The Effects of Water on Compressed Air Energy Storage in Porous Rock Reservoirs. PNL-2869, Pacific Northwest Laboratory, Richland, Washington, March 1979.

3. R.L. Thoms, Laboratory Studies of Salt Response to CAES Conditions, presented at the 2nd Annual Mechanical & Magnetic Energy Storage Contractors Review Meeting, Washington, D.C., 1979.

THIS PAGE

WAS INTENTIONALLY

LEFT BLANK

PROJECT SUMMARY

Project Title:	Advanced Concepts Studies CAES
Principal Investigator:	R.T. Allemann
Organization:	Pacific Northwest Laboratory P.O. Box 999 Richland, Washington 99352 (509) 946-2151
Project Goals:	Develop and assess advanced technologies for CAES that require little or no supplementary firing by petroleum fuels in order to eliminate the dependence of CAES on these fuels.
Project Status:	The advanced concepts studies are screening the major advanced technologies, thermal energy storage (TES), fluidized bed combustion (FBS), and coal gasification (CG). The screening should be completed in FY1980. Test facilities for thermal energy storage and comprehensive cost analysis are the other major tasks and are also directed toward defining criteria and recommending a CAES system to be demonstrated.
Contract Number:	EY-76-C-06-1830
Contract Period:	FY1979
Funding Level:	$575K BO/$700K BA
Funding Source:	Department of Energy, Division of Energy Storage Systems

ADVANCED CONCEPTS STUDIES

R.T. Allemann and M.K. Drost
Pacific Northwest Laboratory
PO Box 999
Richland, Washington 99352

ABSTRACT

The objectives of this program are to reduce or eliminate the dependence of CAES systems on petroleum fuels. The approach has been to evaluate improved cycles, equipment capabilities, coal firing methods, and thermal energy storage as applied to CAES. The evaluations have included both technical and economic studies. Preliminary results show technical promise for CAES systems integrated with coal fired fluid bed combustion, with thermal energy storage, and coal burning steam plants. The latter system uses advanced indirect thermal energy storage that shows economic benefits over direct thermal energy storage. A review of coal gasification shows potential benefits when coupled with a CAES peaking plant.

INTRODUCTION

Compressed air energy storage is a feasible technology that has been demonstrated. Many studies in the U.S. have determined its probable economics and electric power costs. The potential difficulty arises from the use of petroleum fuel in the compressed air energy storage cycle. Such fuels are becoming more expensive and indeed may be unavailable for electrical power generation. The advanced concepts CAES program is directed toward reduction and elimination of the need for petroleum fuels in the CAES cycle. The term "advanced" in this context is used in that sense, not in the sense of more sophisticated equipment. This paper is a review of the 1979 Advanced Concepts Studies being carried out as part of the Compressed Air Energy Storage program by DOE .

CONCEPTS CONSIDERED

This year the advanced CAES studies have been directed toward technical and economic evaluation of reduced or no-oil/CAES concepts. These include the following:

- CAES/Thermal Energy Storage Technical and Economic Studies
- CAES/Coal Gasification Technical Studies
- CAES/Fluidized Bed Combustion Technical and Economic Studies
- CAES Cycle Evaluations Technical.

Specific tasks during 1979 include the following elements, some of which have been or will be submitted as reports:

- Incremental Cost Analysis of Advanced Concept CAES Systems by C.A. Knutsen (Knutsen Research)
- Economics of TES for CAES by S.C. Schulte (PNL)
- Coal Fired Fluid Bed CAES by A.J. Giramonti (UTRC)

- CAES/Solar and CAES/TES Studies by G. T. Flynn (MIT)
- Review of Compressor and Turbine Limitations by H. Bomelburg (PNL)
- Direct Coupled Steam on CAES Cycles by M.K. Drost (PNL)
- Review of Coal Gasification with CAES by G.L. DeHaan and R.T. Allemann (PNL), and
- New Concepts Studies by R.T. Allemann (PNL)

The first of these tasks was reported in a paper presented at a recent IECE Conference in Boston. The next two tasks will be presented at this conference. In this paper, I shall briefly summarize some of the other tasks and outline the direction of the Advanced Concepts Studies.

RESULTS OF REVIEW OF COAL GASIFICATION/CAES

The use of low BTU gasified coal is a potential means for eliminating the need for petroleum fuels by a CAES plant. It has the potential advantage over temperature limited thermal energy storage/CAES and FBC/CAES of being able to supply high temperature air to present and future turbines. Several technical feasible cycles were analysed for near term use. Comparisons were made with longer term coal gasification concepts as described by A.J. Giramonti in the 1978 Energy Storage Symposium and with magnetohydrodynamic long term concepts (also coupled with CAES).

These results, partially shown in Table 1, indicate that coal gasification/CAES appears to be technically feasible in the near term and may have potential improvements in heat rate in the long term. Further development and economic evaluations appear to be needed. It should be noted that in view of the extensive coal gasification research and development conducted by DOE and industry, and in view of the fact that only minor modifications would be required to integrate a coal gasification system into CAES, this task has been primarily concerned with the analysis and evaluation of data to assist the DOE with decisions on which advanced CAES concepts to develop further.

TWO RESERVOIR CLOSED CAES CYCLE

A technical analysis was made of an advanced CAES cycle suggested by H. Bomelburg of PNL. It is a closed cycle in which the air is passed between two high pressure compensated storage caverns by the compressor and turbine. The schematic is shown in Fig. 1. The formula at the bottom is the air path in the cycle. The air goes from low pressure store (AS_1) through

TABLE 1. CAES Performance Summary

Name of System	Base Mode		Generation Mode		Compression Mode	Round Trip	Equivalent
	Output kW (MW)	Heat Rate Btu/kw-hr	Output kW (MW)	Heat Rate Btu/kW-hr	Output kW (MW)	Heat Rate kW (MW)	Storage Efficiency
1A. Base System for Comparison	3,980	10,550	9,020	4,745	-5,280	10,600	94.0%
1B. Cogas/CAES w/Recuperator	2,560	14,220	7,505	4,938	-2,595	13,246	95.0%
1C. Cogas/CAES w/Waste Heat Steam Cycle	4,272	11,638	9,207	5,833	- 881	12,190	89.1%
2. AFBC/CAES	1,400	19,650	6,395	4,440	-3,755	14,614	96.0%
3. PFBC/CAES	1,460	18,000	6,455	4,198	-3,695	13,994	96.0%
4. MHD/CAES Option 1	(961)	7,103	(1,395)	6,021	(+584)	7,941	56.4%
5. MHD/CAES Option 2	(961)	7,103	(1,392)	5,468	(+548)	7,575	77.6%

*Compression time is equal to generation time for all cycles

compressor (C) to high pressure storage reservoir (AS_2). During generation the air goes from AS_2 through turbine (T), trim cooler (q) to lower pressure storage reservoir (AS_1). The advantages of this cycle are a low temperature rise (Fig. 2) due to low pressure ratio of compression and expansion, and high storage efficiency of about 72-75% (Fig. 3). The disadvantage appears to be the relatively large storage volume required (Fig. 4). Table 2 shows a comparison with other systems. The two reservoir concept requires a volume that is nearly three times larger than the underground pumped hydro storage and thus would not appear to be competitive. Because of the very large storage volumes required, we have not proceeded with an economic evaluation.

RESULTS OF REVIEW OF DIRECT COUPLED STEAM/CAES CYCLES

As part of PNL's evaluation of advanced compressed air storage concepts, PNL has evaluated the performance of a direct coupled coal fired steam/CAES plant. The direct coupling of the two types of cycles provides benefits for each cycle and improves the overall performance of the facility. This concept was examined because it gives the potential for substantially reducing or eliminating the use of petroleum fuel and satisfy the peaking power requirements of utilities.

A schematic of the Direct Coupled Steam/CAES cycle is shown in Fig. 5. The steam cycle is typical of current steam power plant technology with multiple stages of feedwater heating and reheat. There has been three modifications to the steam cycle; the steam turbine can be clutched to either the compressor train of the CAES cycle or to a generator, some feedwater heating is provided by the heat of compression from the compressor train of the CAES cycle and the hot reheat steam is used to charge a thermal storage unit. The hot reheat steam is partially desuperheated and returned to the steam plant intermediate pressure turbine.

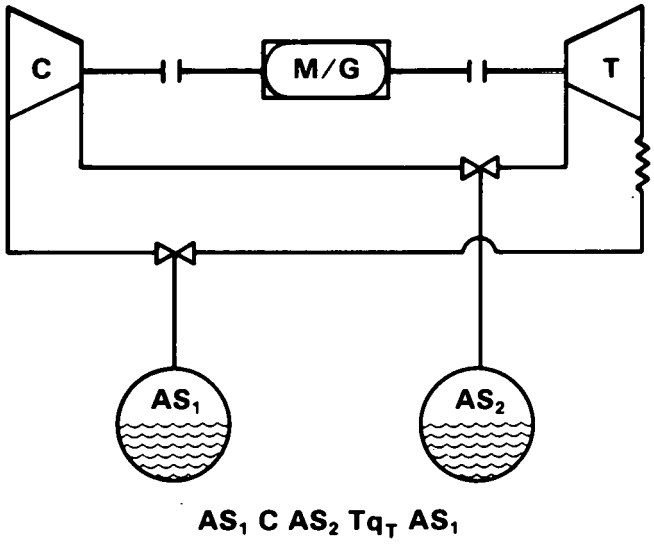

Fig. 1. Two Reservoir Cycle

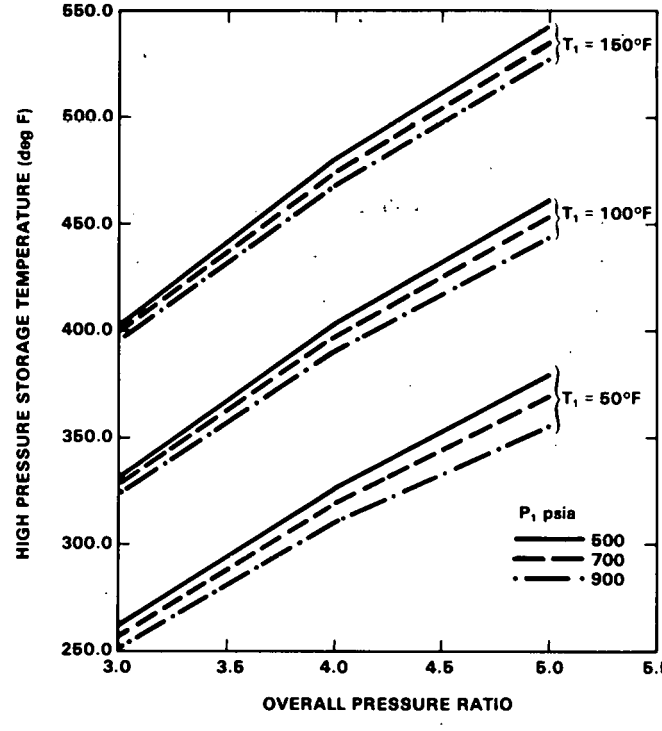

Fig. 2. Storage Temperature (T_2) as a Function of Pr, P_1, and T_1

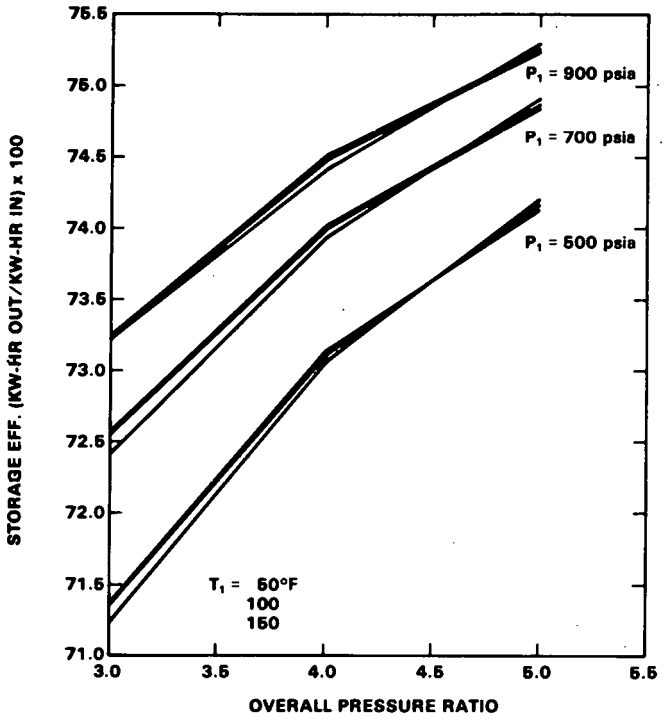

Fig. 3. Storage Efficiency as a Function of Pressure Ratio, Initial Pressure and Initial Temperature

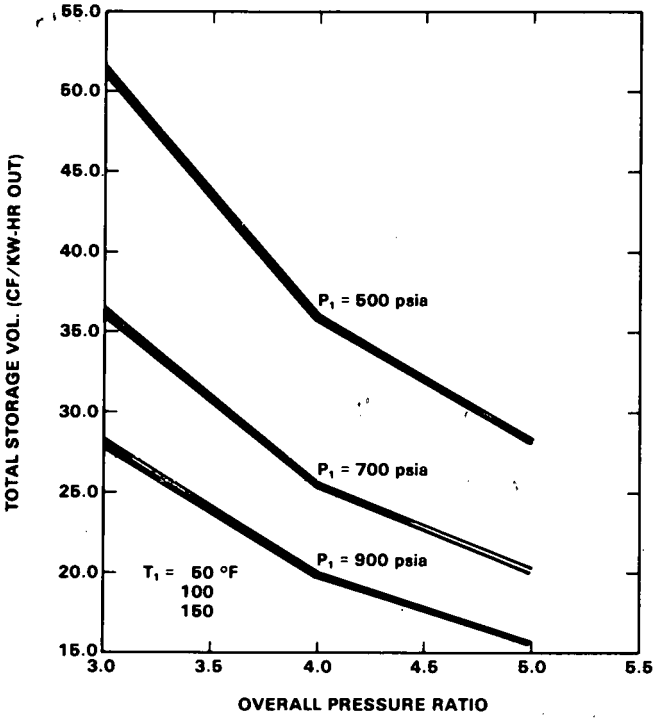

Fig. 4. Storage Volume as a Function of Pressure Ratio, Initial Pressure, and Temperature

TABLE 2. Two Reservoir Cycle Results Comparison

	Two Reservoir Closed System CAES	Double Stage TES/CAES	Underground Pumped Hydro
Storage Efficiency %	~70	~70	~70
Storage Depth (ft)	2000/6500	2000	6500
Specific Storage Volume (ft^3/kW-hr out)	18.3/8.2 Total 26.5	4.45	9.4
Turbine, Compressor Pressure Ratios	3.25	65	
Technology Risk	Low	Moderate	Moderate

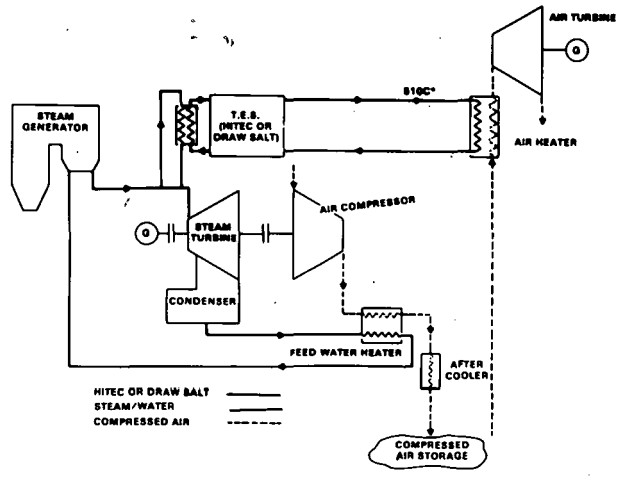

Fig. 5. Cycle Arrangement Close Coupled Steam/CAES Cycle TES Heated with Hot Reheat Steam

The cycle has been modified so that compressed air is heated during discharge by heat stored in the thermal storage unit. The CAES cycle can be either an adiabatic CAES/TES cycle or a hybrid cycle that uses both TES and fuel.

The thermal storage is assumed to be a molten salt thermocline storage, where thermal energy is stored as sensible heat in a mixture of molten salt (HITEC or Draw salt) and rock. This type of thermal storage unit is being developed for solar thermal applications.

During the charge cycle, the steam turbine is clutched to the CAES system compressor train to compress air for storage underground. The heat of compression, which is normally rejected, is used for feedwater heating in the steam cycle. Hot reheat steam is used to charge storage and is the expanded in the steam cycle intermediate and low pressure turbines.

During discharge, the steam turbine is clutched to its generator and steam is extracted for feedwater heating to replace the heat of compression. Discharge air is heated from the thermal storage and expanded in the air turbine which is shafted to a generator.

Using the steam heated TES arrangement, the maximum temperature of air entering the air turbine is around 510°C. Cycle performance can be improved by adding a petroleum fuel combustor on the discharge of the air heater to obtain a higher temperature before expansion in the air turbine.

The Direct Coupled Steam/CAES concept has several advantages over a separate steam plant used to provide power to a CAES plant. Generator, motor and transmission line losses are eliminated for charging power. A substantial fraction of the heat of compression is recovered and petroleum fuel consumption is reduced or eliminated by providing air heating from the thermal storage. It should be noted that the steam generator does not cycle and that the steam cycle and CAES cycle are commercially available.

The arrangement can operate in a no petroleum fuel mode but there is a substantial performance penalty because of the low temperature of the air entering the air turbine. In addition, using hot reheat steam for charging storage reduces the performance of the steam cycle. To avoid these problems, two alternate cycles were considered; one in which the storage media is directly heated in the steam generator and one which uses a fluid bed combustor.

The Direct Heating arrangement is similar to the steam heated arrangement discussed above except that the molten salt is directly heated in the steam generator (see Fig. 6). This gives a slightly higher temperature in storage and improves the performance of the steam cycle particularly in the no petroleum fuel case. This arrangement has the disadvantage of requiring a major redesign of the steam generator.

An advanced arrangement has also been considered (see Fig. 7). In this concept an FBC is used as the steam generator for the steam cycle. In addition, the FBC is used to heat air which in turn is used to charge a pebble bed thermal storage unit. During discharge, air from storage is passed through the thermal storage and is heated. It is assumed that the air temperature on the discharge side of storage reaches 815°C. The air which is used to charge storage goes directly to the air turbine during discharge. This arrangement improves performance of the Direct Coupled Steam/CAES cycle particularly for the no petroleum fuel case. The major disadvantage is that both the FBC and the thermal storage require development.

The performance of the various cycles was determined for a base case, a reduced petroleum fuel case, and a no-petroleum fuel case. The base case is a typical CAES facility with the HP turbine fired to 1000°F and the LP turbine fired to 1500°F. Several reduced petroleum fuel cases were considered and the one with the lowest heat rate was selected. This was a Direct Coupled Steam/CAES plant which used the steam heated TES arrangement and a hybrid Glendenning A-5 cycle for the CAES (Fig. 5). Several no petroleum fuel cases were considered and two are presented. The first is a near term arrangement which used the direct heated TES arrangement and a conventional CAES cycle with both the LP and HP turbines heated (Fig. 6). The second is an advanced arrangement which uses an FBC for the steam generator and a hybrid Gendenning A-5 cycle for the CAES (Fig. 7).

The reduced petroleum fuel case resulted in a 60% reduction in petroleum fuel use from 4400 Btu/kW-hr to 1600 Btu/kW-hr but with an 11% increase in overall heat rate. The no-petroleum fuel cases eliminated the use of petroleum fuel and increase the overall heat rate by 10% for the direct heated arrangement. The advanced arrangement both eliminated the use of petroleum fuel and decreased the overall heat rate (see Table 3).

The results indicate that the direct coupled steam/CAES concept has promise. Further studies will be needed to improve performance calculations and to determine the economics of this concept.

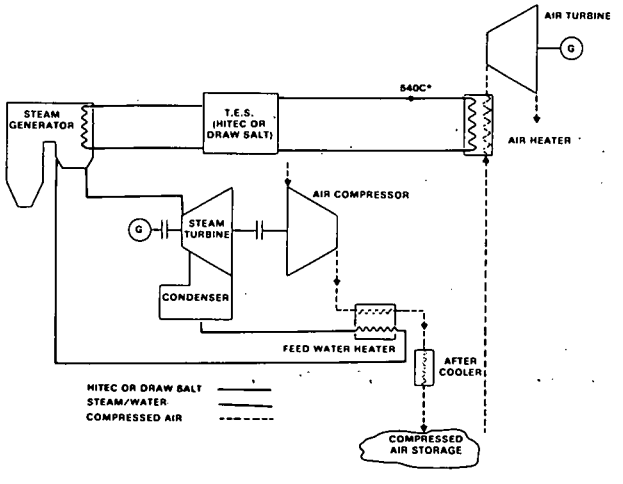

Fig. 6. Cycle Arrangement Close Coupled Steam/CAES Cycle TES Directly Heated

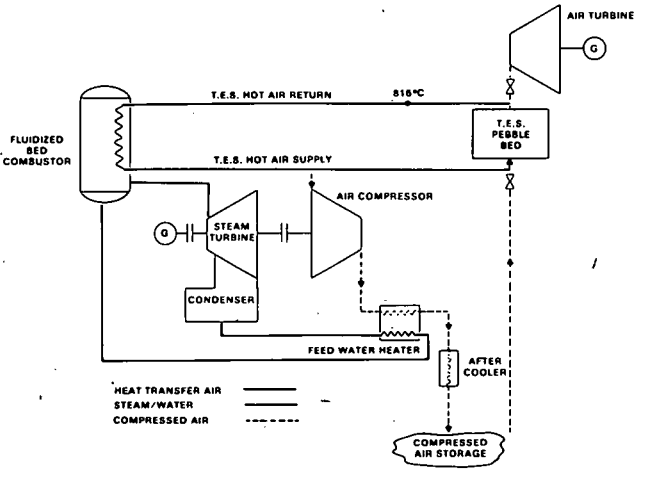

Fig. 7. Cycle Arrangement Close Coupled Steam/CAES Cycle Advanced Cycle

TABLE 3. Summary of Results for Direct Coupled Steam/CAES Cycle

Concept	Arrangement	Net Heat Rate Btu/kW-hr	Petroleum Heat Rate Btu/kW-hr
Base	Separate	10,700	4,400
Reduce Petroleum Fuel	Steam Heated	11,200	1,900
No Petroleum Fuel	Direct Heated	11,900	0
No Petroleum Fuel	Advanced	10,100	0

DIRECTION OF ADVANCED CONCEPTS STUDIES

The thrust of the advanced concepts/CAES work is to develop and evaluate existing information required to assist the DOE in deciding on which advanced concept or concepts to pursue to the demonstration phase. The evaluation depends upon the results of technical and economic studies that have been done. Inputs for the evaluation have come and are expected to come from all areas of the industry. Work by the CAES participants such as EPRI, UTRC, CEGB, TVA PEPCO, Acres American, PSI and Middle South Services, will be especially important to a sound decision. Current planning calls for a recommendation by PNL to the DOE, on which advanced concepts should be considered for the demonstration phase, by the end of FY-1980. A decision by the DOE on the recommendation may be made in FY-1981.

PROJECT SUMMARY

Project Title:	Advanced CAES Concept Studies - Thermal Energy Storage/Economic Analysis
Principal Investigator:	S.C. Schulte
Organization:	Pacific Northwest Laboratory P.O. Box 999 Richland, Washington 99352 (509) 942-4362
Project Goals:	The goals of the thermal energy storage/economic analysis task are to: (1) estimate the costs (e.g., initial capital investment cost, operating and maintenance cost, fuel oil and compression energy cost, levelized energy cost) of alternative CAES advanced TES system concepts relative to the costs of a conventional CAES non-TES system, and (2) examine the sensitivity of these estimated costs to changes in compression energy and turbine fuel costs.
Project Status:	The activities completed thus far this fiscal year are: (1) an incremental cost analysis study focusing on four alternative CAES advanced TES system concepts, and (2) a consolidation/update study that developed "normalized" system cost estimates for previous contractor-generated CAES advanced TES system studies. The incremental cost analysis has been documented in a draft report and in a paper presented at the 14th intersociety energy conversion engineering conference (IECEC). The consolidation/update study is described in a paper that will be presented at the 1979 Mechanical and Magnetic Energy Storage Contractors' Review.
Contract Number:	EY-76-C-06-1830
Contract Period:	FY-1979
Funding Level:	$35K
Funding Source:	Department of Energy, Division of Energy Storage Systems
Budget Number:	C8-03-02
PNL Number:	PNL 85002, 80055

THE ECONOMICS OF THERMAL ENERGY STORAGE FOR COMPRESSED AIR ENERGY STORAGE SYSTEMS

by

S.C. Schulte
Pacific Northwest Laboratory
Richland, Washington 99352

ABSTRACT

The costs of compressed air energy storage (CAES) systems utilizing thermal energy storage are compared with the costs of conventional CAES systems and combustion gas turbine systems. Comparisons are made on the basis of system energy cost levelized over system operating lifetime (mills/kWh). The comparison was performed by Pacific Northwest Laboratory for the Department of Energy using information from reference studies by the Massachusetts Institute of Technology, Central Electricity Generating Board and Knutsen Research Services.

System energy costs were estimated using information from three reference CAES/thermal energy storage studies, a recent PNL research effort, and the EPRI Technical Assessment Guide. Capital investment cost estimates and system operating requirements were obtained from the reference studies. Current turbine fuel and compression energy prices were obtained from a July 1979 PNL research effort. Economic and financial input assumptions and a discounted cash flow-required revenue computational methodology were taken from the Technical Assessment Guide. Use of such a "normalization" procedure results in system energy cost estimates that are both realistic and comparable.

Two principal conclusions resulted from the study. First, given today's fuel prices and the expected fuel prices in the 1980's, conventional CAES systems yield lower energy cost estimates than combustion gas turbine systems. Second, thermal energy storage/adiabatic CAES systems yield equivalent and, in some instances, slightly lower energy cost estimates than conventional CAES systems while requiring considerably less turbine fuel oil.

INTRODUCTION

The cost of energy from conventional compressed air energy storage (CAES) systems is highly dependent upon the cost of the turbine fuel oil used in this system. Due to the uncertainty and rapid escalation of fuel oil prices, this dependence upon fuel oil decreases the economic attractiveness of conventional systems and increases the attractiveness of systems that require little or no fuel.

The purpose of the study described in this paper was to assess the costs of one group of alternative near term CAES system concepts that require little or no turbine fuel. These alternative systems utilize thermal energy storage. In these systems, a thermal energy storage device is heated or charged using the heat of compression. Thermal energy is then stored for use during the system's power generation cycle. During power generation, compressed air is passed through the thermal energy storage device resulting in heating of the compressed air. The additional heat available from thermal energy storage replaces heat that in conventional systems would be generated by burning fuel oil. This substitution results in a decrease in system fuel cost. If the decrease in fuel cost more than offsets increases in compression energy cost and thermal energy storage device cost, the net effect of utilizing thermal energy storage is to reduce system energy costs. Under these circumstances, CAES/thermal energy storage systems are economically more attractive than conventional CAES systems.

The measure of system cost or economic performance used in the comparison is system energy cost levelized over the system's operating lifetime. The cost estimates are reported in 1979 price levels in terms of mills/kWh.

The study was performed by Pacific Northwest Laboratory for the Division of Energy Storage Systems, the Department of Energy.

APPROACH

The approach taken to assess economic performance was to develop and compare alternative system levelized energy cost estimates. Estimates were developed for CAES systems utilizing thermal energy storage, conventional CAES systems, and combustion gas turbine systems. Assessments of economic performance were based on these energy cost estimates.

The procedure used to develop energy cost estimates is shown in Figure 1. It is important to recognize that this paper is not reiterating the findings of the reference studies. The study reported in this paper uses the reference studies as sources of input information only. In most instances, this study's energy cost estimates are different from the reference study estimates. This results from the use of very current (July-August 1979) price information in this study and outdated price information (pre-1979) in the reference studies.

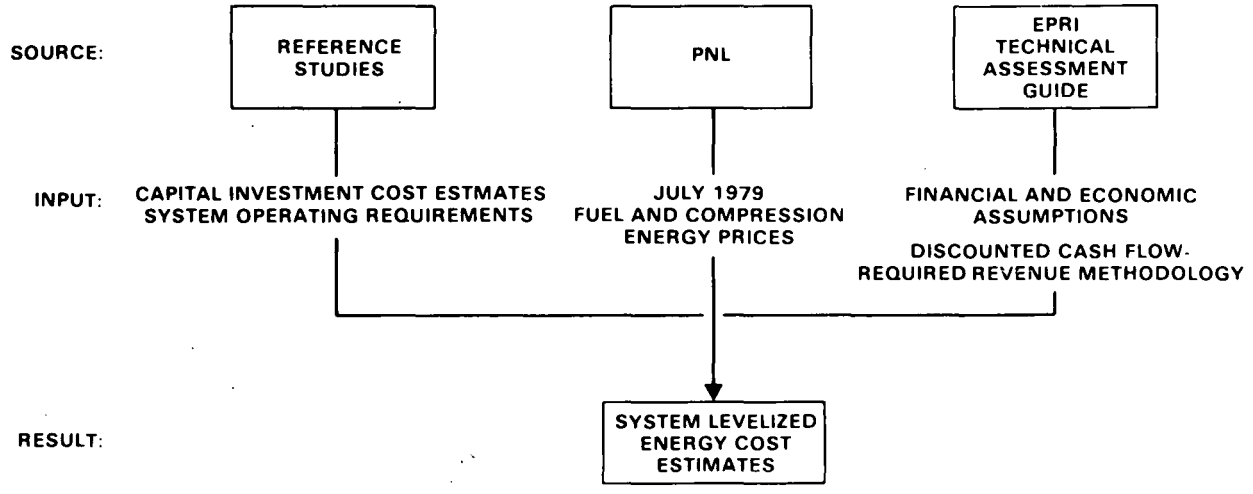

FIGURE 1. Levelized Energy Cost Estimating Procedure

The reference studies are as follows:

- Advanced Compressed Air Energy, Central Electricity Generating Board, March 1979. (Preliminary Draft.)[2]
- Incremental Cost Analysis of Advanced Concept Compressed Air Energy Storage Systems, Knutsen Research Services, July 1979. (Preliminary Draft.)[3]
- Application and Design Studies of Compressed Air Energy Storage for Solar Applications, Massachusetts Institute of Technology, February 1979. (Draft Final Report.)[1]

The type of consolidation/update study described in this paper is useful in two respects. First, such a study reports the results of different studies collectively. Credibility is enhanced when independently generated studies arrive at similar conclusions. Second, this type of study provides for the updating of previously generated studies whose conclusions are invalid because they were based on now outdated input. Often, different yet valid conclusions can be drawn from older studies that are reworked with current input. Both these reasons indicate the usefulness of a consolidation/update study to the compressed air energy storage development program.

SYSTEM DESCRIPTIONS

Four generic near term peaking system concepts were examined in this study. Two compressed air energy storage (CAES) systems utilizing thermal energy storage, one conventional fired CAES

system, and one combustion gas turbine system. The conventional CAES system and combustion gas turbine system were included in the analysis for comparative purposes. The four generic system concepts are as follows:

- CAES/One Stage TES/Hybrid
- CAES/Two Stage TES/Adiabatic
- Conventional CAES
- Combustion Gas Turbine

Simplified system diagrams are shown in Figure 2 for the conventional CAES system concept, in Figure 3 for the one stage thermal energy storage/hybrid system concept, and in Figure 4 for the two stage thermal energy storage/adiabatic system concept. The one stage thermal energy storage/hybrid system utilizes thermal energy storage and is fired (i.e., requires fuel oil to operate). The two stage thermal energy storage/adiabatic system operates adiabatically (i.e., is not fired). The conventional CAES system does not use thermal energy storage and is fired. The reference conventional CAES system is assumed to be of second generation design.

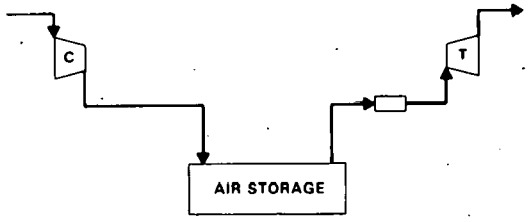

FIGURE 2. Conventional CAES

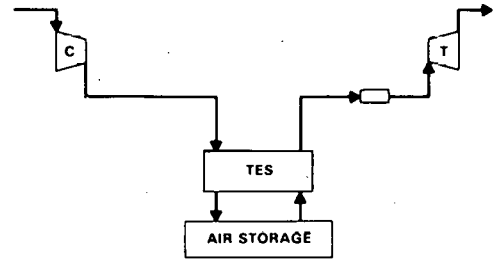

FIGURE 3. CAES/One Stage TES/Hybrid

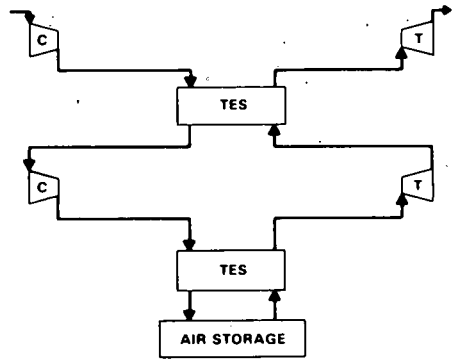

FIGURE 4. CAES/Two Stage TES/Adiabatic

System designs, operating requirements, and capital investment cost estimates were taken from the reference studies. This information was used as input to the calculation of levelized energy cost. This information is shown in Table 1.

TABLE 1. System Descriptions

PNL System Designation	Reference Study	Reference Study System Designation	Fuel Heat Rate (Btu/kWh)	Coefficient of Performance (kWh Out/kWh In)	Capital Investment Cost (1979 $/kW)
CAES/One Stage TES/Hybrid	CEGB[2]	A5-Hybrid	2,646	.95	304.
CAES/One Stage TES/Hybrid	Knutsen[3]	TES-1	4,074	1.31	344.
CAES/One Stage TES/Hybrid	Knutsen[3]	TES-4	3,545	1.13	355.
CAES/Two Stage TES/Adiabatic	Knutsen[3]	TES-3	--	.65	580.
CAES/Two Stage TES/Adiabatic	MIT[1]	Systems A-H	--	.70	334.
Conventional CAES	CEGB[2]	2nd Generation Brown Boveri	4,085	1.20	266.
Conventional CAES	Knutsen[3]	Reference	4,416	1.45	292.
Combustion Gas Turbine	Knutsen[3]	GT	14,000	--	185.

ECONOMIC ANALYSIS

The computational methodology utilized to estimate levelized energy cost was taken from the EPRI Technical Assessment Guide.[4] Economic and financial input assumptions utilized in the analysis were also taken from the Technical Assessment Guide. Turbine fuel prices and compression energy cost estimates were developed specifically for this study by a PNL survey effort.[5,6]

Reference CAES system designs are based on near term (pre-1985) design technology. Estimates reflect expected costs of commercial generating systems existing as part of a mature CAES economy (i.e., tenth plant built of a like technology). Estimates do not reflect costs for prototype or first of a kind systems. CAES systems are assumed to be owned and operated by a regulated electric utility company.

Three sets of input assumptions were used in the analysis. Base case assumptions reflect the most realistic input assumptions. Sensitivity Case 1 assumptions consist of assumptions typical of those used in previous year CAES/thermal energy storage studies. Sensitivity Case 2 input assumptions represent input for a low capacity factor/1000 hour operation per year system. Assumptions are shown in Table 2. In the table, only those sensitivity case inputs that differ from base case inputs are shown.

TABLE 2. Economic Assumptions

	Base Case Most Realistic Assumptions (July 1979)	Sensitivity Case 1 Year 1978 Assumptions	Sensitivity Case 2 Low Capacity Factor Assumption
First Year of Plant Operation	1985		
Plant Capacity Factor	.25 (8 Hr Discharge)		.12
Plant Lifetime	30 Yr		
Cost of Capital	10%/Yr		
Fixed Charge Rate	15%/Yr		
Compression Energy Cost (1979)	15 Mills/kWh	20 Mills/kWh	
Turbine Fuel Cost (1979)	$5/10^6 Btu	$3.33/10^6 Btu	
General Inflation Rate	6%/Yr		
Capital Escalation Rate	6%/Yr		
Operating and Maintenance Escalation Rate	6%/Yr		
Compression Energy Escalation Rate	7%/Yr		
Turbine Fuel Escalation Rate	8%/Yr	7%/Yr	
Gas Turbine Technology	Near Term	Advanced	

RESULTS

Estimates of levelized energy cost for the four system concepts are shown in Table 3. Estimates are reported in 1979 price levels for a construction/ operation scenario where CAES systems would begin commercial operation in 1985. Estimates were developed for each of the reference study design cases. A breakdown of levelized energy cost contributor elements for the base case estimates is shown in Figure 5.

TABLE 3. Levelized Energy Cost Estimates (1979 mills/kWh)

	Base Case Most Realistic Assumptions (July 1979)	Sensitivity Case 1 Year 1978 Assumptions	Sensitivity Case 2 Low Capacity Factor Assumption
CAES/One Stage TES/Hybrid	98	93	121
	108	94	136
	110	96	135
CAES/Two Stage TES/Adiabatic	99	116	143
	77	93	102
Conventional CAES	107	91	127
	108	89	130
Combustion Gas Turbine	206	103	220

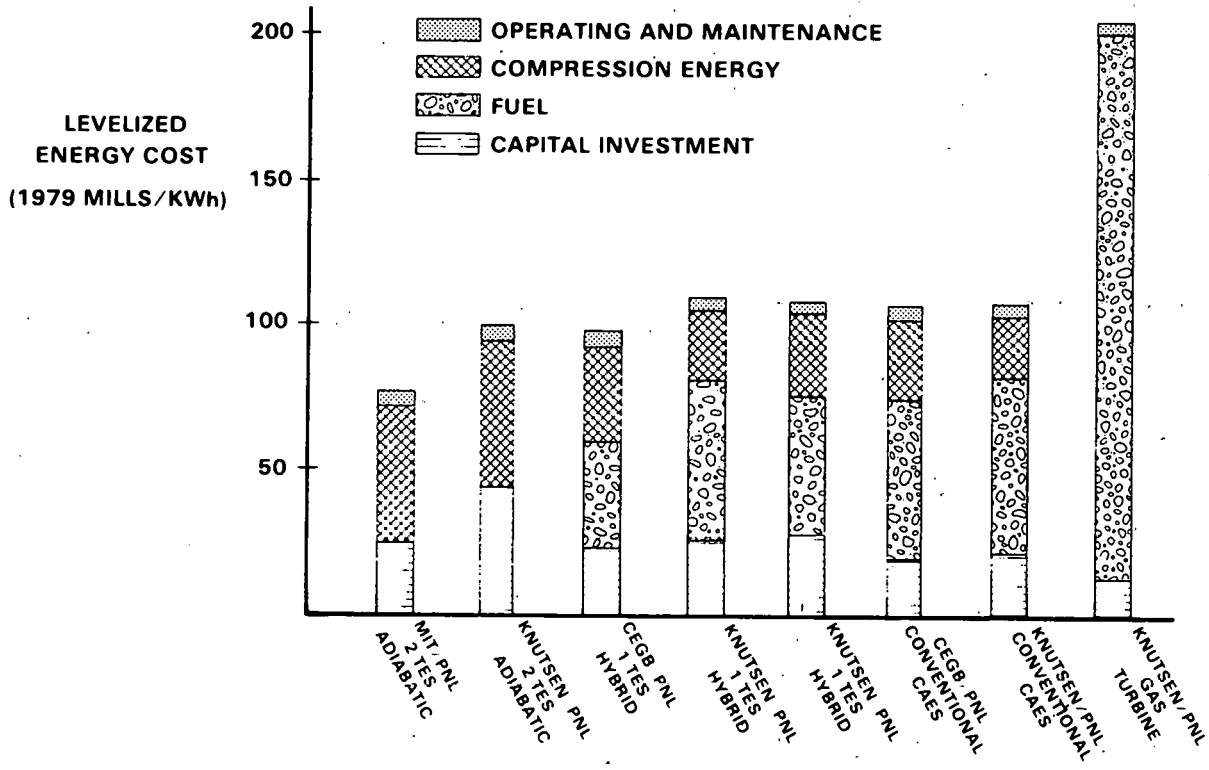

FIGURE 5. Levelized Energy Cost Estimates - Base Case

CONCLUSIONS

A ranking of the economic performance of the four systems is shown in Table 4. Rankings were based on levelized energy cost estimates.

TABLE 4. Ranking of Systems Based on Energy Cost Estimates

	Base Case Most Realistic Assumptions (July 1979)	Sensitivity Case 1 Year 1978 Assumptions	Sensitivity Case 2 Low Capacity Factor Assumption
CAES/One Stage TES/Hybrid	2	2	1
CAES/Two Stage TES/Adiabatic	1	4	1
Conventional CAES	3	1	1
Combustion Gas Turbine	4	3	4

The most significant conclusion that can be made from examination of the rankings is that relative economic performance or ranking is very dependent upon turbine fuel oil and compression energy price. System ranking differs significantly depending upon the set of price assumptions utilized in the analysis. Base assumptions were developed from very current (July 1979) price information. These inputs reflect recent increases and uncertainty in fuel oil prices. Sensitivity Case 1 input assumptions were developed to match assumptions used in reference studies. Recent price increases and uncertainty are not reflected in these earlier year study assumptions. Energy cost estimates for systems that burn fuel oil are very sensitive to input assumptions. Energy cost estimates for systems that burn little or no fuel are relatively insensitive to input assumptions. Relative rankings of systems will vary depending upon the input assumption case utilized due to this difference in assumption sensitivity.

This study makes four conclusions with respect to the economic performance of compressed air energy storage (CAES) systems using thermal energy storage. These conclusions are as follows:

- CAES system energy cost estimates are very sensitive to changes in fuel oil prices and compression energy costs.
- CAES system energy cost estimates are less sensitive to changes in system capital investment cost.
- CAES systems appear less costly than combustion gas turbine systems.
- Previous studies have reported that dramatic fuel oil price increases would make CAES/thermal energy storage systems cheaper than conventional CAES systems. Fuel oil prices have increased dramatically. Adiabatic CAES systems using thermal energy storage now appear slightly less costly than conventional CAES systems.

REFERENCES

1. G. T. Flynn and J. L. Nash-Webber, Application and Design Studies of Compressed Air Energy Storage for Solar Applications, Massachusetts Institute of Technology, Lexington, Massachusetts, February 1979. (Draft Final Report)
2. I. Glendenning, Advanced Compressed Air Energy, Central Electricity Generating Board, Marchwood Engineering Laboratory, Southampton, SEZ, England, March 1979. (Preliminary Draft)
3. C. Knutsen, Incremental Cost Analysis of Advanced Concept Compressed Air Energy Storage Systems, Knutsen Research Services, Bothell, Washington, July 1979. (Preliminary Draft)
4. Technical Assessment Guide, Electric Power Research Institute, Palo Alto, California, EPRI PS-866-SR, June 1978.

5. Platt's Oilgram Price Report, McGraw Hill Publishing Company, New York, New York.

6. Monthly Energy Report, U.S. Department of Energy, Energy Information, DOE/EIA-0035/6(79). June 1979.

PROJECT SUMMARY

Project Title: Assessment of Fluidized Bed Augmented Compressed Air Energy Storage System

Principal Investigator: A.J. Giramonti, R.D. Lessard

Organization: United Technologies Research Center
East Hartford, CT 06108
(203) 727-7361

Project Objective: Conduct a preliminary technical and economic feasibility evaluation of coal-fired fluidized bed combustion (FBC) augmented compressed air energy storage (CAES) systems.

Project Goals: This project is divided into the following five tasks:

(1) Review status of FBC technology and assess application to CAES systems.

(2) Conduct FBC/CAES systems analysis including a review of turbomachinery technology, system integration and performance studies, and a preliminary screening analysis to identify the most promising system configuration.

(3) Prepare a preconceptual FBC/CAES power plant design for the most promising system configurate and estimate the cost of electricity for such a plant.

(4) Perform a preliminary market evaluation based on siting considerations and cost comparisons with commercial power plant alternatives.

(5) Perform an introductory assessment of FBC/CAES system performance and operation under part load conditions.

Project Status: The status of each task is as follows:

(1) & (2) Tasks completed. FBC/CAES concept appears feasible, and configuration using open-bed FBC selected for further study.

(3) Preconceptual designs for major components and overall plant layout near completion. Economic studies to begin shortly.

(4) Market evaluation to begin shortly.

(5) Part load assessment was recently initiated.

Contract Number: B-51299-A-P

Contract Period: November 1978 to March 1980

Funding Level: $250,000

Funding Source: Battelle Pacific Northwest Laboratories

PRELIMINARY EVALUATION OF COAL-FIRED FLUID BED COMBUSTION-AUGMENTED COMPRESSED AIR ENERGY STORAGE POWER PLANTS

Albert J. Giramonti
United Technologies Research Center
East Hartford, Connecticut 06108

ABSTRACT

This paper presents the highlights of an ongoing program to assess the technical and economic feasibility of advanced concepts for generating peak-load electric power from a compressed air energy storage (CAES) power plant incorporating a coal-fired fluid bed combustor (FBC). Specifically, it reviews: the design and operating considerations involved with integrating an atmospheric fluid bed combustor (AFBC) or a pressurized fluid bed combustor (PFBC) with a CAES system to yield practical system configurations; the integration of system configurations; the parametric performance of these system configurations; and the preliminary screening which considered performance, cost, and technical risk and which led to the identification of an open-bed PFBC/CAES system as having the greatest near-term commercialization potential.

INTRODUCTION

An energy storage system which could be attractive for future electric utility peak-power applications is a modified gas turbine power system utilizing underground storage of very high pressure compressed air. In the compressed air energy storage (CAES) concept (1), synchronous gear clutches would be used to uncouple the compressor and turbine so that they could operate during different time intervals. During low-load, off-peak periods the compressed air would be withdrawn from storage, mixed with fuel, burned, and expanded through the turbine to generate power. One such system using petroleum fuel is currently in operation in West Germany (2), and others of this type are deemed likely in the foreseeable future.

A potential long-term weakness of the CAES concept, as presently implemented, is its reliance on petroleum fuels during the power generation mode. It is appropriate, therefore, to investigate advanced CAES concepts designed to substitute a domestically more abundant fuel, such as coal, for petroleum. Direct combustion of pulverized coal in gas turbines was attempted in the 1950's but proved unsuccessful because of problems with ash slagging, erosion, and corrosion associated with high combustion temperatures (3). An improved approach to coal combustion utilizing fluid bed combustors (FBC), offers the promise of solving some of these problems by permitting the combustion process to take place at low temperature.

Application of a FBC to the CAES concept creates the potential for a large number of possible FBC/CAES power plant system configurations incorporating atmospheric fluid bed combustors (AFBC) or pressurized fluid bed combustors (PFBC). In principle, all of these configurations would use a coal-fired FBC to replace the petroleum-fired burner. A very simplified schematic representing possible PFBC and AFBC/CAES system configurations is shown in Fig. 1. If a PFBC were used, high-pressure air could be fed into the combustor. The

combustion gases from the PFBC would then be cleansed and expanded through the turbine. Another possible approach (not shown in Fig. 1) would be to split the airflow prior to the PFBC feeding a portion of the high-pressure air through heat transfer tubes immersed in the bed and the remaining portion into the combustor. The combustion gases would then be cleansed and mixed with the clean heated air prior to expansion. If an AFBC were used, high-pressure air would be heated in tubes immersed in the bed and then expanded through the turbine. The turbine exhaust air would then be fed into the combustor to provide the combustion air. The combustion gases from an AFBC are at atmospheric pressure and could not be mixed with the heated air, as in the PFBC, but would be directed to the stack after transferring its thermal energy to the high pressure air (not shown in Fig. 1).

The purpose of this paper is to review the analysis performed to select a FBC/ CAES system configuration which has the potential for attractive performance and cost characteristics combined with near-term commercialization potential. The study program on which this paper is based is being supported by the Battelle Pacific Northwest Laboratory under Subcontract No. B-51299-A-P as part of their Contract No. EY-76-C-06-1830 with the Department of Energy.

INTEGRATION CONSIDERATIONS

Integrating the fluid bed combustor, gas turbine, air storage and heat transfer equipment into an efficient, uncomplicated, and inexpensive power plant requires an appreciation of the operational and design limitations associated with each of these major subsystems to ensure compatability among them. In previous years, conceptual design studies of petroleum-fired CAES power plant systems have been conducted by several organizations (4, 5, and 6). In these studies considerable effort was expended to ensure that compatability does exist among the gas turbine, air storage, and heat transfer equipment. By effectively using the results from these studies attention can be focused upon the novel feature of the FBC/CAES power plant system, i.e., the substutition of a coal-fired FBC for the petroleum-fired combustor.

BED EXIT TEMPERATURE

The operating conditions which can be expected from both the FBC and CAES turbomachinery are significantly influenced by their designs. In an earlier publication (7), the design technologies associated with both these subsystems were reviewed. From that review it can be stated that the most critical operating condition is the bed exit temperature, because the turbine inlet temperature is dependent on the bed temperature and the means chosen to transfer the thermal energy from the bed to the expansion gas.

The choice of bed temperature is influenced by many considerations, the most important of which are achieving a high combustion efficiency, avoiding ash sintering, maximizing sulfur retention, obtaining high heat transfer rates to in-bed tubes, limiting the temperature of heat transfer surfaces in the bed, and reducing emissions of alkali metal salts. Weighing these sometimes opposing considerations results in an indication that the bed operating temperature should be maintained within the range of 775 to 900 C (1425 to 1650 F) with 850 C (1560 F) being a representative value.

If an open-bed PFBC were used in the CAES power plant and the combustion gases expanded in the gas turbine after particulate cleanup, then the turbine inlet temperature would at most be equal to the bed temperature (Fig. 2a). Turbine inlet temperatures of this magnitude

are characteristic of operating conditions used two decades ago and would not produce the maximum performance potential from current gas turbines that operate at temperatures around 1095 C (2000 F). The reduced temperatures would, however, tend to inhibit potential erosion and corrosion resulting from particulates and alkalies entrained in the hot gases.

If an AFBC or a PFBC with tubes immersed in the bed were used in the CAES power plant, then the turbine inlet temperature might be limited to 550 C (1020 F) for near-term applications. The air in immersed tubes is constrained to this temperature despite the higher bed temperature by a concern for the integrity of tube metal which, while being required to contain pressurized air, is being subjected to a high-temperature corrosive environment in the fluid bed. By maintaining the air temperature below 550 C (1020 F), it is possible to keep the outside tube metal temperature below a level (650 C (1200 F)) which can be considered to be within the corrosion limit of current commercially available materials. Obviously, maintaining the expansion air temperature at this level severely restricts the number of viable system configurations which could be considered because of the reduced performance that would be associated with a turbine inlet temperature of this magnitude.

For an AFBC, one approach around this limitation would be to place convection heat exchanger surface in the freeboard above the bed where it is possible for gas temperatures to reach 1000 C (1830 F) due to combustion in the freeboard (Fig. 2h). Since the corrosive environment in the freeboard is much less severe than in the bed due to the absence of the sulfur acceptor, the outside metal temperature of the convective heat exchanger tubes can approach 800 C (1470 F) for commercial alloys. Accordingly, the exit air temperature could be as high as 750 C (1380 F).

For a PFBC with tubes immersed in the bed, the turbine inlet air temperature can exceed the maximum immersed tube air temperature of 550 C (1020 F) because the combustion gases at 850 C (1560 F) are mixed with the tube exit air prior to the turbine. However, this mixing will result in the turbine inlet temperature being at some level below the bed temperature.

BED PRESSURE AND FLUIDIZING VELOCITY

Bed pressure and fluidizing velocity are also important operating parameters. The selection of operating pressure will influence combustion efficiency, sulfur retention, nitrogen oxides emission, and capital cost. Operation at elevated pressure (PFBC) will produce beneficial results for all of these parameters as opposed to operation at atmospheric pressure (AFBC). The fluidizing velocity must be controlled within fairly narrow limits, i.e., 0.75 to 1.4 m/s (2.5 to 4.5 ft/sec) for a PFBC and 0.75 to 2.5 m/s (2.5 to 8 ft/sec) for an AFBC. Operation within this range will establish good bed fluidization, provide sufficient oxygen for combustion, and limit elutriation of bed particles.

Both pressure and velocity significantly affect combustor capital cost. The size of the FBC is reduced with increasing pressure and fluidizing velocity because the mass flow rate increases, thereby increasing the power output per unit bed area. This effect is graphically illustrated in Fig. 3.

SYSTEM CONFIGURATIONS

The FBC/CAES system integration incorporated the system design philosophy used by UTRC in previous studies (4, 6, and 8) wherein the turbomachinery contains both low- and high-pressure components. In such a system the low-pressure compressor is used to raise the air

to an intermediate-pressure level (typically 16 bar (atm)), after which the booster compressor is used to increase the pressure to a level compatible with the storage reservoir pressure (typically 40 to 80 bar (atm), with 66 bar (atm) used in this study). The high-pressure expansion turbine and low-pressure turbine perform the reverse role. Using this system design philosophy as a basis, it is then possible to introduce the key components associated with the fluid bed combustor and turbomachinery which might be unique to a specific FBC/CAES application.

Several FBC/CAES system configurations were studied; some of the more promising are discussed here. The compression system was unchanged among these configurations; consequently, the only variations in the system configurations are in the manner in which the stored air would be heated and expanded.

PFBC/CAES SYSTEM CONFIGURATIONS

In the open-bed PFBC/CAES configuration (Fig. 4), air from the recuperator at approximately 60 bar (atm) would be expanded through the expansion turbine and used for combustion in an intermediate-pressure (16 bar (atm)) open-bed PFBC. The gases would then be expanded to almost atmospheric pressure in the low-pressure turbine and cooled in the recuperator. The temperature into the expansion turbine would be relatively low, thus, leading to relatively low power output. To increase the power output from the expansion turbine, other system configurations were investigated which would increase the temperature into the expansion turbine.

One approach would be to utilize a very high pressure (VHP) PFBC operating at about 60 bar (atm). Air from the recuperator would be used for combustion in the VHP PFBC (Fig. 5), expanded in the expansion turbine, and then used for further combustion in the intermediate-pressure PFBC. The twice combusted gas would then be expanded in the low-pressure turbine. This system exhibited the best performance of all the FBC/CAES systems that were studied.

Another approach to increase the temperature into the expansion turbine and, thus, increase the expansion turbine output would be to put in-bed air heater tubes in the PFBC. High-pressure air from the recuperator would pass through tubes in an intermediate-pressure PFBC (Fig. 6). The air would be heated to 550 C (1020 F) and then expanded through the expansion turbine. The air would then be used for combustion in the PFBC and expanded through the low-pressure turbine. The air temperature exiting from the in-bed tubes would be limited to 550 C (1020 F) because of the corrosion problems identified previously.

AFBC/CAES SYSTEM CONFIGURATIONS

The use of an AFBC would do away with the potential problems of turbomachinery material corrosion and erosion because only clean air would be expanded through the turbines. Several basic AFBC/CAES system configurations were studied, all of which used immersed tubes in the bed and external convective heat exchangers using energy in the hot AFBC exhaust gases. One of these configurations is depicted in Fig. 7. Air from storage would be preheated in the recuperator, heated to 550C (1020F) in tubes placed within the bed, and then further heated in the convective heat exchanger prior to expansion. The hot AFBC combustion gases (at 1000 C (1830 F)) would be used to heat the expansion and low-pressure turbine inlet air and reheat the combustion air going to the AFBC. The combustion gases are then mixed with

the low-pressure turbine exhaust air which was not used for combustion. The resulting mixture is passed through the recuperator to preheat the air from storage.

Both counterflow and parallel flow heat exchangers were investigated with the objective of obtaining as high a temperature as possible into the turbines while limiting the average heat exchanger metal temperature to 800 C (1472 F). The counterflow arrangements are capable of heating the turbine air up to about 740 C (1370 F), but they would require a maximum metal temperature around 870 C (1600 F). In the parallel flow arrangement a pinch condition would limit the maximum air and metal temperatures to about 690 C (1270 F) and 715 C (1320 F), respectively.

PARAMETRIC PERFORMANCE

The level of performance that a CAES power plant could achieve depends greatly on the system operating conditions and component performance characteristics selected. The pertinent component values for the FBC and turbomachinery were estimated for use in the performance analysis. Operating and performance characteristics for the remaining CAES equipment were based on previous studies conducted by UTRC (Refs. 4, 6, and 8). The more important parameters are identified in Table I, and the performance results are summarized in Table II.

PFBC/CAES SYSTEMS

Four sets of operating conditions were simulated for the open-bed system configuration depicted in Fig. 4. First, the range of operating pressure which could be expected from current PFBC technology and which could be applied to the intermediate-pressure PFBC in a near-term CAES application, i.e., 10 to 15 bar (atm), was bracketed. Next, the effect on performance of an evolution in technology was simulated; first, by increasing bed temperature 50 C (90 F) above existing temperatures to 900 C (1650 F), then by increasing the bed pressure to 20 bar (atm) from 15 bar (atm) along with the elevated temperature of 900 C (1650 F). In reviewing both the output power and round trip heat rate resulting from this exercise, it can be seen that the increase in bed temperature produced a more marked improvement in performance than did the increase in bed pressure.

As noted before, the system configuration of Fig. 5 with a very high-pressure open bed PFBC produced very attractive performance characteristics. Two sets of operating conditions were investigated for the intermediate-pressure PFBC representative of near-term technology (15 bar, 850 C (15 atm 1560 F)) and slightly advanced technology (20 bar, 900 C (20 atm, 1650 C)). The bed temperature for the VHP PFBC was taken to be the same as for the intermediate-pressure PFBC, while the bed pressure corresponded to the air pressure at the exit of the recuperator (58 bar (atm)).

The system configuration of Fig. 6 with immersed tubes was the most extensively investigated system configuration, with seven sets of operating conditions simulated. Five of these seven sets were used to bracket the current technology bed operating condition of 850 C (1560 F) and 15 bar (atm). First, it was bracketed by bed pressure, 10 bar (atm) and 20 bar (atm) then it was bracketed by bed temperature, 775 C (1420 F) and 900 C (1650 F). An effect similar to that observed for the simple open bed resulted; i.e., a variation in bed temperature produced more significant improvements in performance than variations in bed pressure.

To evaluate the effect that air storage pressure would have on system performance, the storage pressure was alternately increased then decreased by 20 percent. In viewing the performance resulting from these two simulations, it can be seen that increased storage pressure leads to increased power at the expense of a slight increase in heat rate. The results of this exercise could also be used to approximate the performance that could be expected in constant volume or porous media storage reservoirs wherein the pressure during compression and generation would vary over a similar range (6). It can be shown that the performance of a variable pressure air storage system would be comparable to that obtained from a constant pressure air storage reservoir when the constant air storage pressure is equal to the average pressure of the variable pressure reservoir.

AFBC/CAES SYSTEMS

Three sets of operating conditions were simulated for the AFBC/CAES system configuration of Fig. 7. The first two simulations provided for counterflow heat exchangers in the convective zone above the free-broad, and the last provided for a parallel flow heat exchanger. In the first of the counterflow simulations, the expansion turbine air bypassed the convective heat exchangers. Consequently, the expansion turbine inlet temperature reflected the immersed tube air exit temperature of 550 C (1022 F). In the second of the counterflow simulations, the expansion turbine air did pass through the heat exchanger where it was heated to 740 C (1370 F). For the parallel flow simulation, the expansion turbine air also passed through the heat exchanger where it was heated to 690 C (1270 F).

The counterflow simulations produced the better performance results because of the higher turbine inlet conditions. Of the two counterflow configurations, the second one in which both the expansion and low turbine inlet air streams were heated to the maximum temperature produced the better performance. However, the maximum metal temperature would be much lower in the parallel flow arrangement.

PRELIMINARY SCREENING ANALYSIS

The objective of the screening analysis was to identify the FBC/CAES system that has the greatest potential for near-term commercialization and also has attractive performance, low cost, and low technical risk. The performance results are covered in the previous section; cost and risk characteristics are presented below.

COST CHARACTERIZATION

Cost characterizations were estimated for each of the major subsystems of the FBC/CAES system: the fluid bed combustor, the heat transfer equipment, and the CAES aboveground and underground equipment. To these direct costs were added approximations for the indirect, owning, and operating costs. The cost values used in this analysis are preliminary in nature, but they are internally consistent and suitable for comparison purposes within the guidelines of the current effort. The relative cost rankings are given in Table III.

RISK ASSESSMENT

A major concern when investigating a novel power system is proper evaluation of the risks associated with its commercialization. Not only is there a technlogical risk in that

the power system may not meet performance expectations, but there is also an economic risk in that the developer may not earn an acceptable return on his investment.

Areas in which R&D on fluid bed combustion is required include: coal and sorbent feeding, coal distribution, combustor design, hot gas cleanup, disposal of output solids, tube bundle design, load following and control, and regeneration of sorbent. The existence of unknowns in these areas poses a potential risk to the commercialization of the FBC/CAES power plant system concept. Obviously, success in some areas is more vital to the concept then in other areas. For the open-bed PFBC/CAES system, hot gas clean up is important. For the FBC/CAES systems with immersed tubes, tube bundle design and load following are important. Consequently, in assessing these systems greater weight was subjectively assigned to those areas.

Relatively little risk is associated with the turbomachinery in AFBC/CAES applications. However, areas in which R&D on turbomachinery for PFBC/CAES applications is required include: hot gas cleanup, particulate erosion, corrosion, combined erosion/ corrosion, deposition, combined deposition/ erosion/corrosion, damage control techniques, and alkali metal control. In this assessment, particulate erosion and alkali erosion received greatest weight.

Many of the corrosion concerns expressed about the turbomachinery are similar to those for the high-temperature convective heat exchangers. These concerns occur primarily for the AFBC systems because hot AFBC exhaust gases bathe the hot side of the convective heat exchangers. Metal operating temperature, therefore, is an important risk consideration.

It should be noted that most of these risk areas are being addressed as part of an extensive DOE combined cycle development effort (9). However, the rapid cycling requirement for CAES systems in peaking applications is significantly different from the intermediate- and base-load requirements of the combined cycle program. Accordingly, some of the load-following requirements of FBC/CAES systems require special attention.

The approach used in this study was to estimate the relative technical risks for each of the three key development areas discussed above -- the FBC system, the turbomachinery and the heat exchangers. A subjective ranking system was used to represent the range from no risk (equipment commercially available) to high risk (design unknowns, R&D required). The result of the risk evaluation is presented in Table III.

COMMERCIALIZATION

The discussion of technical risk, and its associated R&D requirements, leads directly to the issue of commercialization. The term commercialization date, for the purpose of this study, is defined as the earliest date at which both the buyer (electric utility) and the seller (equipment manufacturer) would agree to sign a contract based on standard commercial terms and conditions. Typically, the first date of commercial operation would follow the contract signing by three to ten years, depending on the time required to obtain the necessary permits and construct the plant.

Estimates of the commercialization date are provided in Table IV for the FBC/CAES systems considered. These estimates are based primarily on the development requirements of FBC technology, which was judged to be the pacing item. These projections are consistent with the degree of technical risk reflected in the risk analysis.

PBC/CAES SYSTEM SELECTION

The results of the FBC/CAES screening analysis are summarized in Table III. The open bed PFBC/CAES system was identified as an attractive candidate system. This is based mainly on the relatively low risk for the PFBC design (no tubes in bed), the moderate costs, and the respectable round trip heat rates which this system exhibited. The open bed VHP PFBC/CAES system exhibits superior performance but has high risk. Consequently, this concept may become a future candidate once better design and costing data become available. The PFBC/CAES system with low-temperature air tubes is also an attractive candidate. Its cost and heat rate are lower than for the open-bed PFBC/CAES system; however, because of the tubes in the bed the risk is increased slightly. The AFBC/CAES system with low-temperature air tubes was judged to be questionable for commercial applications. This system would have low risk resulting from the lack of turbine corrosion/erosion problems, but it also has relatively high cost and poor performance.

From the above, it is clear that both the PFBC/CAES-open bed and PFBC/CAES-immersed tube systems are attractive. The latter has lowest cost and heat rate, but it could not become commercial until about 1990. The former has lowest risk and could be commercialized shortly after 1985.

Based upon the potential for earlier commercialization, the PFBC/CAES-open bed system configuration (Fig. 4) was selected for more detailed evaluation. The bed operating conditions chosen for this system are 15 bar (atm) and 850 C (1560 F).

The recommended open bed system has several promising future growth options which tend to reduce costs and lower fuel consumption. Figure 8 graphically depicts two possible evolutionary growth paths from the recommended open bed PFBC system. The upper path contains the nearer term options. Without tubes in the bed, it should be a relatively easy matter to increase bed temperature to 900 C (1650 F) and to increase bed pressure to 20 atmospheres. When the technology for very high pressure beds is developed, one could be added to the system to improve performance. The lower path involves placing tubes in the bed. First, low temperature tubes would be added with metal temperatures limited to about 650 C (1200 F). Eventually, high temperature tubes could be added where the metal temperature would approach the bed temperature.

CONCLUDING REMARKS

The open bed PFBC/CAES system concept seems to be an attractive and logical near-term power plant option. It has low risk, early commercialization potential, and acceptable performance and cost. Furthermore, this system has several growth versions promising lower cost and improved performance. This system is currently undergoing more extensive preconceptual design and analysis.

REFERENCES

1. Giramonti, A. J., Lessard, R. D. Blecher, W. A. and Smith, E. B., "Conceptual Design of Compressed Air Energy Stage Electric Power Systems", Applied Energy, October 1978.

2. Herbst, C. M. Hoeffins, M. and Stys, Z. S. "Huntorf 290 MW Air Storage System Energy Transfer (ASSET) Plant Design, Construction and Commissioning", Proceedings of the 1978 Compressed Air Energy Storage Symposium, Vol. 1, 1979.

3. Tabakoff, W., "Erosion Study in Turbomachinery Affected by Coal and Ash Particles - Phase I", University of Cincinnati Annual Progress Report FE-2465-5, 1978.

4. Giramonti, A. J., et al, "Preliminary Feasibility Evaluation of Compressed Air Storage Power System", United Technologies Research Center Report R76-952161-5, NTIS PB 259-281/4GI, December 1976.

5. Bush, J. B., et al: " Economic and Technical Feasibility Study of Compressed Air Storage", General Electric Company Report COD-2559-1, March 1976.

6. Hobson, M. J. Heath, E. G. Lessard, R. D. and W. A. Adent, " Feasibility of CAES in California", California Energy Resources Conservation and Development Commission Report 500-002, May 1978.

7. Lessard, R. D., Giramonti, A. J. and R. L. Sadala, "Coal Fired Fluid Bid Compressed Air Energy Storage Power Plants: A Preliminary Technical Assessment", Proceedings of the 14th Intersociety Energy Conversion Engineering Conference, August 1979.

8. Davison, W. R. and Lessard, R. D. "Study of Selected Turbomachinery Components for Compressed Air Energy Storage Systems", United Technologies Research Center Report R77-952923-5, November 1977.

9. Fiebus, H. et al, " Commercialization Strategy Report for Advanced Electric Generation Technologies", Department of Energy Report, TID-28839, 1979.

TABLE I. Selected Operating and Design Conditions

Maximum immersed-tube metal temperature	650C (1200F)
Maximum immersed-tube air temperature	550C (1020F)
Storage pressure	66.3 bar (atm)
Storage temperature	49C (120F)
Storage leakage loss	4%
Low-pressure turbomachinery efficiency	.90%
High-pressure turbomachinery efficiency	75-85%
Combustor carbon loss	1%
Combustor radiation loss	1%
Sulfur retention	85%
Overall grid utility heat rate	10,550 kJ/kWh (10,000 Btu/kWh)

TABLE II. FBC/CAES System Performance Summary

System	Bed Exit Conditions bar	C	Power MW	Round Trip Heat Rate kJ/kWh
		PFBC/CAES		
Open bed	10	850	220	14167
(Fig. 4)	15	850	224	13977
	15	900	235	13521
	20	900	238	13414
Open bed,VHP	58/15	850/850	273	12278
PFBC (Fig. 5)	58/20	900/900	281	12134
Immersed tubes	10	850	242	13166
(Fig. 6)	15	850	247	12979
	20	850	247	12942
	15	775	234	13428
	15	900	255	12703
	15(1)	850	254	13069
	15(2)	850	237	12907
		AFBC/CAES		
Immersed tubes	1(3)	1000	218	14263
(Fig. 7)	1(3)	1000	225	13920
	1(4)	1000	213	14528

(1) Storage pressure +20% (79.5 atm)
(2) Storage pressure -20% (53.0 atm)
(3) Counterflow heat exchanger
(4) Parallel flow heat exchanger

TABLE III. FBC/CAES Screening Analysis Results

System	Risk	Cost	Heat Rate	Prognosis
PFBC/CAES-open bed	L	M-L	H-M	Attractive candidate
PFBC/CAES-open bed, VHP PFBC	H	?	L	Future candidate
PFBC/CAES-tubes	M	L	L	Attractive candidate
AFBC/CAES-tubes	L	H	H	Questionable

H = high
M = moderate
L = low

TABLE IV. Commercialization Date Projections

System	Date
PFBC/CAES-open bed	1985+
PFBC/CAES-open bed, VHP PFBC	1995+
PFBC/CAES-immersed tubes	1990-
AFBC/CAES-immersed tubes	1985+

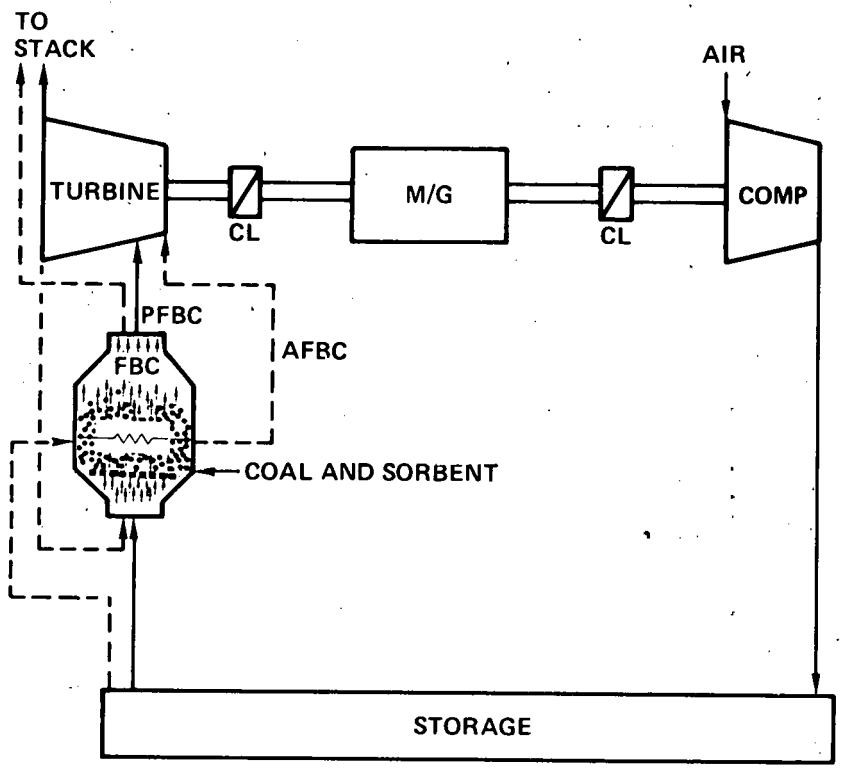

Fig. 1 Simplified coal-fired FBC/CAES system configuration

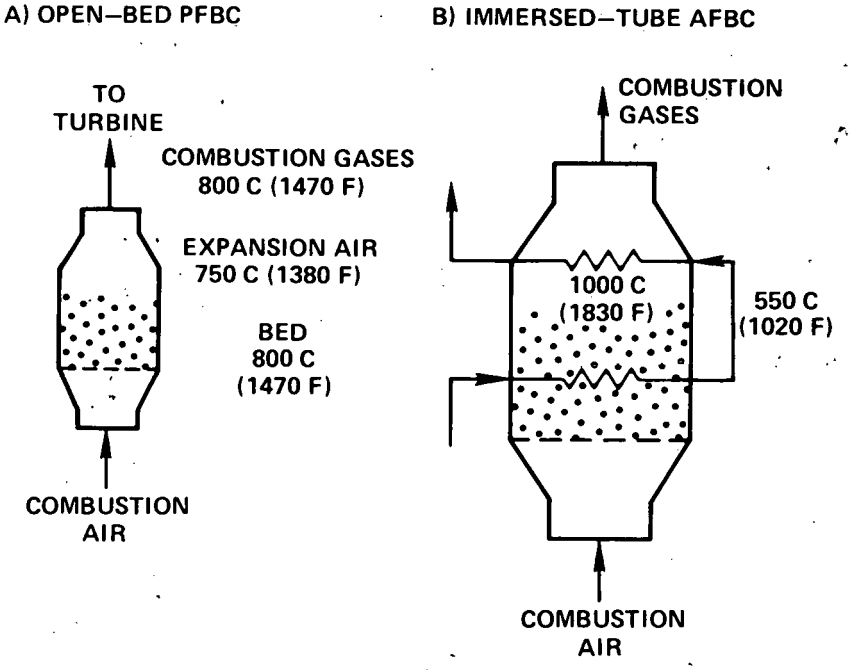

Fig. 2 FBC temperature

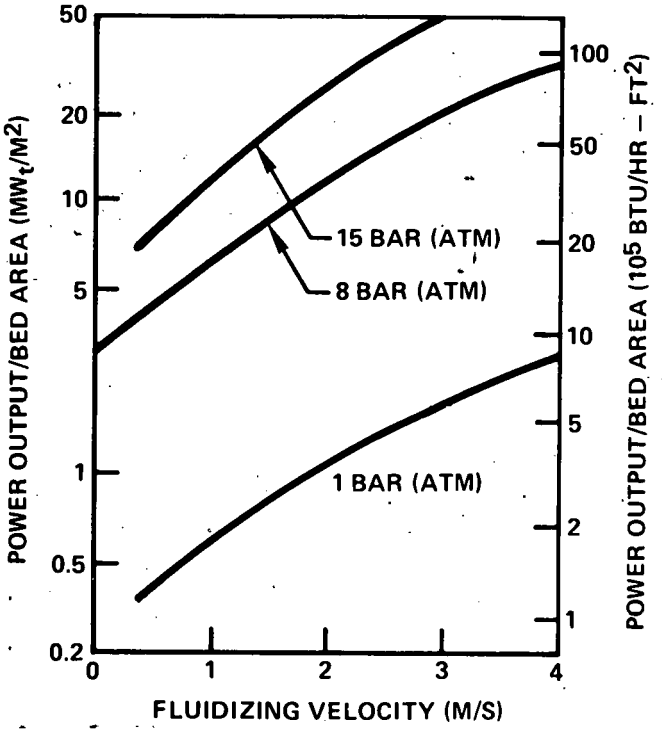

Fig. 3 Effect of fluidizing velocity and operating pressure on power flux

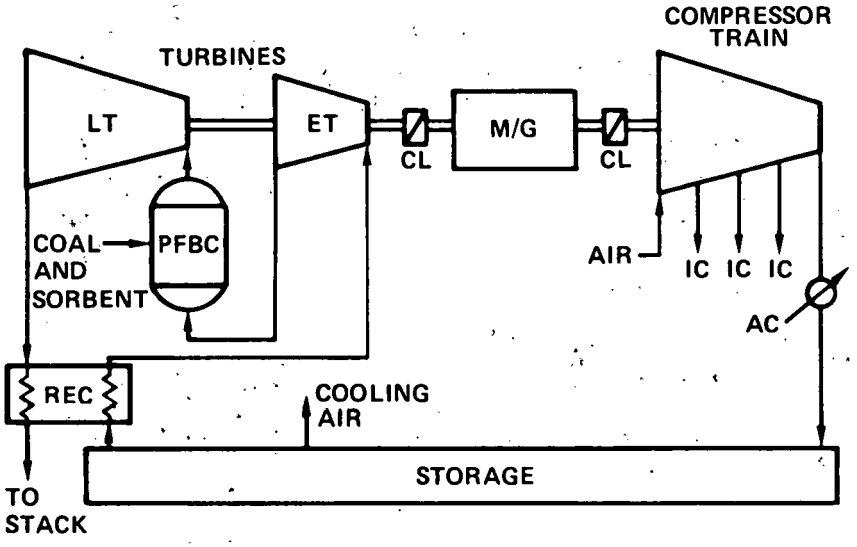

Fig. 4 Coal-fired PFBC/CAES system configuration with open bed

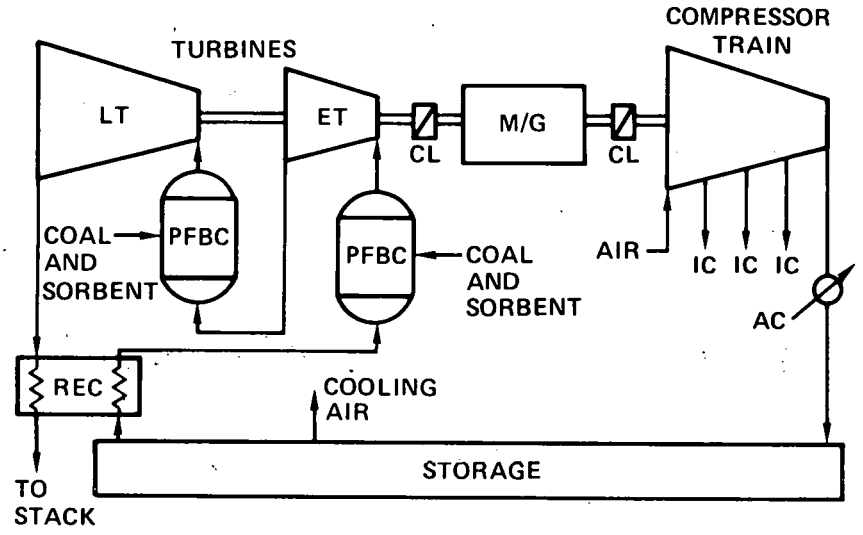

Fig. 5 Coal-fired PFBC/CAES system configuration with open beds and a very high-pressure PFBC

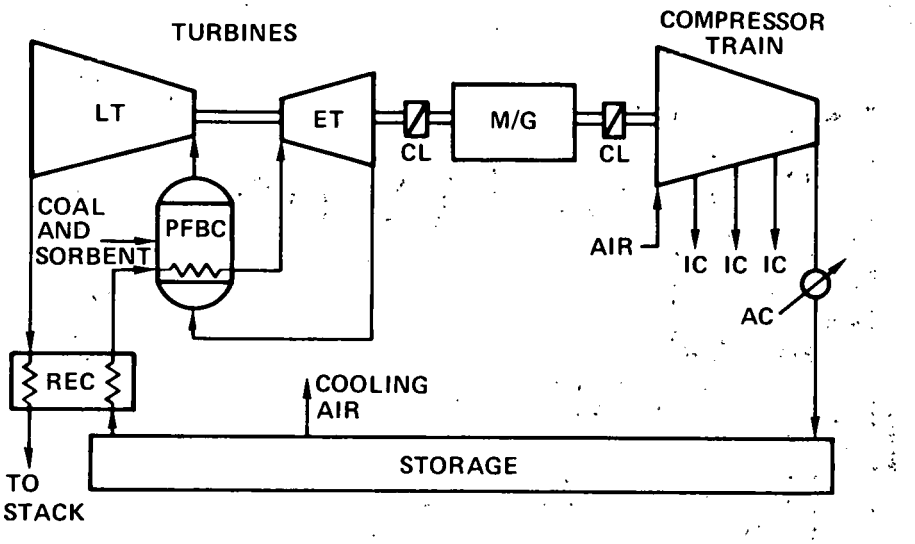

Fig. 6 Coal-fired PFBC/CAES system configuration with tubes immersed in bed

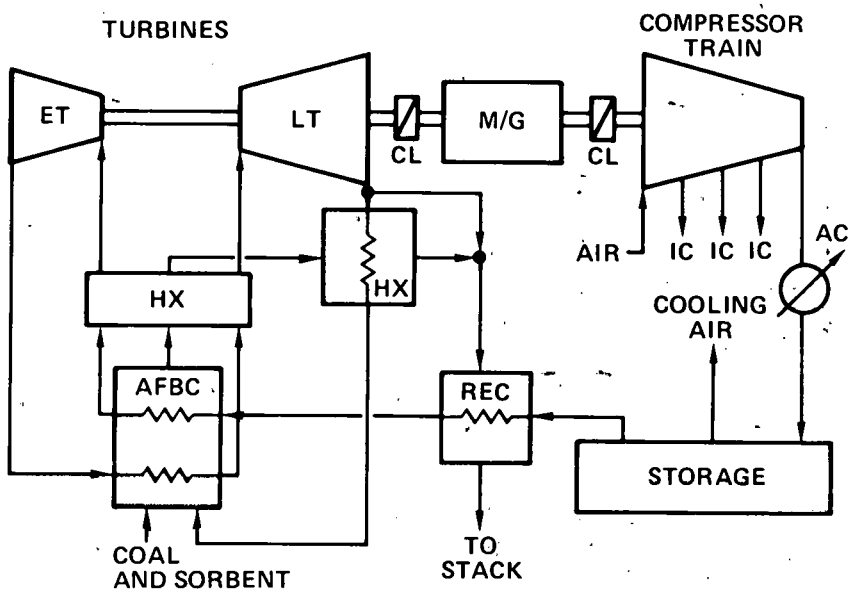

Fig. 7 Coal-fired AFBC/CAES system configuration with tubes immersed in bed and high-temperature heat exchanger

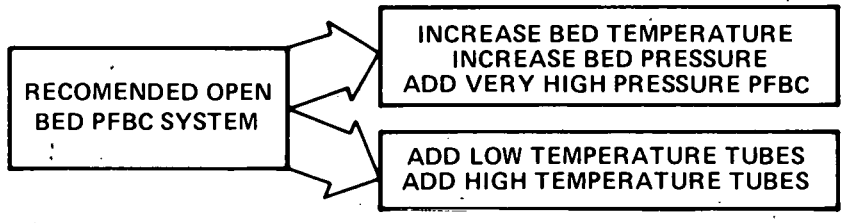

Fig. 8 Growth potential of recommended PFBC/CAES system

SESSION 3: UNDERGROUND PUMPED HYDRO STORAGE

THIS PAGE

WAS INTENTIONALLY

LEFT BLANK

PROJECT SUMMARY

Project Title: "Evaluation of Reversible Pump/Turbines for Underground Hydroelectric Pumped Storage Power Plants"

Principal Investigator: John R. Degnan

Organization: Allis-Chalmers Corporation
Hydro-Turbine Division
P.O. Box 712
York, Pennsylvania 17405
(717) 792-3511

Project Goals: Generation of preliminary machine designs and corresponding hydraulic performance for pump turbines with the following characteristics:

1. 350 megawatt single stage units for rated heat conditions of 500, 750 and 1000 meters
2. 350 megawatt double stage units for rated heat conditions of 1000 and 1500 meters
3. 350 and 500 megawatt multistage units for rated head conditions of 1000, 1250 and 1500 meters.

Project the cost for the various alternate machine designs developed in order to generate parametric cost relations as a function of head and power capacity.

Project Status: It should be noted that this document addresses only the initial two phases of a large development project extending into 1982. The project is concerned with not only the conceptual development of mechanical and hydraulic designs but actual model testing at prototype heads.

The project's first phase was completed and reported during 1978. The second phase is in progress with extensive work being done to develop the multistage concept. Preliminary designs are complete and are currently being analyzed so that the designs can be finalized.

Contract Number: 31-109-38-5078

Contract Period: Phase II - May 25, 1979 - September 30, 1979

Funding Level: $132K

Funding Source: Argonne National Laboratory

COMPARISON OF SINGLE, DOUBLE AND MULTISTAGE PUMP/TURBINE EQUIPMENT FOR UNDERGROUND PUMPED STORAGE SERVICE

John Degnan
Allis-Chalmers Corporation
Hydro-Turbine Division
Box 712
York, Pennsylvania 17045

ABSTRACT

This paper attempts to summarize the significant design considerations found during the development of single, double and multistage reversible hydro machinery for the Underground Pumped Hydro Storage project (UPHS) currently funded through the U.S. Department of Energy (D.O.E.). This year's study involves the following major objectives:

1. Complement the 500 MW Pump/Turbine equipment developed last year for UPHS with 350 MW machinery.

2. In addition, develop efficient multistage pump/turbine designs for the operating conditions used in the designing of all the Allis-Chalmers single and double stage machinery for UPHS so far.

3. Establish parametric relations for the cost of reversible hydro machinery as a function of head, capacity and number of stages.

Examples of the preliminary designs for the different staged machines are included in this paper. Special design considerations and conclusions as to the feasibility and limitations of each type of machine are drawn according to their expected cost, mechanical and hydraulic considerations.

INTRODUCTION

The D.O.E. continued to fund the UPHS program in 1979 in order to extend the design knowledge and cost data developed during the first phase of the program in 1978. With regard to the reversible hydro machinery, the following development work has been reported or is in progress:

- 350 MW single stage pump/turbines were developed for rated head conditions of 500, 750 and 1000 M complementing the larger 500 MW units as documented in (1).

- 350 MW double stage pump/turbines have been designed for rated head conditions of 1000 and 1500 M. These units have been developed according to design criteria consistent with the previously designed double stage units described in (2).

- Development of the multistage concept as it applies to pump/turbine technology is required in order to accommodate a growing demand for higher and higher head conditions. 350 and 500 MW nongated reversible multistage pump/turbines are being developed to accommodate base loads at rated heads of 1000, 1250 and 1500 M.

These designs will provide additional engineering and manufacturing cost data in the prescribed head range while allowing for direct comparison with the gate regulated double stage units as they relate to hydraulic performance, mechanical design, associated powerhouse requirements, etc.

MECHANICAL DESIGN

Fig. 1 exemplifies the single stage concept by showing the 500 M nominal head, 350 MW machine distributor section. Fig. 2 shows some design variations required to accommodate the smaller machine configuration of the 1000 M, 350 MW pump/turbine. Note, for instance, the different gate bushing designs. Due to the small size of the latter unit, it is impossible to access the inside of the headcover for gate placement and removal. The 1000 M machine is therefore equipped with the special bearing cartridge serving both upper journal bearings as well as providing thrust restraint against the upper collar. The special bearing cartridge is inserted and secured to the top headcover deck from the pit area rather than from inside the headcover.

Also note that the 1000 M machine requires an outside gate operating linkage again due to the relatively small machine size. The more conventional inside linkage can fit into the larger 500 M machine. The main disadvantage of the outside linkage arrangement is that it requires a more complex servomotor anchorage into the powerhouse as well as a more expensive pit liner. In spite of this, it is a proven alternative means of gate regulation when the machine size cannot accommodate the conventional linkage arrangement.

The remaining machine components have been sized according to criteria consistent with the 500 MW machines described in (1). The reader may consult the reports and papers listed in the references for details concerning the machine designs.

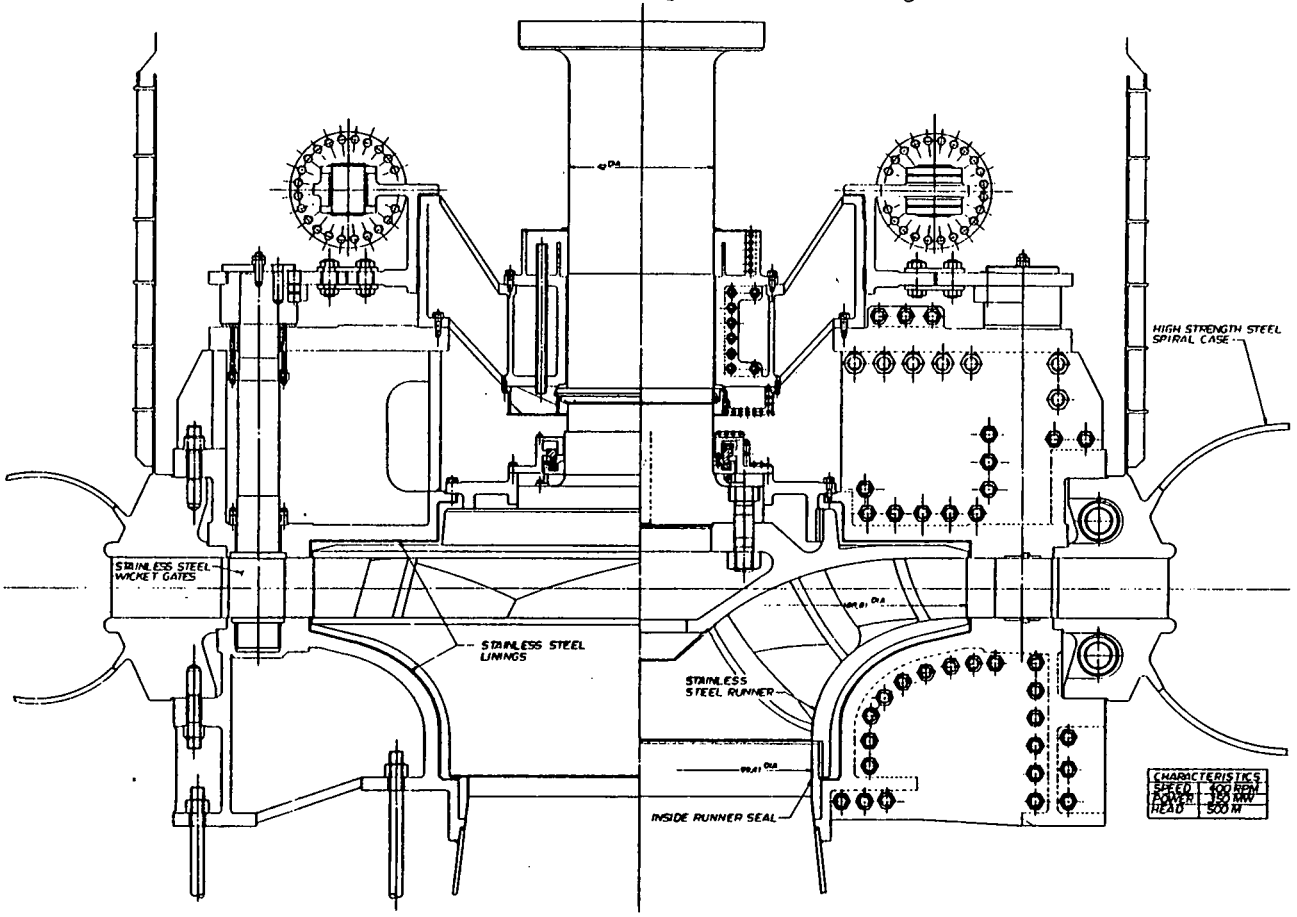

FIG. 1- UNDERGROUND HIGH HEAD P/T PROJECT - ARGONNE NAT'L LAB - 500 METERS

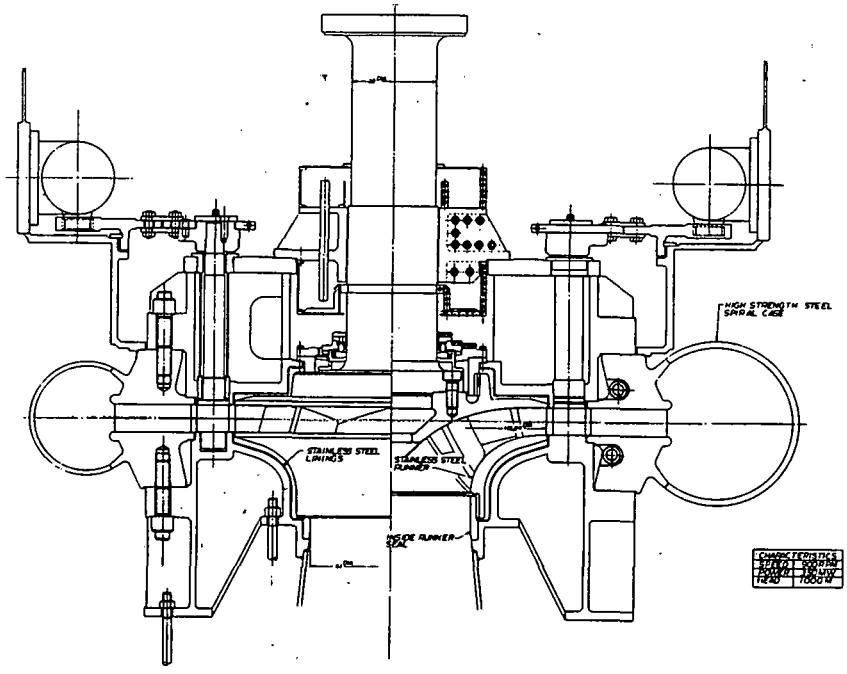

FIG. 2- UNDERGROUND HIGH HEAD PIT PROJECT - ARGONNE NAT'L LAB - 1000 METERS

HYDRAULIC PERFORMANCE

One of the most important parameters characterizing a hydraulic machine is its specific speed. In general, for high head pumping an upper limit in the selection of specific speed can be placed by consideration of the losses attributable to flow in the water casing. This is because at higher specific speeds casing losses have the strongest influence on efficiency. One of the most important parameters characterizing a hydraulic machine is its specific speed. In general, for high head pumping a lower specific speed must be selected relative to the peak efficiency point, however, a lower limit must also exist since losses associated with disk friction and leakage increase rapidly at lower specific speeds. With the impeller and other mechanical losses relatively constant, these considerations leave a rather narrow band of specific speeds from which to choose. A similar distribution of losses must be considered in the turbine mode in order to decide the best specific speed with respect to hydraulic performance. There are advantages to choosing the highest feasible specific speed such as reduced unit and possibly powerhouse size, reduced waterhammer load and increased efficiency. An increased potential for cavitation accompanies these advantages, however, but the resulting increase in submergence may or may not be a significant cost in a UPHS plant since this cost is indeed a small percentage of the overall excavation expenses necessary to develop such a plant.

Related to the selection of specific speed is a problem of matching the prototype speed with an available synchronous speed. This becomes increasingly difficult as the head requirements increase since with the increasing head there are few available synchronous speeds for a given power rating. Fig. 3 shows this. For a given head and unit capacity, specific speed must therefore be adjusted to correspond to an available synchronous speed. With so few synchronous speeds available at high heads, there are many benefits to be derived by close coordination between the customer and designer in selecting unit capacity for high head plants. Such coordination will aid in the selection of a design that has an optimum balance of efficiency, speed, submergence and size.

For the high heads being considered in UPHS, the cavitation phenomena is an especially important design consideration. It is very important that impellers and other water passage obstructions be virtually free of imperfections or discontinuities which could

lead to cavitation bubble formation. During the design and production phases of such a plant, care should be taken to use cavitation resistant material such as A296 GR CA-6NM stainless steel and assure proper water passage finishes avoiding distortion of the as designed shapes. It should be noted here that as machine size decreases, difficulty in accessing critical water passages to do the necessary surface finishing increases. The associated extra manufacturing costs must reflect this.

Table 1 indicates characteristic parameters for the UPHS single stage pump/turbines.

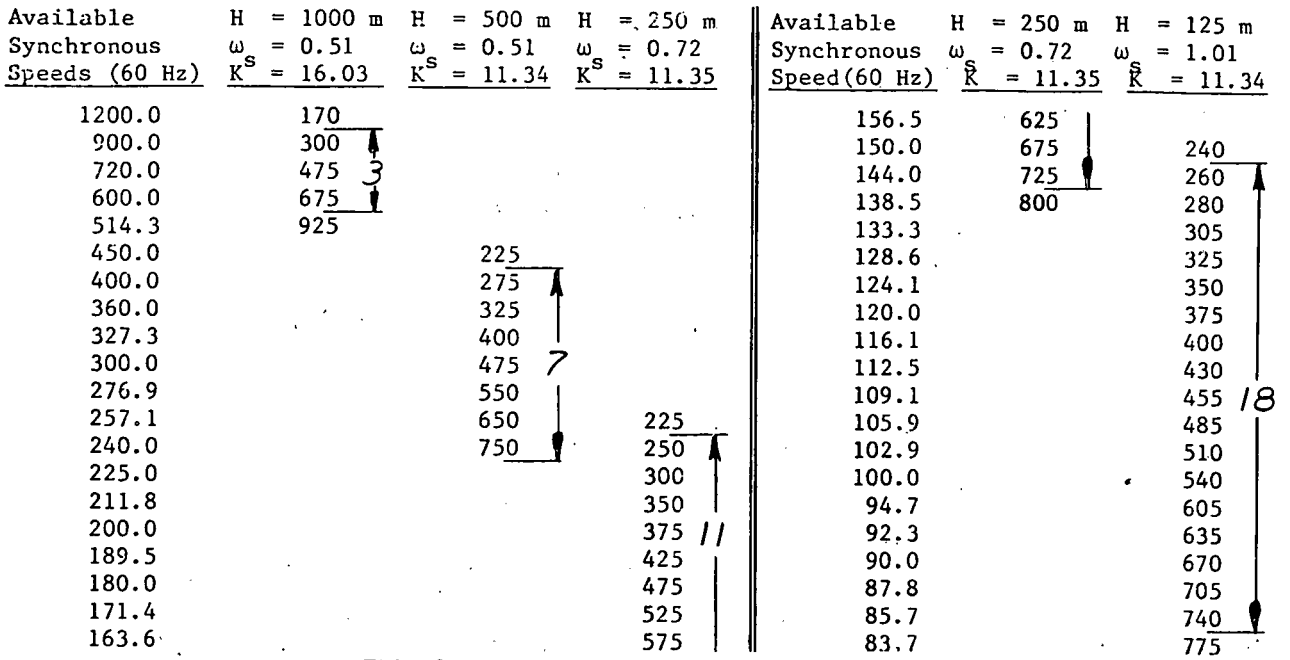

FIG. 3 AVAILABLE POWER SELECTIONS (MW)

TABLE 1 Summary of Single Stage Design Parameters

Nominal Head, H (M)	500	750	1000	500	750	1000
Rated Power (MW)	350	350	350	500	500	500
Flow, Q (M**3/s)	70	50	34	100	70	52
Speed, N (RPM)	400	600	900	327	514	720
Runaway Speed (RPM)	560	840	1260	458	720	1008
Pump Specific Speed, N (q,p) (Units = NQ **.5/H**.75)	31.65	29.60	29.51	30.95	30.02	29.2
Expected Best Efficiency						
Pump (%)	93.0	92.3	91.3	92.6	92.3	91.7
Turbine (%)	92.1	91.5	90.4	92.4	91.8	90.9
Shaft Diameter (M)	1.067	0.927	0.813	1.270	1.118	0.991
Spiral Case Inlet Diameter (M)	2.362	1.810	1.442	2.718	2.007	1.594
Runner Outside Diameter (M)	4.796	3.874	3.003	5.818	4.507	3.701
Runner Pad Height (M)	0.435	0.325	0.262	0.488	0.352	0.274
Number of Runner Buckets	7	7	7	7	7	7
Number of Wicket Gates	20	20	20	20	20	20

DOUBLE STAGE PUMP/TURBINES

MECHANICAL DESIGN

Figs. 4 and 5 show the double stage concept with the top stage gated in a 1000 M, 350 MW application and a 1500 M, 350 MW application. The latter machine as with the 1000 M, 350 MW single stage unit requires a special gate cartridge type bearing and an outside linkage due to its small size. Other than these modifications, the mechanical design criteria for all the major components closely followed those documented in (3).

HYDRAULIC DESIGN

Based on the mechanical considerations of critical shaft speed as described in (2), the mass and power ratios of the top to bottom stages are greater than unity with the top impeller developing about 60% of the power. Since both impellers have the same flow and rotational speed, their specific speeds will differ. Again the highest feasible specific speed was chosen per the arguments presented under the "HYDRAULIC DESIGN" discussion in the single stage portion of this paper. Note that specific speeds of each stage vary slightly between the machines but this is mainly because of having to match prototype speed with an available synchronous speed. Ideally specific speed is kept constant in order to maintain constant efficiency for each head machine.

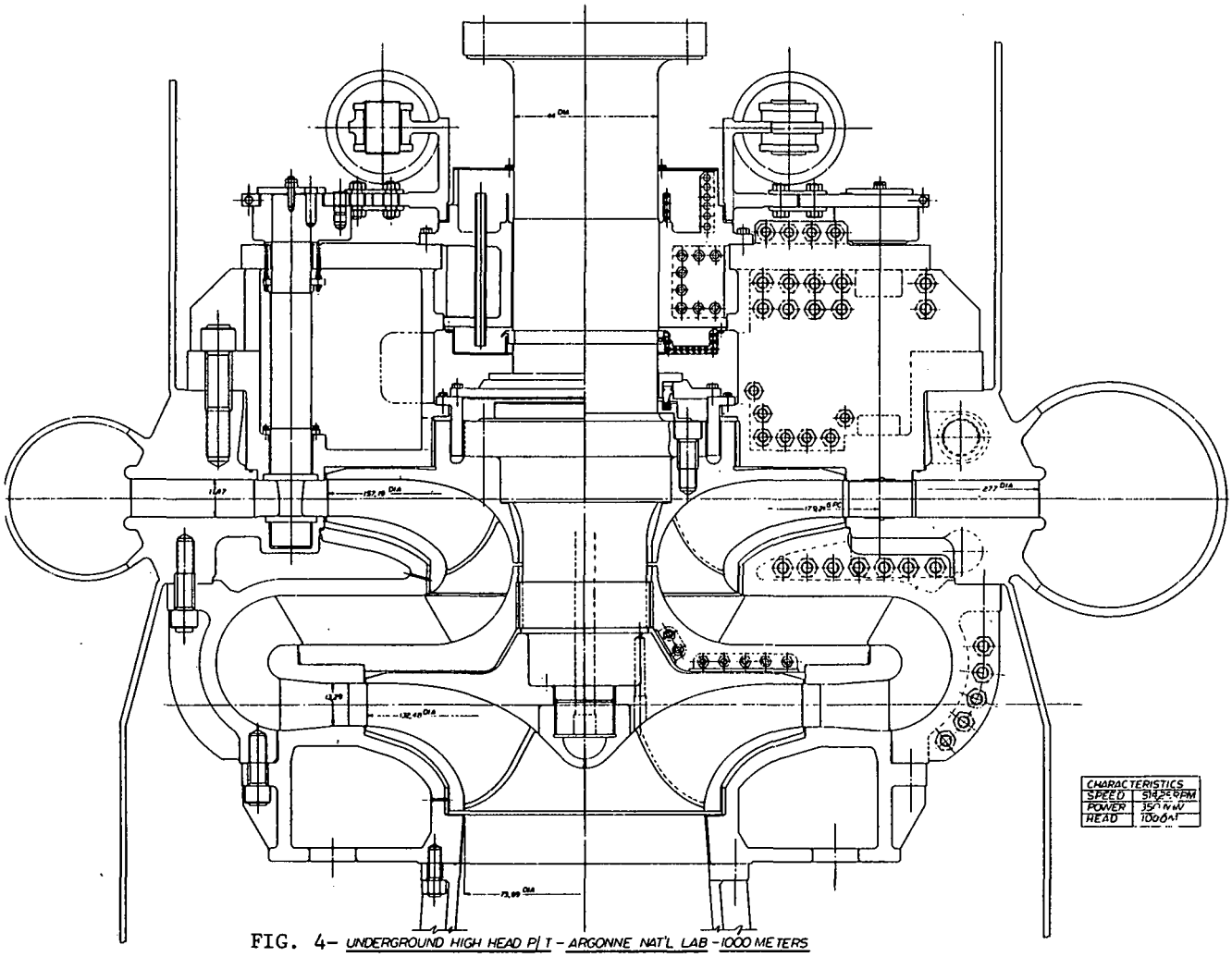

FIG. 4- UNDERGROUND HIGH HEAD P/T - ARGONNE NAT'L LAB - 1000 METERS

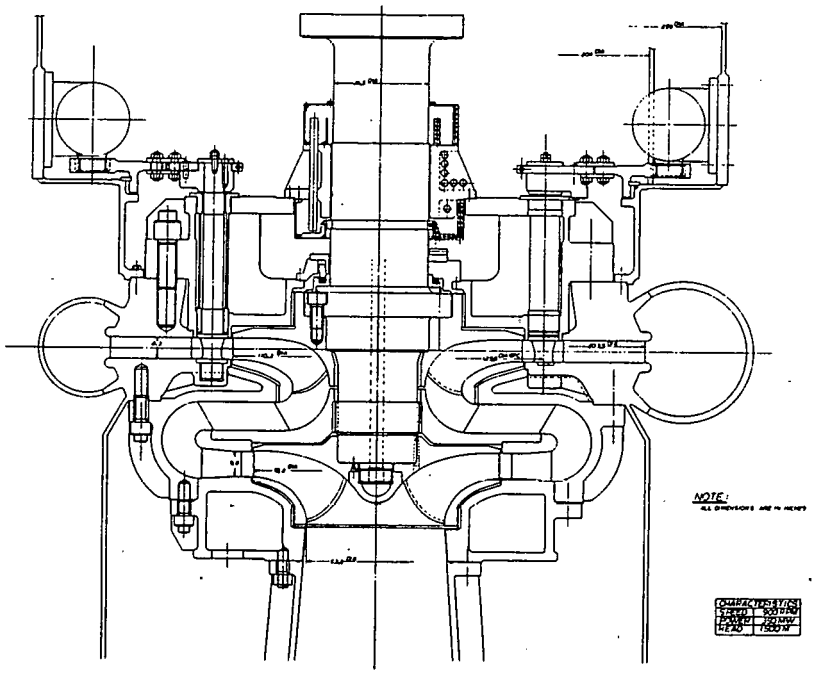

FIG. 5 – UNDERGROUND HIGH HEAD PIT-ARGONNE NATL LAB-1500 METERS

Table 2 indicates characteristic parameters for the UPHS double stage pump/turbines.

TABLE 2 Summary of Double Stage Design Parameters

Nominal Head, H (M)	1000	1250	1500	1000	1250	1500
Rated Power (MW)	350	350	350	500	500	500
Flow, Q (M**3/s)	35.7	28.6	23.8	51.5	40.8	33.6
Speed, N (RPM)	514.3	720.0	900.0	450.0	600.0	720.0
Pump Specific Speed, N (q,p)						
Units = NQ **.5/H **.75						
Top	34.36	36.42	36.22	36.1	36.25	34.43
Bottom	25.35	26.87	26.73	26.64	26.74	25.40
Expected Best Efficiency (%)						
Pump	91.0	90.0	89.0	91.0	90.0	89.0
Turbine	90.1	89.5	88.8	90.0	89.5	88.5
Shaft Diameter (M)	1.118	1.168	0.927	1.321	1.194	1.118
Spiral Case Inlet Diameter (M)	1.676	1.327	1.219	1.873	1.588	1.391
Runner Outside Diameter (M)						
Top	4.552	3.185	3.195	4.552	3.820	3.474
Bottom	3.993	2.680	2.803	3.830	3.216	2.921
Runner Pad Height (M)						
Top	0.286	0.229	0.211	0.318	0.269	0.229
Bottom	0.338	0.267	0.249	0.375	0.318	0.274
Number of Runner Buckets	7	7	7	7	7	7
Number of Wicket Gates	20	20	20	20	20	20

MECHANICAL DESIGN

350 and 500 MW machines are currently being designed at Allis-Chalmers for operational heads of 1000, 1250 and 1500 meters. Theoretically these machines can be of a regulated type with all the stages independently gated or they can be designed as base load type machines with no gates. Practically speaking, only the latter choice is feasible due to the extreme complexity of independently governing the multiple stages not to mention the related expenses, questionable reliability and potential maintenance problems. Actually some degree of load leveling can be realized with a power plant containing several ungated units by choosing to operate a selected number of the units according to the line demand. Fig. 6 shows the preliminary design of a 1500 M, 500 MW unregulated four-stage pump/turbine.

Given capacity and head parameters, the starting point to initiate such a design is to choose the number of stages and specific speed. These will essentially set the machine size and according to the shafting system design, the fundamental critical speed can be determined. As in the double stage units described in (2), the lateral critical speed presents the first major problem in the design process. The designer must decide an acceptable relationship between operational speeds and the critical speeds. The conventional single stage machines can be designed with the first critical a good 40% greater than the maximum runaway speed. This is the safest and most conservative approach and is used whenever possible to ensure avoidance of dynamic problems in the shafting system. In the design of double stage hydro machinery it is very difficult to satisfy this criteria without adding some type of intermediate lateral support or even a lower turbine guide bearing; however, with multistage equipment including 5 and 6 stages it becomes unreasonable to adhere to such a conservative criteria even with the lower turbine guide bearing. In attempting to satisfy this rigid design criteria on multistage hydro machine designs, the tendency is to progressively increase shafting system stiffness which probably increases the runner size and thus mass and machine cost. The increased runner mass substantially detracts from the positive effects on critical speed given by the increased shaft stiffness. Another ill effect is a resulting reduced machine efficiency and increased potential for cavitation (6). Some multistage machinery, especially in the compressor industry, have been designed to operate between the first and second critical speeds with success. Some of these required special journal bearing designs in order to control half frequency whirl, a dynamic phenomena exhibited by the shafting tending to whirl around its journal bearings at half the machine's rotational speed. This dynamic response associated with operational speeds above the critical can cause serious damage to the bearings if left unchecked (7). A 5 stage machine currently being developed at Allis-Chalmers employs special shoe type journal bearings whose wedge effect should alleviate this dynamic problem. The 4 stage machine shown in Fig. 6 has its critical speed 20% above the maximum runaway speed.

Design experience of multistage hydro machinery at heads approaching 1500 M is practically nil. Only one multistage pump/turbine is currently operational: La Coche, France, with an 80 MW capacity and 940 M Head. High head pump design experience is presently being researched in order to verify our preliminary designs. The following points summarize the important design considerations in multistage pump/turbine development uncovered thus far:

- Size and mass of the largest components with respect to the capacity limitations of both foundry and transportation facilities including the limitations associated with underground power plant handling devices.

- High flow velocities and associated corrosive effects.

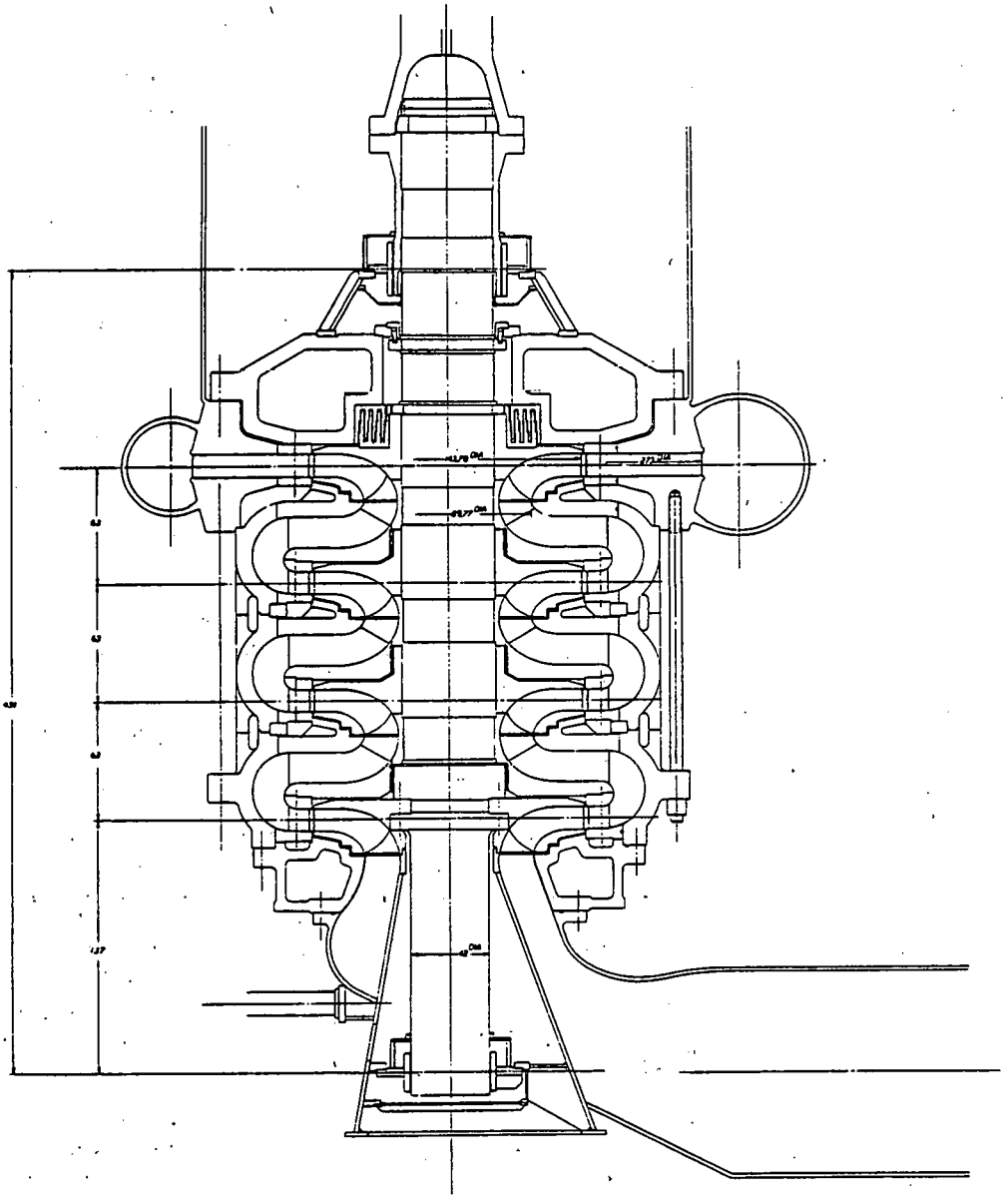

FIG. 6 - UNDERGROUND HIGH HEAD P/T-ARGONNE NAT'L LAB-1500 METERS

CHARACTERISTICS	
SPEED	450 RPM
POWER	500 MW
HEAD	1500M

- Material selection to accommodate corrosion problems and highly stressed components. Fig. 7 shows an axisymmetric finite element model of the 4 stage unit in order to assess the various components' stress levels.

- Vibration and noise.

- Critical speed of shafting system; bearing design and stiffness.

- Design limitations of the electrical generator/motor as it relates to speed selection of the pump/turbine.

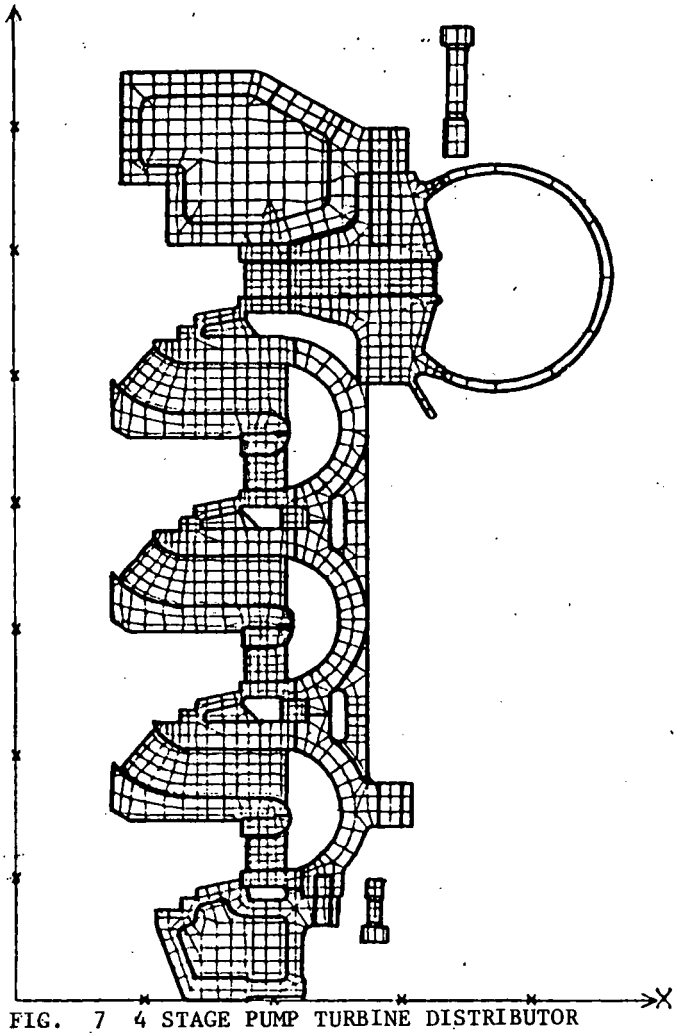

FIG. 7 4 STAGE PUMP TURBINE DISTRIBUTOR SECTION-FINITE ANALYSIS

HYDRAULIC DESIGN

Specific speed selection for multistage pump/turbines are under the same restrictions as mentioned for the double and single stage machines except that the potential hazards due to cavitation are less exaggerated. This is because the total machine head is distributed across a number of stages thus lowering the fluid velocities and allowing higher acceptable specific speeds. A related advantage in using multiple stages is that the submergence need not be as deep as in single and double stage equipment in order to inhibit cavitation. Actually mechanical and manufacturing considerations become more and more a dominant consideration for specific speed selection as more stages are added. This is because specific speed has such a strong influence on machine size which directly relates to the problems associated with critical speed and attaining and inspecting stringent water passage finishes. Another practical limitation in selection of specific speed is the maximum allowable generator rotational speed. Currently, this limiting speed appears to lie between 720 and 900 RPM.

Preliminary designs for the stationary water passage shapes have been determined as a function of minimum head loss and the experience of multistage pump design. Certainly mechanical constraints of the stationary components also influence the water passage shape such as required stay vane strength, lower turbine guide bearing influence on the draft tube design and perhaps most significantly, lateral shaft stiffness dictating shaft diameter as it relates to the critical speed problem.

ECONOMICS

Engineering and manufacturing costs for the single and double stage hydro machinery presented in this paper have been estimated and provide a data base from which generalized cost estimates can be made as a function of head, capacity and machine type. The parametric relations are provided in Figs. 8 and 9. Note that the data has been normalized to a value which is, of course, dependent on the market at a given point in time. For the most part these relative cost values are sufficient in helping to choose the optimum selection of equipment for a given installation. The multistage machine designs are not yet completed and therefore the cost data is incomplete at the time of this writing.

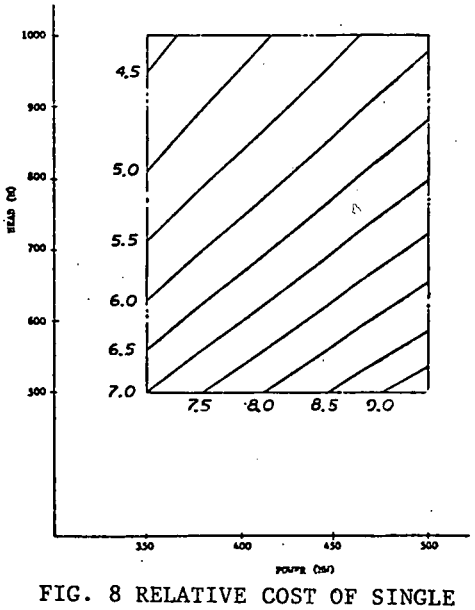

FIG. 8 RELATIVE COST OF SINGLE PUMP TURBINES

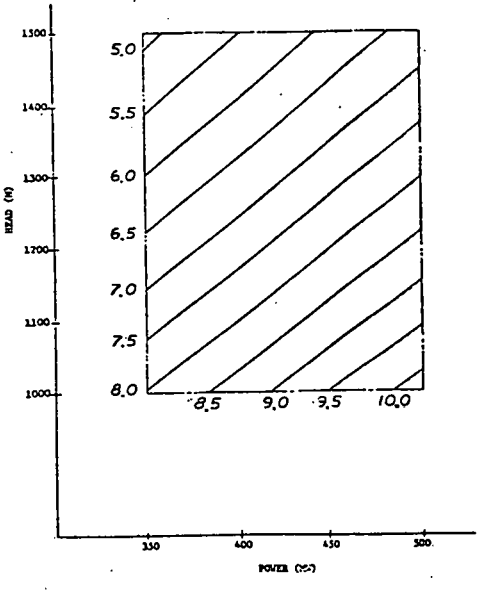

FIG. 9 RELATIVE COST OF DOUBLE STAGE PUMP TURBINES

CONCLUSION

The well established single stage pump/turbine concept is the cheapest, most efficient, most versatile and reliable solution for use in power plants; however, a head limitation of about 1000 M seems apparent today. The double stage concept with its top stage regulated is the next logical solution to accommodate increased head conditions. The concept has been developed with acceptable expected efficiencies and no major obstacles for finalization. The operating conditions of these machines are naturally less flexible due to the narrowing band of near peak efficiency when compared with single stage machinery. Finally, the recent efforts being made to develop a general multistage pump/turbine concept seem to indicate that in spite of its inflexible allowed operating conditions, it has the advantage of accommodating high heads at least twice those of current experience. This ability is an essential factor in considering the feasibility of some UPHS sites. The accompanying price tag includes (6):

- High equipment cost.
- No per unit load regulation.
- An expensive pump priming procedure requiring a "watered up" unit with a relatively large power demand of about 50% of the rated pump capacity. An unwatered pump start with a single stage machine typically needs only about 10% of its rated power.
- Synchronous condensing is not possible without a method to dewater the machine.

REFERENCES

1. "Final Report Underground Pumped Storage Plant For Argonne National Laboratory Development - Task I-A", Allis-Chalmers, Hydro-Turbine Division, September, 1978.
2. "Final Report Underground Pumped Storage Plant For Argonne National Laboratory Development - Task I-B", Allis-Chalmers, Hydro-Turbine Division, September, 1978.
3. "Final Report Underground Pumped Storage Plant For Argonne National Laboratory Development - Task II-A, II-B", Allis-Chalmers, Hydro-Turbine Division, May 30, 1979.
4. Degnan, J., "Evaluation of One and Two Stage High Head Pump/Turbine Design For Underground Power Stations", presented to the U.S. Department of Energy at the Mechanical and Magnetic Energy Storage Technology Meeting, October, 1978.
5. Chacour, S. A.; Degnan, J. R.; LoSasso, D. M.; Webb, D. R.; "Design Considerations For a 1000 Meter Head, 500 Megawatt Single and Double Stage Reversible Pump/Turbine", presented at the ASME Spring Meeting, Niagara Falls, New York, June, 1979.
6. Rodrique, P., "The Selection of High Head Pump/Turbine Equipment For Underground Pumped Hydro Energy Storage Application", presented at the ASME Spring Meeting, Niagara Falls, New York, June, 1979.
7. Pinkus, O., "Experimental Investigation of Resonant Whip", Transactions of ASME Summer Meeting, July, 1956.

PROJECT SUMMARY

Project Title:	"Underground Pumped Hydro Storage Program"
Principal Investigator:	C.A. Blomquist, A.A. Frigo, S.W. Tam
Organization:	Argonne National Laboratory 9700 S. Cass Avenue Argonne, Illinois 60439 (312) 972-7691
Project Goals:	The primary objective of this program is the development of the technology of Underground Pumped Hydroelectric Storage (UPHS) as a viable peak-power-generation alternative which does not require the use of premium fossil fuels for the electric utility industry. Successful commercialization of this energy-storage scheme requires studies of hydraulic turbomachinery, lower reservoir and powerhouse construction, geology, motor generators, environmental issues, and system arrangement and optimization.
Project Status:	This present program has primarily concentrated on hydraulic turbomachinery development and system studies. The Allis-Chalmers Hydro-Turbine Division completed Contractual Studies in FY1978 on the preliminary design, hydraulic performance, and costs of single- and two-stage gated, reversible pump turbines for high-head applications. An extension to this study was completed in June of 1979. From the mechanical and hydraulic viewpoints no major obstacles are foreseen which could hamper the development of these machines for UPHS plants. Detailed reports on this turbomachinery are in preparation. Allis-Chalmers is currently investigating the preliminary design aspects, hydraulic performance, and cost of 350 and 500-MW, multistage, ungated, reversible pump turbines with operating heads of 1000, 1250, and 1500 M. This study will be completed at the end of FY1979. Dr. Alexander Gokhman, EDS Nuclear Corp, has completed an assessment of the application potential of controlled flow rate pumps for energy storage applications. This study has shown the advantage of these machines for several application areas. Argonne National Laboratory had conducted studies on the effects of advanced turbomachinery utilization, pump turbine efficiency, charge-discharge ratio and other factors on the cost of UPHS plants. A report on this work is in preparation. Argonne is also preparing a report on UPHS that is scheduled for completion at the end of FY1979.
Contract Number:	W-31-109-ENG-38
Contract Period:	FY1979
Funding Level:	$370,000 BO*
Funding Source:	Department of Energy, Division of Energy Storage Systems

*Includes $125,000 Contract with Allis-Chalmers, and
$12,000 Contract with EDS Nuclear, Inc.

TURBOMACHINERY CONSIDERATIONS FOR UNDERGROUND PUMPED HYDROELECTRIC STORAGE PLANTS (UPHS)

S.W. Tam, A.A. Frigo and C.A. Blomquist
Argonne National Laboratory
Argonne, Illinois 60439

ABSTRACT

UPHS plant costs for plants equipped with advanced reversible pumped turbines have been considered. Equipment used includes single-and two-stage reversible pump turbines for operating heads from 500 to 1500 m. The effects of machinery costs, operating heads, plant configurations and sizes have been taken into account. The results indicate that the use of advanced machinery seems to push the minimum UPHS plant cost to heads greater than 1500 m. The employment of advanced reversible pump turbines seems to be economically attractive. It is shown that pump-turbine efficiencies and the so-called charge/discharge ratio are very important design parameters for UPHS applications and the interactive effects of these parameters have been analysed. The results show that under certain conditions a pump-turbine option with a higher charge/discharge ratio at the expense of somewhat lower operating efficiency can be desirable.

1. INTRODUCTION

The application of UPHS for electric utility peaking service is enhanced by the use of relatively high head (>1000 m) and large capacity (>350 MW) turbomachinery.[1,7] These constraints are presently not mutual. High-head but small capacity (<150 MW) turbomachines are currently available as multistage reversible pump turbines or tandem units (Pelton-type waterwheel and multistage storage pump). Large capacity Francis turbines are available for low head operation, e.g., 700 MW @ 87-m head. Single-stage reversible pump turbines are under construction for output powers of 315 MW at 625 m, and 508 MW at 384 m. Recent design studies[2] have shown the technical feasibility of advanced machinery such as 500-MW-capacity, single-stage, reversible pump turbines at a 1000-m head, and two-stage, gated, reversible pump turbines with an operating head of 1500 m.

The choice of turbomachinery for UPHS plants rests ultimately on economic considerations. The results of preliminary cost analyses are discussed in this paper. The principal objective is the comparison and contrasting of the costs associated with the utilization of state-of-the-art pump turbines and those associated with advanced machinery.

Recently, UPHS plant costs have been estimated.[3] The turbomachinery options chosen are either state-of-the-art or a slight extension of currently available technology. A total of seven different UPHS plant configurations was considered. The major plant characteristics together with the relevant cost information are listed in Table 1. Major conclusions are:

(1) For a fixed plant size and type of machinery, the minimum plant cost ($/kW) seems to occur in the head range of 1200-1500 m.
(2) Multistage reversible units appear to be the most economical machinery option.
(3) A plant capacity of 2000 MW represents the most economical plant size, when interest during construction and escalation are added.

In this work, advanced turbomachinery is considered for UPHS plant configurations similar to those shown in Table 1, thus providing a common basis for comparison. Civil engineering costs from Reference 3 (updated to Sept 78 dollars) have been utilized. The advanced machinery considered includes single-stage, reversible pump turbines and two-stage, reversible pump turbines. These machines represent considerable extension to the state-of-the-art reversible pump-turbine technology. At present, single-stage, reversible, Francis-type pump turbines have been designed for operating heads as high as 625 m (Bajina Basta Station in Yugoslavia) and for power outputs up to about 500 MW (Bath County Plant in

Virginia, U.S.A.). Theoretically, there are no maximum head limitations for these types of machines. However, manufacturers have acted cautiously in the development of higher-head and power-output equipment. Increases have occurred in small increments rather than in large jumps. At the present time, high-head technology for single-stage pump turbines for power applications is actually lagging that for boiler feed pumps where multistage machines developing heads as high as 1150 m per stage have already been built and operated.

Preliminary engineering design and cost studies of higher-head and greater-output, single-stage, reversible, Francis-type pump turbines (SSRPT) have been conducted by Allis-Chalmers Hydro-Turbine Division for ANL.[2] Three separate high-head machines have been investigated. The three units are designed to produce a power output of 500 MW while operating under heads of 500, 750, 1000 m respectively. (Table 2)

A similar design analysis has been carried out on two-stage reversible pump-turbines (TSRPT) with operating heads at 1000, 1250 and 1500 m (Table 3). At present, there are no known operating gated TSRPT. Performance characteristics[2,4] of these pump-turbines have been utilized to investigate UPHS plant costs for plants equipped with such advanced turbomachinery. Major factors that have been considered include machinery costs, operating heads, plant configurations and sizes. It turns out that pump-turbine efficiencies as well as the so-called charge/discharge ratios of the machines are very important elements. The interacting effects of these factors will be analyzed.

2. UPHS COST ESTIMATES

2.1 MACHINERY COSTS

Using the cost data from the Allis-Chalmers' study, cost functions with operating head as a parameter were generated for both the single- and two-stage machines. The general form of these functions is: cost = $a(\text{head})^b$, where a and b are constants. The cost data and functions for the single- and two-stage machines are shown in Figs. 1 and 2. Over the applicable head range, the data are reproduced with an error of less than 2%. These cost functions are used in subsequent analyses.

Note that the cost per unit for both types of machines decreases as the operating head increases. One major reason for this result is that the machine size becomes smaller as operating head increases.[1,7]

The costs shown in Figs. 1 and 2 are Sept 78 values chosen to be consistent with costs of all other components (such as civil engineering costs) considered in this study. Installation costs of pump turbines are estimated to be 30% of the machinery cost, which is on the high side of such estimates.

2.2 THE EFFECT OF PLANT CONFIGURATION

There are two major UPHS plant configurations -- the one-drop and the two-drop schemes. The one-drop scheme is similar to conventional pumped hydro storage except that the lower reservoir is an underground cavern and the upper reservoir is at ground level. At present, for operating heads considered favorable for UPHS ($\geq$ 1000 m), only multistage reversible pump turbines or tandem units can be utilized for the one-drop scheme.[1,7]

The two-drop scheme has a small intermediate reservoir located halfway between the upper and lower reservoirs. Two powerhouses are located near the lower and intermediate reservoirs, respectively. This arrangement allows the use of turbomachinery with half the total operating head of the UPHS plant. Single-stage reversible machines for this head range (500-600 m) are available.

Recent studies[3] have indicated that the one-drop scheme with multistage units is the most economical choice. A simple estimate was made to determine the possible cost savings if two-stage gated reversible pump turbines are used for the various UPHS plant configurations. The results are listed in Table 4 and indicate that the two-stage unit becomes increasingly favorable when compared to multistage, single-stage (two-drop scheme), and tandem units. Consequently, most of the subsequent cost comparisons will be made between two-stage and

multistage reversible pump turbines. However, other turbomachinery will be considered when the effects of efficiency are addressed.

2.3 THE EFFECT OF PLANT SIZE

The C.T. Main study[3] indicated that the optimum UPHS plant capacity is approximately 2000 MW when multistage, reversible pump turbines are installed. In order to determine if optimum capacity remains unchanged when two-stage machines are used, cost estimates were made for a one-drop UPHS plant with a 1200-m head. Both 500-MW, and 350-MW, two-stage, reversible pump turbines were considered. The resultant percentage savings in plant cost when compared to multistage machines are shown in Fig. 3. These savings are somewhat insensitive to plant size, which means that the selection of multistage or two-stage units does not affect the optimal size of a UPHS plant. Subsequently, all discussions are based on a UPHS plant capacity of 2000 MW.

2.4 COST ESTIMATES FOR UPHS PLANTS

The results of the Main study[3] indicate that multistage reversible units represent the most promising turbomachinery option. Therefore, this machine was chosen to be compared with the two-stage gated unit, which is the only advanced category machine designed to operate above 1000 m.

The cost ($/kW) for a 2000-MW UPHS plant similar to Scheme I in Table 1, but employing four 500-MW, two-stage, reversible pump turbines as a function of operating head, is shown in Fig. 4. For comparison purposes, the plant cost[4] utilizing multistage units is also shown. The two-stage cost curve decreases rather rapidly with increasing head; however, the incremental change in the cost decreases as a 1500-m head is approached. If a minimum cost exists, it is probably beyond a 1500-m head.

For heads above 1000 m, the two-stage reversible pump turbine is the best choice. The point denoted by *single-stage* is the cost for a similar UPHS plant utilizing 900-m-head, single-stage, reversible pump turbines. The cost data shows that it is economically the best machine choice for operating heads less than 1000 m. Other advantages include relative simplicity in design and somewhat better efficiency than multistage or two-stage units. The main drawback of this machine is that the feasibility of its operation beyond 1000 m is currently unknown.

2.5 THE EFFECT OF PUMP-TURBINE EFFICIENCIES

It was shown that the direct cost in using the two-drop configuration or tandem units are, in general, higher than other schemes. However, the single-stage reversible pump turbines used in the two-drop scheme operate at a much lower head (for each drop) and, hence, generally have a better efficiency than two-stage or multistage machines of the same total capacity and total operating head. Tandem units also have a somewhat better operating efficiency. The product of the turbine and pump mode efficiencies $\eta_t\eta_p$ can be one to two percentage points higher than corresponding two-stage units.[1,4] Since the expected UPHS plant lifetime is about 50 years, cost savings or penalties due to differences in $\eta_t\eta_p$ must be considered in evaluating turbomachinery options. The effect will be addressed in a parametric manner.

Pertinent factors that must be considered are:

(1) types of base load plants (nuclear or coal-fired) supplying the pumping energy to the UPHS plant,

(2) fuel costs for each type of baseload plant, and

(3) number of hours of annual operation for the UPHS plant.

The baseline UPHS plant considered has a 50-year life and a 70% overall efficiency. The effective UPHS plant efficiency η_e is given by

$$\eta_e = 0.7\ (1.-\delta). \qquad (1)$$

where δ is a measure of the change in plant efficiency due to a change in the product of the turbine and pump efficiencies, $\eta_t\eta_p$. If the original efficiency product is $(\eta_t\eta_p)_o$, then the new product $\eta_t\eta_p$ is related to δ by

$$1 - \delta = \frac{\eta_t\eta_p}{(\eta_t\eta_p)_o} \quad . \tag{2}$$

The yearly fuel saving or penalty, A ($/kW per year), in year zero dollars was first calculated for various fuel costs, hours of annual operation, and relative differences in pump-turbine efficiencies, δ.

For these values of A, capitalized values, P ($/kW) were calculated using

$$P = A \frac{(1 + i)^n - 1}{i(1 + i)^n} \tag{3}$$

where n = plant lifetime (years) and i = escalation rate.[5] The results of this analysis for n = 50 and i = 0.08 are plotted in Figs. 5 to 8.

Using these figures for a UPHS plant utilizing lower efficiency machinery, the following observations are obtained:

(1) The effective cost penalty, P, resulting from the lower pump-turbine efficiency is less for nuclear baseload plants than for coal-fired ones. This result is basically due to the lower nuclear-fuel cost.

(2) The cost penalty for $\delta \simeq 2\%$ and 1800 hours of annual operation is not negligible. Typically it is approximately 9.6 $/kW for coal and 5.5 $/kW for nuclear baseload plants (Figs. 5 to 8), which tends to reduce the attractiveness of advanced machinery. However, for moderate differences in pump-turbine efficiency, for typical baseload plant fuel costs and for typical UPHS plant utilization, this cost penalty is still not large enough to alter the conclusion that two-stage machines offer the most cost effective option for heads over 1000 m (Table 4).

(3) In situations where pumpturbine efficiency differences are large ($\delta \simeq 4\%$), the fuel costs (coal or nuclear) are high and the UPHS plant is extensively utilized (hours of annual operation $\geq$2500), the effective cost penalty, P, can be a substantial amount (Figs. 5 and 7).

3. CHARGE/DISCHARGE RATIO

3.1 THE EFFECTS OF CHARGE-DISCHARGE RATIO

In designing pump turbines for pumped storage applications, machinery efficiency is an important element to be considered, because of the long lifetime ($\simeq$50 years) of the machinery (see Section 2.5). However, the so-called charge/discharge ratio, r, must also be taken into account in pump-turbine design considerations. This factor is defined as the ratio of the average pumping load to the rated generation capacity. The averaging should be performed over the designed cyclic operating period of the pumped-storage plant. For example, plants can be designed to operate on a daily, weekly or even longer cycle.

A pump turbine that has a charge/discharge ratio of close to 1 is said to have an electrically balanced design, and the output is roughly the same as the pumping load. On the other hand, a high r value (1.3 or 1.4) means the generation time, T_G, is comparable to the pumping time, T_p. Therefore, the pump discharge rate, Q_p, is about the same as the turbine discharge rate, Q_T. The pump turbine is then in a hydraulically balanced mode.

The significance of r is that the larger this ratio, the longer the available generation time for a given amount of pumping time. The generation time T_G is related to the pumping

time T_p by the equation

$$T_G = r\eta_u T_p \quad (4)$$

Here η_u is the overall UPHS plant efficiency. Average values over the charge/discharge cycle of the pumped-storage plant should be used. Typical values of r and the associated energy storage capacity (in hours) for several conventional pumped storage plants are listed in Table 5. Note that except for Cabin Creek all plants listed have a charge/discharge ratio greater than or equal to 1. For Cabin Creek if a plant efficiency of about 70% (which is typical for pumped storage plants) is assumed, a pumping time of 8.9 hours is required to obtain the 5.8 hours of generation time listed in Table 5. In this case, the T_p required is substantially more than T_G, which is reasonable if:

(1) supplementary pumping time (i.e., time in which load demand is relatively low) is available and

(2) the implied additional storage cost is acceptable.

To illustrate these points consider a pumped storage plant that has been designed to supply 6 hours (T_G) of peak power each weekday. Suppose the plant efficiency η_u is 70% and that the charge/discharge ratio is 1.0. From equation 4 a pumping time of 8.6 hours is required each weekday to supply the 6 hours of generation time required by the grid. Assume further that the maximum available pumping time each weekday as allowed by the grid is 8 hours. One way this difference can be taken up is via supplementary pumping during the weekend. The amount of weekend pumping required in this example is $0.6 \times 5 = 3$ hrs, which translates into additional storage of $3 \times 0.7 \simeq 2$ hours. Hence, this pumped-storage plant will have to have a designed storage capacity of about 8 hours instead of the 6 hours storage capacity that the grid actually requires. This result represents 30% more storage capacity with a corresponding increase in the associated storage cost.

However, if the pump turbines used in this hypothetical storage plant have a higher charge/discharge ratio of 1.4 with the same operating efficiency as before then equation 4 predicts that $T_p \simeq T_G$. In this case no supplementary pumping is necessary, and no additional storage capacity beyond the 6 hours needed to supply the utility grid is required. This result represents a substantial cost reduction if the storage component is a significant part of the total plant cost.

On the other hand there are some constraints on developing turbomachinery with high charge/discharge ratios, particularly for reversible machines. A larger r (1.5) means the average pumping load is equal to 1.5 times the turbine load. For a reversible machine it is difficult to optimize performance characteristics for both the pumping and turbining modes with such a significant difference in operational requirements. The necessary compromise generally leads to an overall lower pump-turbine efficiency.

Furthermore, a higher r value will require a higher generator-motor rating to meet the higher pumping load requirement. The turbomachinery (pump turbines) will have to be larger to handle the increased quantity of water. There will be corresponding increases in the size of some structures and equipment (e.g. powerhouse and cranes) to house and handle these larger pieces of machinery. All these factors will lead to a higher plant cost. Previous estimates[5] have indicated that to change the charge/discharge ratio from 1.0 to 1.4 will add about 20% to those affected components of the plant cost (i.e. civil structures such as powerhouses, equipments, motor-generators and pump turbines). In addition, it may be necessary to add the additional (capitalized) cost due to differences in pump turbine efficiencies. Detailed cost differences will depend upon such things as the specific machinery used, powerhouse design, and plant configuration. Balanced against these constraints is the cost savings due to the reduction in storage costs. This cost component is mainly represented (particularly for UPHS plants) by the construction cost of the lower reservoir.

In this section, the results of a parametric analysis of the effects of the charge/discharge ratio on the trade-offs between the general increase in the balance-of-plant cost and the cost reduction in the storage component are presented. The implications on the design

philosophy of high head turbomachinery for UPHS application will be considered.

Section 3.3 is devoted to a performance analysis of single-stage reversible pump turbines over the head range of 500-1500 m. Actual preliminary design data will be utilized. The main focus will be on the charge/discharge ratio. Several modes of turbine operation will be considered.

3.2 PARAMETRIC ANALYSIS

In analyzing the trade-off effects discussed in the previous sections several important parameters need to be brought into consideration including the maximum pumping time per day, the generation time per day as required by the utility grid, underground cavern cost, coal and nuclear baseload plant fuel costs, effective UPHS plant efficiency, charge/discharge ratio and types of turbomachinery employed.

Supplementary pumping during the weekend (if required) will lead to additional storage requirement. The additional specific storage cost ($/kW), ΔS, can be obtained from the following relation

$$\Delta S \ (\$/kW) = C_u \, N_{p/T} \times 3600 \times 5 \times Q_T \times (T_G^d - \alpha T_D^d)/\text{plant capacity} \qquad (5)$$

where

C_u = underground cavern construction cost ($/m^3)

$N_{p/T}$ = number of pump/turbines

Q_T = mean turbine flow rate (m^3/sec)

T_G^d = daily generation time (hrs) required

T_P^d = maximum daily pumping time (hrs) available

α = (charge/discharge ratio) (average plant efficiency (η_u)

In equation 5, a 5 weekday peak generation cycle has been assumed. In the following analysis the baseline case consists of a UPHS plant of 2000MW capacity, operating at a 1200-m head, with an overall plant efficiency of 70%, a charge/discharge ratio of 1 (i.e. an electrically balanced turbomachinery design) and 8 hours of available daily pumping time. The change in ΔS was also calculated for a charge/discharge ratio of 1.4 (i.e. a hydraulically balanced pump/turbine design) with the same turbine mean discharge-rate requirement.

Within this framework factors that were considered include:

(1) different grid requirements of respectively six hours, eight hours, and ten hours of daily generation;

(2) possible reduction in overall UPHS plant efficiency η_u from the baseline case of 70% to 69% and 67%; and

(3) two different sets of turbomachinery--330-MW, multistage, reversible pump turbines (MSRPT)[3] and 500-MW, two-stage, reversible pump turbines (TSRPT).[1,2]

With factor 2, the cost penalty involved for both coal and nuclear baseload plants has been estimated using results already obtained in Section 2.5 and Figs. 5-8. For factor 3, the main effect is on the increase in the balance-of-plant costs. A 20% increase in the cost of the powerhouse, equipment shaft, and equipment such as cranes, motor generators and pump turbines has been considered.[5] Recent construction cost data[3]

(updated to Sept 78 dollars) have been utilized, and for MSRPT leads to an increase of about $21.3/kW in the plant cost. For TSRPT the cost increase is about $18.6/kW.

The results of the analysis are displayed in Figs. 9-12. Some pertinent observations are:

(1) The variations in the balance-of-plant cost and in the capitalized cost from changes in plant efficiency are two important cost components when varying r values are considered. These two cost components can be comparable in magnitude for some ranges of pumping energy costs, plant utilization and plant efficiency changes. (Fig. 9).

(2) For a 6 hour generation time, the savings from a storage cost reduction due to increasing r from 1 to 1.4 is neutralized by the increase in both the balance-of-plant cost and the capitalized cost resulting from a reduction in plant efficiency. In these cases, it is probably not beneficial to design turbomachines for high values of r. (Fig. 9, 11).

(3) When the generation time is 8 hours or more, an increase in r leads to cost savings from reductions in storage costs that outweighs the other associated cost increases. In these cases r should be considered a very important design parameter. Sacrifices in efficiency (within reasonable limits) from increasing r may have to be accepted.

3.3 CHARGE/DISCHARGE RATIO FOR SSRPT

The foregoing discussion is best illustrated with the results of the recent Allis-Chalmers-ANL study.[2] Using actual design data from this study for the SSRPT, the charge/discharge ratio and the ratio of generation time, T_g to pumping time, T_p has been estimated. Two turbining modes were selected to provide a lower and upper bound to the charge/discharge ratio, r, at adequate performance levels. Mode A considers maximum power generation at the minimum head. It provides high power generation over a relatively limited time. Mode B considers power generation at maximum efficiency at the minimum head. This mode provides longer power generation times at a reduced level. Performance characteristics for both modes are summarized in Table 6. It should be noted that the ratio T_g/T_p for Mode A is less than Mode B, which means that Mode B operation is preferable unless power generation at an increased level over a limited time is desirable. An instructive way of looking at the issues is illustrated in Fig. 12, where T_g is plotted against T_p for both Mode A and B at a 1000-m nominal head. For a daily pumping time of say eight hours, a 30% increase in r (from Mode A to B) is equivalent to an almost 40% increase in the effective storage capacity. The high cost of the underground reservoir makes Mode B operation economically attractive illustrating the importance of a high charge/discharge ratio in turbomachinery design considerations particularly when storage cost is significant.

4. CONCLUSIONS

From the results of the system studies presented, the following conclusions can be drawn:

(1) The utilization of advanced turbo-machinery seems to push the minimum UPHS plant cost beyond a head of 1500 m.

(2) The percentage savings in plant costs using advanced machinery is somewhat insensitive to variation in plant capacity (1300-2700 MW).

(3) For heads at or below 1000 m, single-stage, reversible pump turbines seem to be a logical choice. For heads above 1000 m, the present work indicates that two-stage, reversible pump turbines represent an economically attractive option. A significant cost reduction results when a plant with two-stage reversible units is compared with two-drop configuration plants or plants equipped with tandem units. However, this cost reduction may be diminished when differences in pump turbine efficiencies are considered. Because of the long plant and machinery lifetime, seemingly small differences in performance can result in nonnegligible cost penalties or benefits.

4. Increasing the charge/discharge ratio will reduce the relative storage cost. This reduction is accompanied by increases in the balance-of-plant cost and cost penalties resulting from possible reduction in turbomachinery efficiency. The cost benefit will depend on the amount of generation capacity required. For large enough generation time a cost savings from reduction in storage cost will outweigh the other associated cost increases. In these cases some sacrifices in efficiency from increasing the charge/discharge ratio may be acceptable. Both this and other factor[3] discussed in Section 3.2 illustrate the point that evaluation of both capital cost and performance are essential in making a judicious choice of turbomachinery options for UPHS application. Maximizing operating efficiency is only one among several important aspects in pump/turbine selection considerations.

ACKNOWLEDGMENTS

The research activities in underground pumped hydro storage, of which this paper is a part, were funded by the Division of Energy Storage Systems, Office of Energy Technology, U.S. Department of Energy.

REFERENCES

1. C.A. Blomquist, S.W. Tam, and A.A. Frigo, "Turbomachinery Options for an Underground Pumped Hydro Storage Plant," paper presented at the proceedings of the 14th Intersociety Energy Conversion Engineering Conference, Boston, Aug. 5-10, 1979.

2. Allis-Chalmers Corp., unpublished studies for Argonne National Laboratory (ANL), Oct. 1978.

3. "Underground Pumped Hydroelectric Storage. An Evaluation of the Concept," Final Report. Solicitation No. 6-07-DR-50100, Chas. T. Main, Inc., Nov. 1978.

4. C.A. Blomquist, A.A. Frigo, and S.W. Tam, ANL unpublished study.

5. D.G. Newman, "Engineering Economic Analysis: Engineering Press, 1976, pp. 50-53.

6. PSE&G "An Assessment of Energy Storage Systems Suitable for Use by Electric Utilities," Vol. III EM-264 EPRI project 225 ERDA E(11-1)-2501 July, 1976.

7. P. Rodrique, "The Selection of High-head Pump-turbine Equipment for Underground Pumped Hydro Energy Storage Application," Proceedings of the ASME 1979 Spring Meeting, Niagara Falls, New York, June 18-20, 1979.

TABLE 1. UPHS Plant Configurations

Schemes	Capacity (MW)	Average Gross Head (m)	Storage (Hours)	Machinery (No. of Units)	Plant Cost * ($/kW in Sept 1978 Dollars)
I	2000	1200	10	Multistage (6)	362
II	2000	2 x 600 (two-drop)	10	Single-Stage (2 x 4)	374
III	2000	1200	10	Tandem (6)	394
IV	2000	1500	10	Multistage (6)	354
V	2000	900	10	Multistage (6)	400
VI	2700	1200	10	Multistage (8)	344
VII	1300	1200	10	Multistage (4)	398

*Interest during construction and escalation not included.

TABLE 2. Single-Stage Reversible Pump-Turbine Characteristics

Parameter	Numerical Value		
Nominal Head (m)	500	750	1000
Rated Power (MW)	500	500	500
Rotary Speed (rpm)	327.27	514.27	720
Rated Pump Efficiency (%)	93.2	92.3	91.4
Rated Turbine Efficiency (%)	91.0	91.3	90.7
Submergence (m)	75	100	125
Specific Speed[a] $\left(\frac{\text{rpm}(\text{m}^3/\text{s})^{1/2}}{\text{m}^{3/4}}\right)$	31.0	30.0	29.2
Gate Pin Circle Diameter (cm)	680.7	527.3	421.9
Runner Outside Diameter (cm)	581.8	450.7	370.1

[a]Pump Cycle

TABLE 3. Two-Stage Reversible Pump-Turbine Characteristics

Parameter	Numerical Value			
Nominal Head (m)	1000	1250	1250	1500
Rated Power (MW)	500	500	350	500
Rotary Speed (rpm)	450	600	720	720
Rated Pump Efficiency (%)	90.6	89.6	89.6	88.3
Rated Turbine Efficiency (%)	90.0	89.5	89.6	88.4
Submergence (m)	75	85	85	100
First Stage Head (m)	400	500	500	600
Second Stage Head (m)	600	750	750	900
First Stage Specific Speed[a] $\left(\frac{rpm(m^3/s)^{1/2}}{m^{3/4}}\right)$	36.1	36.3	36.4	34.4
Second Stage Specific Speed[a] $\left(\frac{rpm(m^3/s)^{1/2}}{m^{3/4}}\right)$	26.6	26.7	26.9	25.4
Gate Pin Circle Diameter (cm)	519.2	435.6	363.2	396.2
Top-Stage Runner Outside Diameter (cm)	455.1	382.0	318.5	347.5
Bottom-Stage Runner Outside Diameter (cm)	383.0	321.6	268.0	292.1

[a] Pump Cycle

TABLE 4. Percentage Saving in Plant Cost When Two-Stage Reversible Pump Turbines Are Used Instead of the Turbomachinery Listed

Machinery Type	Savings ($/kW)[a]	Percentage Saving (%)
Multistage Reversible Pump Turbine	16	4.4
Single-Stage Reversible Pump Turbine (Two-Drop)	28	7.5
Tandem Unit	48	12.2

[a] 1978 dollars.

TABLE 5. Charge/Discharge Ratio and Energy Storage[a] for Representative Pumped Storage Plants.

Plant	Charge/Discharge Ratio (Pump Load/Plant Capacity)	Energy Storage (hours) kWh/kW of Plant
Taum Sauk	1.07	7.7
Yarks Creek	1.30	8.8
Middy Run	1.05	14.2
Cabin Creek	0.93	5.8
Seneca (Kinzua)	1.29	11.2
Northfield	1.00	8.5
Blenheim-Gilboa	1.13	11.6
Ludington	1.25	9.0
Jocassee	1.11	94.0
Bear Swamp	1.04	5.6
Racoon Mountain	1.01	24.0

[a] adapted from "An Assessment of Energy Storage Systems Suitable for Use by Electric Utilities," Vol. III, EM-264 EPRI Project 225, ERDA (11-1)-2501, July 1976. (Ref. 6)

TABLE 6. Some Performance Characteristics of Single-Stage Reversible Pump Turbines. (Ref. 2)

Nominal Head (m)	Mode	Capacity (MW)	r[a]	Tg/Tp[b]
500	A	430	1.07	0.74
	B	325	1.42	1.00
750	A	475	0.96	0.65
	B	350	1.31	0.91
1000	A	500	0.91	0.60
	B	365	1.24	0.85

[a] Charge/Discharge Ratio.

[b] Generation Time/Pumping Time.

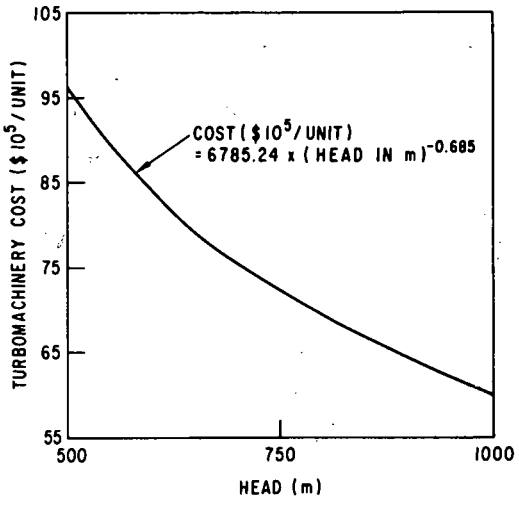

Fig. 1. Single-Stage Reversible Pump-Turbine Cost (500 MW Size)

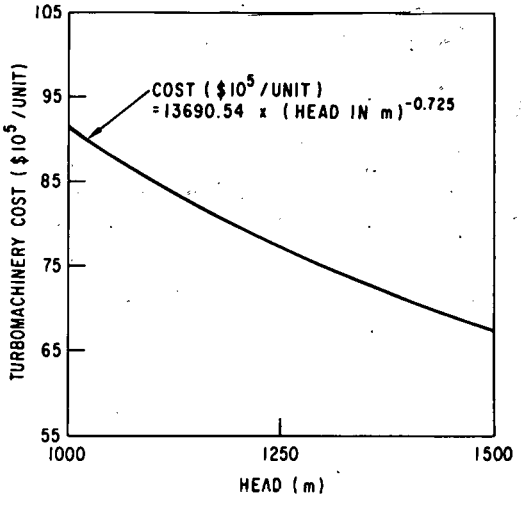

Fig. 2. Two-Stage Reversible Pump-Turbine Cost (500 MW Size)

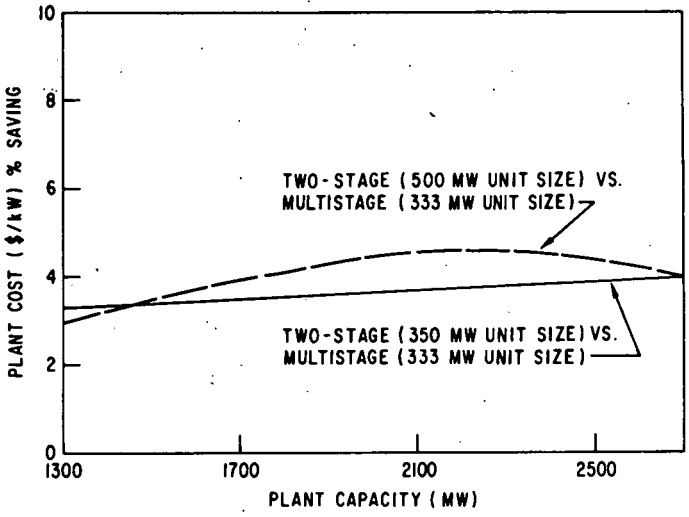

Fig. 3. Percent Savings in UPHS Plant Cost ($/kW) at 1200m Head

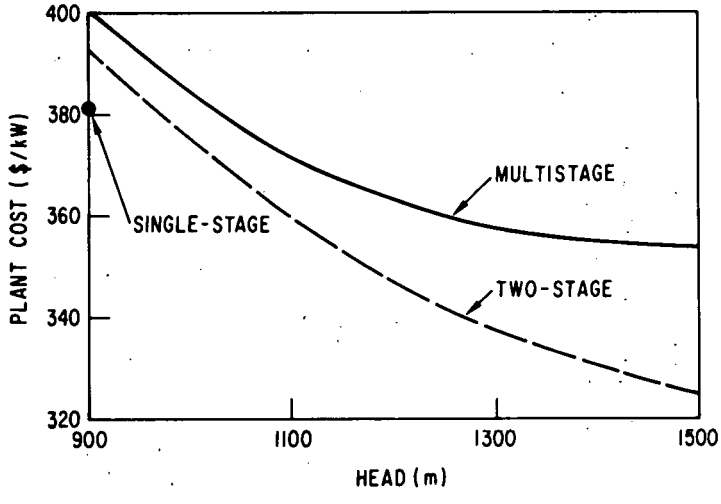

Fig. 4. UPHS Plant (2000 MW) Cost ($/kW)

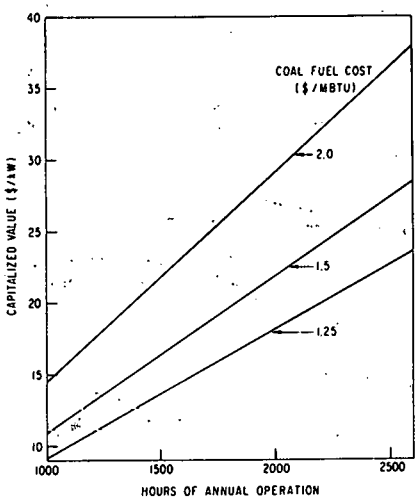

Fig. 5. Capitalized Value ($/kW) for 4% Difference in Pump-Turbine Efficiency (50 Years Lifetime at 8%)

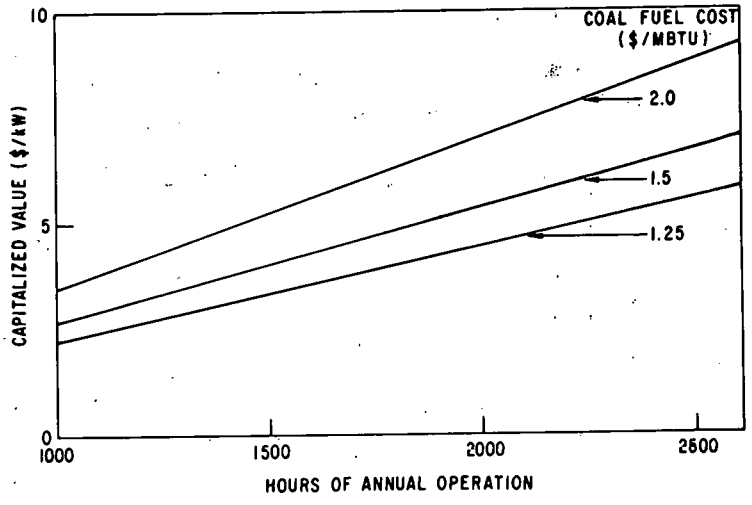

Fig. 6. Capitalized Value ($/kW) for 1% Difference in Pump-Turbine Efficiency (50 Years Lifetime at 8%)

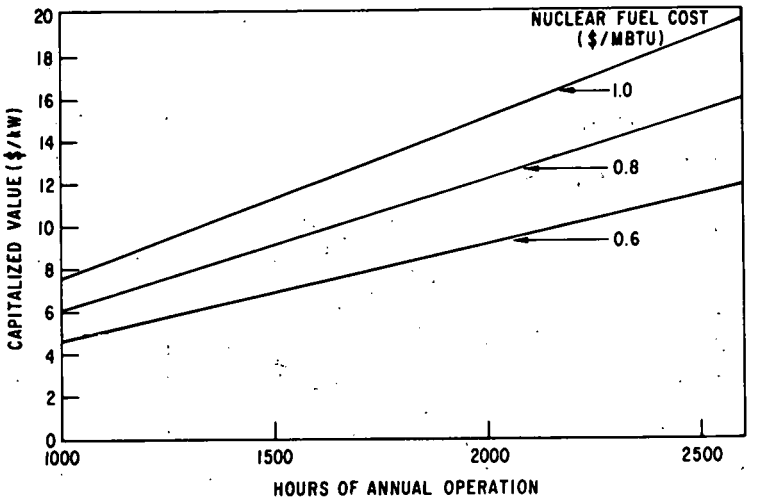

Fig. 7. Capitalized Value ($/kW) for 4% Difference in Pump-Turbine Efficiency (50 Years Lifetime at 8%)

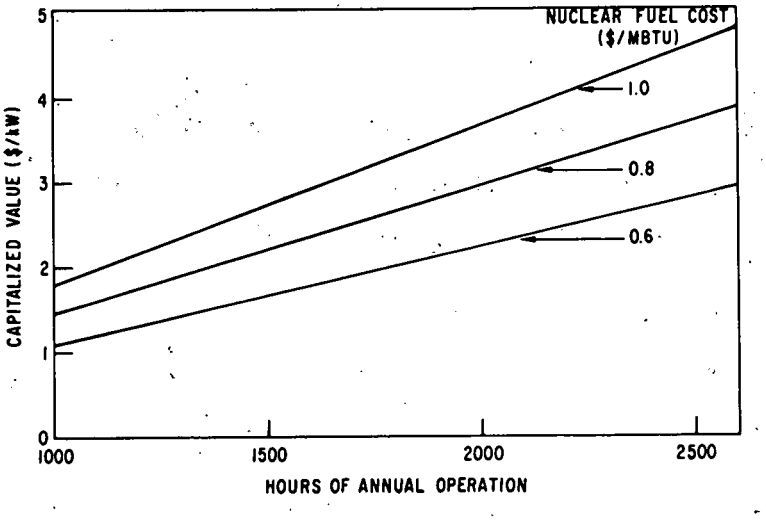

Fig. 8. Capitalized Value ($/kW) for 1% Difference in Pump-Turbine Efficiency (50 Years Lifetime at 8%)

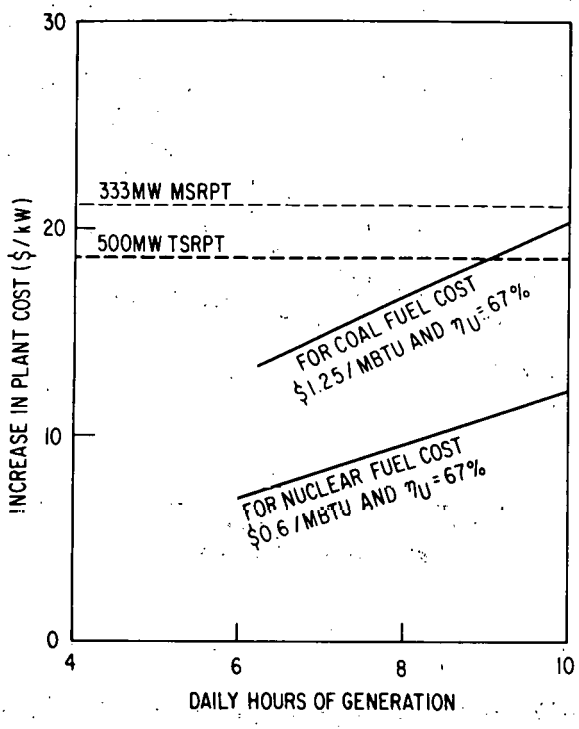

Fig. 9. Increase in Balance-of-Plant Cost and Pumping Energy Cost Vs. Daily Hours of Generation

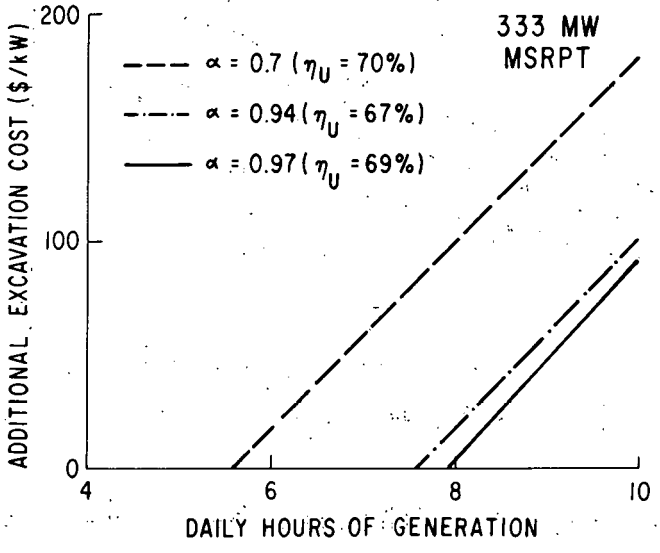

Fig. 10. Additional Excavation Cost Vs. Daily Hours of Generation for 333 MW MSRPT

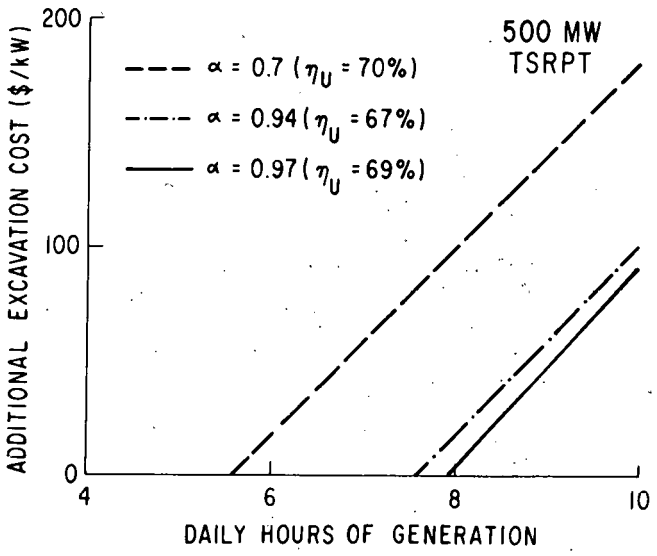

Fig. 11. Additional Excavation Cost Vs. Daily Hours of Generation for 500 MW TSRPT

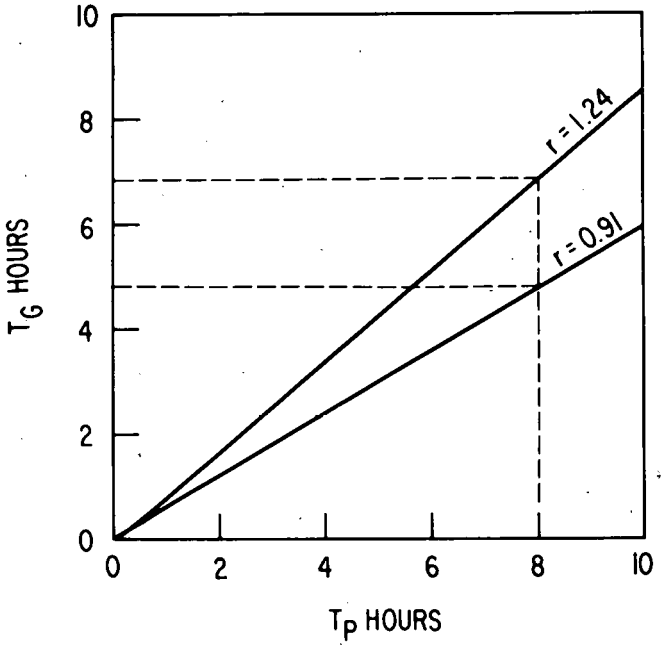

Fig. 12. T_G Vs. T_P for SSRPT with 1000 M Head

PROJECT SUMMARY

Project Title:	Assessment of the Application Potential of the Pumps with Controlled Flow Rate for Energy Storage
Principal Investigator:	Alexander Gokhman
Organization:	EDS Nuclear Inc. 220 Montgomery Street San Francisco, California 94104 Telephone (415) 544-8199
Project Goals:	The goal of this project was to conduct the economical analysis (based on the results of the preliminary design accomplished by the University of Miami in October 1978) in order to justify the spendings of the government and private industries for experiments with model turbine-pumps and for conceptual design of the machine by one of the vendors.
Project Status:	The project was completed in June 1979 and final report was submitted to Argonne National Laboratory in July 1979. The results of the project are being evaluated at Argonne National Laboratory, DOE, EPRI and Bureau of Reclamation (Department of Interior).
Contract Number:	31-109-3810
Contract Period:	April 5, 1979 - July 1, 1979
Funding Level:	$12,000
Funding Source:	Argonne National Laboratory

ASSESSMENT OF THE APPLICATION POTENTIAL OF THE PUMPS WITH CONTROLLED FLOW RATE FOR ENERGY STORAGE

Alexander Gokhman, Nail Ozboya
EDS Nuclear Inc.
220 Montgomery Street
San Francisco, CA 94104

ABSTRACT

The present project covers the comparison of the turbine-pumps and pumps with controlled flow rate with the alternative equipment for the different areas of application. The analyses showed the definite advantage of these new machines for the main areas of application.

INTRODUCTION

The Turbine-Pump with Controlled Flow Rate (TPCFR) was invented in 1975 by Dr. Alexander Gokhman.(1) In this machine the flow rate is regulated by means of change of the water passage height in both turbine and pump modes. In order to change the height of the water passage, TPCFR has additional adjustable hub in the runner and movable upper cover in the wicket gate. Both these additional parts can move along the axis of the machine.(2), (3)

No other Turbine-Pump connected to a synchronous motor-generator can efficiently regulate the flow rate in the pump mode. Neyrpic, a leading hydraulic machinery manufacturer in France, made an attempt to develop a turbine-pump which would regulate the flow rate in the pump mode by means of a wicket gate placed between the spiral casing and runner. Such a pump can regulate the flow rate only by increasing the head losses significantly. Consequently, it has low efficiencies at flow rates smaller than the maximum flow rate.

The effective regulation of flow rate and consequently power in the turbine mode can be provided only in one-stage machines. The conventional multi-stage turbine pumps cannot regulate power in the turbine mode. However, there is a recent development by Allis-Chalmers on two-stage turbine-pumps with the wicket gate in the upper stage which would allow regulation of power in the turbine-mode. This machine has several disadvantages. (4) Consequently with the modern tendency toward high-head pumped-storage plants which require two-stage machines only TPCFR can provide efficient regulation of power in both turbine and pump modes. The ability of TPCFR to regulate flow rate in the pump mode makes it very attractive for pumped-storage plants and storage of energy generated by solar and wind-electrical plants, and solar-mechanical applications.

In 1977, the U. S. Department of Energy funded a research project on the preliminary designs of one and two stage TPCFR's at University of Miami, Coral Gables, Florida. The present study is based on the results of that project which was successfully completed in 1978.(3) The comparisons evaluated in this study are preliminary in order to justify the spendings of the government and private industries for experiments with model turbine-pumps and for conceptual design of the machine by one of the vendors.

The detailed economical comparisons for the commercialization of TPCFR can be based only on the results of the experiments mentioned above and on the conceptual design. In the present project the authors tried to show the positive features of TPCFR by means of the quantitative comparison of this new machine with alternative equipment for typical conditions.

COMPARISON OF THE TURBINE-PUMP WITH CONTROLLED FLOW RATE WITH ALTERNATIVE EQUIPMENT (FOR PUMPED-STORAGE PLANTS)

One of the possible application areas for one and two-stage TPCFR'S is pumped-storage plants. These pumped-storage plants may have the lower reservoirs underground or above the ground. The alternative machines in this case are conventional one and two-stage turbine-pumps, two-stage turbine-pumps with wicket gate at the upper stage (Allis-Chalmers) and one-stage turbine-pumps with wicket gate utilized in the pump mode (Neyrpic).

The daily power demand graph which was chosen for the economical analysis (see Fig. 1.), is a hypothetical graph for a medium size system of the Northern U.S.A. with two peaks of power; one in the morning, and one in the evening. The maximum and minimum powers of the system in December and January are taken to be 4000 MW, and 1050 MW, correspondingly. The technical minimum of system is taken as 1500 MW. It is clear from Figure 1 that the pumped-storage plant can be charged between hours 0:00 and 6:00 (when the demand to the system is lower than the technical minimum) and that pumped-storage plant can work in the evening peak between hours 16:30 and 19:30 augmenting the thermal plants. Consequently the pumped-storage plant does not only redistribute the energy within one day but also decreases the installed power of the thermal-electric plants of the system.

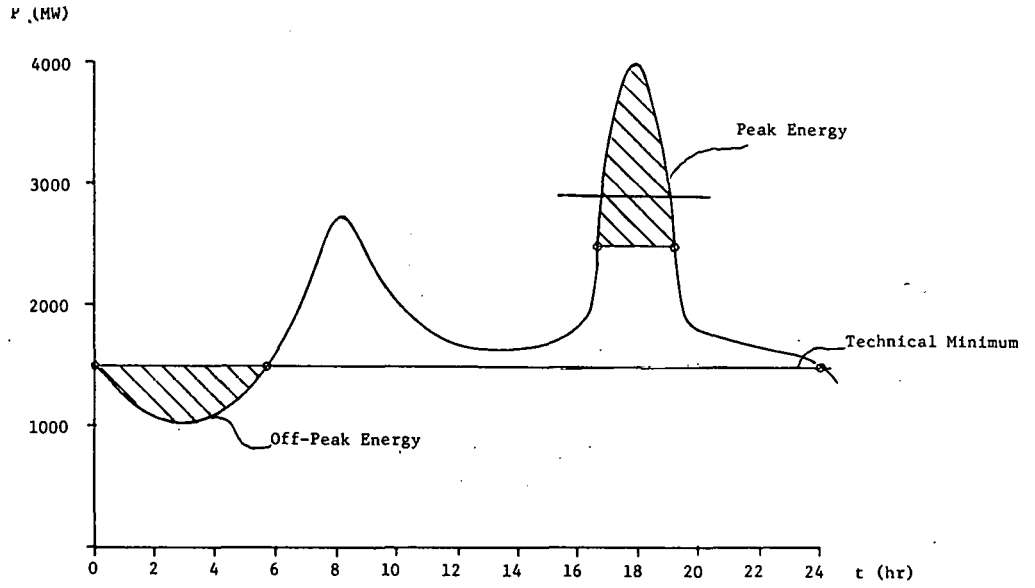

Fig. 1. Daily Graph of the Power Consumption of the System

The graph of the power available for the pumped-storage plant charging, $P_c = P_c(t)$, based on the daily power demand graph for December and January, is presented on Fig. 2. The maximum power of this graph is 450 MW. The graph of peak power $P_p = P_p(t)$ in which the pumped storage has to work is presented in Fig. 3.

For the calculation of energy stored and produced by pumped-storage plant the maximum of $P_c = P_c(t)$ is taken in June and July as 550 MW and the average maximum is as 500 MW. It is further assumed that the curves, $P_c = P_c(t)$, with maximum powers of 450 MW and 550 MW cover 25% of the year and the curve with the maximum power of 500 MW covers 50% of the year. In order to simplify the calculation of the energy available for charging and the calculation of the guaranteed power of the pumped-storage plant during the evening peak, the graphs $P_c = P_c(t)$ and $P_p = P_p(t)$ are considered as symmetric parabolas with vertices at the maximum points. Consequently the analytical representation of $P_c = P_c(t)$ is

$$P_c = \frac{P_{c\,max}}{9} \cdot (6t - t^2) \quad (\text{for } 0.0 \leq t \leq 6.0) \tag{1}$$

where $P_{c\,max}$ is the maximum of the curve. And the analytical representation of $P_p = P_p(t)$ for December and January is:

$$P_p = 4000 - 960 \cdot (t - 18)^2 \qquad (\text{for } 16.5 \leq t \leq 19.5) \tag{2}$$

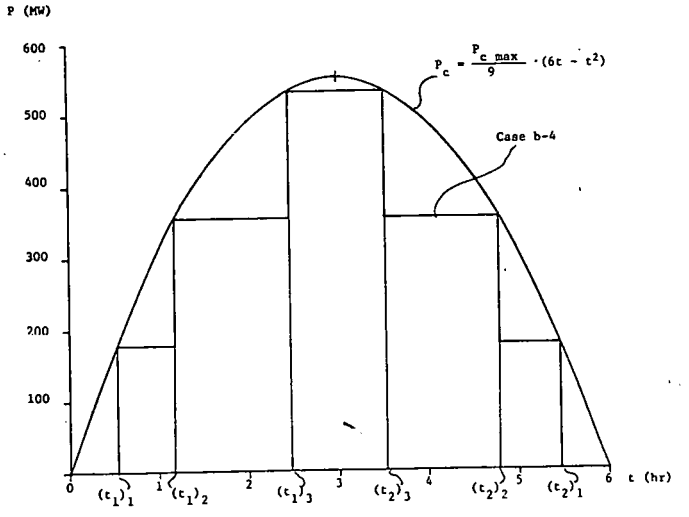

Fig. 2. Daily Graph of the Power Available for the Pumped-Storage Plant Charging

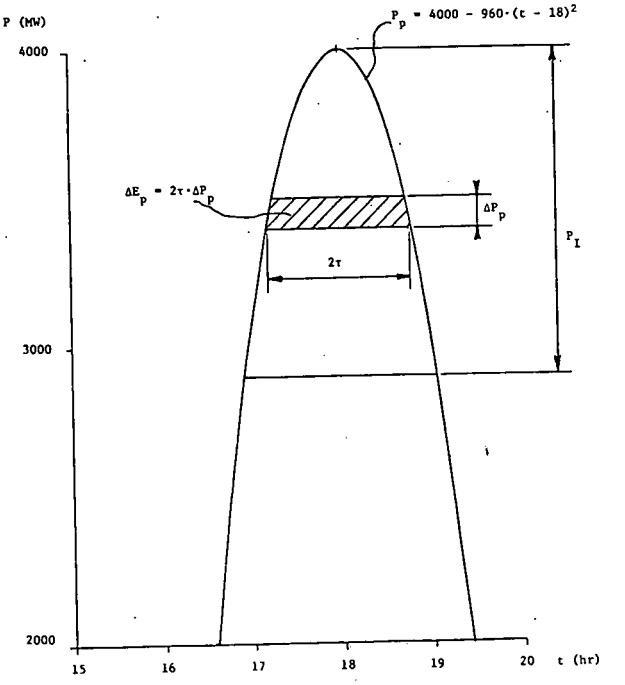

Fig. 3. Daily Graph of Work of the Pumped-Storage Plant in the Peak

For economical comparison, two pumped-storage plants are considered; one equipped with two TPCFR's and conventional machines and the other equipped with alternative equipment.

As given in Reference 5, the capital cost of 1 kW of installed power for Oil Steam Electric Power is \$425 and for Pumped- Storage Plant is \$150 in 1970 dollars, therefore, if the yearly rate of inflation is assumed to be 5%, these costs are approximately 41% higher in 1977 dollars, since $(1 + 0.05)^7 = 1.407$. Consequently in 1977 dollars, for thermal plants, the cost of 1 kW is \$598 and for pumped storage plant, the cost of 1 kW is \$211. The cost of one kW of installed power is taken to be \$100 for the conventional turbine-pumps, and \$120 for TPCFR as it was done in the Feasibility Analysis of the Final Report on the Preliminary Design of TPCFR.(3)

The following rates are used for the electrical energy consumption. For the peak energy, the rate is 4¢/kW-hr, for the off-peak energy, the rate is 2¢/kW-hr.

CONVENTIONAL ONE-STAGE TURBINE-PUMPS

The following alternatives are under consideration.

- Pumped-storage plant equipped with two TPCFR's and conventional one-stage turbine-pumps.

Pumped-storage plant equipped with conventional one-stage Turbine-Pumps.

The head of the pumped-storage plant is taken to be 500 m., since this head is very lose to the most economical head for the one-stage turbine pumps. The combined efficiency of charging and discharging of the energy for both alternative plants under consideration is taken as 0.80.

a) Pumped-Storage Plant Equipped with Two TPCFR's and Conventional Turbine-Pumps

Since the pumped-storage plant can continuously regulate the flow rate, the energy available daily for charging according to (1) is

$$E_c = \int_0^6 \frac{P_{c\ max}}{9} (6t - t^2)dt$$

or

$$E_c = \frac{P_{c\ max}}{9} \left(\frac{6t^2}{2} - \frac{t^3}{3}\right) \Big|_0^6 = 4 \cdot P_{c\ max} \qquad (3)$$

Therefore, the daily available energy for discharging in peak is $E_p = E_c \cdot \eta = 3.2 \cdot P_{c\ max}$. So in December and January $E_p = 3.2 \cdot 450 = 1440.0$ MW-hr.

The installed power of the pumped-storage plant, P_I, is the power of this plant working in December and January in the peak with available energy $E_p = 1440.0$ MW-hr.

Formula (2) introduces P_p as a function of time. But one can use Stieltjes integral in order to find the function $P_I = P_I(E_p)$ (See Fig. 3.), so

$$E_p = 2 \cdot \int_{4000 - P_I}^{4000} \tau \cdot dP_p \qquad (4)$$

where $\tau = t - 18$ and $t \leq 18$.

From formula (2)

$$\tau = \frac{1}{\sqrt{960}} \sqrt{400 - P_p} \qquad (5)$$

or

$$E_p = 0.06455 \cdot \int_{4000 - P_I}^{4000} \sqrt{4000 - P_p} \cdot dP_p \qquad (6)$$

and

$$E_p = 0.06455 \frac{2}{3} P_I^{3/2}$$

therefore,

$$P_I = 8.143 \cdot E_p^{2/3} \qquad (7)$$

Finally the installed power

$$P_I = 8.14334 \cdot (1440.0)^{2/3} = 1038.4 \text{ MW}$$

Consequently the pumped-storage plant can be equipped with five machines with a power of 207.7 MW for each machine. Two of these machines are accepted to be TPCFR and three to be conventional.

The daily energy for charging with maximums 450 MW, 500 MW and 550 MW by equation (3) are

$(E_c)_{450} = 1800$ MW-hr.

$(E_c)_{500} = 2000$ MW-hr.

$(E_c)_{550} = 2200$ MW-hr.

And therefore the total energy available for charging during the year is

$$(E_c)_y = 365 \cdot [0.25 \cdot (E_c)_{450} + 0.50 \cdot (E_c)_{500} + 0.25 \cdot (E_c)_{550}]$$

or

$$(E_c)_y = 7.3 \cdot 10^8 \text{ kW-hr.}$$

And the output of the energy in peak during one year

$$(E_p)_y = (E_c)_y \cdot 0.80 = 5.84 \cdot 10^8 \text{ kW-hr.}$$

b) Pumped-Storage Plant Equipped with Conventional Turbine-Pumps

The energy available for charging can not be completely used by the plant and depends on the power of the smallest unit of the plant. The following cases are under consideration.

b-1) Four machines with the unit power $P_u = P_I/5$ and eight machines with the unit power $\Delta P_u = P_I/40$.

b-2) Four machines with the unit power $P_u = P_I/5$ and four machines with the unit power $\Delta P_u = P_I/20$.

b-3) Four machines with the unit power $P_u = P_I/5$ and two machines with the unit power $\Delta P_u = P_I/10$.

b-4) Five machines with the same unit power ($P_u = P_I/5$).

The charging energy by Pumped-Storage Plant with power of the smallest unit P_u can be obtained using (1). Indeed the power of the plant in pumping mode can be expressed as

$$(P_c)_k = k \cdot \Delta P_u \tag{8}$$

where k is an integer, and

$$1 \leq k \leq k_{max} \leq \frac{P_{c\ max}}{P_u}$$

The values of time $(t_1)_k$ and $(t_2)_k$ corresponding to $(P_c)_k$ are obtained from (1)

$$k\Delta P_u = \frac{P_{c\ max}}{9} \cdot (6t - t^2)$$

or

$$(t_{1,2})_k = 3 \mp \sqrt{9 - \frac{k \cdot \Delta P_u \cdot 9}{P_{c\ max}}} \tag{9}$$

Therefore the Charging Energy (See Fig. 2.)

$$E_c = \sum_{k=1}^{k\ max} \Delta P_u \cdot [(t_2)_k - (t_1)_k]$$

or using (9)

$$E_p = \eta \cdot \sum_{k=1}^{k\ max} 6 \cdot \Delta P_u \sqrt{1 - \frac{k \cdot \Delta P_u}{P_{c\ max}}} \tag{10}$$

Since this plant can regulate the power in turbine mode, the relation between $E_p = \eta \cdot E_c$ and P_I is the same, as for the plant equipped with TPCFR (by formula (7). It is clear from the formula (10) and (7) that the values of P_I for cases b-1, b-2, b-3, and b-4 can be calculated only by means of iterations. The results of calculation of P_u and P_I are presented in Table 1.

TABLE 1. Installed Power and the Power of the Smallest Unit

Case	b-1	b-2	b-3	b-4
P_u (MW)	25.2	49.2	91.7	176.5
P_I (MW)	1008.0	984.0	917.0	838.0

After P_I is calculated it is relatively easy to determine the energy output of the pumped-storage plant. The results obtained by using equation (10) are tabulated in Table 2. Also included in the table are the annual energy output of the pumped-storage plant for each case.

TABLE 2. Available Energy for Daily Charge and Yearly Output

Case	b-1	b-2	b-3	b-4
$(E_c)_{450}$ (kW-hr.)	$1.721 \cdot 10^6$	$1.669 \cdot 10^6$	$1.494 \cdot 10^6$	$1.304 \cdot 10^6$
$(E_c)_{500}$ (kW-hr.)	$1.921 \cdot 10^6$	$1.860 \cdot 10^6$	$1.747 \cdot 10^6$	$1.397 \cdot 10^6$
$(E_c)_{550}$ (kW-hr.)	$2.122 \cdot 10^6$	$2.060 \cdot 10^6$	$1.882 \cdot 10^6$	$1.762 \cdot 10^6$
$(E_p)_y$ (kW-hr.)	$5.619 \cdot 10^8$	$5.431 \cdot 10^8$	$5.015 \cdot 10^8$	$4.278 \cdot 10^8$

The examination of Tables 1 and 2 shows that case b-1 gives the highest annual energy output and the maximum power substitution during the peak. The annual energy output and the maximum peak power substitution would be increased if a storage plant was equipped with machines in case $P_u = P_I/80$. However, there is a limit on the minimum unit power after which it is technically impossible to utilize machines under such a head. For example, in order to use $P_u = P_I/80$, one has to have a machine with P_u = 12.5 MW and with an approximate runner diameter of 0.9m. under 500 m. head. The production of such a machine is technically not feasible. Therefore the case b-1 will be compared with the storage plant equipped with TPCFR's. Conservatively, the increase in the capital cost due to using eight small machines instead of one machine will be neglected (there is no reliable information on the increase of capital cost for this case).

The increase in the capital cost of Pumped-Storage Plant, equipped with TPCFR's (case a) with respect to case b.1.

The construction:

$$(1038.4-1008.0) \cdot 111 \cdot 10^3 = \$3.3744 \cdot 10^6$$

The equipment:

$$(2\ 207.7 \cdot 120 + 3\ 207.7 \cdot 100 - 5\ 201.6 \cdot 100) \cdot 10^3 = \$11.358 \cdot 10^6$$

The decrease in the capital cost in the thermal-electric plants which are substituted by Pumped-Storage Plants equipped with TPCFR'S with respect to case b.1.

$$(1038.4 - 1008.0) \cdot 598 \cdot 10^3 = \$18.179 \cdot 10^6$$

Therefore the gain in the capital investment for the case a in comparison with b.1 is at least:

$$18.179 \cdot 10^6 - (11.358 \cdot 10^6 + 3.3744 \cdot 10^6) = \$3.4466 \cdot 10^6$$

The difference in the profits due to difference in peak and off-peak power costs, in the case a with respect to case b-1

$$(5.84 \cdot 10^8 - 5.61 \cdot 10^8)\ \text{kW-hr} \cdot \$0.02/\text{kW-hr} = \$460{,}000.$$

This analysis shows that the pump-storage plant equipped with TPCFR'S (case a) is definitely more advantageous than the plant with conventional machines both from capital investment and annual profits point of view. In this connection, it should be noted that, the increase in the capital cost of plant with conventional machines was not taken into account when eight small machines were used. It should also be pointed out, that the plant equipped with TPCFR's can maintain the frequency of the system while working in the pump mode and save fuel in the system in comparison with conventional equipment.

CONVENTIONAL TWO-STAGE TURBINE PUMPS

The method of comparison with respect to operation in the pump mode is identical to the ethod described in Section 2.1.1. However, in the turbine mode, conventional two stage urbine-pumps cannot regulate the power and consequently cannot accept the fluctuations in the power of the system and maintain the frequency. Therefore, the frequency of the system has to be maintained by thermal plants which causes additional fuel losses in comparison with storage plants equipped with TPCFR's.

Consequently, in the case of two-stage machines TPCFR is much more advantageous than the conventional machines not only in the pump mode but also in the turbine mode.

TWO-STAGE TURBINE-PUMPS WITH WICKET GATE AT THE UPPER STAGE

This machine is analysed in detail in reference 4. From this analysis it is clear that this machine does not have the main positive feature of two-stage machines which is to divide the total head among the stages. Consequently this machine can be considered as a more complicated and expensive than one-stage conventional machine without any additional positive features and hence, no further analysis is required.

ONE-STAGE TURBINE-PUMPS WITH WICKET GATE UTILIZED IN THE PUMP MODE

This machine is analysed in detail in reference 3. The operation of this machine in the turbine-mode is identical to conventional one-stage turbine-pumps. In the pump-mode the flow rate is regulated only by direct losses of the head as shown in the hydraulic analysis mentioned above. If the machine is designed to pump the water to the upper reservoir height at optimum conditions, it will not be able to pump any water during regulation that is at loads smaller than optimum. If it is desired to pump water at conditions other than optimum, the machine has to be designed for larger power which will consequently increase the capital cost significantly. Therefore, this machine does not offer any advantage at all on the conventional one-stage machines, and hence, no further analysis is required.

COMPARISON OF PUMP WITH CONTROLLED FLOW RATE WITH ALTERNATIVE EQUIPMENT

The possible utilization areas for the pump with controlled flow rate (PCFR) are solar-electric power plants, solar and wind mechanical applications and irrigation and water supply applications. These cases will be analysed in detail in the following sections. The alternative equipment for these application areas are the one-stage conventional pumps.

CONVENTIONAL ONE-STAGE PUMPS FOR SOLAR-ELECTRIC POWER PLANTS

The combination of a solar electrical plant with pumped storage forms the solar complex electrical plant.[6] In this arrangement, the storage plant comprises separate pumps working at night on off-peak energy and during the day time on solar energy and the turbines giving energy to the system during the peak time.

The cost of 1 kW of power of the solar electrical plant is very high compared to the cost of 1 kW of pumped-storage plant. The utilization of conventional pumps in the pumped-storage plant will lead to inevitable losses of power during operation up to the capacity one unit. These losses will drastically increase the cost of 1 kW of power of the solar complex electrical plant. On the other hand, the utilization of the pump with controlled flow rate will eliminate these losses, but slightly increase the price of the 1 kW of the pumped-storage plant still resulting in smaller cost of 1 kW of the solar complex electrical plant. As an illustration of the point let us consider the solar complex electrical plant (SCEP) participating in the electrical system of South Florida (latitude 24°N) without utilizing off-peak energy. Also let us assume that SCEP will reliably work in the period from March through September. Obviously the worst months for the plant are

March and September since the amount of solar energy received is the smallest and the requirement of the plant to the system is highest in these months. If we make the further assumptions that the plant has to work two hours during the peak time with 1109 MW and the ratio of sunny days in this region is 80% during these months, the energy which has to be produced by the solar electrical plant on a sunny day becomes

$$E_{sd} = \frac{1109 \cdot 10^3 \cdot 2}{0.8 \cdot \eta_{ps}}$$

where

$\eta_{ps} = 0.8$ is the efficiency of the pumped-storage plant.

Therefore

$$E_{sd} = 3.467 \cdot 10^6 \text{ kW-hr}$$

The distribution of solar insolation on a sunny day in March can be introduced as a parabola with maximum power P_{oi} at noon and the smallest power of 0.6 P_{oi} at 8.00 and 16.00. For simplicity let us assume the efficiency of the solar electrical plant is constant. Therefore the same curve will represent the power output of the solar electrical plant (see Fig. 4.).

The cost of 1 kW of solar electrical plant is approximately \$2000 and the cost of 1 kW of the conventional pumped-storage plant equipped with pump-turbines is \$211.(5), (7) Let us say there are five pumps with 100 MW capacities at this pumped-storage plant and the cost of the pump with controlled flow rate is 20% higher than the conventional pump, since the conventional pump does not have a distributor and the labor in the case of new pump is more expensive. The cost of the equipment at the pumped-storage plant can be assumed as \$100/kW. Therefore, we can roughly say that the cost of 1 kW of the pumped-storage plant with separate pumps and turbines is approximately \$311 (\$111/kW for the construction, \$100/kW for the turbines and \$100/kW for the pumps).

Now it is possible to compare the cost of SCEP equipped with conventional pumps with that of SCEP comprising the conventional pumps and two PCFR's (two pumps of this kind can provide continuous regulation of power).

a) SCEP Equipped with Conventional Pumps and Two PCFR's

The analytical expression for the parabola representing the output of solar electrical plant is

$$P = P_o \cdot (1 - 0.025 \cdot (t - 12)^2) \tag{11}$$

where P_o is the maximum output of solar electrical plant. Consequently the total energy produced by the plant is

$$E_{sd} = \int_8^{16} P_o \cdot (1 - 0.025 \cdot (t - 12)^2) \cdot dt = 6.933 \cdot P_o$$

$$E_{sd} = 3.467 \cdot 10^6 \text{ kW-hr}$$

Since

$$P_o = 500 \cdot 10^3 \text{ kW}$$

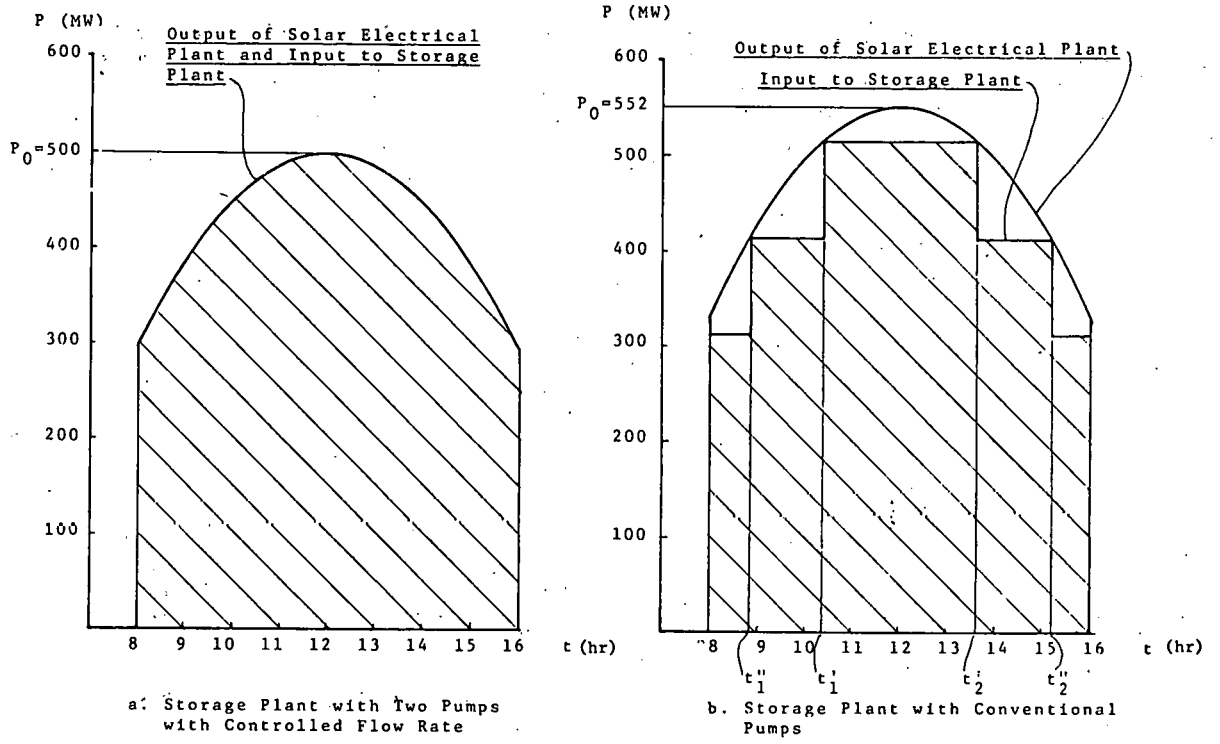

Fig. 4. Pumped Storage as Energy from Solar Electric Plant.

Now it is possible to find the costs of SCEP parts, remembering that there are five pumps, three of them being conventional.

Cost of solar electrical plant $= 500 \cdot 10^3 \cdot 2000$
$= \$\ 1 \cdot 10^9$

Cost of construction of pumped storage plant $= 1109 \cdot 10^3 \cdot 111$
$= \$\ 0.1231 \cdot 10^9$

Cost of conventional pumps $= 3 \cdot 100 \cdot 10^3 \cdot 100$
$= \$\ 0.030 \cdot 10^9$

Cost of two PCFR's $= 2 \cdot 100 \cdot 10^3 \cdot 120$
$= \$\ 0.024 \cdot 10^9$

Cost of turbines $= 1109 \cdot 10^3 \cdot 100$
$= \$\ 0.1109 \cdot 10^9$

Therefore the total cost of SCEP is

$C = \$\ 1.2880 \cdot 10^9$

and the cost of 1 kW of power is

$$k = \frac{1.2880 \cdot 10^9}{1109 \cdot 10^3} = \$\ 1161.41\ /kW$$

b) SCEP Equipped with Five Conventional Pumps

In order to have a reliable comparison, it is necessary to find the optimum capacity of one pump unit which gives minimum P_o which is required for the same value of E_{sd} to be produced by step regulation. As can be seen from Fig. 4., P_o should be larger than $5P_u$, otherwise one unit will never work. Also the the smallest P is equal to $0.6P_o$, therefore, only two steps are possible. As follows from the figure 4 and the formula (11)

$$E_{sd} = 5 \cdot P_u(t_2' - t_1') + 4 \cdot P_u(t_2'' - t_1') \cdot 2 + 3 \cdot P_u(16 - t_2'') \cdot 2 \tag{12}$$

where

$$t_{1,2}' = 12 \mp \sqrt{\frac{1-5 \cdot k_p}{0.025}}$$

$$t_2'' = 12 + \sqrt{\frac{1-4 \cdot k_p}{0.025}}$$

and

$$k_p = \frac{P_u}{P_o}$$

After some manipulation

$$E_{sd} = k_p \cdot P_o \cdot (12.65 \cdot (\sqrt{1-5 \cdot k_p} + \sqrt{1-4 \cdot k_p}) + 24) \tag{13}$$

Now it is possible to find the value of k_p which will give minimum P_o. If we rewrite (13) as

$$P_o = \frac{E_{sd}}{F(k_p)} \tag{14}$$

where

$$F(k_p) = k_p \cdot (12.65 \cdot (\sqrt{1-5 \cdot k_p} + \sqrt{1-4 \cdot k_p}) + 24)$$

The necessary condition for the minimum P_o is

$$\frac{dP_o}{dk_p} = 0$$

or from (14)

$$-\frac{E_{sd}}{F(k_p)^2} \cdot \frac{dF(k_p)}{dk_p} = 0$$

and since $E_{sd}/F(k_p)^2$ is not zero, the condition is

$$\frac{dF(k_p)}{dk_p} = 0$$

or

$$(12.65\cdot(\sqrt{1-5\cdot k_p}+\sqrt{1-4\cdot k_p})+24)-k_p\cdot(31.625\frac{1}{\sqrt{1-5\cdot k_p}}+25.3\frac{1}{\sqrt{1-4\cdot k_p}})=0$$

and

$$k_p=\frac{12.65\ (\sqrt{1-5\cdot k_p}+\sqrt{1-4\cdot k_p})+24}{31.625\frac{1}{\sqrt{1-5\cdot k_p}}+25.3\frac{1}{\sqrt{1-4\cdot k_p}}} \qquad (15)$$

The method of iteration applied to (15) gives $k_p = 0.1877$

Therefore, from (14) $P_o = 552.163\cdot10^3$ kW and $P_u = 103.64\cdot10^3$ kW

In this case, the costs of SCEP parts are:

Cost of solar electrical plant = $552.163\cdot10^3\cdot2000$
= \$ $1.1043\cdot10^9$

Cost of construction of pumped storage plant = $1109\cdot10^3\cdot100$
= \$ $0.1231\cdot10^9$

Cost of pumps = $5\ 103.64\cdot10^3\cdot100$
= \$ $0.05183\cdot10^9$

Cost of turbines = $1109\cdot10^3\cdot100$
= \$ $0.1109\cdot10^9$

The total cost of SCEP is C = \$ $1.3779\cdot10^9$ and the cost of 1 kW of power is

$$k=\frac{1.3901\cdot10^9}{1109\cdot10^3}=\$\ 1253.47/kW$$

So even in the case when PCFR is accepted to be 20% more expensive than the conventional machines, the utilization of this pump decreases the total cost of 1 kW by approximately 8%. However, from the weight comparison it is not clear PCFR is more expensive than the conventional machine at all. All those considerations show that PCFR is very attractive for solar complex electrial plants.

The economical comparison provided above shows not only the advantages of the new pump in comparison to the conventional pumps but it clearly introduces the advantage of using the combinations of solar electrical plants with pumped-storage plants. Indeed the cost of 1 kW of solar plant was accepted as \$ 2000, however, in combination with pumped-storage, the cost of 1 kW of SCEP immediately dropped to \$ 1150.

CONVENTIONAL ONE-STAGE PUMPS FOR SOLAR AND WIND MECHANICAL APPLICATIONS

Two general schemes can be considered for the solar and wind mechanical application.

a) The Mechanical Energy Generated by the Sun (Using a Collector and a Heat Engine) or Wind (Using a Wind Mill Without Generator) is Directly Applied to the Pumps.

In this case the pumps without ability to regulate the flow rate are not directly applicable without significant loss of energy, since it is impossible to adjust the speed of the prime mover (heat engine, propeller of a wind mill) shaft with the speed of a pump shaft wihout additional regulating devices. Consequently, it is more advantageous to use PCFR's in this case.

b) The Energy Generated by the Sun or Wind is First Converted to Electricity Via D.C. or A.C. Generators and then Applied to the Pumps.

For the case in which photovoltaic cells or DC generators are used, the conventional pumps are more advantageous due to their simplicity and lower cost, since it is possible to adjust the speed of the shaft of the DC moter to the power. For the case in which AC generators are used, it is more advantageous to us CPFR'S.

CONVENTIONAL ONE-STAGE PUMPS FOR IRRIGATION AND WATER SUPPLY APPLICATION

In the case of irrigation, PCFR can provide significant savings, especially if the irrigation of hillside fields is considered, since it can regulate the head providing the same flow rate for the top of the hill as well as for the foot of the hill and save water and energy.

For the water supply systems without special elevated water reservoirs, the utilization of CPFR'S will result in considerable energy savings, since the water use demand can be continuously followed. The conventional pump always exceeds the water demand unless the water demand is equal to sum of outputs of the pumps, therefore, causing waste of energy.

CONCLUSIONS

From the analysis of the application potential of the turbine-pumps and pumps with controlled flow rate the following conclusions have been made.

- The most attractive application of the turbine-pumps with controlled flow rate (TPCFR) is for high head pumped-storage plants. Two TPCFR in combination with conventional turbine-pumps will provide the pumped-storage plant with the ability to regulated power continuously and with high efficiency in both pump and turbine modes.

  The utilization of the TPCFR is definitely advantagous both from capital investment and annual profits point of view.

- The most attractive application of the pumps with controlled flow rate (PCFR) is in storage systems of solar-electric plants, etc. since these pumps can continuously regulate power with high efficiency. The utilization of PCFR decreases the capital cost of one kilowat of installed power for these plants.

- It is appropriate to begin laboratory experiments with TPCFR and PCFR and also to initiate the conceptual designs for these machines by one of the vendors.

- There is an immediate demand of solar and wind electrical plant storage systems for rural areas of the U.S.A. In order to satisfy this urgent demand it is possible to start the technical design and production of small machines of this new type. The power of these machine should be no more than 1 MW. and the diameters no more than 1m. These machines will sucessfully operate under a head around 100m.

REFERENCES

1. A. Gokhman, "Multi-Stage Turbine-Pump with Governing", Patent Application No. 618 964, October 2, 1975.

2. A. Gokhman, N. Ozboya, "Multi-Stage Turbine-Pump with Controlled Flow Rate", Proceedings of the 1978 Mechanical and Magnetic Energy Storage Contractor's Review Meeting, U.S. Department of Energy, Luray, Virginia, 1978.

3. A. Gokhman, N. Ozboya, "Multi-Stage Turbine-Pump with Controlled Flow Rate", Final Report for D.O.E., University of Miami, 1978.

4. A. Gokhman, "Assessment of the Application Potential of the Pumps with Controlled Flow Rate for Energy Storage", Final Report for Argonne National Laboratory, #01-0720-1039, EDS Nuclear Inc., San Francisco, 1979.

5. C. Braun, et al., "The Target Capital Costs for the Implementation of Fuel Cells and Electric Storage Devices within the National Energy System", Proceedings of Hydrogen Energy Short Course, Albuquerque, New Mexico, 1976.

6. A. Gokhman, "Complex Solar Electric Plants of Large Capacity", Alternative Energy Sources, An International Compedium, Hemisphere Publishing Corporation, Washington, 1979, volume 3.

7. F. A. Blake, "Central Receiver Solar Thermal Power", Proceedings, Solar Technology in the Seventies, Winnipeg, Canada, August, 1976.

THIS PAGE

WAS INTENTIONALLY

LEFT BLANK

SESSION 4: SOLAR MECHANICAL ENERGY STORAGE

THIS PAGE

WAS INTENTIONALLY

LEFT BLANK

PROJECT SUMMARY

Project Title:	"Mechanical Energy Storage for Photovoltaic/Wind Project"
Principal Investigators:	H. M. Dodd, B. C. Caskey, and H. E. Schildknecht
Organization:	Sandia Laboratories, Division 4716, Albuquerque, New Mexico 87185 (505) 264-8835
Project Goals:	The goal of this project is to identify and develop mechanical energy storage technologies for eventual commercialization, with the emphasis on solar (sun and wind) sources. The project utilizes results of systems analysis, special studies, and detailed design studies to define areas for hardware demonstration projects. The resulting cost and performance data will be available for consideration by industry. The project involves both Sandia in-house analysis and contracts with universities and industries.
Project Status:	System analysis has identified flywheel energy storage as the most promising of the mechanical energy storage technologies for residential applications. Therefore, special study and detailed design study contracts (three with universities, two with industries) address various aspects of stationary flywheel energy storage. These contracts are essentially complete and provide the basis for systems analysis that will yield a recommendation on construction of a demonstration flywheel system. A study of industrial compressed air has been completed. It showed that no compressed air storage was in place that could be used by industry for charging from solar sources. Also, even with "free" underground caverns, economics do not favor solar/wind powered industrial compressed air systems before the year 2000. Initial results from a study of low head underground pumped hydro storage indicate that the system may have economic potential. A detailed evaluation of residential flywheel energy storage systems is under way. In addition to the cost and performance data generated from study contracts, time-of-use pricing and energy sell-back are included in the study. This project will be transferred in its entirety to Lawrence Livermore Laboratory effective October 1, 1979.
Contract Number:	C8-03-02-02-03
Contract Period:	October 1977 - September 1979
Funding Level:	FY1979 - $553,000
Funding Source:	DOE, Division of Energy Storage, Advanced Physical Methods Branch

SOLAR MECHANICAL ENERGY STORAGE PROGRAM OVERVIEW AND SYSTEMS ANALYSIS RESULTS

B. C. Caskey
Sandia Laboratories
Systems Analysis Division 4716
Albuquerque, New Mexico 87185

ABSTRACT

The current status of the Solar Mechanical Energy Storage Program is described, along with the remaining activities before Lawrence Livermore Laboratory assumes program responsibility in October, 1979. Contractor results are presented in other papers; preliminary system analyses results for residential flywheel energy storage systems (FESS) are presented. Various phases of the program have addressed small-to-intermediate applications of photovoltaic/wind energy storage utilizing flywheels, compressed air and low head underground pumped hydro technologies.

INTRODUCTION

In 1977, the U.S. Department of Energy (DOE) assigned to Sandia Laboratories (SLA) the primary responsibility for the Mechanical Energy Storage for Photovoltaic/Wind program. Activities for that year included development of an optimizing systems analysis computer program called ENERA and subsequent analyses using it. Henry M. Dodd, et al., presented a paper in September 1977 entitled "An Assessment of Mechanical Energy Storage for Solar Systems."(1) This paper and subsequent studies, all of which compared only the various mechanical storage concepts with each other, concluded that flywheel systems are the most promising for residential applications. Therefore, the primary emphasis has been on the development of low-cost stationary flywheel technology. Other activities include a more detailed investigation of pneumatic-energy storage systems for industrial applications, low-head pumped-hydro storage, and continuing systems analysis efforts. The program has been described at various times in references 2, 3, and 4.

To continue this work in future years, DOE has asked Lawrence Livermore Laboratories (LLL) to assume the responsibility for the project. Pacific Northwest Laboratory (PNL) will assist LLL in some areas, i.e., compressed air and pumped-hydro activities.

SCOPE

This program is concerned with mechanical-energy storage modes that may be used in conjunction with solar (including wind) inputs supplying small-to-intermediate loads. Since, for central-station utility applications, energy storage would be tied to the grid rather than to a solar energy source, this program does not address central station applications.

Sandia Laboratories is a US Department of Energy (DOE) facility. This work was supported by the Division of Energy Technology, US DOE, under Contract DE-AC04-76DP00789.

CONTRACTS

During FY79, seven contractors (4 industry, 3 university or college) supported this program. All efforts are either completed or close to completion. In subsequent papers at this meeting, the results of each contract will be presented. Additionally, MIT Lincoln Laboratory's Flywheel Energy Storage and Conversion System project will be presented during this session as Sandia is the project's technical monitor.

The seven contracts are:

FLYWHEELS

FESS with Photovoltaic Input	- Wm. M. Brobeck & Associates
FESS with Wind Turbine Supply	- Garrett-AiResearch
Cellulosic Flywheels	- University of Minnesota
Flexible Flywheels	- Texas A&M
Variable Inertia Flywheel	- Union College

LOW-HEAD PUMPED HYDRO

Pumped Aquifer Storage System	- The BDM Corporation

INDUSTRIAL COMPRESSED AIR

Applications for Solar/Wind	- Jalar Associates

SYSTEMS ANALYSIS

SOLSTOR

Improvements to the project-developed ENERA code have resulted in a new code (SOLSTOR) which includes the following significant features:

- Time-of-day electricity pricing
- Energy sellback to the utility
- Off-peak storage charging
- Simple, nonpredictive storage utilization logic

Energy flow paths for SOLSTOR when configured for a FESS and a photovoltaic (PV) collector are shown in Fig. 1.

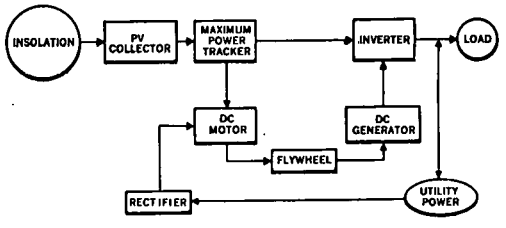

Fig. 1 SOLSTOR Energy Flow Paths Example

Each component in SOLSTOR is characterized by a "size," an efficiency, and a cost. The cost includes fixed and variable terms, with the variable term (cost per unit of size) also allowing for possible economies of scale.

The collector output and load demand are calculated on an hourly basis from TMY weather data (insolation and outside air temperature).

Economic parameters supplied to SOLSTOR include tax rates, tax credits, inflation rates, fuel escalation rates, the electricity sellback ratio, and utility electric rates. These electric rates may vary with time-of-day and with the season of the year.

SOLSTOR performs a search over the multi-dimensional space (maximum of 8 dimensions) to find the lowest life cycle system cost. This "optimal" configuration specifies the sizes of all components.

In order to achieve the best cost performance, all possible energy flow patterns are allowed. Collector energy may 1) satisfy the load, 2) charge storage, or 3) be sold to the utility. Storage may be charged from either the collector or the utility. Simple priority logic dictates the appropriate allocation of energy for each option.

PRELIMINARY RESULTS

Preliminary results have been obtained using SOLSTOR configured with a flat plate PV collector and a FESS. The economic assumptions used for all runs were:

System Life	20 Years
Base/Price Year	1980
Initial Operation Year	1986
Tax Bracket	30%
Property Tax	0%
Tax Credit	20%
Down Payment	20%
Cost of Capital	10%
Inflation Rate	5%
Purchased Electricity Escalation	8% & 11%

These conditions were selected to be representative for an individual homeowner.

Some of the system assumptions were:

ARRAY	$\$117/m^2$ + \$1047; 11% Efficiency; Flat Plate
FESS	$\$748*(\text{size in kWh})^{0.83}$ + \$1500
LOCATIONS	New York, Phoenix
RESIDENCE	1520 ft^2; All Electric with Heat Pump

ELECTRICITY COSTS (¢/kWh) — PEAK:OFF PEAK

		1:1	3:1	6:1
New York	Summer	13.9	22.8:7.6	27.3:4.55
	Winter	11.2	18.5:6.17	21.9:3.65
Phoenix	Summer	5.15	8.14:2.71	9.51:1.59
	Winter	4.51	7.14:2.38	8.33:1.39

O&M	1.5% of Initial Capital

The array costs represent DOE's 1986 goal of 50¢/W_p (1975\$) converted to 1980\$ and with markups, installation, and other system costs added.

The FESS costs were based on preliminary figures from Brobeck on production runs of 100,000 units. The \$1500 fixed cost is for site preparation (underground pit) and installation. An economy of scale factor was calculated from point designs at 10 and 50 kWh sizes. Although Brobeck presented the numbers as production costs (not prices), no markup was included for this preliminary study. The function used results in \$656/kWh and \$415/kWh for the 10 and 50 kWh units, respectively.

The 1:1 electricity costs were provided by the utilities in New York and Phoenix. The 3:1 and 6:1 ratio costs were determined so that the total electric bill for a customer (without this solar/storage system) would not change. Off peak rates were in effect on weekends and from 9PM-9AM in summer or 8PM-8AM in winter.

Figure 2 displays SOLSTOR results for optimal system configurations at Phoenix. The life cycle cost ratio is the annualized life cycle system cost plus net purchased electricity divided by the annualized cost of purchased electricity if no system was used. It provides a measure of the goodness of the system; negative values indicate that the homeowner would make money (receive a check from the utility)--probably an unrealistic condition.

3% Electricity Escalation

Sellback Ratio	Life Cycle Cost Ratio 1:1	3:1	6:1	Array Size (m^2) 1:1	3:1	6:1	FESS Size (kWh) 1:1	3:1	6:1
0.0	0.89	0.80	0.76	43.	47.	48.	0.	0.	0.
0.25	0.87	0.77	0.72	53.	59.	64.	0.	0.	0.
0.50	0.78	0.55	0.44	150.	150.	150.	0.	0.	0.
0.75	0.52	0.22	0.09	150.	150.	150.	0.	0.	0.

6% Electricity Escalation

Sellback Ratio	Life Cycle Cost Ratio 1:1	3:1	6:1	Array Size (m^2) 1:1	3:1	6:1	FESS Size (kWh) 1:1	3:1	6:1
0.00	0.79	0.69	0.65	52.	54.	55.	0.	0.	0.
0.25	0.74	0.59	0.51	89.	150.	150.	0.	0.	0.
0.50	0.50	0.27	0.16	150.	150.	150.	0.	0.	0.
0.75	0.24	-0.05	-0.19	150.	150.	150.	0.	0.	0.

Fig. 2. Preliminary SOLSTOR Results for Phoenix.

These results show that a FESS (with the costs assumed) is not viable in Phoenix in 1986, although PV-only systems are attractive. The array size was limited to 150 m^2, which completely covers the residence roof.

Figure 3 presents SOLSTOR results for New York. Although less insolation is available at New York, the high electricity rates generally yield more cost effective, larger systems when compared to Phoenix. FESSs are used in some combinations of time-of-day and sellback ratios.

		Life Cycle Cost Ratio			Array Size (m^2)			FESS Size (kWh)		
		1:1	3:1	6:1	1:1	3:1	6:1	1:1	3:1	6:1
Sellback Ratio	0.0	0.85	0.77	0.71	50.	55.	76.	0.	0.	11.
	0.25	0.81	0.65	0.58	120.	150.	150.	0.	0.	0.
	0.50	0.62	0.40	0.30	150.	150.	150.	0.	0.	0.
	0.75	0.42	0.15	0.00	150.	150.	150.	0.	0.	24.

3% Electricity Escalation

		Life Cycle Cost Ratio			Array Size (m^2)			FESS Size (kWh)		
		1:1	3:1	6:1	1:1	3:1	6:1	1:1	3:1	6:1
Sellback Ratio	0.00	0.71	0.65	0.58	138.	112.	103.	29.	20.	14.
	0.25	0.67	0.52	0.41	150.	150.	150.	0.	0.	11.
	0.50	0.48	0.27	0.13	150.	150.	150.	0.	0.	16.
	0.75	0.28	0.01	-0.23	150.	150.	150.	0.	0.	43.

6% Electricity Escalation

Fig. 3. Preliminary SOLSTOR Results for New York

Off peak charging is evident when FESSs are used at 6:1 time-of-day ratio, but not at lower ratios.

To portray the relative amounts of energy flows in various paths, Fig. 4 is presented. It represents a case (0.25 sellback, 6:1 time-of-day ratio) that utilizes all possible modes of operation.

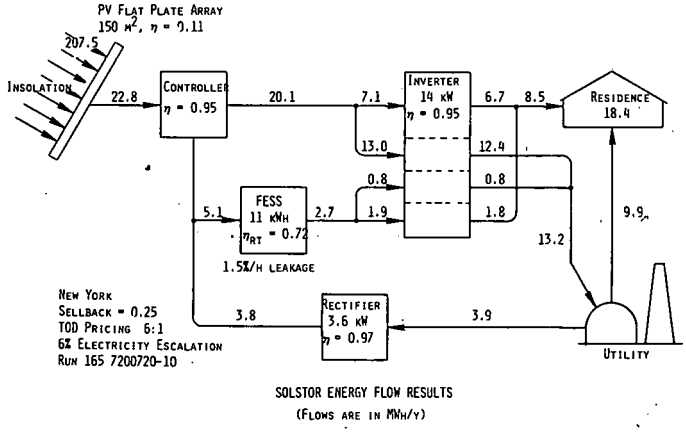

Fig. 4 SOLSTOR Energy Flow Results

By assuming that all energy used by the load or sold back during peak pricing displaces electricity generated with oil, and that all energy purchased off peak is generated by base plants (from coal or nuclear), the system shown in Fig. 4 displaces 25.5 barrels of oil each year. This number, although small when compared to US daily oil imports, is significant in relation to the gasoline consumed by the average household.

PRELIMINARY OBSERVATIONS

When Brobeck FESS production costs are used as prices, reasonable economic and utility pricing assumptions do not favor large scale penetration of FESS systems in 1986. Additional locations and cost/performance data from Garrett-AiResearch will be included in future analyses; these could affect FESS viability. Also, a comparison with competitive storage schemes (batteries) is planned before a final recommendation is forthcoming from Sandia on future FESS development. This work will be completed in September, 1979.

SUMMARY

The Solar Mechanical Energy Storage Program at Sandia is drawing to a close. All Sandia contractors will complete their work this fiscal year; Sandia will assess their results and the results of in-house analysis and provide recommendations to Lawrence Livermore Laboratory on future program activities. Specific recommendations will be made (in September 1979) on flywheels, compressed air and low head underground pumped hydro storage. Preliminary indications do not favor compressed air or flywheel systems; more work is probably justified on pumped hydro.

REFERENCES

1. Henry M. Dodd, et al., in Robert Randolph, ed., "An Assessment of Mechanical Energy Storage for Solar Systems," 12th Intersociety Energy Conversion Engineering Conference Proceedings, Vol. 2 (Washington, DC: American Nuclear Society, 1977), pp. 1174.

2. B. C. Caskey, "Solar Mechanical Energy Storage Project," Proceedings of the 1978 Mechanical and Magnetic Energy Storage Contractors' Review Meeting, Luray, Virginia, October 24-26, 1978, CONF-781046.

3. B. C. Caskey and H. E. Schildknecht, "FY79 Annual Operating Plan, Solar Mechanical Energy Storage Project," November 1978, SAND78-2130.

4. Bill C. Caskey and Harold E. Schildknecht, "Mechanical Energy Storage for Photovoltaic/Wind Project Technical Progress Report as of March 31, 1979," May 1979, SAND79-0874.

THIS PAGE

WAS INTENTIONALLY

LEFT BLANK

PROJECT SUMMARY

Project Title:	Conceptual Design of a Flywheel Energy Storage System
Principal Investigator:	F. C. Younger
Organization:	William M. Brobeck & Associates 1235 Tenth Street Berkeley, California 94710 (415) 524-8664
Project Goals:	The development of a conceptual design for a flywheel energy storage system suitable for on-site interfacing with small scale solar energy sources. The basic design objective is to provide a generous margin of safety and above average reliability and efficiency at the lowest practical cost.
Project Status:	A basic concept for a flywheel energy storage system to interface with solar energy sources has been studied. This concept utilizes a constant voltage motor/generator directly connected to a flywheel rotor. The field current of the motor is controlled to maintain the voltage level at the optimum operating voltage of the array of photovoltaic cells. When a surplus of electrical energy from the solar source occurs, the voltage of the array tends to rise above the set voltage of the motor/generator, and surplus power drives the motor to accelerate the flywheel. When a deficiency in solar energy occurs, the voltage of the array tends to drop below the set voltage, and power is drawn from the flywheel via the generator. A variety of motor types and rotor types have been studied to arrive at a conceptual design to meet the program objectives. A fiber-composite rotor driving a separately-excited dc motor appears as the most economical way to satisfy the basic requirements. Design details have been examined to confirm the dynamic stability of the rotor suspension system and to determine the energy losses and system efficiency. Optimization studies, design layouts, detailed specifications, and cost estimates have been made. A final report is being prepared.
Contract Number:	07-3663
Contract Period:	July 1978 - August 1979
Funding Level:	$139,053
Funding Source:	Sandia Laboratories

FLYWHEEL ENERGY STORAGE SYSTEM CONCEPT FOR A RESIDENTIAL PHOTOVOLTAIC SUPPLY

Francis C. Younger
William M. Brobeck & Associates
1235 Tenth Street
Berkeley, California 94710

ABSTRACT

A conceptual design of a flywheel energy storage system suitable for on-site interfacing with small scale solar energy sources has been developed. The basic design objective was to provide a generous margin of safety and above average reliability and efficiency at the lowest practical cost. This paper describes the basic design concept and the general approach to the conceptual design of the energy storage system. The basic concept to interface with solar energy sources utilizes a constant voltage motor/generator directly coupled to a flywheel rotor. The voltage level of the motor is maintained at the optimum operating voltage of the array of photovoltaic cells and permits peak power tracking. Power is drawn from the flywheel-driven generator when the voltage output of the array drops below its optimum value and power is delivered to the flywheel via the generator (then operating as a motor) when the voltage rises above the optimum value. A variety of motor types and flywheel rotor types has been studied to arrive at a conceptual design to meet the program objectives. A fiber-composite rotor driving a separately-excited motor satisfies the basic requirements. To obtain acceptable efficiency and low rundown losses, the flywheel operates in a vacuum and has a combination of magnetic thrust support and ball bearings to reduce bearing friction in an economical fashion. The need for rotary vacuum seal is eliminated by the use of a hermetically-sealed magnetic power coupling.

INTRODUCTION

The Flywheel Energy Storage System (FESS) is intended to enhance the value and utility of small solar power generating plants. The timely development of economical energy storage concepts is crucial in many solar power applications. The variable nature of solar energy severely limits its applications if some practical storage system is not made available. Batteries, pumped-hydro, compressed air, thermal and mechanical energy storage all offer the potential for suitable systems applications. Economic factors may favor one system in a particular application and yet another in a different application depending upon their performance and cost characteristics. However, at present accurate cost and performance characteristics do not exist for emerging technologies. New designs with generous margins of safety have not yet been demonstrated for mechanical energy storage systems. A concept which could lead toward a practical demonstration is presented.

This paper describes the effort for the development of a conceptual design for a FESS suitable for on-site interfacing with small scale solar energy sources. The new design has as objectives a generous margin of safety, high reliability and efficiency obtained at the lowest practical cost. The design is for a stationary application, in which no cost premiums are allowed for minimizing size and weight. The basic design

objective is a system which can be economically manufactured in existing industrial facilities using conventional production methods.

Attainment of the highest practical charge/discharge efficiency is a high priority goal. This requires very careful attention to design details, as well as the selection of the most appropriate engineering concept.

BACKGROUND

The FESS for use with a small residential solar energy source was studied and conceptually designed under contract to Sandia Laboratories, Albuquerque, New Mexico, as part of a program supported by the U. S. Department of Energy, Assistant Secretary for Energy Technology, Division of Energy Storage Systems. Early work on this program, its goals and objectives were described at a previous review meeting.[1] The goals have not significantly changed since that review meeting, but the conceptual design has evolved during the course of the study as ways of improving the design to give greater reliability, lower losses, and lower costs were uncovered.

The program objective is the design of storage units suitable for use with small to intermediate scale solar sources. The nominal energy storage capacity is in the range of 5 kWh to 100 kWh; the specific requirements are for the detailed design of a 10 kWh storage system and for a detailed cost estimate for a 50-kWh system. The required power rating of the 10-kWh system is 5 kW. These units are to have an electrical interface for 60 Hz/220 Volts single-phase power. The control system must maintain the desired frequency and voltage over the full rotor operating speed range.

The round-trip efficiency for charging and discharging must exceed 70 percent. This requires that the one-way efficiency exceed 84 percent. The rate of loss of stored energy due to friction and windage must not exceed 5 percent per hour.

The design must have a generous factor of safety and high reliability. It must be designed for a life expectancy of at least twenty years during which a minimum of 10,000 charge/discharge cycles may be encountered. These cycles cover the full speed range of the design. Allowance may have to be made for any overspeed tests which might occasionally be performed.

PROJECT DESCRIPTION

The project is divided into four main tasks covering (1) the basic system concept; (2) optimization; (3) design of a 10-kWh unit; and (4) estimate for a 50-kWh unit.

The basic system concept effort and subsystem options consist of an evaluation of workable engineering concepts and the narrowing down of choices to the best subsystem options. Subsystem options include flywheel configuration, materials, flywheel housing and containment, seals, type of motor/generator, suspension system, mounting, controls, auxiliaries, and instrumentation. Problems of safety, efficiency, losses and parasitic loads, manufacturability, maintenance, and economics are considered.

Various flywheel configurations and material combinations have been considered for energy storage systems. It has been shown that high energy density is potentially achievable with materials possessing a high strength-to-weight ratio. In many engineering applications light weight is very important and a premium may be paid for a material with a high strength-to-weight ratio. However, for a utility application, additional expense merely to save weight is unreasonable. The appropriate design criterion is maximum energy at minimum cost.

CONCEPTUAL DESIGN

The FESS concept integrated with a residential photovoltaic (PV) supply is shown in Fig. 1. The FESS acts as an energy buffer between the direct current PV supply and the alternating current utility power source to permit an optimum utilization of the available solar energy. The PV supply represents a variable voltage dc source with its voltage dependent upon its temperature and current and upon the solar insolation. With increasing insolation, the available PV energy will rise and may exceed the load demand of the home; excess power is then diverted for storage in the flywheel shown in the pit below the garage floor. This stored energy is subsequently recovered to supply electrical energy to the home when the available solar energy is inadequate to satisfy the demand.

In addition to providing an energy storage capacity via the flywheel, the FESS provides the necessary energy conversions to match the requirements of the various portions of the integrated system. These include the conversions from mechanical (kinetic) energy to electrical energy, from dc to ac, and the tracking of optimum dc voltages. Figure 2 shows the general flow of power and main system elements. The generator coupled to the flywheel provides the electrical to mechanical energy conversion using adjustable field current to provide control of the power flow. The generator converts mechanical energy into electrical energy to discharge the flywheel when there is a demand for its energy or it acts as a motor to reverse the energy flow when there is a surplus of solar energy.

The link shown between the solar unit, the generator, and the power conditioner is a dc link set at the voltage which optimizes the power output of the PV cells. This optimum value of voltage depends upon the temperature of the PV cells and the solar insolation. The voltage is controlled by the field excitation of the generator and the flywheel speed. As the flywheel speed increases, the field current is reduced to maintain the desired voltage. The power conditioner provides the required dc to ac conversion.

The flywheel/generator system is shown in Fig. 3 and 4. The main elements are the flywheel, motor/generator, vacuum vessel and the flywheel suspension system. The suspension system consists of support bearings to carry the flywheel weight and dynamic loads and damper assemblies to prevent whirl instabilities.

TEN-KWH FLYWHEEL

The flywheel as shown in Fig. 5 is a biannulate rim supported by tension-balanced polar-catenary spokes which bridge the zone between the hub and the rim. This flywheel is similar to the one described at a previous review meeting.[2] For the 10-kWh unit, the biannulate rim, consisting of a fairly thick portion filament wound with E-glass/epoxy and a thin circumferential overwrap of Kevlar 49/epoxy, has an outside diameter of 1.267 m and an inside diameter of 1.038 m. The glass/Kevlar interface diameter is 1.249 m. The rim axial length is 333 mm. The relatively large amount of the inexpensive E-glass keeps the cost down and the high modulus Kevlar 49 overwrap suppresses the radial tension stresses which otherwise would occur in a thick rim. This design permits a high volumetric energy density as a large percent of the swept volume of the flywheel is occupied by highly stressed fiber-composite material. The rim weight is 278 kg and the total weight is 411 kg. For 10-kWh of available energy, the peak stored energy is 13.5 kWh at 9800 rpm, and the energy density is 32.8 Wh/kg.

A 584-mm diameter hub reduces the radial space between the hub and rim to allow the Kevlar 29 spokes to be short enough to provide adequate rigidity to maintain hub/rim concentricity.

The large hub is strengthened by a pre-stressed Kevlar 49 overwrap which partially resists the centrifugal loading on the aluminum portion. The radial stresses in the hub web are minimized by its conical shape.

A high margin of safety for the rotor is provided by designing to a low stress level. The stresses in the fiber-composite biannulate rim are shown in Fig. 6. The Kevlar 49 overwrap has the higher stress primarily because it has a higher modulus of elasticity.

DRIVE MOTOR

The motor generator for converting electrical energy to flywheel kinetic energy is shown in Fig. 7. The motor is a separately-excited three-phase alternator connected to run as a brushless dc motor by using electronic commutation and a shaft position sensor. The design is based on reasonable modifications to an existing 9 kVA aircraft alternator. The unit has two slip rings for field excitation current. An additional slip ring is shown for control of excitation current for the magnet coils for a synchronous magnetic coupling used to transmit power across a non-magnetic vacuum barrier. This magnetic coupling and vacuum barrier are also shown in Fig. 7. The outer portion of the coupling is driven by the motor and holds the magnet coil windings. The inner portion which is attached to the flywheel via a 12.7-mm diameter quill shaft is driven synchronously as a salient pole machine running on reluctance torque. The gap between the inner and outer portion is occupied by a vacuum barrier shown as a "vacuum interface can."

SUSPENSION SYSTEM

The suspension system consists of a combination of precision ball bearings and a magnetic thrust bearing as shown in Fig. 8 and 9. The magnetic thrust bearing support 90 percent of the rotor weight and is shown as two parts in Fig. 8. The upper part labeled "wound lifting mag. (stationary)" is the portion that is electrically energized to attract the lower part labeled "lifting mag. (rotating)." Both parts are silicon iron with an outside diameter of 273 mm and the gap between them is a nearly uniform .76 mm with very little runout. The geometry of the combined bearing system is designed to insure that the gap between these two parts remain constant even if the rotor were experiencing a small precession with nutation.

A small amount of precessional motion is permitted by the flexibility of the suspension system. The upper and lower bearing supports are mounted in rubber pads which permit a limited amount of motion and which provide damping to prevent dynamic instability. The system operates above the critical speed and asynchronous whirl modes can be excited unless adequate damping is provided.

CONTROL SYSTEM

The FESS control system maintains the optimum flow of power from the PV supply by diverting excess power from the PV supply to the flywheel when the available solar power exceed the demand of home and by taking power from the flywheel when the demand is greater than that available from the PV supply. For a given insolation and temperature of the PV cells, there is an optimum dc voltage where the maximum power is drawn from the PV supply. If the load demand increases above this maximum power output, it would cause the voltage output of the PV supply to drop excessively. This voltage drop will be prevented and power diverted from the flywheel if the output voltage of the generator is set at the optimum value. Similarly if the load demand decreases, the voltage of the PV supply tends to rise as the current falls. This rise in voltage and loss of current will also be prevented by having the output voltage set at the optimum value because as the PV output voltage rises, the generator becomes a motor and diverts power to the flywheel.

The FESS control system continuously monitors the dc bus voltage and sets it to a value which maximizes the power output of the PV supply. The set point voltage is produced through an integrated circuit pulse width modulator that regulates the field current of the generator. A schematic diagram for the control system is shown in Fig. 10.

The circuit for the electronic commutation of the three-phase motor is also shown. A three-phase waveform generator develops the control signals for the six power transistors which drive the motor. The developed signal is a periodic three-phase square wave. The frequency of operation is a direct function of the rotor speed as the clock signal is generated from the rotor position sensor. A unique feature is that the line voltage is monitored to prevent common devices from turning on simultaneously. This allows the conduction angle of the waveform to approach a maximum of 120^{0}.

The power transistor circuit for driving the motor is shown in Fig. 11. The drive electronics consists of NPN Darlington Transistors and diodes for the drive and generation modes. The transistors that are referenced to ground are driven directly through current amplifiers while the transistors that are referenced to the positive bus are driven from optical-isolators through current amplifiers. The optical-isolators are referenced to a voltage that is 5 Volts below the positive bus. This voltage is developed through an integrated circuit chopping regulator.

EFFICIENCY AND OPTIMIZATION

Rundown losses at 10,000 rpm are listed in Table 1. Total losses are 150 watts which correspond to 1.5 percent per hour. The pie graph in Fig. 12 illustrates the relative magnitude of the rundown losses.

TABLE 1. Rundown Losses at 10,000 rpm

Component	Losses in Watts
Main bearings	36
Bottom damper bearings	2
Magnetic coupling bearings	23
Magnetic lift excitation	30
Magnetic lift hysteresis	4
Magnetic lift eddy current	20
Oil lube pump	2
Windage	33
Total	150

Rundown losses vary with speed and will decrease as the speed is reduced. A major factor in rundown losses is windage. In order to minimize this the enclosure is evacuated. For the windage loss in Table 1, the vacuum level is 2×10^{-7} atmospheres.

Power conversion efficiency is a function of power level and speed. At the maximum power level of 5 kW, the average efficiency over the operating range is 71 percent. This value drops with lower power level until it reaches zero at zero power.

COST ESTIMATE

TEN-KWH SYSTEM

Layout drawings, specifications and cost estimates for a prototype and for serial production quantities of the 10 kWh, 5 kW flywheel energy storage system have been prepared based upon the developed concepts. Serial production costs are based upon estimates of costs for fabricating components to designs and methods of fabrication typical of mass-production techniques.

In the quantity-production costs estimates the tooling costs has not been estimated and, in general, the material and production cost has been based upon the assumption of production quantities of 100,000 sets of parts where die costs are of the order of a few cents per part. Then for each factor of ten reduction in quantity an increase of 17.6 percent in cost was assumed. This method of estimation is valid for three to four decades in quantity reduction but becomes unrealistic for small quantities where alternate methods of fabrication become dominant.

Table 2 shows the estimated 10 kWh total system cost for various quantities of production. In quantities of 100,000 units per year, the total production cost is estimated to be $5057 or $505 per usable kilowatt-hour stored.

TABLE 2. Estimated 10 kWh Total System Cost

Quantity	Mechanical Parts	Controller Peak Power Tracker	Inverter	Total
10^2	7085	536	795	8416
10^3	5845	478	276[a]	6599
10^4	4955	441	235	5631
10^5	4445	412	200	5057

[a]Represents the change from a commercially purchased unit to an in-house design.

FIFTY-KWH SYSTEM

In estimating the cost of the 50-kWh, 10 kW FESS, heavy dependence was placed upon the methods and unit costs developed for the 10-kWh storage system. Because of the greater weight of materials in the larger unit, break points in material cost occur for a small number of units.

The rotor assembly proper was scaled by a factor of 50/10 for all components in weight and a factor of $\sqrt[3]{5}$ in all dimensions.

Table 3 gives the estimated 50 kWh total system cost including the mechanical assembly, the electrical controller assembly and the synchronous inverter. In production quantities of 100,000 units per year, the estimated total system cost is $18,561. This amounts to a $371 initial capital cost per usable kilowatt-hour stored for the 20-year lifetime unit.

TABLE 3. Estimated 50 kWh Total System Cost

Quantity	Mechanical	Controller	Inverter	Total
10^2	25,860	706	1589	28,155
10^3	22,340	623	485[a]	23,448
10^4	19,560	564	411	20,535
10^5	17,695	516	350	18,561

[a]Represents the change from a commercially purchased unit to an in-house design.

CONCLUSIONS AND RECOMMENDATIONS

This design study indicates that a reliable, efficiency flywheel energy storage system can be manufactured at a reasonable cost.

It is recommended that a prototype model be produced to demonstrate the viability of the concept.

REFERENCES

1. F. C. Younger, "Conceptual Design of a Flywheel Energy Storage System," Proceedings of the 1978 Mechanical and Magnetic Energy Storage Contractors' Review Meeting, Luray, Virginia, October 1978.

2. F. C. Younger, "A Composite Flywheel for Vehicle Use," Proceedings of the 1978 Mechanical and Magnetic Energy Storage Contractors' Review Meeting, Luray, Virginia, October 1978.

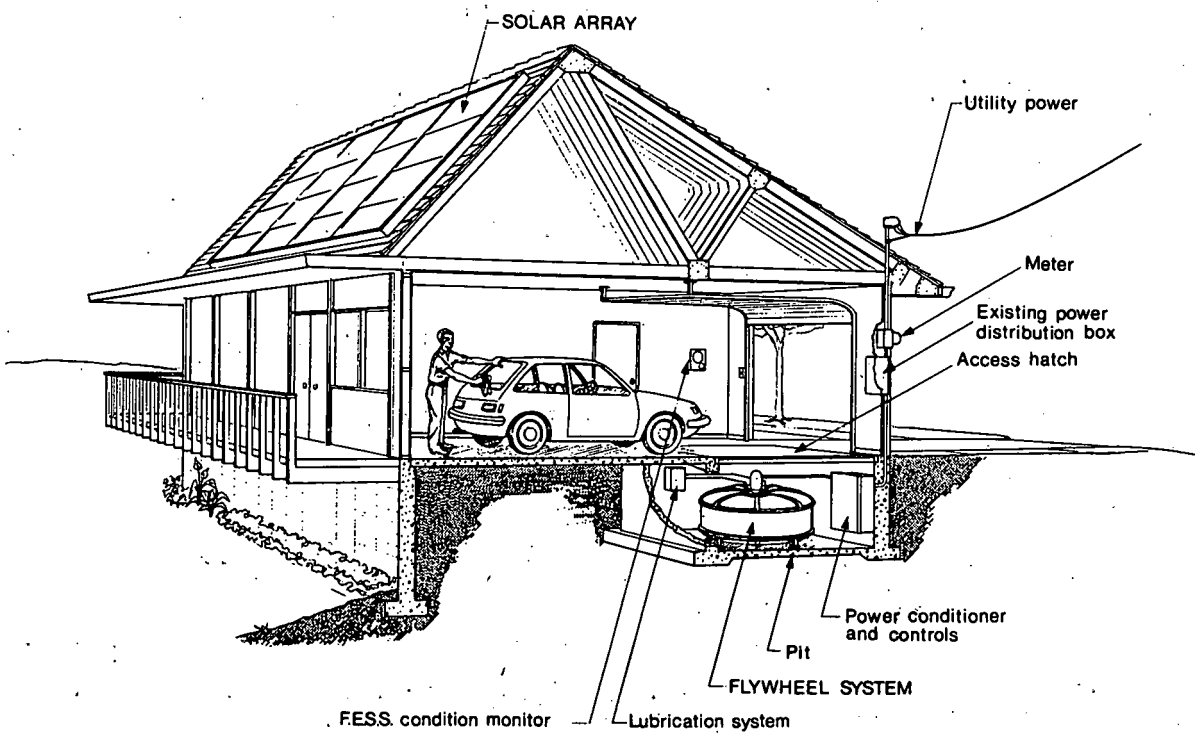

Fig. 1. Ten-kWh Flywheel Energy Storage System for Photovoltaic Supply

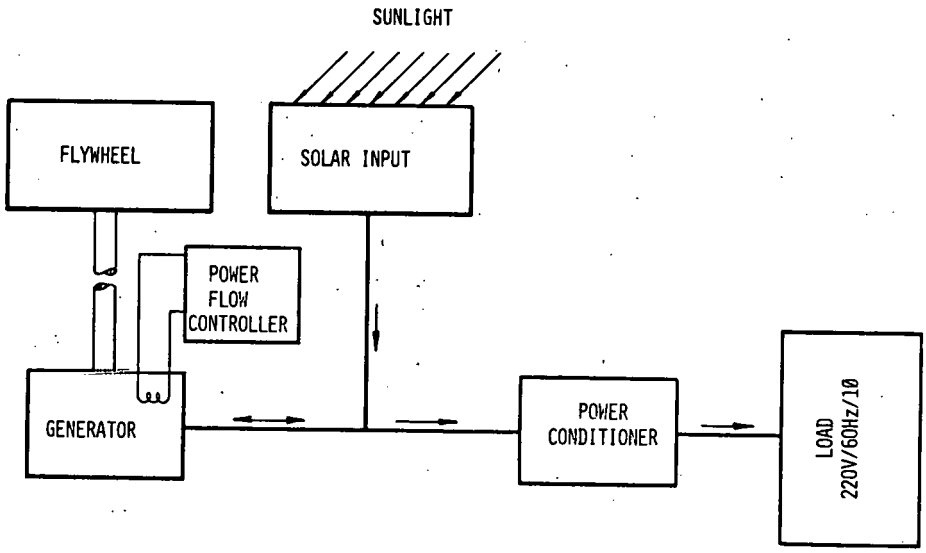

Fig. 2. Power Flow Diagram FESS for Photovoltaic Supply

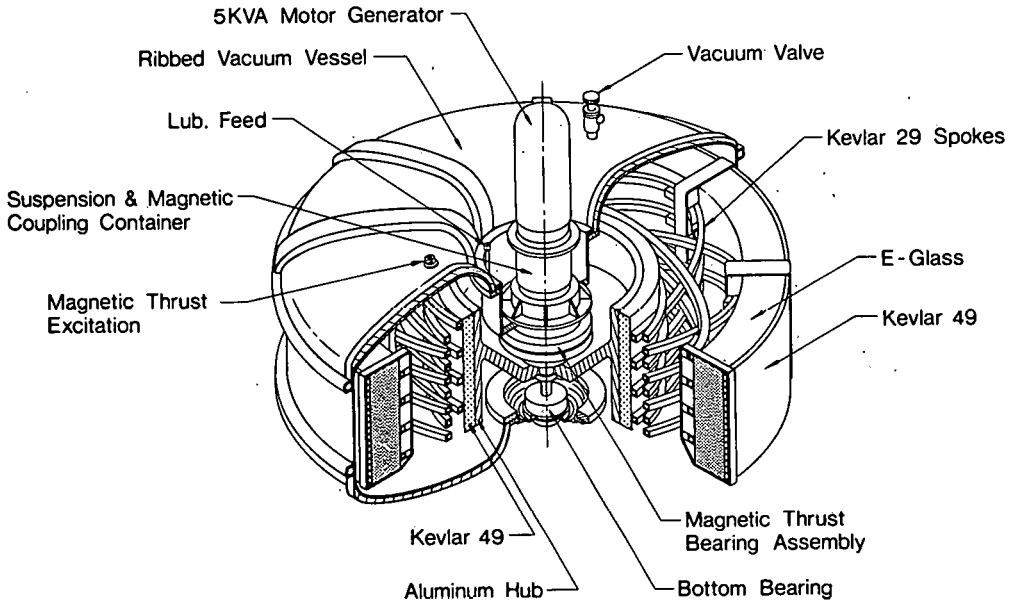

Fig. 3. Ten-kWh System Concept

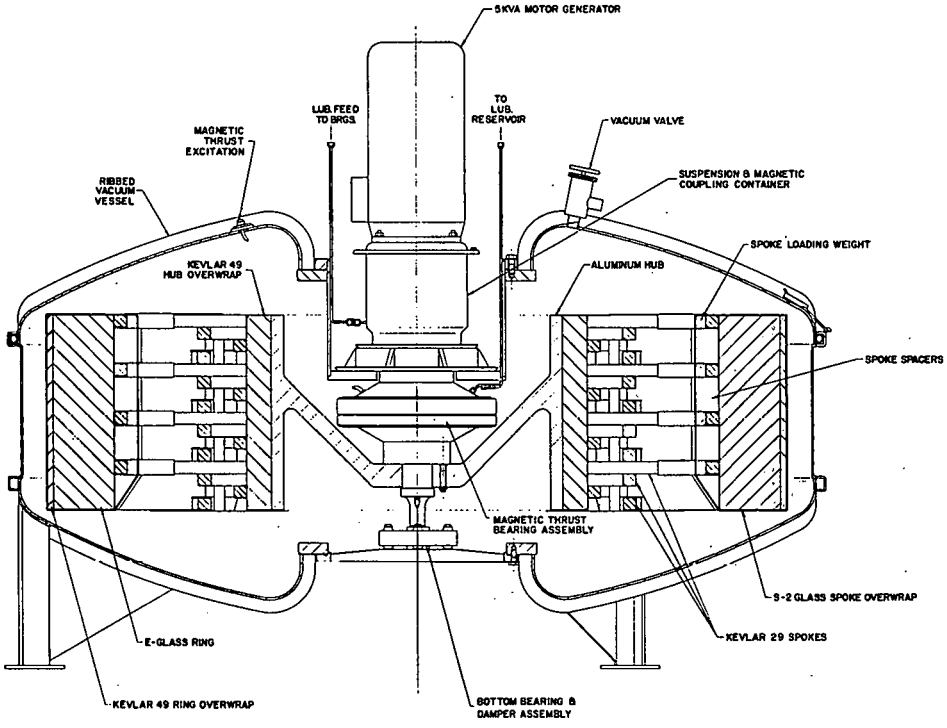

Fig. 4. Ten-kWh Flywheel Assembly

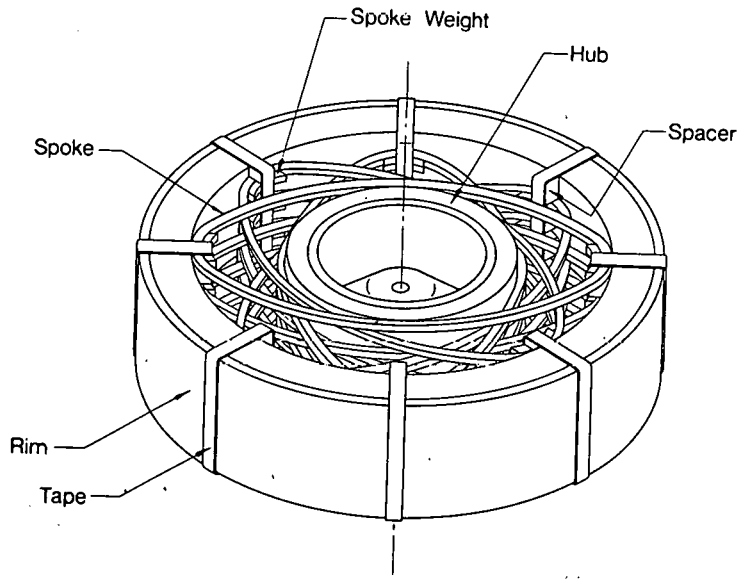

Fig. 5. Ten-kWh Flywheel

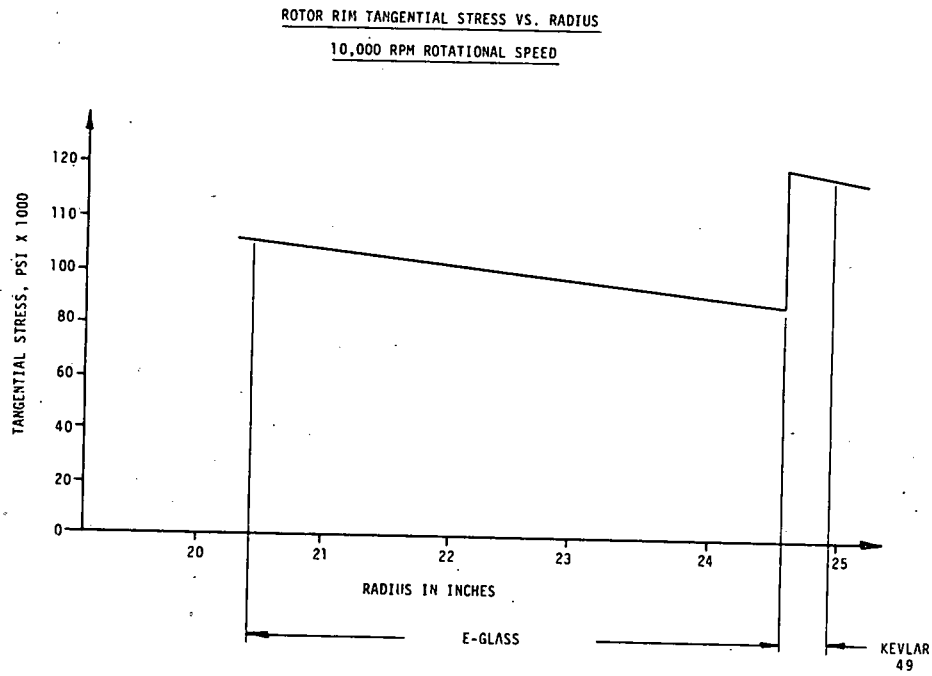

Fig. 6. Stresses in Biannulate Rim of Flywheel

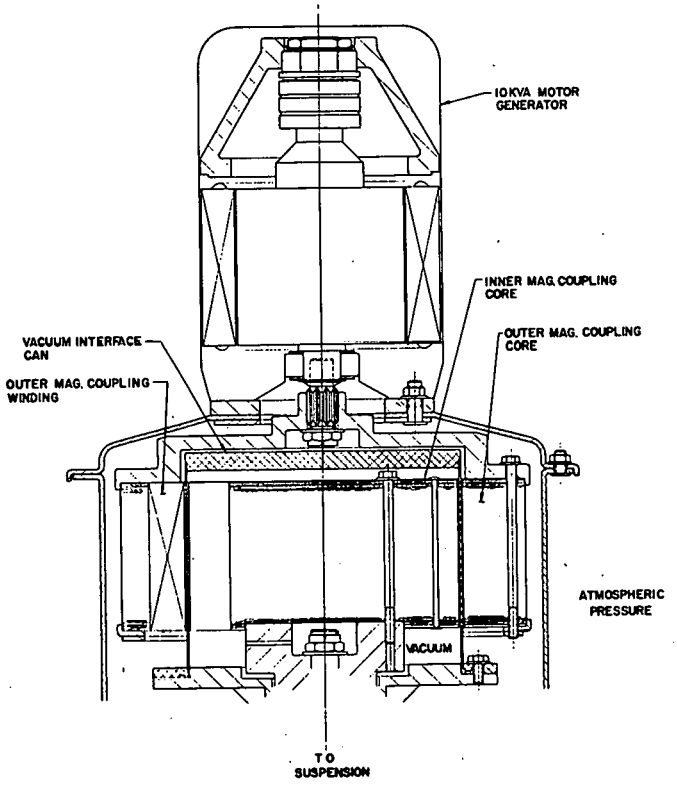

Fig. 7. Motor Generator for FESS

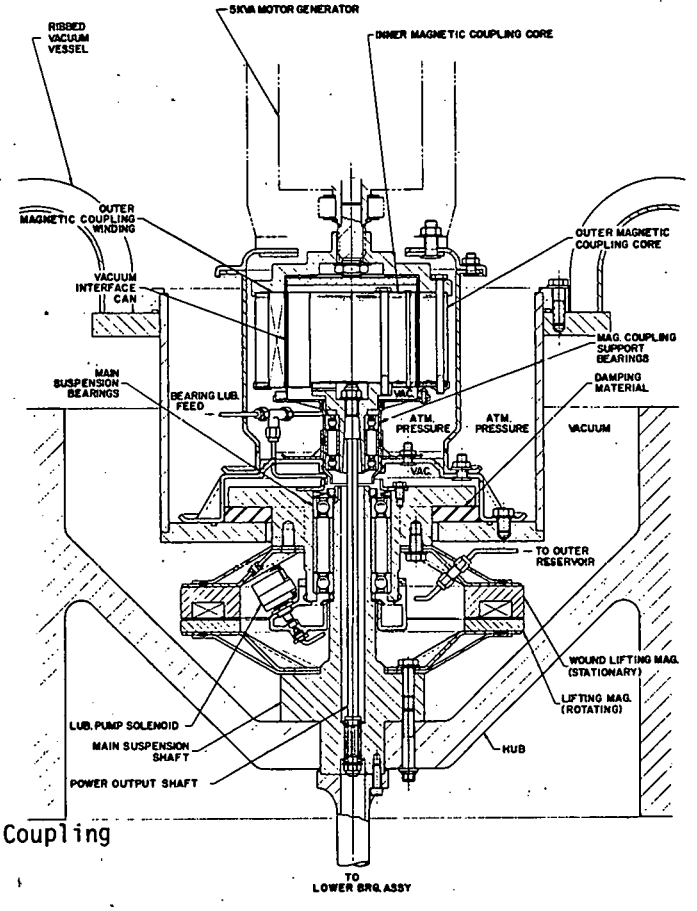

Fig. 8. Upper Suspension and Magnetic Coupling Assembly

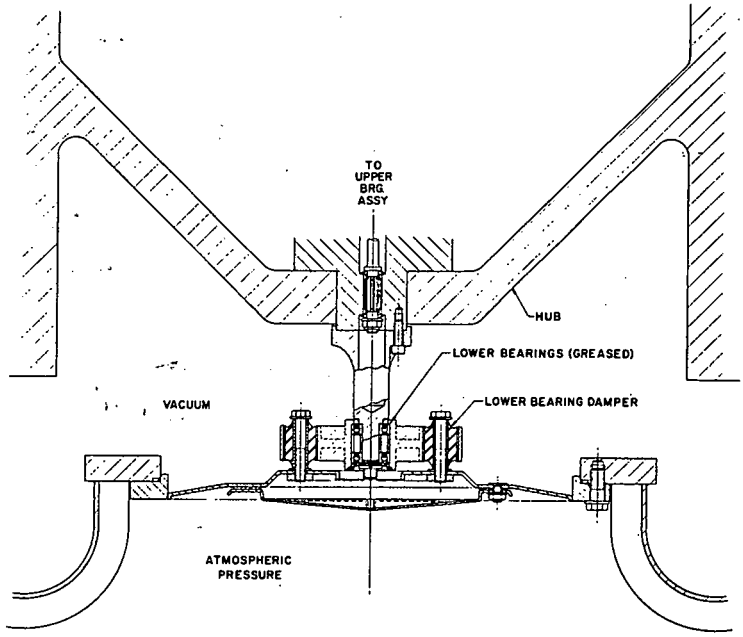

Fig. 9. Lower Suspension Assembly

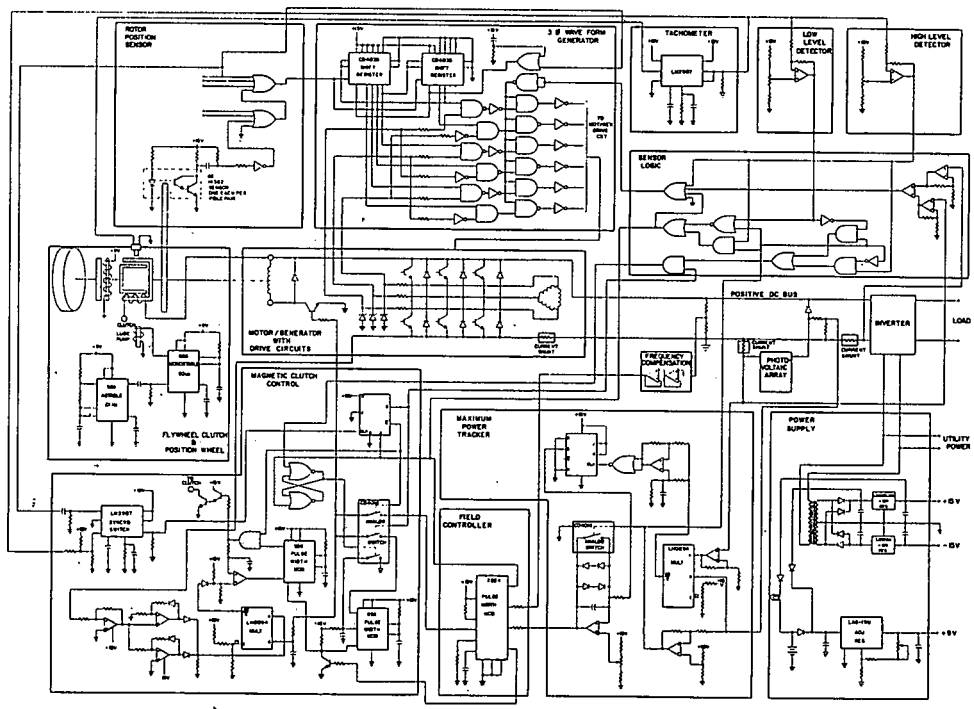

Fig. 10. FESS Control Schematic

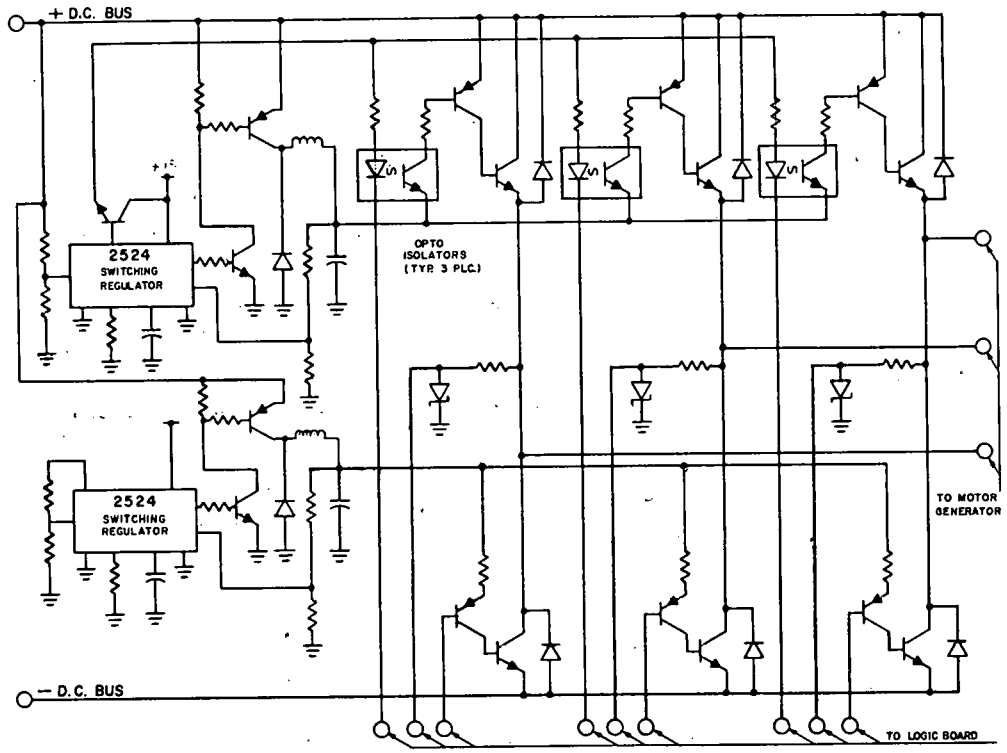

Fig. 11. Power Transistor Circuits

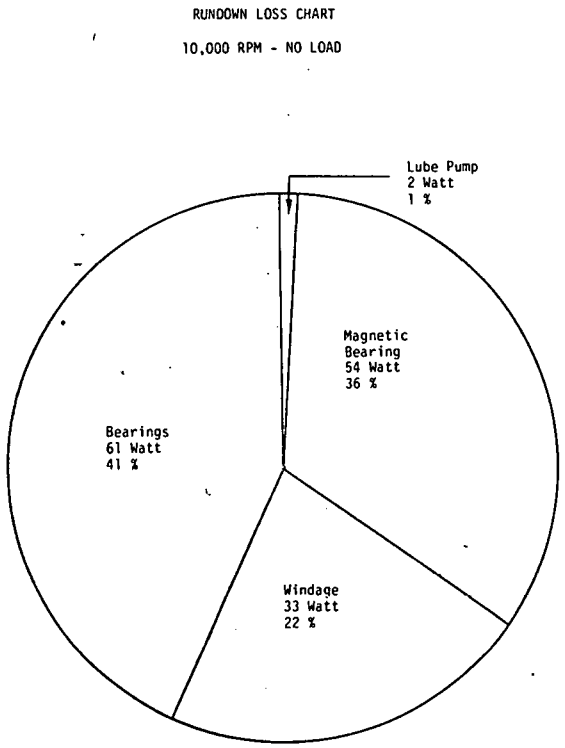

Fig. 12. Rundown Loss Chart

PROJECT SUMMARY

Project Title:	Residential Flywheel with Wind Turbine Supply
Principal Investigator:	Theodore W. Place
Organization:	AiResearch Manufacturing Company of California 2525 W. 190th St Torrance, California 90509
Project Goals:	To identify a cost-effective mechanical storage device, which, when used with a wind turbine, would replace or supplement utility power.
Project Status:	A system composed of a gearbox, variable transmission, a generator, and a hermetically sealed flywheel has been selected. A tradeoff of components resulted in the selection of a synchronous generator; variable belt transmission; and a hermetically sealed, magnetically coupled, magnetically levitated, E-glass composite rotor assembly. The analysis defined the geometry, the safety, and the reliability of the design of a 10 kw-hr system. The 10 kw-hr design was defined in a layout drawing, and then extrapolated to a 50 kw-hr design. Cost estimates of both the 10 kw-hr and the 50 kw-hr systems are complete. A final report has been submitted for approval, thus completing the program.
Contract Number:	07-9093
Contract Period:	FY '78
Funding Level:	$135K
Funding Source:	U.S. Department of Energy, Division of Energy Storage System

RESIDENTIAL FLYWHEEL WITH WIND TURBINE SUPPLY

Theodore W. Place
AiResearch Manufacturing Company of California
A Division of The Garrett Corporation
Torrance, California

ABSTRACT

A flywheel system that stores energy from a wind turbine source and converts the energy to a 60-Hz, 220-v output for residential use is described. The typical residence has a 1500-sq ft floor area, with a maximum power level of 5 kw. The flywheel system was defined in a study to determine the cost benefits of storing wind energy in a flywheel and using it on a demand basis. The systems and the flywheel rotor materials that offer the greatest promise in reducing initial costs were examined. This paper describes the progress to date on this program and the work planned to complete the study.

INTRODUCTION

A Department of Energy contract was issued through Sandia Laboratories to the AiResearch Manufacturing Company in August 1978 for a study to define a cost-effective mechanical energy storage system applicable to wind turbines. The system study has been completed and the mechanical energy system has been defined. The current effort entails completing a design layout and performing life-cycle cost analyses.

In configurations such as American multiblade, high-speed two-blade, or Darrieus vertical blade, the wind turbine converts wind to mechanical energy. This energy is usually more than can be utilized at one time, and is sporadic because wind varies from day to day. The flywheel was selected as a device that could capture the excess energy being generated and store the energy for a windless day (1).*

The objective of the study was to define a system that would take the output from a wind turbine and convert it to household electrical power, store the excess energy, and regulate the wind turbine speed or the electrical frequency. The unit had to be cost-effective and competitive with battery and electrical grid system storage. The study of the residential flywheel system has been completed and the baseline design selection has been made. The baseline system, the reasons for selecting certain components, and system performance are described briefly in this paper.

PROJECT GOALS

One of the project goals was to identify a cost-effective mechanical storage device that would be safe and reliable for 20 years. The study constraints included a 5-kw output generator and a 10-kwh flywheel system; a mechanical storage system utilizing current, rather than future technology; and conventional manufacturing and processing methods. The study was undertaken to stimulate industry to produce and market a mechanical energy storage system that will produce a significant reduction in the use of utility power. Another goal was a low acquisition cost for the energy storage system that would produce a net savings in life-cycle costs.

SYSTEM DESCRIPTION

After evaluation of several candidate systems, the design illustrated in Figure 1 was selected because of its low acquisition cost. The mechanical energy storage system selected for a residential application consists of five major components--a generator system, a gearbox,

*Numbers in parentheses designate references at end of paper.

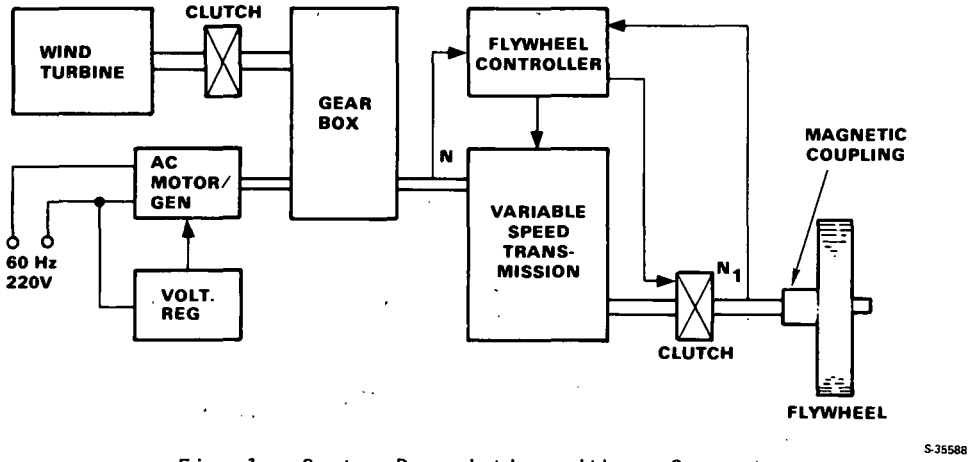

Fig. 1. System Description with ac Generator

a variable-speed belt transmission, a flywheel storage system, and a control system. In the system analysis, candidates for each of the above components were substituted into the performance and cost analysis to finalize the system.

The mechanical design of the system was constrained by the requirement that shaft power be supplied at a constant 125- or 175-rpm speed, depending on which test data were to be evaluated (2). The output of the system was defined by Sandia Laboratories as 5-kw, 60-Hz, 220-v electrical supply.

To evaluate system performance, two preselected test sites were used--one of high and one of low wind activity. The wind data in kilowatt hours were obtained for a typical week in each of the four seasons.

The electrical demand was calculated for an all-electric house with a floor area of 1500 sq ft as a model for the system. The electrical demand data were then correlated with the wind input data for the system.

COMPONENT DESCRIPTIONS

The selection of the components for the total system first emphasized low acquisition cost. Although system performance was secondary, a minimum input/output efficiency of 70 percent was required. In addition, the parasitic losses could not exceed 500 w at the 10 kw-hr storage level. The total unit had to be reliable and meet safety requirements.

FLYWHEEL

The flywheel rotor had to be defined in terms of shape, material, weight, and vacuum environment. The complete flywheel system includes bearings, coupling, and the structure housing the rotor. The variables considered in selecting the baseline flywheel system are discussed below.

Flywheel Material

The flywheel rim materials that were considered and the selected design are shown in Figure 2, which also indicates the relative costs to produce the complete rotor at a modest production rate of 10,000 per year. Material selection was based on the acquisition cost of the rotor; the lowest cost design was selected. The use of a composite material such as E-glass and epoxy also reduced the cost of the flywheel housing.

Flywheel Shape

The shapes of steel or isotropic material flywheels are limited to a solid disc, whereas a concentric ring design is used for the composite material flywheel. Figure 3 illustrates

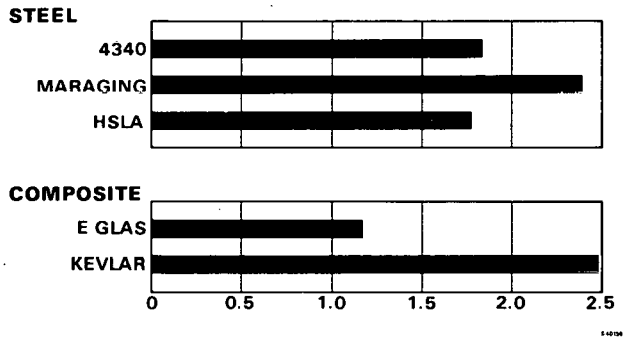

Fig. 2. Flywheel Rotor Manufacturing Cost

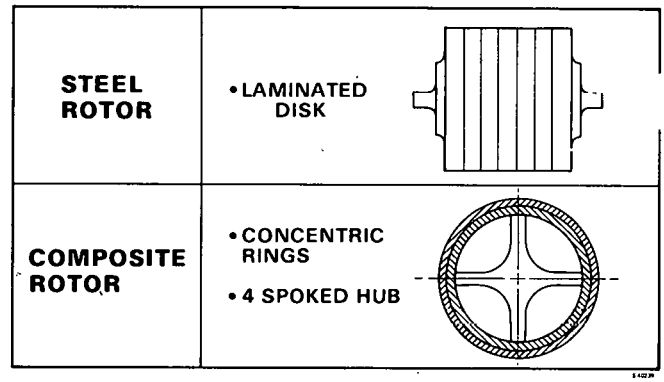

Fig. 3. Flywheel Rotor Candidate Shapes

the shape factor (K_s) that is used in calculating energy density (3). The second variable for consideration was the length-to-diameter ratio; the selected minimum diameter was 2.0 ft, and the selected maximum diameter was 6.0 ft.

Vacuum for Flywheel

The flywheel system windage losses will be insignificant if the cavity pressure is maintained between 1 and 10 microns. Figure 4 shows that the loss is insensitive to the length-to-diameter ratio. The thermal limit is listed on the 100-micron line. Pressures higher than 100 microns will start to deteriorate the outer fibers of the composite flywheel and eventually result in an unuseable flywheel.

Flywheel Sizing

Figure 5 shows a flywheel with an outside diameter of 60 in., a rim internal diameter of 51 in., and a wheel made up of four segments that was recommended as a result of this study. The aluminum center hub is made from aluminum sheet, stamped out, and brazed into a single hub. The rotor weight is 710 lb, and it operates at a speed of 7110 rpm.

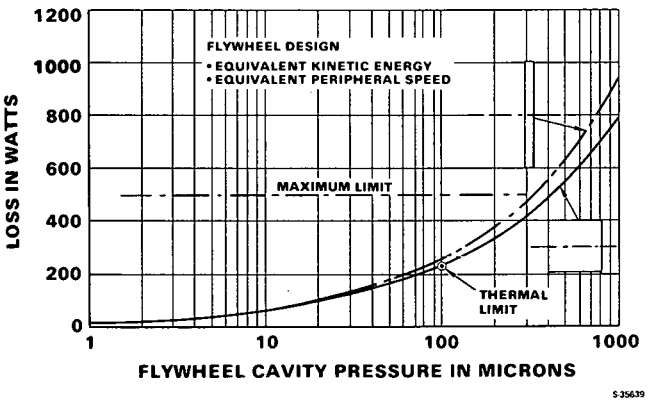

Fig. 4. Effect of Length/Diameter Ratio Versus Windage Losses

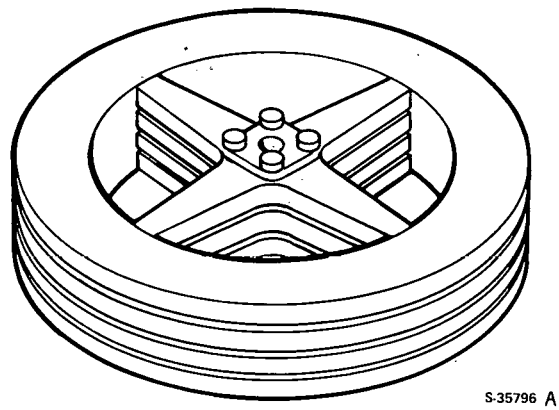

Fig. 5. Ten kw-hr Composite E-glass Flywheel

Flywheel Bearings

Ball, roller, magnetic, and hydrostatic bearings were evaluated for performance and cost. The magnetic bearings were selected because of their low parasitic losses, high reliability, and acceptable cost (4). Although the cost of the magnetic bearings was 1.5 times that of the roller bearings, this increase was considered acceptable because of the low dollar impact.

Flywheel Seals

In addition to a hermetically sealed, magnetically coupled unit, carbon and ferrofluid seals were considered. The magnetically coupled hermetic unit was selected because of its very low parasitic losses, high reliability, and acceptable cost impact.

Flywheel Structure

The flywheel containment housing had to be sealed and evacuated to provide the required environment for the flywheel. The containers considered in the cost evaluation were a hermetically sealed metal container, a metal and concrete container, and a metal container with earth embankment or pit. As a result of the analysis, the simple metal container was selected because it was the least expensive and would contain a composite flywheel failure. In addition, no other structure to dissipate torque reaction from a flywheel failure was required.

TRANSMISSION

The function of the transmission is to provide a variable speed input to the flywheel system to store or extract mechanical energy as a result of a speed change of the flywheel. The transmission was selected from among the candidates listed in Figure 6. Because the transmission is placed between the 1800-rpm gearbox and the flywheel and because the design horsepower is approximately 26 hp, it appeared that either the traction or the variable-pulley rubber belt would satisfy the design. The relative costs listed in Figure 6 show the variable-pulley rubber belt to be most attractive on a first-cost basis. The analysis showed that the belt drive with a simple shift satisfies the starting requirements of the flywheel, and meets the performance and cost requirements (see Figure 7).

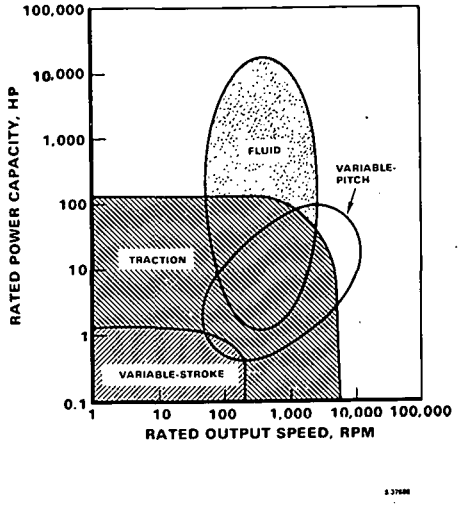

Fig. 6. Design Rationale for Selection of Transmission Options

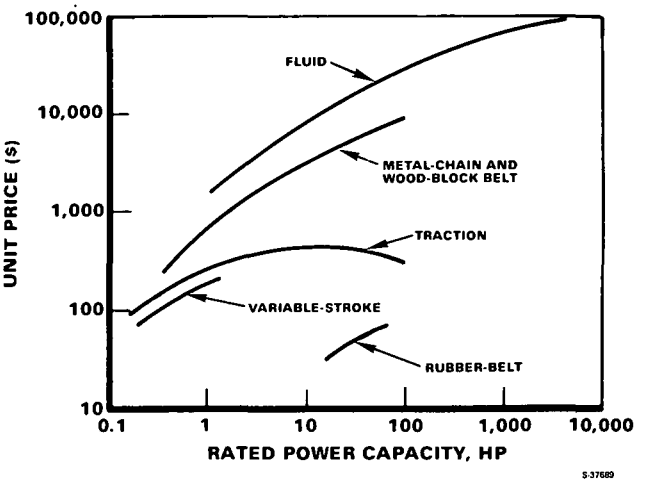

Fig. 7. Cost Rationale for Selection of Transmission Options

MOTOR/GENERATOR

The main function of the motor/generator (M/G) was to provide a nominal 220 rms (110-v, line-to-neutral, single-phase) at a nominal 60 Hz. In the motor mode, it can be used to start the wind turbine, using the utility as a power source.

The motor/generator also could be applied as a velocity governor for the wind turbine if it is referenced to the utility to maintain an accurate 60-Hz frequency. If it is not referenced to utility frequency, the flywheel and continuously variable transmission must be controlled to provide the required frequency. The frequency would then be accurate enough for all household energy loads, except synchronous clocks.

The three M/G types that are commercially available as well as technically acceptable are the (a) salient pole synchronous alternator; (b) squirrel cage induction alternator; and (c) separately excited dc generator.

The salient pole synchronous alternator is the most easily controlled of the three candidates. With slip rings to transfer dc field current to the rotor, voltage regulation can be readily accomplished. It cannot control sudden overloads because it will lose synchronism if pullout torque is exceeded. Amortisseur windings are required if it is to be used as a starting motor.

The squirrel cage induction alternator is capable of continuous, near-synchronous operation despite short-term overloads. However, its efficiency is not as high as that of the synchronous alternator unless it is controlled to a low-slip operation. In general, it is less stable than the synchronous alternator under variable loads and operates at a lower power factor.

The separately excited dc generator is readily voltage-regulated, reasonably efficient, capable of absorbing overloads, and capable of wide variations in speed under loaded conditions. However, it must be augmented with a solid-state inverter to provide the household 60-Hz power; thus the beneficial operating characteristics are offset by the high cost of the required inverter.

The salient pole synchronous alternator was selected as the best unit for the design.

SELECTED DESIGN

The selected design for the flywheel is shown in Figure 8. By mounting the flywheel vertically on a quill shaft, dynamic problems of the flywheel are eliminated. It is significant that the machining of the cover section is confined to the bearing area. The bottom section may be deep-drawn like a bathtub, with wide-open tolerances that would take advantage of controlling cost through minimum machining. The generator and belt drive is mounted in a vertical manner to take advantage of the vertical shaft from the wind turbine supply. Excluding the cost of the wind turbine, the system costs are estimated at $4050 for 10,000 units per year and $2885 for 100,000 units per year.

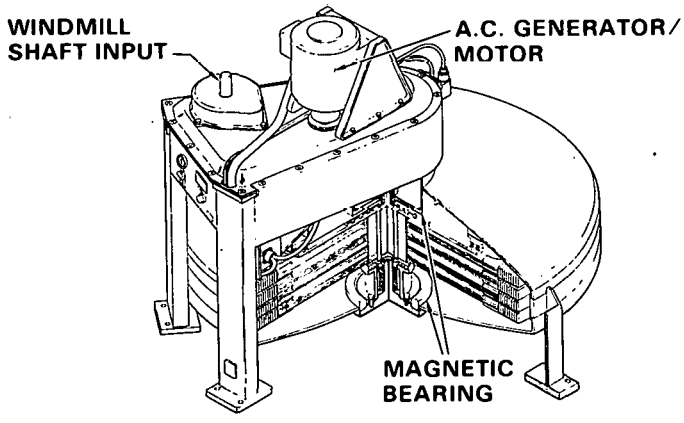

Fig. 8. Ten Kw-Hr Flywheel Energy Storage Unit

SYSTEM PERFORMANCE

System input/output efficiency is 76 percent; that is, 76 percent of the captured wind energy is delivered to the residence as electrical energy. The performance of this system was simulated in a computer, using the performance of the selected components. The wind data and electrical demand were input to the computer program. An example of the computer output using the Blue Hill, Massachusetts test site is as follows:

Season	Residential Energy Demand Supplied by Wind, percent
Spring	33.7
Summer	55.7
Autumn	51.0
Winter	58.0

EXTRAPOLATION OF 50 KW-HR UNIT

The 10 kw-hr unit could be easily converted to a 50 kw-hr unit by increasing the rotor length, and by increasing the rotor length and containment band from 8 to 40 in. No other changes in the flywheel storage module would be required. The generator would be increased from 5 to 10 kw as a study requirement. The transmission or variable-belt unit would be parallel to a differential gear unit that is coupled to the flywheel assembly. A cost analysis shows that while the energy storage capacity is increased by a factor of five, the cost is increased to only three times the baseline unit.

SUMMARY

The flywheel energy storage unit meets the objectives of: (1) low aquisition cost, (2) safety and reliability, and (3) efficiency. The flywheel energy storage unit uses existing technology and is conventionally manufactured.

RECOMMENDATIONS

The technology for developing prototype flywheels with turbine supplies is now mature enough to warrant fabrication of prototype units. Such development, coupled with a modest venture analysis, should be sufficient to encourage the industry to market these units for residential use.

REFERENCES

1. Banas, J. F., and W. N. Sullivan, "Engineering of Wind Energy Systems, Sandia Laboratories, SAND75-0530, January 1976.

2. Blackwell, B. F., "The Vertical Axis Wind Turbine, How It Works," Sandia Laboratories, SAND74-0160, December 1974.

3. Towgood, D. A., "An Advanced Vehicular Flywheel System for ERDA Electric Powered Passenger Vehicle," presented to U.S. Department of Energy, CONF 771053, October 1977.

4. U.S. Department of Energy Report, "Economic and Technical Feasibility Study for Energy Storage Flywheels," HCP/MI066-01, May 1978.

THIS PAGE

WAS INTENTIONALLY

LEFT BLANK

PROJECT SUMMARY

Project Title: "Investigation of the Technical and Economic Feasibility of Using Pumped Well-Water Energy Storage Systems"

Principal Investigator: Gerald E. Weinstein

Organization: The BDM Corporation
2600 Yale Blvd. S.E.
Albuquerque, New Mexico 87106
(505) 843-7870

Project Goals: To determine the technical and economic feasibility of storing surplus solar and wind energy for rural applications using a small hydro/mechanical system that pumps water from an aquifer to a surface reservoir and recovers energy by returning the water to the aquifer.

Project Status: An analysis of user demand, institutional and legal issues, and aquifer characterization has been completed. Determination of engineering feasibility is in progress and economic analysis will begin shortly.

The user demand investigations have identified rural applications where the storage of surplus solar or wind energy is key to these energy sources meeting energy demands. This study has also determined generic load profiles for use with energy availability curves to determine storage requirements.

The institutional and legal issues study has identified water rights as a real property right owned and possessed by the individual user in the State of New Mexico. Certain portions of New Mexico have been declared Underground Water Basins within which the usage and storage of water is regulated. In addition, the Water Quality Control Commission has established regulations and standards for discharges into underground water. Review of all these issues has identified no barriers that rule out the development of aquifer hydro/mechanical energy storage systems.

The aquifer characterization has identified those characteristics which are required for the aquifer to perform according to requirements determined by the system engineering of the entire system. In particular, it was determined that the aquifer should have a hydraulic conductivity greater than 1000 gal/day-ft^2.

Engineering considerations in establishing technical feasibility include: efficiency, control systems, equipment, and sizing. Central to technical feasibility is the integration of energy availability and demand with off-the-shelf equipment capabilities. Off-the-shelf turbine/generators-pump/motors have been identified and control systems are being investigated.

Contract Number: 13-6485

Contract Period: April 11, 1979 to September 30, 1979

Funding Level: $41,000.00

Funding Source: Sandia Laboratories, Albuquerque
Division 2324

FEASIBILITY STUDY OF A SMALL PUMPED AQUIFER STORAGE SYSTEM FOR SOLAR AND WIND ENERGY

Arthur J. Mansure
The BDM Corporation
2600 Yale Blvd., S.E.
Albuquerque, New Mexico 87106

ABSTRACT

The technical and economic feasibility of storing surplus solar and wind energy in rural locations is being investigated for a small hydro/mechanical system that pumps water from a subsurface aquifer to a surface reservoir and then recovers the energy by allowing the water to return to the aquifer. An analysis of rural user energy demands, institutional and legal issues, and aquifer characterization has been completed. The availability of equipment to operate the system has been investigated and it has been determined, with the exception of specialized control equipment, that off-the-shelf equipment exists that meets rural installation and maintenance needs. A system design that integrates the components, based on energy availability and user demand, is in progress. Economic analysis will follow completion of the engineering study.

INTRODUCTION

As a result of today's increased awareness of the environment and limited natural resources, it has become imperative to conserve and/or better utilize the Earth's existing energy, especially the renewable energies -- wind and solar. One reason that these free forms of energy have not been exploited is the lack of economically feasible methods to harness and store these forms of energy so that man can use them to fit his needs. Technological discoveries are continually advancing the state of the art of extracting these energies (i.e., photovoltaics, solar heat collectors, wind machines, etc). However, without efficient storage capability, these advances are of limited usefulness.

The concept of an aquifer based hydro/mechanical energy storage system (Figure 1) may be one feasible solution to this dilemma. Such a storage system is appropriate for rural life styles, because it uses equipment already available and maintainable in rural areas and can be incorporated into existing farm or ranch systems. In principle, it would be based upon equipment such as a turbine/pump that can perform multiple functions and system elements such as wells and reservoirs that have other farm and ranch uses. Thus, the storage system would be an integral part of rural life support systems and would promote a conservation approach to energy usage. In addition, such a system would make maximum use of existing equipment and thereby reduce costs.

CONCEPTUAL SYSTEM DEFINITION

The assessment of the feasibility of any conceptual system is only as valid as the assumptions defining the system. This study is determining the variables that are pertinent to the description and operation of this storage system and evaluating the effects of these parameters on the technical and economic feasibility of the system. Some values have been assumed; some have been determined by engineering and economic data of available equipment; others have been determined from statistical data bases.

A surplus of solar and wind energy is assumed. This energy will be supplied to the storage system in appropriate 60 Hz A.C. form. The purpose of the storage system is to make energy available when needed on a cost-effective basis.

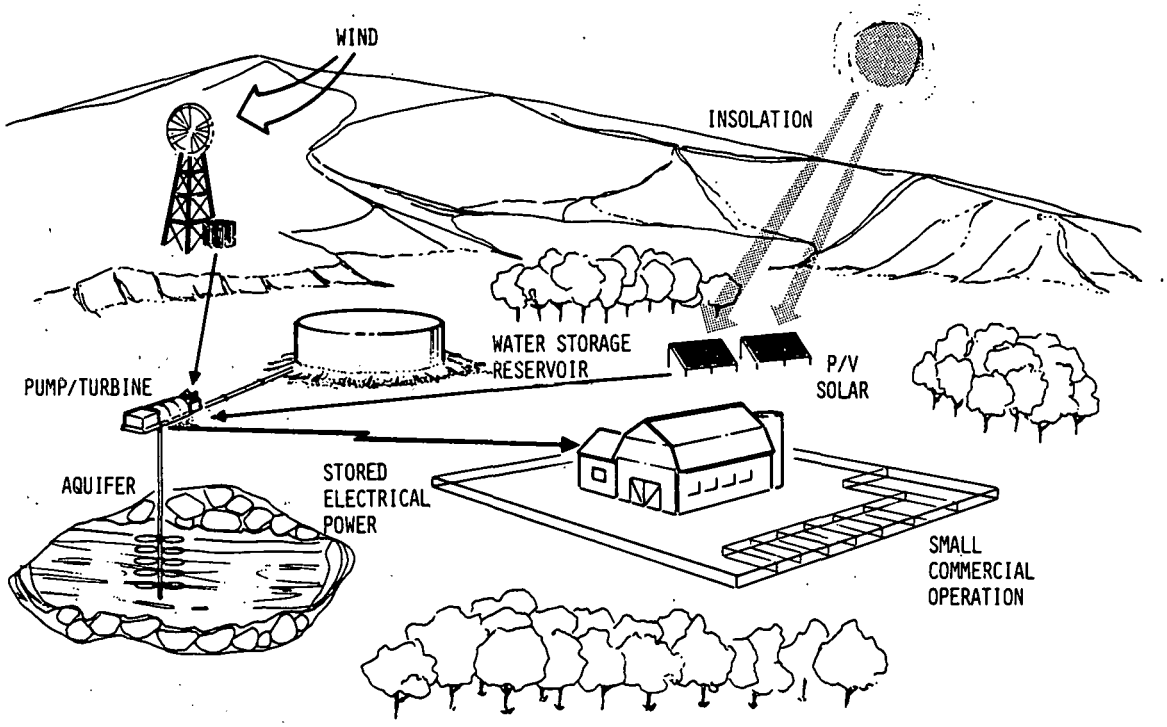

Fig. 1. Aquifer Hydro/Mechanical Energy Storage System

This system is considered for the small farm, ranch, or isolated rural business. Power produced will be used on the premises (i.e., no power will be sold); however, the power system will tie in with a standard commercial power network grid. Utility power will be available for emergency use and for times when statistically unusual weather patterns preclude the production of surplus energy. Utility power will also be used to satisfy the high peak demands occurring occasionally in lieu of oversizing of the equipment. This concept is felt to be more cost-effective.

For the initial concept, it is assumed that power requirements on the storage system do not exceed 5 kW peak and 60 kWh daily. Albuquerque meteorological data has been used to characterize the solar and wind availability throughout the day. Five kW is a reasonable lower limit for this concept; the system could, however, be scaled up to 30 kW, at which point multiple wells will be required.

LOAD DESIGN REQUIREMENTS

This part of the study has identified electrical requirements (peak kW and total kWh of storage) and demand curves for rural applications including dairy, chicken (egg), and pig farms, as well as small beef feedlots and a store/trading post. Each of these units included a dwelling.

For all of these applications, there was found to be insignificant variation between summer and winter demands, as long as no significant space heating load was considered. The chicken farm was determined to have a night-time load of 10 kW and a day-time load of 27.4 kW. The other operations were determined to have night-time loads ranging from 4 to 7 kW and day-time loads of the same range or less indicating a clear need for energy storage so that solar or wind energy collected during the day can be used at night. Figure 2 shows the power required curve for the beef feedlot user, the user considered most representative of the group (excluding the chicken farm).

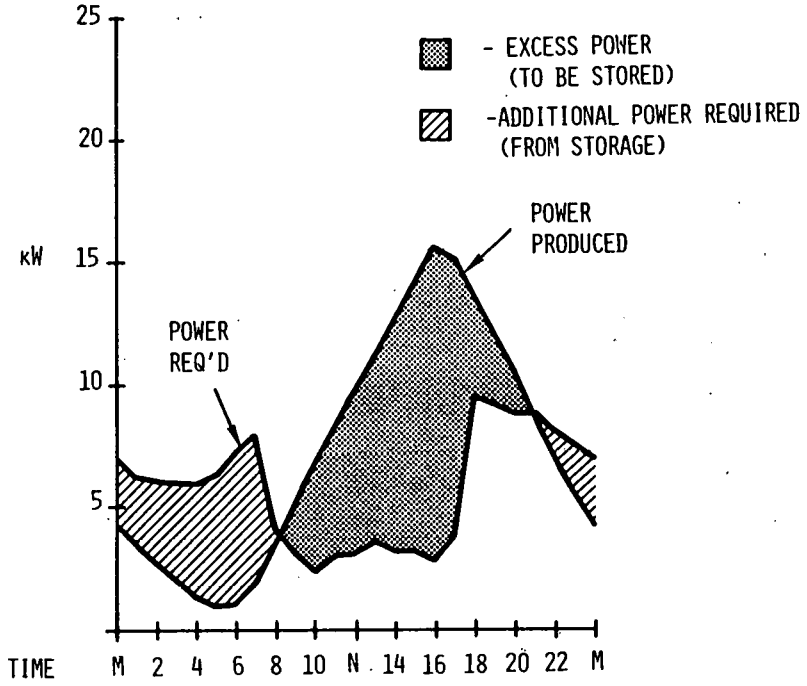

Fig. 2. Feedlot Power Required and Power Availability Curves

AQUIFER REQUIREMENTS

For an aquifer to be suitable for the hydro/mechanical energy storage system, it must have adequate well flow potential and be deep enough below the surface for adequate turbine head. The relationship between these parameters at the system's electrical output is given by(1)

$$P = QH/(5300 \text{ gal-ft/min-kW}) \quad (1)$$

where P is the power in kW, Q is the turbine flow rate in gallons per minute, and H is the turbine head in feet. For an assumed average well flow rate of 300 gal/min, a 5 kW system operating at a 70% efficiency thus requires a minimum turbine head of 126 feet. Because of other head losses such as draw-down/up and well-bore skin effects, the initial conceptual depth for a 5 kW system should be 200 feet.

For the energy storage system to operate efficiently, the power expended against viscous forces in the aquifer must be small compared to the output of the system. This can be insured by aquifer characteristics that keep the draw-down/up a small fraction of the turbine head. In other words, during operation, the distance between the water level in the well and the potentiometric surface should be a small fraction of the distance from that water level to the ground surface. For example, if the draw-down/up is 15 ft. and the depth of the water is 200 ft., then the water will have to be pumped from 215 feet and will give up energy to the turbine while falling to a depth of 185 feet. Thus, the viscous efficiency will be

$$\frac{185}{215} = 86\% \quad (2)$$

Maintaining draw-down/up within such limits is also important to insure the turbine/pump can be properly sized according to head to give maximum mechanical efficiency.

ENGINEERING REQUIREMENTS

The turbine/generator-pump/motor is the key to the storage system. Present state-of-the-art equipment performs at 75% (±5%) efficiency when operated within the limits of the designed head and flow rates. Using the nominal efficiencies of 75% for pumping and 75% for power generation, it is apparent that 2 units of power input are required for each unit to be recovered from storage. This equipment consists of a motor located on the surface that is connected to a long shaft which drives the pump. The pump head is located at the bottom of the well and is a multi-stage vertical turbine. The whole pump assembly is contained in a vertical pump casing. In the recovery stage, the pump impeller would be driven by return flow of water and the motor would become an alternator, which is driven by the pump impeller. It is necessary to control the power generation with some form of a governor. Such a device is not commercially available at this time since this type of pump was not designed to be used as a turbine generator.

Initial design considerations indicate the need for a 15 horsepower pump which would provide a flow rate of about 225 gallons per minute from a well 200 feet deep. This same flow rate must be maintained in the storage recovery cycle and would provide a recovery of approximately 5 kW.

Fundamental to system sizing is an examination of the relationship of the power supply and demand curves. When supply is greater than demand, the excess energy is diverted to storage. Conversely, when demand is greater than supply, the energy must be recovered from the storage system to make up for this deficiency. It follows then, for a plot of either supply or demand (where the ordinate represents kilowatts and the abscissa represents time of day), the area under the curve equates to the daily power produced or required, respectively. The area contained between the curves equals the energy stored or recovered. This relationship is depicted in Fig. 3. Units of the y-axis are kilowatts and the x-axis denotes time of day starting at midnight through noon to midnight the next day. The supply and demand curves (represented by linear functions for simplicity) are labeled "S" and "D". The shaded area on the right represents the energy going to storage; the area on the left represents energy recovered from storage. The area on the right should be approximately twice as large as the area on the left since this system will recover power with a system efficiency of approximately 48%. The demand curve is established by the needs of the farm and is fixed. The supply curve, however, is elastic and can be translated vertically (S') by the addition of equipment (i.e., more windmills and/or solar panels).

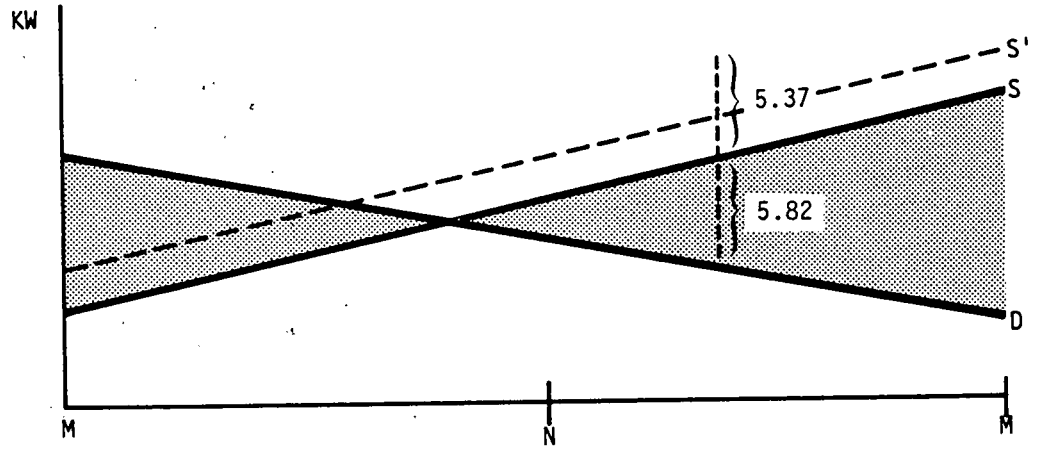

Fig. 3. Power Supply Versus Power Demand Relationship For an Average Day

Also shown on Fig. 3 is the breakeven point. A pump rated at 15 horsepower equates to 11.2 kW. This pump will not run on a power supply of less than 11.2 kW without damaging the motor. Likewise, if more power than 11.2 kW is available, the pump cannot use it to pump additional water. For times when the available surplus power is less than 11.2 kW, a sufficient quantity of power will be purchased from commercial sources to reach the 11.2 kW level so that the pump may operate. Since the system operates at 48% efficiency, we expect to recover only 5.4 kW of energy (11.2 x 48% = 5.4). If 5.4 kW were purchased and 5.8 kW were produced, the system would just break even. This breakeven point is denoted by the vertical dashed line. Energy produced to the left of this line does not economically warrant storage and is wasted. Thus, proper sizing of the equipment requires balancing available power, demand, and minimum motor power requirements.

INSTITUTIONAL AND LEGAL ISSUES

In New Mexico, water rights are a real property right owned and possessed by the individual user. In addition, certain portions of New Mexico have been declared Underground Water Basins within which the usage and storage of water is regulated. The Water Quality Control Commission has established regulations and standards for discharges into underground water. Review of all these issues has identified no barriers that prevent the development of aquifer hydro/mechanical energy storage systems.

AQUIFER CHARACTERIZATION

In addition to aquifer productivity and depth requirements, the requirement that the aquifer draw-down/up be limited places limits on aquifer hydraulic conductivity and thickness. Aquifers can be either confined or unconfined; preliminary calculations indicate that, within safe yield production, differences between draw-down/up for confined and unconfined aquifers are typically only a factor of 2. For this study, the aquifer type with the larger draw-down/up (confined aquifer) has been assumed.

Draw-down/up is the local fluctuation in the water table or potentiometric surface caused by the production or injection of the well. When a well is being produced, the pumping causes a local pressure reduction sufficient to set up the pressure gradient that causes additional water to flow into the well. Unsafe production of the well occurs when local depletion of water exceeds one-half the depth from the water table or potentiometric surface to the bottom of the aquifer. During injection (or in this study, returning the water to the aquifer) the water level in the well must stand sufficiently above the water table or potentiometric surface to supply the necessary force to drive the water back into the aquifer against the viscous forces that retard flow through a porous media.

Table 1 shows the results of quasi-steady state draw-down/up calculations. These calculations assume .7 foot well radius, 1,050 ft. drainage radius, and 300 gal/min flow rate. The table implies the hydraulic conductivity should be greater than 3.8×10^2 gal/day-ft^2.

TABLE 1. Draw-Down/Up as a Function of Aquifer Thickness and Hydraulic Conductivity

	K(gal/day-ft^2)	Thickness (ft)[a]				
		25	75	100	200	400
Gravel	7.2×10^3	3	1	1	0	0
Coarse Sand	3.7×10^3	5	2	1	1	0
Medium Sand	3.8×10^2	-	18	14	7	3
Fine Sand	1.1×10^2	-	-	46	23	12
Sandstone	3.0×10^1	-	-	-	84	42

[a] Draw-down/up is left blank if safe yield conditions would be exceeded.

Time dependent constant production calculations for a medium sand aquifer 75 feet thick indicate the draw-down/up will be 23.8 feet after 12 hours. This is considerably larger than the 18 feet given in Table 1 and is a result of the fact that quasi-steady state calculations assume the water is derived by recharge rather than from storage. This significant draw-down/up, in a period comparable to the usage of the stored energy, indicates the need for detailed analysis of cyclic production (net zero water production) to determine if production and recharge effects cancel, thereby, resulting in small draw-down/ups.

Figure 4 shows the draw-down/up that results from 6 hours of pumping followed by a 6 hour delay before recharge, for a medium sand aquifer 100 ft. thick. The figure indicates that the basic draw-down/up given in Table 1 serves to bound hydraulic conductivities and aquifer thickness.

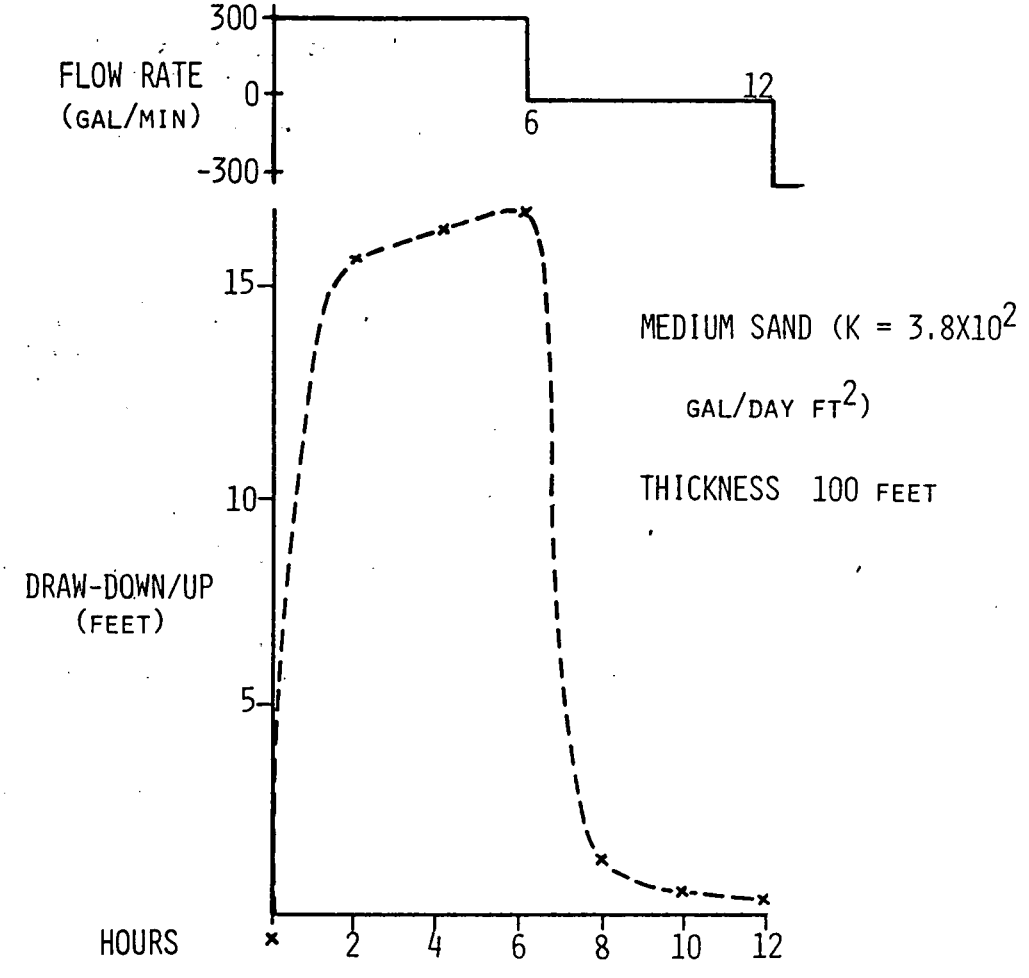

Fig. 4. Draw-Down/Up During Cyclic Production

In summary, the requirements that characterize an aquifer suitable for use in an aquifer hydro/mechanical energy storage system are

(1) Depth to water table or potentiometric surface - 200 feet minimum.
(2) Well productivity - 200 gal/min. minimum.
(3) Hydraulic conductivity greater than 1,000 gal/day-ft^2 minimum.

These requirements, plus considerations of institutional and legal issues, have led to the identification of the regions shown on Fig. 5 as the best regions in New Mexico for aquifer hydro/mechanical energy storage projects.

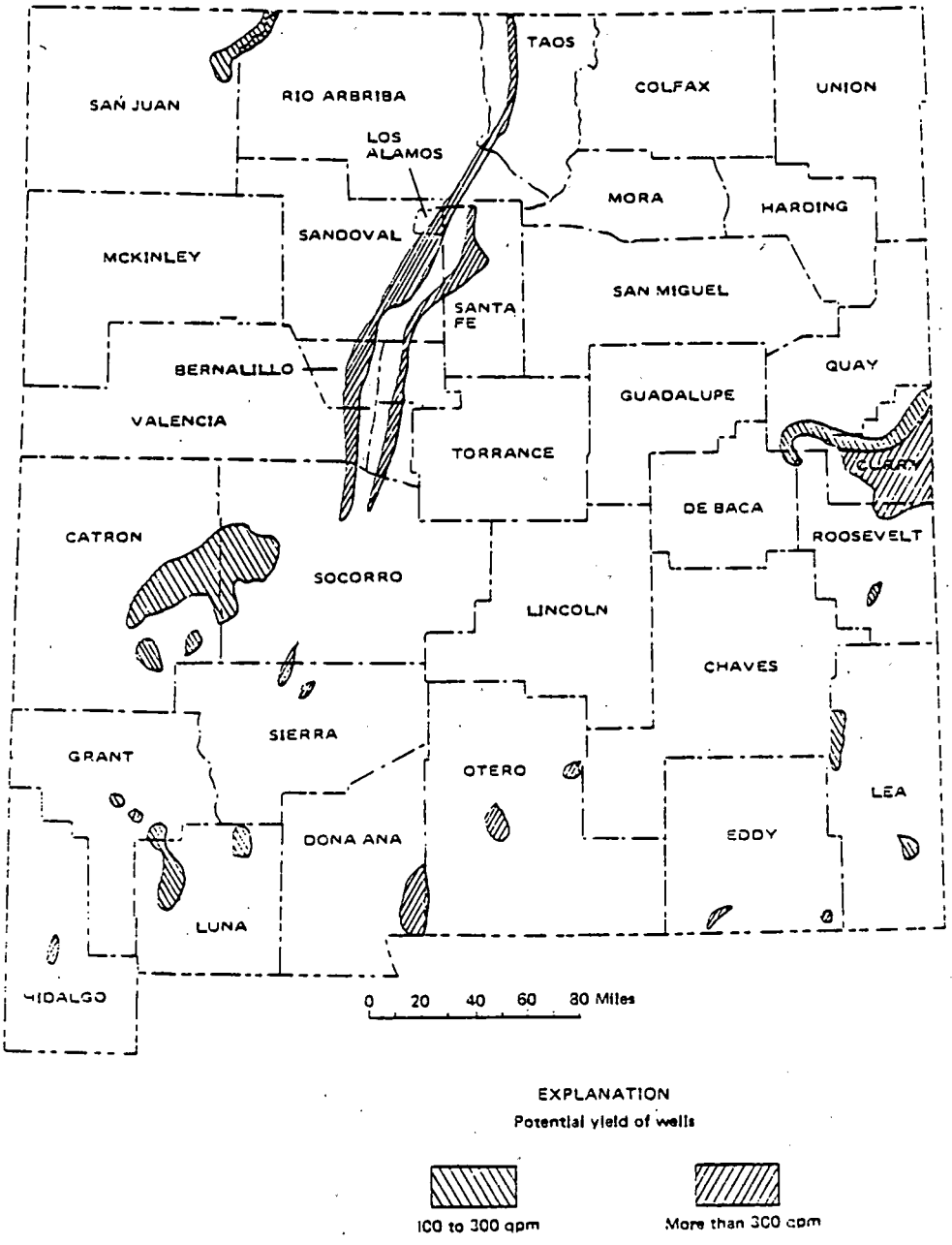

Fig. 5. Regions With Aquifers Suitable For Use as Lower Reservoir of Mechanical Energy Storage Systems

REFERENCES

1. Engineering Manual, R. H. Perry, 1967, p. 8-71.

ACKNOWLEDGMENTS

The work reported in this paper was supported by Sandia Laboratories Systems Analysis Division 4716 and performed by George Collaros, Dick Dascher, Bob Grassberger, A. J. Mansure, Steve Schoderbek, Bob Sheridan, and G. E. Weinstein.

PROJECT SUMMARY

Project Title: Industrial Compressed Air Application for Solar Energy Conversion/ Storage Devices.

Principal Investigator: Laurence B. McEwen

Organization: JALAR ASSOCIATES
1321 Chestnut Street
San Francisco, CA 94123
(415) 771-1544

Project Goals: To ascertain the feasibility of utilizing solar energy devices and compressed air energy storage to supply power for industrial compressed air systems.

Project Status: Contract has been completed, the final report was delivered July 18, 1979.

The fulfillment of this effort entailed the performance of three separate tasks. The first task established a profile of installed industrial compressed air capacity, the characteristics of plant air usage, and quantified the energy required to produce this air. The results of this task provided a perspective for the potential energy savings that might occur from subsequent work.

The second task evaluated the technical feasibility of the concept while the third task determined the economic viability of specific and representative approaches.

The primary conclusions of the study are as follows:

1. Significant fossil energy savings could be accomplished if plant air could be produced from solar sources. (.2 quadrillion BTU's annually).

2. The concept is technologically feasible, and enhanced, in most cases, by the use of energy storage.

3. The concept is not economically viable either currently or in the immediate future.

4. There is a good opportunity for energy conservation in that 90% of all air compressor energy is currently being discarded as waste heat.

Contract Number: 07-9091

Contract Period: FY '77

Funding Level: $68K

Funding Sources: U.S. Department of Energy, Division of Energy Storage System.

INDUSTRIAL COMPRESSED AIR APPLICATIONS FOR SOLAR ENERGY CONVERSION/STORAGE DEVICES

L. B. McEwen and J. W. Swain

JALAR ASSOCIATES

1321 Chestnut Street
San Francisco, CA 94123

40 Denton Road
Wellesley, MA 02181

ABSTRACT

Survey of Industrial Compressed Air, its uses and energy requirements. Investigates the feasibility of utilizing solar/wind energy conversion systems with or without compressed air energy storage devices to supply power for industrial compressed air. None of the scenarios depicted in the study were economically attractive at this time. The main reason this conclusion was scaling the solar energy conversion devices to displace only ten percent of a plant's electrical load, thereby severely limiting the scope of potential savings. Technological improvements, reduction in capital costs, more rapid rises in utility rates or an abrogation of fossil fuel supplies would be necessary before further pursuit of this concept is warranted.

INTRODUCTION

The purpose of this contract effort, managed by Sandia Laboratories and funded by the Energy Storage Systems Division, U.S. Department of Energy, was to determine the feasibility of utilizing solar energy devices and compressed air energy storage to supply power for industrial compressed air systems. The fulfillment of this effort entailed the performance of three separate tasks. The first task established a profile of installed industrial compressed air capacity, the amount of plant air normally used, and the energy required to produce this air. The results provided a perspective for the potential energy savings that might accrue from subsequent work. The second task evaluated the technical feasibility of using energy from solar sources to power industrial compressed air systems either directly or through the employment of energy conversion or storage devices. Should such an arrangement be technically feasible, then the purpose of task three was to determine the economic viability of specific and representative approaches.

The principal findings of this study were as follows:

1. Significant energy savings could be accomplished if plant air could be produced from solar energy (.2 quadrillion BTU's annually).
2. The production of plant air by means of solar energy devices with or without compressed air storage systems is technologically feasible.

3. The economic viability of any such arrangement is not encouraging for the immediate future. This is due primarily to the limitation of savings to compressed air generation only (10% of industrial power costs).
4. There is a good prospect for energy conservation in that 90% of all air compressor energy is currently being discharged as waste heat.

Task I, the investigation of industrial compressed air usage, centered on detailed observations of eighteen industries situated throughout the United States. These collectively account for approximately 40% of the Nation's industrial energy demand. Findings regarding compressed air use and energy demand were then translated to the remaining industries to ascertain the maximum energy savings that might be realized through the application of solar energy to industrial air systems.

The energy required to produce compressed air in 1976 was 0.2 quadrillion BTU's or 1.6 percent of total industrial energy consumption (12.6 quads). Installed compressed air capacity was estimated to be 50 million cubic feet per minute (CFM).

Table I summarizes the expected values for plant air loads and compressed air energy requirements for the eighteen industries studied. Eleven of these industries show a compressed air power requirement of over 1,000 kW, large enough for testing industrial-scale solar energy conversion devices. Compressed air storage facilities were not present in any of the industries studied. Some plants, however, did utilize receivers to dampen surges in demand, thereby reducing compressor cycling.

Task 2 concluded that several applications of solar energy conversion devices were, indeed, technically compatible with industrial air compressor requirements. Although no attempt was made to design an ideal system, several promising scenarios were identified. Both photovoltaic (PV) and wind energy conversion systems (WECS) were found suitable for application to industrial compressed air systems. Because of the relatively minor role which compressed air production plays in industrial energy consumption however, most utility-scaled solar energy conversion schemes (which tend to be capital intensive) were found to be not suitable for this study. Among the photovoltaic and wind energy conversion system approaches, flat-plate photovoltaic arrays, and both horizontal axis and vertical axis wind turbine designs were found to be suitable. Adequate operating data appears to have been compiled on these technologies. Concentrating photovoltaic arrays also appear suitable, but were not regarded as sufficiently developed for consideration in this study.

Rotary screw, reciprocating and centrifugal air compressor designs were found to be suitable for generating compressed air in these applications. Rotary screw compressors were suggested because of their low cost, low starting torque, and high ratio of output to weight. Reciprocating compressors were recommended due to their high efficiency and relatively low operating speeds for direct drive applications. Centrifugal designs were the most commonly employed compressors in applications of over 5,000 cubic feet per minute (CFM). Scroll and other experimental compressors were not deemed suitable as they are still in the developmental stage, and have not been demonstrated at appropriate scales.

Compressed air storage, although technically feasible utilizing either underground caverns or high-pressure vessels, was not deemed to be suitable for industrial compressed air applications due to unfavorable economics of scale. Only in the case of an existing cavern, in which the high initial costs of excavation might be avoided, could compressed air energy storage costs be brought into line for industrial compressed air applications.

Having established the scope of potential energy benefits of the concept and the technological feasibility of the approach, Task 3 then focused on the economic merits. In order to establish the economic feasibility of combining industrial scale compressed air requirements with solar energy sources, three different scenarios were proposed, depicting a range of scales and different applications of solar energy with compressed air energy storage. The first scenario consisted of a small scale energy supplement to an existing plant utilizing a photovoltaic power source with a small (two hour) compressed air storage system. The second application involved a large scale horizontal axis wind turbine farm supplying power for compressed air to a central facility providing heating, cooling and compressed air services to an industrial park. The last scenario involved the application of an intermediate scale vertical axis wind turbine supplying compressed air directly to a remote industrial site situated in an undeveloped country. This application was designed to present the most favorable circumstances for an evaluation of a wind power/compressed air energy storage installation. All three scenarios relied on the availability of an existing cavern that was suitable for the particular compressed air energy storage application.

In order to determine the value of each of the scenarios, it was first necessary to establish a base case cost of providing compressed air service to the industries involved. This was done by annualizing the capital cost of a conventional compressed air system, adding the annual operating and maintenance and utility costs required to provide air service and dividing that sum by the quantity of air produced during the year. These calculations yielded a cost per unit quantity of air. In like manner, the costs of producing air utilizing first solar power, and then solar power with a compressed air energy storage system were calculated. Each of these calculations was then projected for a period of 15 years from a 1985 start date. These projections assumed an annual inflation rate of 8 per cent and an annual increase in the cost of electrical service of 13 per cent; 5 per cent over the assumed inflation rate.

A summary of the results of these economic analyses is contained in Table II. The first scenario fails to yield attractive pay back rates (5 year period) from either the use of photovoltaics or photovoltaics with energy storage until the year 2000, or 15 years after initial operation. Again in the second scenario, in which a central facility provides air to an industrial park, there are no economically attractive options during the first five years of operation. However, beginning in 1995 and continuing throughout the remaining life of the project, savings become attractive with the implementation of wind power, with or without energy storage. These attractive savings depend on utility charges that continue to escalate at an annual rate of 13 per cent. In the last scenario, an undeveloped site in a third world country, although energy storage makes the approach technically feasible, satisfactory savings again do not appear until 1995, or ten years after construction.

The unattractive immediate economic findings in all three scenarios can be attributed to several key economic parameters. The primary constraint on economic benefits is the small portion of utility costs which are subject to savings. Only 10 per cent of utility expenses for the industries concerned are the result of compressed air generation. Therefore the high capital costs required to implement any of these systems for use with compressed air generation can be ammortized over only a small portion of total utility costs. The most promising economics are associated with the second scenario, primarily because any electric power outputs from the wind energy conversion system which are in excess of compressed air energy requirements can displace other plant electrical demand. In the third scenario, the mechanical output of the WECS prevents any alternative uses of output power, and mandates the inclusion of energy storage to even achieve technical viability.

In the last scenario, an evaluation was made of generating electricity by means of an air-driven turbine. The inefficiency of the air turbine at pressures and temperatures compatible with industrial compressed air systems, however, makes the production of electricity by means of air turbines non-competitive with conventional diesel generators. Specifically, power from air is almost three times as expensive as from conventional diesel generators, even given the high fuel costs (150% of projected U.S. prices) used for this exercise.

In conclusion, none of the scenarios depicted in this study, which utilized solar power and compressed air storage devices to supply industrial air, were economically attractive. In every instance, satisfactory rates of return did not appear until ten years after construction. Improvements in technology, reduction in capital costs, more rapid rises in utility rates or an abrogation of fossil fuel supplies would be necessary before further pursuit of this concept is warranted.

Table 1. Compressed Air Requirement Plant Summary

INDUSTRY	AVERAGE PLANT AIR LOAD (CFM)	AVERAGE PLANT AIR REQUIREMENT (kW)	% TOTAL ENERGY CONSUMED
Aircraft Assembly	7,500	1,250	3.4
Appliance Mfg.	8,000	1,300	3
Automobile Assembly	20,000	3,300	4
Automobile Mfg.	30,000	5,000	6
Brewing	6,000	1,000	1.5
Chemical Mfg.	15,000	2,700	3
Construction (Indust.)	185	60	N/A
Food Processing	1,000	170	.5
Glass Container Mfg.	9,000	1,500	3.6
Heavy Construction (Dams)	5,000	840	4.8
Heavy Electrical	13,600	2,350	.75
Mining (Iron)	24,000	4,000	7.5
Oil & Gas Drilling	2,850	475	.1
Packaged Goods Mfg.	1,500	250	2.7
Paperboard Mfg.	9,500	1,600	.6
Steel Production	40,000	6,500	1.8
Textile Mfg.	1,000	175	.4
Tool & Die Mfg.	600	100	2.9
Weighted average of sample industries			1.6%

Table 2. Summary of Economic Analysis (K$)

	Add'l Capital Investment (1985)	Annual Savings			
		1985	1990	1995	2000
Scenario I					
Base Case	452				
(PV, No Storage)	1,170	32	59	108	200
PV + Storage	1,340	37	68	126	231
Scenario II					
Base Case	7,500				
Wind	19,100	--	110	3,660	10,126
Wind + Storage	19,700	--	1,012	5,466	13,652
Storage Only	600	--	--	769	1,586
Scenario III					
Base Case	1,800				
Wind	5,600	--	178*	1,200*	3,000*
Wind + Storage	6,200	--	78	1,000	2,800

* Hypothetical savings, since this option was found to be technically not viable.

PROJECT SUMMARY

Project Title:	"An Overview of Contracts With Colleges and Universities for Advanced Flywheel Concepts"
Principal Investigator:	Harold E. Schildknecht
Organization:	Sandia Laboratories, Division 2324, Albuquerque, New Mexico 87185 FTS 475-2402
Project Goals:	To identify and develop advanced flywheel concepts that offer potential advantages over traditional approaches to flywheel energy storage systems.
Project Status:	A 12-month contract with the University of Minnesota to study cellulosic flywheels is scheduled for completion in September, 1979. A major portion of the work completed to date has been the design and fabrication of the special apparatus required to evaluate strength and durability of plywood test specimens and experimental hub-to-rotor bonds. The plywood specimens are equilibrated at either $\sim$ 12% or $\sim$ 0.1% moisture content and then tensile tested. Comparing the results shows the low moisture-content specimens to have approximately 18% lower average tensile strength. Apparatus has also been designed and fabricated to facilitate bonding metallic hubs to plywood rotors and dynamically balancing the bonded assemblies. A 14-month contract with Union College to study a band-type variable inertia flywheel (BVIF) is scheduled for completion in August, 1979. This concept provides a varying moment of inertia during rotation through the transfer of coiled flexible bands between the flywheel's hollow outer casing and inner hub. The equations of motion were derived for two BVIF design variants and incorporated into computer codes. A proof-of-concept model was designed and built for comparing actual and computer-simulated BVIF operation. Results to date support the viability of the concept for specific load conditions. A 12-month contract with Texas A&M University to study a flexible flywheel concept is scheduled for completion in September, 1979. Primary emphasis has been placed on developing a gimballed support system to suppress the flywheel's nonsynchronous whirl tendencies. This includes designing the system, building a small demonstration model, deriving the equations of motion, developing computer codes, and incorporating the gimbal mechanism into a medium size flexible-flywheel test stand. Results to date indicate that a properly designed gimballed support system will place the whirl instability boundary above a reasonably high maximum working speed.
Contract Number:	C8-03-02-02-3 SOL/100
Contract Period:	FY'79
Funding Level:	$106K
Funding Source:	U. S. Department of Energy, Division of Energy Storage Systems

AN OVERVIEW OF CONTRACTS WITH COLLEGES AND UNIVERSITIES FOR ADVANCED FLYWHEEL CONCEPTS

Harold E. Schildknecht
Sandia Laboratories
Division 2324, P. O. Box 5800
Albuquerque, New Mexico 87185

ABSTRACT

The Solar Mechanical Energy Storage Project work performed under the direction of Sandia Laboratories includes contracts with one college and two universities for studies on advanced flywheel concepts. The three institutions involved and their respective advanced-concept pursuits are as follows: University of Minnesota, cellulosic flywheels; Union College, variable inertia flywheel; and Texas A&M University, flexible flywheel. The primary objectives of the contract with the University of Minnesota are to evaluate the physical properties of cellulosic materials (primarily plywood) relative to suitability for flywheels, and to develop inexpensive methods of metallic-hub attachment and dynamic balancing for cellulosic flywheels. Of particular interest is the effect of prolonged vacuum exposure on plywood strength and durability. The contract with Union College is to characterize the dynamics of their proposed band-type variable inertia flywheel and determine if it offers potential advantages in the areas of economy, reliability and efficiency. The Texas A&M contract is primarily directed at studying the rotational characteristics of a flywheel configuration featuring flexible spokes and rim, with particular emphasis being placed on devising practical methods for suppressing undesirable whirl modes. All three of the above contracts are scheduled to be completed by September, 1979.

INTRODUCTION

In 1977, the U. S. Department of Energy (DOE, formerly ERDA) designated Sandia Laboratories the lead laboratory for the national Solar Mechanical Energy Storage Project. Shortly thereafter, a comparative-analysis was made of leading candidates for mechanical energy storage systems. The results showed flywheel systems to be the most promising for residential applications. By virtue of that finding, major emphasis has been placed on developing low-cost flywheel technology. This is being largely accomplished through contracts with industrial firms, colleges, and universities. The contracts with industry are primarily to obtain design details and cost figures on comparatively state-of-the-art flywheel energy storage systems, whereas the college and university contracts are aimed specifically at studying advanced concepts. The three contracts placed to date for advanced flywheel studies are as follows:

Cellulosic Flywheel -- University of Minnesota, Minneapolis, Minnesota
Variable Inertia Flywheel -- Union College, Schenectady, New York
Flexible Flywheel -- Texas A&M University, College Station, Texas

This paper presents the highlights of each of the above contracts.

CELLULOSIC FLYWHEELS, UNIVERSITY OF MINNESOTA

BACKGROUND

Several leading proponents of flywheel energy storage systems have recognized for some time the potential of wood and other natural forms of cellulose as inexpensive and renewable sources of material for flywheels. The moderately high strengths and low densities typical of natural cellulosic fibers provide specific-energy capabilities (the ratio of tensile strength to density) comparable to some commonly used steels. In addition, cellulosic-materials processing has long been an established technology in this country as evidenced by the abundance of woodworking, plywood, composite board and paper industries. In light of these attributes, the use of cellulosic flywheels in energy storage systems where size and weight are secondary to cost is seen as potentially competitive with flywheels made from more traditional materials such as steel and fiber-composites.(1)

The results from the spin-testing of experimental wood disks at the Applied Physics Laboratory (APL) of Johns Hopkins University suggests the feasibility of utilizing moderate performance wood flywheels in stationary energy storage applications.(2) These tests revealed the tendency of wood disks to fail by shredding. This implies significantly greater inherent safety for wood than for steel flywheels, with the resulting need for less elaborate and costly failure-containment vessels. The APL experimentation also identified a need to develop economical and reliable methods for attaching hubs to wood flywheels.

Preliminary research at the University of Minnesota (U of M) on flywheels in general culminated in a comprehensive review and bibliography on flywheel technology by Professor A. G. Erdman and graduate student D. L. Hagen.(3) Their study showed virtually no work being done outside of APL to further the development of cellulosic flywheels. As a result, they began an investigation into the physical properties of cellulosic materials from the standpoint of suitability for use in flywheels. The investigation served to identify areas of cellulosic-materials evaluation and characterization that were inadequate and in need of additional research. This need and the potential benefits were brought to the attention of Sandia in the form of an unsolicited proposal from the U of M.

CONTRACT ACTIVITIES

A contract was placed with the U of M in 1978 for a study pertaining to cellulosic flywheels. It is 12-months duration, costing $41K, with Erdman and Hagen the principal and assistant investigators, respectively. The main objectives of the contract are:

- Evaluate the physical properties of cellulosic materials relative to suitability for flywheels.
- Develop inexpensive methods of metallic hub attachment and dynamic-balancing for cellulosic flywheels.

What currently appears to be the most promising method for constructing cellulosic flywheels is to laminate individual plywood disks into a rough cylindrical block and then turn and sand the block to finished dimensions. In view of plywood's apparent preeminence among competing forms of cellulose for flywheel use, emphasis is being placed on evaluating the physical properties of plywood tensile-test specimens. Of particular interest is the effect that prolonged vacuum exposure (i.e., such as would be experienced in an evacuated flywheel housing) will have on strength and long-term durability.

A major portion of the work completed to date under the contract has been the design and fabrication of special routing dies, fixtures, and grips. These items were required to form plywood test specimens and to adapt existing tensile and fatigue test machines for the evaluation of those specimens.

The plywood tensile and fatigue testing activity has primarily involved the measurement of changes in strength of the test specimens when vacuum dried from ∿ 12 percent moisture content (representative of 50 percent ambient RH) to less than 0.1 percent. Both the tensile test and fatigue test machines are fitted with environmental chambers for maintaining humidity control during testing. The tensile-test machine has been specially equipped for making high resolution stress/strain and acoustic emission measurements, and for recording and processing the measurements data using microcomputer supplemented data-acquisition equipment (Fig. 1). Statistical analysis of these data is expected to provide valuable insight into the relationship between load and damage rate, and thereby assist in predicting long-term durability for plywood flywheels.

Two existing flexural fatigue-testers were modified into a composite machine that can simultaneously apply a transverse moment (represents rotor imbalance) and a cyclic torque (represents rotor acceleration/deceleration) to a hub/rotor interface. This machine is currently being used to evaluate the strength and fatigue resistance of elastomeric bonds for attaching metallic hubs to plywood rotors. Load cells and position transducers are utilized to monitor flexure-induced stress and creep in the bonds.

The use of an elastomeric bond in the hub/rotor interface avoids the penalty incurred by drilling a hole through the center of the rotor for shaft retention (∿ 50% resultant loss in usable energy-storage capacity), plus assists the composite rotor/hub assembly (flywheel) to spin about its mass moment of inertia at speeds greater than first critical. However, attaching the hubs so that the shaft centerlines will be collinear with each other and the principal spin-axis of the rotor can be both difficult and expensive. Hence, a dynamic balancing machine was designed and built which is used to locate the mass moment of inertia of a spinning rotor. The hubs are attached after the geometrical location of the principal spin-axis is identified.

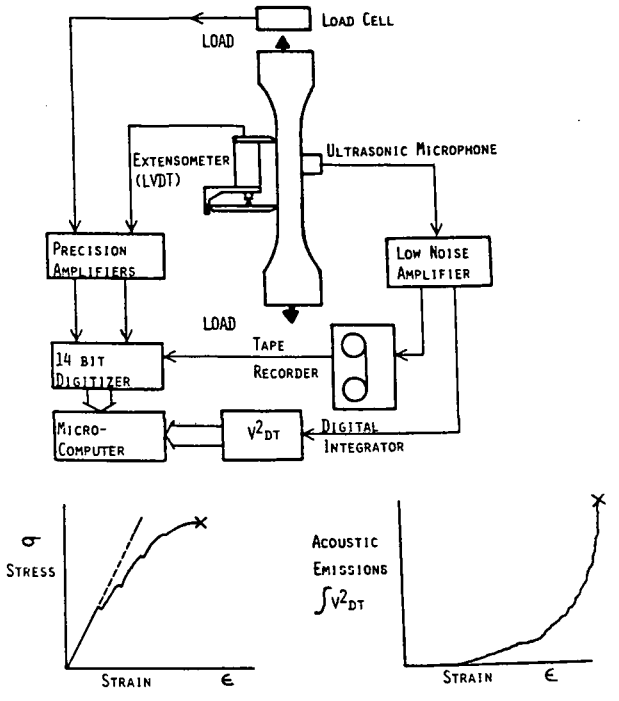

Fig. 1. Tensile-Test Machine Schematic

Birch was selected as the wood species for the plywood test specimens due to its high specific energy and commercial availability. Approximately 300 Finnish birch specimens have been tensile tested to date. The specimens were formed from 9-ply one-half inch plywood so that the face veneers were either parallel, normal, or 45 degrees to the tensile-stress axis. About half were equilibrated at 50 percent RH (∿ 12% moisture content), while the balance were vacuum dried (< 0.1% moisture content). The vacuum dried specimens have measured an average 18 percent weaker than their 50 percent-RH equilibrated counterparts. It is currently theorized that the orientation of the outer veneers with respect to the tensile-stress axis may have been a principal factor in the amount of strength loss. Over 700 16-ply test specimens have been formed for checking that theory.

The fatigue testing of plywood specimens and hub-to-rotor elastomeric bonds is in progress, but insufficient data has been acquired to date to reasonably predict performance trends.

This contract is scheduled for completion in September, 1979.

VARIABLE INERTIA FLYWHEEL, UNION COLLEGE

BACKGROUND

The energy stored in a rotating flywheel is governed by the relation

$$E = 1/2\ I\omega^2$$

where E is kinetic energy, I is the moment of inertia of the flywheel about its spin axis, and ω is the angular rate. Thus, for stored energy to be extracted, the rotational rate must decrease. However, in a typical energy storage application, the device which the storage medium drives is required to provide electrical power at constant frequency. An example is a flywheel driving an alternator. Without provisions to compensate for the flywheel's drop in speed, the alternator's output frequency will drop correspondingly. A commonly used method for reconciling this rotational-rate incompatibility is by adding a continuously variable transmission to the output shaft of the flywheel. This approach, while technically practical, incurs the dual penalties of additional cost and reduced efficiency for the overall system.

Since low cost and high efficiency are essential to the successful commercialization of flywheel energy storage systems, it would be desirable if a means could be devised to extract energy without creating the aforementioned problem of rotational-rate incompatibility. Re-examination of the flywheel energy equation suggests such a possibility; it is to vary the flywheel's moment of inertia around the axis of rotation such as to compensate for the energy outflow with minimal change in rpm. Mechanisms of this type are called variable inertia flywheels (VIF).

Between 1974 and 1977, while at Ohio State University, D. G. Ullman (now Dr.) was the co-investigator in a literature search for information on mechanical VIF's.(4) The most interesting concept encountered was for a coiled band type VIF (BVIF). As shown in Fig. 2, three separate parts comprise the basic configuration; namely, the inner hub, hollow outer casing and flexible band. The hub is mounted in the center of the outer casing and is free to rotate therein within the limits allowed by the coiled band connecting the two parts. The band is similar in appearance and mounting to the mainspring of a clock. During flywheel rotation, centrifugal force causes the band to conform to the inside periphery of the hollow casing; however, if an external load is applied to the inner hub, the band will begin to wrap around the latter part. The amount and rate of band transfer taking place from the casing onto the inner hub will depend on a variety of factors including band stiffness, centrifugal force, applied torque and the rotational-rate difference between the two parts. However, the net effect is a reduction in the moment of inertia of the outer casing about its spin axis with a resulting force imbalance that favors an increase in rotational rate. This induces greater centrifugal force on the band and, due to the attendant increase in the band's reactive-torque capacity, tends to compensate for the load induced slow down of the inner hub.

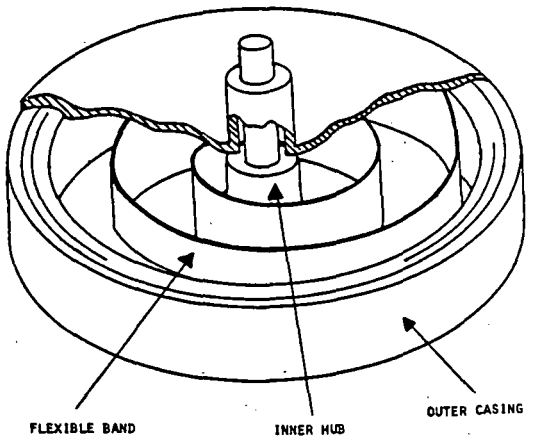

Fig. 2. Coiled Band-Type Variable Inertia Flywheel (BVIF)

The relationships between forces, applied and reactive torques, rotational rate differences and momentum represent a complex problem in dynamic balance, but one that has to be analyzed to adequately understand the potential of the BVIF. When his literature search found no evidence of these kinds of analyses, Ullman undertook the job and made it the subject of his doctoral dissertation.(5) In 1978, Ullman moved to Union College (UC). UC subsequently submitted an unsolicited proposal to Sandia for a BVIF study.

CONTRACT ACTIVITIES

A contract was placed with UC in 1978 for a study pertaining to a BVIF. It is 14-months duration, costing $25K, with Ullman the principal investigator. The objectives of the contract are to characterize BVIF dynamics and to determine if the concept offers advantages in the areas of economy, reliability, and efficiency. This is to be accomplished through the following task assignments:

- Model and analyze dynamics of basic BVIF configuration
- Model dynamics of BVIF with fixed ratio power recirculation
- Construct and test a proof-of-concept model

The first activity after contract placement was to develop the equations of motion for the BVIF in its simplest form. This configuration, called Type I, is where two nested bands connect the outer casing and inner hub, and the external load is applied to the latter. Thus, the rotational rate of the outer casing is in response to the tension in the bands. The equations of motion were derived and written into a computer code for dynamic simulation of the system. The Type I configuration appears to have no practical value for energy storage applications; however, understanding its dynamics was necessary before proceeding to the more promising Type II arrangement.

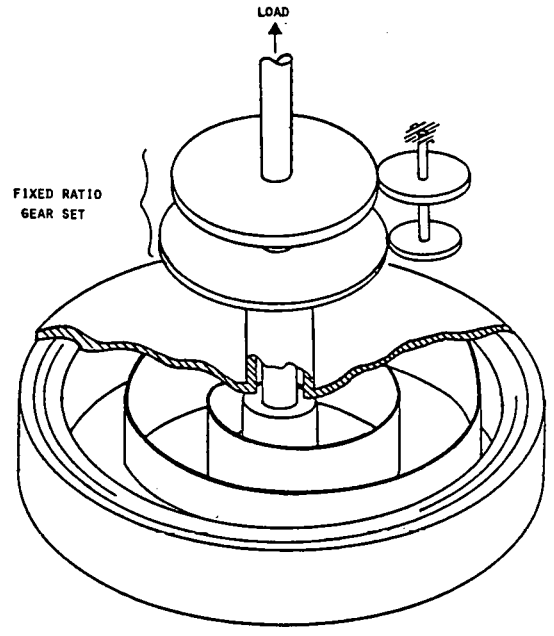

Fig. 3. Type II BVIF With Fixed Ratio Power Recirculation

The Type II BVIF configuration (Fig. 3) is essentially an extension of the Type I in the sense that, in addition to being joined by the coiled bands, the outer casing and inner hub are connected by an integral gear set. The gear set is fixed ratio, meaning that the rotational rates of the two parts will always be in constant ratio. A significant advantage of the Type II configuration is that band transfer is controlled by circulating power through two links rather than one. This provides greater design versatility and increased adaptability to specific load conditions. Primary emphasis has been placed on the analysis and testing of the Type II configuration. This includes the derivation of the highly nonlinear equations of motion for the fixed ratio power recirculation system and the incorporation of those equations into a computer code for dynamic simulation of the system. A linearized adaptation of the computer code was also developed which has proved a useful complement to its nonlinear counterpart.

A more complex gearing system has also been considered which would utilize a planetary gear train. For this system, the load is

connected to the planet gear which joins, and is free to orbit around, the inner hub and outer casing gears. Since three rather than two elements of gearing determine the torque balance, this system is considered to be potentially more versatile than the Type II. However, it has received only cursory examination under this contract.

A proof-of-concept BVIF model was designed and fabricated which can independently incorporate the Type I and Type II configurations for dynamic response testing. The model has been of only limited usefulness through much of the program due to frequent difficulty with the bands binding in the outer casing. However, the recent addition of a band-guidance reel to the head of the inner hub alleviated the problem and permitted reliable data acquisition.

The work of this contract is essentially complete, including the submittal of a draft copy of the final report. The results indicate that the Type II BVIF can be configured as a relatively high density flywheel which will maintain nearly constant rotational rate under specific load conditions while releasing energy. This indicates a probable efficiency advantage for the device over traditional fixed-inertia flywheel designs. However, whether the additional advantages of economy and reliability can be achieved under penalty of the BVIF's greater complexity remains to be proved.

FLEXIBLE FLYWHEEL, TEXAS A&M UNIVERSITY

BACKGROUND

The idea of a flywheel with flexible ring and spokes for storing kinetic energy originated with Dr. R. T. Schneider of the University of Florida (U of F) in 1975.(6) His objective was to develop an economical, reliable and safe energy storage device that would increase the use of solar-derived electrical power for residential and small commercial applications.

A flywheel test facility was established at the U of F in 1976. The subsequent testing of prototype flexible flywheels verified Dr. Schneider's prediction that the configuration would be self-centering and balancing. However, it also disclosed an unexpected problem with rotational instability. Following the discovery of the problem, Dr. J. M. Vance of U of F, a recognized authority in rotor dynamics, joined the project. Shortly thereafter, the nature of the instability was identified as nonsynchronous whirl. The consensus was that internal damping in the flexible ring and spokes provided the driving force for the whirl.

The fundamental flexible flywheel configuration is shown in Fig. 4. It basically consists of a flexible ring which is centrally suspended from an overhead shaft by means of equispaced support lines. The ring is made from a continuous length of synthetic cord or rope that is repetitively coiled into an approximate toroidal shape of the desired size and weight. A moderate amount of cross-sectional support is provided by either a woven sleeve or a single overlay of helically wound cord. Contrary to the conventional fiber-composite flywheel rim, the ring utilizes no bonding material, but depends on spin-induced centrifugal force for circumferential rigidity.

The potential advantages of the flexible flywheel configuration are the following:

- The spinning ring is in pure tension, thereby loading its fibers in the direction (longitudinal) of maximum strength.
- No bonding material present to create elasticity mismatch problem.
- Self-centering and balancing due to its flexible suspension system.

- Simple and economical to manufacture out of either medium or high strength synthetic fibers (e.g., Dacron, E-glass, S-glass, Kevlar).
- Relatively safe failure mode due to unbonded-ring construction.

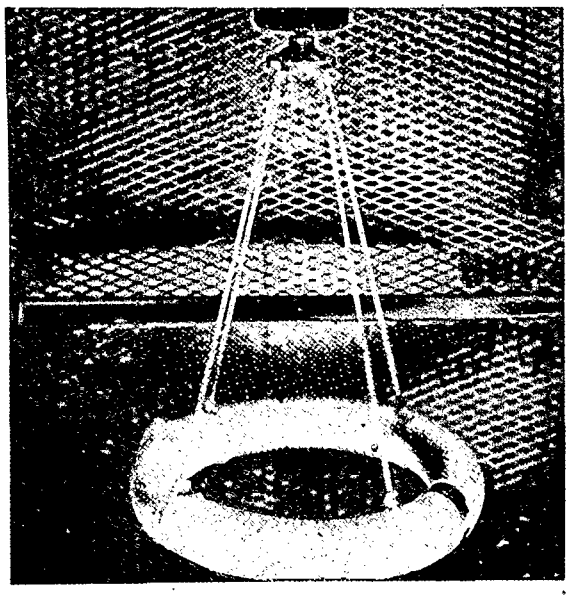

Fig. 4. Flexible Flywheel Configuration

The U of F submitted an unsolicited proposal to Sandia in mid 1978 for a flexible flywheel study. Shortly thereafter, Vance moved to Texas A&M University (A&M) and, per mutual U of F/A&M agreement, the proposal was reassigned to the latter institution.

CONTRACT ACTIVITIES

A contract was placed with A&M in 1978 for a study pertaining to the flexible flywheel. It is 12-months duration, costing $40K, with Vance the principal investigator. The major objectives of the contract are as follows:

- Study the rotational characteristics of experimental flexible flywheels.
- Devise economical and effective methods for suppressing undesirable whirl modes.
- Develop the conceptual design of a small size flexible flywheel energy storage system and estimate the cost.

Since the viability of the flexible flywheel concept hinges on finding a technically and economically feasible solution to the nonsynchronous whirl problem, the contract is structured to emphasize that objective.

Commonly used techniques for suppressing self-excited nonsynchronous whirl in high-speed rotating machinery are as follows: 1) flexible bearing supports, 2) asymmetric bearing support stiffness, 3) bearing support damping, and 4) bearing support mass (dynamic absorber effect). Dr. Vance chose the fourth technique wherein the mass of the drive motor would serve as the dynamic absorber.(7) He proposed to accomplish this by mounting the motor vertically downward in a gimballed support system (nonintersecting axes) and attaching the apex of the support-lines to the end of the motor shaft. Figure 5 illustrates the basic configuration. A table top model was subsequently designed and built for use as a demonstrator and for conducting preliminary studies on the whirl suppression effectiveness of the gimballed support system concept. Work was simultaneously initiated on deriving the basic equations of motion for the system.

The evaluation of the gimballed table-top model got underway in early 1979. Rotational stability observations were made on a 0.3 m (12 inch) diameter, 1.2 kg (2.7 lb) Dacron wheel with the gimbals both locked and unlocked. The testing was conducted in atmospheric air. In the locked condition, nonsynchronous whirling developed at approximately 10.5 rad/s (100 rpm). With the gimbals unlocked and the adjustable vertical separation between the gimbal axes at maximum setting, the flywheel remained stable through 68 rad/s (650 rpm), a significant improvement.

Following the above table-top model experimentation, the regular flexible-flywheel test stand was modified to incorporate a gimballed support system. A 0.61 m (24 inch) diameter,

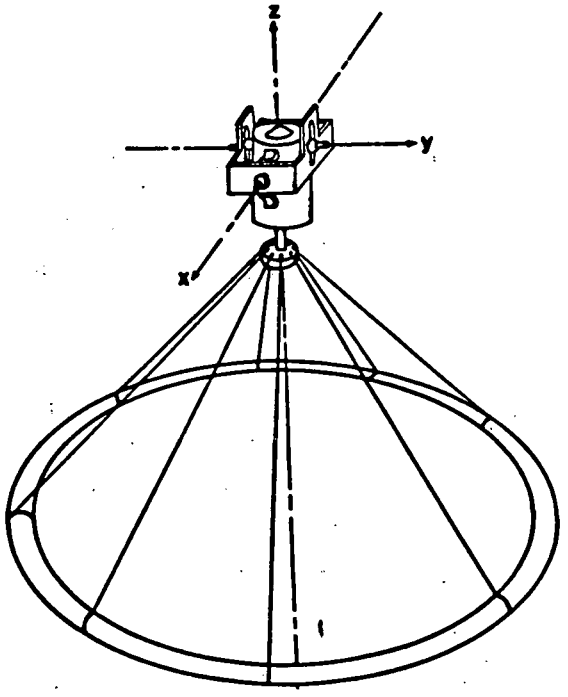

Fig. 5. Gimballed Support System

8.6 kg (19 lb) Dacron flywheel was subsequently spun to 209.3 rad/s (2000 rpm) with no stability problem. It is planned that this rate be increased to 523.4 rad/s (5000 rpm) after strengthening the safety enclosure. If no difficulties are encountered, plans are to place the test stand in an evacuated chamber and spin the flywheel to the maximum capacity of the drive motor.

This contract is scheduled for completion in September, 1979. Results to date indicate that gimball-supporting the flexible flywheel configuration will raise its instability boundary above a reasonably high maximum working speed.

REFERENCES

1. D. W. Robenhorst, "The Applicability of Wood Technology to Kinetic Energy Storage," Johns Hopkins University, Applied Physics Laboratory, APL/JHU Technical Digest, Vol. 11, No. 5, May/June, 1972, pp. 2-12.

2. D. W. Robenhorst, "Composite Flywheel Development Program--Final Report," John Hopkins University, Applied Physics Laboratory, APL/JHU SDO-4616A NSF Grant No. AER 75-20607, May 1978.

3. D. L. Hagen and A. G. Erdman, "Flywheels for Energy Storage: A Review with Bibliography," Design Engineering Technical Conference, Montreal, ASME Paper No. 76-DET-96, September 26-29, 1976.

4. D. G. Ullman and H. R. Velkoff, "The Variable Inertia Flywheel (VIF), an Introduction to its Potential," 1977 Flywheel Technology Symposium Proceedings, October 5-7, 1977, San Francisco, California.

5. D. G. Ullman, "A Variable Inertia Flywheel as an Energy Storage System," Ph.D. Dissertation, Ohio State University, March 1978.

6. J. M. Vance, E. H. Holtzclaw and R. T. Schneider, "A Flexible Flywheel Concept," 1977 Flywheel Technology Symposium Proceedings, October 5-7, 1977, San Francisco, California.

7. J. M. Vance, "A Concept for Suppression of Nonsynchronous Whirl in Flexible Flywheels," Proceedings of the 1978 Mechanical and Energy Storage Contractors' Review Meeting, October 24-26, 1978, Luray, Virginia.

THIS PAGE

WAS INTENTIONALLY

LEFT BLANK

Dup

PROJECT SUMMARY

Project Title:	"A Flywheel Energy Storage and Conversion System for Photovoltaic Applications."
Principal Investigator:	Alan R. Millner
Organization:	Massachusetts Institute of Technology Lincoln Laboratory Energy System Engineering Group P.O. Box 73 Lexington, Massachusetts 02173 617-862-5500
Project Goals:	To develop a flywheel system to store electrical output from a photovoltaic array and convert it to regulated 60 Hz AC for use in residences or load centers, and to analyze its performance, worth, and cost.
Project Status:	Scaling laws have been developed for a baseline design residential scale system. From these a subscale model has been designed, and parts are now 75% fabricated. These include a steel rotor, magnetic bearings, ironless armature motor generator, vacuum and containment housing, and electronics. System testing will begin in November 1979. System analysis has produced an energy budget for the system and an advance in the treatment of whirl modes of such a system. Economic analysis of the system for residential and load center sizes is divided into user worth analysis and manufacturing cost studies. User worth analysis is nearly complete, while cost studies are now under way.
Contract Number:	EY-76-C-02-4094-A002
Contract Period:	FY'79
Funding Level:	$560K
Funding Source:	U.S. Department of Energy jointly by Division of Energy Storage Systems and Division of Distributed Solar Technology.

COO-4094-57

A FLYWHEEL ENERGY STORAGE AND CONVERSION SYSTEM FOR PHOTOVOLTAIC APPLICATIONS*+

Alan R. Millner
MIT Lincoln Laboratory
P. O. Box 73
Lexington, Massachusetts 02173

ABSTRACT

Progress is described on a project to develop a flywheel energy storage unit for use with photovoltaics in residential or load center applications. The unit employs a high-efficiency permanent-magnet motor-generator and cycloconverter electronics to convert DC input to regulated AC output. It also tracks the maximum-power operating point of the solar array. Magnetic bearings are used to support the motor.

The project includes fabrication of a scale model unit, scaling laws for residential and intermediate load center sizes, and worth and cost estimation. Fabrication of a subscale model is 75% complete. Scaling laws have been developed for components and user worth studies performed for this unit; manufacturing cost studies are in progress.

INTRODUCTION

Over the past year MIT/Lincoln Laboratory has been working on a flywheel interface and storage technology (FIST) project to develop a system with the following major components:

Magnetic bearings
Motor generator
Low cost rotor (not part of the project)
Power conditioning electronics
Vacuum housing.

This unit is intended to be a complete interface between a solar photovoltaic (PV) array and an AC load. Applications include a single residence and a 100-kW load center as point designs, with emphasis on the residence as the first and smallest use. The project includes three major tasks[1].

1) To develop scaling laws for designs of a residential and 100-kW load center system.

2) To build a scale model working system.

3) To estimate cost and worth to potential users of a residential and a 100-kW load center system.

---

*This work was sponsored by the U.S. Dept. of Energy.

+Progress Report For the Mechanical and Magnetic Energy Storage Annual Review, 19-22 August 1979, Washington, DC.

The system concept is shown in an artist's sketch in Fig. 1. Design trade-offs showed advantages of a simple rotor interface with a lightweight, inexpensive supporting structure in the choice of bearings above and rotor below. The key system elements are shown in the design layout illustrated in Fig. 2.[2] Magnetic bearings are at the top, motor-generator below them, and the flywheel rotor attached by a quill shaft.

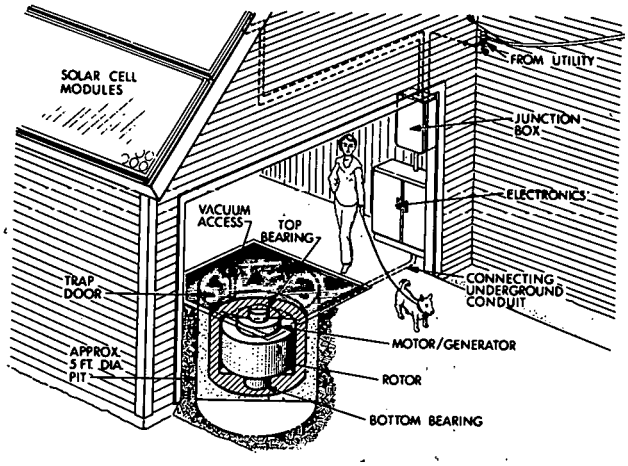

Fig. 1. Residential System Concept

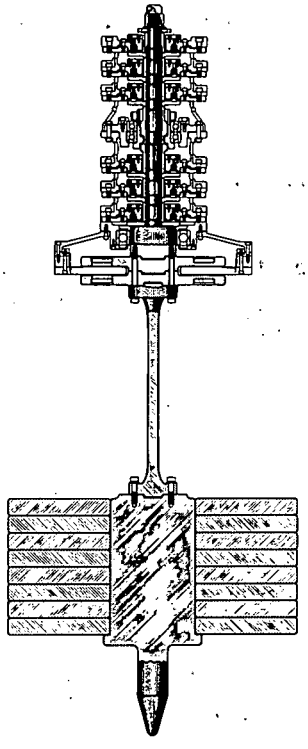

Fig. 2. Subscale System Design Layout

Scaling laws have been derived and will be reported soon. Major conclusions are that the motor-generator and flywheel rotor scale upward with constant shape factor and charge-discharge rate. Scale of the magnetic bearings is slightly different, with the permanent-magnet size growing slowly in relation to the rotor size up to the residential scale. Above this size an electromagnet design should replace the permanent magnet because the resistive losses for a load center application are negligible. At a still larger scale, a combined bearing and motor-generator without permanent magnets becomes feasible but has not been designed in detail. Scaling of system parameters is given in Table 1, while component scaling is given in Table 2.

TABLE 1. Flywheel System Parameters

Parameters	Units	Subscale	40-kWh Residence	500-kWh Load Center
Energy stored	kWh	1 to 4	40	500
Energy available	kWh	.6 to 2.5	25	325
Power input	kW	0.50	8	100
Power output	kW	.625	10	100
Input voltage max. volts	DC	400	400	800
Input current max. amps.	DC	2.5	40	260
Output voltage RMS volts	AC	110	220 c.t.	440
Max. output current FMS amps. per phase		5.6	45	130
Phases	NO.	1	1	3

TABLE 2. Component Point Designs

	Prototype	Residence	Load Center
Rotor			
weight, lb.	500	4000	500,000
diameter, in.	20	36	84
length, in.	20	36	84
max. speed, KRPM	15	15	6.5
Motor/Generator			
peak power, kW.	.625	10	100
avg. power, kW.	.500	8	100
diameter, in.	8	16	34
magnet weight, lbs.	1.1	8.7	108
Magnetic bearing-6 per system			
diameter, in.	3.2	9	32
gap, mils	18	30	57
Nominal dissipation, watts			
perm. magnet design	4	4	4
electromagnet design	300	300	300
50/50 design	72	72	72
PM design			
magnet weight, lbs.	.72	9.6	228
Electronics			
crossover frequency w_cHz	30	23	16
max. switching freq, kHz	1.25	1.25	.54

User worth studies are nearly complete for both sizes and will be reported at a future date. Major results are as follows:

1) Optimum flywheel usable storage capacity in stand-alone systems for a given solar array size is approximately 2 to 4 hours times the array peak rating (energy capacity measured at the system output). As the price of diesel fuel rises, the optimum size of both array and flywheel increases.

2) Storage is desirable at a utility-interactive site only if less than 50% buy-back rates are available on a flat-rate basis. Time-of-use pricing modifies this conclusion.

3) Choice of a stand-alone with diesel backup and storage or a utility-interactive system design without storage is determined by distance from the electric utility, with the cost of interconnection exceeding the benefits between 5 and 15 miles distance, depending on cost assumptions.

Manufacturing cost studies are now being conducted.

The subscale system rotating hardware is shown in Fig. 2. The status of each component is described below:

1) Rotor and containment system: no bids were received for a test (steel) rotor and containment system, so an in-house design has been completed and is now in fabrication. This resulted in a two-month project schedule slip, reported previously. The design will be available to other experimenters.

2) Magnetic bearings have been fabricated. An error in the numerical analysis resulted in a design with excessive leakage and resulting low lifting force. Adjustment of magnetic air gap and reduction of total rotor weight from 500 to 390 pounds has been chosen to permit system testing; a redesigned bearing with full lifting capacity and air gap will be built later to verify the design.

3) Motor-generator fabrication is 90% completed with no technical problems.

4) Cycloconverter electronics have been fabricated and 80% tested on a simulated motor-generator. A design improvement permits operation below design spread with increased harmonic content.

5) Motor-drive electronics are 60% fabricated. The microprocessor-controlled maximum-power-point tracker has been completed and tested.

6) System dynamics analysis has proceeded by simulation. A generalized flywheel whirl stability criterion has been derived, and an application method has been developed which uses linear non-rotating vibrational modes of the system from standard finite element programs. Calculations of damping and torque requirements have been made to traverse whirl modes of the system during initial spin-up. By design, there are no whirl modes in the operating speed range of the system, as shown in Fig. 3.

7) Test system (vacuum tank and support structure) modifications are in progress. These include fabrication of the containment ring and its supports, and are the pacing items on project schedule.

Initial system testing is scheduled to begin in November 1979.

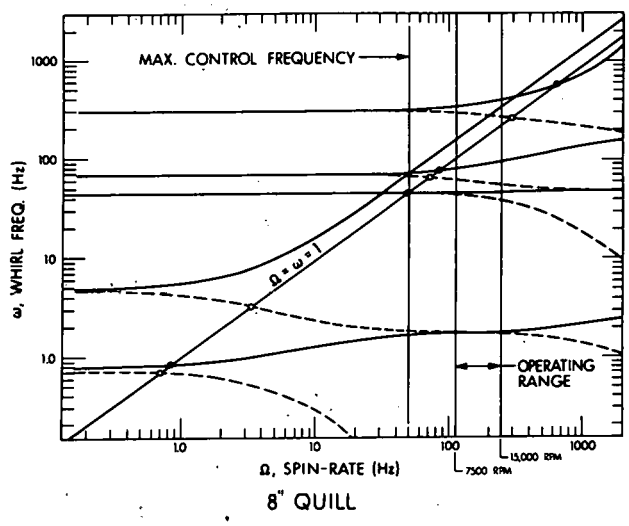

Fig. 3. Spin-Whirl Dynamics.

The predicted system efficiency is calculated from an energy budget for the residential system, shown in Table 3. Using a load profile from the G.E. PV Residential System Design Study[3] and two possible solar input profiles, both giving an energy balance over a day, the system energy round-trip efficiency is approximately 70%. This figure is not very sensitive to details of the input/output profile, as Figs. 4 and 5 show, due to the high efficiency of the input/output equipment.

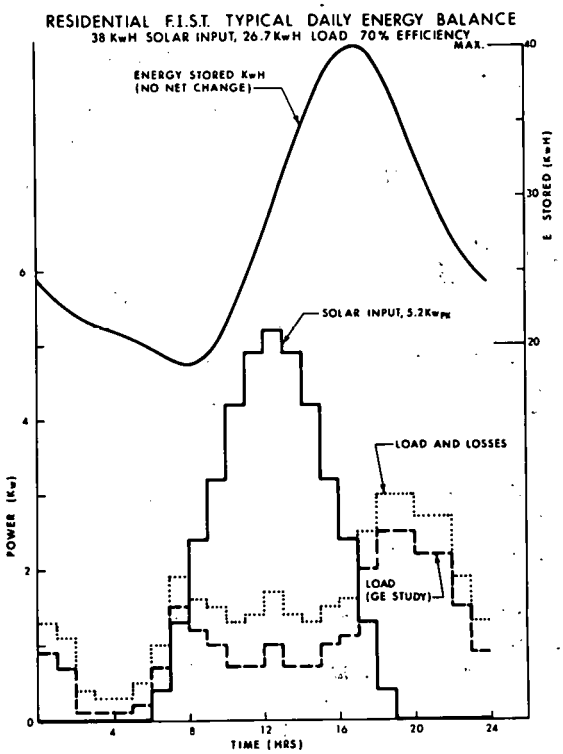

Fig. 4. Load Profile A

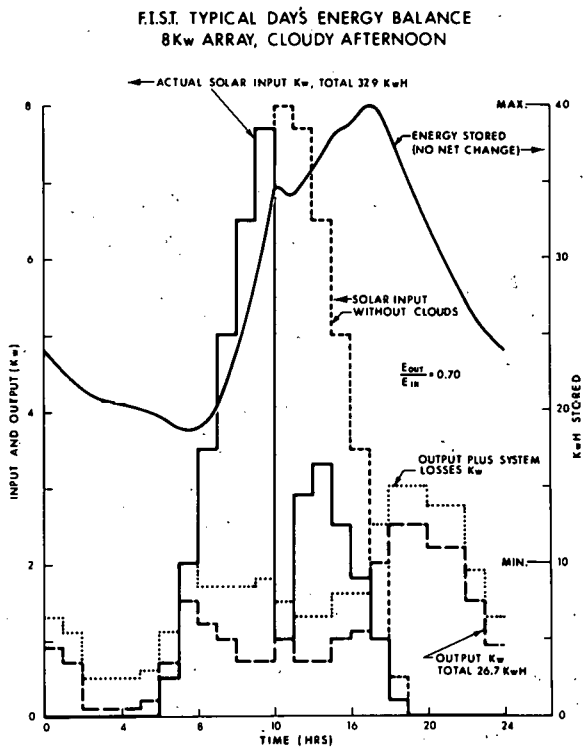

Fig. 5. Load Profile B

TABLE 3. FIST Energy Storage

Fixed loss	200 watts (2% of full load)
Storage loss	0.3% per hour
Input electronics	
Full load	8%
Half load	7%
Output electronics	
Full load	8%
Half load	7%
M/G Loss (input-output)	
Full load	4%
Half load	2%

[a]No vacuum pump power has been assumed.
[b]A 5-micron vacuum level is assumed.
[c]A residential vacuum system might require 160 watts.

In the future, MIT/Lincoln Laboratory hopes to investigate on a subscale basis the implications of:

- Utility-interactive flywheel electronics
- Dynamics effect of low-cost rotors.

Also MIT/Lincoln Laboratory hopes to build a residential-sized system based on the result of this work, assuming that cost analysis results are favorable.

REFERENCES

1. A. R. Millner, "A Flywheel Energy Storage and Conversion System for Photovoltaic Applications," COO 4094-48, International Assembly on Energy Storage, Dubrovnik, 28 May - 1 June 1979.

2. A. R. Millner, R. D. Hay, "Flywheel Energy Storage Interface Unit for Photovoltaic Applications," COO 4094-44, 14th Intersociety Energy Conversion Engineering Conference, Boston, 5-10 August 1979.

3. E. J. Buerger *et al.*, "Regional Conceptual Design and Analysis Studies for Residential Photovoltaic Systems," SAND78-7039, Tech. Vol. II, prep. for Sandia Laboratories by General Electric Space Division, Philadelphia, January 1979.

SESSION 5: FLYWHEELS

THIS PAGE

WAS INTENTIONALLY

LEFT BLANK

PROJECT SUMMARY

Project Title: Mechanical Energy Storage Technology Project

Principal Investigator: Thomas M. Barlow

Organization: Lawrence Livermore Laboratory
P. O. Box 808, Mail Stop L-388
Livermore, CA 94550
(415) 422-8200

Project Goals: The goals of this project are to develop and evaluate mechanical energy storage for both vehicular and photovoltaic/wind applications and to maximize the commercialization potential of the technology.

Project Status: The Lawrence Livermore Laboratory's (LLL) efforts in the development of mechanical energy storage technology (MEST) were initiated in FY75. Our early efforts involved the development and characterization of fiber-composite materials for use in light performance flywheels.

In FY1977 and FY1978, respectively, the Project expanded to include (1) technical management of the development MEST technology for application to electric and hybrid vehicles and (2) evaluation of the laminated disc rotor concept. Funding in the former area was provided under the Electric and Hybrid Vehicle RD&D Act of 1976 (Public Law 94-413).

In FY1979, the project was expanded as the Sandia Laboratory in Albuquerque (SLA) began to transfer its activities to LLL. Included in this transfer are the technical management responsibility for flywheel rotor and mechanical component technology areas, as well that for photovoltaic and wind energy systems applications.

The project consists of into six tasks, as listed below. The estimated FY1979 expenditure levels for each task is included; these estimated costs do not include the work reported separately by SLA.

o Transportation Applications	$1,321,000
o Photovoltaic/Wind Applications	$36,000
o Fiber Composite Materials Characterization	$310,000
o Flywheel Rotor Technology	$520,000
o Component Technology	$213,000
o Project Management and DOE Support	$175,000

For the most part, the Project's activities emphasize subcontracts to private industry. In-house activities include technical management, material characterization, and tapered-thickness rotor concept evaluation.

Contract Number: W-7405-Eng-48

Contract Period: Continuing

Funding Level: $845,000 FY1979 B/O from E&HV Program
$1,730,000 FY1979 B/O from Energy Storage Program

Funding Source: U. S. Department of Energy

THIS PAGE

WAS INTENTIONALLY

LEFT BLANK

PROJECT SUMMARY

Project Title:	Mechanical Energy Storage Technology Development
Principal Investigator:	R. O. Woods
Organization:	Sandia Laboratories Albuquerque, NM 87185 (505) 264-7553
Project Goals:	The selection of those mechanical components of flywheel energy storage systems that can be carried to their next stage of evolution by efforts within the scope of the budget; the funding of developmental work treating such components. The documentation of the state-of-the-art in component technology where such information is scattered or fragmentary.
Project Status:	Efforts have treated the following components: Rolling Contact Bearings Magnetic Bearings - Active and Passive Composite Wheels - Hardware development, development of analytic and testing techniques, material studies. Composite Materials - Analysis, improved properties, vacuum outgassing properties, fabrication and thermal characteristics. Seals - Power dissipation, lifetimes, permeation rates. Funding has been provided to other agencies for the testing of energy storage systems, and the groundwork has been completed for a program to deal with the problems of vacuum technology.
Contract Number:	SOL 78
Contract Period:	FY79
Funding Level:	$980 K*
Funding Source:	DOE, Division of Energy Storage Systems

*Included in this project are the following:
"Rotor Analysis," Keith Miller.
"Flywheel Rotor Analysis," Arlo Nord.

SANDIA ACTIVITIES OVERVIEW

R.O. Woods
Sandia Laboratories
Advanced Energy Projects
Division 4715
Albuquerque, NM 87185

ABSTRACT

This presentation will mention all Sandia efforts in the field of components development during FY79. Particular emphasis will be placed upon activities not reported at the October 1978 review meeting. A complete list of the publications that were generated during the reporting period is included here and will be presented as a handout during the verbal presentation.

INTRODUCTION

This program can most logically be discussed in terms of the four main tasks listed in Viewgraph 1. Table I, which is included in the handout but not reproduced as a viewgraph, lists all the contracts that were active during FY79.

A. 40 WATT-HR/LB COMMERCIAL WHEELS

The largest single item in order of cost was the placing of contracts for the development of composite wheels with a nominal energy density of 40 watt-hr/lb. A strenuous effort was made to bring this part of the program to the attention of all potential suppliers; it was hoped that some new sources would be developed. A note was placed in Commerce Business Daily for December 8, 1977, soliciting expressions of interest. Twenty-three replies were received, of which nineteen were credible candidates. A request for proposals was circulated to those nineteen. Four contracts were placed in August 1978 after proposals had been evaluated by a panel of five Sandia persons working in relevant fields. The successful bidders (Viewgraph 2) were:

1. Garrett AiResearch

This organization proposed a design that was a logical continuation of work that had been done for the Army Mobility Equipment Research and Development Command (MERADCOM). Final testing of the original MERADCOM design had been partly supported by DOE via a Sandia Federal Agency Order. (The wheel was successfully spun to its design speed in September 1978, when a peripheral speed of 2800 FPS was reached. Energy density at this speed was 26 Whr/lb; an impressive level in itself, but all the more significant since much of the weight of the wheel was in a brute force hub/spoke assembly that was used solely to test the rim.) The unique feature of this design is a rim that is wound in concentric layers, isolated from one another by films of teflon which cripple their bending stiffness. This allows the rim to be pressed on the cruciform spoke assembly by deforming it into a slightly square ("subcircular") shape. The same concept was used on the successfully tested rim. Spokes and hub of the present design are formed by using a carbon-filament structure.

The program was concluded on schedule. As of July, we are awaiting delivery of the hardware. The effort was documented in Reference 1. (The list of publications is included in the handout but not shown as a viewgraph.)

2. Rockwell International

The Rockwell design is based upon an earlier version that had been developed for use in spacecraft as an energy-storage and inertial flywheel. Hardware delivery is scheduled near the end of FY79.

3. Hercules

The Hercules wheel is unique in that it is essentially monolithic, with the mass concentrated near the periphery. This gives a very high volumetric energy density. Emphasis is placed upon use of a polysulfone matrix, rather than the more common but less elastic epoxy, to minimize transverse stresses. As with the Garrett wheel, hub attachment is via an elastomeric bond. Hardware delivery is scheduled near the end of FY79.

4. William M. Brobeck & Associates

The Brobeck design incorporates a rim concept that has become almost traditional. Its unique feature is the use of "tension-balanced" spokes, in which an elaborate design matches radial growth of the spokes to the centrifugal dilation of the rim. Stresses at the spoke/rim interface are thereby held constant. One specimen wheel has been shipped as of July 1979. A second is being fabricated.

B. WHEEL ANALYSIS AND TESTING

This has involved two testing campaigns which took place in R.M. Hargreaves' Livermore spin test facility, as well as extensive analytic work that resulted in publications by members of Sandia's staff and consultants at the University of Oklahoma[2-13] This was a tightly-organized effort in which experiments were used to verify analytic predictions of vibrational modes. The program was coordinated by E.D. Reedy, Sandia Laboratories. The objective was not to develop the ultimate wheel, but rather to perfect analytic techniques that would make it possible to predict the behavior of new wheel designs. For this reason, the test wheels themselves were workhorses rather than high-performance hardware.

As a parallel to the classical mechanics approach taken by the University of Oklahoma group, a finite-element analysis using NASTRAN was implemented at Sandia by A.K. Miller. Corresponding analyses were performed using both techniques, and the results were used for mutual checking. An extremely fruitful dialog has resulted that has led to refinements in both computational techniques. Both sides of the effort will be described in presentations that are scheduled to be given at this conference.

A third experimental approach to investigating vibration has been taken by instrumenting wheels with multiple accelerometers, shocking them, and computer processing the accelerometer outputs in real time. This work was done at Sandia's Albuquerque environmental test facility.[14] Experiments of this kind make it possible to analyze vibrational modes without having to spin the wheels. This provides very cheaply yet another check on the accuracy of prediction models. A video tape presentation will display the technique.

Near the end of CY78, negotiations were begun that were aimed at establishing a flywheel test center, either at Union Carbide's Y-12 plant or at the Applied Physics Laboratory, Johns-Hopkins. The choice of locations has not yet been made.

C. BEARINGS

Two bearings studies (Viewgraph 4) were under way at the beginning of the year; one by Draper Laboratory that treated the next generation of ball bearings as specialized for the vacuum environment, the other by Mechanical Technology, Inc., dealing with a hybrid magnetic suspension. A second contract was placed with MTI later in the year, following an open RFP treating a fully magnetic suspension. The Draper Laboratory report[16] was delivered at the end of CY78 and represents a substantial contribution to mechanical bearing technology. In

it, the characteristics of retainerless ball bearings operating in vacuum were investigated experimentally and a computer model was developed that would predict the operating parameters of such bearings over a range of speeds and loadings. These data are now available for use in trade-off studies comparing mechanical (i.e., ball) bearings to other types.

The MTI contracts were also aimed at producing hard data for trade-off studies. In the first, the details of a hybrid magnetic/fluid-film bearing were worked out with enough elaboration to allow realistic estimates to be made of power consumption, load capability, bearing geometry, and lubrication system characteristics. This work was documented in Reference 17. (As of this writing, release of this document has been held up for patent considerations.)

The second MTI study, which was placed with this contractor after an open RFP failed to locate another vendor, provides similar data for a system in which the entire mass of the rotating assembly is to be supported magnetically. The specific intention was to provide input to systems studies where scaling laws are needed to predict bearing operating parameters for units ranging in capacity from 1 kW-hr and intended for use in vehicles, to 100 kW-hr, intended for stationary applications. In all cases, operation in vacuo is assumed. Particular attention is required to the hardware aspects of the system such as: production costs vs. quantity, scaling laws for significant parameters, sensitivity to acceleration and vibration, maintenance considerations, lifetimes, and environmental problems. The contractor is currently in the process of producing the final version of his report.

D. VACUUM TECHNOLOGY

A number of aspects of vacuum technology relevant to flywheel applications were studied during FY79 (Viewgraph 5). These included a program by Ball Brothers Research that measured the outgassing properties of flywheel composite materials, a study by M. Baer, Sandia Laboratories, of the aerodynamic heating of composite wheels, and a study of shaft seals by the Franklin Institute. A contract was also placed with the Applied Physics Laboratory to study ferrofluidic shaft seals, and R.O. Woods issued a publication that discussed the overall vacuum technology problem.[18] The latter is intended as background material to supplement an RFP, if and when an effort is made to locate a contractor capable of handling the entire program.

It has long been recognized that vacuum environment is necessary for the operation of any high-performance flywheel system, but the acceptable pressures and gas loads due to outgassing of composites were matters for speculation. For want of better information, many workers assumed that an adequately low pressure could be maintained by pumping at infrequent intervals and sealing-off the system. A Sandia-sponsored investigation of outgassing properties of the composite materials used in flywheels has established the magnitude of the gas load. In that study, the outgassing rates of six different materials were measured as a function of time up to 100 hours. Similar data were also taken at elevated temperatures. The data are presented in Reference 19.

The similarities between the conditions that exist at the surface of a composite flywheel and those at the skin of a re-entering spacecraft were exploited to make use of existing Sandia aerodynamic heating codes. Peripheral speeds of composite wheels can range as high as 1000 metres/second -- a reasonable speed for a re-entering sounding rocket. Further, atmospheric pressure in the altitude range where re-entry effects become significant is in the vicinity of 10^{-3} to 10^{-4} torr -- a practical range for the pressure in a flywheel enclosure. When the similarities were brought to his attention, M. Baer was able to capitalize upon them by adapting a computer code that had been developed for re-entry heating calculations. This was used to generate boundary conditions for another code that evaluated the internal temperature fields of anisotropic bodies. Baer's work[20] made it possible to set an upper limit to the pressure at which composite wheels could operate. (For steady-state conditions, this will typically be around 10^{-4} torr.)

It is generally thought that mechanical shaft seals will not be suitable for use in composite wheel systems because of the high running speeds and low tolerance of such systems for leakage. A contract was placed with Franklin Institute Research Laboratories aimed at testing this supposition by documenting the practical range of running speeds determined by wear and power consumption and to establish realistic permeation or leakage rates for present state-of-the-art seals. It was also required that the contractor suggest the most fertile line of development for future seals technology. The results of this study were documented in Reference 21.

Another type of seal is being investigated experimentally by the Applied Physics Laboratory, Johns Hopkins University. This is the so-called "ferrofluidic" seal that uses a magnetic fluid held to a shaft by a magnetic field. The APL program is scheduled to conclude in August.

E. MISCELLANEOUS

Funding was provided to MERADCOM to finish testing a complete flywheel energy storage unit that had been developed by Rockwell as a part of a cancelled program. These tests are to be performed during CY79. This unit embodies a number of engineering innovations and is unique as to size and designed performance levels. The test data will represent a substantial contribution to our knowledge of what is practically attainable in energy storage systems. Tests are to be supervised by L. Amstutz of MERADCOM.

Materials research, aimed largely at improving the transverse properties of composites for flywheel use, was conducted by R.E. Allred of Sandia Laboratories. Means were investigated to modify the properties of a matrix by the addition of a rubbery phase, and to improve the filament/matrix bond. These studies necessitated the development of improved test fixtures, which have greatly reduced scatter in the test data. This work has been documented in Reference 15.

PUBLICATIONS

1. SAND79-7019, "High-Energy-Density Composite Flywheel," AiResearch Manufacturing Co. of California, April 11, 1979, Contractor's Final Report.

2. SAND78-7070, "Lateral and Tilt Whirl Modes of Flexibly Mounted Flywheel Systems," The University of Oklahoma, November 17, 1978.

3. SAND78-7073, "Whirling Response and Stability of Flexibly Mounted, Ring-Type Flywheel Systems," The University of Oklahoma, December 12, 1978.

4. SAND78-7049, "Critical Speeds and Natural Frequencies of Rim-Type Composite-Material Flywheels," The University of Oklahoma, November 9, 1978.

5. "Design of Spoked-Rim Composite Flywheels," E.D. Reedy, Jr. and F.P. Gerstle, Jr., Proc. 1977 Flywheel Technology Symposium, San Francisco, CA, October 5-7, 1977.

6. "A Composite-Rim Flywheel Design," E.D. Reedy, Jr., Proc. 23rd National SAMPE Symposium and Exhibition, Anaheim, CA, May 2-4, 1978, SAMPE Quart. 9, (3), p. 1, April 1978.

7. "Model Analysis of Stable Crack Growth," E.D. Reedy, Jr., Eng. Frac. Mech. 10, (2), 1978.

8. "Sandia Composite-Rim Flywheel Development," E.D. Reedy, Jr., Proc. 1st Annual Mechanical and Magnetic Energy Storage Contractors' Information-Exchange Conference, Luray, VA, October 24-26, 1978.

9. "Composite-Rim Flywheels: Spin Tests," E.D. Reedy, Jr. and H.K. Street, submitted for publication 2/29/79, SAMPE Quart.

10. "Prediction of Creep Behavior for Filamentary Composites Under Stress Conditions Encountered in Flywheels," C.W. Bert and T.L.C. Chen, Proc. of the 1977 Flywheel Technology Symposium, San Francisco, CA, October 5-7, 1977, DOE CONF-771053, March 1978, pp. 291-298.

11. "Critical Speed for Standing-Wave Instability in a Filament-Wound-Composite Ring-Type Flywheel," C.W. Bert, Proc. of the 1977 Flywheel Technology Symposium, San Francisco, CA, October 5-7, 1977, DOE CONF-771053, March 1978, pp. 429-433.

12. "On Vibration of a Thick Flexible Ring Rotating at High Speed," C.W. Bert and T.L.C. Chen, Journal of Sound and Vibration, Vol. 61, no. 4, December 22, 1978, pp. 517-530.

13. "Research on the Dynamics of Band-Supported Flywheel Systems," C.W. Bert, C.A. Kocay, T.L.C. Chen, and J.P. Busby, Research Report OU-AMNE-78-8, November 1978; also Sandia Laboratories Report, SAND78-7074, February 1979.

14. Sandia Test Report #060564, "Modal Analysis of Two Composite Flywheels," A.R. Nord and C.M. Grassham, January 1979.

15. "Improvement of Transverse Composite Strengths: Test Specimen and Materials Development," R.E. Allred, H.K. Street, and R.J. Martinez, Proc. 24th National SAMPE Symposium and Exhibition, San Francisco, CA, May 8-10, 1979, pp. 31-50.

16. SAND79-7003, "Final Report on the Development of an Advanced Flywheel Bearing Performance Model," The Charles Stark Draper Laboratory, Inc., January 12, 1979.

17. SAND79-7007, "Application of Magnetic Suspensions and Fluid Film Bearings to Energy Storage Flywheels," Mechanical Technology, Inc., January 1979.

18. SAND78-0944, "Vacuum Technology Requirements for Flywheel Energy Storage," R.O. Woods, August 1978.

19. SAND78-7075, "Outgassing Tests of Fiber/Epoxy Composite Materials," Ball Brothers Research Corp., Aerospace Division, December 13, 1978.

20. SAND78-0957, "Aerodynamic Heating of High-Speed Flywheels in Low-Density Environments," M.R. Baer, October 1978.

21. SAND79-7011, "Seal Studies for Advanced Flywheel Systems," Franklin Research Center, February 1979.

22. "Use of Polymeric Materials in Energy Storage Systems," J.H. Swisher, in: Polymer Materials Basic Research Needs for Energy Applications, Proc. of Workshop, Case Western Reserve University, Cleveland, OH, June 27-29, 1978.

23. Report #ALO-41/1, "Study of Heat Engine/Flywheel Hybrid Propulsion Configuration with Electrical Transmission System," AiResearch Manufacturing Co., Division of the Garrett Corporation, April 1978.

24. SAND79-1151, "Mechanical Energy Storage Technology Development -- Annual Report," R.O. Woods, July 1979.

TABLE I. Contracts Active During FY79

Contractor and Description	Sandia No.	Status (8/1979)	Start Date
Brobeck Wheel	07-0291	Active	7/78
Hercules Wheel	07-0292	Active	7/78
Garrett Wheel	07-0293	Concluded	7/78
Rockwell Wheel	07-6955	Active	7/78
Draper Labs Bearings	07-6996	Concluded	10/77
MTI Hybrid Bearings	07-6997	Concluded	1/78
MERADCOM Garrett	07-7095	Concluded	1/78
Franklin Institute Seals	07-7141	Concluded	1/78
MTI Magnetic Bearings	07-7142	Active	4/78
Ball Brothers Outgassing	07-7150	Concluded	1/78
University of Oklahoma (1979)	13-3832	Active	10/78
MERADCOM Rockwell	13-2369	Active	12/78
APL (J-H) Seals	13-2396	Active	12/78

Viewgraph 1

MAJOR TASKS

40 WATT-HR/LB WHEELS

WHEEL ANALYSIS AND TESTING

BEARINGS

VACUUM TECHNOLOGY

Viewgraph 2

40 WATT-HR/LB WHEELS

BROBECK

HERCULES

GARRETT

ROCKWELL

Viewgraph 3

WHEEL ANALYSIS AND TESTING

SLA IN-HOUSE PROGRAMS:

- SPIN TESTS
- MODAL ANALYSIS
- NASTRAN

UNIVERSITY OF OKLAHOMA

Viewgraph 4

BEARINGS

MAGNETIC

- MTI HYBRID
- MTI FULLY-MAGNETIC

MECHANICAL

- DRAPER LAB RETAINERLESS BALL BEARING

Viewgraph 5

VACUUM TECHNOLOGY

OUTGASSING

- BALL BROTHERS RESEARCH

SEALS

- FRANKLIN INSTITUTE
- APPLIED PHYSICS LABORATORY

AERODYNAMIC HEATING

- SLA

Viewgraph 6

MISCELLANEOUS

MERADCOM TESTS

MATERIALS STUDIES

PROJECT SUMMARY

Project Title: Analysis of Composite-Material Flywheels for Vehicle Applications

Principal Investigator: Charles W. Bert

Organization: University of Oklahoma
School of Aerospace, Mechanical and Nuclear Engineering
Norman, Oklahoma 73019

Project Goals: To develop analytical capability to predict dynamic behavior of rim-type flywheels supported by flexible bands in two configurations: spin-test configuration (quill shaft) and vehicle configuration (end-supported), to correlate predictions with spin-test results, to suggest design changes to improve dynamic behavior, to investigate effects of nonlinearity of support bands, and to investigate analytically problems of containment after band failure.

Project Status: The following linear analyses have been completed for the quill-shaft system: free whirling, stability, and forced whirling (response to rim unbalance and initial tilt). The results have been correlated with spin-test results and certain design improvements have been suggested to improve the dynamic behavior of the system. The effects of a variety of vehicular support parameters (end-supported flywheel shaft) have also been investigated.

A string-column model has been devised to simulate the nonlinear action of the supporting bands connecting the rim to the hub. This model has been used to determine radial restoring force and tilting moment as a nonlinear function of running speed, relative radial displacement, and relative tilting angle. A Runge-Kutta numerical-integration procedure has been devised to determine the time response of the complete system including the nonlinear action.

Regarding containment, some preliminary calculations have been made involving both strength and frictional heating due to rubbing of the rim against the containment housing after failure of the supporting bands. It is difficult to utilize these results until some experimental measurements are made on impact dynamics and heat generation in these material combinations at these speeds.

Contract Number: 07-7843; 13-3832

Contract Period: Dec. 1, 1977-Nov. 30, 1978; Dec. 1, 1978-Sept. 30, 1979

Funding Level: $38 K; $33.6 K

Funding Source: U.S. Department of Energy, through Sandia Laboratories, Albuquerque, NM

ROTOR DYNAMICS:
DYNAMICS OF RIM-TYPE FLYWHEELS SUPPORTED BY FLEXIBLE BANDS

Charles W. Bert
School of Aerospace, Mechanical and Nuclear Engineering
The University of Oklahoma
Norman, Oklahoma 73019

ABSTRACT

Certain high-performance, composite-material flywheel systems for energy storage on vehicles differ significantly from turbine/compressor systems in two respects: the flywheel rim attachment to its hub is very flexible (especially in tilting) and these flexibilities depend upon rotational speed through centrifugal stiffening. This paper describes analysis of free whirling, suggestions for design improvements, stability analysis, response to unbalance and initial tilt, and nonlinear analysis of supporting-band action.

INTRODUCTION AND BACKGROUND INFORMATION

As part of the national effort to conserve petroleum as an energy source, there is interest in storing energy in hybrid automotive vehicles, especially for short-distance, start-stop vehicles such as urban cars, delivery vehicles, etc. One candidate mechanical means of storing energy in such a vehicle is a flywheel. Most flywheels developed to date have been rather heavy, rigid ones made of conventional, homogeneous, isotropic materials, such as high-strength steel. However, with the development of advanced filamentary composite materials, there is considerable promise in the use of these materials in view of their high strength-to-weight values, since the energy storage per unit weight is directly proportional to this parameter. Another advantage is the less catastrophic nature of the failure of such flywheels; this advantage allows a lighter flywheel containment system.

One design concept to achieve high energy storage per unit weight is to have the composite flywheel mass concentrated at fairly large radius (rim) and run at high speed (>30,000 rpm). High speed causes difficulties in attachment to the power-transmitting hub; thus, the attachment must also be of composite material. Composite material in turn results in a very flexible attachment, which causes quite different dynamic problems than those encountered previously in rotating machinery such as turbines and compressors.

In this investigation, the dynamic phenomenon of the whirling mode, generally recognized as one of the most catastrophic ones associated with rotating machinery, is carefully examined. Apparently the only previous analyses in the literature concerning the whirling dynamics of rim-type flywheels existing are due to McKinnon[1] and Bert and Chen[2]. McKinnon considered free whirling of a two-mass system having three degrees of freedom: hub tilting, hub translation, and rim tilting. In Ref. 2 these flexibilities were considered plus the radial flexibility of the hub-flywheel connector.

In the present work, free whirling, forced whirling, and stability analyses are studied for a four-mass, eight degree-of-freedom believed to be the most appropriate model to describe the Sandia flywheel[3] as installed in a quill-shaft, air-turbine-drive test facility.

The Sandia Laboratories experimental flywheel prototype (Fig. 1), for which the present analyses are intended to be applied, has a thick rim of hoop-wound graphite-epoxy attached to a

central aluminum hub by radially wound bands of aramid-epoxy (Fig. 2). The hub is attached to the turbine through a relatively flexible steel flywheel shaft (a quill shaft cantilever-mounted, at the top, inside the turbine shaft). The steel turbine shaft is supported on two ball bearings and carries the air-driven turbine. An external damper is located between the lower bearing and hub on the flywheel shaft. In Ref. 3, Reedy predicted that the design energy-storage goal of 0.56 kwh (49.4 watt-hr/kg) is achieved at a rotational speed of 32,000 rpm and that the governing material strength is reached at 39,850 rpm.

PROJECT DESCRIPTION AND RESULTS

HYPOTHESES

In the analyses presented here, the principal engineering assumptions are:

1. The bearings (ball bearings) are isotropic and act as simple supports.
2. All rotating components are geometrically axisymmetric, but provision is made for rim mass-center eccentricity (static unbalance) and tilt.
3. In the main analyses, all nonlinear effects are neglected. (However, in the latter part of the paper, string/column action of the bands is investigated.)
4. Although the shaft is vertical, pendulum action is small.
5. The shafts and bands are modeled as discrete, massless elements with elasticity and material damping; the damper is assumed to have viscous damping.
6. The flywheel rim, flywheel hub, turbine disk, and damper are considered as discrete rigid bodies. (For the flywheel rim this was confirmed in an earlier contract[4], where it was found that the lowest natural frequency is 56,900 cpm.)

FREE WHIRLING AND SUGGESTED DESIGN IMPROVEMENTS

When a shaft with a rigidly attached rotor, overhung with respect to its supports, is rotated at constant speed, the centrifugal force produced by an eccentricity causes the disk to tilt with respect to the axis of rotation. This tilting action, in turn, produces a gyroscopic couple about the diametral axis of the disk. The sense of the gyroscopic couple is such that it effectively stiffens the shaft at the speeds associated with forward precession and reduces the effective stiffness at the speeds associated with retrograde (or backward) precession.

In the Sandia thick-rim flywheel (Fig. 2)[5], the rim is connected to the hub by means of relatively flexible bands, in contrast to the usual case for overhung compressor disks which customarily are rigidly attached to the shaft. Thus, it is clear that the rim and hub should be considered as two different masses rather than a single one. Except for Refs. 1 and 2 all existing multi-mass disk-shaft system analyses are applicable only to the case when the flexible members connect to ground. In the case of the Sandia flywheel mounted in the spin-test facility, a flexible member (the bands) connects to an otherwise free mass (the flywheel rim).

In the whirling analysis, each rotor has two generalized displacements associated with translation (r) and rotation (ϕ). For the flywheel depicted schematically in Fig. 1, there are eight generalized displacements $\{q_i\} = (r_r, \phi_r, r_h, \phi_h, r_t, \phi_t, r_d, \phi_d)^T$. The subscripts r, h, t, and d refer to the rim, hub, turbine, and external damper, respectively. The corresponding generalized forces are $\{Q_j\} = (F_r, M_r, F_h, M_h, F_t, M_t, F_d, M_d)^T$. The connecting equations can be written in matrix form as follows:

$$\{Q_i\} = [K_{ij}]\{q_j\} \quad ; \quad i, j = 1, 2, \ldots, 8 \tag{1}$$

where $[K_{ij}]$ is the stiffness matrix. Derivation of the compliance matrix, from which $[K_{ij}]$ can be obtained by inversion, was presented in Ref. 5, Appendix E.

Assuming normal-mode whirling with frequency ω, one seeks the following solutions:

$$\{q_i\} = \{\bar{q}_i\} e^{i\omega t} \quad ; \quad i = 1, 2, \ldots, 8 \tag{2}$$

where $\bar{q}_i$ is the amplitude of q_i. Putting Eq. (2) into Eq. (1), one gets the homogeneous linear

algebraic equation set

$$\{[K_{ij}] + [N_{ij}]\omega - [M_{ij}]\omega^2\}\{\bar{q}_i\} = 0 \qquad (3)$$

where $[M_{ij}]$ and $[N_{ij}]$ are 8x8 matrices.

Equation (3), referred to as a generalized eigenproblem, can be reduced to the standard-type eigenproblem by use of an appropriate transformation. Solving the eigenvalue problem, one can obtain modal frequencies as a function of the rotational speed. Plots of these relationships are shown in Fig. 3 for both the forward and the retrograde branches. The intersections of the ω vs. Ω curves with straight lines of the form $\omega = n\Omega$ determine the so-called critical speeds (Ω_{cr}) which correspond to the values of running speed Ω at which dynamic instability may take place. The value $n(= \omega/\Omega)$ is called the order of the critical speed and it is usually either a positive or negative integer or its reciprocal. Lines corresponding to $n = \pm 1$ and $n = \pm 2$ are shown in Fig. 3.

Most investigators have emphasized the first order (n=1) critical speeds; some claim that backward-precession critical speeds are less dangerous than forward-precession ones. However, Yamada[6] observed experimentally retrograde as well as forward critical speeds of orders up to 8, and Thomson et al.[7] detected several critical speeds of both retrograde and forward orders. In Fig. 3 there are shown four first- and at least four second-order forward critical speeds in the rotational speed range up to 50,000 rpm. The first-order critical speeds occur at about 700, 7,600, and 38,100 rpm. In contrast, the experience of Refs. 1 and 7 suggest that higher-mode forward critical speeds of second order are most dangerous. It is noted that the amplitude ratios ϕ_r/ϕ_h and r_r/r_h increase rapidly as the running speed approaches the fourth-mode, second-order forward critical speed (approximately 24,200 rpm). This is consistent with comparison be-between the present results and the experimental results in Ref. 8 as discussed below.

The major differences in System B (twisted bands) as compared to System A are smaller out-of-plane band compliance and larger hub mass and axial moment of inertia (m_h, J_{mh}). It appears that this calculated fourth-mode, second-order forward critical speed was not associated with the excessive amplitudes which occurred during spin tests in the vicinity of 29,000-30,000 rpm. Exactly which critical speed is most important is less certain. However, there is a distinct possibility that it is a first-order forward one at the second mode. Further comparisons with experimental results may be found in Ref. 5.

One of the objectives in designing the flywheel systems is either to eliminate the critical speeds, if possible, in the operating speed range or to move them beyond the maximum operating speed. In the Sandia System A and B designs, the two most dangerous critical speeds are the first-order forward one at the second mode, $(\Omega_{cr})_{12}$, and the second-order forward one at the fourth mode, $(\Omega_{cr})_{24}$. In view of the nearly identical performance of Systems A and B, it is practically sufficient to present numerical results for only one system since these results are applicable to the other system with an error of less than 0.5%.

Practical ways to increase $(\Omega_{cr})_{12}$ are: to increase the flexural rigidity (EI_s) of the flywheel shaft, to decrease the hub's diametral mass moment of inertia, and to increase the angle of the bands with respect to the plane of the rim, $\tilde{\phi}$. It was found that $(\Omega_{cr})_{24}$ is unaffected, but $(\Omega_{cr})_{12}$ is increased by approximately 3% for each one-degree increase in $\tilde{\phi}$, $(\Omega_{cr})_{12}$ is increased by approximately 18% when I_{mh} is reduced by 20%. Critical speed $(\Omega_{cr})_{24}$ remains unchanged for the above two cases and for the case even when I_s and $\tilde{\phi}$ are increased simultaneously. In order to increase critical speed $(\Omega_{cr})_{24}$, it is necessary to increase the stiffnesses of the flywheel shaft and turbine shaft as well as the angle $\tilde{\phi}$ simultaneously. When the foregoing three parameters are doubled simultaneously, critical speed $(\Omega_{cr})_{24}$ is increased from 24,200 rpm to 31,800 rpm and $(\Omega_{cr})_{12}$ is increased from 38,100 rpm to 41,700 rpm.

In addition to the work just described for the Sandia flywheel in the spin-test facility, a series of computations[9] was carried out for the Sandia design mounted between ball-bearing supports, more typical of a vehicular mounting. Twenty-six different combinations of the following parameters were investigated: hub location along the shaft, upper and lower bearing-pedestal

spring constants, and the area moment of inertia of the shaft. Of the 26 cases considered, twenty were deemed to be satisfactory from a dynamic standpoint, in that they had no forward-precession critical speeds of first- or second-order in the desired operating speed range of 3,000 to 32,000 rpm.

STABILITY ANALYSIS

Internal friction (damping) acts in rotating shafts provided that the whirling speed is different from the shaft rotational speed. Internal friction has the effect of resisting shaft motion and causes energy dissipation. It is well known that internal damping reduces the amplitude of a non-rotating vibrating system and thus stabilizes such a system. In rotating machinery, however, if the rotational speed is above the lowest first-order critical speed, the effect of internal damping is reversed, i.e., the amplitude of whirling vibration gradually builds up and finally leads to an unstable motion.

One can bring internal damping in the steel shaft and in the aramid-epoxy bands into the formulation by replacing the Young's modulus with a complex modulus

$$\hat{E} = (1 \mp i\gamma)E \quad ; \Omega \gtrless \omega \tag{4}$$

Also the external force acting on the flywheel shaft at the external damper (with viscous coefficient C_d) is added. Thus, one obtains a matrix characteristic equation of the same form as Eq. (3) except that now the "stiffness" matrix $[K_{ij}]$ is complex rather than real.

The stability criterion is obtained by using the Routh concept directly by numerically determining the complex roots. In general, the whirling frequencies are complex numbers, i.e., $\omega = \omega_R - i\omega_I$. Thus, the solution can be written as $\{q_i\} = \{\bar{q}_i\}e^{\omega_I t} e^{i\omega_R t}$. The quantity ω_R is the damped frequency, while the quantity ω_I is the growth factor. It is noted that if $\omega_I > 0$, the amplitude will grow with time exponentially and the system will become unstable. On the contrary if $\omega_I < 0$, the system is in a stable condition. Values of γ_s and γ_b are assumed to be 0.005 and 0.0172, typical of steel and aramid/epoxy, respectively. Effects of the external viscous damping coefficient C_d on the onset of instability are shown in Fig. 4. If $C_d = 0$, the onset of instability occurs at the lowest first-order forward critical speed. Only a small value for C_d (less than 43.8 N-sec/m or 0.25 lb-sec/in) is required to stabilize unstable motion associated with the first and third modes for $\Omega > \omega$. When the value of C_d is greater than approximately 35.0 N-sec/m or 0.2 lb-sec/in, the onset of instability jumps up to 38,100 rpm. Increasing the value of C_d has very little effect on increasing the onset of instability beyond 38,100 rpm.

FORCED WHIRLING

Although the rotors used for high-speed flywheels can be well balanced in today's technology, it is not possible to eliminate the initial unbalance completely. This initial balance (eccentricity) causes resonance in the neighborhood of first-order critical speeds. In the absence of damping, the resonance response would build up and finally cause the failure of the system. Another source of excitation for first-order critical whirling is unavoidable initial flywheel tilt (equivalent to couple unbalance). To reduce the response amplitudes in the Sandia flywheel system, there is an external damper located on the flywheel shaft as shown in Fig. 1. Here the frequency response of the system is studied, and minimum damping determined for a given maximum response allowance.

If a rotor is unbalanced with an eccentricity of $\tilde{e}$ and initial tilt ϕ_o, the translational displacement (r_c) and tilt angle (ϕ_c) of the rotor mass center can be expressed as

$$r_c = r + \tilde{e}\, e^{i\Omega t} \quad ; \quad \phi_c = \phi + \phi_o\, e^{i\Omega t} \tag{5}$$

The maximum values of eccentricity and initial tilt are 0.025 cm (0.010 in) and 0.13°.

Due to the geometric configuration of the Sandia system it is expected that the unbalance

and initial tilt mostly occur in the rim. Thus, only frequency responses excited by such kinds of geometric imperfections are studied. The governing matrix equation of motion is Eq. (3) with the addition of an excitation column matrix on the right side. Solving this equation on a digital computer, one obtains response as a function of running speed. Typical responses induced b rim eccentricity are presented in Ref. 5.

In the Sandia spin-test setup, there is a "stop" installed in the system, which limits the hub translation to a maximum of 0.071 cm (0.028 in). To prevent the hub from hitting the "stop", an adequate amount of external damping should be present. Hub translational response induced by a combination of an exaggerated value of rim eccentricity, 0.071 cm (0.028 in), and an initial tilt of 0.15 deg. is given in Fig. 5. Even in this extreme, a C_d of 43.8 N-sec/m (0.25 lb-sec/in) is enough to keep the hub from hitting the "stop". Also, calculations related to allowable clearance at the damper show that this same amount of damping should be adequate.

NONLINEAR EFFECTS IN THE SUPPORTING BANDS

From the geometry of the bands supporting the flywheel rim (Fig. 2), an analysis is made to analytically model the radial force and tilting moment as nonlinearly coupled functions of rim-to-hub relative radial displacement and tilt angle, and running speed. To simplify the geometric relationships involved, the geometry is assumed to be that of a string, i.e., the effect of flexural rigidity of the bands on the deflected shape is neglected. However, the effect of flexural rigidity on the buckling load is not neglected, i.e., it is assumed that when the net compressive load (on the compressive side of a tilted rim or on the compressed bands due to in-plane displacement of the rim) in a given band reaches the calculated buckling based on appropriate boundary conditions, that band cannot carry any additional load. The modal shape used to depict the band behavior depends upon the running speed; for example, the point of maximum deflection shifts from the band midpoint ($x/L = 0.5$) to $x/L = 0.57$ when the speed is increased from zero to 30,000 rpm. If this change in deflected shape was not taken into account, the buckling load at 30,00 rpm would be overestimated by about 7.2% (the accurate value is approximately 156% greater than the buckling load at zero speed). Figure 6 is a typical 3-D plot showing tilting moment as a function of displacement (x) and tilt angle (ϕ). The Runge-Kutta numerical-integration technique is used to directly integrate the coupled nonlinear governing equations.

ACKNOWLEDGMENTS

The research reported here was sponsored by the Department of Energy through contracts from Sandia Laboratories. The author also acknowledges the use of computational capability of the University's Merrick Computing Center. Appreciation is due to Drs. E. D. Reedy, Jr. and A. K. Miller of Sandia, and to Professor D. M. Egle of the University for helpful discussions. The computations reported here were ably performed by T. L. C. Chen, former graduate research associate, and C. A. Kocay, graduate research associate. The manuscript was carefully typed by Mrs. Rose Benda.

REFERENCES

1. C.N. McKinnon, Jr., "Rotor Dynamic Analysis", Appendix B of "Evaluation of Selected Drive Components for a Flywheel Powered Commuter Vehicle", Final Rept., Contr. EY-76-C-0301164, Phase I, LMC Corp. (June 30, 1977).

2. C.W. Bert and T.L.C. Chen, "Lateral and Tilt Whirl Modes of Flexibly Mounted Flywheel Systems", Rept. SAND 78-7070, Sandia Laboratories (Dec. 1978); to appear in Shock and Vibration Bulletin 49 (1979).

3. E.D. Reedy, Jr., "A Composite-Rim Flywheel Design", SAMPE Quart. 9(3), 1-6 (Apr. 1978).

4. C.W. Bert and T.L.C. Chen, "On Vibration of a Thick Flexible Ring Rotating at High Speed", J. Sound Vib. 61 (4), 517-530 (Dec. 22, 1978).

5. T.L.C. Chen and C.W. Bert, "Whirling Response and Stability of Flexibly Mounted, Ring-Type Flywheel Systems", Rept. SAND 78-7073, Sandia Laboratories (Feb. 1979); to appear in J. Mech. Design, Trans. ASME.

6. Yamada, Y., "On the Critical Speeds of a Rotor System Having an Asymmetrical Disk", Proc. 4th Japan Nat. Cong. Appl. Mech., 381-384 (1954).

7. W.T. Thomson, et al., "Whirl Stability of the Pendulously Supported Flywheel System", J. Appl. Mech., Trans. ASME 44, 322-328 (June 1977).

8. E.D. Reedy, Jr. and H.K. Street, "Composite-Rim Flywheels: Spin Tests", SAMPE Quart. 10 (3), 36-41 (Apr. 1979).

9. C.W. Bert, et al., "Research on the Dynamics of Band-Supported Flywheel Systems", Rept. SAND 78-7074, Sandia Laboratories (Feb. 1979).

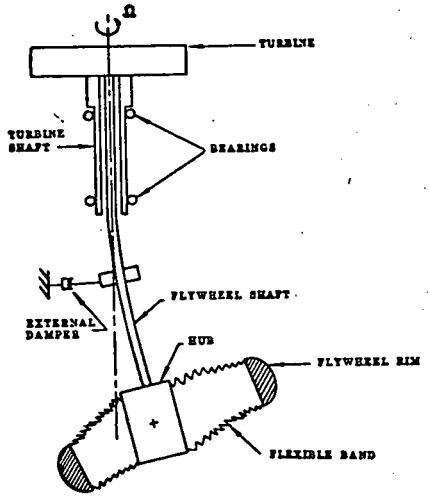

Fig. 1 Schematic Diagram of the Sandia Flywheel System, as Installed in the Sandia-Livermore Spin-Test Facility

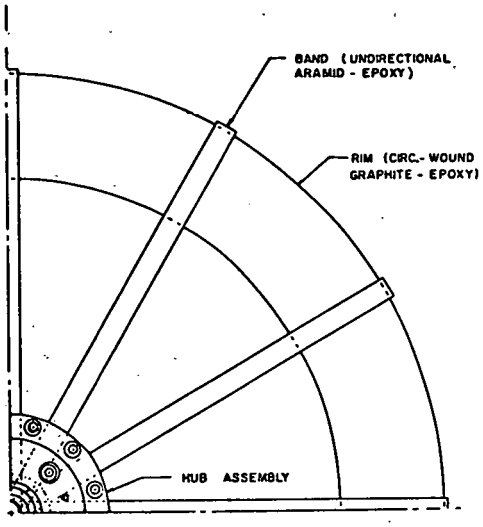

Fig. 2 Plan View of One Quarter of the Sandia Thick-Ring Flywheel (System A)

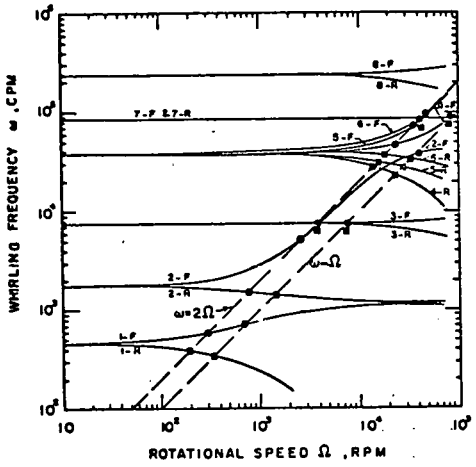

Fig. 3 Free-Whirling Performance of System A. Mode identification: The number denotes the mode number and the suffix denotes the branch (F ∿ forward, R ∿ retrograde). The circles denote first- and second-order forward critical speeds and the squares first- and second-order retrograde critical speeds

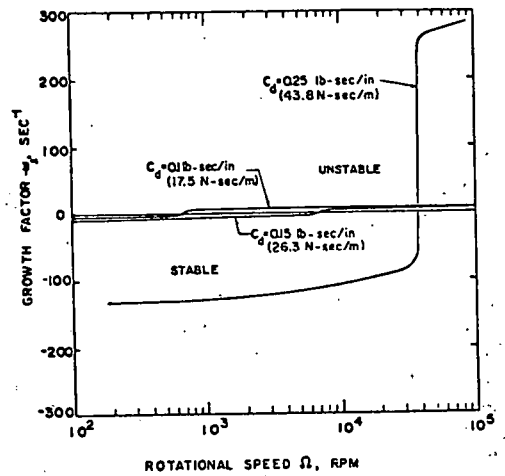

Fig. 4 Effects of External Viscous Damping Coefficients C_d on the Stability Boundary for the Onset of Instability

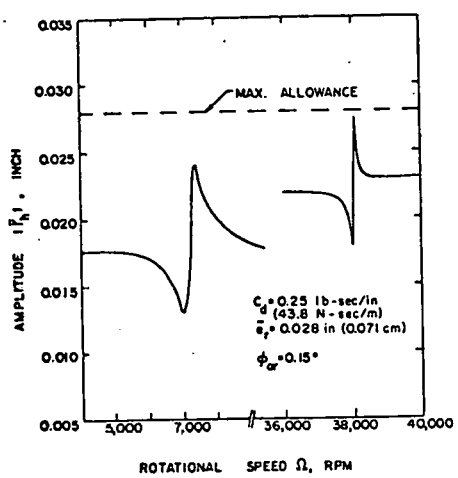

Fig. 5 Hub Translational Amplitude Response to a Combination of Rim Eccentricity and Initial Tilt

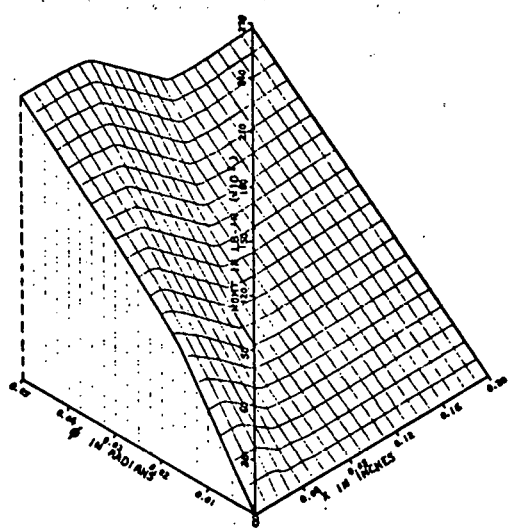

Fig. 6 Restoring Moment About the y-Axis at 20,000 rpm as a Function of Out-of-Plane Tilting about the y-Axis and In-Plane Displacement along the x-Axis

PROJECT SUMMARY

Project Title:	Mechanical Energy Storage Technology Development
Principal Investigator:	R. O. Woods
Organization:	Sandia Laboratories Albuquerque, NM 87185 (505) 264-7553
Project Goals:	The selection of those mechanical components of flywheel energy storage systems that can be carried to their next stage of evolution by efforts within the scope of the budget; the funding of developmental work treating such components. The documentation of the state-of-the-art in component technology where such information is scattered or fragmentary.
Project Status:	Efforts have treated the following components: Rolling Contact Bearings Magnetic Bearings - Active and Passive Composite Wheels - Hardware development, development of analytic and testing techniques, material studies. Composite Materials - Analysis, improved properties, vacuum outgassing properties, fabrication and thermal characteristics. Seals - Power dissipation, lifetimes, permeation rates. Funding has been provided to other agencies for the testing of energy storage systems, and the groundwork has been completed for a program to deal with the problems of vacuum technology.
Contract Number:	SOL 78
Contract Period:	FY79
Funding Level:	$980 K*
Funding Source:	DOE, Division of Energy Storage Systems

*Included in this project are the following:
"Rotor Analysis," Keith Miller.
"Flywheel Rotor Analysis," Arlo Nord.

RECENT SPIN TESTS OF TWO COMPOSITE WAGON WHEEL FLYWHEELS

A. Keith Miller
Applied Mechanics Division 5522
Sandia Laboratories†
Albuquerque, New Mexico 87185

ABSTRACT

This paper briefly discusses some observations made of spin tests performed on two variations of the Sandia "wagon wheel" flywheel. In one design, the graphite/epoxy rim was attached to the aluminum hub with twenty-four thin Kevlar-49/epoxy spokes, while in the other design eight thicker graphite/epoxy spokes connected the rim to the hub. The test objective was to compare the dynamic behavior of the two structurally dissimilar flywheels. The tests were limited to speeds less than 22,000 RPM and only moderate torques were applied during the acceleration phase of the tests in an attempt to detect speeds for previously predicted modes of vibration of the flywheel-spin-turbine system. Using proximity sensors, horizontal disturbances of the flywheel hub were detected for speeds less than approximately 6,000 RPM. These disturbances are believed to be associated with predicted modes of vibration for the flywheel-spin-turbine system. No modes of vibration were sensed for the predicted possible whirl and torsional resonances in the speed range between 6,000 RPM and 22,000 RPM. A squeeze film damper assembly which was attached to the flywheel spindle shaft is believed to have sufficiently dampened possible whirl modes so that they were undetectable in the speed range tested. The tests indicated that the squeeze film damper assembly successfully stabilized the flywheel-spin-turbine system when the damper functioned properly; however, low frequency retrograde instabilities were induced into the system by the damper assembly when it was not operated within prescribed parameters.

---

* This work was sponsored by the U.S. Department of Energy (DOE), under Contract AT(29-1)-789.

† A U.S. DOE facility.

INTRODUCTION

Results from a previous series of spin tests reported at the 1978 Mechanical and Magnetic Energy Storage Contractor's Information Exchange Conference prompted further study into the dynamic response of the "wagon wheel" design [1]. The purpose of these previous tests was to demonstrably spin the flywheels to the design speed. As reported in References 1 and 2, one of the flywheels was actually spun to within six percent of its design goal before failure of either the turbine spindle shaft, or the flywheel occurred. The cause of these failures was not conclusively determined. As reported by Reedy [1], these test results indicated that a better understanding of the dynamics of the rotors needed to be developed.

Basically two designs of a thick-rim rotor were spun in the tests previously reported--the pin-wrapped design, and the wagon wheel design. Detailed descriptions of each of the designs can be found elsewhere [3,4]. In general, the wagon wheel design seemed not to perform as well as the pin-wrapped. The wagon wheel design appeared to have a more severe vibrational response. As reported by Nord [5], the hub of the pin-wrapped flywheel is more compliant than the one for the wagon wheel design, which may be one reason why the pin-wrapped flywheel functioned somewhat better. Flaws in the rims of the wagon wheel flywheels were also detected which may have caused their poorer performance [1]. Additional tests of new wagon wheel flywheels were therefore needed.

During subsequent tests, attempts were made to detect speeds where modes of vibration were predicted, and to determine whether failures of the previous tests were caused by material failure within the rotors or by dynamic instabilities which forced the turbine spindle to break. One wagon wheel flywheel of identical design to those previously tested was fabricated by the Defense Division of the Brunswick Corporation. A variation of design was incorporated into a second flywheel. Instead of having twenty-four thin Kevlar 49/epoxy spokes attaching the rim to the hub, eight graphite/epoxy spokes each three times thicker attached the rim to the hub. This flywheel was also fabricated by the Brunswick Corporation.

BRIEF ANALYTICAL RESULTS

As an initial step in analyzing the dynamic response of the two variations of the wagon wheel flywheel, finite element structural models of both flywheels were constructed. The normal modes of vibration predicted by the structural models of only the flywheels (without the spin turbine) under unrestrained boundary conditions (free-free conditions) were compared to those obtained by experimental modal analysis techniques [5]. The models were refined until the predicted mode shapes and natural frequencies agreed with the experimentally determined ones.

Table 1 lists the modes and the corresponding frequencies obtained from the experimental analysis and those predicted by the models. Vibration modes were identified above 600 Hz but they are associated with rim flexures. These modes have been neglected in Table 1 since the resonant frequencies change very little when the finite element models of the flywheels are attached to the model of the spin turbine. These frequencies are also well above the operating speed of the flywheels. All of the predicted frequencies shown in Table 1 are within fourteen percent of those measured for the twenty-four spoke flywheel, and within two percent for the eight spoke flywheel.

Table 1. Experimentally Measured and Predicted Normal Modes of Vibration for Two Wagon Wheel Flywheels

Mode Number	Experimental Modal Tests: Natural Frequency (Hz)	Experimental Modal Tests: Damping Factor Percent	Mode Description	Model Prediction: Natural Frequency (Hz)
			24-SPOKED FLYWHEEL	
1	101.77	0.78	Axial	86.8
2	376.54	1.00	Torsional	373.4
3	629.19	2.45	Whirl	635.3
			8-SPOKED FLYWHEEL	
1	109.55	2.16	Axial	108.5
2	347.05	1.22	Torsional	344.8
3	412.23	1.59	First Whirl	407.4
4	574.95	0.79	Second Whirl	566.7

The experimentally verified mathematical models of the flywheels were then attached to a finite element structural model of the Model 6100 Barbour-Stockwell air turbine used in the spin tests. The normal modes of vibration of the flywheel-turbine (undampened) system were determined neglecting the damper assembly in the system. The turbine damper assembly is normally attached to the turbine spindle to provide stability to the system as it traverses through critical vibrational speeds. The first normal mode for the flywheel-turbine system, using the twenty-four spoked flywheel, is shown in Fig. 1 as an example of the analytical representation of the flywheel-turbine system.

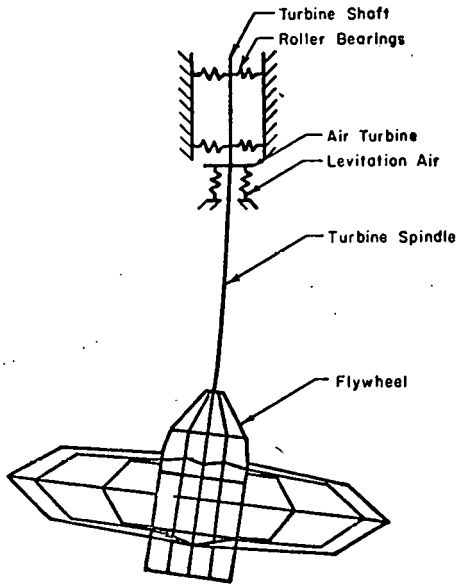

Fig. 1. First Lateral Bending Mode of Flywheel-Turbine Modal Frequency 6.15 Hz (369RPM)

Table 2 lists the normal modes and frequencies predicted from the flywheel-turbine model of the twenty-four spoked flywheel. Note that only one torsional mode is predicted for this system in the speed range between approximately 4,000 and 32,000 RPM. Several vibration modes associated with bending of the turbine spindle and axial motion of the rim are predicted below 4,000 RPM however.

Table 2. Normal Vibrational Modes and Frequencies Predicted for the Twenty-Four-Spoked Flywheel-Turbine System Neglecting Squeeze-Film Damper Assembly

Mode Number	Natural Frequency (Hz)	Mode Description
1	6.15	First Lateral Bending of the Turbine Spindle
2	8.08	Axial Motion of Flywheel and Turbine on Air Support
3	44.08	Second Lateral Bending of the Turbine Spindle
4	66.33	Axial Motion of the Flywheel Rim
5	243.20	Combined Torsional Mode of Flywheel and Turbine Spindle
6	637.00	Combined Third Lateral Bending of the Turbine Spindle and First Flywheel Whirl

Results of the flywheel-turbine system for the eight-spoked flywheel are not presented in detail here because the modes predicted below 20,000 RPM are essentially the same as those shown in Table 1. One additional mode which is associated with the first diametrical rotational mode of the hub (flywheel whirl) is predicted to be near 25,000 RPM for the eight-spoked flywheel mounted to the turbine.

The normal modes of vibration shown in Table 2 were predicted for a static condition of the flywheel-turbine system; i.e., the system was considered not to be rotating. An analysis of possible gyroscopically induced whirl modes for a four-degree-of-freedom model of the twenty-four spoked flywheel indicated that no whirl modes exist within the speed range of interest. This conclusion is the same as that reached by Bert, et al., [6] for a similar four-degree-of-freedom model. However, a more complex, eight-degree-of-freedom model developed by Chen and Bert [7] indicates a possibility that several whirl modes may exist between 10,000 and 25,000 RPM. There was no known way of assessing the strength of these possible modes however. It is possible such modes may be easily dampened to the point they become unobservable.

SPIN TEST DESCRIPTION

During the past year, two series of spin tests were performed at the Sandia Laboratories Livermore facilities using a Model 6100 Barbour-Stockwell six-inch diameter air turbine. Attempts were made to spin both the twenty-four spoked and the eight spoked flywheels in the first series of tests. The maximum speed was limited to less than 20,000 RPM to ensure that the flywheels would not be destroyed.

Horizontal displacements of the adaptor section attached to the top of the flywheel hub were monitored with two orthogonally placed proximity transducers. The test plan was to limit the angular acceleration during the spin-up phase of the tests to a relatively low rate in an attempt to clearly identify speeds where there was disturbance of the horizontal position of the hub which could be associated with critical natural frequencies of the system. Speeds of 10,000; 13,000; 15,000; 17,000; and 20,000 RPM were to be maintained for approximately 60 seconds each during the spin-up portion of the tests in order to access the stability of the flywheels at those speeds. Upon completing the dwelling at 20,000 RPM the flywheels would be allowed to coast down in speed with no reversing torque applied. Critical speeds were expected to be more easily identified by allowing the flywheels to drift through the speed range slowly.

Only the twenty-four spoked flywheel was spun during the second test series. This second series of tests was essentially a repeat of the first, with only the oil feed rate to the squeeze-film damper assembly increased, and the flywheel rebalanced.

TEST RESULTS

Discussion of the test results will concentrate on the phenomenon observed for the twenty-four-spoked flywheel because most of the test time was devoted to this flywheel, and because most of the conclusions were drawn from the information obtained from this flywheel.

Several disturbances in the horizontal position of the hub of the twenty-four spoked flywheel were noted below approximately 6,000 RPM. These disturbances were characterized by rapid increases and decreases in the run-out (variation of the horizontal position) of the hub. Above 6,000 RPM the pattern on the oscilloscope displaying the hub run-out stabilized into a toroidal shape. The diameter of the toroid (which is one indication of horizontal run-out) increased proportionately to approximately the square of the rotational speed. The rotation of the flywheel appeared to be stable at all of the constantly held speeds. However, the amount of horizontal run-out of the flywheel was believed to be approaching an operational limit at the 20,000 RPM mark. No sudden changes in the behavior of the flywheel were noted during the spin-up portion of the test for speeds above 6,000 RPM.

A very low frequency (approximately 3 Hz) retrograde whirl motion developed as the twenty-four spoked flywheel drifted down in speed from 20,000 RPM. The amplitude of this whirl increased approximately exponentially with time until the motion became so violent that the test had to be stopped. Several attempts were made to allow the flywheel to drift down in speed, all resulting in the development of the same, nearly classical, instability.

The horizontal run-out of the hub of the eight-spoked flywheel appeared to be considerably greater at all speeds than observed for the twenty-four-spoked flywheel. A somewhat similar pattern of behavior was noted. Rapid fluctuations in run-out occurred below 6,000 RPM, and more benign motion was noted above that speed. The development of the retrograde whirling instability appeared to be much more serious for this flywheel. The instability would develop when repeated attempts were made to dwell at 15,000 RPM, which forced termination of further testing of this flywheel.

Investigation into the possible cause of the low frequency retrograde whirl of the flywheels during this first series of tests revealed that the oil pressure in the squeeze-film damper assembly was below normally prescribed conditions. An obstruction in the hose which supplies the feed oil to the damper assembly was removed, the oil pressure was increased, and a second series of tests using only the twenty-four spoked flywheel was performed.

The follow-on test plan was identical to that used during the first series of spin tests. Rapid changes in the run-out were again observed below approximately 6,000 RPM. The oscilloscope display of the run-out was not a perfect toroid above 6,000 RPM, as it had been during the first series of tests, as it was distorted into a much more narrow three-point crown shape. However, the amount of hub run-out did not increase with speed as had been observed during the first series of tests. The flywheel had been rebalanced dynamically prior to the second series of tests which

leads one to conclude that the increase in run-out during the first series of tests may have been the result of a slight unbalance.

The flywheel was completely stable at all speeds tested. The instability as the flywheel drifted down in speed from 20,000 RPM was no longer observed. The speed was gradually increased in the final test of this series until a gradual increasing of the hub run-out was observed at 22,000 RPM. The tests were terminated at that speed.

It is important to note that reversing torque had to be applied to slow the flywheel to a stop below the 6,000 RPM level. The relatively large horizontal displacements sustained at the various critical speeds below 6,000 RPM required that those speeds be traversed as rapidly as possible.

DISCUSSION OF RESULTS

While the original test objectives were not achieved, several tentative results have been drawn from the experience.

First, it was demonstrated that the wagon wheel flywheel design could be smoothly driven to 22,000 RPM (the highest speed at which this design failed during the 1977-1978 test series) under proper balancing of the flywheel and under a rather narrow set of operating parameters of the particular drive turbine used. The gradual increase in the run-out as the system was spun to 22,000 RPM in the final series of tests may have been a result of yet a small amount of dynamic unbalance in the rotor. It was concluded that to fully ascertain that possibility, the balance of the flywheel would need to be checked before higher speeds were attempted.

Related to the possible balancing problem, it was found from this experience that instrumentation which could simultaneously monitor the center of the flywheel with respect to the spin axis (the run-out), and the angular position of the flywheel with respect to a fixed reference frame may be needed to better separate dynamic effects caused by unbalance from those associated with possible vibrational frequencies. Gunter [8] has pointed out that, theoretically, the location of possible unbalance in a thin rotor can be obtained from monitoring these two measurements as the system is spun through its first few critical speeds. By also monitoring the planar tilt and knowing its relationship to the angular orientation of a flywheel, it may prove that dynamic unbalance of thick rotors also may be detectable at higher speeds (speeds greater than 5,000 RPM).

A final result found from these spin tests is that a squeeze-film damper assembly attached to the turbine spindle successfully stabilizes the flywheel-turbine system at higher speeds. Theoretical development of the hydrodynamic forces within squeeze film dampers [9, 10, 11, 12] indicates that although dynamic instabilities can result from the use of squeeze-film dampers, such devices should be very effective in damping possible whirl modes induced by either coulomb damping, hysteresis damping in the turbine spindle, or gyroscopic effects. The effectiveness of these squeeze-film damper assemblies in damping whirl modes appears to be rather strongly dependent on maintaining the oil pressure within reasonable operating parameters [12], a fact apparently confirmed by these tests.

It is suggested that further investigation be made into the stabilization of pendulously supported flywheel spin tests using squeeze film damper assemblies.

REFERENCES

1. E. D. Reedy, Jr., "Sandia Composite-Rim Flywheel Development," Proceedings of the First Annual Mechanical and Magnetic Energy Storage Contractors' Information-Exchange Conference, Luray, Virginia, October 24-26, 1978, pp. 87-91.

2. E. D. Reedy, Jr. and H. K. Street, "Composite-Rim Flywheels: Spin Tests," to be published.

3. E. D. Reedy, Jr. and F. P. Gerstle, Jr., "Design of Spoked-Rim Composite Flywheels," Preceedings of the 1977 Flywheel Technology Symposium, San Francisco, California, October 5-7, 1977, pp. 99-110.

4. E. D. Reedy, Jr., "A Composite-Rim Flywheel Design," SAMPE Quarterly, Vol. 9, No. 3, pp. 1-6.

5. A. R. Nord, "Experimentally Determined Modes From Three Composite Flywheels," 1979 Mechanical and Magnetic Energy Storage Contractors' Review, August 19-22, 1979, Washington, D.C.

6. C. W. Bert, T. L. C. Chen, and C. A. Kocay, "Critical Speeds and Natural Frequencies of Rim-Type Composite-Material Flywheels," Sandia Laboratories Technical Report, SAND78-7049, January 1979.

7. T. L. C. Chen and C. W. Bert, "Whirling Response and Stability of Flexibly Mounted, Ring-Type Flywheel Systems," Sandia Laboratories Technical Report, SAND78-7073, February 1979.

8. Gunter, E. J., "Dynamic Stability of Rotor-Bearing Systems," NASH SP-113, Office of Technical Utilization, U.S. Government Printing Office, Washington, D.C., 1966.

9. John M. Vance, and Alan J. Kirton, "Experimental Measurement of the Dynamic Force Response of a Squeeze-Film Bearing Damper," Journal of Engineering for Industry, November 1975, pp. 1282-1290.

10. D. H. Hibner, R. G. Kirk, and D. F. Buono, "Analytical and Experimental Investigation of the Stability of Intershaft Squeeze Film Dampers, Part I: Demonstration of Instability," Journal of Engineering for Power, January 1977, pp. 47-52.

11. P. N. Bansal and D. H. Hibner, "Experimental and Analytical Investigation of Squeeze Film Bearing Damper Forces Induced by Offset Circular Whirl Orbits," Journal of Mechanical Design, Vol. 100, July 1978, pp. 549-557.

12. E. Feder, P. N. Bansal, and A. Blanco, "Investigation of Squeeze Film Damper Forces Produced by Circular Centered Orbits," Journal of Engineering for Power, Vol. 100, January 1978, pp. 15-21.

THIS PAGE

WAS INTENTIONALLY

LEFT BLANK

PROJECT SUMMARY

Project Title:	"Modal Determination - Composite Flywheels"
Principal Investigator:	A.R. Nord
Organization:	Sandia Laboratories Organization 1542 Albuquerque, NM 87185
Project Goals:	To provide experimental verification of the modal changes predicted by both classical and numerical analyses.
Project Status:	The testing program is complete. Data have been furnished to the engineers who are performing the theoretical analyses.
Contract Number:	Does not apply.
Contract Period:	FY79
Funding Level:	$15K
Funding Source:	U.S. Department of Energy, Division of Energy Storage Systems

EXPERIMENTALLY DETERMINED MODES OF THREE COMPOSITES FLYWHEELS*

A.R. Nord
Sandia Laboratories
Vibration and Modal Testing Division
Division 1542
Albuquerque, NM 87185

ABSTRACT

Three composite flywheels were analyzed by the Vibration and Modal Testing Division of Sandia Laboratories. Modal analysis techniques were used to experimentally determine the modal frequencies, damping, and complex mode shapes of the flywheels in a frequency range corresponding to the purposed operating speed range of the wheels. The wheels were suspended from soft supports during testing so the modes characterize the structures for an unrestrained boundary. Since the complex mode shapes for each modal frequency are best appreciated when viewed on a dynamic display, a special videotape has been prepared to show the first mode shapes of the three flywheel configurations. This paper serves as an introduction to and a summary of the videotape and is not intended to be a complete description of the modal analysis work done on the flywheels.

TEST PROCEDURE

The three flywheel configurations were instrumented in a similar manner. The three photographs show the location of accelerometers on the aluminum cubes every 90^{0} around the top and bottom of the hub and around the rim. The 12- and 4-spoked wagon wheel design had accelerometers at the center of the rim only, but the pinwrapped model was instrumented with measurement points both at the top and bottom of the rim. Each measurement point was monitored in the axial, radial, and tangential directions. The flywheels were suspended from soft rubber tubes attached to the hub and the structure was excited by tangential impacts to an aluminum block also secured to the hub.

In Figure 1 ("12-Spoked Flywheel"), an example of a 3-axis mounting block for accelerometers can be seen at station "4." Only the pickoff for tangential acceleration is shown installed. The same is true of Figure 2 ("Pinwrapped Flywheel"). In this case, three tangential-motion sensors are shown at the top of the hub and a number of bare blocks can be seen on the rim of the wheel. Figure 3 ("Four-Spoked Flywheel") shows, in addition to a wheel, the instrumented hammer that was used to shock the wheels. It will be noted that the hammer incorporates an accelerometer which is used to give a time-domain readout of the driving function.

Frequency response functions (transfer functions) were measured by effectively taking the ratio of accelerometer response to the input hammer force in the frequency domain. The modal parameters were extracted from the measured frequency response functions by fitting an analytical expression to the measured data by an iterative routine on the analyzer/computer. The analytical function used to fit the measured response function contains the three modal parameters; frequency, damping, and complex amplitude. After each analytical function has an acceptable fit to the corresponding measured response function, the computer can display the structure at each mode and show the relative motion of each measured point.

*This work supported by the U.S. Department of Energy, DOE.

MODAL RESULTS

The accompanying videotape shows the modes of each of the three flywheel configurations that were found near and below 600 Hz. The film discusses the similarity and the differences of the modes and relates them to the flywheel's structure. The table below is a summary of these first modes on the three flywheels.

Mode	12-Spoked Model	4-Spoked Model	Pinwrapped Model
Axial	102 Hz	109 Hz	70 Hz
Torsional	376 Hz	347 Hz	153 Hz
Rim Twist with Hub Deformation			299 Hz
1st Hub Rotation	629 Hz	412 Hz	486 Hz
2nd Hub Rotation		575 Hz	

The videotape shown at the conference will be archived at Sandia Laboratories, Albuquerque. Arrangements for borrowing it can be made with the author of this paper.

The summary shows the simple axial and torsional stiffness of the two wagon wheel designs are very close, but the pinwrapped model is much softer. The 12-spoked model has one hub rotational mode above 600 Hz which should place this mode above the operating speed range. The 4-spoked flywheel has two hub rotational modes below 600 Hz possibly well within the operation range. The pinwrapped wheel has a rim twisting mode with some hub deformation well in the operating range. This softer system with a much more flexible hub brings a mode into this lower frequency range that was not observed in the other two wheels. The pinwrapped wheel's hub rotational mode is similar to but lower than the 12-spoked model.

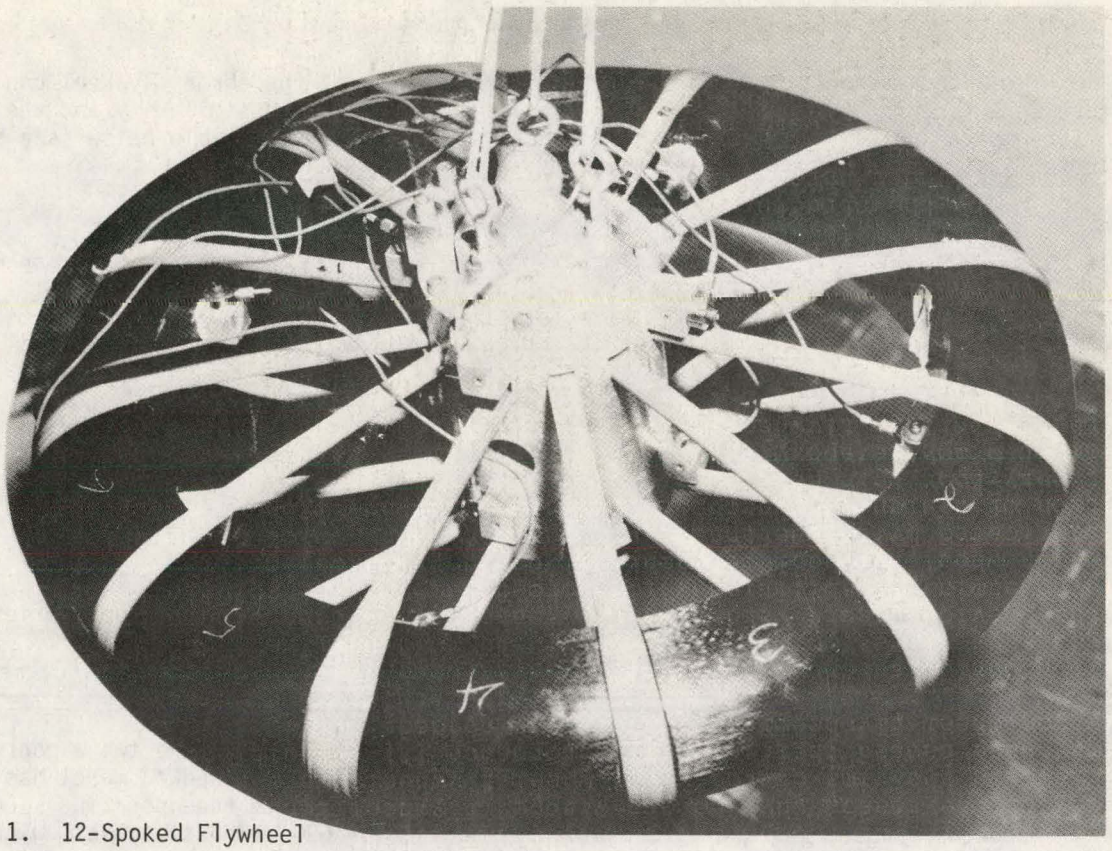

Fig. 1. 12-Spoked Flywheel

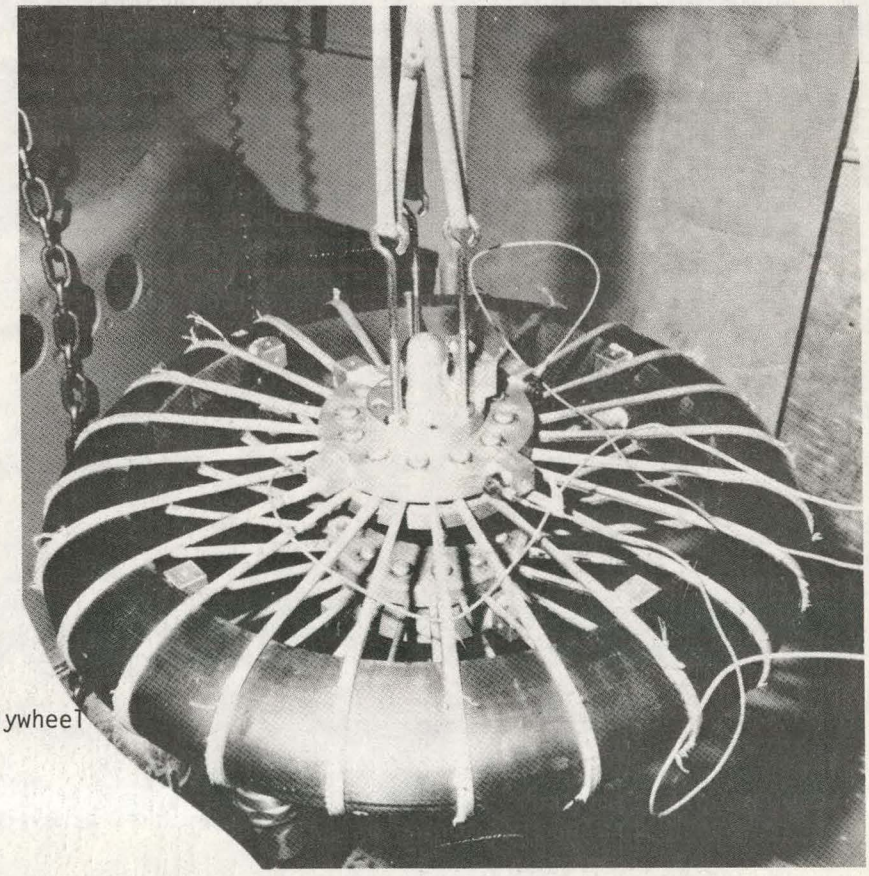

Fig. 2. Pinwrapped Flywheel

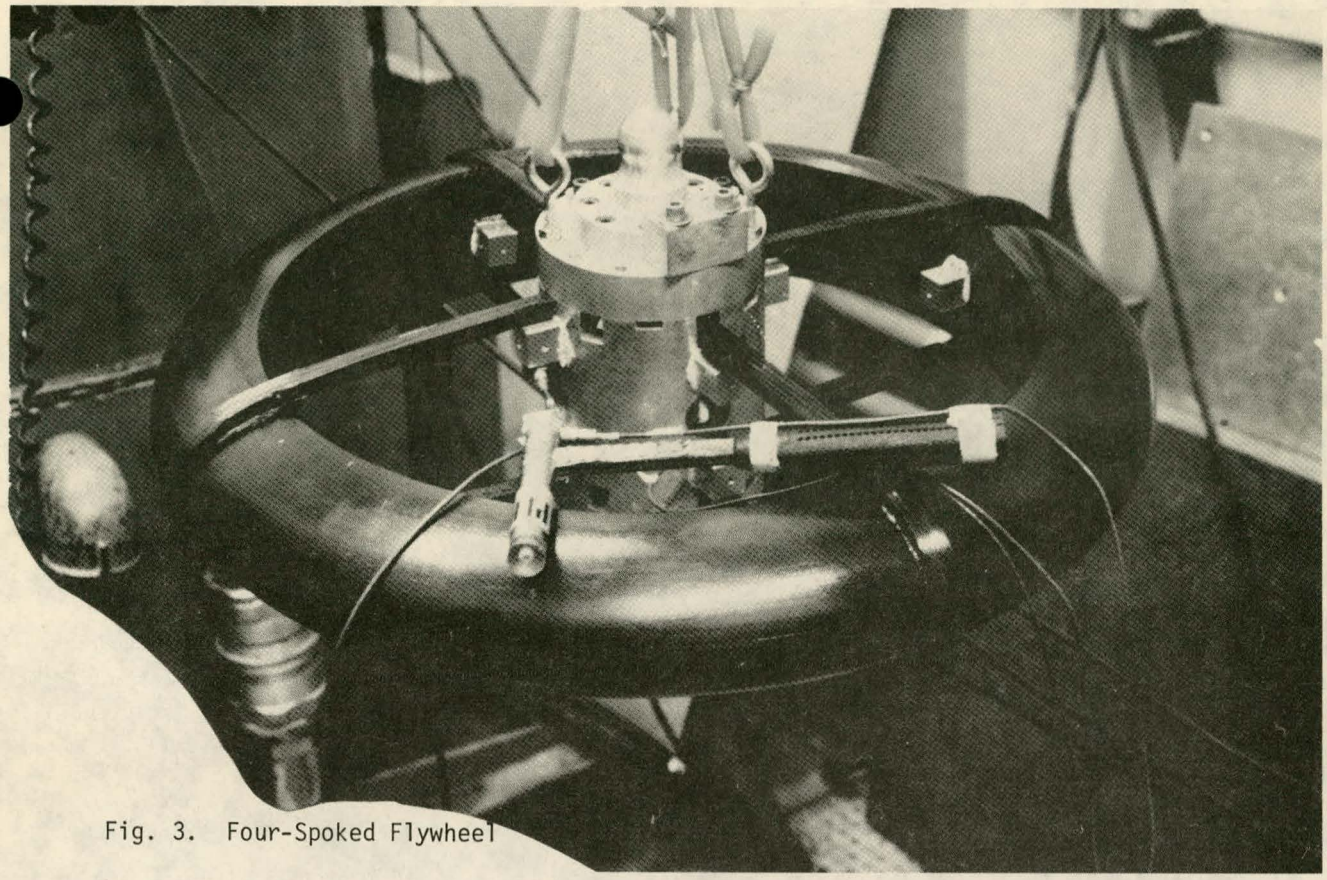

Fig. 3. Four-Spoked Flywheel

THIS PAGE

WAS INTENTIONALLY

LEFT BLANK

Dup

PROJECT SUMMARY

Project Title:	LLL Materials Program for Fiber-Composite Flywheels
Principal Investigator:	J. A. Rinde and Ed Wu
Organization:	Lawrence Livermore Laboratory University of California Livermore, California 94550 (415)422-7077, FTS 532-7077
Project Goals:	The goals of this project are threefold: (1) to accelerate the widespread use of the fiber-composite flywheel by developing the necessary engineering-design data on fiber composites, (2) to demonstrate the high-energy kinetics attainable with fiber-composite materials, and (3) to transfer the technology thus gained to the private sector.
Project Status:	During FY'79 the LLL materials program for fiber-composite flywheels has worked in the areas of matrix resins, stress rupture, static engineering properties, and fatigue or time-dependent engineering properties. We have tested the physical and mechanical properties of a low-cost matrix-resin system suitable for service up to 150°C. Also, we have obtained results from stress-rupture tests on E-glass at load levels of interest to flywheel designers. Lifetimes at these levels are longer than those of S-glass in previous tests. We have also measured static engineering properties on a Kevlar-49/rubberized-epoxy* composite at 25 and 75°C. Properties did not decrease within this temperature range. Creep and fatigue tests have been performed over a wide range of stress levels. Both input loads and material-response strains were measured and used to correlate times to failure under creep and fatigue loading histories. Further development may provide a basis for predicting composite-flywheel structural life from laboratory tests.
Contract Number:	W-7405-ENG-48
Contract Period:	FY'79
Funding Level:	$310K
Funding Source:	U.S. Department of Energy, Division of Energy Storage

*Reference to a company or product name does not imply approval or recommendation of the product by the University of California or the U.S. Department of Energy to the exclusion of others that may be suitable.

LLL MATERIALS PROGRAM FOR FIBER-COMPOSITE FLYWHEELS*

J. A. Rinde and Ed Wu
Lawrence Livermore Laboratory, University of California
Livermore, California 94550

ABSTRACT

During FY'79 the LLL materials program for fiber-composite flywheels has worked in the areas of matrix resins, stress rupture, static engineering properties, and fatigue, or time-dependent engineering properties. Results are reported for physical and mechanical tests of a low-cost matrix-resin system suitable for service up to 150°C. Results of stress-rupture tests on E-glass at load levels of interest to flywheel designers are reported for the first time. Lifetimes at these levels are longer than those of S-glass in previous tests. Static engineering properties on a Kevlar-49/rubberized-epoxy composite are reported for tests at 25 and 75°C. Properties did not decrease within this temperature range. Creep and fatigue tests were performed over a wide range of stress levels. Both input loads and material-response strains were measured and used to correlate times to failure under creep and fatigue loading histories. Further development may provide a basis for predicting composite-flywheel structural life from laboratory tests.

INTRODUCTION

The LLL materials program for fiber-composite flywheels was begun in 1975 to provide reliable engineering-design data on composite materials specifically intended for flywheels. The two main criteria for material selection for this program are high performance and reasonable cost.

Since 1975, in this program we have:

- Generated engineering design data for Kevlar 49, S2-glass, and E-glass composites.
- Spin tested thin-rim flywheel rotors of Kevlar- and glass-fiber composites and correlated the results with the fibers' static strength properties.
- Developed and engineered a new fiber-composite flywheel design--a quasi-isotropic, laminated, solid-disk rotor with a tapered profile.
- Characterized flexible and rubberized matrix resins.
- Investigated the transverse tensile properties as a function of matrix-resin modulus for a series of S2-glass composites.
- Conducted stress-rupture tests on Kevlar 49 and E-glass composites.

During the past year, we concentrated our efforts specifically on new matrix resins, stress rupture of E-glass composites, engineering properties of a composite made with a rubberized resin, and composite lifetime under fatigue.

FORMULATION OF A LOW-COST MATRIX RESIN FOR HIGH-TEMPERATURE SERVICE**

Because commercial flywheels must be of low or moderate cost, we have begun characterizing a low-cost cycloaliphatic epoxy resin cured with a liquid anhydride. This system has good processing properties and high-temperature performance, but will require more care during the filament-winding process to achieve optimum properties. Cost of the resin system is $1.15/lb ($2.50/kg).

The cycloaliphatic epoxy resin used in this formulation offers the advantages of low viscosity, low cost, and high glass-transition temperature when properly cured. Because cycloaliphatic epoxy resin cannot be cured with amines, they are generally cured with anhydrides. The particular anhydride we chose to use offers the advantages of being a liquid at room temperature, being inexpensive, and providing good high-temperature performance. In

*This work was performed under the auspices of the U.S. Department of Energy by Lawrence Livermore Laboratory under contract No. W-7405-Eng-48.
**Principal investigator: J. A. Rinde.

addition to the epoxy resin and anhydride, we have added a small amount of a liquid rubber to the formulation to decrease brittleness, but not enough to lower the glass-transition temperature significantly. The catalyst used is an imidazole that allows curing at relatively low temperatures and yet achieves high glass-transition temperatures. Table 1 presents the resin-system components and the amounts of each used.

TABLE 1. Components of Matrix Resin System Formulated for High-Temperature Service

Component	Parts by weight
Cycloaliphatic epoxy resins; CY–179 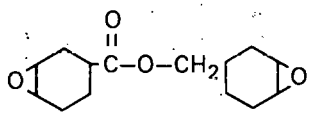	100
Liquid anhydride curing agent 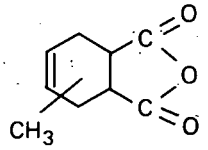	100
Flexibilizer; CTBN rubber 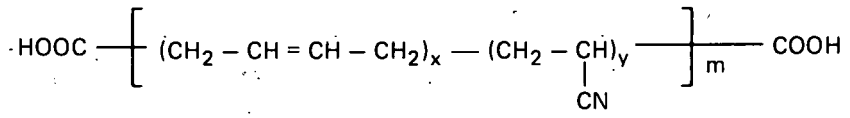	5
Catalyst; 2 ethyl 4 methyl Imidazole 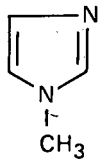	1

The properties of the uncured resin are very good for filament-winding. The resin system has both a low viscosity and long gel time. The initial viscosity is only 0.38 Pa•s, and this increases to 0.72 Pa•s after 8 h at 25°C. Gel time at 25°C is 36.6 h. Gellation of the resin can be accomplished in 2 h at 90°C, and full cure can be accomplished in 4 h at 150°C. Lower-temperature cures of this material are possible if the cure time or the catalyst concentration is increased. We have obtained good cures in 8 h at 120°C or 24 h at 100°C.

It is well known that water affects the cure of anhydride-cured epoxy resins by reacting with the anhydride to form a diacid. The diacid will react with epoxy groups but with a functionality of one, whereas the anhydride functionality is two. The overall result of moisture is to reduce the cross-link density of the cured epoxy and therefore the glass-transition temperature. Because of this moisture sensitivity, more care must be taken in any manufacturing processes involving these resins to reduce moisture pick-up. To measure the effect of moisture on the properties of the cured resin, we added liquid water to the resin system during mixing and cast resin sheets in the normal fashion. Figure 1 shows the effects of adding 1.0 and 2.3% water to a anhydride-cured resin system. In this case, the glass-transition temperature is reduced by 20 to 25°C for each 1% water added. Also shown by the figure is the decrease in cross-link density with increasing water content. In the rubbery region above T_g = +40°C the cross-link density is proportional to the shear modulus.

The tensile properties of this resin system are presented in Table 2 for temperatures from 25 to 150°C. These preliminary data show that the modulus decreases by a factor of two and the strength by a factor of 2.4 over this temperature range. We are performing tests to obtain more precise values for the tensile properties on 150°C aged and unaged specimens.

TABLE 2. Tensile Properties of Matrix Resin System of CY 179/CTBN/MTHPA/1MI (100/5/100/1) Cured 2 h at 90°C plus 4 h at 150°C

Temperature, °C	Modulus, GPa	Maximum stress, MPa	Maximum strain, %
25	2.9	70	3.1
100	2.1	56	5.2
125	2.0	42	3.5
150	1.5	29	3.4

We have measured dynamic shear modulus on the cured resin in the temperature range from -150 to 250°C. These measurements confirmed the trends of the above tensile results and extended the temperature range over which we observed these trends. The shear modulus is approximately constant, decreasing by about a factor of two as temperature went from -50 to 150°C. This temperature range is the region of most interest to flywheel designers. Results of these shear measurements are presented in Fig. 2. We see that the glass-transition temperature for this resin cured at 150°C is above 200°C. The moderate size of the loss modulus peak in the temperature range from -110° to -50°C shows that this resin is more brittle than amine-cured epoxy resins.

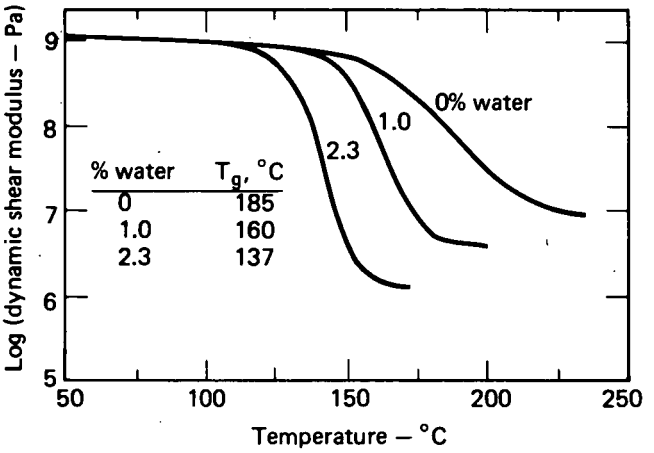

Fig. 1. Effect of Water Content on the Dynamic Shear Inodulus and Glass-Transition Temperature for an Ambydride-Cured Epoxy Resin

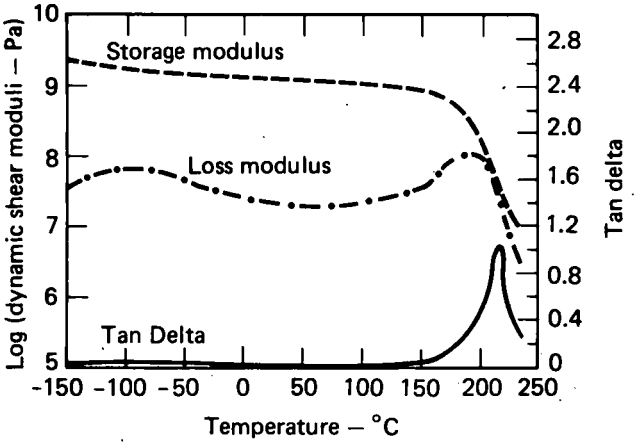

Fig. 2. Dynamic Shear Moduli of CY 179/CTBN/ MTHPA/1MI AT 1 Hz

ENGINEERING PROPERTIES OF KEVLAR 49/EPOXY COMPOSITES*

In a continuing effort to develop a data base for engineering design, we have characterized thermomechanical properties of Kevlar-49/epoxy composites. Initially, the epoxy system chosen was XD7575.03/XD7114/Tonox 60-40 (called epoxy A). However, because XD7575.03 became no longer commercially available, we later substituted an equivalent system, DER 332/Kelpoxy G293/Heloxy 68/Tonox 60-40 (called epoxy B).

*Principal investigator: H. T. Hahn.

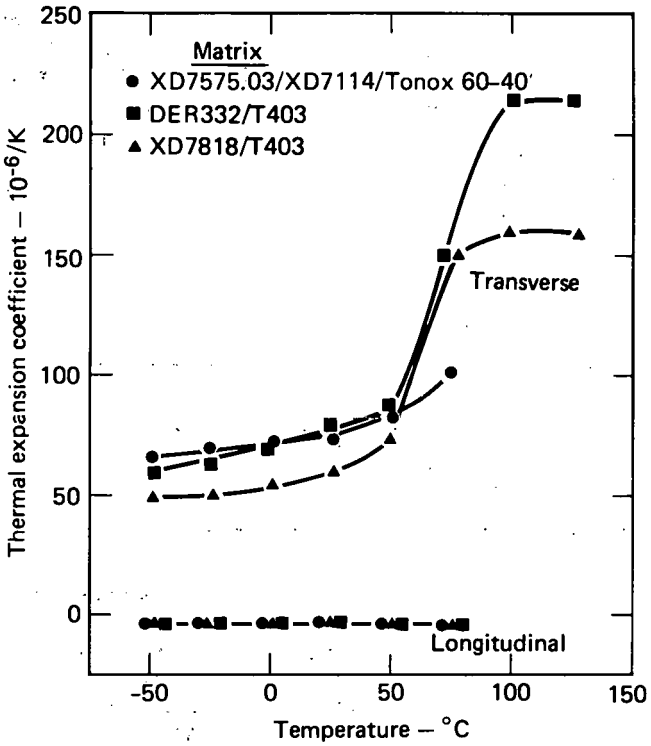

Fig. 3. Effect of Epoxy Type on Thermal-Expansion Coefficients for Kevlar 49 Composites

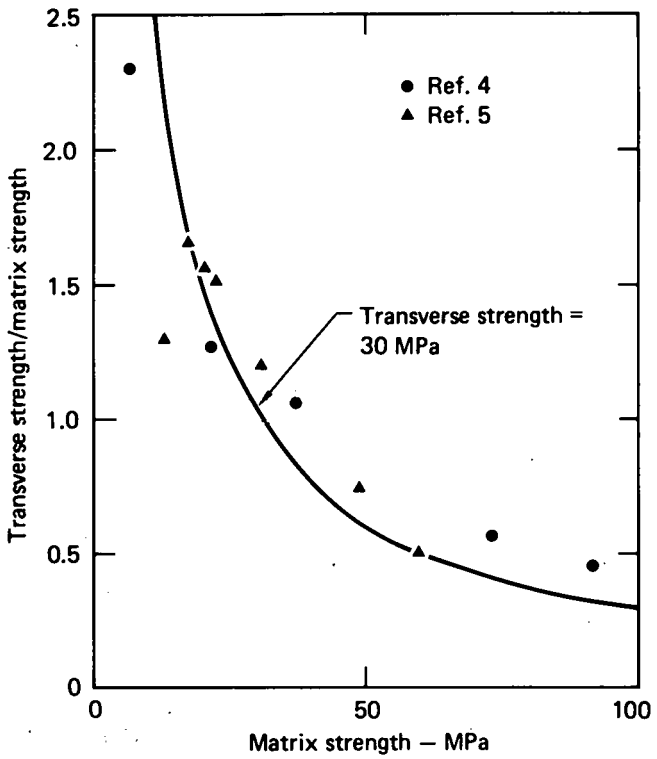

Fig. 4. Insensitivity of Transverse Strength to Matrix Strength for Fiber Composites

Mechanical properties of Kevlar 49/epoxy A were reported at the 1978 Annual Review.[1] Since then we have determined its thermal properties. Figure 3 shows the effect that the type of epoxy has on the thermal-expansion coefficients of the composite. Because the other two epoxy systems shown in the figure have lower glass-transition temperatures (~87°C for DER 332/T403 and ~76°C for XD7818/T403[2]) than epoxy A (~104°C[3]), the rapid increase in the transverse thermal-expansion coefficient occurs at a higher temperature for epoxy A. Up to 50°C, however, the transverse thermal expansion is fairly independent of epoxy type. The longitudinal thermal expansion is very independent of epoxy type throughout the temperature range studied.

We determined some of the mechanical properties of Kevlar 49/epoxy B both at room temperature and at 75°C, which is the operating temperature expected in flywheels. The preliminary data (Table 3) indicate very good retention of mechanical properties at 75°C. Additional tests are in progress.

To delineate the effect of matrix properties on matrix-controlled composite strength, we critically examined the data available in the literature.[4,5] Because we report the details in reference (6), we here only summarize our conclusions:

- The transverse and shear strengths are rather insensitive to the matrix strength. (Figure 4 shows the transverse-strength behavior.) Thus, failure strain can be increased by using a flexible resin with little sacrifice of failure stress.
- Whereas the elastic analysis predicts the composite-to-matrix strength ratio to be less than unity and to increase with the matrix strength and the fiber content for the composites studied, the experimental data show the opposite trend (Fig. 4). Thus, the elastic analysis alone is not sufficient to model the composite. However, this experimental observation can be explained by a model based on the average constituent stresses if the matrix ductility is assumed to increase with lower strength.

TABLE 3. Mechanical Properties of 60 vol% Kevlar 49 Epoxy Composite

Property	Room temperature	75°C
Elastic moduli, GPa		
Longitudinal	76.0	71.2
Transverse	5.5	3.1[a]
Shear	1.8[b]	1.5[b]
Strength, MPa		
Longitudinal tension	1569	1542
Transverse tension	8.0[a]	7.2[a]
Shear (0.2% offset)	25.0[b]	21.3[b]

[a]66 vol% fiber.

[b]70 vol% fiber.

- When a composite fails prematurely at the interface between the fiber and matrix before the matrix undergoes inelastic deformation, the composite strength follows the elastic prediction.
- If the fiber-to-matrix bond is strong, a matrix that is both strong and highly ductile will yield a higher composite strength.

STRESS-RUPTURE BEHAVIOR OF E-GLASS/EPOXY COMPOSITES*

Reliable long-term use of composite materials in flywheels requires that lifetime data on the composite be available and that the long-term behavior of the composite be understood. Recognizing such needs, we have been testing E-glass/epoxy strands in stress rupture. The epoxy system is DER 332/T403, and a strand contains about 2050 E-glass filaments.

Table 4 shows the status of our stress-rupture tests as of mid-July, 1979. Five different stress levels were chosen for study. The higher stress levels are necessary to generate lifetime data within a short time, and we expect the lowest to yield information about possible endurance limit. Tests are complete at 86 and 78% UTS, and no failure has yet occurred at 60 and 40% UTS.

The lifetime data shown in Fig. 5 were analyzed by using a two-parameter Weibull distribution of the form

$$R(t) = \exp\left[-\left(\frac{t}{t_0}\right)^{\alpha}\right],$$

TABLE 4. Results (to Date) of Stress-Rupture Testing of E-Glass/Epoxy Strands

Applied stress, % UTS[a]	Total No. of specimens	No. of failures	Ongoing tests: Last failure time, h	Ongoing tests: Elapsed time, h	Shape parameter	Characteristic lifetime, h
86	40	40	_	_	0.681	1.027×10^{-1}
78	66	66	_	_	0.267	2.894
70	50	31	2051	4968	0.277	1.146×10^{3}
60	50	0	_[b]	4968	_[b]	_[b]
40	50	0	_[b]	2736	_[b]	_[b]

[a]Average ultimate tensile strength.

[b]No failures yet; testing is continuing.

*Principal Investigator: H. T. Hahn.

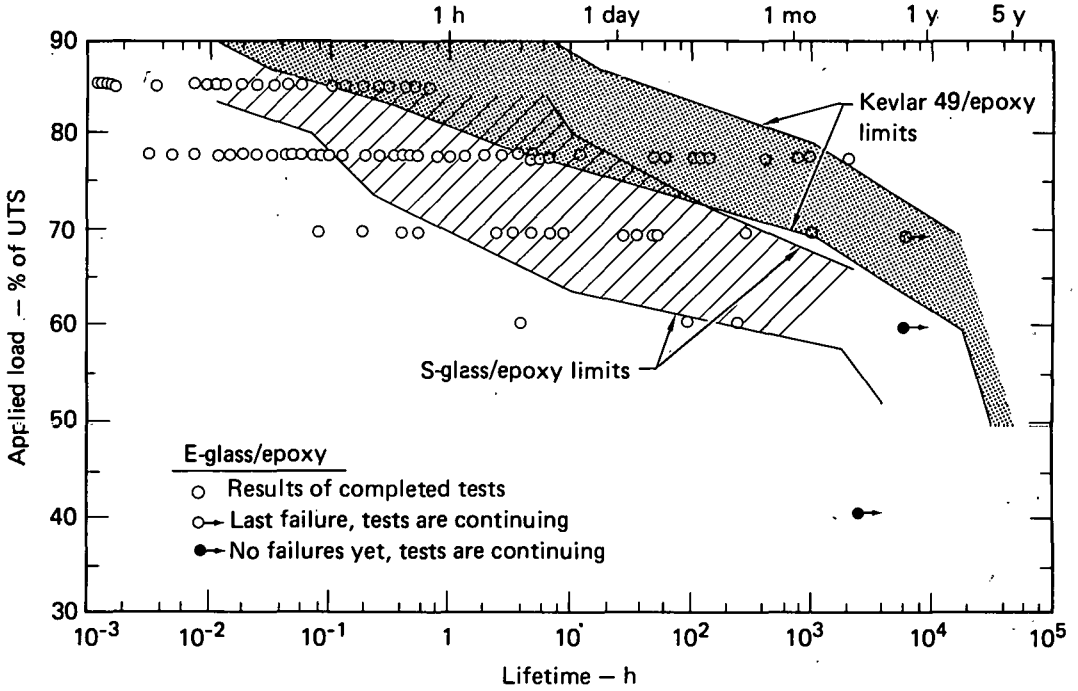

Fig. 5. Comparison of Lifetime Data for Composite Strands, where the Curves Represent 1% (Left) and 99% (Right) of Failures

where R(t) is the probability of lifetime greater than or equal to t. The shape parameter α and the characteristic lifetime t_0 were determined by the method of maximum likelihood at each stress level, and the results are given in Table 4. For comparison, Fig. 5 also shows the 1-to-99% failure bands of S-glass/epoxy and Kevlar 49/epoxy strands.[7-9] The stress-rupture behavior of E-glass/epoxy at the stress levels studied differs from those of the other materials in that the shape parameters are much smaller than unity, indicating a failure rate that decreases with time and large scatter.

The decreasing failure rate can be explained by the following failure process. Cracks created by fracture of weak fibers can grow either normal or parallel to the fibers. Initially, these cracks are more likely to grow normal to the fibers, leading to a catastrophic failure. In such cases, the failure rate is high. After the initial period of possible normal-crack propagation, the cracks tend to grow parallel to the fibers, thereby relieving stress concentrations on the neighboring fibers. Thus the failure rate of specimens that survive to this period is lower because the ultimate failure is a result of stress rupture of fibers without stress concentrations. Over the entire life span, therefore, the failure rate decreases with time.

Once an E-glass/epoxy strand survives the initial period of high failure rate, it out performs S-glass/epoxy at the same fraction of UTS (Fig. 5). Two factors seem to be responsible for such behavior in our testing. First, the E-glass/epoxy strands used were much larger than the S-glass/epoxy strands, i.e., ~2050 filaments versus ~200 filaments. Second, the test environment for the E-glass/epoxy was controlled better than for the S-glass/epoxy; the maximum relative humidity during testing was only 20% for the E-glass/epoxy but was about twice as high for the S-glass/epoxy. The larger size and lower humidity allow much less moisture concentration at the fiber/matrix interface of the E-glass/epoxy strands. Therefore, the E-glass/epxoy will outlive the S-glass/epoxy because water accelerates crack growth in glass through stress-corrosion. This conclusion is borne out by the excellent stress-rupture resistance of the E-glass/epoxy strands at 60% UTS.

Our study of stress-rupture behavior thus far indicates that the long-term lifetime of E-glass/epoxy at low stresses in a controlled environment can be much larger than expected from short-term lifetimes at high stresses. Because a flywheel is run in a vacuum, the problem of stress-corrosion does not exist in service. It seems possible that E-glass/epoxy can be used more effectively in vacuum than in a moist environment.

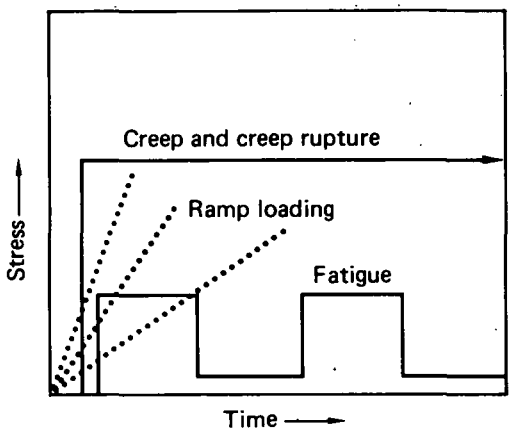

Fig. 6. Mechanical Tests Performed to Determine the Time-Dependent Behavior of Kevlar 49 Composites in the Tension-Tension Mode

FATIGUE LIFETIME OF KEVLAR 49 COMPOSITES*

Knowledge of time-dependent deformation and strengths is essential for the design of flywheels to ensure minimum dimensional change, maximum dynamic stability, and long-term safety of operation. Kevlar 49 composites are among the most important candidate materials for flywheels. Many engineering materials (e.g. most metals and composites of graphite) are independent of time and stress rate, and therefore their life can be predicted by cumulative-damage relations in terms of the number of service cycles (i.e. the S-N curves).

In contrast, Kevlar composites are significantly time-dependent in both fiber-controlled and matrix-controlled properties. To predict the life of Kevlar composites, we must extend conventional fatigue-analysis techniques to account for dependence on time and history. Such extension needs an adequate data base in conjunction with formulation of realistic theory and analysis. In this program, we are providing all of these.

We are characterizing the time-dependent properties of Kevlar 49 composites in the fiber direction by fitting test results to equations of viscoelasticity. Tests being conducted are illustrated in Fig. 6. Creep compliances are obtained from static-weight tests. The onset of nonlinearity depends on both stress level and loading rate, and we are identifying it by comparing creep tests and ramp loading tests at several loading rates. We are using low-frequency fatigue tests (1 Hz) to identify the effects of cyclic stress history on the composite deformations and lifetimes. By comparing the fatigue data with our stress-rupture data, we will obtain the design curves that can be used to estimate composite lifetimes in accordance with current engineering practice (e.g., curves of S-N or stress vs number of cycles to failure). We are also exploring a theoretical correlation via the damage-function formulation in an attempt to increase the utility of these fatigue data to generalized applications.

A second part of our fatigue program is to test small Kevlar 49 rings by tension-tension load cycling at the stress levels expected in operating fiber composite flywheels (i.e., 50 to 75% of UTS). We believe that this cyclic test simulates the ring-type flywheel and that the test results will be useful as a direct estimate of flywheel structural performance.

In our work we are relating materials-response properties to the input loads. In this manner, we not only produce immediately usable engineering data; we also lay the groundwork for a generalized failure theory for fiber composites. Much of our effort and resources have been directed toward the instrumentation and data-acquisition systems necessary to measure the strain responses of the composite. Examples of the creep responses are shown in Fig. 7 for nine samples, loaded to creep level of 88% of UTS. In Fig. 7, the vertical lines are the abrupt strain increases due to sample failures. We can readily observe the scatter of failure times and the strain increase immediately preceding failure. We performed 36 such creep-rupture tests at four stress levels (80, 84, 86, and 88% of UTS). Also, we are performing 20 additional creep tests at lower stress levels. These tests have been proceeding for over four months, and they have not yet reached rupture.

*Principal investigator: E. M. Wu.

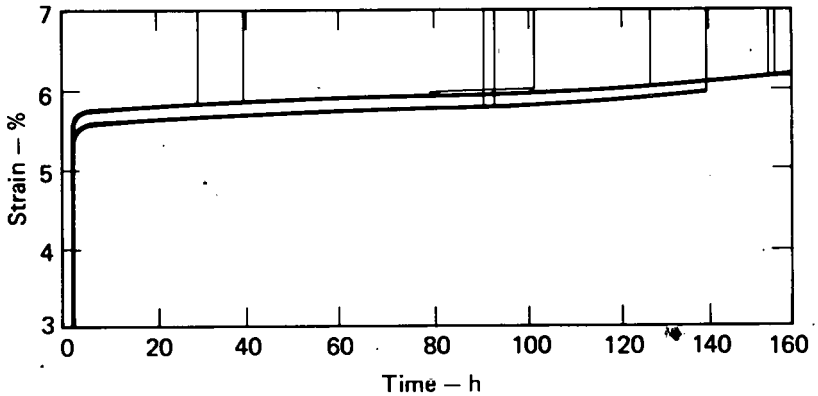

Fig. 7. Creep Strain and Distribution of Failure Times of Creep-Rupture Tests (at 88% of Static Ultimate Strength)

Typical data recorded for a fatigue test are shown in Fig. 8. Figure 8(a) is the strain history induced by a square-wave fatigue such as is shown in Fig. 6; we can observe strong time-dependent effects in the creep and recovery during loading and unloading. One such complete strain history is recorded every 100 cycles up to failure. Figure 8(b) is the envelope of the maximum and minimum strains for the fatigue cycles. We can observe a creep superimposed on the fatigue and, most importantly, a notable strain increase immediately preceding failure.

We conducted fatigue tests at five load levels (50, 65, 75, 80, and 88% of UTS) and recorded associated data. Extensive recording of detailed materials responses for creep and fatigue is unique to this program; preliminary analysis of these data suggest encouraging potentials in engineering design. First, in Fig. 9, we present the failure points in the conventional format of stress level (i.e. input load) vs the time to failure (i.e. number of load cycles). Under our test conditions, conventional theory of linear damage accumulation (i.e. Miner's rule) would predict the time to failure under fatigue loading to be twice the time to failure under creep. This would be the prediction because, in the square-wave fatigue, the sample is loaded only half of the time. Figure 9 shows that this prediction is not

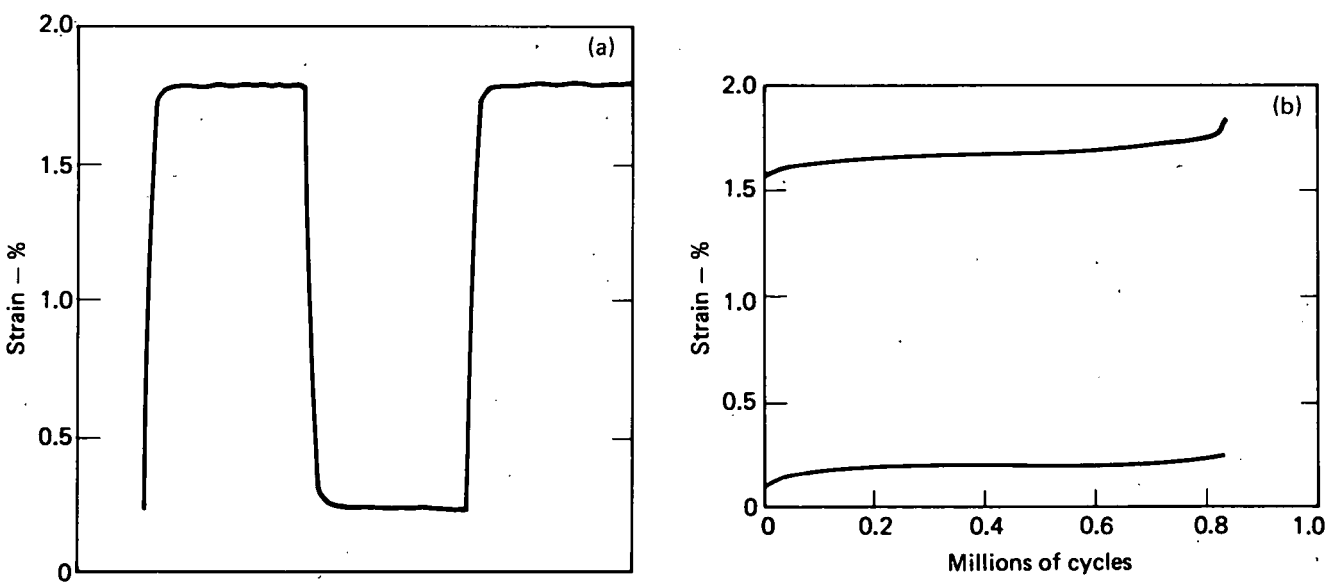

Fig. 8. Response of Kevlar 49 Composite to Cyclic Strain: (a) Response to Individual Cycles, (b) Envelope of Maximum and Minimum Strain

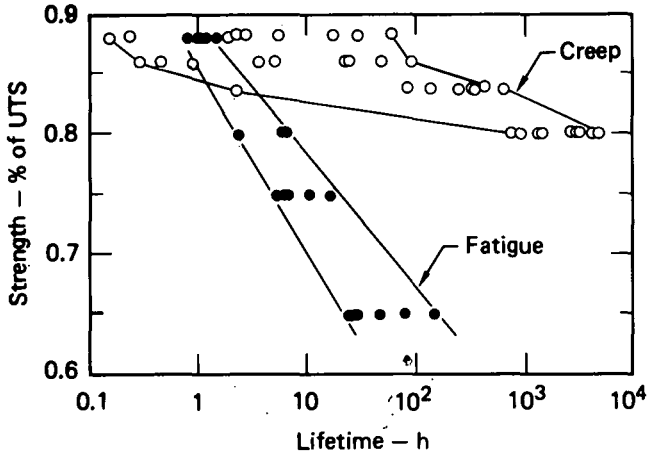

Fig. 9. Stress-Rupture and Fatigue Life of Kevlar 49 Composite

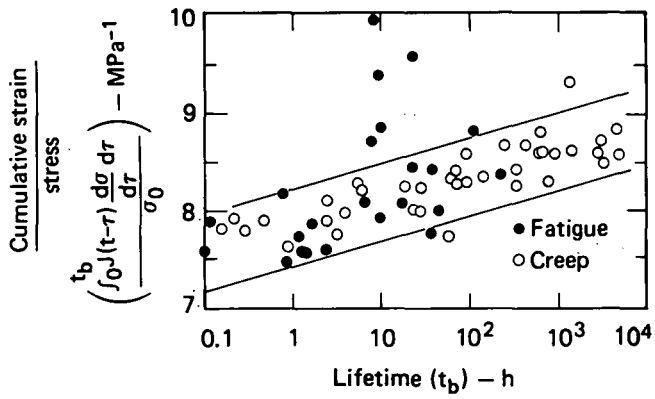

Fig. 10. Cumulative Strain per Unit Stress, for both Creep and Fatigue of Kevlar 49 Composite

supported by our data, where the fatigue time to failure is shorter, instead of longer, than the creep time to failure. Our interpretation is that, for a time-dependent Kevlar composite, the life under one load history cannot be used to predict the life under another load history when only the load-input information is available. The practical consequence is that if laboratory data collection is limited to recording the load input without also recording the material response, the laboratory data will not yield satisfactory predictions of the life of a composite flywheel under a given service loading history. However, including the recorded materials response in the data analysis yields much improved correlations. Figure 10 shows the cumulative strain (the response) at failure vs the time to failure for creep and fatigue. We can observe a general merging of both the creep-rupture and fatigue data. This indicates to us that monitoring both the load input and the materials responses yields data that can be used to predict life under general-service loading.

We also observed interesting results from the simulated structural-fatigue test of the rings. The loading fixture is a split "D" fixture. We applied axial cyclic loading (1 Hz) at 50% of UTS. In this configuration, most of the ring is under cyclic tension but the point at the split is under a complex contact stress concentration. We estimate this test to simulate the contact stress where a spoke attaches to the rim in an actual flywheel. We have tested five rings in this manner and periodically monitored the strain. The rings were tested up to 10^6 cycles and did not fail. They were subsequently tested at a slow loading rate until failure. (The times to failure for this final destructive test were on the order of 10 h.) We observed two important phenomena: After 10^6 cycles at 50% load, the residual strength decreased slightly, by approximately 5%. Also, strain accumulated as in the tension tests, and the material exhibited significant strain recovery when cycling loading was interrupted. The effect of the strain recovery on the life of the ring is now being explored.

In summary, in the fatigue life-time program we have collected a significant and comprehensive amount of creep-rupture and fatigue data. These include recordings of both the load inputs and the material-response strains. Correlation between life-times under different load histories appeared to be possible with these data. Further development may provide the basis of predicting flywheel structural life from laboratory testing. We have also conducted structural testing of rings to simulate rim-type flywheel stress states to bridge the gap between laboratory tests and flywheel applications.

REFERENCES

1. J. A. Rinde, Materials Program for Fiber Composite Flywheels, Lawrence Livermore Laboratory, Rept. UCRL-81724 (1978).

2. L. L. Clements and R. L. Moore, "Composite Properties of an Aramid Fiber in a Room-Temperature-Curable Epoxy Matrix," SAMPE Quarterly 9, 6 (1977).

3. J. A. Rinde, E. T. Mones, R. L. Moore, and H. A. Newey, An Epoxy Resin-Elastomer System for Filament Winding, Lawrence Livermore Laboratory, Rept. UCRL-81254 (1978).

4. R. M. Christensen and J. A. Rinde, Transverse Tensile Characteristics of Fiber Composites with Flexible Resins: Theory and Test Results, Lawrence Livermore Laboratory, Rept. UCRL-79983 (1977).

5. J. B. Snell and J. N. Schurb, "Scotchply Prepregs for Flywheel Applications," in Proc. 1975 Flywheel Technology Symposium, U.S. ERDA document 76-85 (1975), p. 203.

6. H. T. Hahn, Effect of Constituent Properties on Composite Strength, Lawrence Livermore Laboratory, Livermore, CA, UCRL-82051 (1978).

7. T. T. Chiao, J. K. Lepper, N. W. Hetherington, and R. L. Moore, "Stress-Rupture of Single S-Glass/Epoxy Composites," J. Composite Mat. 6, 358 (1972).

8. T. T. Chiao, J. E. Wells, R. L. Moore, and M. A. Hamstad, "Stress-Rupture Behavior of Strands of an Organic Fiber/Epoxy Matrix," in Composite Materials: Testing and Design (Third Conference), ASTM Special Technical Publication 546 (American Society for Testing and Materials, Philadelphia, 1974) p. 209.

9. R. H. Toland and T. T. Chiao, Stress-Rupture Life of Kevlar/Epoxy Spherical Pressure Vessels, Lawrence Livermore Laboratory, Rept. UCID-17755, Part 2 (1978).

THIS PAGE

WAS INTENTIONALLY

LEFT BLANK

PROJECT SUMMARY

Project Title:	"High Energy Density Flywheel"
Principal Investigator:	David L. Satchwell
Organization:	AiResearch Manufacturing Company of California 2525 West 190th Street Torrance, California 90509 (213) 323-9500
Project Goals:	Fabricate two flywheel rotors, for later test, which have an energy density of 80 Wh/Kg.
Project Status:	The contract is completed. Two 80 Wh/Kg rotors are ready for tests that will be conducted on a later contract.
Contract Number:	AT(29-1)-789
Contract Period:	August 1978 - May 1979
Funding Level:	$267,759
Funding Source:	Sandia Laboratories, U.S. Department of Energy, Division of Energy Storage Systems

HIGH-ENERGY-DENSITY FLYWHEEL

David L. Satchwell
AiResearch Manufacturing Company of California
2525 W. 190th Street
Torrance, California 90509

ABSTRACT

This paper describes the design and fabrication of a flywheel rotor with an energy density of 80 Wh/kg. The design features a multi-ring, S-glass and Kevlar composite material rim that is mounted on a graphite composite spoked hub. Composite material flywheels have been constructed with identical rim design using spoked aluminum hubs. These aluminum hub flywheels have been successfully tested to energy densities of 53 Wh/kg. The use of high strength-to-weight graphite composite material in place of the aluminum material significantly reduces the weight of the rotor assembly and thereby increases the energy density. Graphite epoxy composite is chosen for the hub because of its high modulus of elasticity, because of its light weight, and because of its high ultimate flexural strength.

The hub consists of multiple slats, alternately bonded one upon another to form a four-spoke hub with rigid cruciform shape. Hub testing was conducted on three hub sections 19.5 inch dia. by 1 inch thick; and consisted of compression testing across one opposite set of spokes to determine the location, mode, and load at failure. Two hubs were cycled to an increased stress level that is equivalent to a full-life test. Two complete assembled rotors were made available for testing in a following phase.

INTRODUCTION

A flywheel has been designed and fabricated by Garrett-AiResearch to demonstrate a high energy density of 80 w-hr/kg in the rotor. This is a 50% increase over existing flywheel rotors. The rotor design consists of a multi-ring, sub-circular, S-glass/epoxy composite and Kevlar/epoxy composite material rim that is mounted on a star hub of graphite composite material (see Figure 1). This work is being performed under a contract with the Sandia Laboratories for the Department of Energy, Division of Energy Storage Systems.

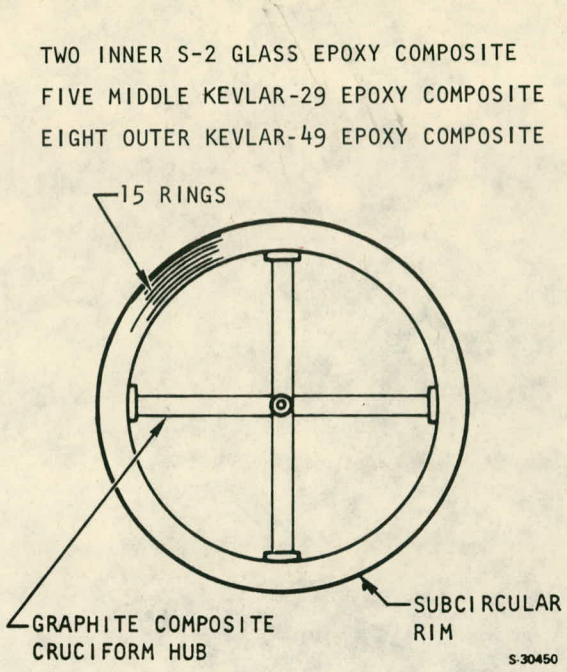

Fig. 1 Flywheel Rotor Configuration

Because of its multiring design, the rim can accommodate the radial stresses caused by centrifugal forces. Upon assembly, the rim is distorted from its round shape so that when placed on an oversized star hub, the forces resulting from the rim trying to assume its round shape hold it onto the hub. The graphite/epoxy composite material hub has a small cross section and is very light, yet can withstand the forces imposed on it.

Two flywheel rotors have been fabricated that meet the above specifications, producibility studies have been completed, and a test plan has been written for a 100 cycle test with deceleration from 28,800 rpm to 9,500 rpm at a 37 kw power level.

MATERIALS SELECTION AND HUB FABRICATION PROCESS PROOF

Rings were made of S-2 Fiberglass/epoxy composite and of Kevlar-49 and Kevlar 29/epoxy composite. The epoxy matrix material, DOW DER 332, was qualified by hydrostatic testing of 19 inch diameter rings. Figure 2 is a photograph of the hydrostatic test fixture used to determine modulus of elasticity from tests of ring stretch vs. internal pressure. Ultimate strength data also was obtained on the test rings by bursting them in the fixture. Placement of the test ring in the fixture is shown in Figure 3.

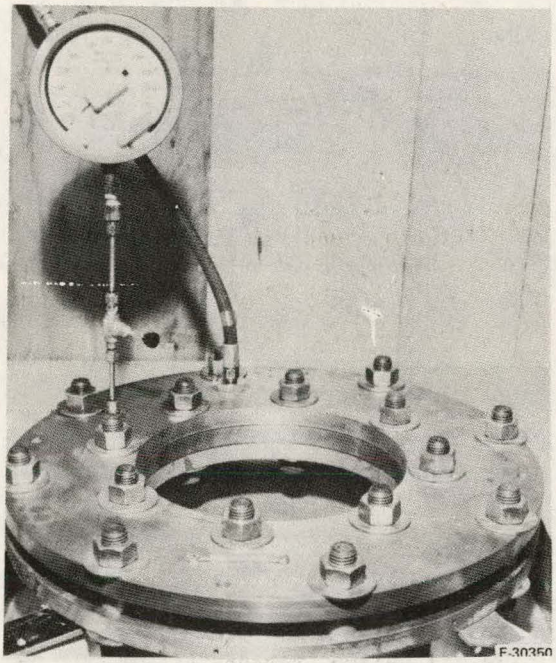

Fig. 2. Hydrostatic Test Fixture

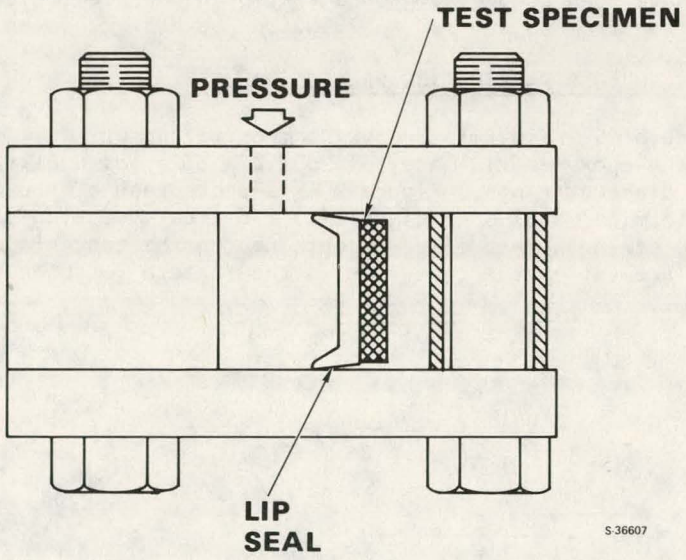

Fig. 3. Hydrostatic Test Section

The hub, made of a graphite/epoxy composite, was fabricated by Structural Composites Industries, Inc. of Azusa, California. Graphite composite is chosen for this application because of its modulus of elasticity of 18 X 10^6 psi, its light weight of 0.05 lb/cu. in., and its ultimate flexural strength of 210,000 psi. The combination of these properties allows reducing the hub weight from 22.5 lb for an aluminum hub to 6.5 lb for the graphite epoxy composite hub.

Three 1 inch axial length test hubs were fabricated to prove the fabrication process, and to allow testing of a hub under axial compression. These 1 inch test hubs are made from 15 slats stacked to form a 19.5 inch diameter rigid cruciform hub. Figure 4 is a photo of the graphite slat, and Figure 5 is a photo of the 1 inch test hub.

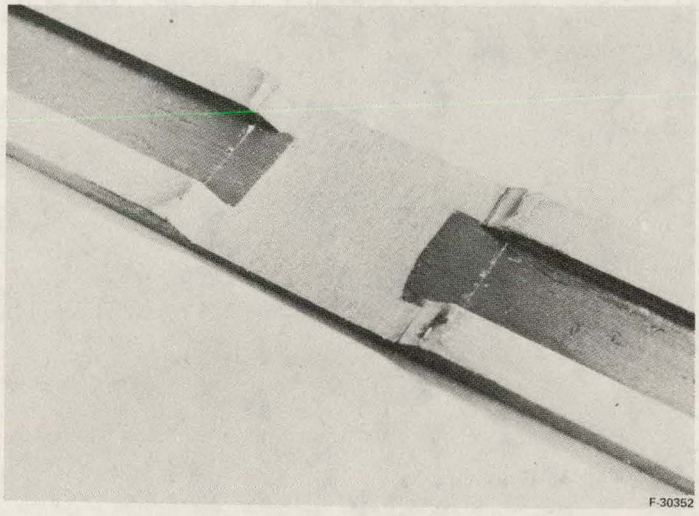

Fig. 4. Slat with Peal Ply in Place

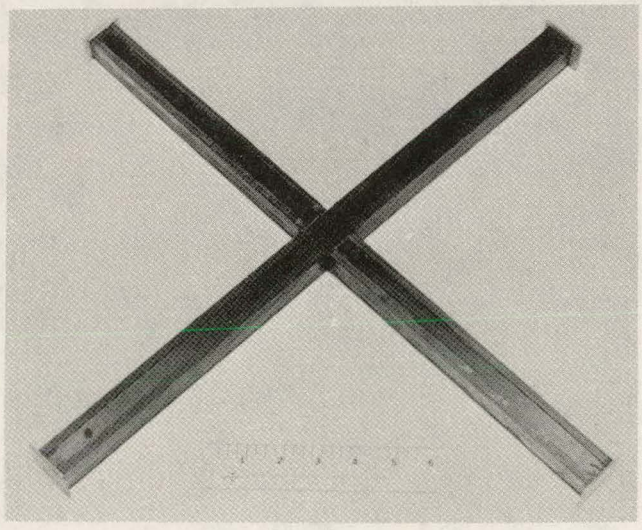

Fig. 5. 1 Inch Test Hub

Two hubs were cycled to simulate 100 speed cycles between full speed and 33 percent speed. The cycle tests were completed with no deterioration, and the stress strain slope remained constant through the tests. These hubs were tested in compression along the axis of the spoke to determine failure strength, and failure mode (see Figure 6). The hub failed in splitting between fibers near the spoke tip at 37,350 psi, four times the stress that will be imposed during the operational cycle.

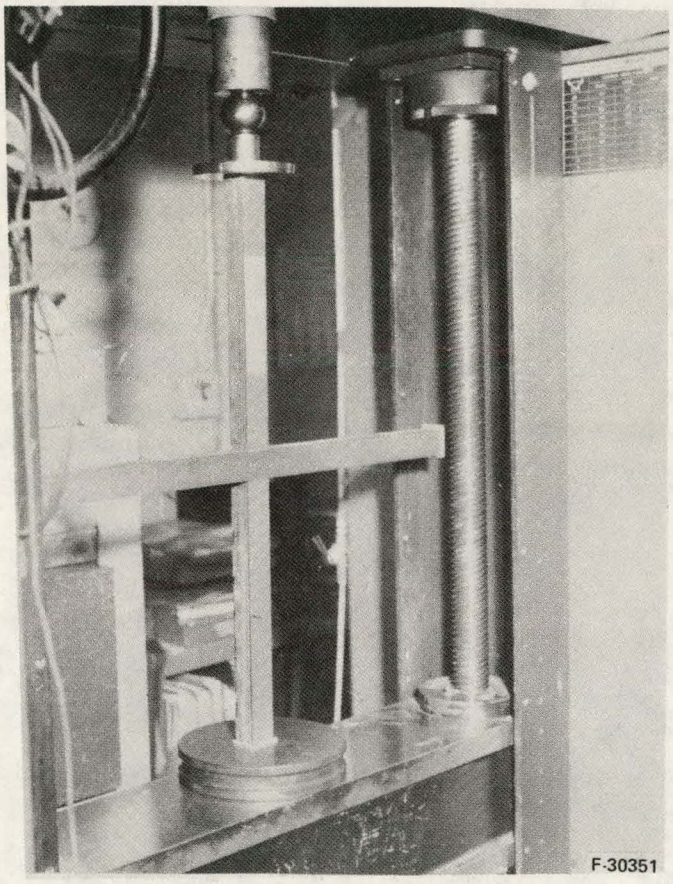

Fig. 6. Hub Compression Test

DESIGN

During operation, the rim is subjected to tangential (hoop) stresses, bending stresses and shear stresses. The tangential stresses are caused by the high centrifugal forces. The bending stresses are caused by the change in curvature of the rim over the spoke tips as the rim changes diameter under operation. The maximum hoop stress of 165.8 ksi occurs in the 8th ring at maximum speed. This stress is 92 percent of the design allowable of 180.0 ksi.

The maximum bending stress of 21.5 ksi, which is 60 percent of the design allowable of 36.0 ksi, also occurs in the 8th ring, but this stress occurs at zero speed, the condition of greatest rim out-of-roundness. Therefore, the maximum values of hoop and bending stresses do not occur together.

In addition to the above loads, the innermost ring is subjected to loads at the spoke tip interface. A radial compressive force is developed between the rim and the spoke tip. This force is shown as a function of operating speed and rim material modulus in Figure 7.

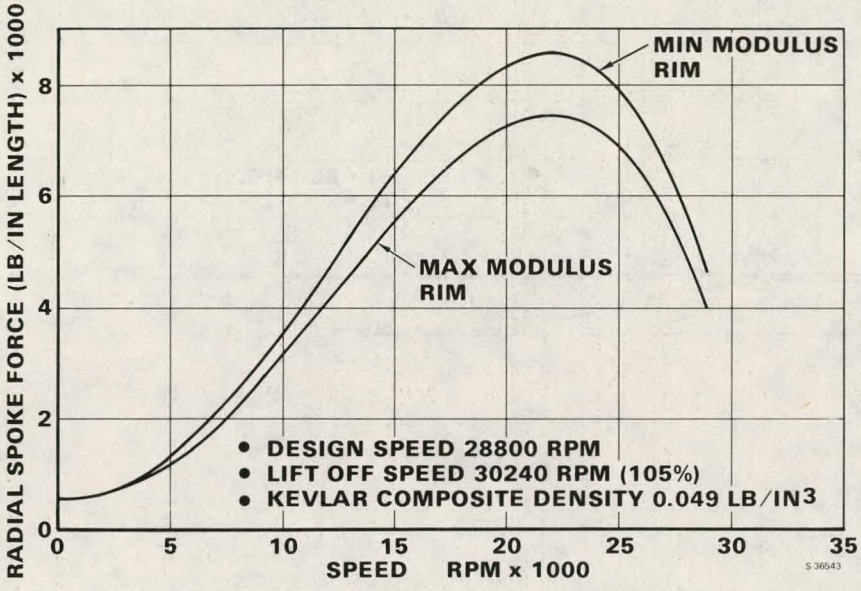

Fig. 7. Spoke Tip Radial Force

The peak radial force is 8500 lbs per unit axial length at 22,800-rpm. The average compressive stress in the inner ring due to this force is 5.7 ksi. This is 50 per cent of the design allowable compressive stress.

The hub supports the flywheel rims and must transfer all transient and steady loads to and from the rim. Another load on the hub is its own centrifugal load. The variation with rotational speed of the steady stress at the tip section and the root section is given on Figure 8. For the root, the maximum tensile stress of 81.5 ksi occurs at 28,800 rpm. This stress is well below the expected 180 ksi fatigue limit for 10^4 cycles at a stress ratio of 0.1. The highest compressive stress of 9.7 ksi occurs in the tip at 20,000 rpm. This stress which is 4 percent of the ultimate strength is expected to be well below the required fatigue limit at 10^4 cycles.

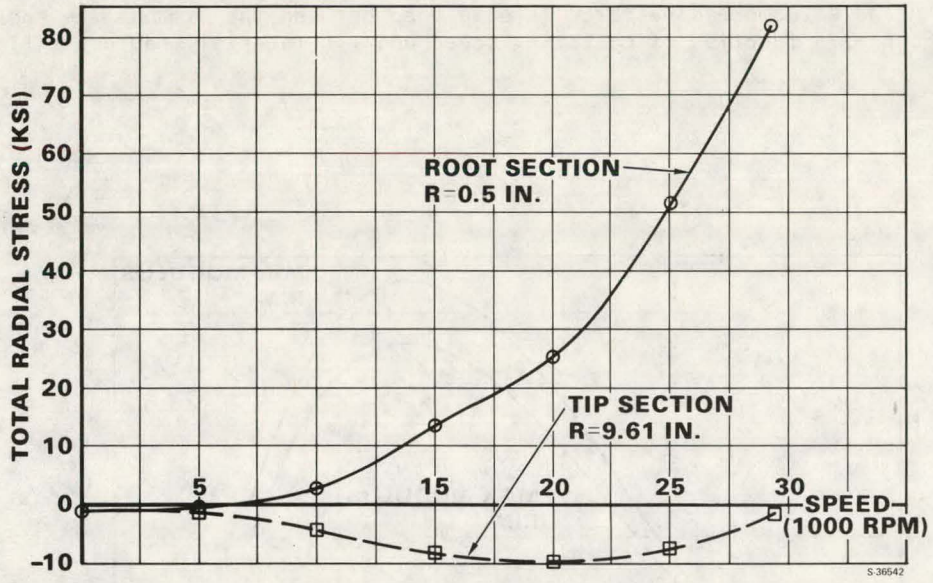

Fig. 8. Spoke Stress Variation with Speed

A detailed finite element analysis has been performed at the spoke tip to determine the magnitudes of the local stresses. Because of the relatively low transverse strength of the unidirectional graphite epoxy hub, it is important to ensure that the compressive forces at the spoke tip result in transverse stresses that do not exceed the allowable strength.

Combining the radial forces, the bearing area available, the selected rim-to-hub interference, and material properties, allows the geometry of the spoke tip to be determined, as shown in Figure 9.

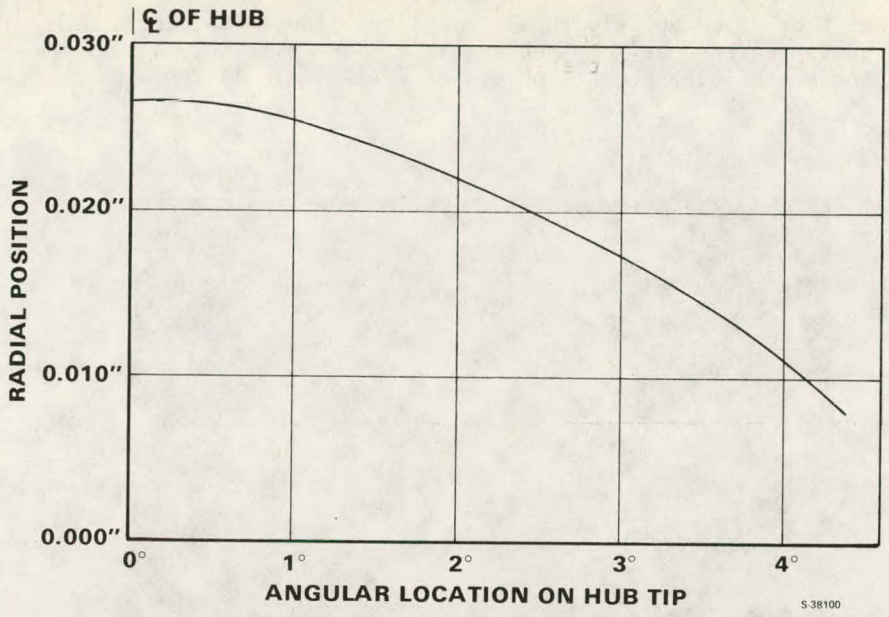

Fig. 9. Hub Tip Profile

HUB AND RIM FABRICATION

Two assembled rotors, as pictured in Figure 10, have been fabricated.

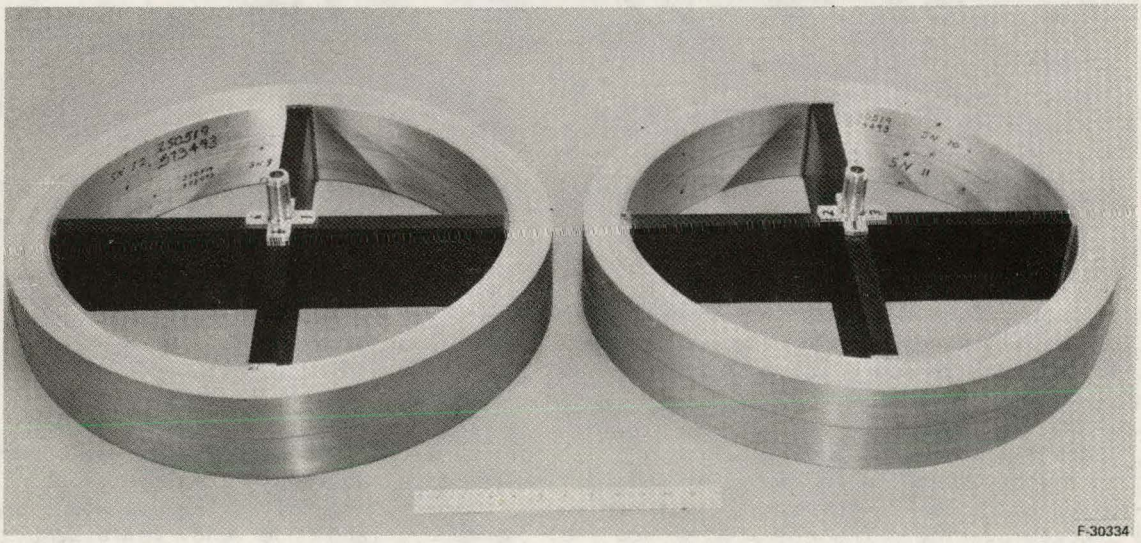

Fig. 10. Two Assembled Rotors

The hub was fabricated by Structural Composites Industries, Inc., using the methods developed and proven on the one inch hub sections. The rim is similar to the one developed for a vehicular propulsion system (see Figure 11).

Fig. 11. Flywheel Rim Modules

The hub slats were molded from multiple layers of pre-preg graphite fiber tape. Individual slats were stacked into a cruciform shape in an assembly mold. The stack was loaded to a pressure at a specified stack height, and heated to cure the adhesive bond.

Each rim was wound individually on a cylindrical aluminum mandrel. The roving was run at a controlled tension and the fiber volume fraction was kept within the range of 71-75 percent. Each ring was gelled after winding. Each successive ring was wound upon the preceeding ring. The rim was removed from the mandrel and made ready for assembly upon the hub.

The rotor was assembled in the fixture shown in Figure 12. The rim was stretched squarish so that the diametral measurement at the spoke was enlarged enough to allow the oversized 4-spoke hub to be placed inside of the rim. The ram pressure was lowered, allowing the rim to spring tight upon the hub.

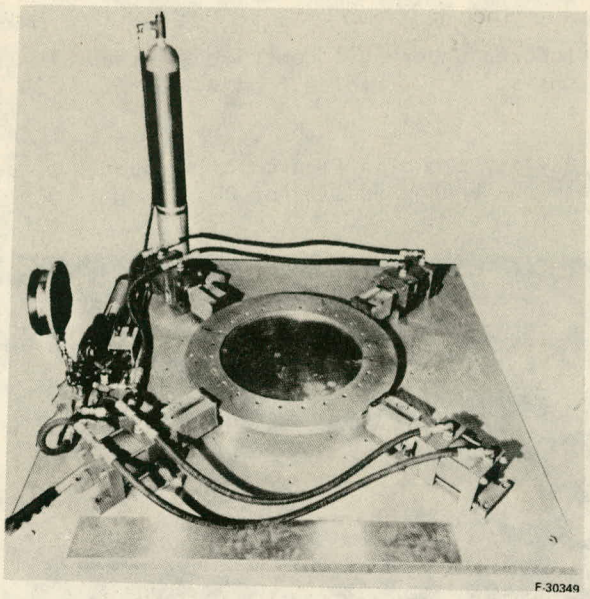

Fig. 12. Assembly Fixture

PRODUCIBILITY AND COST ANALYSIS

The costs and processes involved in the production of the flywheels were analyzed. Cost-effectiveness is affected mainly by the design configuration, by scaling for economic use of materials, and by effective tooling and production techniques. Table 1 summarizes the cost/producibility results.

TABLE 1. Flywheel Rotor Production Cost

Cost Element	1979 Cost, $			1984 Cost, $
	100/yr	1000/yr	10,000/yr	10,000/yr
Material	370.44	342.52	232.68	169.17
Labor:				
Hub	1560.00	748.00	62.40	62.40
Rim	1872.00	249.60	74.88	74.88
Total $/unit	3802.44	1340.12	369.96	306.45
Total tooling, $	37,500	110,500	525,000	525,000

TEST PLAN

The flywheel rotors produced under this contract are ready for test under a separate contract. The test will consist of 100 cycles from 9,500 rpm to 28,800 rpm and back to 9,500 rpm at 37 kW power.

The AiResearch test facility shown in Figure 13 is capable of performing testing to this flywheel to demonstrate the energy density of 80 Wh/kg.

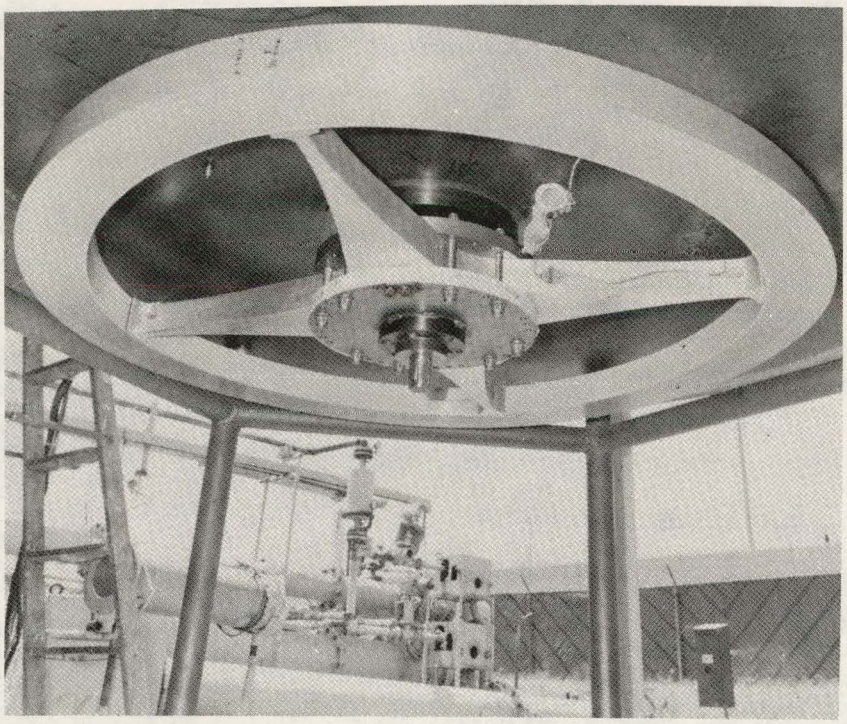

Fig. 13. Composite Flywheel in Test Facility

PROJECT SUMMARY

Project Title:	"Composite-Laminate Flywheel-Rotor Development Program"
Principal Investigator:	Satish V. Kulkarni
Organization:	University of California, Lawrence Livermore Laboratory P.O. Box 808, Mail Stop L-338 Livermore, CA 94550 FTS 532-7128
Project Goals:	To develop a practical and economical prototype high-energy density, composite-laminate rotor for hybrid flywheel/electric/ICE vehicles and stationary applications. In terms of energy density, the objective is to obtain 88-Wh/kg (40 Wh/lb) at failure with an operational range of 44-55 Wh/kg (20-25 Wh/lb) and an energy storage capacity of approximately 1 kWh.
Project Status:	The program is being conducted at the Lawrence Livermore Laboratory (tapered thickness 'Stodola' rotor concept) and the General Electric Company (α-ply constant-thickness rotor concept). The LLL effort has been in the following three areas. Proof-of-concept: (a) redesign of the 'Stodola' rotor by edge thickening and filament winding of ring around the disc to increase energy density; (b) develop a modified layup pattern to increase the strength anisotropy of quasi-isotropic laminates; and (c) fabricate S2-glass and graphite/epoxy tapered-thickness rotors. Design/test correlation studies: (a) perform tests on various S2-glass, graphite and Kevlar-49/epoxy quasi-isotropic laminate coupons to obtain design data and determine the laminate strength anisotropy; (b) spin test S2-glass, graphite and Kevlar-49/epoxy constant-thickness rotors to establish a relationship between design data and failure speed; and (c) evaluate these rotors non-destructively to determine damage accumulation during spinning. Materials and processes: (a) utilize the matched metal-die-compression molding process for fabricating rotors; and (b) investigate the feasibility of making low-cost rotors from structural sheet-molding compounds. Joint cooperative programs have been established with Owens-Corning and PPG Fiberglass in this area. During FY 1980, the above mentioned tasks will be continued.
Contract Number:	W-7405-ENG-48
Contract Period:	FY 1979
Funding Level:	$520K (Total for LLL and GE)
Funding Source:	U.S. Department of Energy

COMPOSITE-LAMINATE FLYWHEEL-ROTOR DEVELOPMENT PROGRAM*

Satish V. Kulkarni
Lawrence Livermore Laboratory, University of California
Livermore, CA 94550

ABSTRACT

The composite-laminate flywheel program is being conducted at the Lawrence Livermore Laboratory (LLL) (tapered thickness 'Stodola' rotor concept) and at the General Electric Company (alpha-ply constant-thickness rotor concept). The major thrust of the FY 1979 LLL program was directed towards identifying the pacing issues and implementing the steps undertaken to improve the performance of the rotor. To that end, the following tasks were initiated: (1) redesigning the 'Stodola' rotor to increase the energy density; (2) testing laminate coupons to establish the degree of strength anisotropy of various quasi-isotropic laminates; (3) spin testing of constant-thickness composite-laminate rotors to establish a relationship between design data and failure speed; (4) developing a matched-metal-die compression-molding process to fabricate thick, high-fiber volume, low-void-content composite panels; and (5) exploring the feasibility of manufacturing low-cost rotors from structural sheet-molding compounds. The progress to date in each of these areas is reported here.

INTRODUCTION

The Lawrence Livermore Laboratory (LLL) and the General Electric Company (GE) have been involved since 1977 in the development of fiber-composite flywheels. It has been concluded from these studies that a most promising rotor design is a disk composed of a number of laminae of fiber-composite materials oriented at different directions. The emphasis at LLL is on the tapered-thickness disk; GE is investigating an alpha-ply disk with a rim overwrap.

The objectives of this program are to develop the technology for high-energy density, fiber-composite flywheels based on the laminated disk concept and to demonstrate a prototype for a practical flywheel of this design. Our goal is a working energy density in prototype wheels of approximately 50 Wh/kg with a capacity of 1 kWh. We also expect to demonstrate model wheels failing at energy densities of about 88 Wh/kg. From a practical design viewpoint, the approach is to optimize the total flywheel-energy system with respect to weight, volume, manufacturability, and economy.

This effort consists of three primary subtasks: (1) design/analysis, (2) materials and processes/fabrication, and (3) test and evaluation. Only the LLL program will be discussed here; the progress of the GE effort is reported elsewhere in this proceedings.

BACKGROUND

Progress during FY 1978 has been reported in Refs. 1 and 2 and is summarized here.

DESIGN/ANALYSIS

A uniform-strength, graphite/epoxy, quasi-isotropic, laminate-composite, 'Stodola' disk was designed.

*This work was performed under the auspices of the U.S. Department of Energy by Lawrence Livermore Laboratory under contract No. W-7405-Eng-48.

A finite-element analysis of a truncated, graphite/epoxy, 'Stodola' rotor was conducted to determine the stress redistribution resulting from the truncation and to determine the magnitude of interlaminar stresses.

MATERIALS AND PROCESS/FABRICATION

A 1-in. thick, high-strength, Celion* 6000/5213 graphite/epoxy (0/±45/90), quasi-isotropic laminate was fabricated by Babcock & Wilcox, Alliance, Ohio, by utilizing the vacuum-bag/press-molding technique.

Bonding of hub was accomplished by Lord Corp., Erie, Pa., by employing elastomeric interlayers.

Precision machining of rotor to the tapered thickness profile was done at LLL. Figure 1 shows the rotor with the hub attachment.

TEST AND EVALUATION

Spin testing of rotor was performed at Johns Hopkins University, Applied Physics Laboratory. Table 1 indicates the diagnostics of the spin test. The energy density

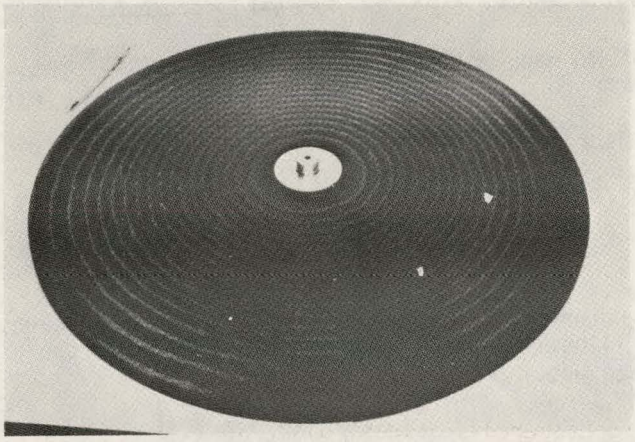

Fig. 1. Tapered-Thickness Graphite/Epoxy Quasi-Isotropic Composite-Laminate Rotor.

TABLE 1. Diagnostic of Tapered-Thickness, Celion 6000/5213, Graphite/Epoxy Flywheel Test

Predicted failure speed	50,000
Predicted energy density	54 Wh/lb
Actual failure speed	36,000 rpm
Actual energy density	28.4 Wh/lb
Predicted maximum strain[a] at 50,000 rpm	0.0102
Actual maximum strain at failure	0.0062
Failure strain from (0/±45/90) laminate test (along 0° layer)	0.0095
Failure strain from (0/±45/90) laminate test (at 22.5° to 0° layer)	0.0066

[a] ($\varepsilon_r = \varepsilon_\theta$).

*Reference to a company or product name does not imply approval or recommendation of the product by the University of California or the U.S. Department of Energy to the exclusion of others that may be suitable.

obtained was about half the predicted value. Also, the actual strain at failure (0.0062) was in close agreement with that obtained from the off-axis laminate test (0.0066).

SUMMARY OF EFFORT DURING FY 1979

Because of the lower-than-expected performance of the 'Stodola' rotor, the program tasks were evaluated critically and certain pacing issues were identified. These areas of concern are listed below:

- Truncation of infinite 'Stodola' rotor reduces efficiency.
- Finite-element analysis may not accurately predict interlaminar stresses.
- Thick laminate technology is in an infant stage. Vacuum bag/press-molding process is not amenable to a low-cost production type environment.
- Machining of rotor is a time-consuming (and expensive) task requiring tight tolerances. Also machining of a built-up composite part is contrary to the concept of building from scratch to avoid material waste.
- Quasi-isotropic laminates are not isotropic in strength (see Fig. 2). Hence full-strength potential of laminate is not fully realized.
- Effect of biaxial stress field on laminate strength is not fully understood (also see Fig. 2).
- Both material and manufacturing costs are high.
- Incomplete understanding of rotor/shaft dynamics leads to premature failures during testing.
- Failure mode is catastrophic for graphite/epoxy.
- Test diagnostics are inadequate.

Effort during FY 79 was directed primarily towards addressing these issues.

DESIGN/ANALYSIS

To increase the rotor efficiency, the rotor edge was thickened to "buy" back mass (Fig. 3a). Figure 4 illustrates that the energy density for the graphite/epoxy rotor can indeed be increased about 5-10% by this approach.

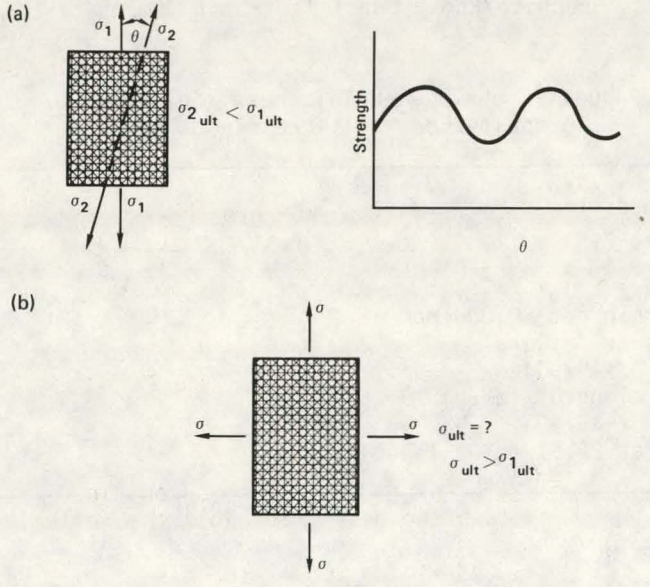

Fig. 2. Certain Features of Quasi-Isotropic Composite-Laminate Strength. (a) Strength Anisotropy. (b) Effect of Biaxial Stress.

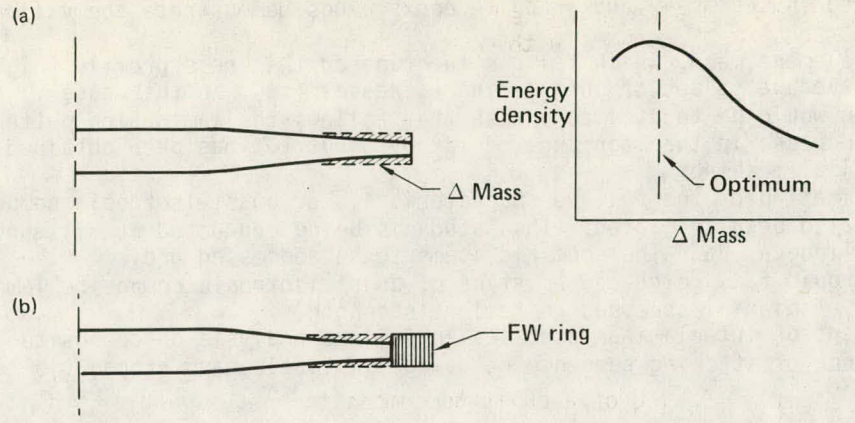

Fig. 3. Design Modifications to Improve Rotor Efficiency. (a) Edge Thickening. (b) Containment of Rotor in a Ring.

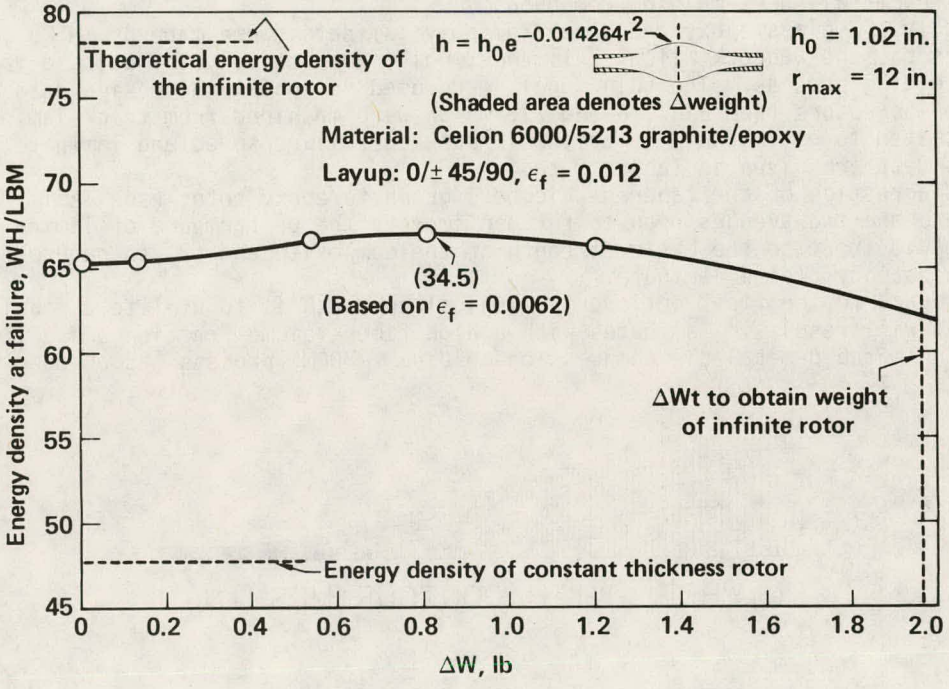

Fig. 4. Variation of Energy Density with Edge Thickening of Rotor.

If, in addition to the edge thickening, the rotor is contained in a filament-wound ring of a higher specific modulus than the disk (Fig. 3b), the following would be the added advantages:

- A compressive pre-stress would be induced in the disk.
- A benign failure mode can be precipitated in the ring.

Such a "hybrid" concept is also being employed by GE for the constant-thickness alpha-ply flywheels.[3] Parametric finite-element studies conducted for chopped-fiber

rotors contained in Kevlar-49 and graphite/epoxy rings demonstrate the validity of this concept.

A finite-element mesh, which follows the tapered thickness profile (Fig. 5a), can determine the average values of interlaminar stresses (τ_{rz}, in this case). A preferred approach would be to utilize a mesh that follows the lamination pattern shown in Fig. 5b. An increase in the magnitude of τ_{rz} by about 10% has been obtained by using the parallel meshing.

An investigation of the failure characteristics of quasi-isotropic composite laminates has also been initiated. This study is being conducted at Villanova University, Villanova, Pa. The specific items to be addressed are:

- Anisotropic failure characteristics of quasi-isotropic composite laminates.
- Effect of biaxial stresses on failure strength.
- Treatment of interlaminar stresses in failure analysis of composite flywheels.
- Influence of stacking sequence on damage initiation and propagation in laminated composite rotors.

MATERIALS AND PROCESSES/FABRICATION

The major thrust of this subtask in FY 1979 has been in the areas of (1) fabricating by the matched-metal-die compression-molding process, continuous-fiber S2-glass, Kevlar-49, and graphite/epoxy panels for both coupon testing and machining constant and tapered-thickness rotors and (2) exploring the feasibility of making low-cost rotors by utilizing structural sheet-molding compounds.

Initially, S2-glass/epoxy and graphite/epoxy laminates were made by 3M Co., St. Paul, Minnesota, and Babcock Wilcox, Alliance, Ohio, respectively, by using a vacuum bag/press-molding process. The thin panels were used for obtaining design data. Constant thickness rotors (see Figs. 6 and 7), which were machined from thick laminates, were spin tested to establish a relationship between failure speed and laminate test data. Test data are given in Tables 2 to 4.

Test diagnostics of the tapered-thickness graphite/epoxy rotor (see Table 1) suggest there are two avenues open to further improve the performance of laminated-disk rotors: (1) to increase the basic strength of the composite and (2) to reduce the strength anisotropy of the laminate.

With regard to the first option, the logical approach is to utilize a fabrication process that will result in laminates with a high fiber-volume fraction and a low void content. The matched-metal-die compression-molding (MMDCM) process (as opposed to the

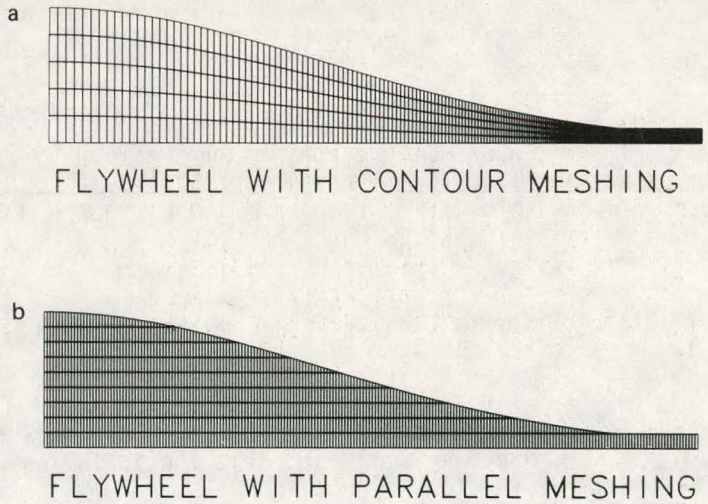

Fig. 5. Finite-Element Meshing for Tapered-Thickness Rotor. (a) Flywheel with Contour Meshing. (b) Flywheel with Parallel Meshing.

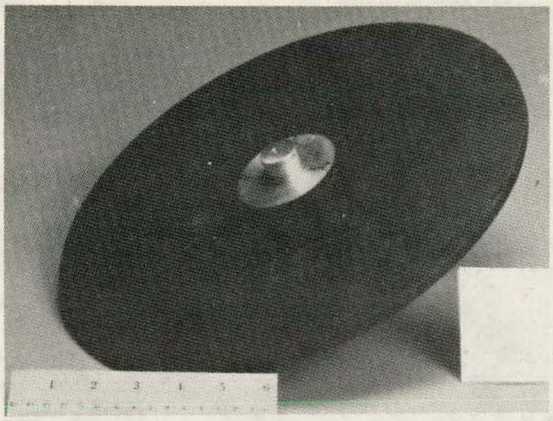

Fig. 6. Constant-Thickness Graphite/Epoxy Quasi-Isotropic Composite-Laminate Rotor.

Fig. 7. Constant-Thickness S2-Glass/Epoxy Quasi-Isotropic Composite-Laminate Rotor.

TABLE 2. Summary of Test Data for Various Quasi-Isotropic Composite Laminates

Material	Layup pattern[a]	Ply thickness (mils)	Nominal fiber-volume fraction	Test direction[b] (deg)	Modulus (msi)	Poisson ratio	Ultimate strength[c] (ksi)	Ultimate strain (%)
Celion 6000/5213 Graphite/epoxy	[90/0/±45][d]	6.3	~0.6	0.0	7.37	0.32	69.6	0.98
Celion 6000/5213 Graphite/epoxy	[90/0/±45][d]	6.3	~0.6	22.5	7.55	0.26	50.0	0.67
Celion 6000/5213 Graphite/epoxy	[90/0/30/60/ -30/-60][d]	6.1	~0.6	0.0	7.66	0.32	74.1	0.91
Celion 6000/5213 Graphite/epoxy	[90/0/30/60/ -30/-60][d]	6.1	~0.6	15.0	7.48	0.33	50.4	0.69
3M SP-250 S2-Glass/epoxy	[90/0/±45][d]	8.5	~0.55	0.0	3.2	0.30	83.8	4.2
3M SP-250 S2-Glass/epoxy	[90/0/±45][d]	8.5	~0.55	22.5	3.4	0.32	43.9	1.6
3M SP-250 S2-Glass/epoxy	[90/0/30/60/ -30/-60][d]	8.4	~0.55	0.0	3.3	0.30	70.8	2.9
3M SP-250 S2-Glass/epoxy	[90/0/30/60/ -30/-60][d]	8.4	~0.55	15.0	3.35	0.31	48.6	2.0
3M SP-250 S2-Glass/epoxy	[0/80/160/240/ 320/40/120/ 200/280][e,f]	7.5	~0.65	10.0	4.8	0.33	79.5	1.6
3M SP-250 S2-Glass/epoxy	[0/82/163/245/ 327/49/131/ 213/295/16/ 98][e,f]	7.6	~0.65	8.2	4.4	0.29	64.4	1.6
3M SP-250 S2-Glass/epoxy	[0/82/163/245/ 327/49/131/ 213/295/16/ 98][e,f]	7.6	~0.65	8.2	4.1	0.28	60.5	1.7

[a] All laminates are symmetric with respect to the midplane.
[b] With reference to a fiber direction.
[c] Average of five tests.
[d] Vacuum-bag/press-curing (VB/PC) fabrication method used.
[e] Matched-metal-die compression molding (MMDCM) process used.
[f] Alpha-ply quasi-isotropic laminates (see Ref. 3).

TABLE 3. Shear Strengths of S2-Glass/Epoxy Composite Laminate Made from MMDCM Process

Laminate	Test	Ultimate strengths[a] (ksi)
$[0]$	Short-beam shear	11.5 (interlaminar)
$[\pm 45]_s$	Uniaxial tension	14.0 (in-plane)

[a]Average of five tests.

TABLE 4. Test Data Summary of Various Constant-Thickness, Quasi-Isotropic Laminate Rotors

Material	Lay-up	Nominal thickness (in.)	Diam. (in.)	Predicted failure speed (rpm)	Actual failure speed (rpm)	σ_{max} at failure (ksi)	Energy density at failure (Wh/lb)
Gr/Ep	$0/\pm 45/90$	0.285	12.3	53,500	44,500[a]	49	16.5
Gr/Ep	$0/\pm 45/90$	0.285	13.5	48,800	48,200	69	23.4
S-G/Ep	$0/\pm 45/90$	0.42	16	35,100	30,000[b]		
S-G/Ep	$0/\pm 30/\pm 60/90$	0.42	16	37,100	30,000[a]		
S-G/Ep	$0/\pm 45/90$	0.42	15	39,900			
S-G/Ep	$0/\pm 30/\pm 60/90$	0.42	15	42,200			
K-49/Ep	$0/\pm 22.5/\pm 45/\pm 67.5/90$	--	16				

[a] Rotor failure attributed to shaft failure.
[b] Test purposely stopped to conduct non-destructive evaluation.

conventional, vacuum-bag, autoclave-curing process) appears to be ideally suited for this purpose and offers the advantages of:

- High volume production.
- Excellent part reproducibility.
- Low labor requirement per unit produced.
- Minimum material scrap.
- Excellent design flexibility (simple to complex shapes).
- Fully mechanized production capabilities.

This process has not been extensively used to date for fabricating fiber/epoxy-resin composites for aerospace applications because of the following reasons:

- Capital investment for the mold is high.
- Release of part from the mold when using epoxy resins is difficult.
- The motivation for obtaining the optimum strength as a function of increasing fiber-volume fraction did not exist.

The aerospace industry typically utilizes the autoclave-curing process where the applied pressures are of the order of 100 to 150 psi. One approach to increase the fiber-volume fraction is to increase the curing pressure (~300 to 500 psi). It is not practically feasible to obtain these pressures in an autoclave. Hence the MMDCM process was used.

Also, it should be borne in mind that an increase in fiber-volume fraction will result in an increase in the density of the composite. Based on analytical calculations, the increase in strength more than compensates for the increase in density. Furthermore, there is an optimum fiber-volume content beyond which the composite strength will actually decrease. In this regard, care must be taken to avoid excessive bleeding of the resin.

For the present program, three steel molds were fabricated by Ewald Associates, Detroit, Michigan, for the purposes of molding laminates of different sizes and thicknesses. In this manner, the scale-up of the process could be accomplished in a methodical manner. Also, special mold-release film was used to facilitate release of the part from the mold after curing.

As mentioned earlier, the second option available for increasing the energy density is to modify the lay-up pattern to reduce the strength anisotropy. The various laminate lay-up or stacking patterns are indicated in Fig. 8. The optimum pattern depends on the trade-off between the through-the-thickness local and global laminate-strength anisotropy. Such an optimum lay-up pattern has been used in the fabrication of the thick laminates.

In summary, nine thick S2-glass/epoxies and high-strength graphite/epoxies (Celion 6000/5213) are being molded presently for the following purposes:

- To demonstrate an energy density of 40 Wh/lb (proof-of-concept).
- To compare matched-die compression molding and vacuum-bag low-pressure press-molding processes.
- To assess the edge-thickening effect.
- To determine the effect of various lay-up patterns.

The strength anisotropy of quasi-isotropic laminates indicates that the most optimum use of materials is achieved for a random orientation. Thus random chopped-fiber composites are possible candidates for flywheel applications. Data[4] for 1-in., chopped, S2-glass/polyester sheet-molding compound (SMC) with 65% weight of fiber show a tensile strength of 35 ksi. The potential exists to increase this value further to about 45 ksi. This is comparable to the off-axis strengths of some continuous-fiber quasi-isotropic laminates (see Table 2). In addition, the low material and manufacturing costs provide the motivation to use these materials.

Joint cooperative programs have been established with Owens-Corning Fiberglass Corp., and PPG Fiberglass Co. during FY 1979 to develop high-fiber-content, chopped

- Single pattern through the thickness

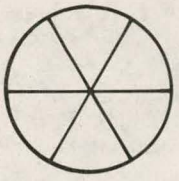

0/60/–60

- Single pattern rotated through-the-thickness

$\underbrace{0/60/-60}_{X}, X+\theta, X+2\theta, \text{etc} \ldots$

- All layers having different orientations
- Layup symmetric WRT mid-plane only
- Layup symmetric locally as well as WRT mid-plane

Fig. 8. Various Quasi-Isotropic-Laminate Lay-up Patterns for the Flywheel Rotor Configuration.

S2-glass SMC (ultimate strength objective: 45 ksi) and to utilize the MMDCM process to fabricate constant- and tapered-thickness rotors in a single step.

Two steel molds are currently being made for LLL by Gougler Industries, Kent, Ohio, for molding these rotors. The actual molding process will be developed jointly with Owens-Corning.

It is also important to identify the areas of concern associated with the use of SMC and MMDCM.

- The curing process may induce residual stresses and internal cracking.
- Appropriate placement of charge (SMC sheets) in the mold is necessary to insure adequate flow and material homogeneity.
- Fatigue/creep of SMC (partially alleviated by outer ring) may occur.

In summary, the design goal is to obtain low-cost, moderate-energy-density rotors.

Finally, since the "hybrid" (disk/ring) design is being actively considered, another processing area being investigated both by LLL and GE is the direct filament winding of the outer ring on the disk.

TEST AND EVALUATION

In FY 1979 these activities consisted mainly of testing various composite laminates to obtain design data and spin testing constant-thickness rotors.

In addition, the objectives of testing various quasi-isotropic laminates were to establish degree-of-strength anisotropy and to determine the improvements in laminate properties by utilizing the MMDCM process.

Table 2 shows the test results for the laminates made from both the vacuum-bag/press-curing and the MMDCM processes.[5] These data demonstrate the following:

- The laminates are quite anisotropic in strength.
- A major improvement in the modulus and strength of S2-glass epoxy laminae can be obtained by using the MMDCM technique.

The cured ply thickness is a measure of the increase in fiber-volume fraction. Table 3 shows the in-plane and interlaminar strength of the S2-glass/epoxy laminates. The high values attest to the superior quality of the laminates. This process has been utilized for graphite/epoxy test panels and scaled up for molding 1-in.-thick S2-glass and graphite/epoxy laminates. The ultimate measure of the adequacy of this will be, of course, determined by the increase in the energy densities of laminated disc rotors.

Spin testing of constant thickness rotors was conducted primarily to establish a relationship between laminate data and failure speed and to ascertain the effect of biaxial stress on strength.

The results of the spin tests (conducted at GE, Schenectady, N.Y.) are tabulated in Table 4. It is clear that the confidence level in predicting failure speeds has improved. Also, a moderately high value of energy density (23.4 Wh/lb) was obtained for one of the graphite/epoxy rotors. Figure 9 illustrates the failed rotor in the spin test chamber.

Because of the laminar nature of composite laminates and the existence of a strong phase (fiber) and a weak phase (matrix), fabrication defects are commonplace. Sometimes, these defects have an adverse effect on performance. Consequently, all the laminates were evaluated nondestructively by utilizing the ultrasonic C-scan procedure. The objectives were to detect manufacturing defects (interlaminar debonds) after fabrication, to detect flaws resulting from machining and handling, and to detect damage accumulation in rotors after spinning to a predetermined rpm.

For the graphite/epoxy rotor (Table 4), no significant damage was detected after spinning it up to 35,000 rpm. However, for the S2-glass/epoxy rotor, damage was evident after 30,000 rpm.

During spinning, the laminated composite rotor is subjected to a biaxial state of stress, and the effect of biaxial-stress field on laminate strength is not fully understood. Ideally, the spin test is the best suited to obtain failure under a biaxial-tensile test. However, it is expensive to conduct such a test and to obtain sufficient data points to develop a certain confidence level. Alternative test methods,

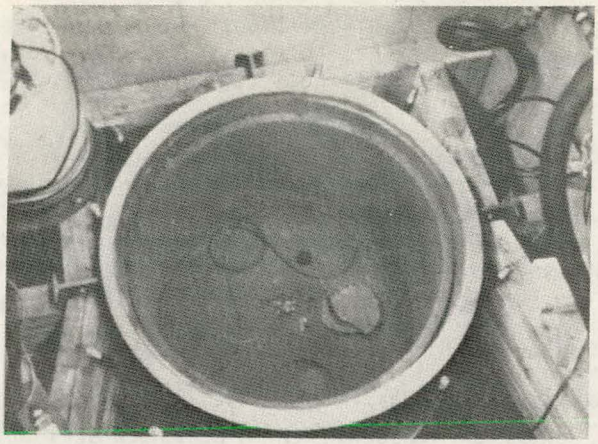

Fig. 9. Remnants of the Failed Constant-Thickness Graphite/Epoxy Rotor in a Spin-Test Chamber.

such as the pressurized tube and the cruciform section, also have some major disadvantages. Consequently, a new test fixture is currently being designed at LLL. This fixture consists of a circular specimen in which a biaxial-stress field is generated by applying radially-outward loads.

ADDITIONAL EFFORT IN FY 1979

In addition to the subtasks related to the laminated composite rotor, the following programs were initiated in FY 1979:

DESIGN GUIDE FOR COMPOSITE MATERIAL FLYWHEEL DYNAMICS

The analyses to be performed for this study at the University of Oklahoma, Norman, Oklahoma, include a continuum analysis of the composite-material flywheel rotor itself to obtain natural frequencies of various vibrational modes; and a system analysis of the flywheel system, including rotor supports, flywheel shaft, and some features of the driving system (both cantilever and end supports).

EVALUATION OF BIDIRECTIONALLY WOVEN COMPOSITE MATERIALS FOR FLYWHEELS

The objective of this program at AVCO Systems Division, Wilmington, Mass. is to assess, by analysis and test, the potential of bidirectionally (radial and circumferential) woven composite materials for flywheels.

FATIGUE TESTING OF COMPOSITE LAMINATES

This activity was initiated primarily in response to the recommendations of the Jet Propulsion Laboratory (California Institute of Technology) Review Board investigating the Garrett AiResearch NTEV (Near Term Electric Vehicle) flywheel failure. It consists of three separate tasks: (1) S2-glass/epoxy [0] laminate tension/tension fatigue tests (Boeing/Vertol, Philadelphia, Pa.); (2) Kevlar-29/epoxy [0] laminate tension/tension fatigue tests (GE, Space Division, Valley Forge, Pa.); and (3) Kevlar-49/epoxy ring tension/tension fatigue tests (Garrett AiResearch).

S2-glass and Kevlar-29/epoxy composite test panels are being filament wound at LLL.

COMPOSITE CONTAINMENT STUDIES

Important aspects of the composite flywheel design problem are the failure of the rotor and the associated safety requirements. Consequently, a rational approach for the

design of the containment must be evolved. To that end a program has been initiated at GE Space Division, Valley Forge, Pa. to assess the applicability of jet-engine fan-blade containment technology to flywheel containment.

PLANS FOR FY 1980

Effort during FY 1980 will essentially involve either the completion or the continuation of the ongoing tasks. However, the emphasis will shift from exploratory development to the testing of prototype rotors. These spin tests will include rotors developed under Sandia sponsorship. Also, studies in the containment area will be augmented.

SUMMARY

The status and progress of the composite-laminate flywheel-rotor development program during FY 1979 have been described. A critical evaluation of the effort was made initially, and certain pacing issues and areas of concern were identified. Appropriate steps were undertaken to address these issues. It is believed that improvements and modifications made in the design/analysis, processing/fabrication, and testing area will lead to the realization of the project goals.

ACKNOWLEDGMENTS

I wish to acknowledge the contributions of Richard A. Larder and Michael A. Gerhard of LLL to the finite-element analysis studies.

REFERENCES

1. R. G. Stone, "The Laminated Disc Flywheel Program," in Proceedings of the 1978 Mechanical and Magnetic Energy Storage Contractors' Review Meeting, U.S. Department of Energy CONF-781046 (Luray, Virginia, October 1978); also Lawrence Livermore Laboratory, Report UCRL-81772, 1978.

2. S. V. Kulkarni, R. G. Stone, and R. H. Toland, Prototype Development of an Optimized Tapered Thickness Graphite/Epoxy Composite Flywheel, Lawrence Livermore Laboratory, Report UCRL-52623, November 1978.

3. R. P. Nimmer, K. Torossian, J. Hickey, and J. P. D. Wilkinson, Laminated Composite Disc Flywheel Development, Lawrence Livermore Laboratory, Report UCRL-13973, January 1979.

4. J. Kay, Owens-Corning Fiberglass Corp., Granville, Ohio (private communication).

5. J. C. Duke, Jr., Investigation of the Strength of the Fiber Reinforced Composite Laminate Specimens, Virginia Polytechnic Institute and State University, VPI-79.26, prepared for Lawrence Livermore Laboratory under P.O. No. 4914709, August 1979.

PROJECT SUMMARY

Project Title: Laminated Disc Flywheel Development Program

Principal Investigator: Ronald P. Nimmer

Organization: General Electric Research and Development Center
P. O. Box 43
Schenectady, New York 12301
(518)385-2370

Project Goals: To design, fabricate, test and evaluate laminated discs with filament wound outer rings for application in high energy density flywheel energy storage units.

Project Status: A plane stress analysis of the laminated flywheel disc with filament wound outer ring has been carried out and the radial thickness of the ring has been optimized to attain maximum energy density. Several different materials have been considered and parametric studies have been conducted to determine the impact of property variability upon the proposed design concept. The design offering the highest energy densities uses an S2-glass laminated disc with a filament wound outer rim.

One-inch thick laminated discs with 11-inch outside diameters are now being hydroclaved routinely with void contents on the order of 1.6% by volume and fiber volume ratios of 48%. Development of filament winding techniques incorporating computer controlled winding equipment have been completed. Fiber volume ratios of 69 - 70% have been achieved for Kevlar-49 rings and 63% fiber volume fractions have been attained for graphite rings. Production of rings for flywheel assembly is now underway.

Tests of laminated composite discs have been initiated. Three tests have been completed on S2-glass discs and an additional three tests have been made with laminated graphite discs. The largest energy density attained for the S2-glass discs was 40 Wh/Kg (18.4 Wh/lb). The highest energy density recorded for the graphite test was 50 Wh/Kg (23 Wh/lb). Tests on flywheels fabricated with filament wound outer rings around laminated S2-glass discs are scheduled to begin next.

Contract Number: LLL Subcontract No. 2479309

Contracting Period: FY 79

Funding Level: $199.4K

Funding Source: U. S. Department of Energy/Lawrence Livermore Laboratories

LAMINATED FLYWHEEL DISC WITH FILAMENT WOUND OUTER RING

R. P. Nimmer
Corporate Research and Development
General Electric Company
Schenectady, New York 12301

ABSTRACT

Lustenader and Zorzi[1] have shown that the energy density of a laminated composite flywheel can be improved if an outer ring of unidirectional composite is added to the rotor. In addition, they established the existence of an optimum thickness for the outer ring which provides maximum energy density. The current work expands upon this basic concept and encompasses the design, fabrication, test and evaluation of such a flywheel as a high energy density, mechanical energy storage unit. Analysis of this design concept has identified failure criteria as well as potential advantages and disadvantages dependent upon material choice. Parametric design studies have been conducted to evaluate the impact of mechanical property variation upon the available energy density. A laminated S2-glass disc with a filament wound, graphite outer ring has been identified as offering the highest potential energy density for this design concept. The hydroclaving technique has been applied to manufacture laminated S2-glass discs with void contents of 1.6%. Computer controlled filament winding has been applied for fabrication of the unidirectional outer rings. Burst tests to date have been conducted on laminated S2-glass discs without outer rings indicating energy densities in the 30 - 40 Wh/Kg (15 - 18 Wh/lb) range. Improved material and addition of filament wound outer rings are expected to raise these values.

INTRODUCTION

The composite flywheel concept currently under consideration of the General Electric Company and illustrated in Figure 1 is a hybrid design using a laminated central disc with a unidirectional outer ring. The laminated composite disc received high ratings in the survey of design concepts conducted by Huddleston, et al.[2] and has also been pursued by Hatch[3], Rabenhorst[4] and Kulkarni, Stone and Toland[5]. High energy storage per unit swept out volume and favorable dynamic characteristics are among its most often cited advantages. Lustenader and Zorzi[1] have illustrated that the energy density of such a flywheel could be substantially improved with application of a unidirectional composite outer ring. The current program addresses the design, fabrication, test and evaluation of such a flywheel.

DESIGN AND ANALYSIS

Several different composite materials have been examined for application in the hybrid disc-ring composite flywheel. Since some of the material combinations require interference fits between the components, the effect of this interference parameter upon achievable energy density has also been investigated. In addition, the impact of mechanical property variability in the composite material has been examined from the standpoint of its impact upon energy density. Since the flywheels designed and built in this program are flat, one-inch-thick discs, an orthotropic plane stress analysis has been applied.

LAMINATED E-GLASS DISC WITH KEVLAR-49 OUTER RING

The first material combination considered analytically was made up of a laminated, E-glass central disc with a filament wound Kevlar-49 outer ring. Based upon considerations of thermal contraction the interference parameter $\bar{\delta}$ for this analysis was set at 0.002 where

$$\bar{\delta} \triangleq \frac{\delta}{R_o} \qquad (1)$$

and δ is the interference dimension and R_o is the outside radius of the ring. The composite material properties pertinent to the analyses in this paper are collected in Table 1. The optimization curves for this baseline design are presented in Figure 2, which plots the energy density at burst for four specific failure criteria versus the ratio of inside to outside radii of the ring. The first failure considered is an α-disc fracture in biaxial tension and fiber breakage at its center. Second, the unidirectional outer ring could fail circumferentially through fiber breakage. Alternately, the outer ring could fail transversely. Finally, the outer ring could simply spin away from the inner disc.

Considering these four modes of failure, it becomes apparent that the α-disc strength and the radial ring strength govern the operating envelope for the E-glass Kevlar-49 design. Analysis indicates that the optimum inside to outside radius ratio for the outer ring is approximately 0.85, and the corresponding energy density at burst for this design is approximately 26.5 Wh/lb. This is a 30.7% improvement in predicted energy density over an E-glass disc without a Kevlar-49 outer ring. It is noteworthy also that the interface pressure between disc and ring (at rest) for this optimized design is only about 2300 psi. The limiting value for this interface stress is considered to be 7400 psi for the Kevlar ring. Finally, it is interesting to note that, as previously mentioned, for sufficiently thin outer rings ($R_I/R_o > 0.95$) no separation will occur. For thicker rings, analysis indicates that a shrink fit is necessary to prevent separation within the wheel's operating range.

The interference fit chosen for the design of this hybrid wheel has a definite impact upon the attainable energy density. Figure 3 describes the variation in the baseline design which can be achieved by changing the interference fit between the disc and the ring. It can be seen from Figure 3 that the energy density at burst for the shrink fit parameter $\bar{\delta} = 0.001$ is 10% less than the attainable energy density for the baseline design with $\bar{\delta} = 0.002$. Increasing the interference parameter from $\bar{\delta} = 0.002$ to $\bar{\delta} = 0.003$ adds only about 4% in energy density. The benefit of increasing the shrink fit above $\bar{\delta} = 0.003$ becomes increasingly less rewarding, since the breakage of the circumferentially wound fibers in the ring now begins to govern, largely offsetting the improvements in the radial stress distribution of the ring. It should be pointed out that on the basis of ease in fabrication, an interference parameter on the order of $\bar{\delta} = 0.002$ seems desirable.

In addition to the interference fit, the relative stiffnesses of the disc and the ring also play a vital role in the design's performance. To prevent separation, the ring should be made of a material with a larger specific circumferential stiffness (E_L/ρ) than the disc. However, the longitudinal stiffness of Kevlar-49 composite can vary depending upon the fiber volume fraction achieved in winding. With this point in mind, analyses show that if the longitudinal moduli of the Kevlar-49 ring is reduced 10% to 10.8×10^6 psi, from the 12.0×10^6 psi assumed in the design characterized by Figure 2, then the resulting energy density is reduced 13%.

Another material property which may vary based on the winding technique applied to ring fabrication is transverse strength. This property can also play a role in performance optimization. However, parametric analyses indicated that the expected variation in transverse strength would result in only about a ± 4% variation in attainable energy density with respect to the baseline design of Figure 2.

LAMINATED S2-GLASS DISCS WITH KEVLAR-49 OR GRAPHITE OUTER RINGS

In order to improve the stored energy density of this flywheel design, S2-glass was also examined as a candidate for the laminated central disc. In laminated form with an α-9 stacking sequence, the S2-glass offers almost 34% more strength than the E-glass as measured by standard tensile test. Since energy density is directly proportional to strength-to-density ratio, this could mean a substantial improvement in flywheel performance. On the other hand, the laminated S2-glass disc is also about 20% stiffer than the laminated E-glass. This increased stiffness has a detrimental effect upon the failure of the flywheel due to separation of disc and ring.

In order to quantify these effects, an optimization analysis was also applied to a hybrid flywheel design consisting of a laminated S2-glass disc with a circumferentially wound outer ring made of Kevlar-49. Results of this analysis indicated that although the S2-glass disc offered higher energy-density levels than the E-glass, an interference parameter of $\bar{\delta} = 0.003$ would be

required to attain a 20% improvement in energy density by application of a Kevlar-49 outer ring. As can be seen from Fig. 2, application of a Kevlar-49 ring to an E-glass disc resulted in a 30% increase in energy density while also allowing smaller interference fits ($\bar{\delta}$ = 0.002). Finally, the longitudinal stiffness of the Kevlar-49 outer ring would have an even more substantial effect upon the S2-glass Kevlar-49 hybrid flywheel's performance.

Since an outer ring made of a material with a larger specific modulus (E/ρ) than Kevlar-49 could significantly improve the hybrid flywheel's performance, filament wound graphite epoxy was considered as an alternative material for use in the outer ring. The disc and ring properties used in this design optimization are also displayed in Table 1 and the resulting design curves are shown in Fig. 4. The performance of the hybrid flywheel with graphite ring characterized in this figure is substantially different than the flywheel with a Kevlar-49 outer ring. First, the predicted energy density is substantially higher, approaching 88 Wh/Kg (40 Wh/lb). At the same time, lower interference fits can be used, thus simplifying assembly procedure. An interference parameter of $\bar{\delta}$ = 0.001 was used in this analysis. However, as can be seen from Fig. 4, substantial energy densities can be reached without any interference fit if the outer ring is designed with an inside-to-outside radius ratio greater than 0.78.

FABRICATION

LAMINATED S2-GLASS DISCS

Material quality is always an important consideration in any structural member. For flywheels, quality as measured by strength-to-density ratios translates directly to improved energy density. In addition, the previously discussed design analysis illustrated the impact of stiffness on the performance of the hybrid disc-ring flywheel. As a result, product quality has been closely monitored during this program. Consideration has been given to fiber-volume content, void fraction, and product uniformity of the wheels. In addition, fundamental gel characteristic data has also been measured to insure similar cure and resulting quality in scaled up wheels to be manufactured later in the program.

The laminated S2-glass discs under consideration are one-inch thick with nine or eleven inch outside diameters and are fabricated with the hydroclaving technique. Variation in thickness has been held to ± 0.002 inch. During a typical hydroclaving cycle the laminate disc is first held under a vacuum at elevated temperature. For relatively thick discs, it is felt that this method more efficiently eliminates the voids caused by trapped air and solvent vapor than the platen pressure applied during compression molding. Furthermore, in the second phase of the hydroclaving process, heat and hydrostatic pressure are applied to the laminates through a heat-and-pressure transfer medium in a compounding tank. This approach enhances uniformity of thick laminates in comparison to compression molded discs. After lay-up and cure, the unmachined discs are elastomerically bonded to an aluminum hub. The outer diameter is then machined using the hub as the center and the flywheel disc is dynamically balanced to within 0.25 gm-cm. Twenty laminated discs have been produced to date.

A number of these laminated wheels have been subjected to destructive tests to determine fiber-volume content, void fraction and uniformity. Uniform, quality material has been attained in both the 10 and 12-inch discs. Void content has been held below 2% and the photomicrographs in Fig. 5 illustrate the marked improvement in this area with respect to previous 1-inch thick laminated discs manufactured with compression molding techniques. The 48% fiber volume content attained is perhaps 4 - 5% less than what might be expected from compression molding of thinner laminates and can probably be explained in terms of the lower pressures (~ 100 psi) applied during consolidation with hydroclaving in comparison to compression molding.

FILAMENT WOUND OUTER RINGS

The outer rings for the hybrid flywheel will be filament wound on mandrels with the use of computer controlled filament winding equipment. Details of the process used to produce these rings are given in Ref. 6. The void content in the Kevlar-49 rings ran from 4.5 - 5.5% while the void content in the graphite rings was measured as 0.95%. The relatively large void content of the Kevlar-49 rings in comparison to the graphite can be attributed to better wettability of the graphite fibers. Vacuum bagging of the Kevlar-49 ring during cure did not appear to improve the void content. The fiber volume fraction for the Kevlar-49 rings has been measured as 69 - 70% while the fiber volume fraction for the graphite is approximately 63%. The photomicrographs of

Fig. 6 compares the cross section of a filament wound Kevlar-49 ring with the cross section of a ring manufactured from preimpregnated Kevlar-49 tape. The superiority of the filament wound product in terms of fiber volume content is already visible. This sort of quality improvement translates directly into higher circumferential stiffnesses and strengths, both vital ring characteristics previously discussed in the design analysis.

TESTING

The spin-pit facility used in this program is instrumented to collect a variety of data. The RPM-time history is monitored digitally as well as recorded on a strip chart. A second strip chart simultaneously displays the time histories of turbine RPM, tank vacuum pressure and shaft orbit magnitude. Tests are generally conducted at vacuum levels of 50 to 100 μ of mercury. In addition, an attempt is being made to photograph failure of the flywheels. Breakage of thin wire wound on a shroud surrounding the flywheel is designed to set off a photographic flash during failure.

Six spin tests have been conducted to date and the associated test results are presented in Table 2. Three of the tests involved laminated S2-glass discs without outer rings and three have involved laminated graphite discs supplied by the Lawrence Livermore Laboratories. One of the S2-glass tests terminated in a system failure associated with the air turbine bearings and is not considered indicative of a flywheel failure. The highest energy density attained with a laminated S2-glass test was 40.1 Wh/Kg (18.2 Wh/lb). One of the graphite wheel tests was nondestructive. C-scans were taken of the wheel before and after spinning the wheel to 35,000 RPM. Comparison of the results of these C-scans revealed no noticeable damage accumulating in the wheel at this level. The flywheel was subsequently broken at 48,200 RPM reaching an energy density of 51.5 Wh/Kg (23.4 Wh/lb). The initial results displayed in Table 4 for both the S2-glass and the graphite laminated discs, indicate tip speeds attained to date in experiment are less than the levels that were originally expected. For the S2-glass, it was originally expected[6] that a disc without holes should reach approximately 884 m/s (2900 f/s). This corresponds to roughly 52 Wh/Kg (24 Wh/lb) energy density. These predictions were fundamentally based upon the assumption that failure would occur when the stress in the center of the disc reached a level sufficient to break fibers at that location.

The lower failure speeds of the laminated S2-glass discs tested to date, and the presence of very fibrous debris after wheel bursts seem to call initial assumptions with regard to failure mechanisms in the laminated S2-glass flywheels into question. Although initial estimates with respect to the ultimate strengths and speeds of these wheels were based upon the assumption that the wheel would fail when fibers were broken, burst tests to date have resulted in very fibrous debris indicating minimal fiber breakage. Figure 7 compares debris from an elastomerically bonded S2-glass test with debris from a previous test made on an E-glass disc with bolted attachments. In two of the S2-glass tests, failure was associated with a rapid decrease in turbine speed as shown in Fig. 8. It has been hypothesized that this effect is a result of a sudden increase in the flywheel's moment of inertia. In this light, failure modes associated with matrix damage must be considered more closely. It is experimentally established that matrix damage occurs at stress levels substantially less than the ultimate stress during tensile tests of laminated coupons. This matrix damage in laminae oriented at an angle to the loading direction can be identified by a change in the Young's modulus of the laminate. The approximate stress level at which such damage occurs can also be identified with classical laminate analysis. The effect of such matrix damage upon a flywheel disc at relatively low tip speeds must be called into question.

The presence of the balanced biaxial stress state at the center of the disc, forces the stresses in the individual layers of the disc to be identical throughout the thickness. As a result, all of these laminae will fail transversely at the same average stress level. A classical laminate analysis of an S2-glass disc reveals that the matrix at the center of the disc will begin to experience transverse failure at a balanced biaxial stress of only 134 MPa (19 ksi). This corresponds to a tip speed of approximately 387 m/s (1271 f/s). Of itself, this matrix failure is not catastrophic since it is extremely localized in nature. The fibers still carry load through the center and are "potted" in undamaged epoxy farther out along the radius of the disc. However, as the wheel accelerates from 387 m/s the area of matrix failure will spread out from the center over larger areas of the laminated disc. Eventually, the region of matrix failure may spread over a region substantial enough to cause the ultimate failure of the disc - either as a result of associated wheel imbalance and shaft failure or as a result of final, rapid damage

propagation to the edge of the disc.

Although this sort of failure criterion is consistent with the debris observed to date, additional information is still required to measure its validity. C-scan information will be utilized in an attempt to identify this type of failure. It appears that in the nondestructive test of the graphite wheel, a speed high enough to initiate substantial matrix damage may not have been attained before the second C-scan. If such damage does indeed contribute to the failure of laminated flywheels, a more flexible resin or stiffer fibers could help alleviate the problem.

CONCLUSIONS

The hybrid disc-ring flywheel design has been analytically optimized for maximum energy density. Parameter studies have been made to establish effects of mechanical property variation. The S2-glass disc with graphite outer ring appears most attractive from these analyses. Quality fabrication of both laminated S2-glass discs and filament wound Kevlar-49 and graphite outer rings has been achieved. Tests are underway to experimentally determine achievable energy density levels with this design. Initial results indicate that matrix damage of the laminated disc should be closely considered.

REFERENCES

1. Lustenader, E. L. and Zorzi, E. S., "A Status of the 'Alpha-Ply' Composite Flywheel Concept Development," presented at SAMPE meeting, Anaheim, California, May 3, 1978.

2. Huddleston, R. L., Kelly, J. J., and Knight, C. E., "Composite Flywheel Development Completion Report," (May 1 - September 30, 1976), Oak Ridge Y-12 Report Y-2080, May 1977.

3. Hatch, B. D., "Alpha-Cross-Ply Composite Flywheel Development," presented at 1977 Flywheel Technology Symposium, October 5-7, 1977, San Francisco, California.

4. Rabenhorst, D. W. and Small, J. R., "Composite Flywheel Development Program: Final Report," Johns Hopkins Applied Physics Laboratory Report SDO-4616A, April 1977.

5. Kulkarni, S. V., Stone, R. G., and Toland, R. H., "Prototype Development of an Optimized, Tapered-Thickness, Graphite/Epoxy Composite Flywheel," Lawrence Livermore Laboratory Report UCRL-52623, November 1978.

6. Nimmer, R. P., Torossian, K. A., Hickey, J. S., and Wilkinson, J. P. D., "Laminated Composite Disc Flywheel Development, First Semiannual Report," General Electric Research and Development Center Report SRD-79-016, January 31, 1979.

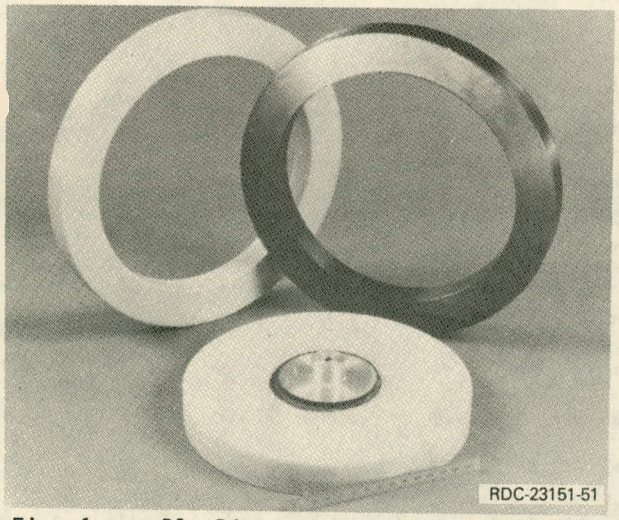

Fig. 1. α-Ply Disc with Kevlar-49 and Graphite Outer Rings.

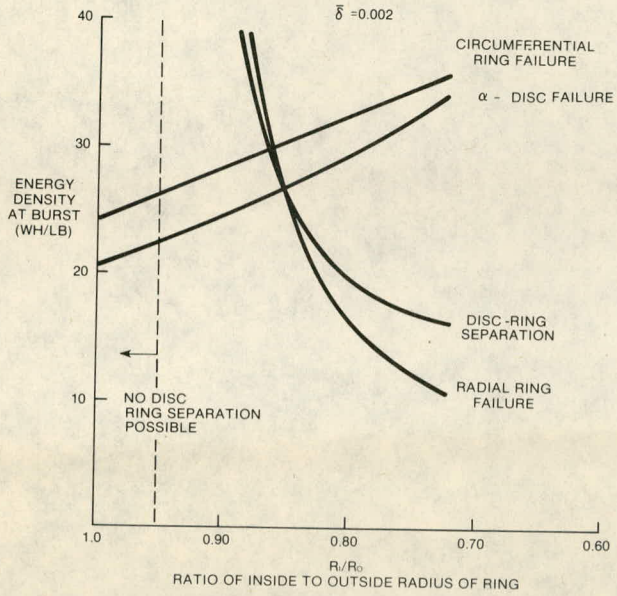

Fig. 2. Optimization Curves for the Baseline Shrink Fit Design; E-Glass, α-9 Disc with Kevlar-49 Outer Ring.

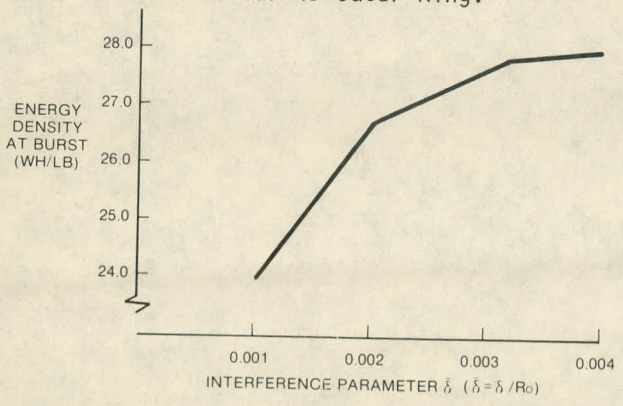

Fig. 3. The Effect of Interference Fit Parameter $\bar{\delta}$ on Flywheel Energy Density for the Baseline E-Glass Disc with Kevlar-49 Ring.

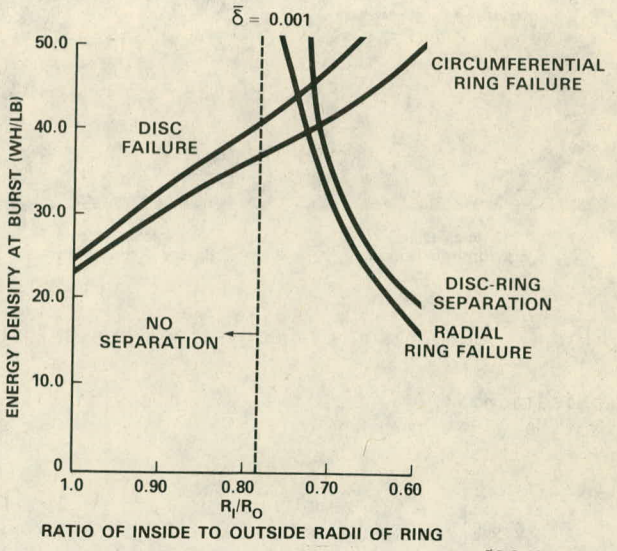

Fig. 4. Design Curves for an S2-Glass Disc with Graphite Outer Ring.

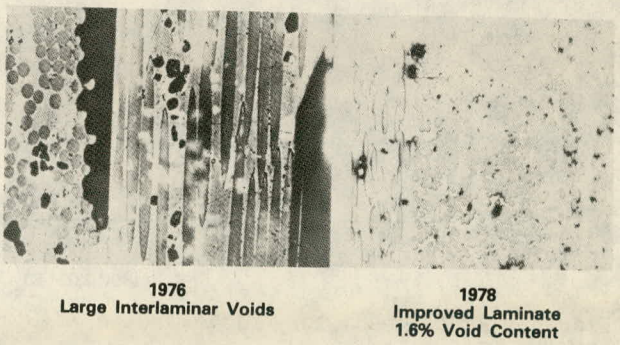

Fig. 5. Reduced Void Content.

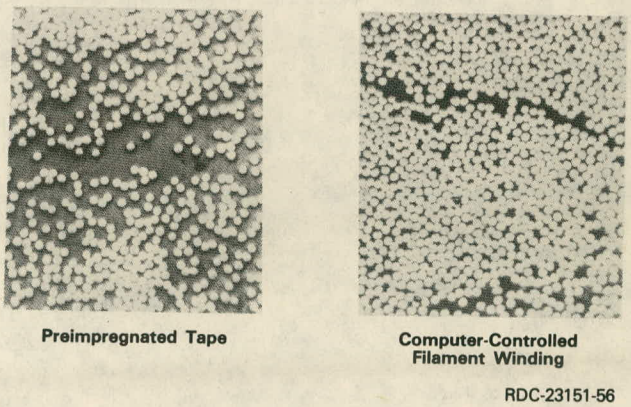

Fig. 6. Improved Fiber Volume Content in Outer Rings.

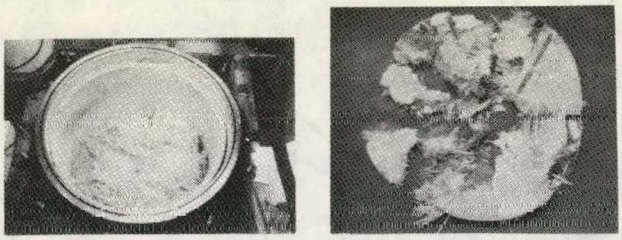

S2-glass Disc; Elastomeric Bond

E-glass Disc; Bolted Attachments

RDC-23151-57

Fig. 7. Comparison of Debris from Burst Tests.

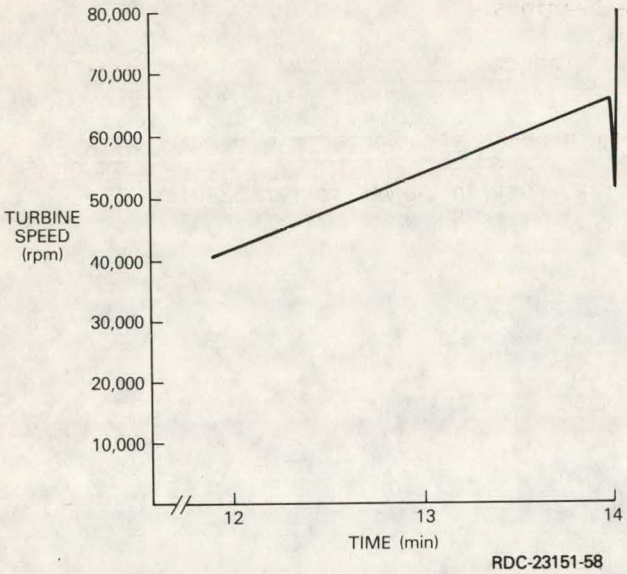

RDC-23151-58

Fig. 8. RPM Time-History of Laminated S2-Glass Burst Test.

TABLE 1
MATERIAL PROPERTIES USED IN ANALYSIS

α-9 E-Glass Disc Properties

$E = 2.6 \times 10^6$ psi
$\nu = 0.3$
$\sigma_{\text{biaxial ult}} = 70$ ksi
$\rho = 0.066$ lb/in^3

α-9 S2-Glass Disc Properties

$E = 3.05 \times 10^6$ psi
$\nu = 0.264$
$\sigma_{\text{biaxial ult}} = 85$ ksi
$\rho = 0.066$ lb/in^3

Kevlar-49 Outer Ring Properties

$E_L = 12.0 \times 10^6$ psi
$E_T = 0.7 \times 10^6$ psi
$\nu_{LT} = 0.35$
$\sigma_{L\ ult} = 190$ ksi
$\sigma_{T\ ult} = 1.6$ ksi
$\rho = 0.05$ lb/in^3

Unidirectional Material Properties for Typical Graphite Epoxy Composite

$E_L = 21.0 \times 10^6$ psi
$E_T = 1.4 \times 10^6$ psi
$\nu_{LT} = 0.3$
$\sigma_{L\ max} = 259$ ksi
$\sigma_{T\ max} = 7.0$ ksi
$\rho = 0.056$ lb/in^3

RDC-23151-59

TABLE 2
TEST DATA SUMMARY

MATERIAL	STACKING SEQUENCE	OUTSIDE DIA. cm (in)	TIP SPEED AT BURST m/s (f/s)	ENERGY DEN. AT BURST Wh/Kg (Wh/lb)
S2-Glass -Epoxy	(0/-45/45/90)	22.54 (8.8)	760 (2495)	40.1 (18.2)
S2-Glass -Epoxy	α-9†	22.54 (8.8)	732 (2230)	31.9 (14.5)
S2-Glass -Epoxy	α-9†	22.54 (8.8)	619 (2032)	26.6 (12.1)
Graphite -Epoxy	(0/90/45/-45)	31.1 (12.25)	725 (2378)	36.3 (16.5)
Graphite -Epoxy	(0/90/45/-45)	34.3 (13.5)	628* (2061)	27.4* (12.42)
Graphite -Epoxy	(0/90/45/-45)	34.3 (13.5)	862 (2827)	51.5 (23.4)

† $\alpha \triangleq$ Angle Between Fibers of Adjacent Plies
$\triangleq 90 - \frac{90}{n}$

*Nondestructive Test

RDC-23151-60

PROJECT SUMMARY

Project Title:	"Low Cost Flywheel Demonstration"
Principal Investigator:	David W. Rabenhorst
Organization:	Applied Physics Laboratory The Johns Hopkins University Johns Hopkins Road Laurel, Maryland 20810 301/953-7100
Project Goals:	Demonstrate feasibility of producing flywheels for $50 per kwh, or better. Develop low loss, long life bearings. Demonstrate low cost flywheel and low loss bearings in a complete energy storage system.
Project Status:	Project was successfully completed on May 31, 1979, and all goals were satisfactorily achieved. The principal recommendation was for the engineering development of a full scale home-sized flywheel energy storage system.
Contract Number:	EC-77-C-01-5085
Contract Period:	FY 1978 and 1979
Funding Level:	$355,190
Funding Source:	U. S. Department of Energy, Division of Energy Storage Systems

DEMONSTRATION OF A LOW COST FLYWHEEL IN AN ENERGY STORAGE SYSTEM

David W. Rabenhorst
Applied Physics Laboratory
The Johns Hopkins University
Laurel, Maryland 20810

ABSTRACT

The Applied Physics Laboratory has been engaged for the past eighteen months in a program for the Department of Energy involving the development of very low cost flywheels, such as those which would be used in individual home or factory energy storage systems. A significant part of this program also included the development of low loss, long life bearing systems.

The flywheel development explored a number of promising low cost materials and produced flywheel configurations which were projected for a large scale production cost of about $50 per kilowatt hour. While this is comparable to the initial cost of competing lead-acid batteries, it is noted that, unlike the batteries, the flywheel would not have to be replaced several times during the life of the system.

The bearing systems evaluated were based upon the use of otherwise conventional ball bearings which were arranged in special configurations so as to minimize their requirements for size and rotation speed. Bearing configurations were demonstrated which exhibited losses of the order of one watt per one hundred pounds of flywheel.

The success of this program warrants consideration of proceeding with a full scale system demonstration, based upon the design projections of the subject program.

INTRODUCTION

The Applied Physics Laboratory of The Johns Hopkins University (APL) has been engaged for the past ten years in a variety of programs dealing with modern flywheel technology, flywheel component and system design, flywheel applications, and the study of various flywheel programs in the United States and throughout the world. During the course of these programs it was concluded that many important flywheel applications would depend upon the development of very low cost flywheels and flywheel system components. It was noticed that most of the flywheel research programs throughout the world were aimed at the development of flywheels capable of high energy to weight ratios and energy to volume ratios, with relatively little concern for the energy per unit cost that would justify the use of the flywheels in these applications. At the Applied Physics Laboratory emphasis was placed on the development of flywheel configurations having a very low cost potential. And here it should be noted that a low cost flywheel not only involves very low cost flywheel materials, but also very definitely requires consideration of simple, low cost fabrication procedures.

The APL/Department of Energy low cost flywheel demonstration program was initiated on October 1, 1977, and was brought to a successful conclusion on May 30, 1979. Total cost of this program was $355,190. All primary objectives were successfully achieved as follows: A full-size, 1000 watt hour flywheel was demonstrated which had an estimated cost in large volume production of approximately $50. per kilowatt hour. A ball bearing system was developed whose total losses were comparable to the total losses in a totally magnetic suspension system. The low cost flywheel was successfully and repeatedly demonstrated in a complete flywheel energy storage system based upon the use of ordinary house voltage and frequency. The experience gained in the hardware program was used to project the system design into a complete full-scale 30 kwh home type flywheel energy storage system.

DISCUSSION OF APPLICABLE FLYWHEEL CONFIGURATIONS

The Laboratory had been experimenting with two flywheel configurations which appeared to offer significant possibilities in the area of very low cost flywheels. The first of these was called the pseudo-isotropic or quasi-isotropic disc flywheel. The basic configuration of this

flywheel is illustrated in Figure 1, where it can be seen that the flywheel is composed of alternate layers of unidirectional composite material arranged precisely so that the resulting overall composite exhibits an isotropic stress capability in the plane of the flywheel. The most obvious advantage of the pseudo-isotropic configuration is the fact that it has a very high energy per unit volume, inasmuch as it occupies 100% of the spinning swept volume of the flywheel. It was believed that a second major advantage was the overall simplicity of fabrication of this type of configuration; however, it was subsequently determined that the fabrication of the pseudo-isotropic flywheel material was quite labor-intensive, and therefore involved higher fabrication costs than was initially believed to be applicable.

Another problem was that for a given energy level, the pseudo-isotropic disc flywheel would have to spin at approximately twice the rotational speed of a wound flywheel configuration. The system studies had shown that anything that could be done to reduce the effective rotational speed of the flywheel, and particularly of the rotating bearing elements, would constitute an extremely important cost-reduction factor over the 10-year life cycle of a flywheel energy storage system. Also, since the design intent for optimum economy in the pseudo-isotropic flywheel is to equalize the stress throughout the flywheel disc, it follows that the failure would be catastrophic. This catastrophic failure releases all of the energy in the flywheel at essentially the same time, which is considerably more difficult to contain than in the case of the wound bare filament flywheel failure, where the failure is distributed over a much greater time. This is illustrated dramatically in Figure 2. Here we see the failure effects on two steel containment rings made from one-quarter inch cold rolled welded steel. The fragments of the ring in the background result from a single spin test to destruction of an eleven pound pseudo-isotropic flywheel containing a total energy of only 300-watt hours. The ring in the foreground made from the same material to the same general construction, is one which has survived more than 50 bare filament flywheel tests to destruction, many of which were at a much greater energy to weight ratio and total energy than was the pseudo-isotropic flywheel involving the ring in the foreground.

The flywheel configuration selected as having the most desirable features for the very low cost flywheel is the wound bare filament configuration illustrated in Figure 3. Here it can be seen that, since all of the bare wound filaments are lined up nearly precisely with the tangential force field, and since these tangential stresses vary as the square of the radius from the center of rotation, it is theoretically impossible for all of the tangential filaments to fail at the same time. This fact has been proven repeatedly through dozens of spin tests of this bare filament flywheel configuration.

The absence of the matrix material throughout most of the flywheel also serves to improve the material use efficiency in the flywheel fabrication. Like in other wound flywheel configurations, the performance is also related to the relationship between the inside wound diameter and the outside wound diameter of the flywheel. Maximum performance is achieved when the ratio of inside to outside diameters is unity. If the inside wound diameter were zero (that is, a wound solid disc), then the performance of the flywheel is exactly one-half of what it would be in the case of unity ratio.

Since the wound portion of the flywheel is a relatively thin ring, it was necessary to develop a suitable hub arrangement to permit the connection of this ring to the flywheel metal attach hub and rotating shaft. The requirement that the hub be capable of surviving at least as high a rotational speed as the wound filament without the presence of these filaments was easily met with hubs made from birch plywood. It was found that tapering plywood hub provided additional structural efficiency of the hub material, by allowing a reduction in its weight and associated cost. In the final configuration the plywood hub arrangement accounted for about four or five percent of the total weight of the flywheel. The metallic hub, which was used to provide the junction with the flywheel shaft, was bonded to the cellulosic hub by means of a suitable elastomeric bonding process. The elastomeric material readily accommodated the difference in expansion rate (due to rotation) between the metal hub and the cellulosic hub.

The inner flange of the metallic hub was arranged to be adjusted radially in any direction in order to permit shifting the spin axis of the flywheel in the direction of imbalance, in order to achieve proper spin balance of the entire assembly. Once the correct location was established, the inner movable flange was epoxied in place. The installation of the flywheel in the energy storage system involved the use of a relatively long thin flexible shaft which could easily accommodate any residual imbalance resulting from the initial balancing procedure. Cost studies of this configuration showed that in large scale production the target of $50. per kilowatt hour of the fabricated flywheel could be readily achieved.

APPLICABLE LOW COST FLYWHEEL MATERIALS

The primary requirement for the low cost flywheel material is of course strength to weight per unit cost, which translates simply to energy per unit cost. However, while this is clearly the most important requirement, there are certain other requirements which must be met in any material considered for low cost flywheel application, and many materials were eliminated by virtue of not being able to meet these secondary requirements. The materials must be available in billions of pounds. The material must be available in a form which will readily permit economical fabrication into a flywheel without introducing other complications which would mitigate its intrinsic low cost capability. In consideration of all of these things, three materials appear to be outstanding at the present time for applicability to the very low cost flywheel. The first of these is steel wire. The type of steel wire considered for this program is that which is used in making high pressure hoses, and in automobile tire manufacture. Its properties are well known, including its static fatigue and cyclic fatigue capabilities. Its large volume production cost can be ascertained with great accuracy, and its availability and suitability for low cost flywheel construction is adequate. Flywheels wound with low cost, nigh strength steel hose wire can store approximately 14 watt hours per pound, which, with their projected cost of around $.60 per pound, result in a rather marginal energy to cost ratio as demanded by the program objectives.

The principal problem areas encountered in this program with the steel wire flywheel fabrication all appear to be capable of satisfactory solution. The first of these is the "slickness" quality. This tends to make the steel wire difficult to hold in place without employing severe helix winding angles, etc. A number of solutions to the "slickness" problem are immediately apparent. The wire can be coated with any number of surface roughening techniques in the process of manufacture, such as cadmium plating, etc.

The main problem which was encountered in the program involving the steel wire low cost flywheels was that of the wire "cast". The cast of a wire is determined simply by cutting a length of the wire (usually one meter) and letting it drop on the floor and measuring the free diameter that the coil forms. If this diameter is much less than the working diameter of the flywheel winding process, the flywheel is likely to have a wavy pattern once it is taken out of the winding mandrels. Fortunately, wire straighteners are employed throughout the wire manufacturing and processing community which can be installed in the flywheel fabrication process. The wire straightener is a relatively simple device consisting of a number of orthogonally located rollers having been ground to notches in the shape of the outside surface of the wire. The bare filament wire wound flywheels tested in this program to date have been consistently successful, and material efficiencies of the order of 80% have been achieved.

The second low cost flywheel material selected for evaluation in this program is vinyl-impregnated fiber glass. This material is similar in some respects to the fiber glass tire cord used in the manufacture of automobile and truck tires, with one notable exception. This is that the flywheel vinyl impregnated fiber glass is extremely tough, and can even be bent and flattened on itself with a sharp crease without failure. In contrast, the fiber glass cord used typically in tire manufacture will instantly break when it is bent on itself. The process for the impregnation of the fiber glass strands is a proprietary development of PPG Industries, Inc. of Pittsburgh, Pa. Tensile strength of this composite over relatively long periods (minutes) appears to be of the order of 264,000 pounds per square inch.

The vinyl impregnated fiber glass material appears to have excellent characteristics as applied to the flywheel fabrication process. The material stays in place and packs very densely. Often the completed flywheel has the appearance of being a fiber glass epoxy structure, when in fact, there is no epoxy matrix in the areas in between the radial bonded areas. The ruggedness of this material is also evident from spin test to destruction, and at least one of these test flywheels has been spin tested four times after being inadvertently dropped to the chamber floor at peripherial velocities exceeding 2000 feet per second. The loose strands were merely trimmed off, and in severe cases the flywheel was rebalanced and then respun successfully.

There are two principal difficulties which have been encountered in the use of the vinyl impregnated fiber glass in the present program. First, the fiber glass wound flywheel occupies more volume because of its lower useable strength (50% of the ultimate tensile strength was assumed). This fact is somewhat compensated perhaps in other flywheel applications by the fact that the vinyl impregnated glass flywheel exhibits considerably higher energy to weight ratio than the other two types tested, being closer to 20 watt hours per pound. The second problem which was encountered is the fact that during the course of the program the vinyl impregnated

fiber glass material suddenly became unavailable, since PPG elected to cease its experimental production. Assurances were given that the reasons for PPG abandoning this material had nothing whatever to do with its technical feasibility, but that the market for which it had been developed did not materialize. It was stated, on the other hand, that the process by which this material was made could readily be licensed to any material processer who would so desire.

The third material to be evaluated in the low cost flywheel program was Metglas* amorphous metal ribbon. This material is a proprietary substance being developed by the Allied Chemical Corporation of Morristown, New Jersey. Metglas ribbon is a metallic alloy which, being amorphous, exhibits many glass-like properties. The form primarily used in the subject program was a one half inch wide ribbon having a .002 inch thickness. Thus it can be seen that one of the principal advantages of Metglas ribbon in the flywheel fabrication process is the fact that it can be wound to a given form about two orders of magnitude more quickly than a filamentary material.

One of the problems with Metglas amorphous metal ribbon is that it has been a difficult material to achieve effective bond with the conventional epoxy materials. Allied Chemical reports that considerable progress has been made on the Metglas ribbon bonding problem, and a number of promising thermo-setting resins are now available for this purpose.

Also, Metglas ribbon is a relatively new material, and consequently it would be some time before its actual production cost will have been established. It appears that in large quantities a Metglas metal alloy suitable for the low cost flywheel could cost in the range of $1. per pound or less.

Another problem, also associated with the newness of the material, is the relative inconsistency of the tensile strength in a given spool of Metglas ribbon. The Metglas ribbon used to date has been in the so-called "as-cast" condition, wherein the ribbon has somewhat ragged edges when viewed under a microscope. Processes for chemically polishing these edges to result in a 20 or 30 percent improvement in the tensile strength are well along, and should be well stabilized within the next several months.

Once these problems with Metglas ribbon have been resolved, this promising new material will be applicable to the low cost flywheel field, and also will be the subject of a number of future programs in the vehicular flywheel field. This projection stems from the fact that the Metglas offers a very high energy per unit volume, primarily by virtue of the fact that its ribbon format allows nearly 100% of the wound structure to be occupied by structural elements, as contrasted to the round steel wire format which typically only occupies 60% to 70% of the wound structure.

LOW LOSS, LONG LIFE BEARING INVESTIGATIONS

The Applied Physics Laboratory's basic approach to the low loss bearing problem is to consider variations of configurations of conventional rolling contact bearings. By focusing the design efforts on bearing load relief and bearing rotating element low rotational speeds, a series of bearing concepts have been demonstrated which appear to have extremely low losses and projected long life times in the flywheel environment. Effectively, by lowering the bearing loads to an absolute minimum and by holding the rotational speed to an absolute minimum, the bearings themselves can be made exceptionally small. It is obvious then that the smallest bearing will produce the lowest losses for a given mass supported. It is equally obvious upon further study that the bearing rotating at the lowest effective rotational speed will also produce the minimum losses, while at the same time achieving orders of magnitude longer projected lifetime.

By hanging the flywheel on a vertical shaft, it can be seen that the principal axial load on the bearing is that from gravity on the spinning mass. This axial load is reduced by the application of permanent magnets, which are designed to remove 95% of the gravity load of the spinning mass. This simple passive magnetic system (costing about $2. in production) could easily have been designed to remove 100% of the load; however, the bearings require a certain pre-load in order to operate most effectively. With the flywheel shaft in a vertical position, the lateral loads imposed on the bearings result solely from flywheel imbalance. The residual imbalance loads are effectively eliminated by placing the flywheel on a flexible shaft, which shaft nutates

---

*A registered trade mark of Allied Chemical Corporation.

less than 1/1000th of an inch due to the residual imbalance loads in the flywheel. Thus, in its final installation, the bearing loads are operating at only 5% of the initial axial load and probably less than 1% of the initial radial loads. As a result, the bearings required to support the rotating equipment can be a tiny fraction of the size that would otherwise be required, thus allowing further reduction in losses.

The effective rotational speed of the bearings can easily be reduced by one of the following methods. First, if the bearings are functionally placed one within the other, as illustrated in Figure 4; and, if the geometry is so arranged that each bearing is the same diameter at the same time, then the effective rotational speed of each of the bearings will be approximately half of what it otherwise would have been without this series bearing arrangement. Spin tests of such a bearing configuration (Figure 5) indicate that a bearing system of sufficient size to support the flywheel assembly had a total drag at 10,000 rpm of less than one watt, which is considerably lower loss than one would anticipate with a totally magnetic suspension system.

A second means of reducing bearing element effective rotational speed is illustrated in the Figure 6 sketch. Here the bearing rotating elements are simply placed inside of a much larger roller, so that the effective rotational speed can be reduced considerably, (sometimes as much as a factor of ten). This concept will be particularly applicable to even higher performance flywheels, where the rotational speed is considerably higher.

Due to the size of the flywheel and the energy level achieved, the nominal maximum rotational speed is 14,400 rpm. Using the series concept alone, the effective rotational speed is reduced to 7200 rpm. If, in addition to this, a slow roller configuration having only 5 to 1 roller ratio were also employed, the effective rotational speed on the bearings would be 1440 rpm. Needless to say, a bearing having only 5% of its design load and 10% of its design rotational speed would represent a considerable improvement in bearing losses and bearing projected lifetime.

FLYWHEEL ENERGY STORAGE DEMONSTRATION SYSTEMS

As stated in the foregoing, one of the principal objectives of the flywheel low cost demonstration program was to incorporate the flywheel into a complete energy storage system capable of operating in the typical individual home voltage and frequency requirements. Two systems were developed during the program for this purpose. The first system involved an early checkout of the electrical equipment using off-the-shelf rugged components, etc., and an aluminum slab flywheel. This ruggedized system known as System #1 was utilized to check out the operating characteristics of the electrical equipment while the development work on the low cost bare filament wound flywheel configuration was in process. In addition to working out the electrical system problems, the System #1 served a useful purpose in allowing the development of the proper flywheel suspension system to enable operation of the flywheel throughout its complete rotational speed range without encountering dangerous vibration at the various critical speeds.

The flywheel in this system is a laminated aluminum disc which, while storing only half the energy of the final flywheel assembly, nevertheless operates at essentially the same rotational speed range as the #2 demonstration system. The motor/generator and control system are the same as those in system #2. The rotating machine is a squirrel cage induction motor designed to operate between 3600 and about 15,000 rpm. Its design is based upon an off-the-shelf unit having moderately high performance.

The control system is designed to accept the energy from a 115 VAC source, transfer this energy into the flywheel, allow storage of the energy in the flywheel for an unspecified period, and finally to transfer the energy from the flywheel into a 115 VAC electrical load. It receives 115 volt, one phase, 60 Hertz input power, rectifies it to a controlled level DC voltage, and inverts it to controlled frequency three phase AC voltage. The control system is arranged to provide constant current per phase, so that the motor produces a constant torque up to the point where the line voltage reaches 230 VAC at 120 Hertz. At this point the motor is producing in excess of four HP. However, over the entire rotational speed range, the average power input and output is of the order of two kilowatts. A block diagram of the electrical system is shown in Figure 7, while Figure 8 illustrates the system components used in the #1 demonstration unit.

System #2 incorporates the optimized components to demonstrate the very low cost flywheel in its operating environment. The system itself was not intended to be a very low cost system, inasmuch as off-the-shelf parts were used throughout, and typically these were not optimized for

the system. The principal differences between this and System #1 were as follows: First, the bare filament flywheel (Figure 9) was substituted for the aluminum flywheel used in System #1. Secondly, small, magnetically unloaded oiled bearings were used in place of the ruggedized sealed, greased bearings of System #1. The magnetic relief system is illustrated in Figure 10. This system employing inexpensive ceramic magnets is relatively small compared to the rest of the system. It should serve to increase the projected life of the bearings in this flywheel energy storage system to at least 10 years duration.

CONCLUSIONS AND RECOMMENDATIONS

There are a number of interesting conclusions and recommendations that can be drawn from the subject program as follows:

CONCLUSIONS:

1. The very low flywheel production cost - $50. per kilowatt hour can be achieved with several available materials.

2. The best flywheel configuration for the low cost application appears to be the bare filament flywheel.

3. Magnetically load-relieved mechanical bearings look very promising for the low cost, long life flywheel system, as well as for other flywheel applications.

4. Operation of a flywheel energy storage system appears to be definitely feasible for the individual home and other stationary applications.

5. The subject program involved a variable speed induction generator electronically controlled to produce a constant electrical output. The component costs of the system chosen seem to warrant a thorough investigation of a constant speed generator with a variable transmission and flywheel system.

RECOMMENDATIONS:

1. The successes of the subject program appear to warrant the immediate institution of a full-scale home storage flywheel energy storage system program involving perhaps a 30 kilowatt hour unit.

2. An in depth investigation of the merits of a constant speed generator system should be conducted.

3. Continued R&D on Metglas flywheels should be initiated in order to determine their ultimate potential, not only for stationary flywheel energy storage systems but for vehicular flywheel systems as well.

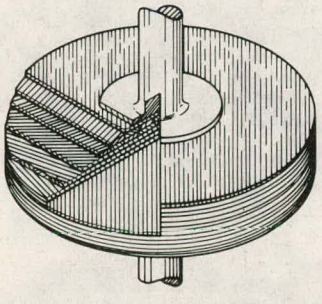

Fig. 1 Pseudo-isotropic flywheel concept.

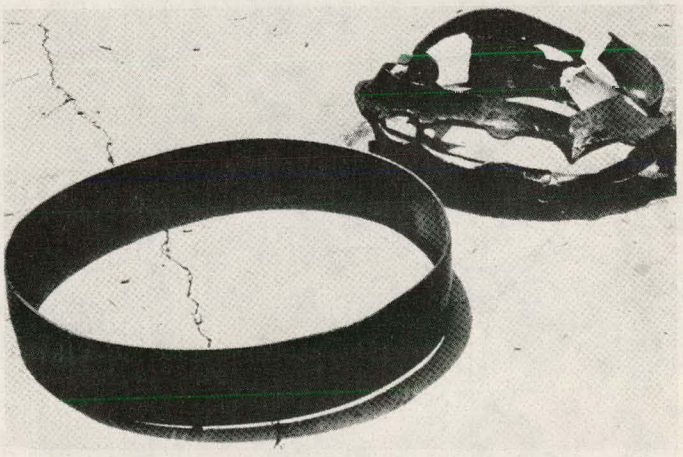

Fig. 2 Containment comparison between P-I disc and bare filament flywheels.

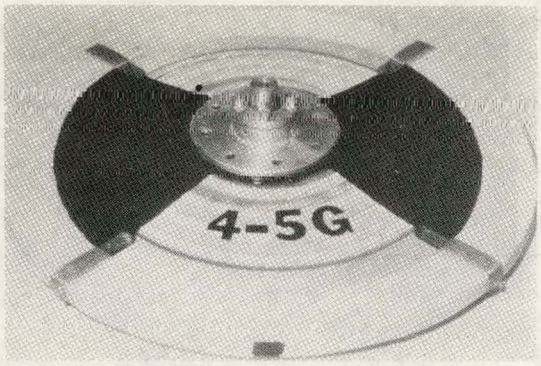

Fig. 3 Typical bare filament test rotor.

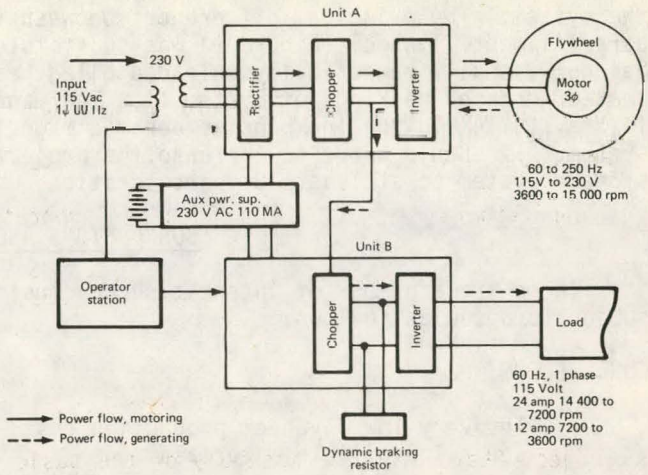

Fig. 7 Block diagram of energy storage system.

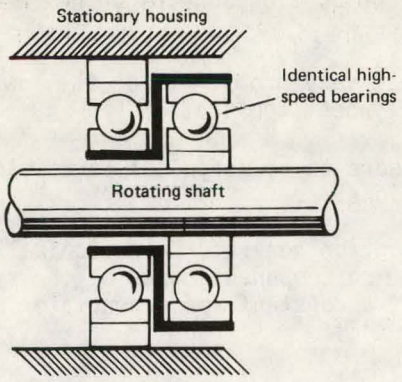

Fig. 4 Series bearing concept.

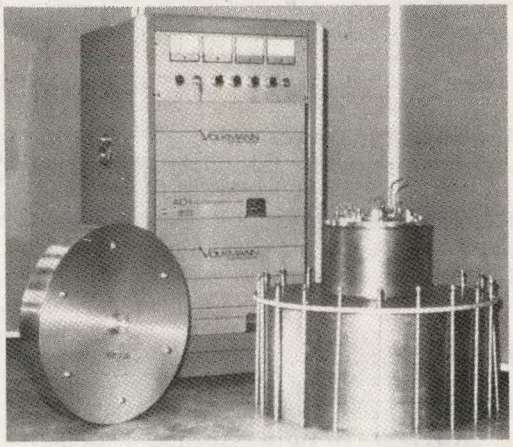

Fig. 8 Demonstration system components.

Fig. 5 Series bearing test assembly.

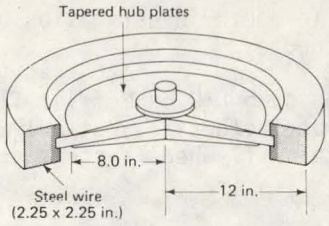

Fig. 9 Sketch of one kWh rotor.

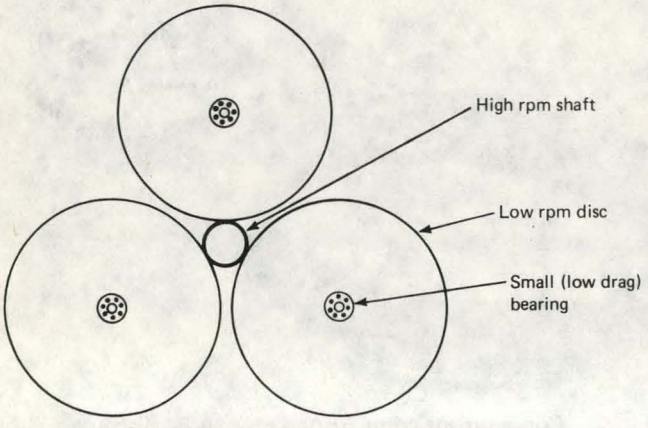

Fig. 6 Slow-roller bearing concept.

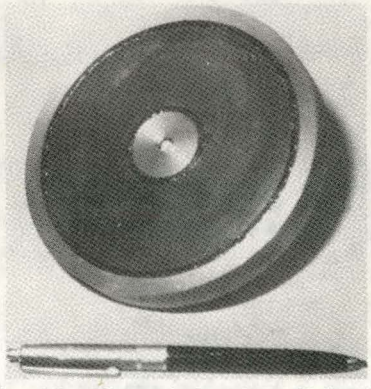

Fig. 10 Magnetic bearing relief unit.

PROJECT SUMMARY

Project Title: "Flywheel Evaluation Program"

Principal Investigator: Robert S. Steele, Jr.

Organization: Union Carbide Corporation
Nuclear Division
P. O. Box Y, 9998 MS-2
Oak Ridge, TN 37830
FTS 624-1837

Project Goal: To provide DOE with the ability to comprehensively evaluate high performance composite flywheels.

Project Status: Assembly of the basic spin test facility is complete. Facility capabilities will be demonstrated at the completion of FY 1979. These basic capabilities include determination of the ultimate speed and momentum transfer at failure of flywheels performing at energy levels up to 2 kWh.

Contract Number: W-7405-eng-26
Contract Period: October 1, 1978 - September 30, 1979

Funding level: $175,000

Funding Source: Lawrence Livermore Laboratories

OAK RIDGE FLYWHEEL EVALUATION LABORATORY

R. S. Steele
Union Carbide Corporation, Nuclear Division
P. O. Box Y, Building 9998, MS 02
Oak Ridge, TN 37830

ABSTRACT

The final assembly and proof testing of the Oak Ridge Flywheel Evaluation Laboratory (ORFEL) spin test facility has been completed as specified in the FY 1979 goals for the Oak Ridge Y-12 Plant's flywheel program. The spin facility is qualified to test flywheels with energy levels of up to 2 kWh.

The comprehensive evaluation of a flywheel design requires that it be subjected to several destructive and nondestructive tests, including detailed quantitative analysis of the test data. The consideration of these requirements is a major feature in the immediate plans of the ORFEL.

INTRODUCTION

The FY 1979 Oak Ridge Y-12 Plant* Flywheel Program goal is to complete the initial assembly begun in FY 1978 of the Oak Ridge Flywheel Evaluation Laboratory (ORFEL) and to begin the evaluation of prototype flywheels. This is in keeping with our overall goal of providing DOE with the ability to comprehensively evaluate high-performance flywheels.

The current Y-12 program is an extension of the UCC-ND Composite Flywheel Development program[1,2] initiated on May 1, 1976. That program was completed in September 1977 with the design, fabrication, and testing of a band-wrap flywheel design. The FY 1978 Flywheel program[3] at Y-12 was concerned with the fabrication of a spin test facility capable of testing rotors with up to 2 kWh energy levels. This work was not completed in FY 1978 but carried over into FY 1979. The current status of that program is the subject of this paper.

---

* Operated by Union Carbide Corporation, Nuclear Division for the US Department of Energy.

The funding level in FY 1979 has been $175,000 and began in April 1979. The schedule for the Oak Ridge Flywheel Evaluation Laboratory is presented in Figure 1.

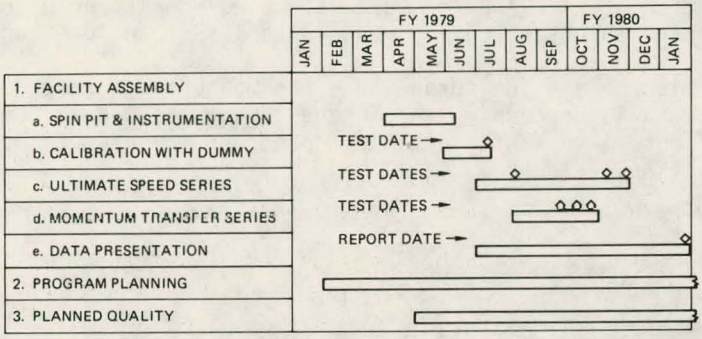

Fig. 1. Current Schedule for the Flywheel Evaluation Laboratory

FACILITY STATUS

The spin test area is located in Building 9766 at the Oak Ridge Y-12 Plant site. The 10- x 10-foot spin pit and its instrumentation and control console are arranged in a 50- x 34-foot room as indicated in Figure 2.

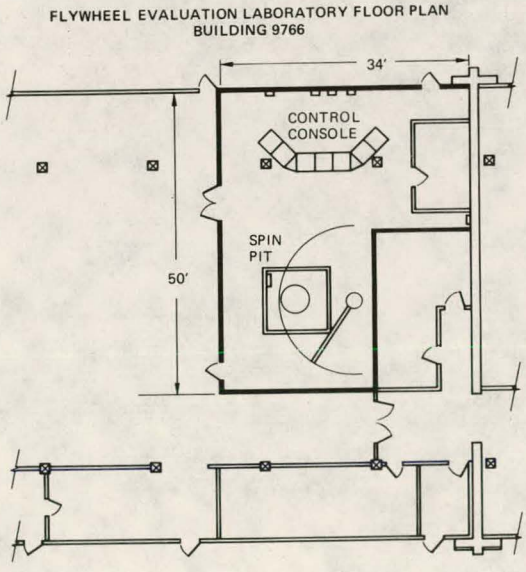

Fig. 2. Floor Plan of the Flywheel Evaluation Laboratory

The flywheel spin tank shown in Figure 3 is centered in the 4-foot-deep pit. It is 45 inches in diameter and 26 inches deep. This tank has walls of 1 1/2-inch-thick ASTM A285 alloy steel, the 2-inch-thick tank bottom and the removable 2 1/2-inch-thick lid are fabricated from the same material. Inside the spin tank are two rotatable cylindrical rings 25 inches tall, the inner steel ring has a wall thickness of 2 inches; and the outer ring wall thickness is one inch providing a useable space of 30 inches diameter. The tank lid supports the flywheel drive system and measurement instrumentation, twelve 7/8-inch-diameter toggle bolts hold the lid in place. The pressure in the spin tank can be reduced to less than 10^{-2} torr.

At the far left of Figure 3 is the torque tube for measuring torque during a catastrophic failure. Details concerning the torque tube are found in our FY 1977 Completion Report 2. Figure 4 shows the ultimate speed and momentum transfer configurations in cross section.

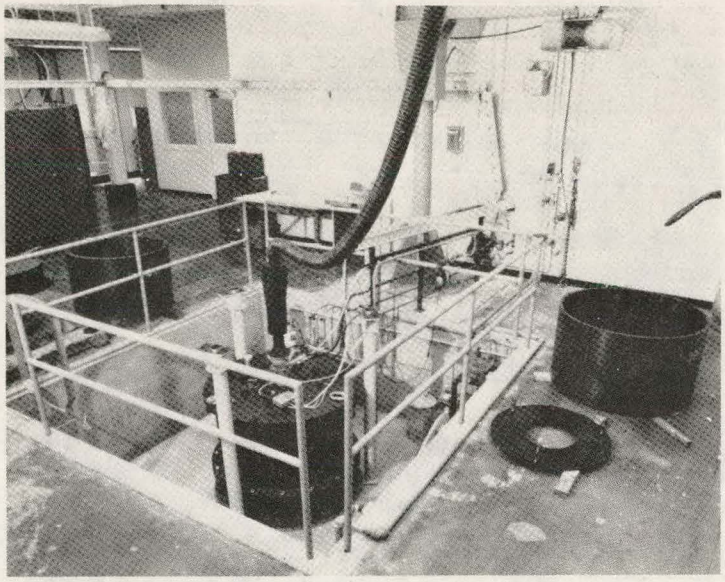

Figure 3. Photograph of the ORFEL Spin Tank

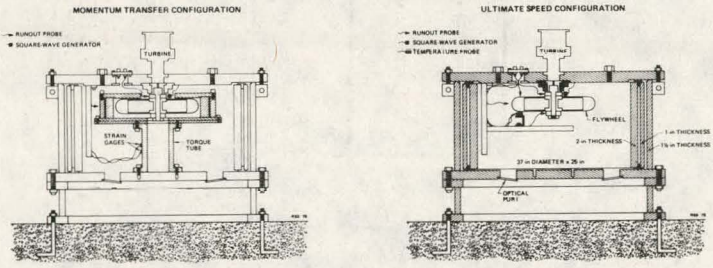

Figure 4. Ultimate Speed and Momentum Transfer Tank Configurations

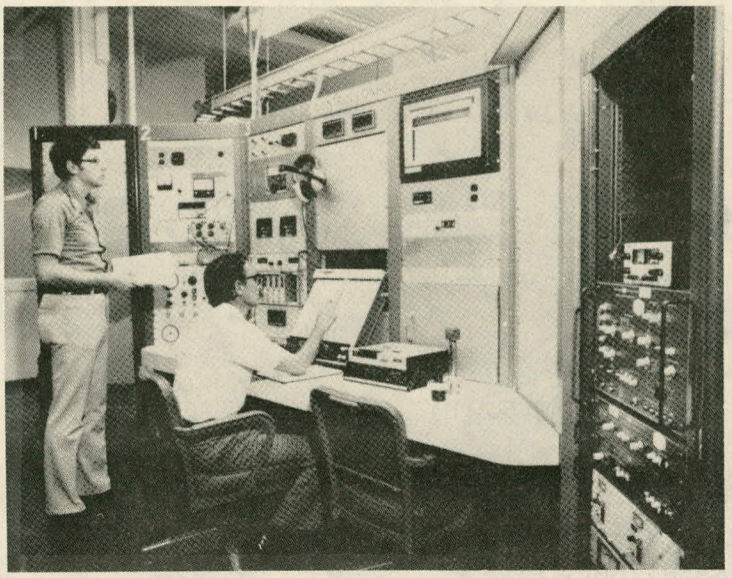

Fig. 5. ORFEL Instrumentation Console

The instrumentation and control console is currently configured as shown in Figure 5. The operational limits for the ORFEL test stand are as follow:

- Maximum kinetic energy of the test flywheel can be up to 2 kWh.
- Maximum rotational velocity can be up to 60,000 rpm.
- Maximum tank pressure during a test will be less than 10^{-2} torr.
- Maximum mass eccentricity of the test unit can be up to 0.020 inch during the test.
- Maximum couple unbalance of the test unit can be up to 175 in·lbs during the test.
- Test unit must fit within a 30-inch-diameter by 25-inch-tall cavity.

APPLIED PHILOSOPHY OF TESTING

The effort to develop a capability for comprehensive evaluation has required the Y-12 program to determine not only what tests must be preformed but to develop a philosophy of how they are to be carried out. First in our mind is that the facility be safe for personnel. Several extensive safety reviews, drawing upon the wide expertise available in Oak Ridge, have been performed in an effort to meet this criterion. Secondly, data acquired during a test must be quantitative rather than

FY79 TEST STAND DATA CAPABILITY

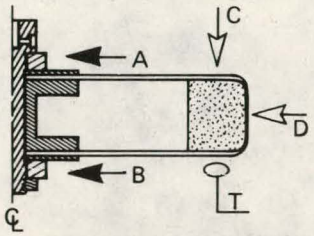

A, B – ELECTRONIC PROXIMITY PROBES

C, D – ELECTRO-OPTICAL PROXIMITY PROBES

T – PYROMETER

SENSOR LOCATIONS FOR DYNAMIC MEASUREMENTS

DATA

- **RUNOUTS AT A, B, C, AND D**
- **STANDOFF AT A, B, C, AND D**
- **TEMPERATURE AT T**
- **ROTATIONAL FREQUENCY**
- **PRESSURE**

Fig. 6. FY 79 Test Stand Data Acquisition Sensor Locations

subjective. Figure 6 reveals the heavy reliance upon proximity probes for dynamic and steady-state dimensional measurements. Thirdly, these data must be analyzed in a quantitative manner. The ORFEL approaches this requirement in its ability to monitor the frequency components of each probe signal and to record and recall those probe signals after failure. The ORFEL is prepared to perform vector manipulations and statistical analysis as may be required using the extensive computational facilities available in Oak Ridge. Fourth, the tests must subject the flywheels to conditions beyond the actual operation ranges of speed and temperature. And, finally, a sufficient number of these tests must be performed to allow the results to be reported with statistical significance. A relatively large number of flywheels will be required for these tests.

The actual tests required were identified in an examination of the end requirements for the flywheel, namely safety and effectiveness. A list of destructive tests which require a spin testing facility must include ultimate speed, momentum transferred during failure, fatigue life and stress life. Nondestructive tests which may run concurrent with the destructive ones include vibrational analysis, strain gage analysis, dimensional variations with stress, dynamic stability, and relative motion between parts.

Knowledge of flywheel characteristics gained from such a test plan should provide the needed data to determine failure modes, containment requirements, energy storage capability, and life estimates all as a function of operational demands placed on the flywheel. This list is not complete. Other tests will undoubtedly develop, but these tests are a required minimum.

ORFEL will develop additional capability of providing reliable measurements to meet future flywheel research demands.

IMMEDIATE FUTURE

By January 1980 the ORFEL will have demonstrated its basic capabilities by completing the ultimate speed and momentum transfer tests using the UCC-ND bandwrap design flywheel. At that time we expect to begin evaluation of prototype flywheel designs for the Department of Energy's Mechanical Energy Storage program.

Concurrent with that work we must expand our capabilities to meet our user's needs. Of immediate need is a failure imaging technique and a flywheel brake for use in fatigue testing. A third highly desirable testing capability is an early-warning-of failure detection technique. The quantity and quality of these development programs, of course, depend the funding support they receive.

SUMMARY

The Oak Ridge Flywheel Evaluation Laboratory will complete its FY 1979 objectives and become a productive member of the high performance flywheel effort early in FY 1980. Our basic capabilities will be testing for ultimate speed, failure mode, and containment requirements of prototype flywheel designs. A great potential exists for their comprehensive evaluation using the considerable expertise available in the Oak Ridge complex. The only constraints are time and money.

REFERENCES

1. R. L. Huddleston, J. J. Kelly, and C. C. Knight, Jr.; "Composite Flywheel Development Completion Report" (May 1 - September 30, 1976), Y-2080; Union Carbide Corporation Nuclear Division, Oak Ridge Y-12 Plant, Oak Ridge, Tennessee, May 11, 1977.

2. R. L. Huddleston, J. J. Kelly, C. E. Knight, R. E. Pollard, and D. W. Post, "Composite Flywheel Development Completion Report" (October 1, 1976 - September 30, 1977), Y-2117; Union Carbide Corporation-Nuclear Division, Oak Ridge, Y-12 Plant, Oak Ridge, Tennessee, May 1978.

3. B. B. Smith, "Flywheel Test Facility" in Proceedings of the 1978 Mechanical and Magnetic Energy Storage Contractors' Review Meeting, Conf-781046, pg. 76.

THIS PAGE

WAS INTENTIONALLY

LEFT BLANK

PROJECT SUMMARY

Project Title:	Army Flywheel Program
Principal Investigators:	C.J. Heise, L. I. Amstutz
Organization:	Army Mobility Equipment Research and Development Command DRDME-EA Fort Belvoir, Virginia 22060 (703) 664-4587
Project Goals:	To develop flywheel energy storage technology appropriate for averaging peak loads on mobile electric power sources.
Project Status:	A steel flywheel energy storage module of 30 kWh capacity has been designed and built by Rocketdyne under contract number DAAG53-75-C-0278. This equipment is being subjected to a thorough checkout and evaluation. It will subsequently be incorporated into an electric power supply for further evaluation. In an attempt to improve safety while reducing weight and volume composite rotor development has been undertaken in parallel with the steel flywheel effort. Contract DAAG53-75-C-0270 with AiResearch has resulted in multiring rim type rotors with storage capability in excess of 20 Wh/lb. These rotors are at a stage of development where they may be seriously considered for incorporation in future energy storage systems demonstrations. Contract DAAG53-75-C-0269 with AVCO has partially developed a more compact biaxial strength rotor which has recently demonstrated storage capability greater than 30 Wh/lb.
Contract Number:	13-2369
Contract Period:	FY 79
Funding Level:	$132k
Funding Source:	Sandia Laboratories, Albuquerque

ARMY FLYWHEEL PROGRAM

C. J. Heise
L. I. Amstutz
US Army MERADCOM
Fort Belvoir, Virginia 22060

ABSTRACT

This paper describes the U.S. Army MERADCOM flywheel program with emphasis on the evaluation of a 30 kWh energy storage module. In this module advanced steel flywheel technology is used to achieve a high energy storage density. The systematic evaluation being undertaken will serve to confirm the design procedures and indicate where changes are needed. This information will be useful in guiding future energy storage systems developments.

INTRODUCTION

This paper is the result of cooperative DOE and DOD funding in the exploratory development of flywheel technology. The Army Mobility Equipment Research and Development Command, MERADCOM, at Fort Belvoir, became interested in mechanical energy storage for use with Army electric power generating equipment in FY75. Since then MERADCOM has managed a development program totaling $1,688,000 including $162,000 of DOE funds. This participation by DOE has been of critical importance in terms of realizing the greatest technological advancement from these efforts. The overall program includes three contracted efforts:

30 kWh steel flywheel energy storage module, Rocketdyne.

Multiring rim type composite rotor, AiResearch.

Biaxial strength composite rotor, AVCO.

DOE funds were used last year to partially fund testing of a multiring rim type rotor which had been built using Army funds. The results obtained contributed to further development work which has been funded exclusively by DOE. This multiring rim approach has been extensively discussed in earlier proceedings [1, 2] and will not be further treated here. DOE funds were not directly applied to the biaxial strength rotor program, however, DOE participation in our overall program contributed to our ability to fund the July 79 rotor tests at the Naval Air Propulsion Test Center. The test results were instructive and encouraging (>30 Wh/lb). This type of rotor is expected to be more expensive than the multiring rim type but also considerably more compact. Additional exploratory development will be required before such composite rotor is ready for incorporation in an energy storage system development. The main topic of this paper is the 30 kWH steel flywheel energy storage module. This module was designed and built using DOD funds. DOE is providing a substantial portion of the cost of a systematic check out and evaluation of the module. It is expected that the information gained during this phase of the effort will contribute to future mechanical energy storage projects.

This paper describes the 30 kWh module, gives anticipated performance characteristics, and describes the tests which are presently underway.

FLYWHEEL SYSTEM DESCRIPTION

The Army flywheel electric power system consists of a flywheel module, a gas turbine engine and variable speed generators. In the module, energy is stored in four flywheels mounted in pairs on two counter-rotating shafts which are interconnected by means of a four-in-line 1 to 1 ratio gear-box. Figure 1 shows one of the assembled shafts. It consists of a pair of end stub shafts and a pair of flywheels all of which are flanged and bolted together to avoid a through shaft which would lead to disruptive center-disc holes.

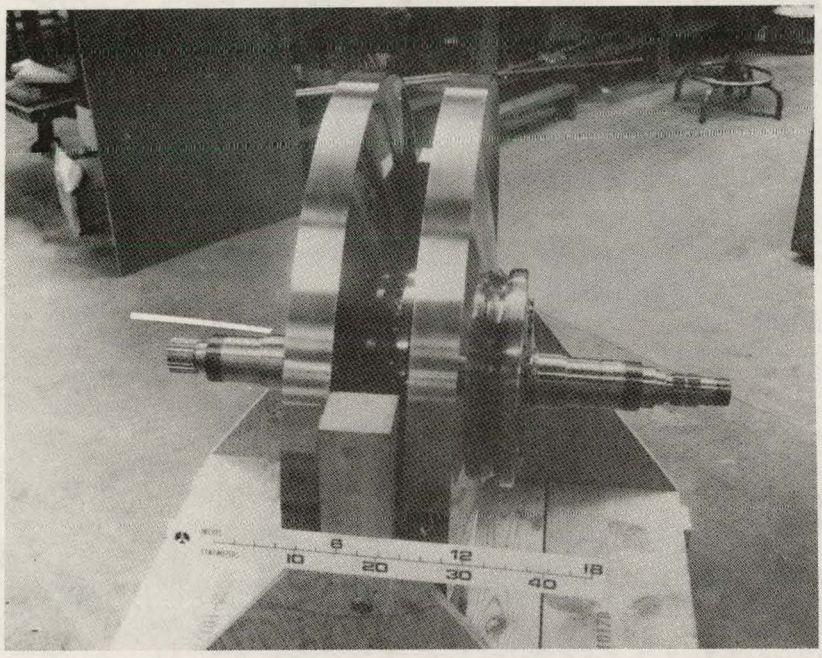

Fig. 1 Assembled Shaft with two Flywheels

The power flow in the module is from the gas turbine engine to the gearbox, to the two horizontally aligned parallel flywheel rotors through over-running clutches and finally to the two directly coupled generators. The module housing consists of three 356-T6 aluminum alloy castings. This housing is used to accomodate the flywheel rotors and to mount the gearbox, gas turbine and the two generators, bolted directly to the housing. The arrangement of the flywheels in the housing can be seen in Fig. 2 which shows the module partially assembled. The flywheels are of the modified constant stress type made of forged and heat-treated low nickel alloy steel HP9-4-30[3], which had been identified as the optimum isotropic flywheel material for the intended service through tests at Rocketdyne. The diameter of each of the four flywheels is 37.1 inches, the weight of each is 650 lbs and rated energy storage at 14,500 RPM is 7.5 kWh per wheel. In order to improve safety in case of flywheel failure, each wheel has a rim and under the rim a section which will be the most highly stressed part of the wheel. In case of overspeed the rim will break off and relieve the rest of the flywheel thus prevention of further damage can be achieved. A subscale rotor was fabricated and tested to prove this failure mode; it was concluded that in the extremely unlikely event of overstress to the failure point only about 20% of the stored energy would be released.[4]

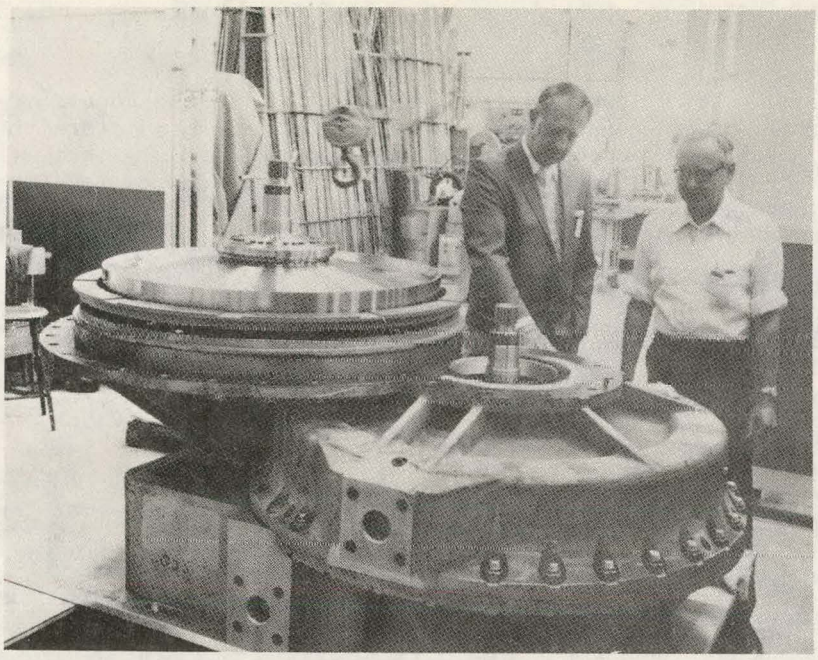

Fig. 2 Partially Assembled Housing

In the module all four wheels will be surrounded by a barrier ring, the clearance between this ring and the flywheel rim will be used as a measure for the stress level in the wheel. It was concluded in the subscale test that observing the reduction of barrier ring clearance is an effective indicator of rotor growth beyond the elastic limit whether due to overspeed or overheating. If a flywheel does contact a ring, the ring will begin to rotate causing immediate loss of energy and deceleration of the rotor. Size and weight of the assembled module not including the turbine engine and the two generators are shown in Table 1.

TABLE 1. Dimensions and Weight of Module

Dimensions (inches)	
Width	77.5
Height	49.8
Length	62.4
Weight (lbs)	
Gearbox	527
Housing	2021
Shafts & Clutches	75
Barrier Rings	1142
Rotor Assemblies	2990
Misc.	602
Total	7357

Characteristics of the flywheel module based on final calculation are shown in Table 2.

TABLE 2. Flywheel Module Characteristics

Energy storage at 14,500 RPM		30 kWh
Operating speed range	min.	10,500 RPM
	max.	16,000 RPM
Material yield speed		17,600 RPM
Critical speeds	6,000 and	21,000 RPM
Energy storage per lb of rotor weight at 14,5000 RPM		10 Wh/lb

This energy storage module is intended by the Army to be a high-performance unit with a moderate cycle life. One could view this same hardware as having a lower energy storage rating but a long cycle life and large safety factor. From this latter perspective, the planned tests and subsequent Army use represent evaluation of the safety margins and accelerated life testing. Fig. 3 shows the fully assembled module at the Rocketdyne's plant.

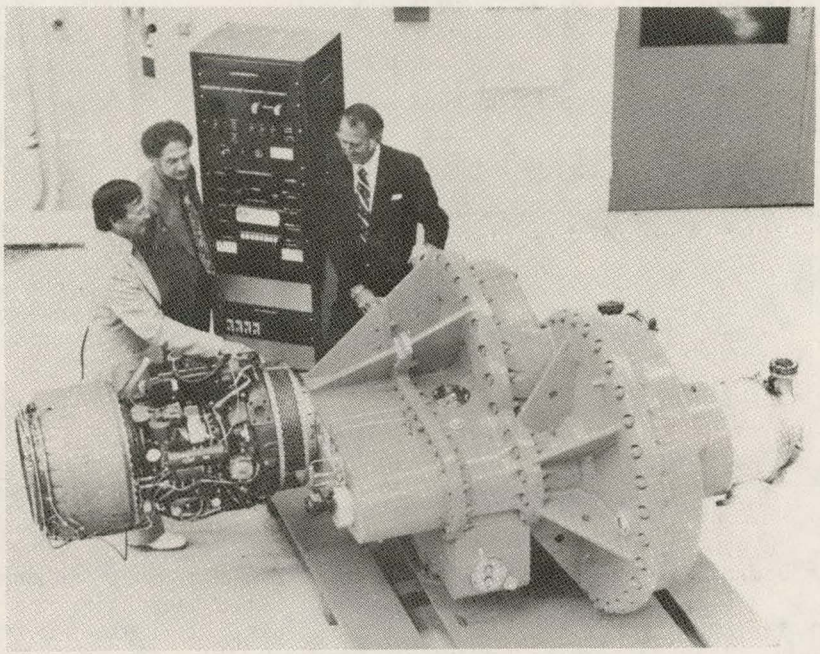

Fig. 3 Fully Assembled Module

TEST PLAN DESCRIPTION

The objective of these tests is to perform a systematic characterization and evaluation of the 30 kWh energy storage module. It is the complete module including the necessary auxilliary equipment which is the subject of the tests now in progress. Since this phase of the work is mainly concerned with the mechanical energy storage, the generators have been replaced by air turbines for the test. The air turbines can be used either as brakes or as drivers during the tests. The testing is divided into four tests, I-IV. The plans for each of these tests will be described in turn. Fig. 4 shows the schedule for the test.

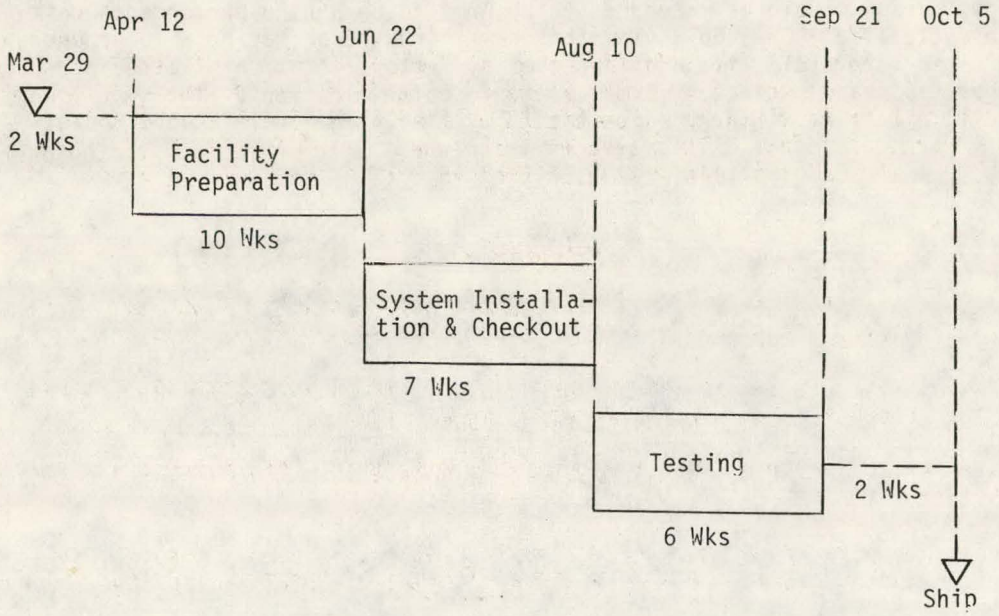

Fig. 4 Test Schedule

TEST I.

This test is a preliminary check out of the ancillary equipment and the data system. The air turbines will be used to operate the flywheels below their first critical speed. This test will verify the operation of vacuum pumps, seals, lubrication system, etc.

TEST II.

This test will evaluate the performance of the system as it passes through the first shaft critical speed, which is below the normal operating speed range. Both rotors will be driven through the resonance using the gas turbine engine. The performance of the bearings and supports will be noted and any adjustments indicated will be made before proceeding to other tests. It is expected that the module will not be harmed by slow passes through this resonance zone.

TEST III.

This test will evaluate the effects of temperature and pressure on the module. When successful operation through the first critical speed has been demonstrated measurements of friction and windage losses will be made at moderate speed. These losses will be characterized over a range of lubricating oil temperatures and over a range of housing pressures up to about 100 torr. Temperature of the rotor, barrier ring and housing will be monitored. The parasitic loss will also be similarly evaluated at higher speed but with the variations in temperature and pressure more restricted in order to avoid damaging the equipment. Within the constraint of not damaging the module an attempt will be made to characterize an elevated pressure shut down.

TEST IV.

This test will evaluate the performance of the module in its intended operating range. The strain of the rotors will be monitored as a function of speed and temperature. The energy storage module will be cycled using the gas turbine engine to charge and the air turbines to brake. This test will include a brief excursion to the overspeed limit where the rotor strain will nearly close the gap between the rotors and the barrier rings.

REFERENCES

1. Satchwell, D. L., "High Energy Density Flywheel," Proceedings of the 1978 Mechanical and Magnetic Energy Storage Contractors' Review Meeting, October 1978.

2. Satchwell, D. L., "Rim Type Rotor," Proceedings of the 1979 Mechanical and Magnetic Energy Storage Contractors' Review Meeting, August 1979.

3. Anon., "Properties of Productive Product of HP 9-4-30 (Cr, Mo)," Republic Steel Research Center, December 8, 1965.

4. Davis, Hodson, Heise, "Rocketdyne's High Energy Storage Flywheel Module for the U.S. Army," Proceedings of the 1977 Flywheel Technology Symposium, October, 1977.

THIS PAGE

WAS INTENTIONALLY

LEFT BLANK

PROJECT SUMMARY

Project Title:	Application of Inertia Welding Technology to Steel Disc-Type Flywheels
Principal Investigator:	Douglas L. Kerr
Organization:	General Electric Company Corporate Research and Development Schenectady, New York 12301
Project Goals:	Investigate the feasibility of applying inertia welding to the fabrication of steel flywheel assemblies for transportation application.
Project Status:	The project has been completed. It consisted of three phases. In Phase I, the inertia welding characteristics of three steel alloys (Hy-Tuf, 4340, and D6AC) were investigated by welding both solid bars and tubular specimens. In Phase II, the feasibility of various "flash trap" designs was explored. The objective of these designs was to contain or shape the weld flash in such a manner as to make it unnecessary to machine the weld flash after welding. Tubular specimens were again used. In Phase III, two simulated flywheel discs approximately 6 inches in diameter were joined by inertia welding, then evaluated. Major conclusions are as follows: a) Inertia welding of both Hy-Tuf and 4340 steel alloys is readily accomplished in configurations desired for flywheel applications. b) Hy-Tuf is somewhat preferable to 4340. c) Crack-free inertia welding of D6AC appears to be difficult to achieve, d) A flash trap has been developed which prevents the radial V-notch in the weld flash, but it has an axial notch area which might cause fatigue problems. It is recommended that work be performed in evaluating fatigue characteristics of inertia weld configurations, including further development of configurations which might enhance fatigue properties.
Contract Number:	W-7405-ENG-48, Subcontract 2867209
Contract Period:	25 September 1978 through 29 June 1979
Funding Level:	$53,835
Funding Source:	U.S. Department of Energy through Lawrence Livermore Laboratories

APPLICATION OF INERTIA WELDING TECHNOLOGY TO STEEL DISC-TYPE FLYWHEELS

Douglas L. Kerr
General Electric Company
Corporate Research and Development
Building 37-380
1 River Road
Schenectady, New York 12301

ABSTRACT

This paper summarizes a program which investigated the feasibility of applying inertia welding to the fabrication of multiple disc, steel flywheel assemblies for transportation application. The program was divided into three phases: Phase I - Establish Inertia Weldability; Phase II - Joint Geometry Considerations; and Phase III - Simulated Flywheel Disc Assembly.

It is concluded that inertia welding of certain steel alloys (Hy-Tuf and 4340, for example) is readily accomplished in configurations desired for flywheel applications. Welds are sound and have good short term tensile properties. Future effort should be applied to evaluating fatigue characteristics, including further study of configurations which might enhance fatigue properties.

INTRODUCTION

Work on flywheel energy storage was initiated by the Department of Energy (DOE) as part of the energy conservation program. Initial emphasis has been on the application of flywheels to electric vehicles. In this connection, the General Electric Company has performed a series of flywheel design studies associated with the application of an inductor motor/flywheel energy storage package for transit bus applications. These studies have been primarily aimed at determining a preferred steel flywheel configuration and evaluating various manufacturing techniques.

It has been concluded[1] that the flywheel configuration that best matches the inductor motor flywheel package concept is a multidisc design in which the individual flywheel discs are attached to each other and to the motor shaft by welding, by bolting, or by a shrink fit. In the case of a shrink fit, impracticably high shrink fits are required to achieve the energy density desired. In the case of the bolted construction, stress concentration factors in the vicinity of the bolt holes must be taken into account. In the welded configuration, the stress concentration factors are assumed to be negligible, but consideration must be given to the possible effects of reduced material properties in the vicinity of the weld.

If a suitable means of welding flywheel discs together can be found, this form of construction is expected to provide much better rotor performance (including lower weight) for a given value of ultimate tensile strength than the bolted construction. The inertia welding concept may be applicable to a modular steel flywheel assembly. It accomplishes the weld by friction and pressure -- the parts are literally spun together. General Electric's Aircraft Engine Group has developed and applied the inertia welding concept in other applications.

In accordance with the foregoing, this program was established to investigate the feasibility of applying inertia welding to the fabrication of steel flywheel assemblies

for transportation application. All of the experimental work was performed by personnel of the Aircraft Engine Group of the General Electric Company. Program direction was provided by personnel of the General Electric Company's Research and Development Center. Reference 2 is the final report for the program.

BACKGROUND ON INERTIA WELDING

In this process, rotational mechanical energy is dissipated between work pieces under axial pressure, resulting in weld without melting. For this reason inertia welding is regarded as a solid-state joining process. One piece that rotates at a high speed is pressed against a second piece which is fixed rigidly and is stationary. This rotational friction removes the metal interfaces away from the weld, producing a clean, defect-free product. This process is rapid and does not require an inert atmosphere even for welding active metals such as titanium.

The metal that is extruded away from the interface during welding results in a weld flash appearing at the free surface(s). This weld flash forms a typical pattern as shown schematically in Figure 1, which indicates the flash that would form in an annular weld. This flash looks somewhat like a double breaking wave, with a radial V-notch forming between the two halves. The depth and sharpness of this V-notch is a function of the materials and also of the weld parameters utilized.

In general, it is undesirable to have notches in parts, especially when subjected to cyclic stresses. Consequently, this weld flash and the V-notch are normally machined off after the weld is completed to form smooth, notch-free surfaces.

In the configuration of Fig. 1, however, it is not possible to machine off the V-notch on the inside radius. Since this type of configuration is desirable in multidisc flywheel applications (See Fig. 2), one of the purposes of the program was to explore the feasibility of various methods of containing or shaping the weld flash on the inside radius in such a manner as to eliminate the V-notch and reduce the possibility of fatigue failures due to such a notch. Of course, it is also possible that with proper design, such a notch could be tolerated safely. However, determination of whether this is a real possibility requires experimental evaluation for specific designs which was not part of this program.

PROGRAM DESCRIPTION

The program was divided into the following three phases:

PHASE I -- ESTABLISH INERTIA WELDABILITY

The inertia welding characteristics of three steel alloys (Hy-Tuf, 4340, and D6AC), were determined by welding both solid bars (1-inch outside diameter) and tubular specimens (2-inch outside diameter by 0.1-inch-thick wall). In addition, characteristics of the weld and the weld flash (that material extruded from the weld mating surfaces during the welding process) were evaluated.

In Phase I, a total of 13 solid bar welds were made, approximately four for each of the three alloy steels. Eighteen tubular welds were made, six for each of the alloy steels. All welds were austenitized, plus oil-quenched, tempered, then welded and post-weld tempered. Estimated ultimate tensile strengths of the materials just prior to welding, based upon the heat treatment used, were 230,000 psi, 190,000 psi, and 220,000 psi respectively for Hy-Tuf, 4340, and D6AC.

All welds were cross sectioned and examined for weld defects, heat-affected zone pattern, and notch sensitivity.

PHASE II - JOINT GEOMETRY CONSIDERATIONS

The purpose of this phase was to explore the feasibility of various "flash trap" designs, whose objective is to contain or shape the weld flash in such a manner as to make it unnecessary to machine the weld flash after welding. Tubular specimens (2-inch outside diameter by 0.1-inch-thick wall) were again used.

A total of 38 welds and over a dozen flash trap designs were utilized in Phase II. (See Fig's. 3 and 4 for some of the designs.) All of the welds were appropriately heat treated before and after welding, and a minimum of two cross sections from each weld were cut and metallographically examined up to a magnification of 400X. Special polishing procedures were utilized to reveal the presence of cracks (if any) and/or voids.

PHASE III - SIMULATED FLYWHEEL DISC ASSEMBLY

In this phase, two simulated flywheel discs approximately 6 inches in diameter were joined by inertia welding, (see Fig. 5) then evaluated by sectioning and metallography to determine the weld characteristics. Tensile tests were also performed on welded portions of the disc assembly. This assembly has shaft extensions. It was also sectioned, and a 75° segment was polished, photomicrographed, and delivered to Lawrence Livermore Laboratories.

RESULTS

Phase I work demonstrated the good welding characteristics of Hy-Tuf and of 4340 and indicated that D6AC was questionable as a candidate material because of cracking. No cracks were observed in any of the Hy-Tuf or 4340 specimens except one 4340 solid bar which was water quenched immediately after welding to see how severe a treatment it could take. All three solid bar D6AC specimens showed cracks, and two out of six tubular D6AC specimens showed cracks.

In Phase II, the D6AC alloy showed poor welds in the first few samples and was dropped from further consideration on this program. Hy-Tuf exhibited somewhat more blunt V-notch characteristics than 4340, and so the remaining portion of the program concentrated on Hy-Tuf material. However, it is believed that 4340 would make acceptable welds if other reasons, such as cost or availability, made it desirable to use this material.

The first flash trap samples (butt weld, angle weld, and J-groove welds of Fig. 3) revealed cracks in nearly all of the welds. These are believed to be due to excessive restraint on the inward flow of weld flash and/or the asymmetry of these configurations from a heat flow and thermal stress standpoint.

Two modifications were then made to the J-groove design. These eliminated the cracking, but had numerous notch-sensitive areas. The plain slot configuration of Fig. 4 was then tried as a means of allowing some inward flow of weld flash but also to mechanically constrain it in a manner as to eliminate the V-notch at the weld centerline. It is also a more symmetrical configuration. Results were promising, but not completely satisfactory. Welds did not exhibit cracks, and the radial V-notch was eliminated. One side of the welds was smooth, but the other side exhibited an axial notch (or cold shut area) along the inner diameter of the tube. (See the schematic of Fig. 6.) Several modifications of this slot configuration were then tried, including one configuration which used stainless steel as an interface between the two pieces being welded. Results were of mixed success. The stainless steel samples produced results no better than those obtained without use of stainless steel, and this approach was dropped.

The most promising flash trap configuration resulting from the Phase II work is the 0.025 slot configuration of Fig. 4. It has somewhat more symmetry than the plain slot

configuration, yields welds without cracks, and eliminates the radial V-notch, but still has the axial notch shown schematically in Fig. 6.

Program constraints made it necessary to do no more work on flash trap configurations on this program.

The Phase III simulated flywheel disc assembly was then made without use of flash traps according to the configuration of Fig. 5. Successful welds were made on the first try by scaling parameters from Phase I and Phase II.

Weld evaluation, including microexamination up to 400X, revealed no defects of any kind. An attempt was made to run short-term tensile tests of specimens cut from the annular weld area C of Fig. 5, but the annular geometry made this impracticable. Therefore, two tensile test specimens were cut from the axial welds A and B of Fig. 5, and short-term room temperature tensile tests were performed on these specimens. Results indicated short term ultimate tensile strength of these welds to be about 85% or more of the ultimate tensile strength of the parent material.

Figure 7 is a photograph of the 75° segment that was cut from this simulated flywheel disc assembly.

CONCLUSIONS AND RECOMMENDATIONS

This program has demonstrated that inertia welding of certain steel alloys is readily accomplished in configurations desired for flywheel applications. Welds are sound and have good short term tensile properties. It is not known, however, whether these welds have adequate fatigue characteristics. In this respect, application of flywheels to transit bus and other transportation applications requires fatigue cycle life on the order of 10^6 cycles(1). This is considerably higher than used heretofore in flywheel applications and imposes a considerable constraint upon the design.

Because of these stringent fatigue requirements, it is recommended that additional work be performed in evaluating fatigue characteristics, including developing better, i.e. more fatigue resistant, flash trap or other types of configurations.

ACKNOWLEDGEMENT

Special recognition should be given to R. Dreisig of the Aircraft Engine Business Group of the General Electric Company, who carried out all of the experimental work on this program.

REFERENCES

1. "A Study of Flywheel Energy Storage for Urban Transit Vehicles," Phase 1 - Final Report, Contract DOT-UT-60096T, General Electric Company, (16 September 1977).

2. "Application of Inertia Welding Technology to Steel Disc-Type Flywheels," Final Report, Lawrence Livermore Laboratories Subcontract No. 2867209, General Electric Company (29 June 1979).

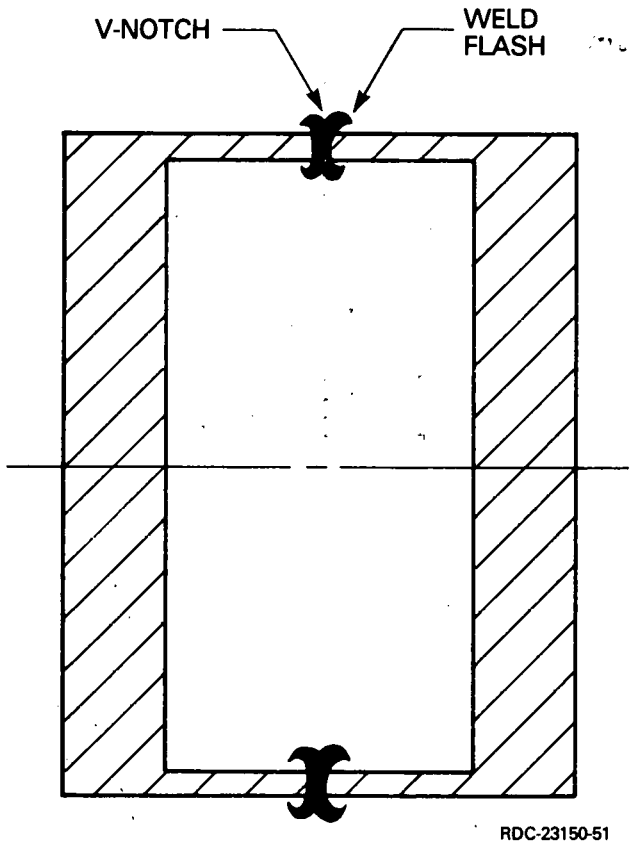

Fig. 1. Schematic of Weld Flash.

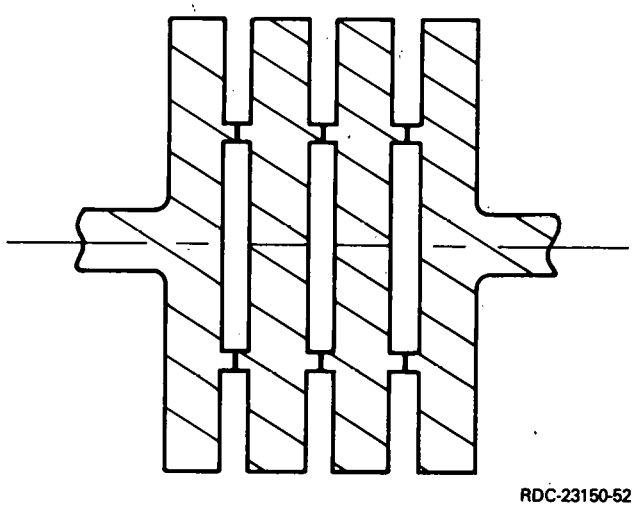

Fig. 2. Flywheel Rotor Schematic.

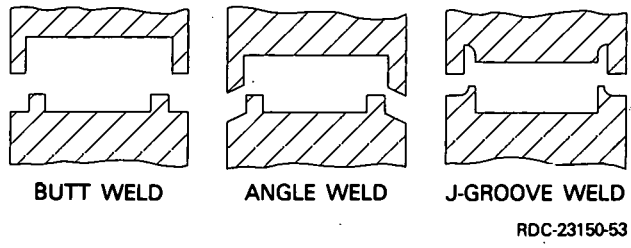

Fig. 3. Initial Flash Trap Configurations.

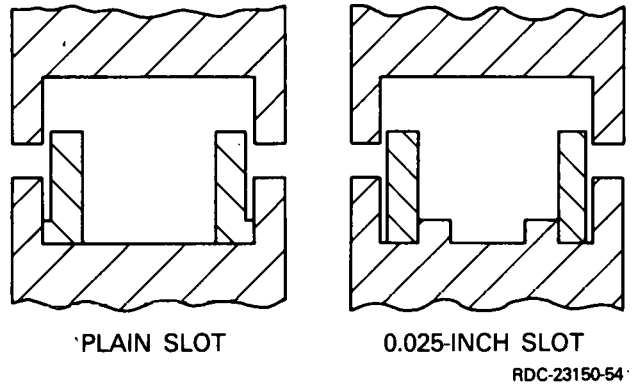

Fig. 4. Slot Flash Trap Configurations.

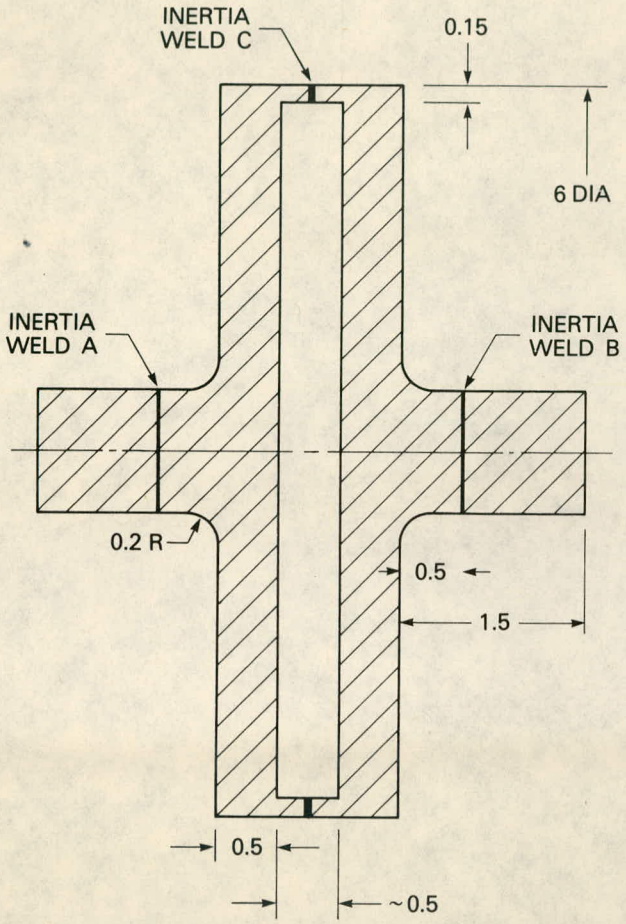

Fig. 5. Phase III Assembly.

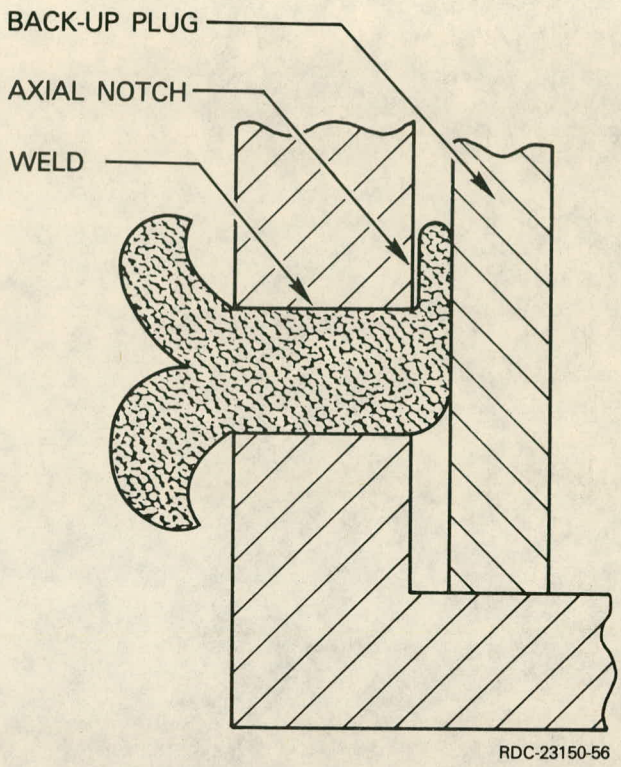

Fig. 6. Axial Notch with Slot Type Flash Trap.

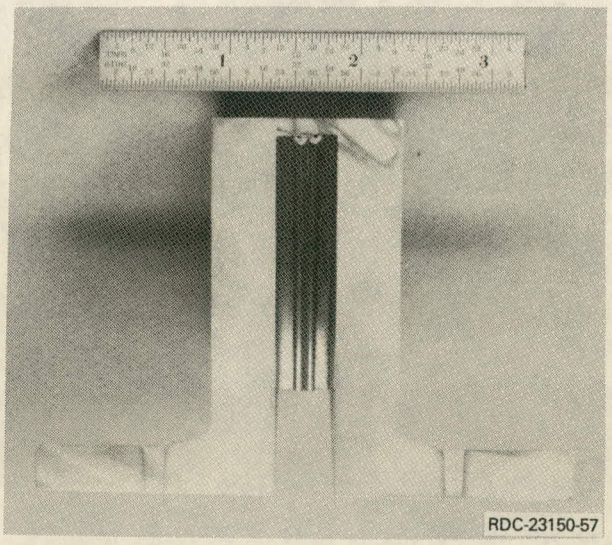

Fig. 7. Section of Simulated Flywheel Disc Assembly (Direct View).

THIS PAGE

WAS INTENTIONALLY

LEFT BLANK

PROJECT SUMMARY

Project Title:	"Flywheel-Engine Powerplant Research and Development Studies"
Principal Investigators:	Norman H. Beachley and Andrew A. Frank
Organization:	College of Engineering University of Wisconsin-Madison 1513 University Avenue Madison, WI 53706
Project Goals:	The basic objective is to provide a design analysis of a flywheel-engine power unit for a passenger automobile. The detailed tasks are: 1) evaluate the potential of alternative powerplants for use with flywheel, 2) determine the lower level of friction that may be practically achieved in driveline components, 3) determine the most promising continuously variable transmission (CVT) concept for a 2nd generation flywheel vehicle, 4) design safety features for the flywheel system, 5) prepare a preliminary layout drawing of the complete flywheel powerplant system suitable for installation in a production automobile chassis.
Project Status:	A preliminary study of alternative heat engine powerplants (Stirling, gas turbine, diesel piston, and gasoline piston engines) has been performed to determine their relative fuel mileage potentials. Other practical aspects still need to be investigated, such as the effect on engine efficiency and life of an on-off mode of operation. Three continuously-variable transmission concepts have been identified as having efficiency, size, and weight characteristics satisfactory for a second generation experimental flywheel car. Preliminary design configurations have been developed based on these three principles, and design work is being continued with the goal of further simplification and reduction of friction losses. Basic packaging configurations have been determined that will permit the flywheel powerplant systems (for each of the three chosen CVT concepts) to fit in the engine compartment of a conventional front wheel drive automobile. There is still much work to be done, however, on the details of mounting and interconnecting the various powerplant components. Considerable information on the friction characteristics of bearings and gears has been collected that will aid in system efficiency calculations, and also in the determination of what fuel economy improvement might be obtained by attention to and optimization of these components in the driveline.
Contract Number:	SUBCONTRACT 4492309
Contract Period:	Feb. 5, 1979-Dec. 31,1979
Funding Level:	$93,286.00
Funding Source:	Lawrence Livermore Laboratory

MECHANICAL CONTINUOUSLY-VARIABLE TRANSMISSION DESIGNS FOR FLYWHEEL ENERGY-STORAGE AUTOMOBILES

Norman H. Beachley and Andrew A. Frank
University of Wisconsin-Madison
1513 University Avenue
Madison, Wisconsin 53706

ABSTRACT

In order to further investigate the concept of an energy storage flywheel powerplant system, a second-generation experimental automobile is planned. The purpose of the vehicle will be to demonstrate the commercial potential of the concept, its performance and fuel-saving characteristics, and to serve as a test bed for further research and development of the basic concept. Three continuously-variable transmission concepts are being evaluated and compared to determine the best design to use in the experimental automobile. They are: 1) multi-speed gearbox with slipping clutch system; 2) hydrostatic power-split system; and 3) van Doorne steel V-belt system. The major transmission requirements are: 1) minimum energy losses under urban driving conditions; 2) low weight and a size envelope that allows compact packaging; and 3) the capability of having torque control, and automatic control of all other required functions. The three concepts being considered all appear attractive, and will be carried through to an assembly drawing stage with concurrent analysis before a final choice is made for the construction of the experimental model.

INTRODUCTION

The concept of flywheel energy storage appears very attractive for significantly improving the fuel economy of passenger car vehicles under urban driving conditions. Studies have shown that a 100% gain over current vehicles is clearly possible, and an experimental car based primarily on off-the-shelf components has experimentally demonstrated savings of about 50%.[1,2]

The basic configuration that we have been investigating is shown schematically in Fig. 1. Although some of the power from the engine will pass directly to the drive axle, one can best describe the concept by saying that the car is driven by the flywheel, and that the engine is run (at wide open throttle) to recharge the flywheel only when its speed drops below some predetermined value. The improvement in fuel economy comes from two factors: 1) the engine is run only under most efficient conditions or not at all, and 2) the system allows efficient regenerative braking.

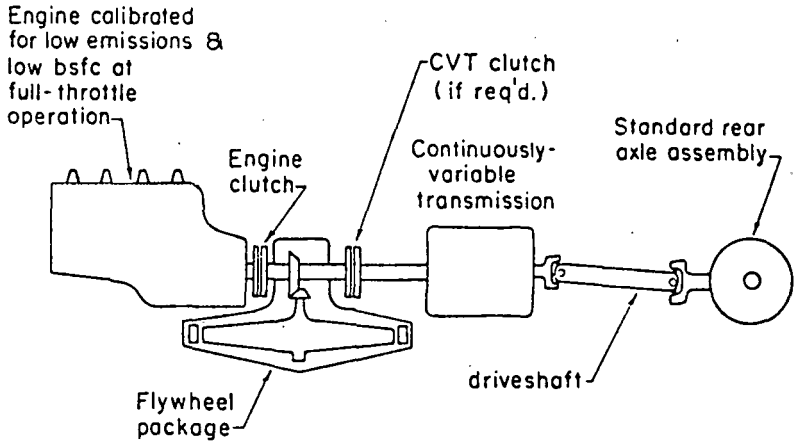

Fig. 1. Schematic diagram of a flywheel hybrid automobile.

In order to match the speed of the flywheel and that of the car under all conditions, a continuously-variable transmission (CVT) is required. Theoretical and experimental studies[1,2] have shown that, with current technology, the CVT is the most critical component of the system; i.e., the component most likely to have the highest energy loss over a typical driving cycle. Table 1 shows the approximate breakdown of the energy produced by the engine in the University of Wisconsin experimental flywheel Pinto when driven over the EPA-CVS Federal Urban Driving Cycle. The average CVT efficiency in this case has been calculated to be about 76%.

TABLE 1. Approximate Energy Breakdown for the University of Wisconsin First-Generation Flywheel Hybrid Automobile (EPA-CVS cycle, 2750 lb Test Weight).

Energy required from engine	10,126 hp-sec
Energy recovered in regenerative braking	1,278 hp-sec
Road load energy	3,392 hp-sec
Energy lost in non-regenerative braking	209 hp-sec
Energy lost in CVT	3,159 hp-sec
Energy lost in 4-speed gearbox	516 hp-sec
Energy lost in rear axle	516 hp-sec
Energy lost in clutches	1,280 hp-sec
Flywheel spin loss energy	686 hp-sec
Energy lost in flywheel gears	181 hp-sec
Energy lost to engine inertia	185 hp-sec

Corrected fuel consumption = 32 mpg.

Even though a CVT may have high efficiency at conditions close to its design point, its average efficiency will be much lower when operated over a typical driving cycle. Consider that a typical 3,000 lb car may need a CVT capable of transmitting about 100 hp to provide what most drivers would consider to be satisfactory performance. Over the EPA-CVS driving cycle, however, the average road load (average power required at the drive wheels of a car with regenerative braking)is about 2 3/4 hp with streamlining, tire characteristics, etc., that are typical of today's cars. The problem then is to develop a CVT that is capable of, say, 100 hp, but has very low losses in the 0 to 5 hp range. The efficiency at or near full power is much less significant since it can be used for only a few seconds at a time except in hilly terrain.

In analyzing and evaluating CVT's, we have found it advantageous to work with loss values rather than efficiencies. This is advantageous for several reasons. First of all, cars are often driven at or near a condition of zero torque (i.e., coasting), and the concept of efficiency is meaningless at zero power output. All transmissions have zero efficiency at zero power output, even though they may be dissipating widely differing amounts of friction power. The friction power, of course,decreases the fuel economy, and the required analysis is handled in this case by loss data. Friction data plotted on the basis of loss rather than efficiency also permit more accurate interpolation and extrapolation near values of low torque and/or low speed.

In order to further investigate the flywheel powerplant concept, a second-generation experimental vehicle is planned. In order to approach a true prototype vehicle, and thereby learn as much as possible about the concept that would apply to a production vehicle, the design specifications will be quite strict. First of all, the vehicle will have front wheel drive, since this reduces the chance of vehicle instability from regenerative braking and also maximizes the amount of regenerative braking that can be used. The total powerplant-drive train system should fit under the hood of a conventionally-proportioned automobile with no intrusion into the passenger volume. Control must be essentially automatic, so that driving the car is no different than driving a conventional automatic transmission car. The additional powerplant system components must add no more than 100 lb to the weight of the car. The efficiency of all system components must be high enough to demonstrate a high fuel efficiency under city driving conditions, with 45 mpg on gasoline over the EPA-CVS cycle being the approximate goal for a 3,000 lb inertia weight vehicle whose present city mileage is about 22 mpg.

Since there is no off-the-shelf CVT available that would allow the above requirements to be satisfied, it is necessary to design and build a CVT specifically for this project. Within the constraints of size, weight, efficiency, and the avoidance of major developmental problems in

the basic CVT itself, the following three concepts appear attractive:

1. A multi-speed gearbox (e.g., 12 speeds) with a slipping clutch to match the flywheel and vehicle speeds in between the discrete ratios. At higher speeds (above about 45 mph), the flywheel would be declutched, and the car driven by the engine through the gearbox alone.
2. A hydrostatic power-split transmission in series with a 4 or 5-speed gearbox. This is the system concept used in the present experimental flywheel vehicle.
3. A van Doorne steel V-belt system in combination with a two-speed gear change unit.

All of the above three concepts appear as if they would meet the CVT requirements, and it is difficult at this stage of the program to determine which is the most promising. We, therefore, plan to carry all three concepts along at least to the stage of a final assembly drawing. It is possible that prototype models suitable for testing the efficiency and control characteristics will be constructed for two, or even all three, based on an evaluation of the final designs and the cost of construction. More details of the three concepts and their current stage of analysis and design are given below.

SLIPPING CLUTCH DESIGNS

Figure 2 shows schematically the basic idea of the slipping clutch concept. In this figure a 5-speed gearbox is placed in series with a two-speed box with clutches to give 10 discrete gear ratios optimally spaced. One of the two clutches will be engaged at all times (unless the car is coasting or at rest) with the loading pressure set by the driver to give a particular clutch slippage torque which results in the desired vehicle drive torque.

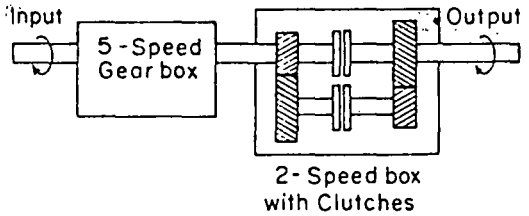

Fig. 2. Schematic diagram of a ten-speed gearbox with slipping clutch CVT.

At first glance, the slipping clutch concept may appear to be an undesirable type of CVT, since the clutch slippage is a pure loss. Its attractiveness lies in the fact that all of the required components other than the slipping clutch surfaces themselves should have very high efficiency (or, more specifically, low friction losses) under all operating conditions. If the clutch slip is kept to 15% maximum, then the basic clutch efficiency would be at least 85% and average about 92% over a driving cycle, regardless of the amount of torque being transmitted. If the other losses (gears, bearings, etc.) are minimal, the result is excellent CVT efficiency. In comparing this concept to the other CVT candidates, it should be remembered that in contrast to a slipping clutch, the friction losses inherent in the other CVT principles (e.g., traction drives and hydrostatic systems) are not proportional to the torque transmitted and constitute a higher percentage of the power transmitted at lower power levels.

One important consideration for slipping clutch designs is the frequency of shifting. An extreme condition would be hard acceleration, say from zero to fifty mph in 10 seconds through 10 speeds. This operation would require a gear shift every second on the average. A satisfactory system would need to automatically shift gears when required in a very short time increment, estimated to be about 1/10 of a second to give the impression of smooth, continuous acceleration with no apparent jerkiness. It appears that this requirement can be met with proper mechanical design. Another consideration is that, for a given combination of vehicle and flywheel speeds, a gear shift would be necessary to change from positive driving power to regenerative braking, since a slipping clutch can transmit torque only in the direction of slip. This should increase the shifting frequency only slightly, however, since the controls would be designed to provide regenerative braking only when the brake pedal was actually pushed. When the driver's foot was simply raised from the accelerator pedal, the car would be allowed to coast, i.e., the clutch would be disengaged.

In developing detailed designs, other important requirements are: 1) a clutch that is

"disengaged" must have no significant drag, 2) the drive train must have no friction loss when the car is at rest (e.g., stopped for a traffic signal), 3) gear and bearing friction must be minimized.

Although the slipping clutch system of Fig. 2 could be implemented satisfactorily, there are other designs that appear to be more attractive. Figure 3 illustrates one of the designs that is currently being pursued, a twelve speed version in this case. Although Fig. 3 is a scale drawing, it is at an early stage of development, with all mechanical details not yet resolved. The two side shafts appear in the side view as if they were 180° apart for clarity of detail. In actuality they are to be positioned as shown in the end view to provide a more compact package.

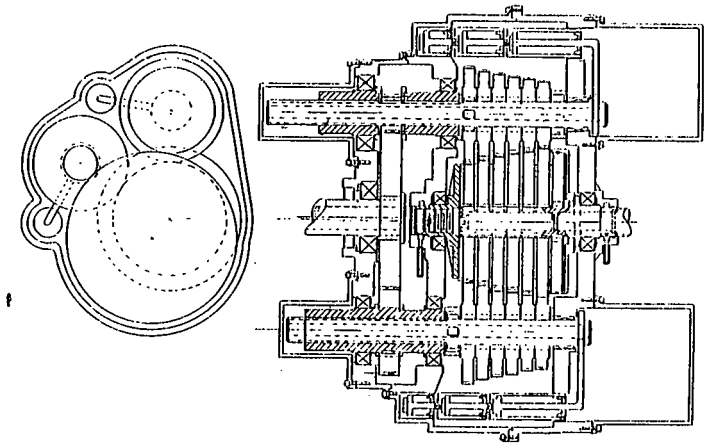

Fig. 3 A twelve-speed slipping clutch CVT with hydraulic clutch actuation and a binary digital piston shifting mechanism.

The center group of six gears has a clutch friction element between each two adjacent gears, and at the outer surfaces of the two end gears. The clutches are loaded by a hydraulic piston at the right. The gears are free to rotate on the center shaft except as restricted by the clutches. The two side shafts each have six gears that are in constant mesh with the gears of the center shaft. The side shafts are moved by sets of digital hydraulic pistons. The short splined section on each of these will thereby lock one gear at a time to its shaft, setting a transmission speed ratio. One or more of the clutch elements will slip to properly match the transmission input and output speeds (i.e., the flywheel and vehicle speeds). When gears are being shifted, the loading of the clutch elements is reduced to zero, and then quickly reset at the required control value as soon as the shift is completed.

Figure 3 as drawn shows the transmission in first (low) gear with the gear on the top left engaged by the splined shaft. Second gear would find the second gear from the left engaged, and so on, up through the first six speeds. For seventh gear the top spline would be moved to the right beyond its stack of gears, and the bottom spline moved to engage the first gear on the left. Note that the two side shafts are both geared to the output shaft.

The first advantage of this particular concept is that it doesn't matter which or how many clutch elements slip; therefore, there can be no detrimental clutch drag. Shifting can be done quickly by a small shaft movement. When shifting occurs, the speed difference between the external and internal splines will be only about 15% so that no further "synchromesh" system is required. One disadvantage of the design is that there are 12 gear pairs in constant mesh, with resulting losses, but it is felt that these should be minimal.

Figure 4 is a variation of the above design. Here, the shifts alternate between the two side shafts, so that the upcoming gear can be "preselected". The two clutches are engaged (and slipped at the desired torque level) alternately. There should be virtually no dead time during a gear change with this design since the engagement and disengagement of the two clutches will occur simultaneously.

Other variations of the above design concepts are under investigation.

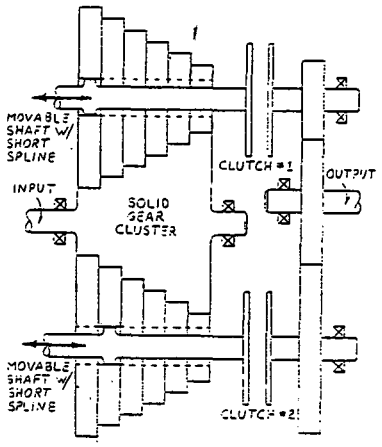

Fig. 4. Schematic diagram of a twelve-speed slipping clutch CVT with a gear preselection feature.

HYDROSTATIC POWER-SPLIT DESIGNS

The basic principle of the hydrostatic power-split CVT is illustrated in Fig. 5. Only part of the power passes through the hydrostatic transmission itself (the hydrostatic pump and motor, one or both with variable displacement), the rest passing through a more efficient direct mechanical path. The two components of power are then added by the gear differential. The overall CVT has higher efficiency but less ratio range than a straight hydrostatic CVT. Figure 5 also shows a gearbox in series with the power-split CVT. This extends the ratio range of the overall system, permitting even smaller hydrostatic units to be used, decreasing size and weight requirements and improving overall efficiency.

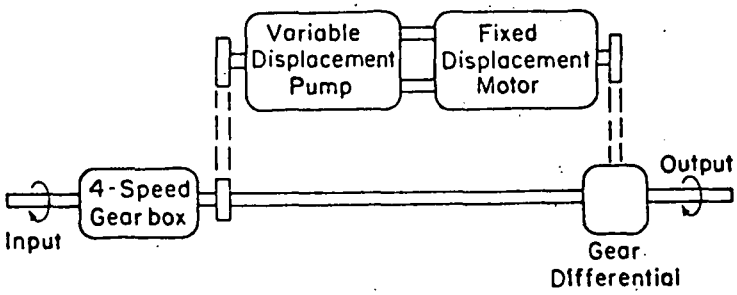

Fig. 5. Schematic diagram of a hydrostatic power-split transmission.

The hydrostatic power-split transmission designed and built for the first generation experimental flywheel car[3] has shown the practicality of this concept, even though its efficiency is much too poor to demonstrate truly significant fuel savings. The main problem with that particular transmission was that it had to be built primarily from off-the-shelf components, which limited the efficiency possible, restricted the use of design optimization, and also resulted in a large and heavy unit. The design did demonstrate the ruggedness, smooth operation, and ease of control possible with hydrostatics, however.

Figure 6 shows the basic hydrostatic power-split design currently under investigation. The radial ball piston concept is used for the pump and motor, both having variable displacement for maximum versatility. The gear differential is the planetary unit at the right of the figure. A 4- or 5-speed gearbox with optimized ratios is to be put in series with the unit. The design is very similar to that developed by General Electric Corporation[4,5] for use in trucks and tracked vehicles.

The main advantages of the design (Fig. 6) are small size and light weight. Another potential advantage is that radial ball piston hydrostatic units apparently have low spin losses under zero or low power conditions even though their full load efficiency may be no greater than other designs. Unfortunately, we have so far been unable to obtain actual experimental data to

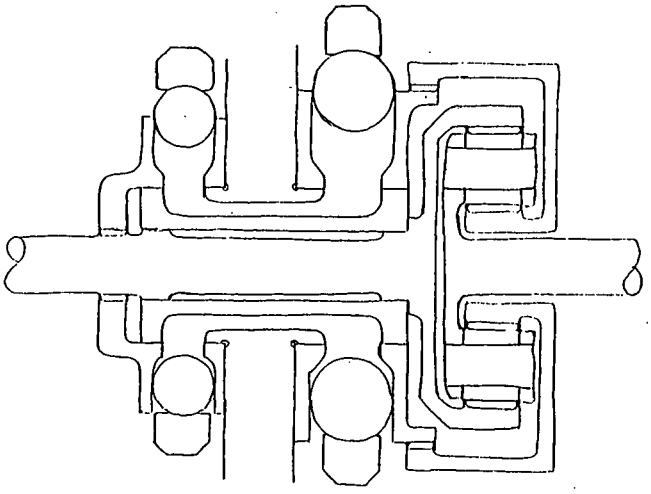

Fig. 6. Sketch of a hydrostatic power-split CVT with radial ball piston pump and motor and a planetary gear differential.

confirm these characteristics. Simulations based on reasonable assumptions have shown that this design should provide satisfactory efficiency for a flywheel car if used in series with a 4- or 5-speed gearbox whose ratios have been optimized.

Experience with the first generation flywheel vehicle has shown the control of this type of transmission to be quite straightforward. To obtain direct control of the output torque (and therefore, the acceleration or deceleration of the vehicle), it is necessary only to control the hydrostatic pressure.* This can be accomplished by a pressure control valve with feedback in which pressure is directly proportional to the position of a control lever.[3] This lever can be connected by a direct mechanical linkage to the accelerator and brake pedals.

In order to more fully investigate the potential of this design, and to carry out parameter optimization studies, it will be necessary to obtain experimental loss data over the full range of operation for the radial ball piston units. If the packaging details look attractive after the design work is completed, such experimental studies may be done. Since the balls and outer ring of a ball piston unit could be taken from a standard ball bearing, construction of a model for experimental studies would be a reasonable task.

BELT DRIVE SYSTEMS

Variable V-belt drives have been demonstrated to have power transmission capabilities that are adequate for small cars. Snowmobiles, for example, use this type of CVT, with racing versions often transmitting well over 100 hp. The life of the rubber belts is not great under such continued high power conditions, however, The DAF automobile, built in the Netherlands (with the company recently purchased by Volvo) has for many years used a rubber V-belt CVT for its transmission, for engines with power ratings up to about 45 hp (higher in racing versions).

A new development is a steel segmented V-belt system with variable sheaves (the "TRANSMATIC") that has been developed by van Doorne's Transmissie B.V. of the Netherlands.[6,7] Figure 7, from Borg-Warner literature, shows the basic design features. The efficiency characteristics of this unit are quite good, and the allowable ratio range is 4:1 or slightly higher. In order to properly handle the range requirements of a flywheel car, a two-speed gearbox in series with the steel V-belt system (or something equivalent) is required.

The basic unit (sheaves and belt) is quite compact. It is currently being developed for use in otherwise conventional cars by Volvo, Fiat and Borg-Warner. They expect to begin making cars with the van Doorne CVT within a couple of years. The controls required for a conventional car are quite different from those needed for a flywheel car, however.

*This is strictly true only if the displacement of the hydraulic motor is fixed. If not, torque is proportional to the product of pressure and motor displacement.

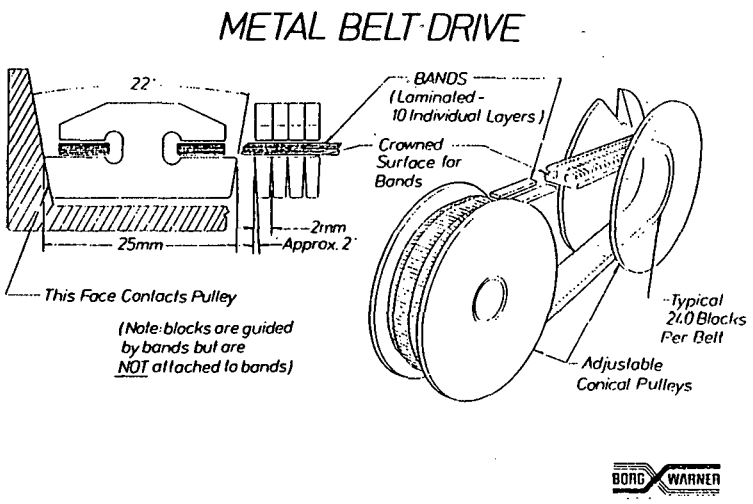

Fig. 7. Details of the van Doorne metal V-belt CVT.

Designs based on this steel V-belt are currently being developed by us for the flywheel car application. Since the basic belt and sheave system is apparently well developed, our work lies primarily in designing the two-speed gearing system, the overall packaging, and the control system.

There are two control aspects to be taken care of: 1) the loading ("squeeze") on the belt from the sheaves must be proportional to the torque being transmitted and inversely proportional to the effective sheave diameter in order to keep spin losses low under conditions of zero or low power transmission; 2) the rate-of-change of the sheave diameters must be controllable since it is the parameter that sets the vehicle driving torque. Present design concepts are based on hydraulic loading of both sheaves, and logic systems will be necessary to set the absolute loading of each sheave for all possible operating conditions. It has been tentatively decided to run the engine continuously and bypass the flywheel under conditions of high speed cruise, but with the power still passing through the van Doorne steel V-belt so that the engine operating conditions can be optimized for this relatively steady-state condition of higher power.

A van Doorne V-belt and sheave system is being procured to allow testing of efficiencies and to provide a "breadboard" model for development of the control system. Many of the control system parameters will need to be determined by a combination of theoretical and experimental work.

OTHER CVT POSSIBILITIES

There are many other continuously-variable transmission concepts that look attractive, especially those in the rolling-contact traction drive category. Unfortunately, there are virtually no such transmissions available as prototype units that could be readily used in the second-generation experimental vehicle. Experimental units could be built for us by a number of companies that are developing such units. However, the cost would in general be quite high and there would be a high likelihood of significant developmental problems in the traction drive unit itself that would impede progress on the overall second-generation flywheel car. We feel that rolling contact traction drive development should be handled separately from this project, even though such CVT's could ultimately prove to be best for flywheel cars.

SUMMARY AND CONCLUSIONS

Three basic CVT concepts have been identified as potentially satisfying the stringent requirements of an i.c. engine-flywheel energy storage automobile. Designs are currently being developed for all three. Ultimately, a choice will need to be made as to which design will be best to use in a second generation experimental flywheel car. In addition to a comparison of the mechanical configurations developed, some experimental studies to determine loss characteristics will be performed, and simulations made to determine net energy losses of the different designs over standard driving cycles.

Since all three concepts appear attractive, and since there are many factors to consider in

the final selection, it is difficult at this time to predict which CVT will be used. There is a strong possibility that engineering models of two and possibly all three will be built and tested to help in the evaluation, depending upon how much this would cost. An attempt will be made to design the overall system packaging so that more than one CVT design could be used in the vehicle with a minimum of other system changes. Ideally, in terms of the overall development program, the CVT packages should be completely interchangeable.

ACKNOWLEDGMENTS

Figure 3 was developed by Michael Nohr, and Fig. 6 by Hans Noeldner, both Research Assistants assigned to this project.

REFERENCES

1. N.H. Beachley and A.A. Frank, "Flywheel Energy Management Systems for Improving the Fuel Economy of Motor Vehicles", Report No. DOT/RSPA/DPB-50/79/1, prepared for U.S. Dept. of Transportation, December, 1978.

2. A.A. Frank and N.H. Beachley, "Evaluation of the Flywheel Drive Concept for Passenger Vehicles", SAE Paper 790049, 1979.

3. N.H. Beachley and A.A. Frank, "Final Report-Increased Fuel Economy in Transportation Systems by Use of Energy Management-Third Year's Program," Report DOT-TST-77-21, prepared for U.S. Dept. of Transportation, Dec. 1976.

4. D.M. Latson, et al., "A Hydromechanical Transmission Development", SAE Paper 670932, 1967.

5. D.M. Latson, et al., "Hydromechanical Transmission Fares Well in Truck Tests", SAE Journal, Vol. 76, No. 6, June 1968, pp. 64-66.

6. Olaf Fersen, "Transmatic", Autocar, 17 February, 1979, pp. 42-43.

7. S.C. van der Veen, "Stufenloser Drehmoment/Drehzahlwandler Transmatic", Ant-Antriebstechnik-16 (1977) Nr. 4, pp. 217-222.

THIS PAGE

WAS INTENTIONALLY

LEFT BLANK

PROJECT SUMMARY

Project Title:	"Vehicular Applications of Mechanical Energy Storage--FY79"
Principal Investigator:	William T. Crothers
Organization:	Lawrence Livermore Laboratory Mail Stop L-209 P.O. Box 808 Livermore, CA 94550 (415) 422-8200
Project Goals:	The goals of this project are to develop and evaluate mechanical-energy storage technology for application to electric, hybrid, and heat-engine vehicles and to maximize the commercial potential of the technology.
Project Status:	Four studies were completed in FY79. Performance improvement related to mechanical-energy storage was the subject of two reports. Continuously variable transmission design was discussed in a third. Elastomeric braking was evaluated in a fourth. Two flywheel/electric systems were fabricated and partially tested. An elastomer-braking system design was initiated. Criteria for a vehicle powered by a flywheel/heat engine were formulated.
Contract Number:	W-7405-ENG-48
Contract Period:	FY1979
Funding Level:	$845,000 EHV Prog. (FY1979); $476,000 Ener. Stor. Prog. (FY1980 B/O)
Funding Source:	U.S. Department of Energy

VEHICULAR APPLICATIONS OF MECHANICAL ENERGY STORAGE--FY79

William T. Crothers
Lawrence Livermore Laboratory
P.O. Box 808, L-209
Livermore, CA 94550

ABSTRACT

The Department of Energy, Division of Energy Storage Systems, has designated the Lawrence Livermore Laboratory (LLL) as the technical manager arm for conducting research in the area of mechanical energy storage. This paper describes developments regarding vehicular applications of that management effort. A five-year project plan, with supporting rationale, is presented.

INTRODUCTION

This paper describes the technical management of vehicular-related, mechanical-energy storage projects at the Lawrence Livermore Laboratory. This year's technical progress will be detailed in other papers at this 1979 MES Review meeting. Additional information can be obtained from the reports listed in the bibliography. Because the management task includes planning, emphasis is placed on future work as it relates to completed and ongoing investigations. Therefore, an overview on how the program goals are to be attained is included.

BACKGROUND

Two sources of funds have supported this work for FY79 (1). The early funding originated under the Electric and Hybrid Vehicle Act. A second more recent source, is through the Division of Energy Storage Systems. This funding has increased the scope of the projects considered with the result that studies of storage applications to vehicles now include heat-engine propulsion as well as electric-driven types.

HIGHLIGHTS OF FY1979

A list of the subcontracts which have been active this year are:

Project	Subcontractor	Status (Ref. No.)
Analysis of Flywheel Energy Storage for Automotive Use	R. F. McAlevy III & Associates	Report published, UCRL-13980 (2)
Energy Storage Assessment Related to E&HV	Lawrence Livermore Laboratory M. W. Schwartz	Report published, UCRL-52773 (2 volumes) (3)
Continuously Variable Transmissions	N. Beachley and A. Frank	Report published, UCRL-15037 (4)
Elastomeric Regenerative Braking Study	Eaton	Report published, UCRL-15044-1 (5)
Elastomeric Braking, Design and Hardware	Eaton	Subcontract initiated 6/28/79
Energy Storage System for EV's	General Electric	Nearing completion
Energy Storage Unit for EV's	Garrett AiResearch	Hardware in test
Heat Engine/Flywheel Vehicle Analysis	University of Wisconsin	Design phase one-half complete
Inertia Weld Development for Flywheels	General Electric	Report published, UCRL-15045 (6)

RESULTS TO DATE

The primary accomplishments of the projects are as follows:

- Energy-storage devices are technically feasible for urban driving conditions.
- Electric vehicles with present and forecast battery capabilities cannot in this century meet the performance standards now needed for city and freeway driving patterns. Energy-storage systems can overcome this disadvantage.
- Flywheel storage with electric drive is at the prototype stage of development--250 W•h capacity, 30 kW power attainable in an 80 lb (36 kg) unit.
- Heat engine/flywheel systems are technically feasible. The transmission needed to couple engine, flywheel, and drive train into a functioning unit is the key to a successful demonstration.
- Elastomers have low specific energy storage capabilities. Relatively simple hardware designs are possible, however, which may make the elastomer an attractive candidate for vehicular use.

ELECTRIC VEHICLE DEVELOPMENTS

Electric vehicles now on the market, and those now being proposed as near-term substitutes for petroleum-fueled vehicles, cannot accelerate adequately in city and freeway traffic to meet the present performance capabilities of vehicles powered by the internal-combustion engine. The implications of this fact to future electric vehicle sales has been and is the subject of much debate. A more tangible and explorable factor is the possible increased petroleum consumption as a result of heavy traffic conditions where vehicles of varied performance capabilities are mixed. Results obtained by using a computer code by Collins and Epps (7), which closely simulates traffic flow on multi-lane freeways, show vehicle-flow interruptions that were directly caused by slow-accelerating vehicles such as tractor-trailer rigs. The increased fuel consumption was obvious and calculable. Three solutions could avoid this problem:

a. Segregate vehicles of greatly differing performance capabilities by street and freeway restrictions.

b. Reduce the high performance of internal combustion engine (ICE) light vehicles (passenger cars). This is a strong possibility as economy can be improved and emissions lowered.

c. Improve the performance of the slow vehicles.

If more uniform performance in the vehicle fleet conserves fuel, mechanical-energy storage systems could prove the equalizer. Our project goal is to demonstrate the usefulness of mechanical energy storage (MES) for this purpose as well as to demonstrate the range extension gained from regenerative braking and load leveling. During the next few years, development will concentrate on the flywheel and electric-input/output energy transfer.

Units now under test appear to offer storage capacities of about 3 to 5 W•h/lb, which is a lower specific energy than today's batteries. The power rating at 30 kW (375-W/lb), however, makes them interesting possibilities. A second generation unit may need to be initiated (Fig. 1). Control systems for such devices are now under development and must be perfected to offer a small, lightweight, economical mate to the energy storage unit (ESU). It is anticipated that these two tasks will allow initial vehicle modifications to begin early in FY81. This vehicle should be in operation in 18 months (mid FY82), and a second-generation follow-on would repeat the process with an updated design during FY82-84.

If funds are available, research will also be directed toward electric-input/output machines with higher efficiencies. Results in this area can be utilized in the proposed vehicles and in a next generation of the Urban Mass Transit Authority (UMTA) bus program now sponsored by the Department of Transportation.

HEAT-ENGINE VEHICLE DEVELOPMENTS

Fuel economy in automobiles has been improving over the past few years. Mandated CAFE (Corporate Average Fuel Economy) standards are to advance from 19 mpg in 1979 to 27.5 mpg in 1985. Volkswagen has already demonstrated a 60 mpg, composite, driving-cycle average with a modified Rabbit. How far these economy feats can be carried with new technology is not clear. Most improvements increase the vehicle cost, a fact which becomes more palatable with rapidly increasing fuel prices. Again mechanical-energy storage can play an important role. Providing the performance of these future automobiles is not degraded, the anticipated minimum improvement of 50% (urban EPA cycle) in mpg because of a flywheel storage system should apply proportionally even to the higher CAFE figures and future anticipated improvements.

Figure 2 shows the intended array of tasks planned to have the first ICE/MES prototype operating by FY82. These tasks define the design and construction of the transmission, flywheel package, engine, and chassis. These components are identified separately and responsibility for their construction will rest with those industrial firms experienced in these fields. The staff of the University of Wisconsin will continue to share the responsibilities with LLL throughout the project.

The key to this project's success lies in the ability to build a transmission. Possible designs and sources have been investigated, research under government and private sponsorship is underway, and cautious optimism has been expressed by those involved. Past attempts at producing a continuously variable design have, at best, been only partially successful. The major difference today is the need. Flywheels must have the flexibility. Prior vehicle design using the internal combustion engine viewed such broad transmission requirements as a nicety. Major emphasis will be placed on the transmission development, and the FY81 vehicle construction relies on a first-generation transmission being built and tested successfully during FY80-81.

A possible addition to the heat engine work is a thorough investigation of gas turbines. Gas turbines for automobiles remain elusive because of high-temperature-material problems. Gas turbines also tend to have above normal brake-specific fuel consumption at low loads. Load-leveling energy-storage flywheels, also operating at high speeds, may be very compatible with the turbine machinery. The present design group will review all types of heat engines. A favorable decision on turbines could involve much more time and funding to reach a demonstration stage than would be the case with a piston engine design. In the event the turbine is a desirable alternate, work will continue with the less exotic engines. Then, depending on fund availability, a second- or third-generation demonstration vehicle would feature the turbine design.

REGENERATIVE BRAKING

Regenerative systems using elastomers are discussed separately as the hardware can be applied to electric or heat engine vehicles driven in urban environments. Results of the first study indicate the energy can be stored efficiently by twisting a cylindrically shaped elastomer. This characteristic implies simple design hardware to transfer energy to and from the rotating drive line of the vehicle. Testing of a full vehicle-sized elastomer will occur in the next few months. Reduced-size versions have elastomeric efficiencies (energy in and out or round trip) of 90%. Similarly encouraging results of the full-size model can lead to several new designs. Vehicle prototypes can be expected in FY81. Figure 3 shows the individual project tasks that must be addressed and the anticipated schedule.

REFERENCES

1. T. M. Barlow, W. T. Crothers, S. V. Kulkarni, and J. A. Rinde, "Mechanical Energy Storage Technology Project: Annual Report 1978," Lawrence Livermore Laboratory, Livermore, Calif., UCRL-50056-78 (1979).

2. Robert F. McAlevy, III, "A Logical Basis for Evaluating the Impact of Flywheel-Transmissions on Automotive Vehicle Performance," Lawrence Livermore Laboratory, Livermore, Calif., UCRL-52758 (1979).

3. Martin W. Schwartz, "Assessment of the Applicability of Mechanical Energy Storage Devices to Electric and Hybrid Vehicles:" Vols. 1 and 2, Lawrence Livermore Laboratory, Livermore, Calif., UCRL-52773 (1979).

4. Norman H. Beachley and Andrew A. Frank, "Continuously-Variable Transmissions, Theory and Practice," Lawrence Livermore Laboratory, Livermore, Calif., UCRL-15037 (1979).

5. L. O. Hoppie, F. S. Chao, I. Kalns, F. G. Mossey-Shaw, D. Speranza, and D. M. Trela, "The Feasibility of an Elastomeric Regenerative Braking System for Automotive Applications," Phase I Final Report, Eaton, Lawrence Livermore Laboratory, Livermore, Calif., UCRL-15044-1 (1979).

6. E. Lustenader and D. Kerr, "Application of Inertia Welding Technology to Steel Disc-Type Flywheels," General Electric, Lawrence Livermore Laboratory, Livermore, Calif., UCRL-15045 (1979).

7. Private Communication with Richard Epps, Lawrence Livermore Laboratory, July 16, 1979.

This work was performed under the auspices of the U.S. Department of Energy by Lawrence Livermore Laboratory under contract No. W-7405-Eng-48. Reference to a company or product name does not imply approval or recommendation of the product by the University of California or the U.S. Department of Energy to the exclusion of others that may be suitable.

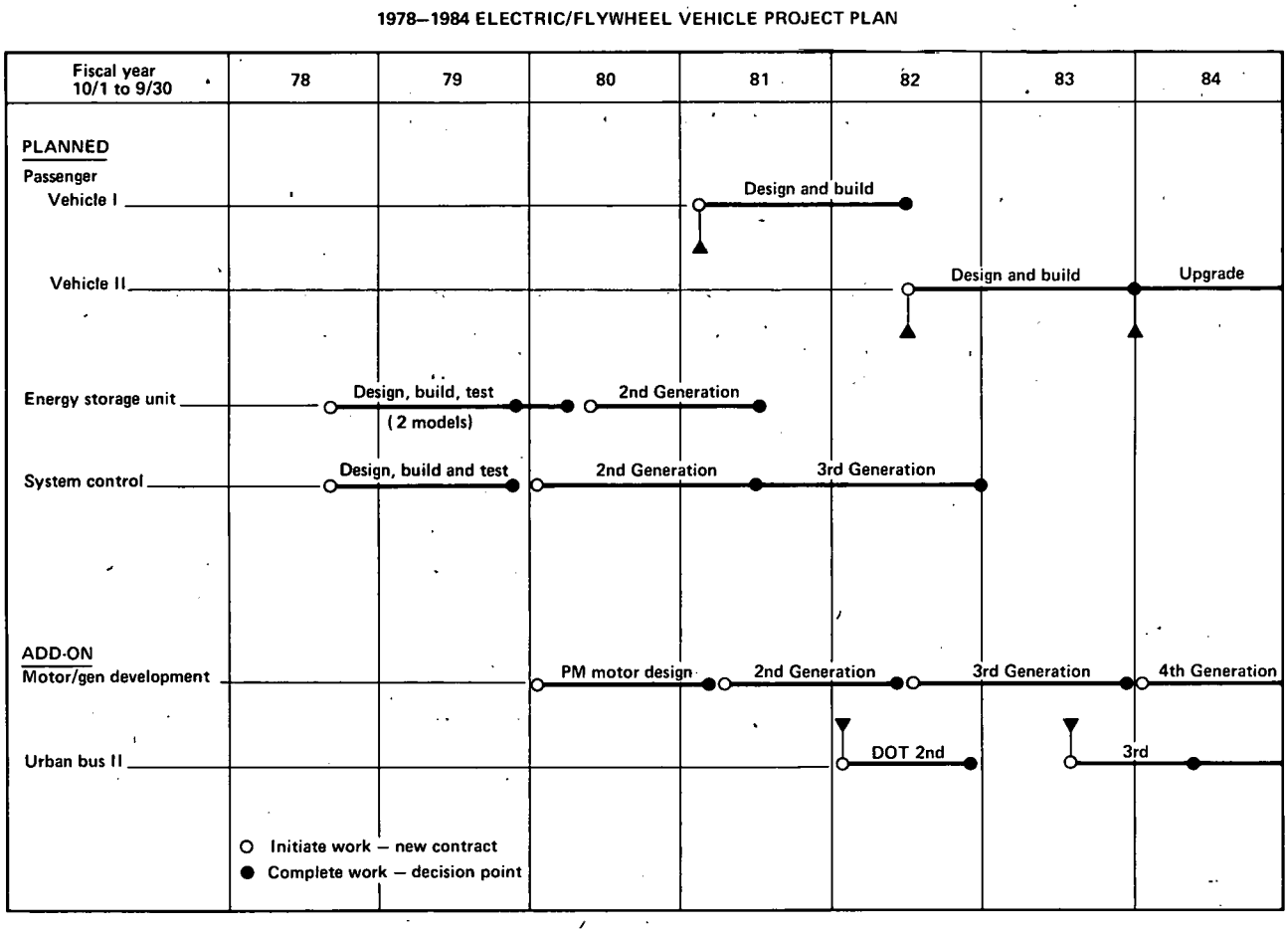

FIG. 1. 1978-1984 Electric/Flywheel Vehicle Project Plan.

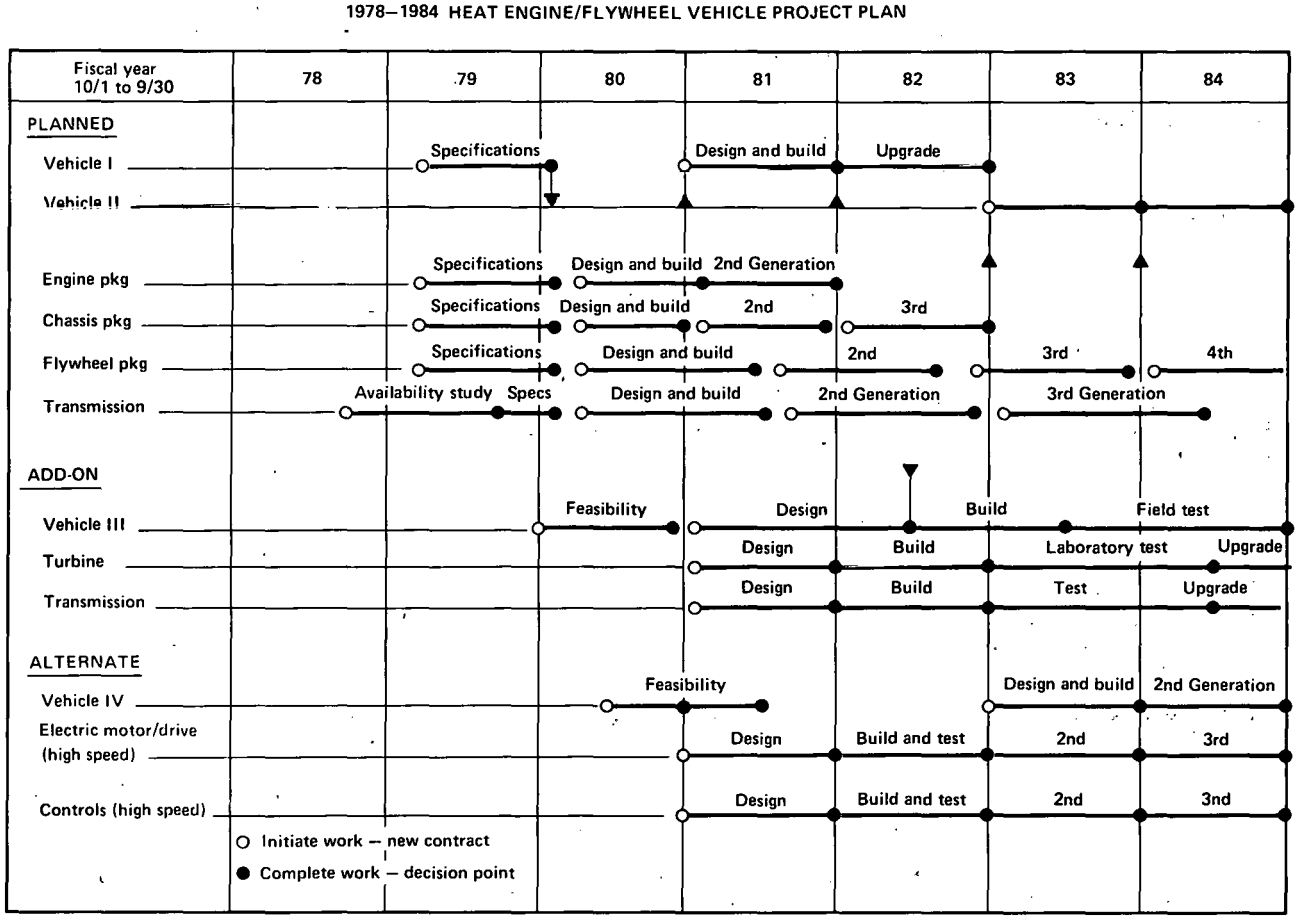

FIG. 2. 1978-1984 Heat Engine/Flywheel Vehicle Project Plan.

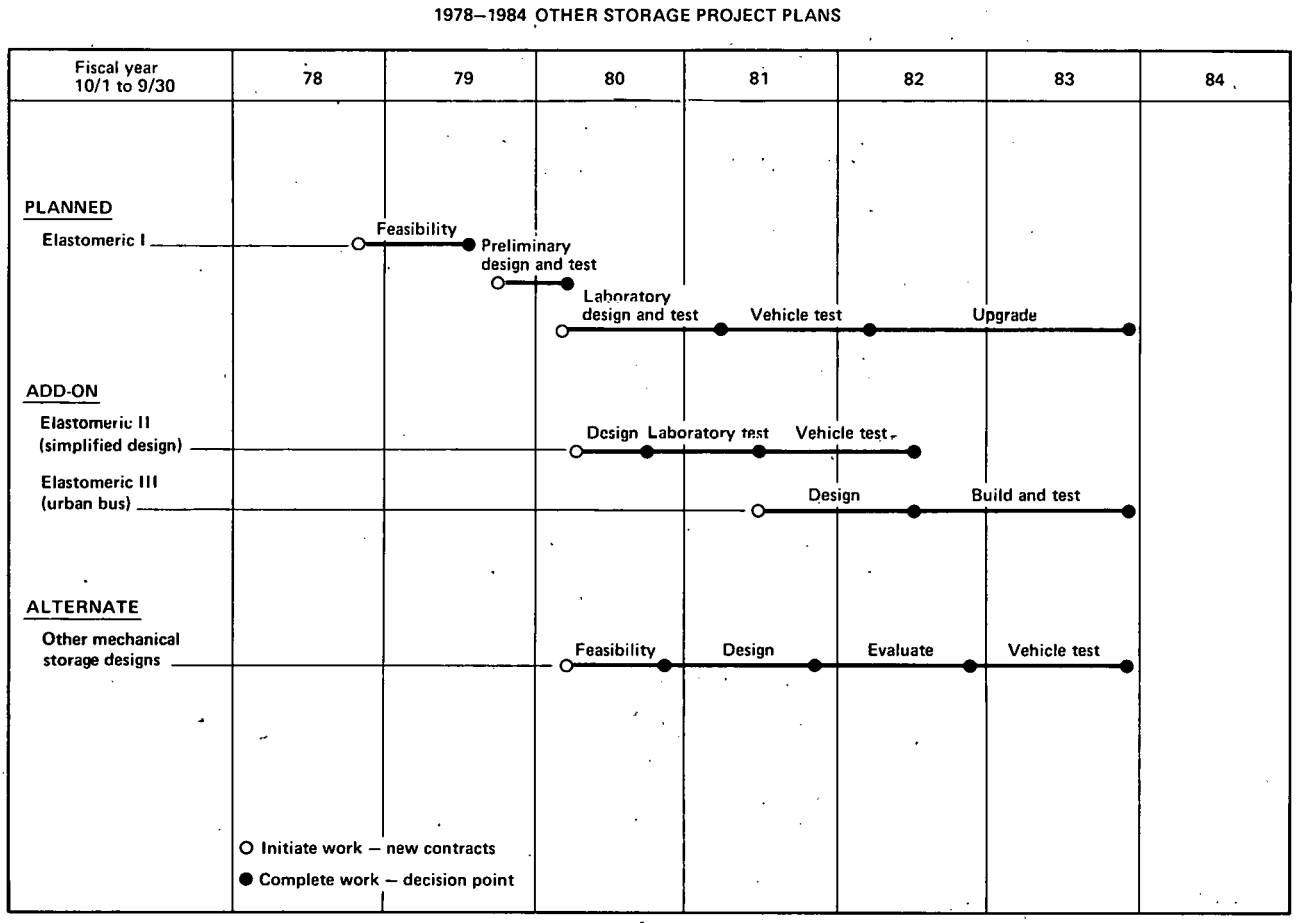

FIG. 3. 1978-1984 Other Storage Project Plans.

PROJECT SUMMARY

Project Title:	Regenerative Braking Through Elastomeric Energy Storage
Principal Investigator:	Lyle O. Hoppie
Organization:	Eaton Corporation Engineering & Research Center P.O. Box 766 26201 Northwestern Highway Southfield, Michigan 48037
Project Goals:	Determine the technical and economical feasibility of an elastomeric regenerative braking system (ERBS) for automotive applications.
Project Status:	During Phase I (Sept. '78 - March '79) theoretical and experimental efforts were focused on: • determining which commercially available elastomer is best suited to this application. • determining which method of stressing an elastomer is best suited to this application. • conceiving and comparing several methods of controlling torque. • predicting the range improvement which would result if a system based on a preliminary design were constructed. • determining the maximum initial cost such a system could have, yet still be cost effective. The Phase I results were felt encouraging enough by both Eaton Corporation and Lawrence Livermore Laboratory to proceed with Phase IIA, during which full-scale elastomeric subassemblies will be designed, constructed, tested and evaluated. If the results of this effort continue to be encouraging, Phase IIB will be initiated without interruption; in Phase IIB, a complete full-scale ERBS will be laboratory tested and evaluated.
Contract Number:	University of California Purchase Order 2617509
Contract Period:	July '79 - Feb. '80 for Phase IIA
Funding Level:	$172,000 for Phase IIA
Funding Source:	Lawrence Livermore Laboratory

REGENERATIVE BRAKING THROUGH ELASTOMERIC ENERGY STORAGE

L. O. Hoppie
Eaton Corporation
Engineering & Research Center
P. O. Box 766
26201 Northwestern Highway
Southfield, Michigan 48037

ABSTRACT

A theoretical and experimental investigation into the use of elastomers as the energy storage element of a regenerative braking system for urban vehicles was carried out. This work culminated in the preliminary design of a complete full-scale system, the prediction of its performance and efficiency, the specification of its control system with the required actuators and sensors, and an analysis of its possible failure modes. The results of this work indicate that such a system could be constructed from materials and components requiring neither new technology nor major development, but significant engineering problems need to be carefully addressed. Incorporation of the system would result in a savings of prime energy required at the drive line of at least 18 percent for the EPA Urban Driving Cycle, and would be cost effective if it can be manufactured and sold at less than about 12 percent of the selling price of the vehicle for which it is intended.

INTRODUCTION

The dramatic increase in petroleum based fuel prices over the past few years has given rise to various research and development efforts in the area of energy conservation. An example of such efforts is that aimed at regenerative braking systems for land vehicles. With such a system, vehicular kinetic energy would be converted to another form and stored as the vehicle stops; the stored energy would subsequently be converted back into vehicular kinetic energy when the vehicle next accelerates. Since some of the energy normally dissipated as heat in the vehicle's brakes would thus be used to help accelerate the vehicle, the amount of prime energy required to propel the vehicle would have been reduced.

The prime energy so conserved when such a system is used clearly depends on the driving cycle and the efficiency of the system. For example, an over-the-highway truck, which typically travels on the order of one hundred miles between stops, would show little or no energy savings even if the regenerative braking system had an efficiency of unity. On the other hand, urban driving typically includes one or more stops per mile and the energy savings could be quite significant. Figure 1 shows two portions of the EPA Urban Driving Cycle, and an accounting of the energy required at the driveline to propel a typical automobile over these two cycles is shown in Fig. 2. Notice that when the freeway portion is included, 34.3 percent of the energy supplied to the driveline is ultimately dissipated in the brakes, whereas 42.5 percent is dissipated in the brakes when the freeway portion is excluded. Thus, if an ideal regenerative braking system were available, the range per unit of prime energy as measured at the driveline could theoretically be increased by 1.52 and 1.74, respective, over the corresponding value of the standard vehicle for these two driving cycles. Obviously, if a driving cycle is such that there are more stops per mile, even higher improvements would be possible. Consequently, applications such as city buses, delivery vans, subways, etc. are particularly attractive applications of regenerative braking systems.

There are two essential features which a regenerative braking system must have in order that the prime energy saved (over a specified lifetime) does offset the initial cost, size and weight penalties of the system:

- The energy storage unit itself must be compact and capable of handling high power levels efficiently.
- Any auxiliary equipment required to convert vehicular kinetic energy into a form suitable for storage and vice-versa must be efficient, compact, and of reasonable cost.

As discussed in what follows, a regenerative braking system based on elastomeric energy storage promises to be capable of demonstrating both of these features.

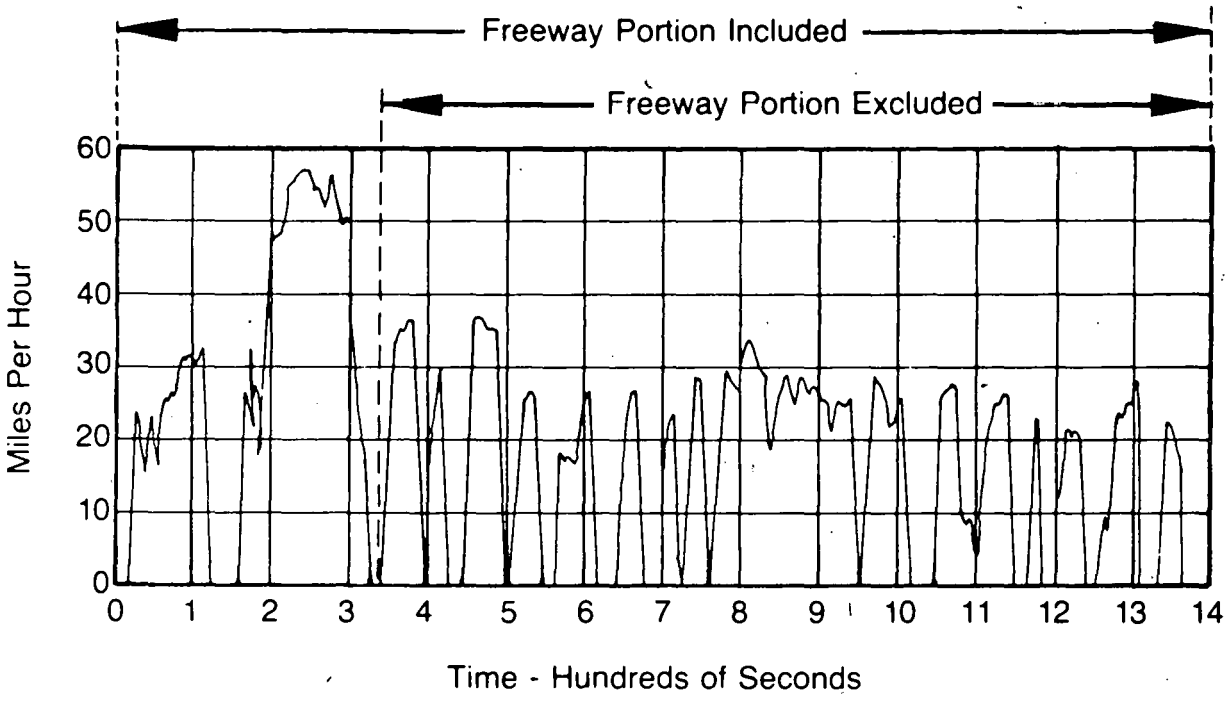

Fig. 1. Portions of the EPA Urban Driving Cycle

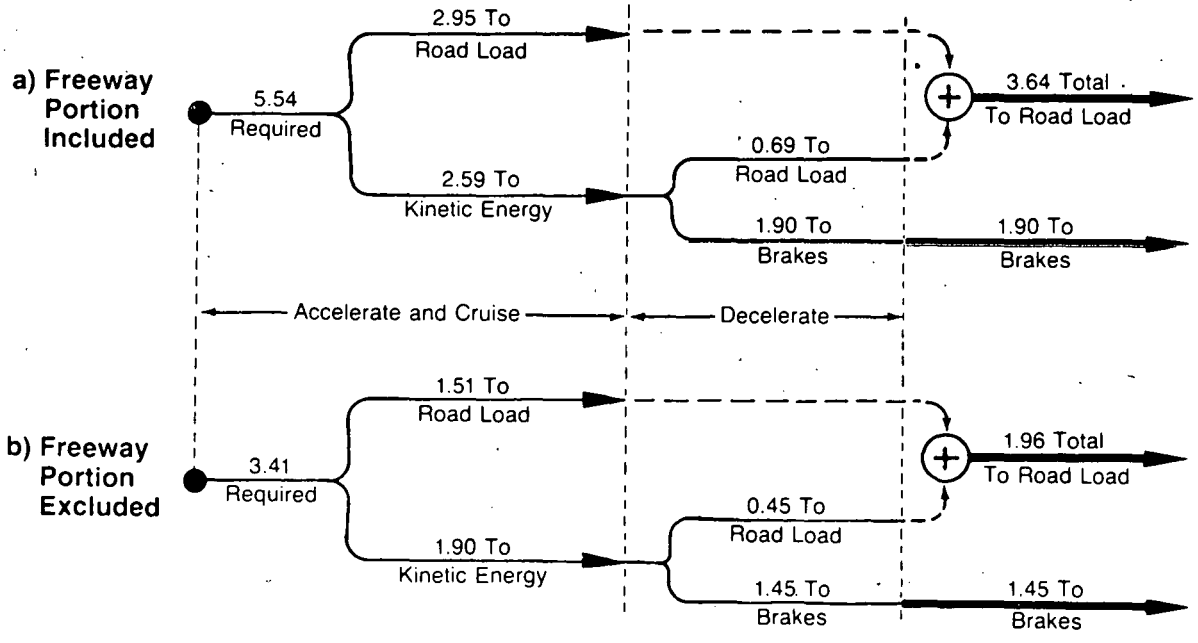

Fig. 2. Accounting of Energy (M Joules) Required to Propel a Vehicle Over the Two Cycles of Fig. 1.
Vehicle Mass: 1400 kg
Drag Coefficients: C_1 = .12 N/kg
C_2 = .001 N·sec/kg·m
C_3 = .53 N·sec^2/m^2

ELASTOMERIC REGENERATIVE BRAKING SYSTEMS

Perhaps the single most important aspect of an elastomeric energy storage system for vehicular applications is its inherent simplicity. The elastomer and vehicle form a "spring-mass" combination which will naturally oscillate; consequently, they can exchange energy quite efficiently with absolutely no control. Thus, to decelerate a vehicle and simultaneously convert its kinetic energy into stored potential energy, one need only connect the axle or driveline of the vehicle to an elastomer such that the vehicle motion stresses the elastomer: this can be done with a simple clutch. Other energy storage systems for vehicular applications require more complex energy transfer equipment. In particular, if the energy storage methods mentioned below are to have system efficiencies high enough to make them attractive, the systems must include the following energy conversion and/or energy transfer equipment:

- flywheel system - continuously variable transmission with a wide speed range
- battery system - electrical machine and electrical power conversion equipment
- compressed gas system - hydraulic pump/motor
- pumped liquid system - hydraulic pump/motor
- magnetic system - electrical machine

Furthermore, the deceleration and acceleration characteristics of a basic elastomeric system (consisting of an elastomer and nothing more complicated than a clutch) are quite similar to actual stop-start driving characteristics. The basic system would thus be nearly ideal for vehicles which exhibit a repetitious stop-start velocity profile, such as subways, people-movers, certain city buses and delivery vans, etc.

Unfortunately, the basic system would need to be modified for use on an automobile to be operated in an urban environment since in this application, there is considerable variation in successive stop-start cycles, primarily due to traffic congestion. The challenge, then, is to modify the basic system as little as possible in order to provide variation in the acceleration-velocity characteristics while simultaneously keeping the system efficiency high. The description and a comparison of the various torque control schemes which have been considered for this application are presented elsewhere.[1]

COMPARISON OF ELASTOMERS

As shown in Table 1, the synthetics polybutadiene, polyester, and polyurethane were evaluated for use as the energy storage media and rejected on the basis of low fatigue life and/or high hysteresis loss. Unfilled natural rubber and synthetic natural rubber (cis-polyisoprene) were found to be the most promising for this application.

TABLE 1. Properties of Various Elastomers

Material	Hysteresis Loss	Fatigue Life-Cycle	Comments	Hardness (Durometer)
Polybutadiene	50%	3	Poor Tear Resistance	60A
Hytrel-Polyester	50%	3	High Modulus Low Fatigue Life	65D
K-Prene Polyurethane	50%	4	High Modulus Low Fatigue Life	60D
Polyisoprene Synthetic Natural Rubber	10-20%	>400 Not tested to failure	Acceptable Hysteresis and Fatigue Life	45A
Filled Natural Rubber	5-10%	500 Unlubricated	Acceptable Hysteresis Low Fatigue Life	45A
Unfilled Natural Rubber	5-10%	>95,000 Lubricated	Acceptable Hysteresis and Fatigue Life	35A

Based on small-scale test data, it is projected that the kinetic energy of a 1400 kg vehicle traveling at 13.5 m/sec could be stored in about 32 kg of material with a round-trip energy transfer efficiency of about 90 percent. Fatigue life is a function of initial and final strain limits, surface lubrication and environment, and a fatigue life in excess of 50,000 cycles is being sought. The preparation of tests designed to determine the energy density, hysteresis loss and fatigue life of full-scale elastomeric subassemblies is currently underway.

COMPARISON OF STRESSING SCHEMES

Various methods of stressing an elastomer were also investigated. As shown in Table 2, pure tension was found to have the highest energy per unit volume of elastomer, as expected.

TABLE 2. Comparison of Elastomeric Energy Storing Schemes

ENERGY STORING SCHEME	STRAIN	E/V_{Elas}	E/V_{Total}
a) TENSION 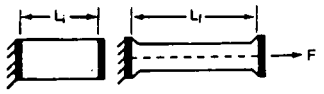	$\frac{L_f-L_i}{L_i}$	$\frac{1}{2} E \epsilon^2$	$\frac{1}{2} E \epsilon^2 \left(\frac{1}{1+\epsilon}\right)$
b) LINEAR SHEAR 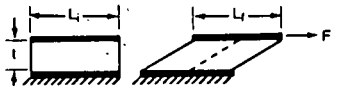	$\frac{L_f-L_i}{t}$	$\frac{1}{2} G \epsilon^2$	$\frac{1}{2} G \epsilon^2 \left(\frac{1}{1+\epsilon t/L_i}\right)$
c) COMPRESSION 	$\frac{L_i-L_f}{L_i}$	$\frac{1}{2} G \epsilon^2 \left(5+\frac{10\epsilon}{3}\right) \leq \frac{1}{2} G \epsilon^2 \left(\frac{1.078}{\epsilon^2}\right)$	
d) ROTATIONAL SHEAR 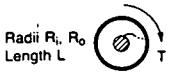	$\frac{2\theta}{1-(R_i/R_o)^2}$	$\frac{1}{2} G \epsilon^2 \left(\frac{R_1}{R_o}\right)^2 \leq \frac{1}{2} G \epsilon^2 \left(\frac{1}{4}\right)$	
e) TORSION 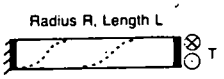	$\frac{R\theta}{L}$	$\frac{1}{2} G \epsilon^2 \left(\frac{1}{2}\right)$	
f) GRADED TORSION BAR 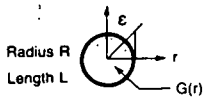	$\frac{R_o\theta}{L}$	$\frac{1}{2} G \epsilon^2 \left(\frac{1}{2} F(n,\rho)\right)$	
g) TORSIONALLY INDUCED TENSION 	Unknown	See Equation 5.	

The scheme referred to as torsionally induced tension, however, promises to have the highest energy per unit of total occupied volume and to be considerably easier to implement for an automotive application. In this scheme, one or more rods are arranged parallel to one another and then sufficient torque is applied to induce buckling. The resultant stress distribution and torque-rotation characteristics have not lent themselves to mathematical derivation, but it was empirically determined that the torque-rotation characteristics in the region of interest shown in Fig. 3 could be specified in terms of the following quantities:

$$K_o = \frac{\pi}{2} GR^4/L \tag{1}$$

$$K_n = \frac{2}{3} n^2 K_o \tag{2}$$

$$\theta_{min} = \frac{\pi L/R}{n+1} \text{ radians} \tag{3}$$

$$T_{min} = K_n \theta_{min} \tag{4}$$

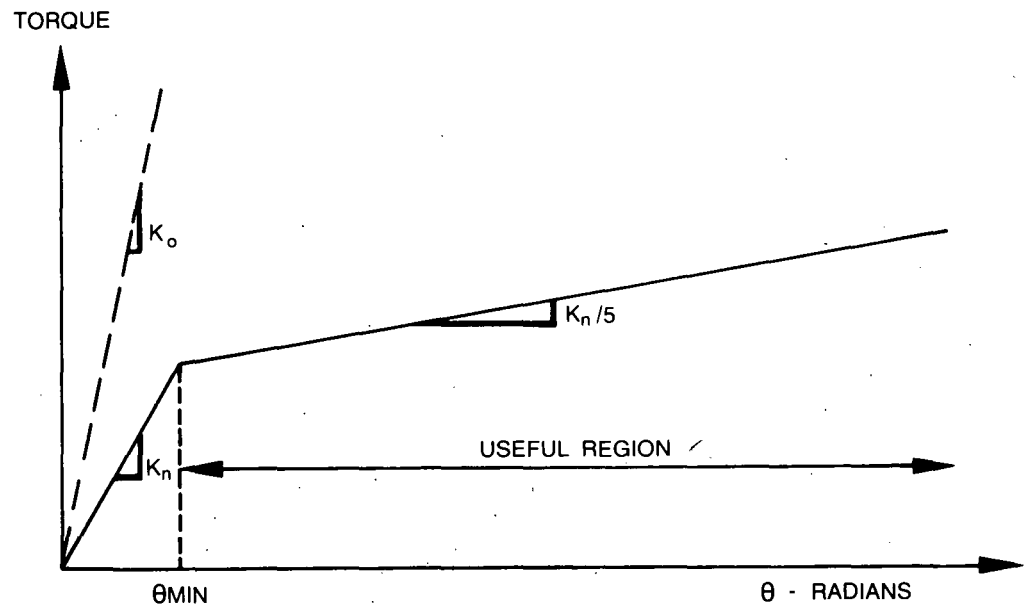

Fig. 3. Empirical Torque-Rotation Characteristics of Elastomeric Torsion Bars in the Buckling Region

In terms of these quantities, it was found that

$$T(\theta) = T_{min} + \frac{1}{5} K_n (\theta - \theta_{min}) \qquad \theta \geq \theta_{min} \tag{5}$$

where R and L are the radius and length of each elastomeric rod, G is the shear modulus, and n is the number of rods.

The full-scale elastomeric subassembly is currently being designed around the torsionally induced tension scheme with n = 4 to be fabricated with cis-polyisoprene by incorporating two molded racetrack shapes of circular cross section.

BREAK-EVEN COST ANALYSIS

Rather than attempt to predict the life cycle cost of a vehicle equipped with a regenerative braking system, the difference in the life cycle cost of such a vehicle and an identical vehicle having no such system can be compared. This greatly minimizes the number of cost figures required and more readily points out the initial-cost vs. energy-savings relationship a regenerative braking system must have in order that it be cost effective.

Assume the standard vehicle has the following known life cycle cost parameters:

C_{INIT} - original vehicle cost per mile, depreciated

C_{ENG} - cost of energy to operate per mile, with taxes excluded

C_{OTHER} - other operating costs per mile, including taxes, insurance, tolls, parking fees and maintenance costs

Then the life cycle cost of operating such a vehicle is

$$\text{Cost/Mile} = C_{INIT} + C_{ENG} + C_{OTHER} \tag{6}$$

Next consider the same vehicle equipped with a regenerative braking system. The corresponding three costs would be C'_{INIT}, C'_{ENG}, and C'_{OTHER} where

$$C'_{INIT} = (1 + \alpha)C_{INIT} \tag{7}$$

$$C'_{ENG} = \frac{1}{1 + \beta} C_{ENG} \tag{8}$$

In these expressions, $(1 + \alpha)$ is the ratio of the purchase prices of the vehicles with and without the regenerative braking system, and $(1 + \beta)$ is the ratio of the miles per gallon or miles per kw-hr of the vehicles with and without the system.

C_{OTHER} and C'_{OTHER} can be estimated by considering the data published by Liston and Aiken[2] of the U. S. Department of Transportation, which has been reproduced as Tables 3 and 4 below.

TABLE 3. Life Cycle Cost Values for Suburban-Based Operation of Compact Vehicles in 1976

Type of Cost	Cost - Cents per Mile
C_{INIT}	3.8
C_{ENG}	2.5
C_{OTHER}	8.3
Total	14.6

TABLE 4. Breakdown of C_{OTHER} Appearing in Table 3

Type of Cost	Cost - Cents per Mile
Taxes	1.2
Insurance	1.6
Garage, Parking, Tolls	2.1
Subtotal	4.9
Maintenance	3.4
Total	8.3

These data show that of the three contributions to total cost, C_{OTHER} is the dominant term, being nearly 57 percent of the total. Maintenance itself, however, is only about 23 percent of the total, suggesting that maintenance costs would have to be increased quite significantly to have much impact on total costs. As a first approximation, therefore, assume that

$$C'_{OTHER} = C_{OTHER} \tag{9}$$

in which case the life cycle cost of a vehicle with a regenerative braking system would be

$$(Cost/Mile)' = (1 + \alpha)C_{INIT} + \frac{1}{1 + \beta} C_{ENG} + C_{OTHER} \tag{10}$$

The differential life cycle cost of a vehicle with and without the system is thus

$$\Delta(Cost/Mile) = (Cost/Mile)' - (Cost/Mile) = \alpha\, C_{INIT} - \frac{\beta}{1 + \beta} C_{ENG} \tag{11}$$

In order that the regenerative braking system be attractive strictly from the economic point of view, therefore, the above quantity must be negative, leading to:

$$\alpha \frac{1 + \beta}{\beta} \leq \frac{C_{ENG}}{C_{INIT}} \tag{12}$$

Thus, if Eq. 9 proves to be a valid assumption, substituting from Table 3 into Eq. 12 leads to

$$\alpha \frac{1 + \beta}{\beta} \leq 0.658 \tag{13}$$

as the relationship between initial cost and range improvement that a regenerative braking system must have in order that it be attractive strictly from the cost point of view.

Results of the analysis on a preliminary design of a complete ERBS[1] indicate a range improvement ratio of 1.22, i.e., $\beta = 0.22$, equivalent to a fuel saving of 18 percent, for the EPA Urban Driving Cycle. Substituting this value into Eq. 13 leads to

$$\alpha \leq 0.12 \tag{14}$$

Thus, if the ERBS can demonstrate a range improvement ratio of 1.22, it would be cost effective if it can be manufactured and sold at less than about 12 percent of the original cost of the vehicle for which it is intended.

REFERENCES

1. L. O. Hoppie, et al., "The Feasibility of an Elastomeric Regenerative Braking System for Automotive Applications," Phase I Final Report, Eaton Engineering & Research Center, Lawrence Livermore Laboratory, UCRL-15044-1 (1979).

2. L. L. Liston and C. A. Aiken, "Cost of Owning and Operating an Automobile - 1976," U. S. Department of Transportation, Federal Highway Administration, Washington, D.C., 1976.

PROJECT SUMMARY

Project Title:	Flywheel System Development for a USPS Delivery Vehicle
Principal Investigator:	Arthur E. Raynard
Organization:	AiResearch Manufacturing Company of California A Division of the Garrett Corporation 2525 West 190th Street Torrance, California 90509
Project Goals:	To develop an experimental flywheel system that will substantially improve the performance of a battery-electric postal delivery vehicle.
Project Status:	The flywheel propulsion system has been designed, fabricated, and developed. System development tests have been performed using a dynamic simulator to operate the propulsion system in a cyclic manner with a vehicle load. The vehicle has been modified to incorporate the flywheel propulsion system and vehicle checkout tests are in progress. The development program has been delayed from the original schedule as a result of changes to the design as required from the development tests. The principal effort was directed towards the development of a power transistor inverter for the electronically commutated motor. Additional major development efforts were required to develop the control logic for propulsion system command and control and to develop the flywheel power unit. The use of a low voltage traction battery was required so that a comparison can be made between the original electric propulsion system vehicle performance and the modified vehicle using a flywheel system. However, this low voltage system has required a larger current capability for the electric power inverter than originally expected. This resulted in major modifications in the inverter design with replacement of the power transistor. The redesigned inverter is operating in a satisfactory manner. The incorporation of a flywheel into a combined-function assembly that includes the flywheel clutch, the electric motor, and a gear reduction unit resulted in excessive oil churning losses. A program to reduce these losses has resulted in a satisfactory level of flywheel mechanical loss.
Contract Number:	DE-AC04-77CS03748
Contract Period:	11/22/76 to 8/31/79
Funding Level:	$426K
Funding Source:	U.S. Department of Energy, Division of Energy Storage Systems and Electric Vehicle Systems; and the U.S. Postal Service

ELECTRIC/FLYWHEEL POWERED POSTAL VEHICLE DEVELOPMENT PROGRAM

Arthur E. Raynard
AiResearch Manufacturing Company of California
A Division of the Garrett Corporation
2525 West 190th Street
Torrance, California 90509

ABSTRACT

A review of the DOE/USPS/AiResearch electric battery/flywheel powered DJ5E Postal Vehicle development program is included in this paper. The program goals are stated. The design and development of the flywheel energy storage unit including a description of the components is reviewed. The program status, including development problems and solutions, is discussed. A DJ5E Postal Vehicle has been modified by removal of the D.C. electric motor and controller, and a flywheel power unit replaces the original system. The new propulsion system features a small steel flywheel, a brushless D.C. motor, and a mechanical vari-belt transmission.

INTRODUCTION

There exists a recognized petroleum fuel shortage and air pollution problem. Since the USPS operates one of the nation's largest vehicle fleets, it must make every effort possible to reduce fuel consumption and air pollution. As a result, the USPS has procured 350 electric vehicles for use on selected park and loop delivery routes. However, the performance of these 350 electric vehicles is limited in range and in number of starts and stops between battery charges. The purpose of this project is to develop a flywheel system which will increase the performance capabilities of electric vehicles so that they can perform the postal delivery mission over a greater number of routes.

The DOE/USPS/AiResearch development program involves the design, fabrication, and installation of a flywheel system in a 1/4-ton postal delivery vehicle. The AM General DJ5E Electric Vehicle has been modified by removal of the electric motor and its controller which is replaced by a flywheel regenerative boosting system, along with associated control and charging systems. The purpose of installing the flywheel system is to demonstrate the performance benefits that are possible when operating the vehicle in start-stop cyclic operation. These benefits apply to both the acceleration rate and the number of start-stop cycles that can be achieved on a single battery charge.

PROGRAM GOALS

The primary program goal is to determine that the vehicle performance can be improved by incorporation of the flywheel system into an existing electric vehicle. The performance comparison is shown in Table 1.

	POSTAL SUPPLIED AM GENERAL DJ-5E	IMPROVED DESIGN
ACCELERATION	0-30 MPH IN 25 SEC	0-30 MPH IN 12.5 SEC
TOP SPEED	33 MPH	33 MPH
GRADEABILITY	10% GRADE @ 10 MPH	10% GRADE @ 20 MPH
SIMULATED POSTAL ROUTE	350 START/STOPS OVER DISTANCE OF 10 MILES	500 START/STOPS OVER DISTANCE OF 14 MILES
RANGE	27 MILES AT 30 MPH	27 MILES AT 30 MPH

Table 1. Flywheel Powered Vehicle Performance Comparison

An additional goal is to provide a vehicle propulsion system that is ready for operational use.

PROGRAM SCHEDULE

The program was started in December, 1976, and has proceeded through design, fabrication, component development, system testing and vehicle checkout. Currently, the vehicle is being prepared for acceptance testing in September.

FLYWHEEL PROPULSION SYSTEM

In the Postal Delivery Vehicle (Figure 1) AiResearch is applying a multiple thin-disc flywheel energy storage system to a battery-powered vehicle to increase its useable stop-start capability, useful range, and acceleration into traffic, while reducing the maximum battery current demand from 600 amp to 270 amp.

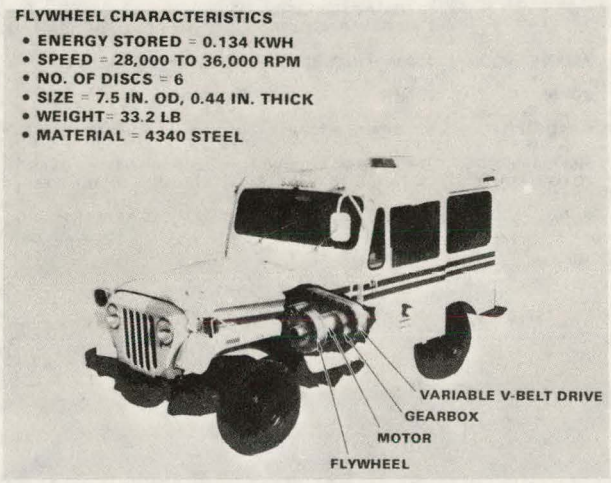

Fig. 1. DOE/USPS Delivery Vehicle with Multiple Thin-Disc Flywheel ESU

The flywheel power unit replaces the original electric motor, and the flywheel assists the electric motor in propelling the vehicle, reducing the power required from the battery during peak-demand transient operating periods. The flywheel is also used to regenerate the braking energy. The electric motor drives the vehicle to 7 mph, reaching its full 36,000-rpm speed. At that point the flywheel fluid coupling is engaged and the flywheel is used to drive the vehicle to its 33-mph cruise speed through the variable-ratio V-belt drive. The process is reversed during braking; the traction wheels supply energy to the flywheel while slowing to 7 mph. Below 7 mph and during emergency stops, the service brakes halt the vehicle. During idle, the fluid coupling is disengaged and the flywheel is the only component that is rotating. A propulsion system block diagram is shown in Figure 2. The original battery is used with a revised controller and power train.

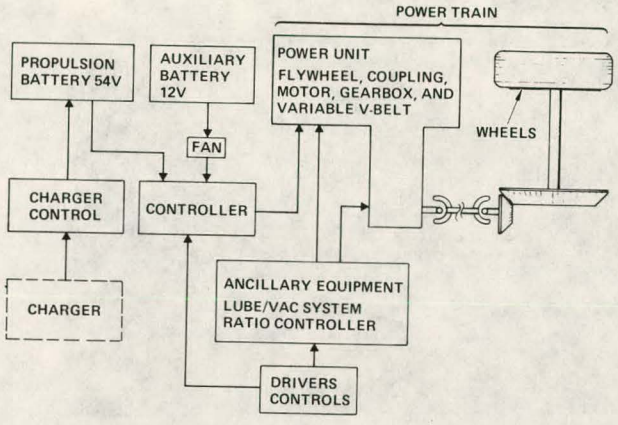

Fig. 2. Propulsion System Block Diagram

ELECTRICAL POWER INVERTER

The inverter provides a means to switch the D.C. battery power by electronically commutating at a frequency synchronous with the motor speed. The motor contains three position pickups that provide the commutating signal for the application of current to the 3 phase motor stator. In this manner, the inverter frequency varies as the motor changes speed and is always "locked in" in a synchronous manner.

The inverter driver circuit also pulse-width modulates the transistors to control the motor torque and to limit the maximum allowable transistor current. Appropriate snubbing devices and free-wheeling diodes dissipate the electrical energy remaining in the motor winding when each transistor is switched off. The inverter is shown in Figure 3, which is a photograph of the inverter and flywheel power unit installed in the vehicle chassis.

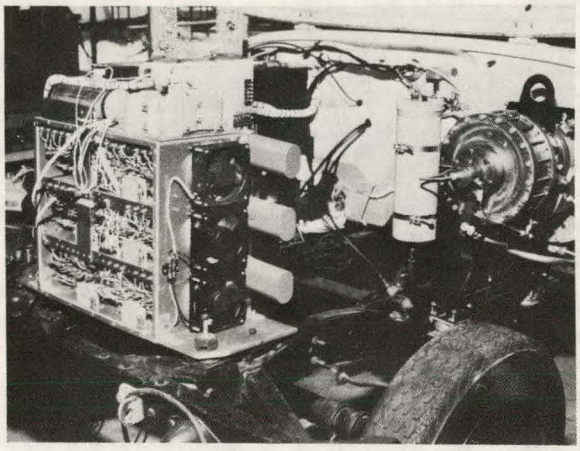

Fig. 3. Inverter and Power Unit Installation

Each of the six inverter legs is constructed by paralleling 16 transistors to achieve the required current carrying capacity to supply motor power. The transistor installation is shown in Figure 4.

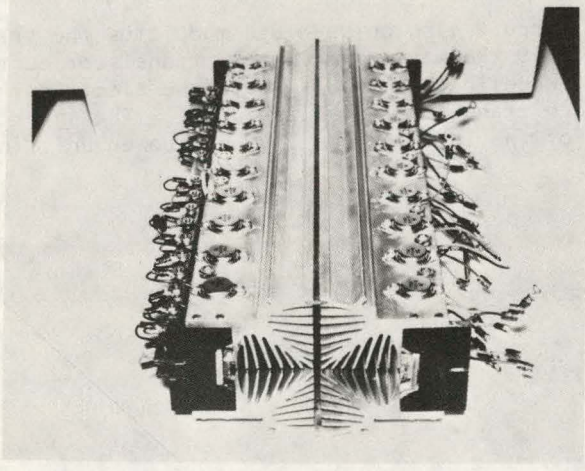

Fig. 4. Inverter Transistor Installation

CONTROLLER

The controller installation is shown in Figure 5.

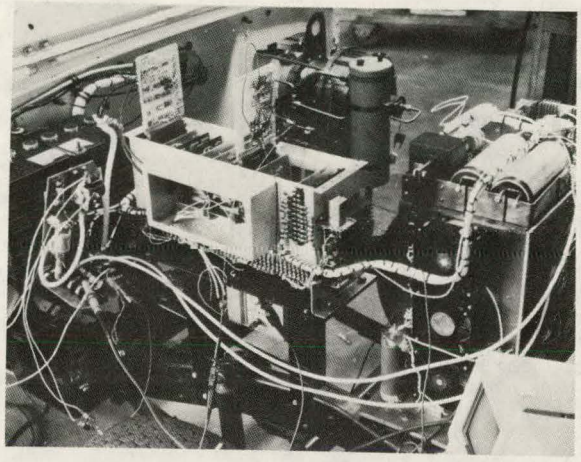

Fig. 5. Controller and Inverter Installation

The controller contains 13 circuit cards that include both the inverter logic and the various driver to power unit commands and control logic. Driver inputs are the foot pedal position of the accelerator pedal and the brake pedal. Additional inputs are the forward and reverse switch and the ignition and start switches.

The controller also senses the vehicle and flywheel speeds, flywheel engagement, and the mechanical transmission V-belt torque and ratio limit.

Commands are given to control the transmission ratio, to engage and disengage the flywheel, to modulate the inverter-to-motor power level, and to maintain the flywheel speed at a programmed value. The motor power is reversed to drive the vehicle in reverse.

SENSORS

The control system includes a number of sensors, which provide the required input signals. Some of these are continuously monitoring (such as flywheel speed), some indicate a specific condition (such as V-belt pulley limit), and others are operator controlled (such as the accelerator). The function of each of these sensors is described below.

Motor Rotor Position

There are three pickups which sense rotor position to provide information to the inverter logic so as to properly phase the stator field with respect to the rotor magnetic poles.

Motor Speed

A signal is taken from one of the rotor position sensors, which generate pulses whose frequency is proportional to speed, to perform these functions:

1. A signal for motor-flywheel speed match for fluid coupling engagement.

2. A signal to indicate motor overspeed, which initiates these actions:

   a. De-energize the fluid coupling solenoid to disconnect the fluid coupling. This prevents flywheel overspeed.

   b. Shut off power to the motor.

   c. Put the V-belt pulleys into min-min condition. This prevents motor overspeed by regeneration from the vehicle.

3. To provide an indication of low motor speed at "full" accelerator when under V-belt control. This is one condition required to initiate a V-belt ratio change to a lower ratio (lower gear) to prevent motor stall when climbing hills.

Flywheel Speed

A speed sensor is located at the outboard end of the flywheel shaft to provide these functions:

1. Information for flywheel energy management.

2. Prevent flywheel overspeed:

   a. De-energize the fluid coupling.

   b. Shut off power to the motor.

   c. Put the V-belt pulleys into min-min condition.

3. Indicate motor-flywheel speed match for fluid coupling engagement.

4. Provide signal for "at speed" condition which de-energizes the start switch holding relay.

FLYWHEEL POWER UNIT

The flywheel power unit block diagram is shown in Figure 6 and the interior view is shown in Figure 7.

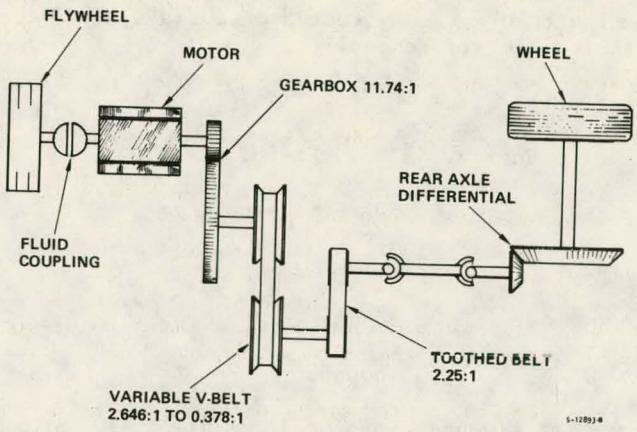

Fig. 6. DOE/USPS Delivery Vehicle Power Train

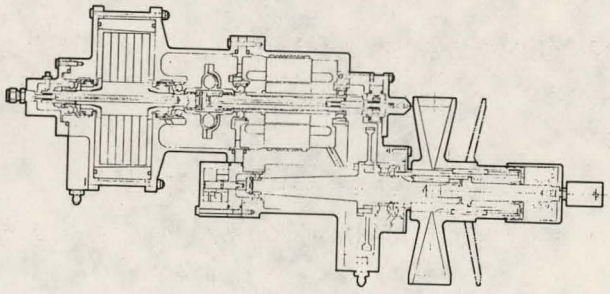

Fig. 7. Flywheel Power Unit

FLYWHEEL ASSEMBLY AND GEARBOX

Rotor - the rotor is constructed of 6 disks of 4340 steel that are attached to the shaft by a thermal interference fit.

Rotor Characteristics -

Kinetic Energy, 357,000 Ft-lb, at 36,000 RPM

Ip , .0502 Ft-lb-sec^2

O.D. , 7.5 in.

Length , 2.64 in.

Weight , 35 pounds

Housing - the flywheel housing forms the mounting and containment structure for all of the rotating components. The housing is shown in Figure 8 with the motor rotor and shaft also shown.

Gearbox - the gearbox reduces the motor and flywheel speed through a two step gear ratio of 11.74 to 1. The gears are helical, ground and hardened to minimize noise and reduce wear. All bearings are rolling element type to reduce losses.

Lube/Vacuum - the lube and vacuum pump is a single internal gear pump that provides both pumping functions. Oil and air are pumped from the flywheel cavity and pumped into an external tank. Atmospheric pressure in the tank provides the head to supply the lubrication and cooling circuits for the flywheel, motor and fluid coupling.

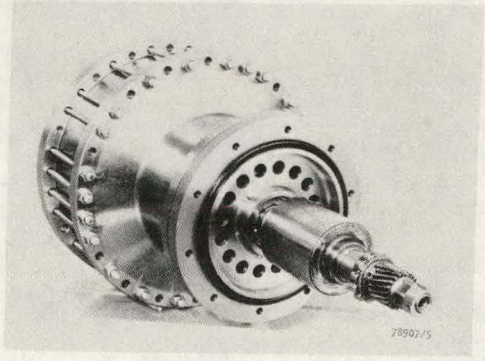

Fig. 8. Flywheel Housing

Fluid Coupling - the fluid coupling acts as a clutch to engage the flywheel and motor when the propulsion system is accelerated to flywheel speed. The fluid coupling minimizes shock engagement and wear. Operation of the clutch occurs when lube oil fluid is introduced through an axial port in the rotating shaft into the coupling. A continuous bleed through the clutch prevents overheating the fluid.

The coupling consists of three separate details (1) a driving half, (2) a driven half, (3) a shroud that is fastened to, and rotates with the driving half, but encloses the outer periphery of the driven half.

MOTOR

The brushless D.C. motor consists of two principal elements; a 3 phase stator winding, and a 4-pole permanent magnet rotor. In addition, 3 proximity probes are attached to the motor housing to supply position signals to the inverter.

The rotor uses samarium-cobalt magnets encased in a high strength inconel jacket. These magnets provide the field excitation required to generate the electro-magnetic rotating field for electrical torque between rotor and stator. This torque is constant for any given value of stator current. Motor torque is increased or decreased by changing the stator current. The motor rotor and stator are shown in Figure 9 which also shows the mechanically commutated D.C. motor used in the original electrical propulsion system installation.

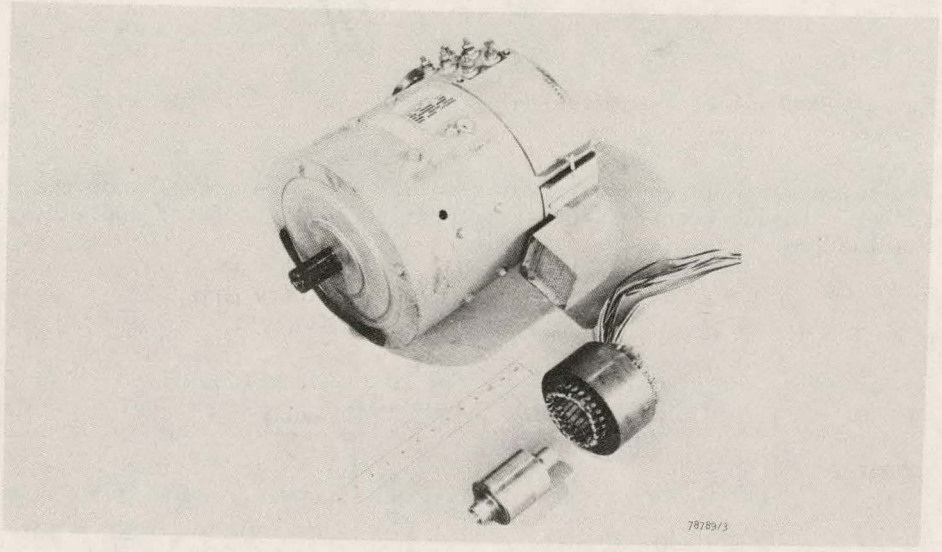

Fig. 9. Original and Replacement Electric Motors

MECHANICAL TRANSMISSION

The mechanical transmission provides an overall ratio change of 7 to 1 to transmit power from-and-to the flywheel and the vehicle wheels.

The variable belt transmission consists of two pulleys, connected by a V-section belt, both of the pulleys being adjustable to vary the operating pitch diameter. A photograph of the transmission is shown in Figure 10.

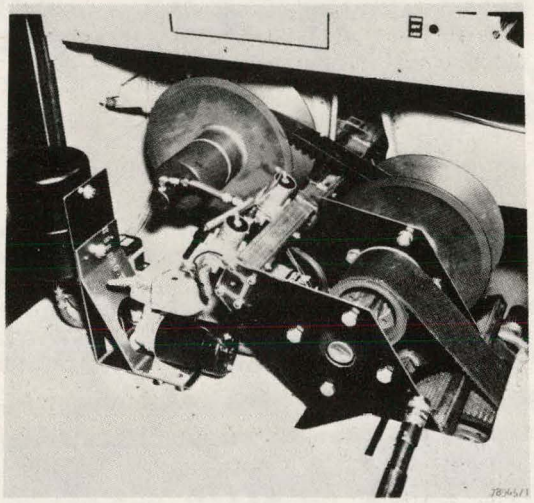

Fig. 10. Vari-belt Mechanical Transmission

The transmission ratio is controlled by reducing the axial spacing of the driver pulley, when accelerating. Torque transmission is proportional to the force applied against the pulley. The actuation system is shown in Figure 11.

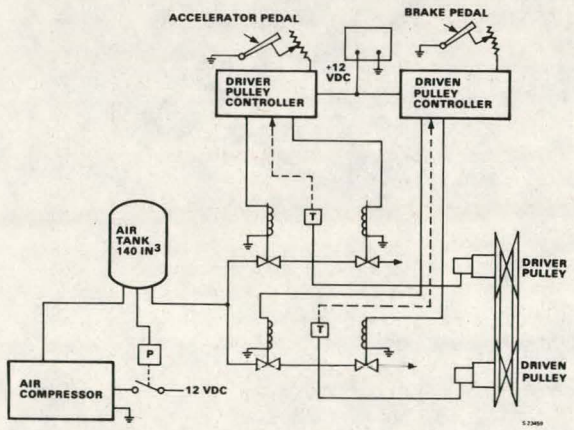

Fig. 11. V-Belt Actuation System

This procedure is reversed when the vehicle is braked.

The driver command is servo controlled by applying pneumatic pressure against a rotating actuation cylinder in the driver pulley that is proportional to the foot pedal position. The driven pulley is pressurized with sufficient pressure to prevent belt slip. This process is reversed when the ratio is changed back to its starting position.

VEHICLE ACCEPTANCE TESTS

Vehicle acceptance tests will be performed when the vehicle checkout, which is currently in process, is completed. The acceptance tests are summarized in Figure 12.

FACILITY FEATURES	TESTS CONDUCTED
LEVEL PAVED TEST COURSE 1400 FT BY 430 FT LEVEL PAVED	• FORWARD-REVERSE CYCLES • GENERAL DRIVEABILITY • ACCELERATION 0-30 MPH • DECELERATION 30-0 MPH • POSTAL CYCLES
CITY STREET > 1/2 MILE STRAIGHT LEVEL ROAD WITHOUT CROSS STREETS	• MAXIMUM SPEED • DASH
CITY STREET WITH APPROXIMATELY 10% GRADE FOR 150 FEET	• GRADEABILITY

Fig. 12. Postal Vehicle Acceptance Tests

The tests will be conducted in a level, paved parking lot and in city streets located in Torrance, California.

THIS PAGE

WAS INTENTIONALLY

LEFT BLANK

PROJECT SUMMARY

Project Title:	Regenerative Flywheel Energy Storage System
Principal Investigators:	E.L. Lustenader, I.H. Edelfelt, D.W. Jones, A.B. Plunkett, E. Richter and F.G. Turnbull
Organization:	General Electric Company Corporate Research and Development Schenectady, New York 12301
Project Goals:	To laboratory test a flywheel energy recovery system sized for a 3000 pound class battery/flywheel electric vehicle. To perform propulsion system tests simulating an electric vehicle operating under various SAE driving cycles (schedules A,B,C,&D). Establish the range improvements attributed to the flywheel. Conduct a life cycle cost comparison of three vehicles: ICE, Battery & Battery/Flywheel.
Project Status:	All hardware for the flywheel energy propulsion system has been designed, fabricated and installed in the laboratory. Components include: • An energy storage package comprised of a 20,000 rpm, six pole, solid rotor inductor type flywheel drive motor coupled to a steel flywheel. This energy storage package is designed to recover 105 watt hrs. of braking energy. • An 8 SCR load commutated inverter, a hybrid reverser and an inverter control for powering the energy storage unit. • A separately excited DC propulsion motor, a flywheel to simulate vehicle inertia, an electrical load machine to provide road loss, and a torque transducer to measure the propulsion motor torque. • A 108 volt lead acid battery bank to provide the propulsion energy. System control and data acquisition will be done using two computers operating in real time. The computer software has been written and is now being debugged. The system has been operated in the following modes: • Acceleration of the flywheel from the battery. • Transfer of energy from the flywheel to traction motor. • Operation of traction motor from battery source. • Regeneration from traction motor to flywheel unit. Operation of the total system on the SAE J227a D cycle has not yet been accomplished. The life cycle cost comparison has been completed.
Sub-contract Number:	8990503
Contract Period:	FY 78, 79
Funding Level:	$538,878
Funding Source:	U.S. Department of Energy, Lawrence Livermore Labs.

REGENERATIVE FLYWHEEL ENERGY STORAGE SYSTEM

E.L. Lustenader, I.H. Edelfelt, D.W. Jones,
A.B. Plunkett, E. Richter and F.G. Turnbull
General Electric Company
Corporate Research and Development
1 River Road
Schenectady, New York 12301

ABSTRACT

This paper describes the current status of a program to develop and evaluate a regenerative flywheel energy storage system. The system has been designed for a battery/flywheel electric vehicle in the 3000 pound class. Planned laboratory tests will simulate this electric vehicle operating over the SAE J227a Schedule D driving cycle. The range improvement attributed to the use of the flywheel will be established. The flywheel energy storage system will consist of a solid rotor, synchronous inductor-type flywheel drive machine electrically coupled to a DC battery electric propulsion system through a load commutated inverter. The motor/alternator unit is coupled mechanically to a small steel flywheel which provides a portion of the vehicle's accelerating energy and regenerates the vehicle's braking energy. The laboratory simulation of the electric vehicle propulsion system will include a 108 volt lead-acid battery bank, a separately excited DC propulsion motor coupled to a flywheel which simulates the vehicle's inertia, and the flywheel energy storage system comprised of the motor/flywheel unit, the load commutated inverter and its control.

INTRODUCTION AND BACKGROUND

A flywheel energy storage system was initially conceived by General Electric and proposed for demonstration to the Department of Energy, Division of Energy Storage Systems. The overall objective of the program was to demonstrate new technology associated with a flywheel energy storage system comprised of a composite flywheel coupled directly to an AC synchronous motor/alternator. The motor/alternator/flywheel unit would be hermetically sealed with the rotating assembly operating in a low pressure helium atmosphere. The motor/alternator would receive power from a solid state inverter/rectifier unit designed to provide the necessary frequency control from a constant DC voltage power supply.

A follow-on to Contract EY-76-C-02-4010, which is the subject of this paper, was initiated in March 1978. The specific objective of this new program is to laboratory test an improved flywheel energy recovery system sized for a battery/flywheel electric vehicle weighing about 3500 pounds. Laboratory tests will be made to simulate the electric vehicle operating under the SAE J227a Schedule D driving cycle. The objective is to determine the range improvement that can be attributed to the use of a small flywheel in combination with the battery bank.

SCOPE OF CURRENT PROGRAM

To achieve the program objective, an improved flywheel energy recovery propulsion system was designed, fabricated, and installed in the laboratory. The scope of the overall program was as follows:

- Establish specifications for the regenerative flywheel energy storage system and prepare a test plan. These specifications were based on tradeoff studies among system weight, component efficiency, and performance.
- Design a new, improved, inductor motor/flywheel energy storage package for a 3000 pound class electric vehicle. Test results from the first phase of the DOE program were utilized in arriving at this design.

- Design a new inverter. The fourteen SCR inverter/rectifier which was demonstrated on the first contract was replaced by a new eight SCR unit and a hybrid reverser. The use of a hybrid reverser, composed of diodes and a power contactor, obviates the need for the six additional SCR's originally proposed for braking.
- Test the regenerative flywheel energy storage propulsion system in the laboratory. In order to simulate an actual driving cycle, a load flywheel was designed to simulate the inertia of the 3000 pound vehicle. This was coupled directly to a new separately excited DC propulsion motor.

The simulated propulsion system consists of a 108 Volt lead-acid battery bank, the DC propulsion motor with load flywheel, and the regenerative flywheel energy storage system. Tests will be conducted on the equipment to simulate the vehicle in operation. The equipment will be operated to establish the performance of the regenerative flywheel energy storage system as if it were performing in an electric vehicle. It will be operated over the simulated driving cycle, and measurements will be made to determine the energy required per cycle. Data will be reduced and the results analyzed and compared to the predicted performance. Results will provide an estimated range and power consumption for a 3000 pound class electric vehicle with this type of flywheel/battery propulsion package.

OVERALL VEHICLE SYSTEM STUDIES

In analyzing the performance of a flywheel/battery powered vehicle operating on a duty cycle such as the SAE J227a Schedule D, a number of operating modes were evaluated.

The final mode selected is shown in Figure 1. The shaded area represents energy supplied by the flywheel.

Energy stored in the flywheel is used to supply the drive motor armature power during the initial stage of acceleration. This results in power not being required from the battery by the motor armature until the back EMF of the traction motor exceeds battery voltage. At this point, flywheel energy is used uniformly over the remainder of the accelerating period with the additional required armature power being supplied by the battery. Cruise power is supplied totally by the battery. Braking energy is recovered and stored in the flywheel. System losses are supplied to the flywheel from the battery during the idle period.

The projected range of the vehicle in this mode of operation is shown in Figure 2.

FLYWHEEL ENERGY STORAGE PACKAGE

ELECTRICAL DESIGN

The electrical machine finally selected from tradeoff studies was a 6-pole machine operating with a maximum speed of 20,000 rpm, with a rotor radius of 3.6 inches and a rotor length of 3.44 inches. A cross section of the machine is shown in Figure 3.

MECHANICAL DESIGN

The inductor machine portion of the rotating assembly, including the six poles and the central shaft, is machined from a magnetic steel billet (AISI 4340). Steel shafts of non-magnetic, austenitic steel are welded to both ends of the pole bearing section in order to minimize flux leakage, which tends to saturate the magnetic iron and magnetize the ball bearings, making them traps for magnetic wear particles. The stub shafts are hollow to reduce weight.

DESIGN STRESSES

The energy stored in the inductor motor rotor is approximately 15 watt-hours over the speed range of 10,000 to 20,000 rpm. An additional 90 watt hours is stored in the flywheel.

The flywheel operates at a relatively modest stress level in order to produce a factor of safety of 2.0 relative to the 10^7 cycle curve for alternating stress.

POWER CONDITIONER & CONTROL

POWER CONDITIONER

The power conditioner is a load commutated inverter similar to the system provided by General Electric under the previous contract (EY-76-C-02-4010). The new unit, however, is lighter and smaller than the original load commutated inverter (LCI), since it requires only six power thyristors instead of twelve. Reversal of power flow is provided by a hybrid reverser (two diodes and two contactors) rather than a second set of six thyristors. Figure 4 shows the new eight SCR inverter. A block diagram of the entire laboratory system is shown in Figure 5. The four major components for the electrical portion of the drive system (battery, propulsion motor, hybrid reverser, and load commutated inverter/rectifier) are shown together with the electromagnetic contactors that connect the various components in the several configurations in which the system operates.

Figure 6 shows the power and auxiliary thyristors of the load commutated inverter/rectifier. In this system, power flow is accomplished by reversing the direction of the DC voltage while maintaining the current flow from the thyristors in the same direction. The two auxiliary thyristors and the single commutating capacitor connected to the synchronous motor neutral terminal for starting are similar to those provided in the previous contract.

This configuration of the power circuit was chosen to permit recharging of the flywheel from the battery during conditions of either vehicle stopped or cruise speed operation.

The electrical requirements of the load commutated inverter (relating to its DC side) when operating over a simulated SAE J227a Schedule D driving cycle are given in Figure 7. Negative current indicates power flow either from the propulsion motor, which acts as a generator during braking, to the flywheel or from the battery to the flywheel. During the condition in which the battery is supplying power to the propulsion motor or to the flywheel motor, the voltage will be in the range of 75 to 108 volts depending on the state of battery charge.

SYSTEM CONTROL

The control system is required to regulate the operation of both the energy storage flywheel system and the vehicle traction motor. The control system uses two computers operating in real time. The first is a Digital Equipment Corporation PDP 11/34 used primarily in an overall supervisary role controlling driving cycle modes, acquiring the data from the sensors, outputing lower speed analog and digital signals to the second computer and printing out the summary data. The second computer is an Electronic Associates Inc. EAI 681 hybrid controller used for the high speed real-time analog control loops for the load commutated inverter together with high speed calculations of analog parameters. The digital portion of this computer is used for the initial starting and accelerating of the flywheel together with the determination of several of the driving cycle mode transitions. Figure 8 shows the interrelationship between the two computers and the experimental set-up together with the interface between hard-wired control cards and sensors and software control accomplished on the computers.

Figure 9 shows the location of the electrical and mechanical signals used by the control system for data acquisition and control of the entire flywheel energy storage and simulated vehicle systems. In order to scale the electrical signals and provide electrical isolation, commercially available transformer isolated gain modules were provided.

The primary control loop for the load commutated inverter consists of an outer current regulator together with an inner angle loop to maintain synchronism between the synchronous

motor and the load commutated inverter. This control system does not require a mechanical shaft position sensor.

In addition to the primary control system, two field current controls are required. One is for the flywheel motor, which will simply vary the flywheel motor field current as a fixed function of inverter DC link current, flywheel speed, and DC link voltage. The second control is for the traction motor field which will remain fixed at low vehicle speeds but must be varied at high speeds to regulate the armature current during those periods when the battery supplies all the power to the propulsion motor. The two field currents are also controlled as a function of the mode of operation of the system. For example, during mode 3 (steady-speed operation), the flywheel is inactive and its field current is programmed to a fixed low value. This will reduce the machines losses when integrated over the duty cycle, thereby improving its energy efficiency. Sufficient field excitation must be provided in order that the inverter control can always be synchronized with the machines back EMF. Similar reductions in the traction motors' field current occur during mode 6 when the vehicle is stopped and there is no need for field excitation.

In a similar manner, the armature current from the traction motor (IA) and the DC current from the flywheel energy storage system (IDC) are also controlled and regulated as a function of the vehicle operating mode. This system is more complex than the field current regulators because during mode 2 (acceleration above the motoring corner point) both current regulators must be active in order to share the total current supplied to the traction motor. A more detailed block diagram of the DC current regulating loops that are active in each mode of vehicle operation is shown in Figure 10.

SYSTEM TEST

An existing laboratory test facility has been modified for use on this contract. The facility includes a new separately excited DC propulsion motor, a flywheel simulating vehicle inertia, an electrical load machine to provide road loss, and a torque transducer to measure the propulsion motor torque. Figure 11 shows this assembly installed in the laboratory. This equipment together with a 108 volt battery bank, the inverter/rectifier, the inductor motor/alternator/flywheel package, and the hybrid controller has been assembled in the laboratory for component and system testing.

Figure 12, from left to right, shows the computer programmable DC power supplies used to provide field current to the three rotating machines, the breadboard load commutated inverter, the DC contactor panel and on the right, the hard wired inverter logic and gating control cards. At the far right is an eight channel recorder used for data presentation and system debugging.

The two digital computers used for system control, data acquisition, and repetitive driving cycle control were existing laboratory equipment programmed for this specific project. Each computer has associated with it a set of peripheral equipment for input/output and communication with the operator. Examples are graphics terminals with hard copy capability, disks for program and data storage and line printers. Figure 13 shows the system programmers operating the PDP 11/34 terminal and in the background, the EAI 681 analog panel.

Major computer sub-routines are programmed on the digital portion of the EAI hybrid computer. Since the system operates in a real-time mode, the entire program is interrupt driven from a fixed time increment clock. A start sub-routine is used to control the initial start up of the flywheel energy storage system. This separate operation is not repeated during the driving cycle tests as it is not one of the normal repetitive modes of operation.

In a similar manner, the PDP 11/34 computer sub-routine operates in real-time interrupt mode. The repeat time internal is 100 milliseconds. This rapid and repetitive acquisition of the data provides for accurate integration and summation of the rapidly changing measured quantities. The data is written to a file for later data analysis and graphing after the series of driving cycles has been completed.

STATUS

At the time of preparation of this paper, the system has operated in each of its control modes. The flywheel has been charged from the battery, this energy transferred to the traction motor, traction motor operated at full speed and regenerated to the flywheel. The control is being debugged and a complete D cycle with measurements is anticipated shortly.

ACKNOWLEDGEMENT

This work is sponsored by the U.S. Department of Energy under a subcontract (No. 8990503) from the University of California Lawrence Livermore Laboratory. Mr. Thomas Barlow of LLL has been the Technical Monitor for the program.

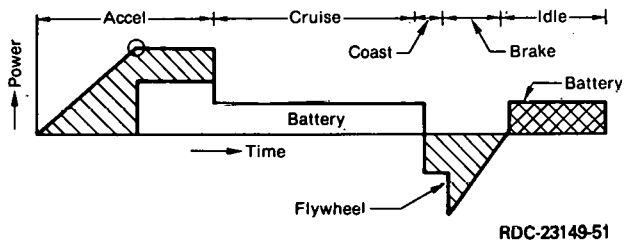

Fig. 1. Power Time Profile for Driving Cycles.

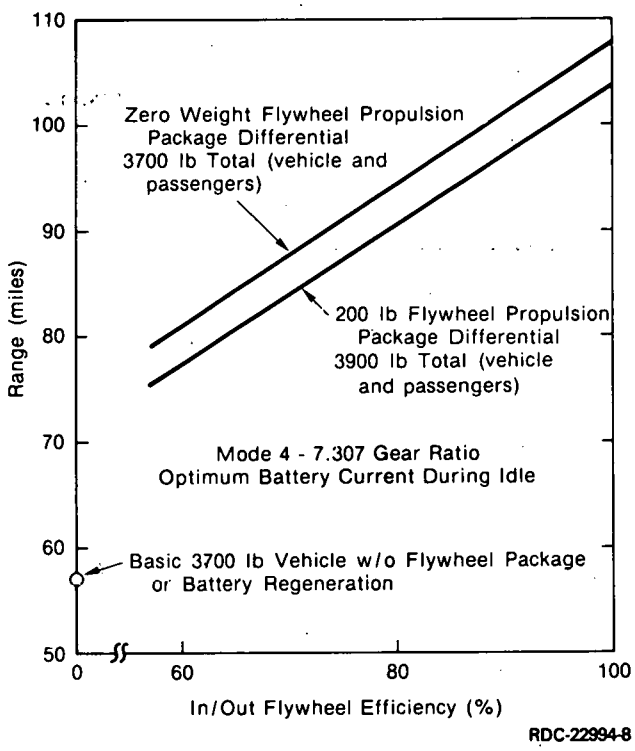

Fig. 2. Flywheel Augmented Vehicle Range.

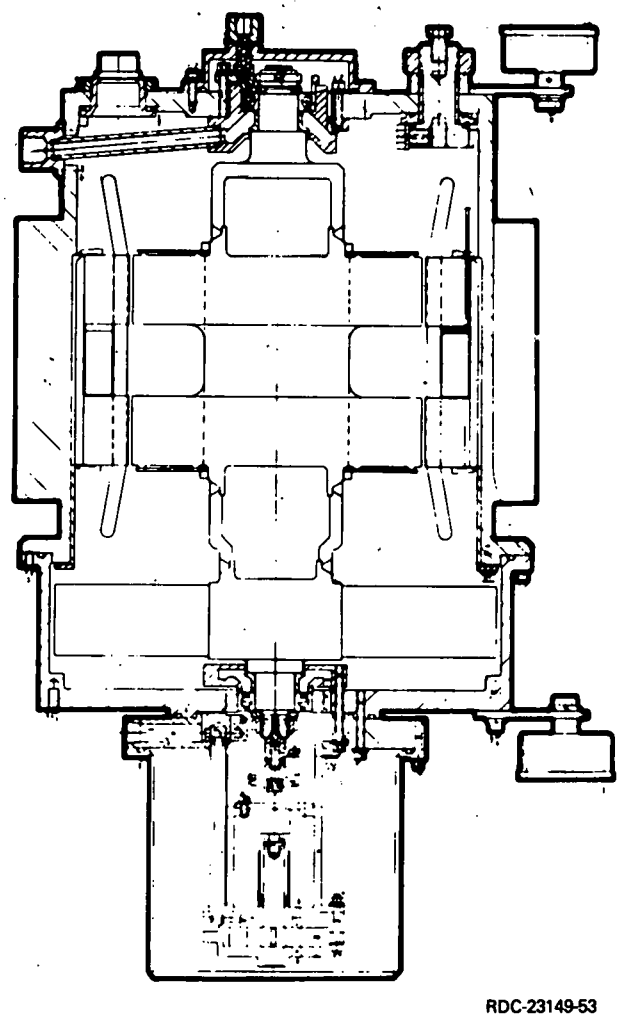

Fig. 3. Detailed Layout of Flywheel Energy Recovery Unit.

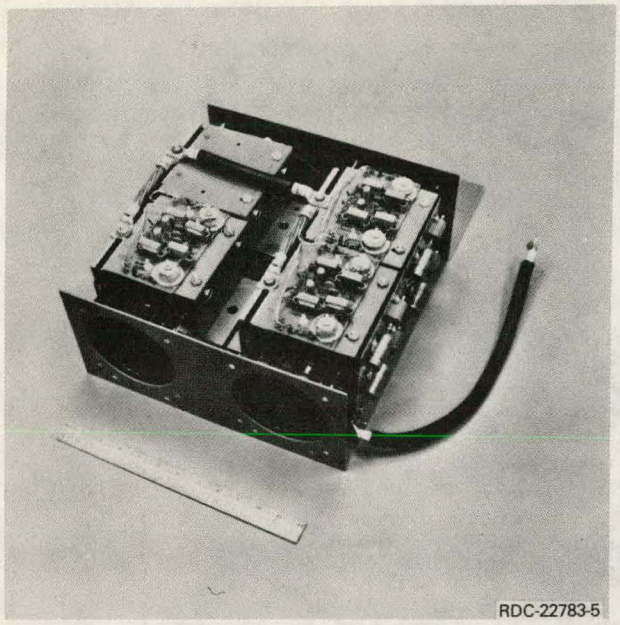

Fig. 4. Load Commutated Inverter.

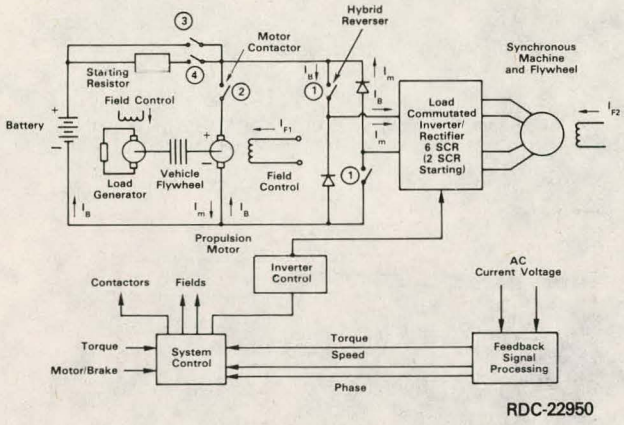

Fig. 5. Schematic Diagram of Simulated Propulsion System.

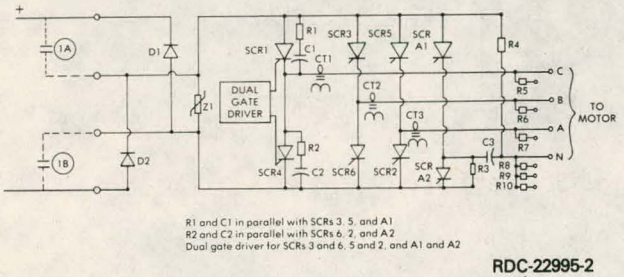

Fig. 6. Load Commutated Inverter/Rectifier Power and Commutating Circuit.

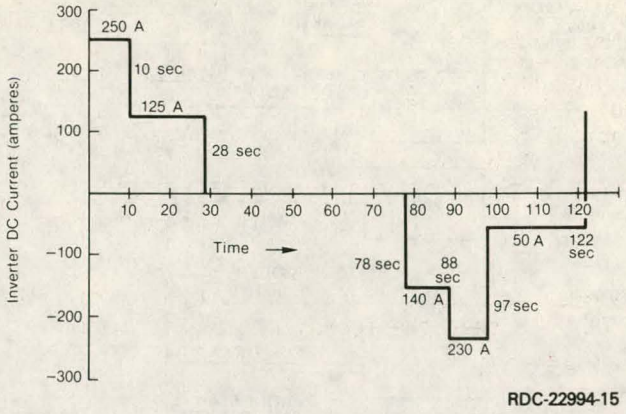

Fig. 7. Inverter DC Current vs. Time.

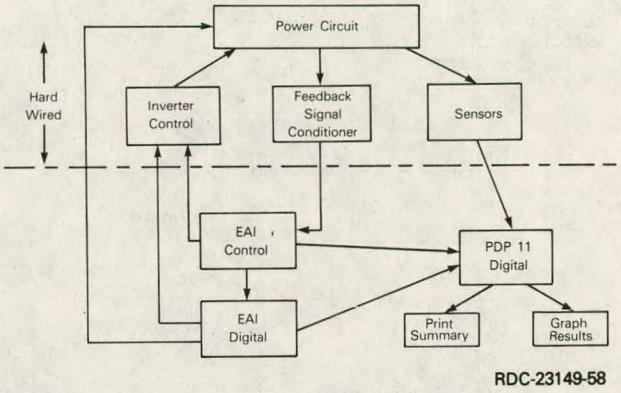

Fig. 8. Control System Block Diagram.

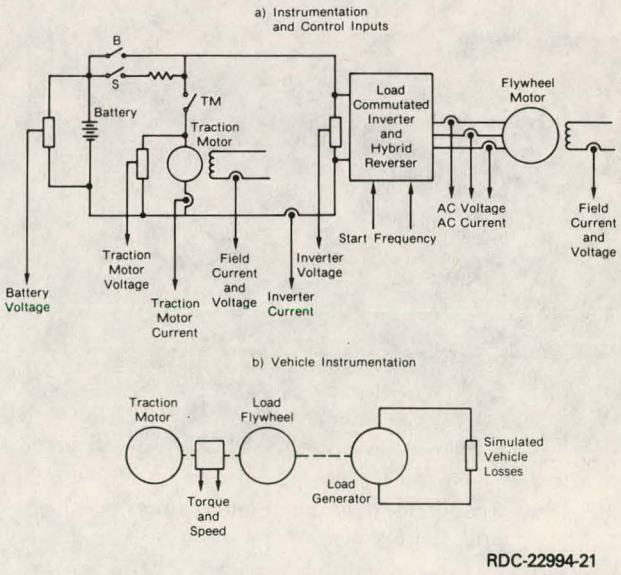

Fig. 9. Electrical and Mechanical Signals for Control and Data Acquisition.

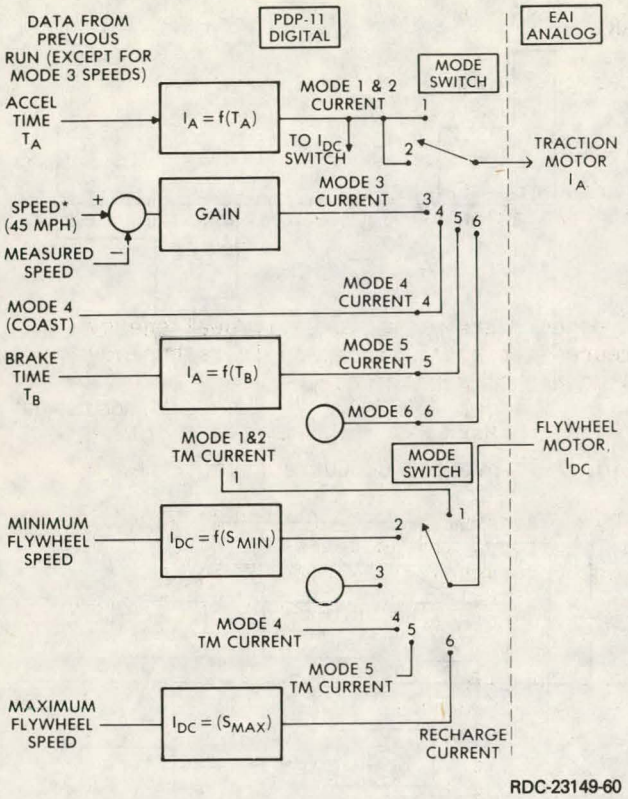

Fig. 10. DC Armature Current Control Modes.

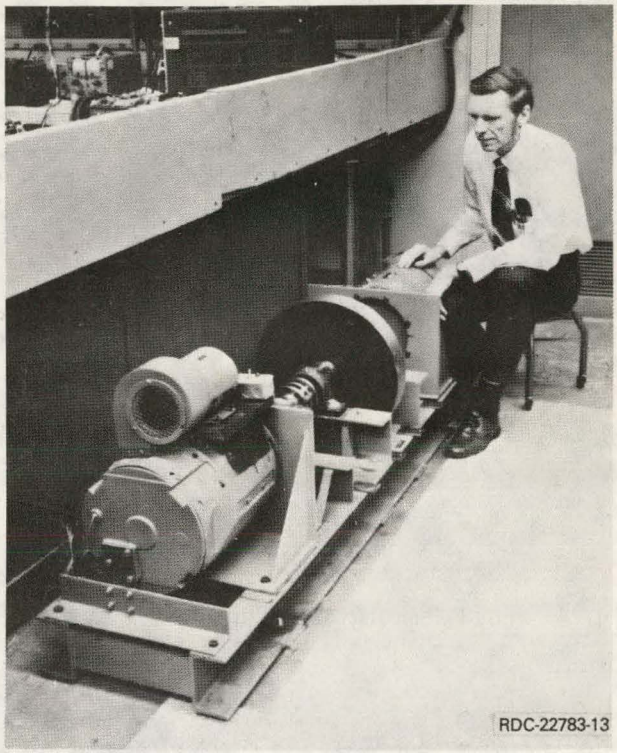

Fig. 11. Propulsion Motor, Torque Transducer, Flywheel and Road Loss Generator.

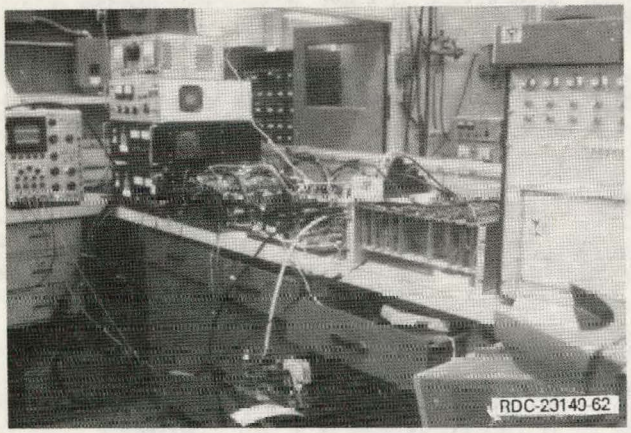

Fig. 12. Breadboard Power Conditioner and Control.

Fig. 13. Computer System in Operation.

PROJECT SUMMARY

Project Title:	LLL/AiResearch Advanced Energy Storage Unit Development Program
Principal Investigator:	Leo V. Norrup
Organization:	AiResearch Manufacturing Company of California A Division of the Garrett Corporation 2525 West 190th Street Torrance, California 90509
Project Goals:	To design and build an advanced state-of-the-art flywheel energy storage unit (ESU) that represents a step increase in technology and provides a baseline standard of performance.
Project Status:	The ESU has been designed and the hardware fabricated. A summary of the testing is as follows: Testing Status - the maximum lube-coolant pump power was determined to be 35 W. The variable frequency, variable voltage electrical power drive is in place and operational. The electronic controller, which is used to automatically control the ESU, has been checked-out in the system. Problems Encountered - the major effort has been expended trying to trim balance (at speed) the ESU rotating group. During the balancing process it was determined that the molecular pump was not performing to specification, i.e., the minimum flywheel cavity chamber pressure attained was 40-microns at 40,000 rpm. The successful balancing of the unit was nearly completed when the motor rotor failed during test. A failure investigation determined that 2 to 3 bars of the cast copper rotor had failed due to casting porosity. Corrective Action - the molecular pump stator geometry was changed from 4 lands and grooves to 3. Prior to the motor failure, it was determined that the ESU had a moment unbalance. An additional probe will be attached at the lower end of the rotating group to aid in trim balancing during test. A high strength back-up rotor, fabricated using extruded zirconium-copper, is available. This results in a porosity free rotor.
Contract Number:	9676603
Contract Period:	May 1, 1978 to November 30, 1979
Funding Level:	$593K
Funding Source:	University of California, Lawrence Livermore Laboratory

LLL/AIRESEARCH ADVANCED ENERGY STORAGE UNIT DEVELOPMENT PROGRAM

Leo V. Norrup
AiResearch Manufacturing Company of California
A Division of the Garrett Corporation
Torrance, California

ABSTRACT

This paper includes a review of the LLL/AiResearch advanced flywheel energy storage unit (ESU) development program. The program scope and goals are stated. A description of each of the major hardware subassemblies is included. The development test program tasks are defined and a summary of the testing in terms of status, development problems, and corrective actions is discussed.

The energy storage unit is a self-contained, hermetically sealed, package that features a light-weight composite material flywheel and a high-power density electrical input/output machine. The ESU was designed for a vehicular application.

INTRODUCTION

The need to reduce dependence on petroleum sources for energy generation has created a substantial interest in the investigation and development of energy storage devices. The flywheel energy storage unit can provide substantial benefits to transportation propulsion systems. The flywheel can supply high power demands and thereby provide a method for load leveling the primary energy supply. This energy supply can be an electrochemical battery or a liquid-fueled heat engine power converter. In addition, the flywheel can accept vehicle kinetic energy during braking (regeneration) at a rate limited only by the transmission power capability. This method of vehicle energy storage can also be applied to third rail, electrically-powered vehicles, or station-charged electrically-powered vehicles.

The LLL/AiResearch flywheel energy storage unit (ESU) technology development program was initiated to demonstrate the advanced state-of-the-art in flywheel ESU technology and to provide actual hardware that is suitable for integration into a vehicular propulsion system. The availability of the hardware will allow the benefits of flywheel mechanical energy storage (MES) to be assessed in an operational environment.

PROGRAM GOALS

The program was established with two goals in mind:

- To design and build an advanced state-of-the-art flywheel ESU that represents a step increase in technology and provides a baseline standard of performance, and
- To configure the ESU such that it may serve as a test bed for demonstration and evaluation of other flywheel concepts.

The current state-of-the-art ESU technology for a unit with a total energy storage capacity of 250 Whr is 1.1 Whr/lb (Fig. 1). The specific energy goal for this program's unit is 3.0 Whr/lb. It is evident that as the amount of stored energy increases for a fixed power output, the specific energy of the ESU will increase (Fig. 1).

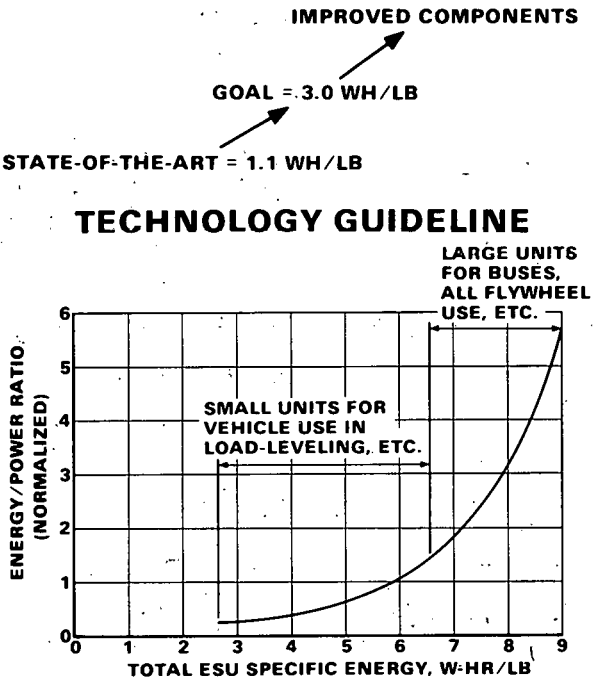

Fig. 1. Program Goal and Technology Guideline

ESU DESIGN APPLICATION

The maximum benefits that may be gained by the incorporation of mechanical energy storage (MES) into vehicular propulsion systems are obtained by combining the concepts of load-leveling the prime source(s) and recovering vehicle kinetic energy by regeneration. These benefits are inutitively achievable and large, and have been indirectly demonstrated in past programs. There has been extensive analytical work done to configure and evaluate vehicles with hybrid heat-engine propulsion arrangements. These evaluations have covered a spectrum of vehicles from a 40-ft bus to a 4-passenger commuter car.

A flywheel MES/heat-engine hybrid propulsion system was designed for a 1985 family sedan that incorporates the LLL/AiResearch ESU, (Fig. 2). The sedan has a curb weight of 3000 lbs and is equipped with a transverse-mounted 1.5-liter spark-ignition heat engine. The flywheel/heat engine hybrid propulsion system shown in this figure provides the sedan with transient performance that is normally associated with vehicles equipped with large V-8 engines. The fuel economy of the sedan over the Federal urban driving cycle (FUDC) is predicted to be 40 mpg.

ESU DESIGN APPLICATION

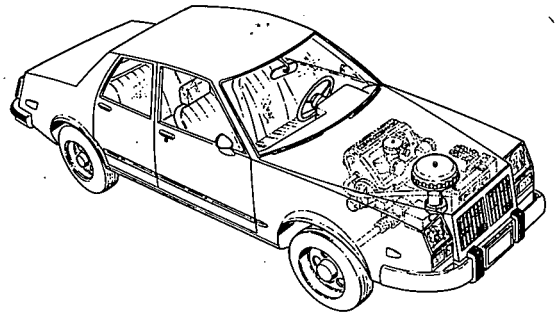

SALIENT FEATURES
- 1985 FAMILY SEDAN
- 3600 LB. TEST WEIGHT
- 1.5L ICE (GASOLINE)
- 0.250 KWHR FLYWHEEL
- 40 MPG (FUDC)
- 0-60 MPH 13 SECONDS

Fig. 2. ESU Design Application (Vehicular Use)

A summary of the ESU program scope is shown in Fig. 3. The four major tasks are identified and their relative time phasing depicted. The 19-month program was initiated May 1, 1978 and is scheduled to be complete November 30, 1979. The purpose of Task 1, Design Tradeoffs, was to determine the best flywheel/electrical input-output machine/ bearings/lubrication/and vacuum system combination such that the resulting ESU assembly meets the program goals and design criteria that was established for the vehicular application. Task 4, Testing and Evaluation, is currently in progress and is scheduled to be complete within the identified 9-month period.

PROGRAM SCOPE

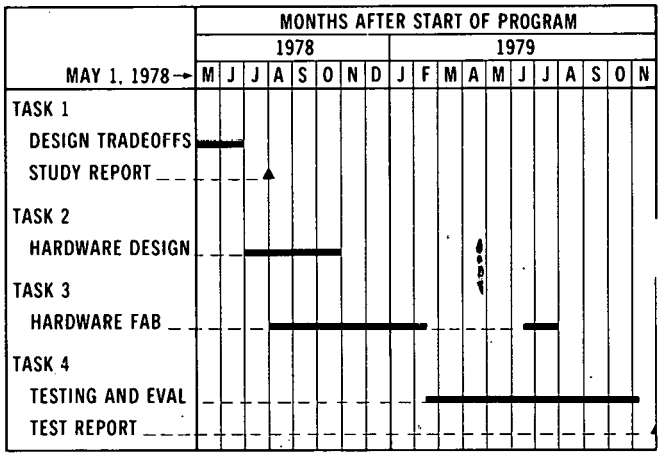

Fig. 3. Program Scope

TRADEOFF RESULTS

The major tradeoffs were performed for the flywheel and the electrical machine.

FLYWHEEL TRADEOFFS

The flywheel tradeoffs considered weight, speed, material, and containment. Two materials were included, Kevlar and S-glass. The rim velocity limits were 2500 fps and 2200 fps, respectively.

The weight shown on Fig. 4 includes rotor, containment, molecular pump, and flywheel housing. This weight is plotted against flywheel diameter and reaches a minimum at 42,000 rpm for the S-glass 12 inch diameter configuration. However, Kevlar was chosen as the rim material because of the experience derived by development work on composite flywheel rotors for the Department of Energy Near Term Electric Vehicle program. The weight difference between the two materials is minor and the program risk was minimized.

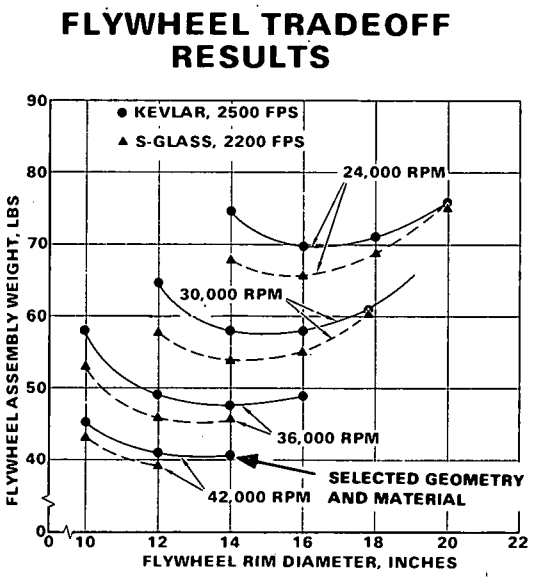

Fig. 4. Flywheel Tradeoffs

ELECTRICAL INPUT/OUTPUT MACHINE TRADEOFFS

Five types of machines were parametrically designed in terms of weight, speed range, and part power efficiencies. They are identified in Fig. 5. Each machine's best weight, which corresponds to its weight at the indicated speed, is listed along with its characteristic efficiency. The upper limit on speed was established based on mechanical constraints (vibratory and strength) in terms of rotor length/diameter ratio and tip speed.

The induction machine was determined to be the most compatible with the composite flywheel technology in the energy level of interest. The composite flywheel/induction machine combination results in a minimum weight ESU. The induction machine is also the least costly of the candidates to produce in quantity.

ELECTRICAL MACHINE TRADEOFF RESULTS

MACHINE TYPE	BEST WEIGHT LB.	100% SPEED RPM	CHARACTERISTIC EFFICIENCY %
SALIENT POLE SYNCHRONOUS	28.5	25,000	89
ROUND ROTOR SYNCHRONOUS	23	36,000	83
INDUCTION	16	42,000	92
HOMOPOLAR INDUCTOR	25	60,000	89
IRONLESS PERMANENT MAGNET	NO SOLUTION	<14,000	

SELECTED MACHINE

Fig. 5. Electrical Machine Tradeoffs

FLYWHEEL ESU DESIGN DESCRIPTION

A full cross-section isometric view of the hermetically sealed ESU is shown in Fig. 6. The transfer of energy in and out of the unit is accomplished by the electrical induction machine that is coupled directly to the composite flywheel.

The slip control method used to modulate the power is based on comparing electrical machine speed, inverter frequency, and commanded power. The machine speed is provided by a digital sensor that uses a six-tooth pickup and is mounted within the ESU.

The ESU design utilizes a dual-pressure chamber concept wherein the flywheel cavity is maintained near 1-micron (at maximum speed) during operation while the remainder of the unit is pressurized to 1 to 2-torr. This pressure differential is provided by the molecular pump. When the unit is at rest, the internal pressure in both cavities equalizes at approximately 1-torr.

The ESU has a self-contained lubrication and cooling system that includes a lube/coolant pump. The cooling system interfaces with an external heat exchanger through ports contained in the ESU main housing.

The ESU is mounted through four shock/vibration isolators. The isolators have two primary functions: (1) to isolate the unit from low frequency external disturbances that will be encountered when used in a vehicular application, and (2) to acoustically decouple the unit from supporting structure to which it may be mounted. The isolators have natural frequencies between 12 and 14 Hz in the lateral mode.

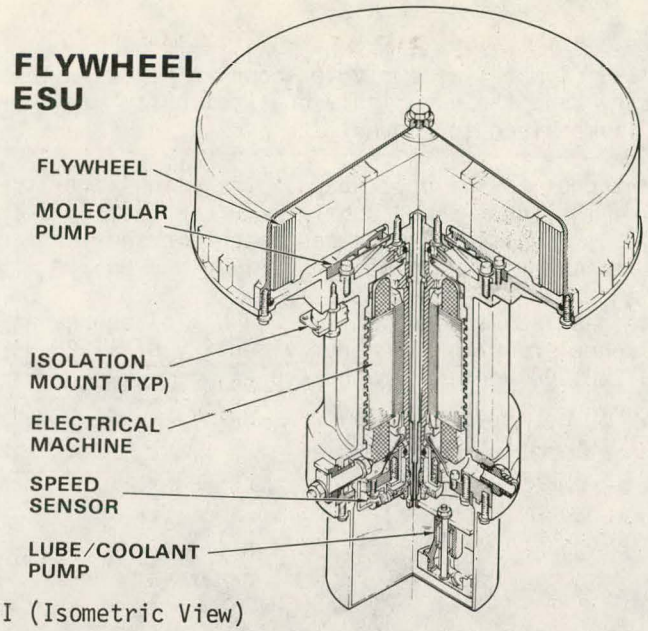

Fig. 6. Flywheel ESI (Isometric View)

FLYWHEEL ENERGY STORAGE UNIT

A photograph of the hermetically sealed flywheel ESU assembly is shown in Fig. 7. The unit is 19.3 in. high and has a maximum diameter of 15.1 in. The upper cover/containment vessel is made of steel, and the main housing and lower cover/sump are made of aluminum. The three electrical power connectors are visible in the photograph, as well as the multi-pin connector that is used for instrumentation.

The electrical input/output machine maximum power transfer is 45 kW which is available at all operating speeds between 21,000 and 42,000 rpm.

The total weight of the ESU is 79 lb. This weight corresponds to a total ESU specific energy of 3.16 W-hr/lb and a specific power of 569 W/lb. The ESU specific energy exceeds the LLL/AiResearch program advanced state-of-the-art goal of 3.00 W-hr/lb. It is estimated that the unit will have a maximum quiescent loss 205 W.

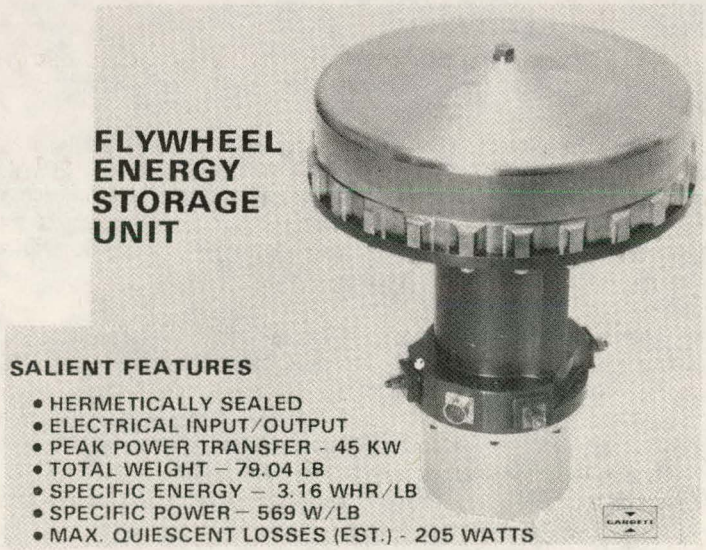

Fig. 7. Advanced State-of-the-Art Flywheel ESU

FLYWHEEL ASSEMBLY

A photograph of the ESU flywheel assembly is shown in Fig. 8. The six-bolt attachment method, the hub geometry, and the nine individual composite rings are visible in the figure. The hub geometry is machined to approximate a constant stress configuration.

The flywheel rotor attaches to the upper end of the main shaft assembly by means of six high-strength bolts. The four-spoked hub is machined from 7075-T7351 aluminum alloy plate. The flywheel rim is composed of nine concentric annular rings of circumferentially wrapped composite material consisting of fiber and epoxy.

The flywheel rotor weighs 14.5 lbs and stores 250 Whr of energy at a peripheral speed of 2500 fps. The flywheel rotor has an energy density of 17.25 Whr/lb, and a design cycle life of greater than 100,000 deep discharge cycles.

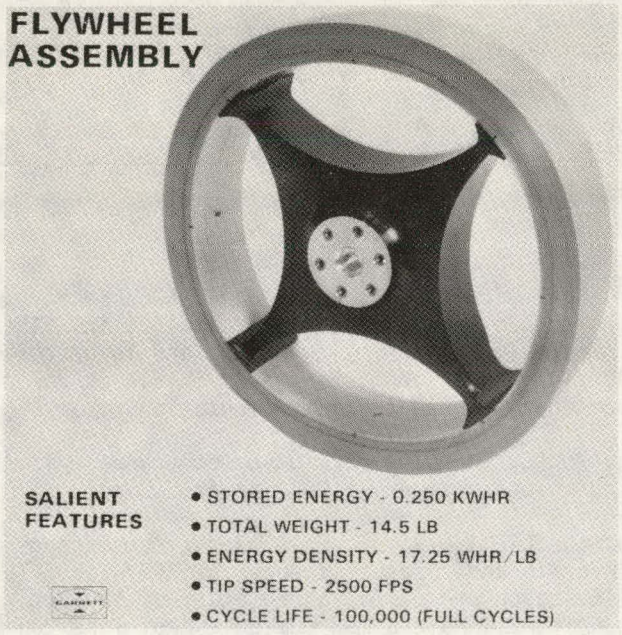

Fig. 8. Flywheel Assembly

FLYWHEEL CONSTRUCTION FEATURES

The flywheel construction features are shown in Fig. 9. The assembly has an overall diameter of 13.70 in., and a hub diameter of 11.44 in., with a radius ratio of 0.835. The composite rim is made up of nine concentric rings with a total thickness of 1.13 in. and a width of 2.70 in. The innermost ring is made of S-2 glass/epoxy. The use of nine separate rings reduces the bending stresses in the rings caused by flexing during rotational speed changes and prevents ring delamination.

The method of attaching the rim to the hub provides a positive load path under all operating conditions. Attaching the two components is accomplished by distorting the circular rim into a semi-rectangular shape and slipping it onto the hub. The rim is held upon the hub by the residual forces in the rim as it tries to become circular again. These residual forces are controlled by the relationship between the hub spokes outside diameter and the rim inside diameter. The hub OD is always greater than the rim ID. The wound concentric ring design utilizes the composite fibers in nearly uniaxal tension.

A continuous operating temperature limit of 175°F is established for the flywheel by the strength-temperature characteristic of the epoxy matrix material.

In this design, the hub stores 20 percent of the energy, which is a relatively large percentage. The remaining 80 percent is stored in the composite rim.

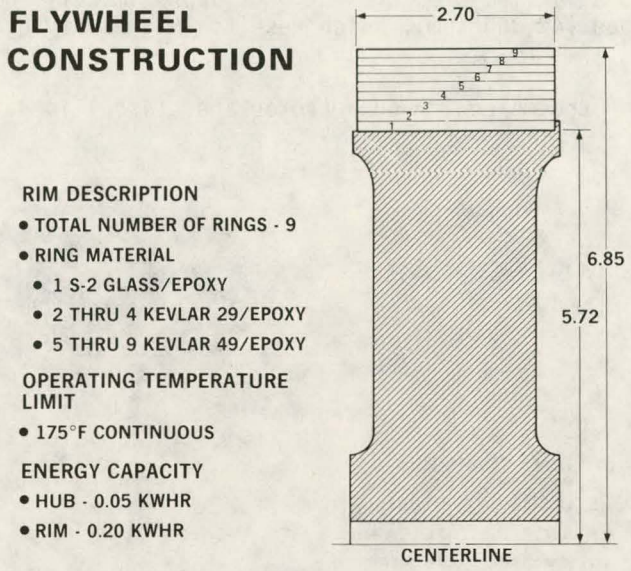

Fig. 9. Flywheel Construction Features

ESU ELECTRICAL MACHINE

A photograph of the ESU electrical machine components (rotor and stator) is shown in Fig. 10. The machine is a 3-phase, 2-pole, induction device that is 4.80 in. long and 4.51 in. in diameter. It has a maximum operational tip speed of 423 fps, a peak efficiency of 93 percent, and a total weight of 19.84 lb. The machine is designed for continuous operation over a duty cycle based on the SAE J227 (A) schedule D driving cycle. It is optimized to operate between 21,000 and 42,000 rpm with corresponding line-to-neutral voltages varying between approximately 44 and 58 v. These voltage levels are compatible with a 180-vdc battery pack.

Fig. 10. Electrical Machine's Components and Features

MOLECULAR PUMP

A photograph of the molecular pump components (rotor and stator) is shown in Fig. 11. The pump is used to provide a very high vacuum level in the flywheel cavity during ESU operation to minimize the aerodynamic losses. When the flywheel is at rest, the ESU internal ambient pressure is approximately 1-torr. As the flywheel speed is increased, the molecular pump begins to evacuate the flywheel cavity. At one-half flywheel speed the pressure ratio across the pump is approximately 20:1, which translates to a cavity pressure of 50-microns. A maximum pressure ratio of approximately 700:1 is reached at 100 percent flywheel speed (42,000 rpm), which results in a cavity pressure of 1.4-microns.

The total weight of the molecular pump (rotor and stator) is 3.7 lb.

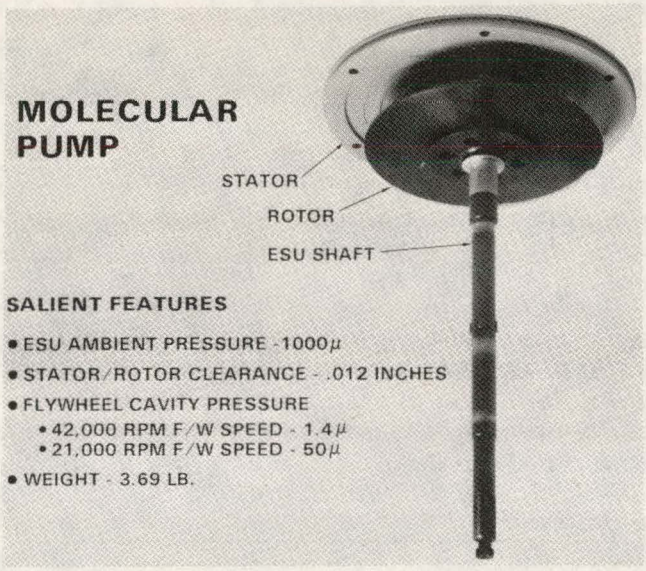

Fig. 11. Molecular Pump Components and Features

LUBE/COOLANT PUMP

A photograph of the unit's lube/coolant pump assembly is shown in Fig. 12. The pump assembly is mounted to the bulkhead, which also contains the lower bearing support. Thus, the pump can be installed and mechanically checked (gear alignment, backlash, etc.) prior to installation of the oil pump cover. The pump is driven by a pinion gear that is machined directly on the end of the ESU main shaft.

The gear ratio is 7 to 1, which provides a design speed range of 3000 to 6000 rpm for the pump. The pump is an unshrouded centrifugal type that provides a minimum flow of 1 gpm at a speed of 3000 rpm. The pump operates with an inlet head of 1-in. of oil. The lube/coolant fluid is a phosphate ester, tradenamed Fyrquel 150, that was selected because of its low vapor pressure, good lubricity, low viscosity, and chemical stability. The fluid operating temperature will be held between 180^{o} and 200^{o}F. The maximum power consumption of the lube/coolant pump assembly is 35 watts. It weighs 1.40 lb.

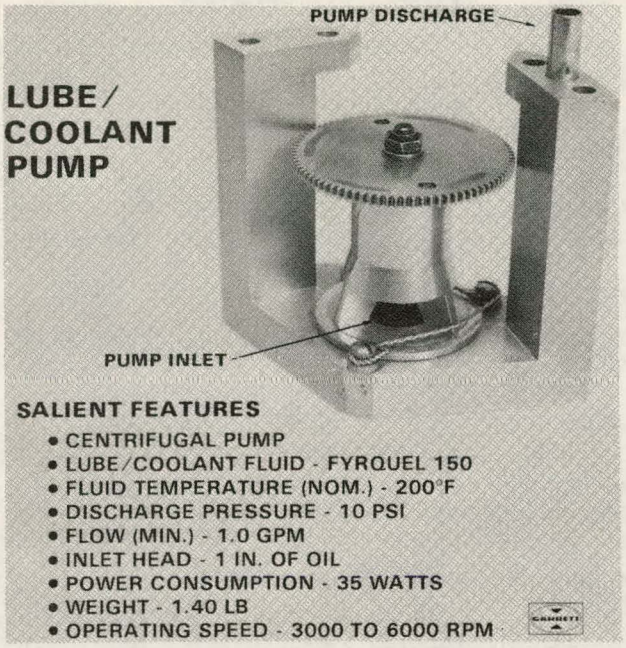

Fig. 12. Lubrication/Coolant Pump Assembly

TESTING AND EVALUATION TASKS

The total ESU test effort is divided into three main subdivisions: (1) performance tests, (2) proof of design, and (3) environmental (Fig. 13). The definition and purpose for each test task are discussed in the following paragraphs.

The purpose of the performance tests is to determine the spin-down losses of the ESU. The procedure for determining the losses is a step-by-step series of tests to assess the loss contribution of each component. When the electrical input-output machine is in the standby mode, the remaining losses are defined as the spindown losses. These losses include flywheel windage, bearing friction, molecular vacuum pump, and the lubrication pump losses. These losses are primarily caused by viscous drag forces of the related gas or liquid in contact with the rotating surfaces. The drag forces are a function of the viscosity or the quantity of the fluid or gas molecules at the surface of the affected part. For this reason, the flywheel chamber will be maintained at a substantially reduced pressure, and the oil temperature will be regulated to obtain low drag torque.

The proof-of-design tests are performed to demonstrate the general operational feasibility of the unit and to assess its basic characteristics (such as vacuum level, internal vibration, noise and heat generation, and input/output efficiency). This information also will serve as a norm for evaluation of changes in performance under externally imposed vibration and maneuvering loads, or elevated temperature.

The environmental tests will provide information on the sensitivity of the ESU to various externally imposed conditions, including external vibration, maneuvering, and temperature. During all testing, the vacuum stability will be monitored and evaluated. The approach used during environmental testing will be to continue to increase the test conditions without destroying the unit or exceeding the maximum established values.

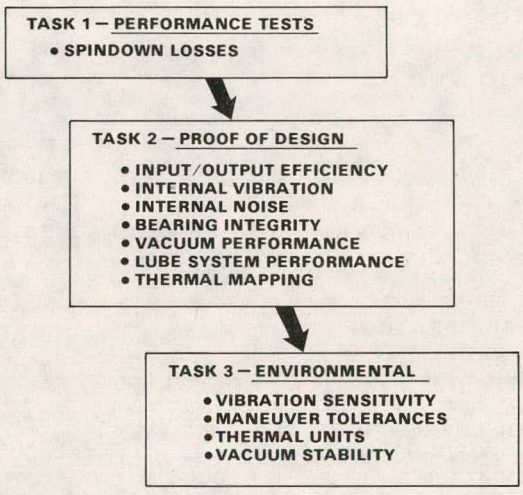

Fig. 13. Testing and Evaluation Tasks

PERFORMANCE TESTS LABORATORY SETUP

A photograph of the laboratory setup for the ESU performance tests is shown in Fig. 14. The test specimen is shown mounted on the dc motor drive test rig. The torque head is also visible. The test console is shown to the left of the test unit. The performance tests are currently in process.

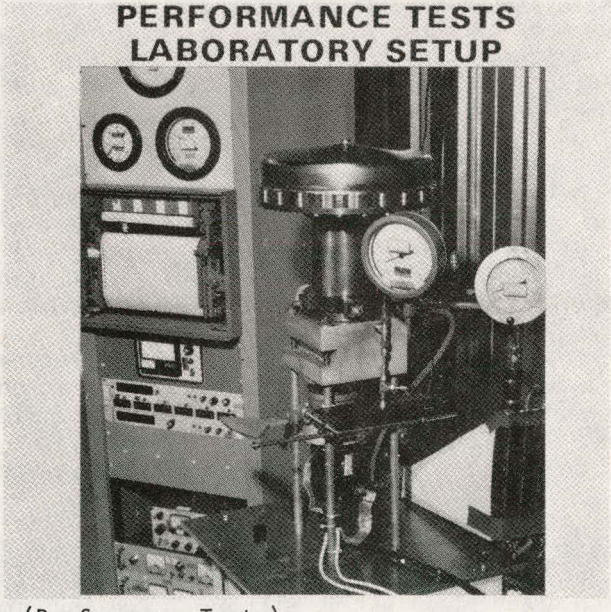

Fig. 14. Laboratory Setup (Performance Tests)

TESTING AND EVALUATION SUMMARY

The development testing status, problems encountered, and planned corrective actions are discussed in the following paragraphs.

TESTING STATUS

The maximum lube/coolant pump power was determined to be 35 W. This is the first of the performance tests.

The variable frequency, variable voltage electrical power drive is in place and operational.

The electronic controller, which is used to automatically control the ESU, has been checked-out in the system.

PROBLEMS ENCOUNTERED

Several problems have been encountered during the five months of development testing that have been completed. The major effort has been expended trying to trim balance (at speed) the ESU rotating group. During the balancing process it was determined that the molecular pump was not performing to specification, i.e., the minimum flywheel cavity chamber pressure attained was 40-microns at 40,000 rpm.

The successful balancing of the unit was nearly completed when the motor rotor failed during test.

A failure investigation determined that 2 to 3 bars of the cast copper rotor had failed due to casting porosity. The machine's rotor and stator shorted and were destroyed.

CORRECTIVE ACTION

The molecular pump stator geometry was changed from 4-lands and grooves to 3. This was done to reduce the leakage between grooves by increasing the land width. Proof of design tests will be performed on the new stator to verify the design.

Prior to motor failure, it was determined that the ESU had a moment unbalance. This type of unbalance is difficult to isolate with displacement probes only at the upper end of the rotating group. An additional probe will be attached at the lower end of the rotating group to aid in trim balancing during test.

A backup electrical machine rotor and stator were manufactured and are available. The rotor was fabricated, instead of cast, using extruded zirconium-copper material. This results in a higher strength rotor that is free of porosity. The rotor will be hot-spin tested in a pit to verify its mechanical integrity prior to being assembled into the ESU.

THIS PAGE

WAS INTENTIONALLY

LEFT BLANK

PROJECT SUMMARY

Project Title:	"Flywheel-Engine Powerplant Research and Development Studies"
Principal Investigators:	Norman H. Beachley and Andrew A. Frank
Organization:	College of Engineering University of Wisconsin-Madison 1513 University Avenue Madison, WI 53706
Project Goals:	The basic objective is to provide a design analysis of a flywheel-engine power unit for a passenger automobile. The detailed tasks are (1) evaluate the potential of alternative powerplants for use with flywheel, (2) determine the lower level of friction that may be practically achieved in driveline components, (3) determine the most promising continuously variable transmission (CVT) concept for a 2nd generation flywheel vehicle, (4) design safety features for the flywheel system, (5) prepare a preliminary layout drawing of the complete flywheel powerplant system suitable for installation in a production automobile chassis.
Project Status:	A preliminary study of alternative heat engine powerplants (Stirling, gas turbine, diesel piston, and gasoline piston engines) has been performed to determine their relative fuel mileage potentials. Other practical aspects still need to be investigated, such as the effect on engine efficiency and life of an on-off mode of operation. Three continuously-variable transmission concepts have been identified as having efficiency, size, and weight characteristics satisfactory for a second generation experimental flywheel car. Preliminary design configurations have been developed based on these three principles, and design work is being continued with the goal of further simplification and reduction of friction losses. Basic packaging configurations have been determined that will permit the flywheel powerplant systems (for each of the three chosen CVT concepts) to fit in the engine compartment of a conventional front wheel drive automobile. There is still much work to be done, however, on the details of mounting and interconnecting the various powerplant components. Considerable information on the friction characteristics of bearings and gears has been collected that will aid in system efficiency calculations, and also in the determination of what fuel economy improvements might be obtained by attention to and optimization of these components in the driveline.
Contract Number:	SUBCONTRACT 4492309
Contracting Period:	Feb. 5, 1979-Dec. 31, 1979
Funding Level:	$93,286.00
Funding Source:	Lawrence Livermore Laboratory

COMPARISON OF ALTERNATIVE HEAT ENGINES FOR FLYWHEEL MECHANICAL TRANSMISSION AUTOMOBILES

Andrew A. Frank and Norman H. Beachley
University of Wisconsin-Madison

ABSTRACT

The feasibility of various heat engines to be used with a flywheel-transmission are investigated. Four possibilities are considered: (1) gas turbine; (2) Stirling engine; (3) gasoline piston engine; and (4) diesel piston engine. These four heat engines are studied to assess their fuel economy capability with one specific flywheel-transmission combination. Their relative fuel economies are compared for engines unmodified from present design.

Design changes possible with each engine are further explored. These changes would improve efficiency, save weight, simplify and reduce the cost of the engine.

The preliminary simulations for the EPA-CVS Federal Urban Driving Cycle (FUDC) with a 3,000 lb. vehicle show the following mpg values (gasoline equivalent) based on engine maps available in the literature: 1) Turbine - 47.9 mpg; 2) Stirling - 51.3 mpg; 3) Gasoline - 41.2 mps; and 4) Diesel - 41.2 mpg. Project improvements are discussed.

INTRODUCTION

The objective of this effort is to investigate via simulation[1] how the flywheel-transmission system can be adapted to existing and future prime movers and to explore prime mover modification to take full advantage of the flywheel transmission concept. The study takes into account a flywheel transmission vehicle with parameters assumed to be (1) vehicle weight 3000 lbs., (2) flywheel size from .3 to .5 hp hrs., (3) flywheel transmission requiring 8640 hp-sec to drive the EPA FUDC[2]. This amount of energy implies an average continually variable transmission efficiency of 77% over the FUDC, and (4) an engine assumed to operate at its best efficiency while producing 60 hp. Thus some prime movers will have a maximum hp of as much as 170 hp while other prime movers will have a maximum hp of 60 hp. The maximum hp available from a prime mover is dependent upon where the best efficiency occurs with respect to maximum power.

The implication of these assumptions are that there will be four charges for the EPA-FUDC when using the University of Wisconsin "on-off" principle. The prime mover will be "on" 30-60 sec depending upon its characteristics. With "on-off" operation there are various simplifications to the prime mover that can be made. Each prime mover type has its own characteristic which can be taken advantage of due to this narrow operating range requirement. Figure 1 illustrates the engine operation characteristics for a "high performance" standard transmission conventional gasoline vehicle over the EPA-FUDC. Figure 2 shows the influence of lower performance. It should be noted that the lower performance vehicle has more of the efficient islands of the prime mover covered by the driving cycle. Thus the lower the performance the better the fuel economy in a standard transmission vehicle. The flywheel transmission on the other hand allows the engine to operate at its best efficiency or not at all and over a narrow speed range. This is shown in Fig. 3. Since the flywheel supplies the power for high acceleration the vehicle performance is less sensitive to engine size. Thus a flywheel transmission vehicle with either a 30 hp or 60 hp engine will have identical 0 to 60 MPH acceleration times. The difference of course is how long it takes to charge the flywheel when it runs down and how fast the vehicle can climb a given constant grade lasting more than a mile or so. Further, the power available from a flywheel transmission is restricted only by the size of the transmission components, thus a 30 hp prime mover can have the performance of 250 or more hp due to the flywheel.

Various prime mover types are examined, they are the Brayton cycle or "gas turbine", the Stirling engine, the gasoline piston engine and the diesel engine. Comparing their relative efficiencies at part load, we find that the turbine is poor, the Stirling is better but still not too good (there are improvements in Stirlings which are projected to give better, values [3]), the gasoline engine is better, and finally the diesel engine is best, i.e., has the broadest efficient operating characteristics (See Fig. 4). The flywheel transmission system, however, does not require the prime mover to have good efficiency except at maximum torque and over a 2 to 1 speed range. Normal speed range for a prime mover in a standard transmission vehicle is at least 5 to 1, while the torque must be modulated from maximum through 0. Therefore in a flywheel transmission vehicle a prime mover can be greatly simplified.

SOME IMPLICATIONS OF FLYWHEEL DRIVE TRANSMISSION SYSTEMS

"On-off" engine operation implies that special care must be taken in engine design. Heat control is necessary since if during the few minutes of "off" it is allowed to cool, energy is lost and therefore must be resupplied to the system by fuel in order to bring the engine back up to proper operating temperature. Start-stop bearing wear is another potential problem with on-off operation which must be taken into account. Loss of the fluid film in hydrodynamic bearings might result in high wear in on-off operation. The cooling system should be redesigned for the narrow operating range, etc.

Since the engine operates only at maximum torque, one of the advantages of the "on-off" system is that it does not require an operating control system. Most standard prime movers require a great amount of design effort in making the engine controllable at part load. Since there is no part load requirement, a turbine can operate only at the maximum torque condition; a Stirling can operate with fixed geometry and fixed gas pressure; the gasoline engine can have a fuel carburetion or injection system which does not have to be modulated for power (because this particular engine does not have to idle, and because items such as valve train design, cylinder head shape, etc., can be designed for optimum conditions). Diesel engine controls can be greatly simplified since the fuel injection system no longer has to have a variable stroke. The engine can be tuned for optimum fuel efficiency and will not have to be adjusted for varying loads since the load is fixed.

Idle fuel flow rates in present prime movers relative to each other form the following order: the turbine is the highest, the Stirling next, the gasoline engine next with the best or lowest being the diesel engine. However, the turbine and Stirline engines have the most to gain from flywheel transmissions without idle requirements because these engines have high fuel consumptions in idle. With all accessories driven off the flywheel, engine idle has no useful purpose. Note also that accessories are being driven with the best fuel efficiency that can be produced by the particular engine.

ENGINE DESIGN OBJECTIVES

In line with the above discussion the engine for a flywheel transmission system should be designed with the following factors in mind: (1) minimum flexibility and only maximum torque operation, (2) minimized internal friction at wide open throttle only, (3) minimized heat loss during the "off" condition, (4) optimized induction system, (5) optimized combustion, (6) exhaust system tuned for fixed conditions, (7) optimum exhaust gas recirculation for emission controls (if required) set for this single operating condition.

It should be pointed out that best efficiency for an engine occurs somewhere between 1/4 to full power. Where the best efficiency for a particular prime mover occurs is dependent upon many factors. In a gas turbine, for example, best efficiency may occur at maximum power. On the other hand for a gasoline piston engine best efficiency normally occurs somewhere between 1/4 and 1/3 of maximum power. For example a conventionally rated gasoline piston engine of 87 hp has its best efficiency of approximately .455 lbs. of gasoline per hp-hr at approximately 28 to 30 hp. Therefore if a flywheel drive system requires a 30 hp gasoline engine, it must be obtained from an engine with the displacement equivalent to a conventional engine currently producing 87 hp.

SPECIFIC ENGINE STUDIES

TURBINE

A gas turbine-flywheel transmission system was studied using a standard two shaft turbine by General Motors, model GT-404-3. This turbine was scaled and compared with a Volkswagen diesel and a Honda CVCC gasoline engine. All engines were scaled for maximum efficiency at 60 hp. Note, because of the characteristics of these individual engines, the peak hp in the piston engines are much higher than the turbine. Thus the scaled Honda CVCC has a peak hp of 178 hp, the Volkswagen diesel a peak of 97 hp while the turbine has a peak of 60 hp. It is assumed that these engines can be scaled without affecting brake specific fuel consumption. This may not be accurate for a turbine since it is size sensitive. Further, the numbers that we are using are for an advanced turbine, that is, a paper turbine (not currently existing). On the other hand since this particular turbine with the flywheel must operate over an extremely narrow range and does not have to be designed for flexibility, it may be possible to design it in such a way that the peak efficiency is easily obtained. Using the turbine characteristics published in (4) the turbine operates between 54 and 60 hp. This range compares with the piston engine characteristic which allow operation between 30 and 60 hp. The piston engine characteristics are from (5,6).

Comparing the turbine average brake specific fuel consumption we find that the turbine on the average is creating energy at .411 lbs. of fuel per hp/hr vs. .463 for a gasoline piston and .425 for a diesel. The simulated EPA-FUDC fuel economy during city driving in a turbine flywheel vehicle is 46.5 MPG on JP4 or 47.9 MPG on "gasoline equivalent", for the diesel it is 45.25 for No. 2 diesel or 41.1 MPG on gasoline equivalent, and for the gasoline vehicle it is 41.1 MPG. The "gasoline equivalent" for the turbine and deisel were made based upon the heating values of the different fuels.

Design considerations for a turbine to be coupled with a flywheel transmission imply a number of factors. One of the first factors to be considered is whether or not a multishaft turbine is required. Since the flywheel is a high speed rotating device it is possible to have a single shaft high temperature turbine with a maximum power around 75 to 80 hp. In order to maintain high efficiency for this low power rating tight aerodynamic tolerances must be maintained and a trade off between air bearings or ball bearings for tolerance maintenance needs to be considered. Air bearings may be used for a high speed turbine-flywheel system, while ball bearings could be used if the turbine-flywheel system operated at a lower speed. Higher speed turbines may operate at speeds around 80,000 RPM while the low speed turbine may operate at speeds around 30,000 RPM. Because of the small size of these turbines, ceramic materials could be used to accommodate much higher operating temperatures.

According to Fig. 5 it may be advantageous to use a multistage power turbine because of the constant load operation, thereby maximizing the kinetic energy extraction for the best possible efficiency. Notice in this figure that a series of system cut-off valves is shown to create a partial vacuum to minimize spin losses when the engine is "off". Further this partial vacuum would help retain the heat within the operating parts of the system. Insulation is still necessary on the outside portions of the turbine in such places as the combustors, etc. Insulated or heat dissipating mechanisms on the main shaft would allow the use of low temperature bearings and lubrication. An optimized design should produce a minimum brake specific fuel consumption around .38 for a mileage of approximately 51.8 MPG gasoline equivalent.

STIRLING

A Ford/Phillips 95 hp and a United Stirling A,B 170 hp engine were studied (5,7). The Ford/Phillips engine was studied in a standard 4-speed manual transmission vehicle with 3,000 lb. inertia weight. This achieved a fuel economy of 29.99 with an average efficiency of 19.68% over the EPA-FUDC city cycle. A United Stirling engine installed in the same vehicle would achieve 31.9. These figures compare with a production of 90 hp vehicle mileage of 24. A flywheel Stirling system would have an engine operating range dependent upon the particular engine characteristics. For example the Ford/Stirling engine would operate between 1350 and

2700 and between 20 and 60 hp, whereas a United Stirling engine would operate between 570 and 1140 and between 31 and 60 hp. The average brake specific fuel consumption for the Ford engine would be .396 and the United Stirling engine .372. The associated Flywheel-Stirling city fuel economy would be 48.1 MPG for the Ford and 51.3 with the United Stirling. The United Stirling highway mileage at a constant 60 would be approximately 42.8. It should be noted that the United Stirling engine obtains better fuel economy in the city than in the highway. It has been claimed by United Stirling that a variable stroke version of their engine can obtain 42 on a combined cycle at a 3500 lb. inertia weight (3). This would translate to an even higher city mileage at 3000 lb. inertia weight. This variable stroke mechanism provides characteristics similar to a continuously variable transmission (CVT) except that it is incorporated within the engine itself.

The advantages of a flywheel drive Stirling system over the variable stroke Stirling are (1) higher mileage is possible in the city due to generative braking; (2) the Stirling engine internal design is simplified by the requirement of a constant load, no idle, and a limited speed operating range; (3) the flywheel-transmission replaces the torque converter transmission which is still required with a variable stroke Stirling; and (4) there is a control system simplification due to a torque controlled continuously variable transmission rather than a controlled engine stroke. This controlled engine stroke requires hydraulic energy and is a rather sensitive mechanism.

Due to the limited range of operation of the Stirling-flywheel system optimum burners, heat exchangers, regenerators, etc. can be choosen. Finally, it is felt that lower brake specific fuel consumption can be obtained because of the possibility of optimum sizing of all components, fewer engine peripheral equipment controls, and the possibility of lowering internal engine friction because of the simpler mechanism and geometry. A Stirling engine designed specifically for use with a flywheel should produce a minimum brake specific fuel consumption of around .35, giving a fuel economy of around 54.5 for the FUDC.

GASOLINE PISTON ENGINE

A gasoline piston engine in a 3,000 lb. present day vehicle apparently can obtain a city fuel economy of about 24 and about 35 at a constant highway cruise speed of 60. If the engine is unmodified and installed into a flywheel vehicle, the expected city fuel economy is between 41 and 48 depending upon the particular transmission used. We will now examine the potential of a flywheel-transmission vehicle with the piston engine designed from the ground up. First the requirement for the engine speed range is approximately 2 to 1. It could be between 1000 and 2000 RPM. The torque range would only be the maximum torque, the operating time would be from 30 seconds "on" and 2 minutes to 5 minutes "off" to continuous operation. Conservation of heat in the "off" condition is an important feature.

With these requirements, designs for a piston gasoline engine should concentrate on reducing parasitic or internal friction losses. This could be accomplished by reducing the size of the water cooling system, minimizing camshaft friction by using either pressure operated poppets or a resonant valve system, optimum bearings, minimized piston scrubbing, lower oil churning, etc.

The fuel and combustion systems can also be greatly simplified since only maximum fuel delivery is required; therefore, no manifold vacuum need contend with such problems as manifold wetting, etc. For example, it may be possible to use a constant flow fuel injection system at the intake ports. Better combustion characteristics due to factors such as high swirl at fixed load, higher compression for a given octane number, etc. could also be achieved.

A change from a four cycle system to a two cycle could further reduce the effect of engine friction by a large factor. Current two cycle engines were designed for power density and not efficiency. With a flywheel transmission system it is possible to design a two cycle engine for efficiency rather than power density and achieve BSFC values better than a four cycle engine.

It is estimated that a two stroke brake specific fuel consumption around .35 lbs. per hp-hr on gasoline is feasible, producing a mileage of about 54.3 MPG in the city and about 45.5 MPG in highway cruise at 60 MPH.

DIESEL ENGINE

The "ground up" design of a diesel flywheel system would require the same features as the gasoline engine discussed above. A simplified injector system could be used since only maximum delivery is required. Better combustion characteristics could occur since the injector angle, prechamber design, etc. could be optimized. Better combustion could also be achieved by using an optimum compression ratio on the diesel, because starting and low power "knock" would no longer be a problem. The flywheel could provide the starting power required to turn the engine over. It is further possible to use a two cycle instead of a four cycle diesel because a two cycle diesel has less effective internal friction.

The optimized design could provide a brake specific fuel consumption on the order of 0.32 lbs. per hp-hr of diesel fuel providing a city mileage of 59.6 MPG for this 3,000 lb. vehicle and a highway mileage of 49.8 MPG at a constant 60 MPH.

CONCLUSIONS

For the first time since the flywheel energy storage program has started, we have looked in some detail at the prime mover design. What we have concluded is that the prime mover can be improved in efficiency considerably over designs currently being proposed for conventional transmission vehicles. The resulting projected improvement in fuel efficiency can provide city gas mileages up to 60 MPG with highway mileages close to 50 MPG with the flywheel-transmission concept. Of course all of these mileage projections are based upon the 3,000 lb. vehicle with the road load obtained from the standard vehicle of today. With aerodynamic improvements the highway mileage can be increased substantially. Further, with lower rolling resistance tires and attention to bearing friction within the drive line from the transmission onwards it is possible to increase the city gas mileage somewhat. The existing vehicle on which all these simulations were based requires 23 hp at 60 MPH. It is clear that many researchers have achieved rolling resistances much less than the 23 hp at 60 MPH. However, this standard was used so that a valid comparison can be made. Even with this relatively poor road load characteristic it has been demonstrated that it is possible to achieve a very high fuel efficiency.

While the suggestions are easy to make on paper, each one made above would require a great deal of research. The possible gain from this research is the capability of improving the fuel efficiency from approximately 42 MPG in the city to about 60 MPG in the city for a 3,000 lb. flywheel transmission vehicle. This is approximately a 30% improvement due to redesign of the prime mover itself. Thus a combined cycle 50 MPG vehicle is possible. The long range potential fuel efficiency is great enough to warrant the investment in such an extensive program. This improvement when compared with conventional vehicles of this weight class is better than 100%.

REFERENCES

1. Le, Sanh, "A Speed-Torque Matrix Method For Analyzing Flywheel Hybrid Vehicle Performance," Master of Science Thesis, University of Wisconsin - Madison, 1978.

2. Harter, Richard, "Optimization Study of A Power Split Hydrostatic Transmission," Master of Science Thesis, University of Wisconsin - Madison, 1977.

3. Fourteenth Intersociety Energy Conversion Engineering Conference, Vol. 1.

4. Fourth International Symposium on Automotive Propulsion Systems, Fig. 14. "Design and Layout of Energy Efficient and Low Polluting Diesel Engines."

5. Fourth International Symposium Automotive Propulsion Systems. April 18-22, 1977, pp. 131-132, Vol. 1.

6. Honda Fuel Map (private correspondence with Honda Corporation).

7. Hallare, B., "The Development of 40-150 KW Stirling Engines in Sweden and Their Application in Mining Equipment, Total Energy Systems and Road Vehicles," pp. 248-268, Automotive Propulsion, Feb. 1978.

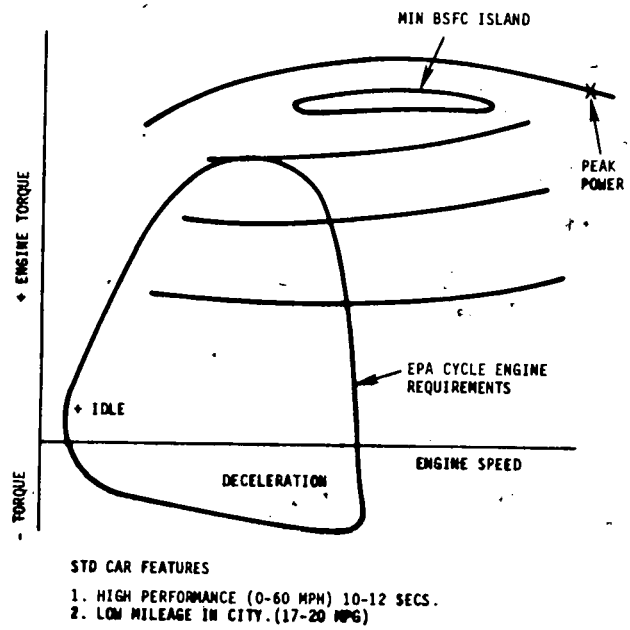

Fig. 1. Standard Transmission High Performance Vehicle Engine Requirements.

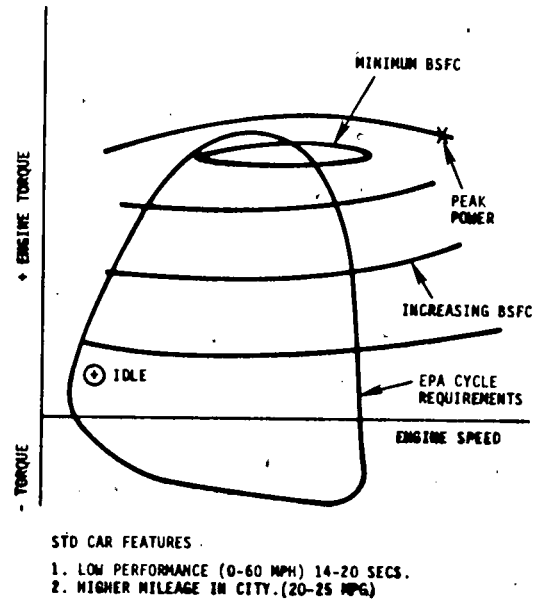

Fig. 2. Standard Transmission Low Performance Vehicle Engine Requirements.

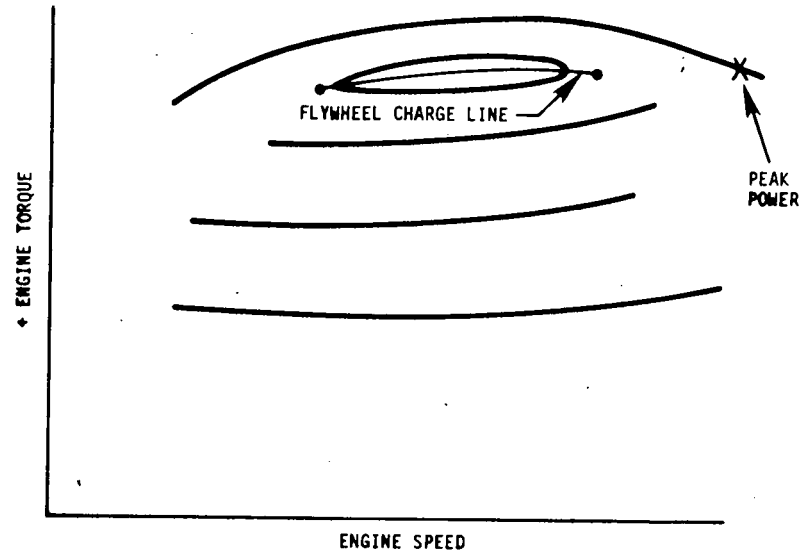

FEATURES: SPEED RANGE 2:1
TORQUE RANGE MAX ONLY ON
POWER 1/3 TO 1/2 MAX
"ON-OFF" OPERATION
DECLUTCHED WHEN "OFF"
(40-50 MPG)

Fig. 3. Flywheel Transmission Engine Operating Requirements.

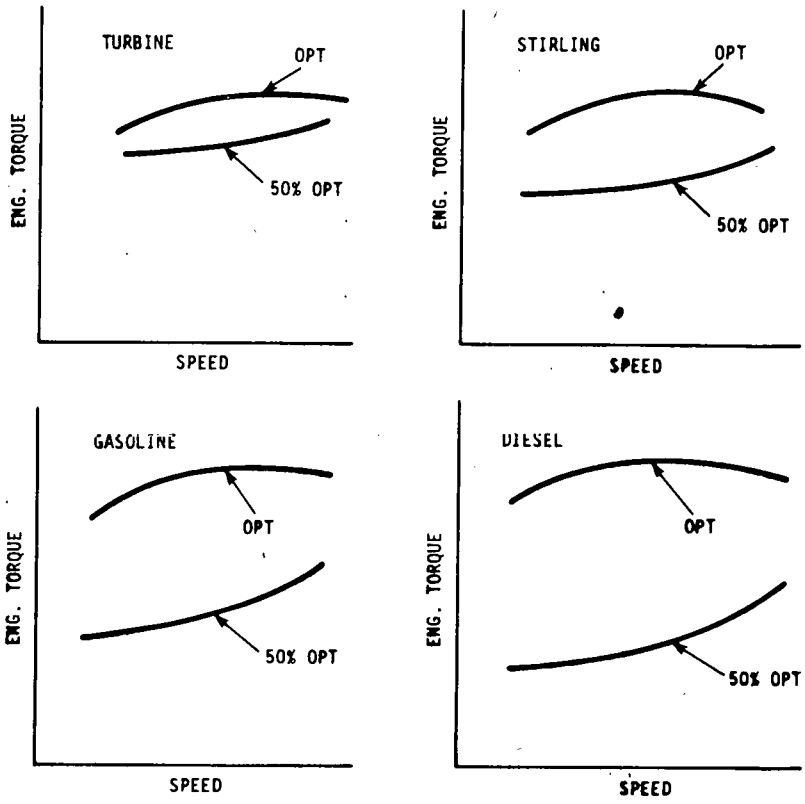

Fig. 4. Comparison of Characteristics of Various Primemovers.

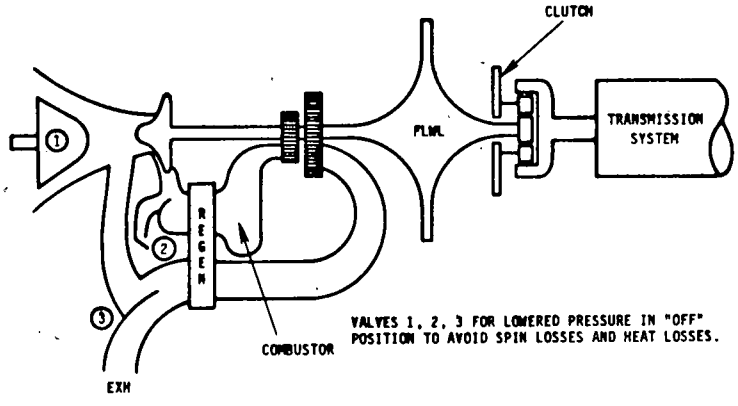

ADVANTAGES OVER STANDARD TURBINE

1. SIMPLE SINGLE SPOOL TURBINE.
2. COMBINED PRIME MOVER-FLYWHEEL SYSTEM (LIGHT WEIGHT).
3. "ON-OFF" COMBUSTION SYSTEM.
4. LOW "OFF" LOSS.
5. FLYWHEEL MECHANICAL CLUTCH SYSTEM.
6. POSSIBLE CATALYTIC REGENERATOR.

Fig. 5. Proposed Turbine Flywheel System.

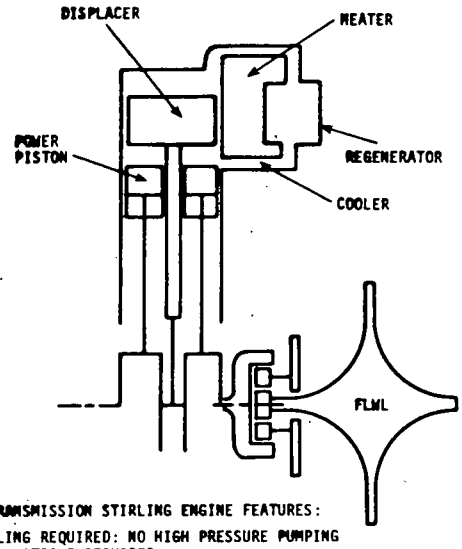

FLYWHEEL - TRANSMISSION STIRLING ENGINE FEATURES:

1. NO THROTTLING REQUIRED: NO HIGH PRESSURE PUMPING OR VARIABLE STROKE REQUIRED.
2. OPERATION ONLY AT OPTIMUM PRESSURES AND STROKES.
3. SIMPLER GEOMETRY.
4. MULTIFUEL CAPABILITY.

Fig. 6. A Possible Stirling Flywheel System.

THIS PAGE

WAS INTENTIONALLY

LEFT BLANK

APPENDICES

THIS PAGE

WAS INTENTIONALLY

LEFT BLANK

1979 MECHANICAL AND MAGNETIC ENERGY STORAGE
CONTRACTORS' REVIEW

Capital Hilton Hotel
Washington, D.C.

August 19-22, 1979

SPEAKERS AND SESSION CHAIRMEN

Mr. B. Alleman
Pacific Northwest Laboratory
P.O. Box 999
Richland, Washington 99352

Dr. L. Amstutz
U.S. Army Mobility Equipment
Research and Development
Command, Lab 3000
Ft. Belvoir, Virginia 22060

Mr. Thomas M. Barlow, Program Manager
Energy and Resource Program
Lawrence Livermore Laboratory
P.O. Box 808
Mail Stop L-209
Livermore, California 94550

Dr. Norman H. Beachley
University of Wisconsin
1513 University Avenue
Madison, Wisconsin 53706

Dr. Charles W. Bert
University of Oklahoma
School of AMNE
Normon, Oklahoma 73019

Dr. James D. Blacic
LASL
Mail Stop 978
Los Alamos, New Mexico 87545

Mr. C. A. Blomquist
Argonne National Laboratory
9700 South Cass Avenue
Argonne, Illinois 60439

Mr. B. C. Caskey
Sandia Laboratory
P.O. Box 5800 - Division 5716
Albuquerque, New Mexico 87115

Dr. George C. Chang
Division of Energy Storage Systems
U.S. Department of Energy
600 E Street, N.W.
Room 416
Washington, D.C. 20585

Mr. Alan F. Clark
National Bureau of Standards
Boulder, Colorado 80302

Mr. W. T. Crothers,
University of California
Lawrence Livermore Laboratory
P.O. Box 808, L-209
Livermore, California 94550

Mr. John Degnan
Mgr. Mechanical Development
Allis Chalmers
Box 712
York, Pennsylvania 17405

Mr. Roger Derby
Division of Energy Storage Systems
U.S. Department of Energy
600 E Street, N.W.
Washington, D.C. 20585

Mr. Henry H. Dodd
Sandia Laboratory
P.O. Box 5800
Division 5743,
Alburquerque, New Mexico 87115

Mr. T. Doherty
Pacific Northwest Laboratory
P.O. Box 999
Richland, Washington 99352

Mr. Fred R. Fickett
Physicist
National Bureau of Standards
Boulder, Colorado 80302

Dr. Arlo F. Fossum
RE/SPEC Inc.
P.O. Box 725
Rapid City, South Dakota 57701

Dr. Andrew A. Frank
Department of Electrical &
Computer Engineering
University of Wisconsin
Engineering Research Building
1800 Johnson Drive, Room 909
Madison, Wisconsin 53706

Mr. J. R. Friley
Pacific Northwest Laboratory
P.O. Box 999
Richland, Washington 99352

Mr. Alexander Gokhman
EDS Nuclear Corporation, Inc.
220 Montgomery Street
San Francisco, California 94104

Mr. A. J. Giramonti
United Technologies Research Center
East Hartford, Connecticut 06108

Dr. P. F. Gnirk
RE/SPEC Inc.
P.O. Box 725
Rapid City, South Dakota 57701

Dr. Lyle Hoppie
Principal Engineer
Eaton Corporation
Engineering and Research Center
26201 Northwestern Highway
P.O. Box 766
Southfield, Michigan 48037

Mr. D. Kerr
General Electric Company
P.O. Box 43
Schenectady, New York 12301

Mr. Satish Kulkarni
Larence Livermore Laboratory
P.O. Box 808, L-502
Livermore, California 94550

Dr. Walter V. Loscutoff
Pacific Northwest Laboratory
P.O. Box 999
Richland, Washington 99352

Mr. Ed L. Lustenader
General Electric Company
Research & Development Center
1 River Road
Building 37, Room 311
P.O. Box 43
Schenectady, New York 12301

Mr. Arthur J. Mansure
BDM Corporation
2600 Yale Boulevard, S.E.
Albuquerque, New Mexico 87106

Mr. Osmond K. Mawardi
School of Engineering
Case Western Reserve University
Cleveland, Ohio 44106

Mr. L. B. McEwen, Jr.
Jalar Associates
2104 Windsor Road
Alexandria, Virginia 22307

Mr. A. Keith Miller
Sandia Laboratory
P.O. Box 5800
Albuquerque, New Mexico 87115

Mr. Alan Millner
Massachusetts Institute of Technology
Lincoln Laboratories
Room 1-302
P.O. Box 73
Lexington, Massachusetts 02173

Mr. Ron Nimmer
General Electric Company
P.O. Box 43
Schenectady, New York 12301

Mr. Arlo Nord
Sandia Laboratory
P.O. Box 5800
Albuquerque, New Mexico 87115

Mr. Leo Norrup
Garrett AiResearch Corporation
2525 West 190th Street
Torrance, California 90509

Mr. Terrence O'Rourke
Special Counsel to Alfred Kahn
Office of the Advisor to
the President on Inflation
Old Executive Office Building
Room 200
Washington, D.C. 20500

Mr. Theodore W. Place
Garrett AiResearch Corporation
2525 West 190th Street
Torrance, California 90509

Mr. John Purcell
General Atomics
P.O. Box 81608
San Diego, California 92138

Mr. D. W. Rabenhorst
Applied Physics Laboratory
Johns Hopkins University
Johns Hopkins Road
Laurel, Maryland 20810

Mr. Art E. Raynard
Garrett AiResearch Corporation
2525 W. 190th Street
Torrance, California 90509

Mr. James A Rinde
Lawrence Livermore Laboratory
P.O. Box 808, L-338
Livermore, California 94550

Dr. John D. Rogers, Jr.
Los Alamos Scientific Laboratory
Org. CTR-9, Mail 464
Los Alamos, New Mexico 87545

Mr. Carl Rosner
Intermagnetics General Corporation
Charles Industrial Park
New Karner Road
Guiderland, New York 12084

Mr. David L. Satchwell
Garrett AiResearch Corporation
2525 W. 190th Street
Torrance, California 90509

Mr. Robert Schermen
Los Alamos Scientific Laboratory
Los Alamos, New Mexico 87545

Mr. Harold Schildknecht
Sandia Laboratories
Division 2324
Albuquerque, New Mexico 87185

Mr. S. C. Schulte
Research Engineer
Battelle Pacific Northwest Laboratories
Battelle Blvd
Richland, Washington 99352

Mr. James J. Skiles
University of Wisconsin
531 Engineering Research Building
Madison, Wisconsin 53706

Rob Steele
Oak Ridge Y-12 Plant
Oak Ridge, Tennesee 37830

Mr. J. A. Stottlemyre
Pacific Northwest Laboratoy
P.O. Box 999
Richland, Washington 99352

Dr. James H. Swisher
Division of Energy Storage System
U.S. Department of Energy
600 E Street, N.W.
Room 416
Washington, D.C. 20585

Mr. S. W. Tam
Argonne National Laboratory
9700 South Cass Avenue
Argonne, Illinois 60439

Dr. Robert L. Thoms
Geomechanics Group
Louisana State University
Institute for Environmental Studies
Rm. 42 Atkinson Hall
Baton Rouge, Lousiana 70803

Professor S. van Sciver
531 Engineering Research Building
15000 Johnson Drive
University of Wisconsin
Madison, Wisconsin 53706

Dr. Jack Vanderryn
Director Office of Technical
Cooperation - Office of Intn'l
Affairs
U.S. DOE
&G-090 M.S. 7F-031
Forestal Bldg.
1000 Ind. Avenue
Washington, D.C.

Mr. L. Wiles
Pacific Northwest Laboratory
P.O. Box 999
Richland, Washington 99352

Ms. Bette Winer
Arthur D. Little, Inc.
Acorn Park
Cambridge, Massachusetts 02140

Mr. Ed Wu
Lawrence Livermore Laboratory
P.O. Box 808
Livermore, California 94550

Mr. Robert O. Woods
Sandia Laboratories
P.O. Box 5800
Albuquerque, New Mexico 87115

Mr. Francis C. Younger
William M. Brobeck & Associates
1235 Tenth Street
Berkeley, California 94710

1979 MECHANICAL AND MAGNETIC ENERGY STORAGE CONTRACTORS' REVIEW

Capital Hilton Hotel
Washington, D. C.

August 19-22, 1979

LIST OF ATTENDEES

ACKERMAN, Sam L.
Director, Advanced Magnet Systems
General Dynamics, Convair Division
10170 County View Road
La Mesa, California 92041

ADOLFSON, William F.
Project Engineer
Booz, Allen & Hamilton
4330 East West Highway
Bethesda, Maryland 20014

ALLEN, Bob
Research Scientist/Engineer
Pacific Northwest Laboratory
Battelle Boulevard
Richland, Washington 99352

BAHADUR, Sher
Senior Engineer
Acres American Incorporated
329 Clark Building
Columbia, Maryland 21044

BERVIG, Dr. Dale
Managing Project Engineer
Black and Veatch
10235 Oakmont Circle
Lenexa, Kansas 66215

BEULINGMANN, Dr. R. F.
Program Director, Energy Systems
General Dynamics, Convair Division
8215 Prestwick Drive
La Jolla, California 92037

BOCART, S. Locke
Staff Scientist
Science Application, Incorporated
8400 Westpark Drive
McLean, Virginia 22102

BORTZ, Susan E.
Management Analyst
OAO Corporation
2101 L Street, N. W., Suite 800
Washington, D. C. 20037

BRANDSHAUG, Terje
Staff Engineer
RE/SPEC Incorporated
P. O. Box 725
Rapid City, South Dakota 57709

BYERLY, R. T.
Advisory Engineer
Westinghouse Electric Corporation
2040 Ardmore Boulevard
Pittsburgh, Pennsylvania 15221

CALLAHAN, Gary D.
Vice President
RE/SPEC Incorporated
P. O. Box 725
Rapid City, South Dakota 57709

CAMPBELL, Jim
Program Manager
Department of Transportation
400 7th Street, S. W.
Washington, D. C. 20590

CAPOZZI, Danelle M.
Consultant
OAO Corporation
2101 L Street, N. W., Suite 800
Washington, D. C. 20037

KAPNER, Mark
Senior Engineer
Hittman Associates, Inc.
9190 Red Branch Road
Columbia, Maryland 21045

KATZ, Donald L.
Professor
University of Michigan
College of Engineering - Ann Arbor
Ann Arbor, Michigan 48109

KAY, John F.
Advanced Engineer
Owens Corning Fiberglass
Technical Center
Granville, Ohio 43023

KING, Dennis
Technical Manager
Lawrence Livermore Laboratory
P. O. Box 808
Livermore, California 94550

KUBO, Larry
Member of Technical Staff
Aerospace Corporation
2350 East El Segundo
El Segundo, California 90245

LANGILL, Richard
Consultant
20150 Wynnfield Drive
Germantown, Maryland 20767

LAVERICK, C.
49C LaBowe Vie Drive
East Patchogue, New York 11772

LEHMAN, Leo J., Jr.
Project Engineer
Acres American, Incorporated
Clark Building, Suite 329
Columbia, Maryland 21044

LEMMENS, Joseph R.
Consultant
Kinergy Research & Development
(Marshall Oil Company, Incorporated)
P. O. Box 1128
Wake Forest, North Carolina 27587

LORENZEN, Harro
Vice President
PB-KBB, Incorporated
800 West Commerce Road
Harahan, Louisiana 70123

LUCAS, Edward J.
President
Magnetic Corporation of America
179 Bear Hill Road
Waltham, Massachusetts 02154

MC ALEVY, R. F., III
Senior Associate
R. F. McAlevy III & Associates
P. O. Box 300
Hampton Bays, New York 11946

MC DONALD, Alan T.
Professor
Purdue University
School of Mechanical Engineering
West Lafayette, Indiana 47907

MC LAUGHLIN, Dr. Philip V., Jr.
Associate Professor of
Mechanical Engineering
Villanova University
Department of Mechanical Engineering
Villanova, Pennsylvania 19081

MC PHERSON, Anna
Registration Staff Member
OAOCO/GREYHOUND
1625 K Street, N. W.
Washington, D. C. 20037

MARSHALL, H. K.
President
Kinergy Research & Development
(Marshall Oil Company, Inc.)
Wake Forest, North Carolina 27587

MARTI, Dr. Joaquin
Senior Engineer
Dames and Moore
123 Mortlake High Street
London SW 4 85N
United Kingdom

MOORE, John E.
Staff
Los Alamos Scientific Laboratory
3458-B Urban Street
Los Alamos, New Mexico 87544

MORAN, Bill
Physicist
Lawrence Livermore Laboratory
P. O. Box 808
Livermore, California 94550

NOLAN, Barbara K.
Conference Coordinator
OAO Corporation
2101 L Street, N. W., Suite 800
Washington, D. C. 20037

MUELLER, Barbara Jo
Program Manager
U. S. Department of Energy
9800 South Cass Avenue
Argonne, Illinois 60439

PAGE, Donna
Registration Staff Member
OAOCO/GREYHOUND
1625 K Street, N. W.
Washington, D. C. 20037

O'Neil, W. K.
Chief Engineer
Eaton Corporation
Northwestern Highway
Southfield, Michigan 48076

PARADIS, L. R.
Principal Engineer
Raytheon Company
Hartwell Road
Bedford, Massachusetts 01730

PARDOEN, Dr. Gerard
Chief Engineer
U. S. Flywheels, Incorporated
1882 McGaw Avenue
Irvine, California 92714

PATRICK, Jan
Manager
Energy Business Development
AVCO

PEDERSEN, Lester T.
Associate Manager, Projects
Battelle-Pacific Northwest Laboratories
Battelle Boulevard
Richland, Washington 99352

PEZDIRTZ, Dr. George F.
Director
Division of Energy Storage Systems
U. S. Department of Energy
600 E Street, N. W.
Washington, D. C. 20585

PHILLIPS, Jerry J.
Projects Manager
Tennessee Valley Authority
350 Commerce Union Bank Building
Chattanooga, Tennessee 37401

PIERSON, William R.
Research Scientist
Battelle Columbus Laboratory
505 King Avenue
Columbus, Ohio 43201

PITKIN, H.
Contracts Administrator
Lawrence Livermore Laboratory
P. O. Box 808
Livermore, California 94550

PODDER, Amitava
Manager, Energy Group
Hittman Associates, Incorporated
9190 Red Branch Road
Columbia, Maryland 21045

POST, Stephen F.
Engineer
William M. Brobeck & Associates
1235 Tenth Street
Berkeley, California 94710

Poubeau
European Aerospace

REED, Arnold
Senior Engineer
Bradford National Corporation
2 Research Place
Rockville, Maryland 20850

REIMERS, Eberhard
MERADCOM
8807 Strause Court
Springfield, Virginia 22153

ROHDE, Dr. Steve
Senior Research Scientist
General Motors Research Laboratory
Mechanical Research
Warren, Michigan 48090

SCHRAMM, Henry
Management
OAO Corporation
2101 L Street, N. W., Suite 800
Washington, D. C. 20037

SUPOWITH, Alan
Section Chief, Materials
AVCO Systems Division
201 Lowell Street
Wilmington, Massachusetts 01887

SCHWARTZ, Dr. Martin W.
Mechanical Engineer
Lawrence Livermore Laboratory
P. O. Box 808
Livermore, California 94550

SCRIBNER, Dean
Physicist
U. S. Coast Guard
Commandant (G-DSA-3/TP 54)
Washington, D. C. 20590

SKARDA, Carol
Management Analyst
OAO Corpoation
2101 L Street, N. W., Suite 800
Washington, D. C. 20037

SMITH, J. C.
Section Chief
LM&STOR APPS
U. S. Department of Energy
20 Massachusetts Avenue, N. W.
Washington, D. C. 20845

SOLIMAN, Dr. Frank Y
Manager
Ewald Associates, Incorporated
18301 Weaver Road
Detroit, Michigan 48228

STEFONEK, David M.
General Engineer
Bonneville Power Administration - DOE
12th & Pennsylvania Avenue, N. W.
Washington, D. C. 20161

STEKLY, Z. J. J.
Chairman/Technical Director
Magnetic Corporation of America
30 Hampshire Road
Waltham, Massachusetts 02154

STEVENS, William A.
Project Manager
Thermal & Mechanical Energy Storage, EPRI
3412 Hillview Avenue
Palo Alto, California 94303

STONE, Richard G.
Engineer Consultant
Lawrence Livermore Laboratory
P. O. Box 808
Livermore, California 94550

STUART, Judi
Administrative Assistant
OAO Corporation
2101 L Street, N. W., Suite 800
Washington, D. C. 20037

SWARTOUT, Bruce E.
President
U. S. Flywheels, Incorporated
1882 McGaw Avenue
Irvine, California 92714

THOMPSON, Phil
Program Management
U. S. Department of Energy
600 E Street, N. W.
Washington, D. C. 20585

ULLMAN, David G.
Assistant Professor
Department of Mechanical Engineering
Union College
Schenectady, New York 12309

VAN ORDEN, Stuart D.
OAO Corporation
50/50 Powdermill Road
Beltsville, Maryland

WILLETT, D. C.
Vice President
Acres American, Incorporated
900 Liberty Bank Building
Buffalo, New York 14202

WOODBRIDGE, Dr. David D.
Group Manager
Hittman Associates
9190 Red Branch Road
Columbia, Maryland 21045

YOUNG, J. L.
Manager Magnet Programs
Westinghouse Electric
1310 Beulah Road
Pittsburgh, Pennsylvania 15235

ZUCKERBERG, Harry
Mechanical Engineer
Transportation Systems Center
55 Broadway
Cambridge, Massachusetts 02142

ZWEBEN, Dr. Carl
Staff Engineer
General Electric Company
Space Division - M4018
P. O. Box 8555
Philadelphia, Pennsylvania 19101

*U.S. GOVERNMENT PRINTING OFFICE : 1979 0-620-309/1468